7 January 2011 | $10

Science

AAAS

EDITORIAL

NEWS OF THE WEEK

NEWS FOCUS

LETTERS

BOOKS *ET AL.*

POLICY FORUM

PERSPECTIVES

REVIEW

CONTENTS continued >>

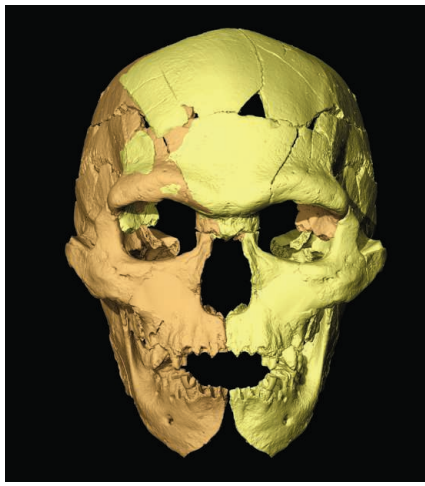

page 20

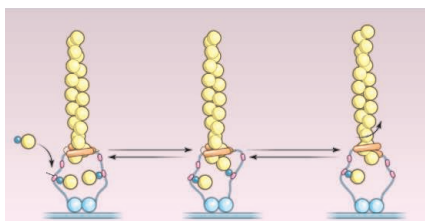

pages 39 & 80

COVER

Multiwavelength extreme ultraviolet image of the Sun taken by the Solar Dynamics Observatory's Atmospheric Imaging Assembly. Colors represent different gas temperatures: ~800,000 kelvin (K) (blue), ~1.3 million K (green), and ~2 million K (red). New observations reveal a link between hot plasma and jets propelled upward from the region immediately above the Sun's surface and help explain why the Sun's outer atmosphere, or corona, is much hotter than its surface. See page 55.

Image: NASA/Solar Dynamics Observatory/ Atmospheric Imaging Assembly

DEPARTMENTS

Published by AAAS

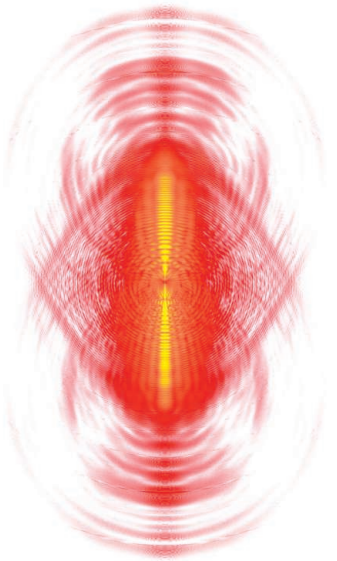

page 61

page 73

BREVIA

RESEARCH ARTICLE

REPORTS

Published by AAAS

SCIENCEONLINE

SCIENCEXPRESS
www.sciencexpress.org

Discovery of Powerful Gamma-Ray Flares from the Crab Nebula
M. Tavani et al.
10.1126/science.1200083

Gamma-Ray Flares from the Crab Nebula
A. A. Abdo et al.
Gamma-ray observations of the Crab Nebula by two different space telescopes challenge particle acceleration theory.
10.1126/science.1199705

Astronomy in the Time Domain
E. Bernardini
10.1126/science.1201365

Seismic Detection of the Lunar Core
R. C. Weber et al.
Reinterpreted Apollo-era seismic data from the Moon reveal a solid inner core and a fluid outer core.
10.1126/science.1199375

A Persistent Oxygen Anomaly Reveals the Fate of Spilled Methane in the Deep Gulf of Mexico
J. D. Kessler et al.
Methane released during the Deepwater Horizon blowout was degraded by methanotrophic bacteria.
10.1126/science.1199697

Human Tears Contain a Chemosignal
S. Gelstein et al.
Merely sniffing women's negative emotional tears reduces sexual arousal in men.
10.1126/science.1198331

Global Tissue Revolutions in a Morphogenetic Movement Controlling Elongation
S. L. Haigo and D. Bilder
The ellipsoid shape of the *Drosophila* egg is controlled by global tissue revolutions that polarize the matrix.
10.1126/science.1199424

SCIENCENOW
www.sciencenow.org
Highlights From Our Daily News Coverage

Collisions Cleared as Cause of Galactic Infernos
Study leaves astronomers puzzling over why the hearts of some galaxies spew radiation.

To Fight Global Warming, Eat Bugs
Farming insects to eat could produce less heat-trapping gas than raising cows and pigs.

Bumblebee Decline Confirmed Across United States
Populations of some species have dwindled by up to 96% in broad regions.

SCIENCESIGNALING
www.sciencesignaling.org
The Signal Transduction Knowledge Environment

EDITORIAL GUIDE: 2010—Signaling Breakthroughs of the Year
E. M. Adler
The editors highlight the year's cell signaling breakthroughs.

RESEARCH RESOURCE: A Genome-Wide RNAi Screen Identifies Core Components of the G_2-M DNA Damage Checkpoint
S. Kondo and N. Perrimon
The DNA damage response in *Drosophila* requires the replication preinitiation complex and the MUS312 nuclease complex.

JOURNAL CLUB: Protein *S*-Nitrosylation in Plants—Photorespiratory Metabolism and NO Signaling
K. J. Gupta
S-nitrosylation of mitochondrial proteins induces cell death in the plant pathogen defense response.

PODCAST
M. B. Yaffe and A. M. VanHook
Chief Scientific Editor Michael Yaffe reviews the year in *Science Signaling*.

SCIENCECAREERS
www.sciencecareers.org/career_magazine
Free Career Resources for Scientists

Taken for Granted: Stormy Weather
B. L. Benderly
Recent reports from the National Academies see no break in the clouds over the scientific labor market.

Seizing Career Opportunities in Turkey
C. Wald
A few researchers trained in the United States and Europe are seeking—and often finding—careers in Turkey.

SCIENCETRANSLATIONAL MEDICINE
www.sciencetranslationalmedicine.org
Integrating Medicine and Science

REVIEW: The p53 Pathway as a Target in Cancer Therapeutics—Obstacles and Promise
A. Mandinova and S. W. Lee
The complex role of the tumor suppressor p53 in normal and malignant cells complicates efforts to target it for cancer therapy.

SCIENCESIGNALING
Signaling breakthroughs of 2010.

RESEARCH ARTICLE: Epigenetic Modification of the *FMR1* Gene in Fragile X Syndrome Is Associated with Differential Response to the mGluR5 Antagonist AFQ056
S. Jacquemont et al.
An antagonist for the metabotropic glutamate receptor improves symptoms in some fragile X syndrome patients.

RESEARCH ARTICLE: Improving Drug Potency and Efficacy by Nanocarrier-Mediated Subcellular Targeting
M. Murakami et al.
Polymeric micelles containing a chemotherapeutic drug carry it adjacent to the DNA target in tumor cells, enhancing the drug potency.

SCIENCEPODCAST
www.sciencemag.org/multimedia/podcast
Free Weekly Show

Download the 7 January *Science* Podcast to hear about sexual ornamentation in butterflies, early human migration out of Africa, your letters to *Science*, and more.

SCIENCEINSIDER
news.sciencemag.org/scienceinsider
Science Policy News and Analysis

SCIENCE (ISSN 0036-8075) is published weekly on Friday, except the last week in December, by the American Association for the Advancement of Science, 1200 New York Avenue, NW, Washington, DC 20005. Periodicals Mail postage (publication No. 484460) paid at Washington, DC, and additional mailing offices. The title SCIENCE is a registered trademark of the AAAS. Domestic individual membership and subscription (51 issues): $149 ($74 allocated to subscription). Domestic institutional subscription (51 issues): $990; Foreign postage extra: Mexico, Caribbean (surface mail) $55; other countries (air assist delivery) $85. First class, airmail, student, and emeritus rates on request. Canadian rates with GST available upon request, GST #1254 88122. Publications Mail Agreement Number 1069624. **Printed in the U.S.A.**

Change of address: Allow 4 weeks, giving old and new addresses and 8-digit account number. **Postmaster:** Send change of address to AAAS, P.O. Box 96178, Washington, DC 20090–6178. **Single-copy sales:** $10.00 current issue, $15.00 back issue prepaid includes surface postage; bulk rates on request. The identification code for *Science* is 0036-8075. *Science* is indexed in the *Reader's Guide to Periodical Literature* and in several specialized indexes.

AAAS
ADVANCING SCIENCE, SERVING SOCIETY

CREDIT: DUNCAN SMITH/THINKSTOCK

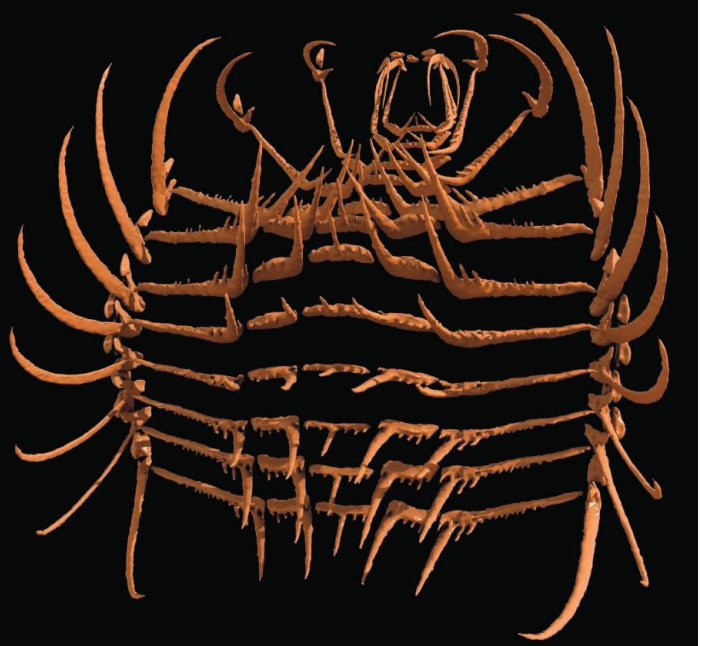

Ammonite, Reconstructed > >

Ammonites were an abundant marine organism that went extinct about the same time as the dinosaurs—roughly 65 million years ago. Although their shells make good fossils, other ammonite structures are rarely discerned. **Kruta *et al.*** (p. 70; see the Perspective by **Tanabe**) have used synchrotron-based x-ray microtomography to visualize and reconstruct the mouthparts of three specimens. The morphology of the jaws and radula suggests that ammonites fed on small marine invertebrates—indeed, tiny crustaceans and snail-like gastropods were found among the jaws of one specimen.

Heating the Solar Atmosphere

The question of why the Sun's outer atmosphere, or corona, is much hotter than its surface is one of the main unresolved issues in solar astrophysics. By combining measurements from NASA's Solar Dynamics Observatory and the Japanese Hinode satellite, De Pontieu *et al.* (p. 55) show that jets of plasma propelled upward from the region immediately above the Sun's surface are implicated in the heating of the solar corona. The results challenge current models for coronal heating and show that the interface region between the surface of the Sun and its corona plays a crucial role in energizing the solar atmosphere.

Spinning the Unspinnable

Weaving and spinning can take a weak material like straw or yarn and turn it into a much tougher rope. **Lima *et al.*** (p. 51) found that by using carbon nanotubes as a support material, they could spin and weave a range of materials that otherwise are considered intractable to such manipulation, ranging from superconductors to sutures containing biomedical agents. The desired materials were deposited onto a web of multiwalled carbon nanotubes, using an electrostatic powder coating gun, and then twisted into yarns, which could be knotted and sewn, and showed excellent retention of the guest particles when subjected to solvents or a mechanical washing cycle.

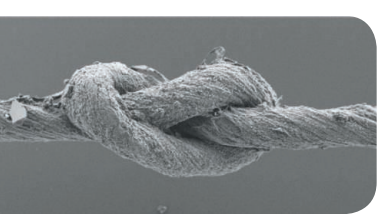

Toward Perfection?

When physicists tried to re-create the conditions believed to have existed microseconds after the Big Bang, they found, to their surprise, that the resulting "soup" of quarks and gluons behaved not like a gas, but like a perfect (frictionless) liquid. **Cao *et al.*** (p. 58, published online 9 December) have studied one such candidate for a perfect liquid at a convenient scale—a dilute gas of fermionic Li-6 atoms—and measured its viscosity in a wide temperature range. The results were consistent with expectations that a resonant Fermi gas would have properties dependent only on density and temperature. Although the estimated viscosity/entropy ratio approached the perfect fluid limit, it still exceeded it by fivefold. Nevertheless, these measurements can now be compared with advanced theoretical models.

Spinning for Naught

Large-scale structures or discontinuities in Earth's interior are typically caused by transformations in the physical or chemical properties of minerals that occur when pressure increases with depth. For example, an electronic spin transition in iron atoms within minerals that are stable at high pressures and temperatures has been predicted to influence some minerals' compressibility and, hence, the speed of sound waves passing through the lower mantle. Using an inelastic x-ray scattering technique at high pressures, **Antonangeli *et al.*** (p. 64) show that the spin transition in fact does not influence how ferroperriclase (a major lower-mantle mineral) is compressed, but it does appear to affect anisotropy (i.e., directionally dependent properties) within ferroperriclase, which may account for the observed directional dependence of some seismic waves in the lower mantle, even though the spin transition itself, which should occur at a defined depth, does not correspond to any specific structure or anomaly in the lower mantle.

Seasonal Behavioral Plasticity

The African butterfly *Bicyclus anynana* shows a sex-role reversal in courtship behavior, which is set during larval development and controlled by larval rearing temperature. In the wet season form, the males court and the females choose, while in the dry season form, females court and males choose. **Prudic *et al.*** (p. 73) show that these changes in mating behavior correlate with a cryptic change of the sexual ornament in both sexes. In the wet season, males have brighter sexual signal in the ultraviolet (UV) range, and in the dry season, females have a brighter sexual signal in the UV range. These changes in both sexual roles and signal are also correlated with a change in costs and benefits to mating among the different seasonal forms. Females have both increased longevity and reproductive output if they mate with dry season males, but dry season males have a reduced life span when mated, while wet season males do not. Thus, reciprocal patterns of sexual selection through the seasons result in mutual ornamentation.

CREDITS (TOP TO BOTTOM): KRUTA & LETHIERS, UMR 7207; LIMA *ET AL.*

Steady As She Goes

Most of the chemical oxidation of atmospheric gases and particles is done by the hydroxyl radical (OH). However, the concentration of atmospheric hydroxyl radicals is extremely difficult to measure, so it must be inferred from measurements of the abundance of other species, like methyl chloroform. Past studies of atmospheric methyl chloroform have indicated that OH can undergo large annual shifts in concentration, although atmospheric models predict a less variable history. Taking data since 1998 and advantage of the Montreal Protocol in limiting methyl chloroform emissions, **Montzka *et al.*** (p. 67; see the Perspective by **Isaksen and Dalsøren**) calculated a more precise estimate of OH variability and find that it varies in concentration less than has been assumed. The results help resolve differences between earlier results, other proxies, and global photochemical models.

Chill Wind

For many plants, the chilly temperatures of winter act to coordinate flowering with the more favorable growth environment that follows in springtime. This process of vernalization translates environmental temperatures into developmental responses through a cascade of molecular responses that depend on epigenetic regulation of the floral repressor. **Heo and Sung** (p. 76, published online 2 December; see the Perspective by **Turck and Coupland**) have identified an RNA that is transcribed from an intron of the repressor gene, but that itself does not encode a protein. Instead, this non-coding RNA, called COLDAIR, adds a histone-methylating complex onto the repressor locus. With the repressive gene itself repressed, the stage is then set to allow flowering.

Nitrogenase Assembly Pathway

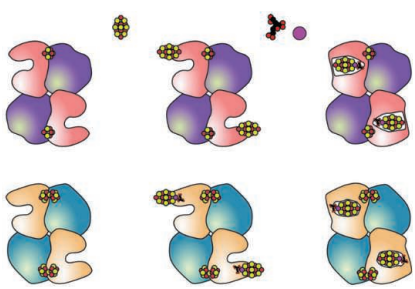

A key step in the global nitrogen cycle is the reduction of atmospheric dinitrogen to ammonia by nitrogenase, a complex metalloenzyme. The catalytic component of this enzyme, the molybdenum-iron protein NifDK, comprises two unusual metallo-clusters, the [8Fe-7S] P cluster and the [Mo-7Fe-9S-X-homocitrate] M cluster. Likewise, the protein NifEN displays sequence similarity to NifDK, but it plays a role in nitrogenase assembly: It converts an iron-only precursor form to the mature molybdenum cluster and delivers this to NifDK. **Kaiser *et al.*** (p. 91) describe the crystal structure of NifEN. By making a structural comparison with apo and holo NifDK, the pathway of cluster insertion can be inferred, which indicates that it is similar in both NifEN and NifDK proteins.

The Mechanics of Movement

Within cells, formin proteins promote the elongation of cytoskeletal actin filaments by associating with filament tips. This activity has the potential to harness actin-generated pushing forces to change cellular architecture. **Mizuno *et al.*** (p. 80, published online 9 December; see the Perspective by **Pollard**) have devised a simple method to analyze the movement of single molecules of a member of the formin family, mDia1, along the growing actin filaments; they discovered that formin molecules mechanically rotate on the end of actin filaments, both during growth and depolymerization of the filament, and can thus influence cell shape during important stages in the cell cycle.

Mind the Gap (Junction)

The role of chemical synapses in learning and memory in the adult mammalian brain is well established. In contrast, the more rapid neuronal transmission that is mediated by electrical synapses is not fully understood. Using a variety of different manipulations—including fear conditioning, drugs, and electrophysiological recordings—in freely moving rats, **Bissiere *et al.*** (p. 87) discovered that blocking neuronal gap junctions containing connexin 36 controls the acquisition and the consolidation of fear memories within the dorsal hippocampus. It appears that interfering with gap junction–mediated neuronal transmission selectively prevented the formation of a memory during aversive experiences such as fear conditioning.

CREDIT: KAISER *ET AL.*

Published by AAAS

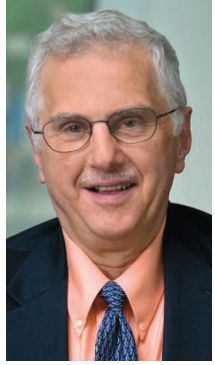

Bruce Alberts is Editor-in-Chief of *Science*.

A New College *Science* Prize

TO START THE NEW YEAR, *SCIENCE* IS PLEASED TO ANNOUNCE THE "*SCIENCE* PRIZE FOR Inquiry-Based Instruction" to highlight outstanding "modules" for teaching introductory college science courses that can readily spread to other settings and schools. Therefore, a unit can neither be unusually expensive nor require highly specialized expertise. To be eligible, a module must provide a coherent piece of coursework in a field such as biology, chemistry, physics, or earth sciences and require 8 to 50 hours of student effort. It should also be free-standing: that is, suitable for teaching as a discrete unit, independent of other modules in the course. How do inquiry-based science modules differ from other science lessons, and why does *Science* care enough about them to create a special prize?

Inquiry-based classes focus on activating students' natural curiosity in exploring how the world works, differing from traditional lectures that focus on transmitting facts and principles derived from what scientists have discovered. Inquiry-based teaching is often associated with hands-on activities. But not all hands-on activities involve inquiry. Consider the laboratory work that traditionally accompanies an introductory college science course. As a science major, I spent three afternoons a week in such laboratories throughout my first 2 college years. Most of us who later became scientists recall these laboratories as tedious "cooking classes," where we learned to follow directions. True, we encountered various pieces of scientific apparatus, such as measuring devices for weights and liquids, and we learned how to keep a laboratory notebook. But we gained neither any real understanding of the nature of science nor experience in generating and evaluating scientific evidence and explanations—two central elements of a modern definition of "science education."* Many college laboratory exercises remain deficient in precisely these ways today.

Science is looking for lessons in which students become invested in exploring questions through activities that are at least partially of their own design. Instead of a typical laboratory exercise that begins with an explanation and results in one correct answer, an inquiry-based lesson might begin with a scenario or question and then require students to propose possible solutions and design some of their own experiments.

In addition to honoring the 12 winning modules, we will attempt to disseminate them as widely as possible. To this end, each winner will write a brief essay describing the module, to be published in *Science*, with complete details in the supporting online material that accompanies the printed article. Direct applications from the course organizers are welcome, as are nominations from former students and colleagues. Different submission forms have been provided for these two groups, posted at http://scim.ag/inquiryprize, along with instructions describing the information required by our judges. The deadline for receiving the short nomination form is 28 February 2011; the longer application form is due from the course organizers on 15 April.

The 1990s science education standards movement in the United States revealed that teachers at the precollege level cannot be expected to teach "science as inquiry" unless they themselves have previously participated in such inquiry as students. Incorporating inquiry into college science teaching will thus be critical for the future teachers of science in all nations. But it will also be crucial for many other adults, because successful modern societies need large numbers of citizens who are skilled, rational problem-solvers—both in the workplace and in their daily lives. Every society also requires citizens who understand the nature of science and value "science as a way of knowing" about important issues. In fact, our new award has been stimulated by the fact that the world badly needs a revolution in science education—a revolution that must begin at the college level.

– Bruce Alberts

10.1126/science.1202096

*B. Alberts, *Science* **323**, 437 (2009).

Published by AAAS

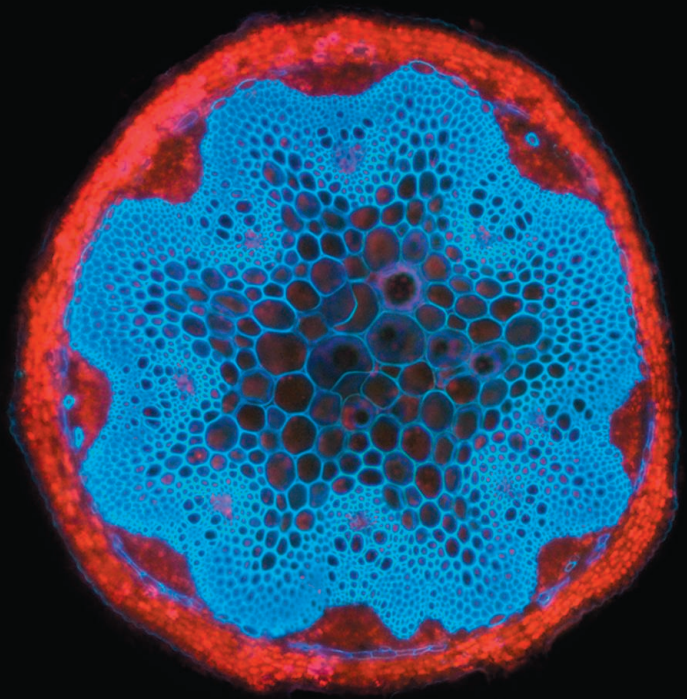

PLANT SCIENCE

Boosting Biofuels

The cell walls of plant stems that are stiffened by lignocellulose not only support an upright growth habit but are also coincidentally used as the starting materials for biofuel production. Studying *Arabidopsis* and *Medicago*, Wang *et al.* now show that WRKY transcription factors control the stiffening of cell walls in some tissues. The authors identified mutations in *Medicago* that resulted in plants with increased lignin content. Related genes were identified in *Arabidopsis* and poplar. In *Arabidopsis*, cells in the central pith of the stem normally have thin cell walls. Cells in the next layer out have thicker cells walls filled with lignin and cellulose. Deletion of WRKY transcription factors resulted in pith cells whose cell walls are thickened with lignin and cellulose; the resulting plants deliver more biomass per plant. Cell walls in other layers of the stem were unaffected, and overall growth of the plant appeared normal. Such insights into the molecular regulation of lignocellulose formation point to a possible way to increase biomass yield for biofuel production. — PJH

Proc. Natl. Acad. Sci. U.S.A. **107**, 22338 (2010).

MICROBIOLOGY

A Boring Life

In the deep oceans, carbonate minerals precipitate slowly, forming the building blocks of limestone or the shells of many marine organisms. Some filamentous bacteria, including photosynthetic autotrophs, can bore deep into these carbonates, but this biological mining process remains a paradox; photosynthesis usually causes carbonates to grow, not dissolve. Garcia-Pichel *et al.* showed how one type of cyanobacteria—originally isolated from a marine snail shell—was able to bore into chips of calcite ($CaCO_3$) in laboratory experiments by controlling the saturation state of calcium. A number of tests, including enzyme-inhibition assays and fluorescence microscopy, suggest that these bacteria used a calcium-ion pump to transport calcium from the boring front, through the cell, and then back out toward the top of the bore hole. Furthermore, based on experiments in both light and dark conditions, boring was probably not directly related to photosynthetic activity. If this mechanism is widespread in other marine carbonates, inhibiting calcium-ion pumps in some cyanobacteria could slow the destructive dissolution of coral reefs and shellfish. — NW

Proc. Natl. Acad. Sci. U.S.A. **107**, 21749 (2010).

SCIENCE POLICY

Electrifying Success?

Liberalization of the UK electricity sector beginning in the 1990s restructured the market by privatizing assets and reforming regulations. The goal was to improve the efficiency of the industry by increasing competition. Jamasb and Pollitt have now analyzed the impact on UK patenting activity and R&D investment in the electricity sector. They noted that whereas government R&D investment had already been declining, this trend was amplified after liberalization, although some increase has been seen in recent years, particularly in renewable energy. Private R&D also diminished after liberalization. Patenting activity, a marker of technology innovation, initially increased, probably reflecting increased emphasis on commercialization of R&D in the electricity industry. In recent years, though, UK patenting has slowed, which the authors attribute to decreased investment in basic R&D and increased foreign ownership of large utilities, which may lead to the transfer of R&D efforts out of the United Kingdom. They highlight efforts such as the Energy Technologies Institute and Innovation Funding Incentive, which aim to integrate public investment and market incentives to promote long-term R&D needed to ensure industry innovation. — BW

Concept House, site of the UK Intellectual Property Office.

Res. Policy 10.1016/j.respol.2010.10.010 (2010).

CHEMISTRY

Hothouse Catalysis

Although some have said that physical organic chemistry is a field whose time has passed, it still is possible, with a bit of creativity, to extract provocative ideas from the growing compendium of chemical data collected on those most interesting of catalysts, enzymes. Stockbridge *et al.* begin with Arrhenius plots, which relate the logarithm of the rate constant to the reciprocal of temperature. They use these to estimate the rates of reaction of a variety of conversions, such as the hydrolysis of peptide bonds and of phosphate monoesters, and find large enhancements as the temperature increases from the common laboratory setting of 25°C to the primordial environment of 100°C, which turn out to be 3000-fold for the former and 10^7-fold for the latter. Why should we care? Because the rates of the slowest reactions increase the most, and thus the synthesis and transformation of small organic molecules would have flourished at 100°C. Enzymes, which make these reactions go fast enough at 25°C to sustain life today, would have been highly sought after as the ambient conditions cooled. Furthermore, lowering enthalpic barriers, as most enzymes do, is a more effective catalytic strategy than boosting entropy as temperatures drop. — GJC

Proc. Natl. Acad. Sci. U.S.A. **107**, 22102 (2010).

CREDITS (TOP TO BOTTOM): SCOTT MCNEIL; INTELLECTUAL PROPERTY OFFICE

www.sciencemag.org

Science

1200 New York Avenue, NW
Washington, DC 20005
Editorial: 202-326-6550, FAX 202-289-7562
News: 202-326-6581, FAX 202-371-9227
Bateman House, 82-88 Hills Road
Cambridge, UK CB2 1LQ
+44 (0) 1223 326500, FAX +44 (0) 1223 326501

Subscription Services For change of address, missing issues, new orders and renewals, and payment questions: 866-434-AAAS (2227) or 202-326-6417, FAX 202-842-1065. Mailing addresses: AAAS, P.O. Box 96178, Washington, DC 20090-6178 or AAAS Member Services, 1200 New York Avenue, NW, Washington, DC 20005

Institutional Site Licenses please call 202-326-6755 for any questions or information

Reprints: Author Inquiries 800-635-7181
Commercial Inquiries 803-359-4578

Permissions 202-326-7074, FAX 202-682-0816

Member Benefits AAAS/Barnes&Noble.com bookstore www.aaas.org/bn; AAAS Online Store www.apisource.com/aaas/ code MKB6; AAAS Travels: Betchart Expeditions 800-252-4910; Apple Store www.apple.com/eppstore/aaas; Bank of America MasterCard 1-800-833-6262 priority code FAA3YU; Cold Spring Harbor Laboratory Press Publications www.cshlpress.com/affiliates/aaas.htm; GEICO Auto Insurance www.geico.com/landingpage/go51.htm?logo=17624; Hertz 800-654-2200 CDP#343457; Office Depot https://bsd.officedepot.com/portalLogin.do; Seabury & Smith Life Insurance 800-424-9883; Subaru VIP Program 202-326-6417; VIP Moving Services www.vipmayflower.com/domestic/index.html; Other Benefits: AAAS Member Services 202-326-6417 or www.aaasmember.org.

science_editors@aaas.org	(for general editorial queries)
science_letters@aaas.org	(for queries about letters)
science_reviews@aaas.org	(for returning manuscript reviews)
science_bookrevs@aaas.org	(for book review queries)

Published by the American Association for the Advancement of Science (AAAS), *Science* serves its readers as a forum for the presentation and discussion of important issues related to the advancement of science, including the presentation of minority or conflicting points of view, rather than by publishing only material on which a consensus has been reached. Accordingly, all articles published in *Science*—including editorials, news and comment, and book reviews—are signed and reflect the individual views of the authors and not official points of view adopted by AAAS or the institutions with which the authors are affiliated.

AAAS was founded in 1848 and incorporated in 1874. Its mission is to advance science, engineering, and innovation throughout the world for the benefit of all people. The goals of the association are to: enhance communication among scientists, engineers, and the public; promote and defend the integrity of science and its use; strengthen support for the science and technology enterprise; provide a voice for science on societal issues; promote the responsible use of science in public policy; strengthen and diversify the science and technology workforce; foster education in science and technology for everyone; increase public engagement with science and technology; and advance international cooperation in science.

Information for Authors
See pages 352 and 353 of the 15 January 2010 issue or access www.sciencemag.org/about/authors

EDITOR-IN-CHIEF **Bruce Alberts**
EXECUTIVE EDITOR **Monica M. Bradford** NEWS EDITOR **Colin Norman**
MANAGING EDITOR, RESEARCH JOURNALS **Katrina L. Kelner**
DEPUTY EDITORS **R. Brooks Hanson, Barbara R. Jasny, Andrew M. Sugden**

Editorial senior editors/commentary Lisa D. Chong, Brad Wible; **senior editors** Gilbert J. Chin, Pamela J. Hines, Paula A. Kiberstis (Boston), Marc S. Lavine (Toronto), Beverly A. Purnell, L. Bryan Ray, Guy Riddihough, H. Jesse Smith, Phillip D. Szuromi (Tennessee), Valda Vinson, Jake S. Yeston; **associate editors** Kristen L. Mueller, Jelena Stajic, Sacha Vignieri, Nicholas S. Wigginton, Laura M. Zahn (San Diego); **book review editor** Sherman J. Suter; **associate letters editor** Jennifer Sills; **editorial manager** Cara Tate; **senior copy editors** Jeffrey E. Cook, Cynthia Howe, Harry Jach, Lauren Kmec, Barbara P. Ordway, Trista Wagoner; **copy editor** Chris Filiatreau; **editorial coordinators** Carolyn Kyle, Beverly Shields; **publications assistants** Ramatoulaye Diop, Joi S. Granger, Emily Guise, Jeffrey Hearn, Michael Hicks, Lisa Johnson, Scott Miller, Jerry Richardson, Jennifer A. Seibert, Brian White, Anita Wynn; **editorial assistants** Emily C. Horton, Patricia M. Moore, Miriam Weinberg; **executive assistant** Alison Crawford; **administrative support** Maryrose Madrid; **editorial fellow** Melissa R. McCartney

Editorial director, web and new media Stewart Wills; **senior web editor** Tara S. Marathe; **web editor** Robert Frederick; **research associate** Corinna Cohn; **web development manager** Martyn Green; **web developer** Andrew Whitesell; **intern** Sophia Cai

News deputy news editors Robert Coontz, David Grimm (Online), Eliot Marshall, Jeffrey Mervis, Leslie Roberts; **contributing editors** Elizabeth Culotta, Polly Shulman; **news writers** Yudhijit Bhattacharjee, Adrian Cho, Jennifer Couzin, Jocelyn Kaiser, Richard A. Kerr, Eli Kintisch, Greg Miller, Elizabeth Pennisi, Lauren Schenkman, Robert F. Service (Pacific NW), Erik Stokstad; **web developer** Daniel Berger; **intern** Sara Reardon; **contributing correspondents** Jon Cohen (San Diego, CA), Daniel Ferber, Ann Gibbons, Sam Kean, Andrew Lawler, Mitch Leslie, Charles C. Mann, Virginia Morell, Gary Taubes; **copy editors** Linda B. Felaco, Melvin Gatling, Melissa Raimondi; **administrative support** Scherraine Mack; **bureaus** San Diego, CA: 760-942-3252, FAX 760-942-4979; Pacific Northwest: 503-963-1940

Production director Wendy K. Shank; **assistant manager** Rebecca Doshi; **senior specialists** Steve Forrester, Chris Redwood, Anthony Rosen; **Preflight director** David M. Tompkins; **manager** Marcus Spiegler; **specialist** Jason Hillman

Art director Yael Fitzpatrick; **associate art director** Laura Creveling; **senior illustrators** Chris Bickel, Katharine Sutliff; **illustrator** Yana Hammond; **senior art associates** Holly Bishop, Preston Huey, Nayomi Kevitiyagala; **art associates** Kay Engman, Matthew Twombly; **photo editor** Leslie Blizard

***Science* International**

Europe (science@science-int.co.uk) **editorial: international managing editor** Andrew M. Sugden; **senior editor/commentary** Julia Fahrenkamp-Uppenbrink; **senior editors** Caroline Ash, Stella M. Hurtley, Ian S. Osborne, Peter Stern; **associate editor** Maria Cruz; **locum editor** Helen Pickersgill; **editorial support** Samantha Hogg, Alice Whaley; **administrative support** John Cannell, Janet Clements, Louise Hartwell; **news: europe news editor** John Travis; **deputy news editor** Daniel Clery; **contributing correspondents** Michael Balter (Paris), John Bohannon (Vienna), Martin Enserink (Amsterdam and Paris), Gretchen Vogel (Berlin); **intern** Jennifer Carpenter

Latin America contributing correspondent Antonio Regalado

Asia Japan Office: Asca Corporation, Tomoko Furusawa, Rustic Bldg. 7F, 77 Tenjin-cho, Shinjuku-ku, Tokyo 162-0808, Japan; +81 3 6802 4616, FAX +81 3 6802 4615, inquiry@sciencemag.jp; **asia news editor** Richard Stone (Beijing: rstone@aaas.org); **contributing correspondents** Dennis Normile [Japan: +81 (0) 3 3391 0630, FAX +81 (0) 3 5936 3531; dnormile@gol.com]; Hao Xin [China: cindyhao@gmail.com]; Pallava Bagla [South Asia: +91 (0) 11 2271 2896; pbagla@vsnl.com]

EXECUTIVE PUBLISHER **Alan I. Leshner**
PUBLISHER **Beth Rosner**

Fulfillment Systems and Operations (membership@aaas.org); **director** Waylon Butler; **customer service supervisor** Pat Butler; **specialists** Latoya Casteel, LaVonda Crawford, Vicki Linton, April Marshall; **data entry supervisor** Cynthia Johnson; **specialists** Shirlene Hall, Tarrika Hill, William Jones

Business Operations and Administration director Deborah Rivera-Wienhold; **business systems and financial analysis director** Randy Yi; **manager, business analysis** Eric Knott; **manager, business operations** Jessica Tierney; **financial analysts** Priti Pamnani, Celeste Troxler; **rights and permissions: administrator** Emilie David; **associate** Elizabeth Sandler; **marketing director** Ian King; **marketing managers** Allison Pritchard, Alison Chandler, Julianne Wielga; **marketing associates** Aimee Aponte, Mary Ellen Crowley, Wendy Wise; **senior marketing executive** Jennifer Reeves; **director, site licensing** Tom Ryan; **director, corporate relations** Eileen Bernadette Moran; **publisher relations, eresources specialist** Kiki Forsythe; **senior publisher relations specialist** Catherine Holland; **publisher relations, east coast** Phillip Smith; **publisher relations, west coast** Philip Tsolakidis; **fulfillment supervisor** Iquo Edim; **fulfillment coordinator** Carrie MacDonald, Destiny Pinson; **marketing manager** Christina Schlecht; **marketing associate** Laura Tutino; **electronic media: manager** Lizabeth Harman; **project manager** Trista Snyder; **assistant manager** Lisa Stanford; **senior production specialists** Ryan Atkins, Christopher Coleman, **computer specialist** Walter Jones, Kai Zhang; **production specialists** Antoinette Hodal, Nichele Johnston, Kimberly Oster; **director, web and new media** Will Collins

advertising director, worldwide ad sales Bill Moran
commercial editor Sean Sanders: 202-326-6430
assistant commercial editor Tianna Hicklin 202-326-6463

Product (science_advertising@aaas.org); **midwest** Rick Bongiovanni: 330-405-7080, FAX 330-405-7081; **east coast/e. canada** Laurie Faraday: 508-747-9395, FAX 617-507-8189; **west coast/w. canada** Lynne Stickrod: 415-931-9782, FAX 415-520-6940; **uk/europe/asia** Roger Goncalves: TEL/FAX +41 43 243 1358; **japan** ASCA Corporation, Nanako Ide +81 (0) 3 6802 4616, FAX +81 (0) 3 6802 4615; ads@sciencemag.jp; **senior traffic associate** Deiandra Simms

worldwide associate director of *Science* Careers Tracy Holmes: +44 (0) 1223 326525, FAX +44 (0) 1223 326532

Classified (advertise@sciencecareers.org); **u.s.: midwest/west coast/south central/canada** Tina Burks: 202-326-6577; **east coast/industry** Elizabeth Early: 202-326-6578; **sales administrator:** Marci Gallun **sales coordinators** Rohan Edmonson, Shirley Young; **europe/row sales:** Susanne Kharraz, Dan Pennington, Alex Palmer; **sales assistant** Lisa Patterson; **japan** ASCA Corporation, Jie Chin +81 (0) 3 6802 4616, FAX +81 (0) 3 6802 4615; careerads@sciencemag.jp; **advertising support manager** Karen Foote: 202-326-6740; **advertising production operations manager** Deborah Tompkins; **senior production specialist/graphic designer** Amy Hardcastle; **production specialist** Yuse Lajiminmuhip; **senior traffic associate** Christine Hall

AAAS Board of Directors retiring president, chair Peter C. Agre; **president** Alice Huang; **president-elect** Nina Fedoroff; **treasurer** David E. Shaw; **chief executive officer** Alan I. Leshner; **board** Linda P. B. Katehi, Nancy Knowlton, Stephen Mayo, Cherry A. Murray, Julia M. Phillips, Sue V. Rosser, David D. Sabatini, Thomas A. Woolsey

AAAS
ADVANCING SCIENCE, SERVING SOCIETY

EDITED BY LAUREN SCHENKMAN

Cavemen Craved Carbs, Too

Thank goodness they didn't brush. Plaque stuck to the teeth of three Neandertals who died more than 35,000 years ago has yielded evidence that the hominids ate plant food, including cooked plants, and not exclusively meat, as some scientists have suggested.

No one knows why Neandertals disappeared about 25,000 to 30,000 years ago, as modern humans spread across Europe. Some data have suggested that they ate almost exclusively big game, which led to a hypothesis that they couldn't get enough calories to compete with modern humans.

But Amanda Henry, a graduate student of physical anthropology at George Washington University (GWU) in Washington, D.C., thought their teeth might tell a different tale. Like a dental hygienist to the Paleolithic, Henry used dental tools to scrape tiny patches of calculus, or hardened plaque deposits, off Neandertal teeth from museum collections. Through a microscope, she saw grains of starch from seeds of cereal-like grasses; grains of cooked starch; legumelike starches; and hard structures, known as phytoliths, from date palms. Henry, along with anthropologist Alison Brooks of GWU and archaeobotanist Dolores Piperno of the Smithsonian National Museum of Natural History, reported the results online 27 December 2010 in the *Proceedings of the National Academy of Sciences*.

"Here you have good research putting nails in the coffin of the 'meat-eating Neandertals,' " says Harvard University archaeologist Ofer Bar-Yosef, who did not work on the project. He says this shows that, like modern humans, Neandertals ate what was available. "So the question, what caused the demise of the Neandertals and the success of the modern humans—I'm afraid we are not going to find this in the kitchen," Bar-Yosef says.

Chubby Little Guys

Baby fat may be cute, but in extreme cases it could doom young children to a lifetime of dangerous weight troubles, according to a study published in the January/February issue of the *American Journal of Health Promotion*.

Obesity researchers Brian Moss of Wayne State University in Detroit, Michigan, and William Yeaton of the University of Michigan, Ann Arbor, studied data from 16,400 children in the United States born in 2001. At 9 months, 31.9% of the children were either obese or at risk for becoming obese by the standards of the U.S. Centers for Disease Control and Prevention. By age 2, the proportion of at-risk or obese children jumped to 34.3%; 44% of the obese babies were still obese, and 20% of the at-risk babies had grown into obese toddlers. "We were surprised that kids seemed pretty disposed for obesity at such a young age," Moss says.

Hakon Hakonarson, a geneticist and obesity researcher at Children's Hospital of Philadelphia in Pennsylvania, says the study highlights the importance of early intervention in preventing obesity. "It's pretty much what people envisioned to be the case, but now there's data to back it up," he says.

Rose Is a Rose Is a Rose

A rose by any other name may smell as sweet, but duplicate scientific names—and for the rose genus, there are at least 191—are pitfalls for botanists. Now there's a solution. On 29 December 2010, a team from the Missouri Botanical Garden in St. Louis and the Royal Botanic Gardens, Kew, in the United Kingdom announced the completion of The Plant List (www.theplantlist.org), a searchable online compendium of all 1,040,426 species names ever recorded.

Before computers, it was nearly impossible to exhaustively search the literature before naming a new species, so duplicates started to pile up. For about 3 decades, both botanical gardens have been working on electronic databases. In 2008, they joined forces and set computers to the task of sorting out synonyms (*Science*, 10 September 2010, p. 1274). The result: Only 298,900 of the million or so names describe unique species; 477,601 are synonyms.

Another 263,925 names remain unresolved. The team hopes botanists worldwide will help edit the list as they use it. "This is just the start," says botanist Peter Raven, president emeritus of the Missouri Botanical Garden. "But it's a big start."

They Said It

"When the idea first arose of a miniseries on materials science, my first thought was, 'Who will watch this?' Unlike chemistry, physics, biology, who has even heard of materials science? But as I came to see, … there's a reason, after all, why great historical ages are all named for stuff, the Stone Age, the Bronze Age, the Iron Age. Learning that was my personal 'duh' moment."

—Paula Apsell, executive producer of NOVA's *Making Stuff*, a four-part television series on materials science. The first episode airs on the U.S. PBS network on 19 January.

CREDITS (TOP TO BOTTOM): AMANDA HENRY; THINKSTOCK (2)

Published by AAAS

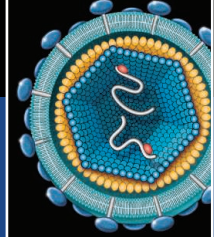

XMRV:
A contaminant?
17

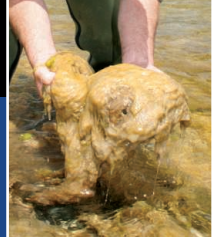

Rock snot invades
Patagonia
18

U.S. SCIENCE POLICY

The Battle Over the 2011 Budget: What's at Stake for Research

The 112th Congress convened this week amid cries from fiscal conservatives to shrink the federal budget and reduce the deficit. With revenues unlikely to grow much now that the outgoing Congress has extended Bush-era income tax cuts for the next 2 years, the immediate task of deficit hawks will be to convince their colleagues that individual agencies should receive less in 2011. But that begs an important question: Less than what?

As federal officials ring in the new year, they are essentially marking time, fiscally speaking. Late last month, Congress agreed to extend 2010 spending levels until 4 March, a date nearly halfway through the 2011 fiscal year, while prohibiting agencies from starting anything new or canceling anything now under way. That means the new Congress—with Republicans controlling the House and Democrats holding a slim margin in the Senate—will decide what agencies can spend for the remainder of the fiscal year ending on 30 September. In the same week, the 111th Congress passed legislation giving some research agencies very specific orders about what to do—or not do—with any money they might receive.

How will Congress play the 2011 budget card? The answer could shape U.S. science for years to come.

The new House speaker, Representative John Boehner (R–OH), says he wants to cut $100 billion from the current $1.1 trillion discretionary budget on the way toward reducing spending to 2008 levels. President Barack Obama has already embraced a 3-year freeze on nonsecurity discretionary spending. But that doesn't necessarily mean a flat science budget, he insists. "If we want to keep our competitive edge, we've got to invest in basic research—the same basic research that resulted in the Internet … [and] in GPS. All those things originated in research funded by the government," Obama explained in a 22 December press conference.

Aversive stimulus. Tea Party activists want the new Congress to roll back initiatives such as the massive 2009 spending package, which included billions for research.

Budget breakdown

It's not that the previous Congress ignored the budget process. Take the National Science Foundation (NSF). In 2010, legislators debated half a dozen bills with proposed 2011 funding levels for NSF that ranged from no increase to a 7.2% boost in its current $6.9 billion allocation.

One of the bills, the America COMPETES Act of 2010, was actually passed by the lame-duck Congress on 21 December, 1 day before it adjourned. Among other things, it endorses annual increases for NSF of 7.2%, 5.1%, and 6.4% in 2011, 2012, and 2013, respectively. The first number matches what President Obama requested for NSF in his 2011 budget submission to Congress last February. A version of COMPETES passed in May by the House of Representatives would have been even more generous to NSF, with annual increases of 8%, 8.6%, and 7.8%.

But as Winnie the Pooh might say, COMPETES is the wrong sort of budget bill. It's an authorization, meaning it sets guidelines but doesn't provide money to expand existing activities or implement any new policies and programs. The same thing happened to NASA in September, when Obama signed legislation that spells out a new policy for space exploration that would rely more heavily on commercial vehicles but doesn't appropriate the money to achieve that goal.

What's going on? The answer is that a federal budget process that has always been hideously complex has become even more fragmented. Congress is supposed to pass 12 separate appropriations bills to fund all branches of government by the start of the fiscal year on 1 October. That has happened less and less often in recent years, however. Instead, procrastinating legislators have adopted one or more short-term continuing resolutions (CRs), holding spending to current levels, before eventually wrapping several individual spending bills into something called an omnibus bill.

PHOTO CREDIT: BOB WEEKS

2010 JAN | FEB | MAR | APR | MAY | JUN | JUL

Unfinished business. The 2011 budget is still a work in progress.

- Appropriations bill
- Authorization bill
- Continuing resolution

1 February: President Obama submits 2011 request to Congress.

28 May: House passes COMPETES reauthorization.

15 July: Senate spending panel approves agriculture and homeland security bills.

22 July: Senate spending panel approves science (NSF, NASA, and Commerce Dept.) and energy bills.

29 July: Senate spending panel approves NIH bill.

16 September: Senate spending panel approves defense bill.

30 September: CR extended to 3 December.

Published by AAAS

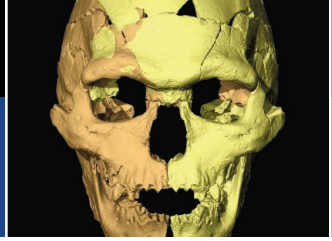

Out of North Africa?
20

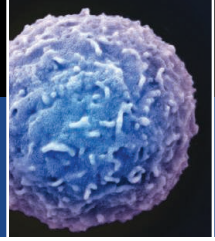

Taking the measure of single cells
24

This year, even that hope-and-a-prayer approach couldn't get the job done. Fresh from what Obama called an electoral "shellacking" by voters, the lame-duck Democratic majority in the House of Representatives passed in early December a modified CR for the rest of the year that would have exempted a few federal agencies and programs from being held to 2010 spending levels. None of the major funders of basic science—NSF, the National Institutes of Health (NIH), and the Department of Energy's Office of Science—was mentioned, meaning that their budgets would have remained flat.

Senate Democrats, who lost six seats in the midterm elections but retain a three-seat majority, took a different approach. Senator Daniel Inouye (D–HI), chair of the appropriations committee, cobbled together an omnibus spending bill that provided detailed guidance and specific funding levels for every agency, including a 6% increase for NSF and a 2.5% increase for NIH. But that bill also contained $8 billion in so-called earmarks, spending that individual legislators have sought to benefit their constituents that was not requested by the agency whose budget would pay for these projects. On 16 December, Inouye withdrew his omnibus bill in the face of a threatened filibuster from Republicans, who have designated earmarks as Public Spending Enemy #1. The next week, both the House and the Senate approved the current CR, which maintains the status quo until 4 March.

COMPETing for clout

In parallel with appropriations bills, Congress also periodically reauthorizes programs at various federal agencies. These bills, both sweeping and detailed, can require or encourage agencies to move in new directions and can block or discourage activities deemed undesirable.

Authorization bills sometimes carry great weight. The annual authorization bill for the Department of Defense, for example, typically lays down guidance for the year's spending bill that, as one congressional staffer notes, "appropriators ignore at their peril."

Historically, authorization bills for science agencies have had much less impact on spending panels. But the first COMPETES Act, in 2007, was an exception to that rule. Based on a 2005 National Academies report that Congress requested, it gained political strength from the endorsements of both President George W. Bush and Democratic congressional leaders. And Congress used the massive 2009 stimulus package to supplement funding for many of its provisions. In contrast, the 2010 COMPETES reauthorization quickly became partisan, with Democrats calling it the best way to ensure long-term economic prosperity and Republicans complaining that its cost would stifle job creation rather than encourage it.

> ***"[We] will have to answer an increasingly urgent question: 'How do we cut spending that we don't need while making investments that we do need?'"***
>
> **—PRESIDENT BARACK OBAMA**

Even so, the 2010 law retains many of the features in the original authorization. It backs a 10-year doubling of the budgets of NSF, the Department of Energy's Office of Science, and the National Institute of Standards and Technology, as well as demanding better coordination across the federal government of science and math education and training programs. It also directs NSF to do things that don't require more money. For example, it nixes a proposed merging of programs to help minority undergraduates, orders NSF to shift some of the cost of its Graduate Research Fellowships from the education to the six research directorates, and tells the National Science Board, NSF's oversight body, to focus on NSF in its recommendations to Congress and the White House rather than cast its net across the entire government.

NSF officials are prepared to implement those mandates, even if they may not like all of them. But congressional action on the 2011 and subsequent budgets could alter them. In particular, a future CR or appropriations bill could override some of those nonmonetary provisions, either through a blanket prohibition on "new starts" or by specifying what is kosher under a budget freeze.

Within the confines of that debate, the idea of doubling the budget of any federal agency is unlikely to get much traction. "There's going to be downward pressure on budgets, and the House will drive that process," predicts one Senate aide. Joel Widder, a science lobbyist for the Washington, D.C., firm of Oldaker, Belair &Wittie, says he's "always hated" the concept of a freeze because of its imprecision—"When does it start and how long does it take?"—but that it's especially inappropriate in the current political climate. "Whether they get to 2008 levels or not, doubling doesn't seem to be on the minds of the new House leadership," he notes.

Although congressional Republicans have yet to describe the role of basic research in their overall philosophy of reducing the size and scope of government, Obama says his Administration is ready to rumble on the subject. "I expect we'll have a robust debate about this when we return from the holidays," Obama said at his recent press conference. "[That] debate will have to answer an increasingly urgent question: 'How do we cut spending that we don't need while making investments that we do need—investments in education, research and development, innovation, and the things that are essential to grow our economy in the long run, create jobs, and compete with every other nation in the world.' "

–JEFFREY MERVIS

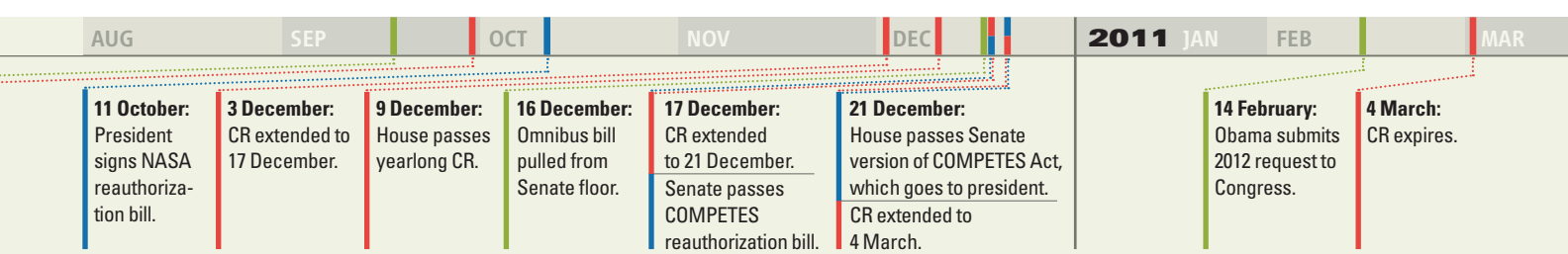

Published by AAAS

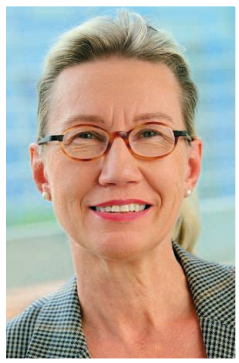

Home front? ESF chief Marja Makarow says no decision has been made on the future of the agency's HQ in Strasbourg, France.

EUROPE

ESF Moves Toward Rebirth, But Change Worries Some

2011 will likely see the end of the European Science Foundation (ESF), at least in its current form. After 37 years of funding researchers, organizing collaborations, and convening meetings across the continent, ESF is expected to transform into a lobbying and strategy organization. But even as the details continue to be worked out, some observers are lamenting the change, particularly as certain science academies may be excluded from the resulting body. "The new organization will lose diversity, and … networking [among scientists] will be much weaker than promoted by the present ESF," says Jüri Engelbrecht, president of ALLEA (All European Academies).

The planned overhaul of ESF into a still-unnamed body, revealed by *Science* last year (*Science*, 11 June 2010, p. 1340), aims to produce a unified voice for the national research agencies that provide the vast majority of Europe's roughly €29 billion annual science spending. Those agencies finance 85% of Europe's science, while the European Union's (E.U.'s) research programs account for only about 5%. Yet E.U. research commissioners are arguably calling the shots on supranational science policy, with initiatives such as the European Research Area and the Innovation Union. The national agencies, which act collectively through an informal grouping called EUROHORCs, felt they should have more influence on regional science strategy.

Those same agencies also form the majority of ESF members. (Other members currently include academies of science and learned societies.) Last year, the agencies decided to transform ESF from a funding body—with an annual budget of about €50 million—into an organization that will focus on research strategy and lobbying on behalf of EUROHORCs members. Because ESF is a formal body bound by statutes, the proposed transformation has had to be studied in detail, and decisions will be made at a special general assembly of ESF members in May. Yet signs of change are already apparent. ESF has canceled calls for proposals for two of its funding programs, which involve setting up cross-border collaborations and networks of researchers. Marja Makarow, chief executive of ESF, emphasizes that most existing projects will be honored.

ESF's EUROCORES program supports large and complex cross-border collaborations between labs, but Makarow says non-ESF programs do a similar job. The European Union, for example, already funds the long-standing Cooperation in Science and Technology program and is also starting an initiative known as Joint Programming that identifies "grand challenges" such as neurodegenerative disease and then coordinates national agencies to collaborate on them rather than duplicating efforts. And then there are smaller groups of countries working together, such as the Scandinavian nations and the German-speaking grouping of Germany, Austria, and Switzerland. "If EUROCORES vanishes, it doesn't leave a void," Makarow says.

Engelbrecht and others remain to be convinced, however. Geophysicist Enric Banda, a former ESF chief who is now president of Euroscience, an association of researchers, also regrets the loss of the current ESF, which he says was "a very good instrument" that didn't have the confidence of its member organizations. "It never really flew," Banda says. Efforts such as Joint Programming are simply too bureaucratic, he adds. "It doesn't make sense that after 60 years of European union, [collaboration] is still done through formal intergovernmental agreements. We're not very European yet." Banda thinks that what Europe really needs is "a reinforced ESF, concentrating on collaboration, with real money."

EUROHORCs wants to limit membership of the new body to organizations that fund research or carry out research, and that means excluding those national academies that operate principally as learned societies, such as the Royal Swedish Academy of Sciences. Engelbrecht says it would be a blow to the science community to exclude those academies because ESF, with its mix of members, was greater than the sum of its parts. Makarow says the new body will strive to maintain its relationship with the learned societies, possibly through an annual conference bringing together the new ESF-EUROHORCs organization, ALLEA, the European Union, universities, and the big European labs.

So, without the funding and networking activities of ESF, what will the new body do? That's under discussion by a working group that is drawing up the body's mission statement. The EUROHORCs agencies, Makarow says, "are very powerful organizations, but they've been fragmented in the past. Now it is time to gather their strengths and direct science policy in Europe—align national policies and supranational policy." Makarow says the new body will use scientific expertise to predict trends for policymakers; promote cross-border cooperation between member agencies; and, most urgently, help the European Union plan its next 7-year research program, which begins in 2014. Banda, for one, is surprised that the new body will focus so much on E.U. funding. "Why worry so much about this 5% of the cake and not the other 95%?" he says. Europe's science voice, it seems, still has some way to go before being unified. **–DANIEL CLERY**

CREDITS: (PHOTOS) EUROPEAN SCIENCE FOUNDATION; EUROHORCS

Published by AAAS

CHRONIC FATIGUE SYNDROME

Studies Point to Possible Contamination in XMRV Findings

The stormy debate over a potential cause of chronic fatigue syndrome (CFS) is nearing hurricane force. Last month, it prompted headlines suggesting that researchers have reached a dead end, scores of blog posts from disappointed patients, and accusations that scientists had gone beyond their data. The 14-month-old row intensified when four papers appeared in *Retrovirology* suggesting that reports linking the virus XMRV to CFS were based on false positives.

The debate began in 2009 with a report in *Science* that XMRV, a retrovirus recently reported to have been found in prostate tumors, had been detected in 67% of a set of CFS patients but in only 4% of controls (*Science*, 9 October 2009, p. 215). Since then, one other group has found XMRV-like viruses in CFS patients' blood. But several teams have failed to detect the virus in CFS or cancer patients or in healthy people. Researchers have struggled to explain the discrepancies (*Science*, 17 September 2010, p. 1454).

The potential link to CFS has had important consequences: Some CFS patients have begun taking antiviral drugs, which can have side effects. Last month, after being briefed on the original XMRV studies, advisers to the U.S. Food and Drug Administration recommended that CFS patients be barred from donating blood.

The *Retrovirology* papers point to contamination as a possible source of positive results in previous studies. The polymerase chain reaction (PCR) test used to detect XMRV (a mouse retrovirus adapted to infect humans) could actually be picking up minute amounts of mouse DNA or similar mouse viruses.

Two of the four studies in *Retrovirology* used highly sensitive assays for mouse DNA and found that samples positive for XMRV-like viruses also tested positive for mouse DNA. Another study found mouse viral RNA in a commercial PCR kit. And the fourth study argues that XMRV sequences previously reported in patient samples don't show the diversity expected if the virus were spreading through the human population. Instead, these authors report, the sequences are similar to those found in a popular prostate cancer cell line, 22Rv1. This cell line, used in lab experiments, was already known to contain an XMRV-like sequence.

Greg Towers of University College London (UCL), who led the study of XMRV diversity, says the evidence linking this virus and human disease "is really looking pretty shaky now." The Wellcome Trust, which cosponsored the research, and UCL issued a press release last week declaring flatly that the Towers study showed that "chronic fatigue syndrome is not caused by XMRV," a message some newspapers repeated. Towers says he was "comfortable" with the release. But John Coffin of the U.S. National Cancer Institute (NCI) and Tufts University Sackler School of Graduate Biomedical Sciences in Boston, who co-authored two of the contamination papers, is wary. He says these studies "just point out how careful one must be."

Virologists who have found a virus-disease link disagree with coverage of the Towers paper. "The data shown … do not justify some of the sweeping statements made," says Ila Singh of the University of Utah, Salt Lake City, who has reported XMRV in prostate cancer samples. Moreover, the lead author of the *Science* paper on CFS and XMRV, Judy Mikovits of the Whittemore Peterson Institute (WPI) in Reno, Nevada, points out that PCR wasn't the only test her studies used: For example, Mikovits's team also showed that XMRV-positive patients make antibodies to the virus and that XMRV isolated from their blood can infect cultured human cells. Mikovits said in a statement, "Nothing that has been published to date refutes our data."

One outspoken scientist wavered on the significance of the *Retrovirology* papers. Columbia University virologist Vincent Racaniello, who runs a popular virology blog and podcast, initially e-mailed a *Chicago Tribune* reporter to say that they were "probably the beginning of the end of XMRV and CFS." But he retracted that statement (and a similar comment to *Science*) after reviewing the studies more closely. "It's pretty complicated," Racaniello concludes.

Some had hoped that a project in which several U.S. labs are testing for XMRV in the same samples would clear up the picture. But so far this effort has been inconclusive. Four CFS patients' blood initially tested positive for XMRV at WPI and the U.S. Centers for Disease Control and Prevention but not at an NCI lab. When all three labs tested new samples from the same patients, none found XMRV—for reasons that aren't yet clear, says Coffin. The group now plans to test blood from several dozen CFS patients and controls.

A bigger study is now under way. Funded by the U.S. National Institute of Allergy and Infectious Diseases, virologist W. Ian Lipkin of Columbia University is leading a project that will collect blood from 150 CFS patients and 150 controls from six U.S. clinical sites. The samples will be tested blindly by several labs. Because all the clinicians have agreed on standard methods, the study should help resolve concerns that differences in how CFS patients are selected or how samples are handled could explain clashing conclusions, Lipkin says: "Results will be definitive."

As the new study gets started, some wonder whether it's worth the $1.3 million it will cost. Jonathan Stoye of the MRC National Institute for Medical Research in London concedes that the Towers study was "overhyped." But he says "it's pointing people in a certain direction," away from chasing an elusive link to XMRV. Still, he says, a larger study may be the only way to satisfy patients.

–JOCELYN KAISER

With reporting by Martin Enserink.

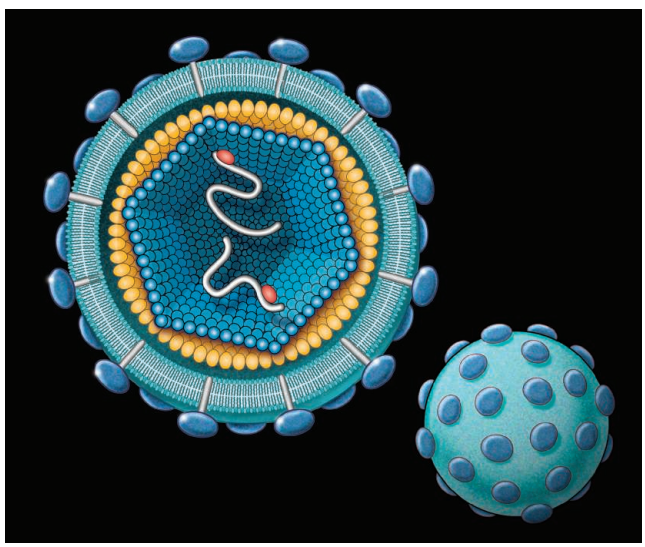

Elusive. Scientists are still debating whether the XMRV virus has any connection to human disease.

CREDIT: REPRINTED WITH PERMISSION, CLEVELAND CLINIC CENTER FOR MEDICAL ART & PHOTOGRAPHY © 2009

Published by AAAS

ECOLOGY

A Slimy Invader Blooms in the Rivers of Patagonia

Biochemist William Horvath was the first to sound the alarm. A Patagonian guide to kayakers from all over the world, Horvath was taking U.S. clients on the pristine Futaleufú River in Chile last year when he saw something that stopped him cold. In the water there "appeared to be toilet paper," he says. Afraid of hepatitis, the kayakers turned back. Horvath decided to investigate. After ruling out pollution from a local water-treatment plant, he sent samples to the U.S. Geological Survey (USGS) in Fort Collins, Colorado. USGS ecologist Sarah Spaulding determined that it was natural material: the mucilaginous stalks of the algae known as *Didymosphenia geminata*, or Didymo.

The discovery caused a stir, as Didymo is unwelcome wherever it blooms. It forms large colonies of brownish slime that cling to vegetation and streambeds, extending leathery trailers into the current. Known to hikers as "rock snot," it is established in several Northern Hemisphere locations—including in Canada and the eastern United States, Europe, and Asia. But it was not seen in the Southern Hemisphere until 2004. That's when Didymo appeared in New Zealand; it has now spread to more than 40 watersheds in the country's South Island. In 2010, to the dismay of naturalists and Chile's tourism industry, it gained a foothold in Patagonia.

Coming to Chile? The invasive alga *Didymosphenia geminata* recently swept through New Zealand's South Island.

CREDIT: NEW ZEALAND FISH AND GAME

A single water drop is enough to carry the diatom into new territory. The nontoxic organism is the only large-scale invasive species known in oligotrophic freshwater environments—those poor in phosphates, nitrates, and organic matter. It is capable of completely covering riverbeds with up to 20 centimeters of gunk, sometimes blocking water intakes for hydro plants and degrading fish breeding habitats.

After Didymo's presence was confirmed in the Futaleufú River, Brian Reid, a limnologist at Chile's Center for the Research of Patagonian Ecosystems (CIEP) based in Coyhaique, in the Aysén Region, organized a survey in June of other rivers whose habitat, configuration, and stability made them potential reservoirs. Massive blooms of Didymo were confirmed in two spots within the Chilean Patagonia watershed, the Espolón River (a tributary of the Futaleufú) and Cea Creek; a macroscopic amount was found in the Cochrane River, part of the Baker Basin. Researcher Viviana Sastre of the Universidad Nacional de la Patagonia in Argentina reported a limited Didymo bloom in the Grande-Futaleufú River, which flows through Argentina and Chile.

In October, a joint report by CIEP, the National Fisheries Service, and the Bureau of Water Management (DGA) identified three common factors in blooms: They occur in stable rivers downstream from lakes, near a main road that offers recreational access, and downriver from sources of nutrients such as waste treatment plants and fish farming operations. The link to nutrient sources does not jibe with earlier analyses. Historically, before its expansion in the United States and New Zealand, it was found in clean waters and places that weren't significantly impacted by humans—mostly in high latitudes and high elevations. Spaulding, who went to Chile in July to study the blooms, says, "We still don't understand why it is spreading so rapidly."

The propagation of *D. geminata* may be unstoppable, although officials in Chile have launched a massive effort to halt it. Since June, a permanent committee of state offices, research centers, and tourism operators has been coordinating fieldwork and educating communities on how to limit its spread. In October, authorities declared the Espolón and Futaleufú rivers "plagued areas" and the Simpson River as threatened.

Pallaoor V. Sundareshwar, an associate professor of atmospheric sciences at the South Dakota School of Mines and Technology in Rapid City, who inspected the blooms in Chile last summer with Spaulding, says researchers plan to determine through DNA analysis whether Didymo in Patagonia is the same type detected in New Zealand and North America. Next they want to compare the environmental aspects of water in the affected regions. And Sundareshwar hopes they will be able to "solve the mystery of how *Didymosphenia* came to Chile, what is it doing, and why is it blooming." He adds: "Maybe if we are lucky we will be able to figure out how to control it."

Sample takers themselves can be a problem, says Jorge O'kuinghtons of DGA. They're being trained in procedures for disinfecting gear and instruments. Training tourists and fishers will be more difficult. The immediate objective is to hold the line and prevent Didymo's expansion to other rivers on Patagonia and to the north of the country. "We are facing a threat to the primary patrimony of regional tourism products," says Fabien Bourlon, director of the Patagonian Center for Scientific Tourism.

The campaign has focused on prevention for a simple reason: "There is no effective and proven method that allows the eradication of Didymo" but also leaves the ecosystem intact, explains Manuel Martínez, an aquaculture engineer who is coordinating regional efforts to intercept the algae. Biocides can kill many organisms and have been ruled out.

Three years ago, Spaulding warned in a paper that "rivers in the southern hemisphere are particularly at risk" to invasion and degradation by new species. The 2007 analysis, co-authored with conservationist Leah Elwell, said that environmental protection agencies in Australia, Argentina, Chile, and Peru should be aware of the "urgency of implementing decontamination procedures" to keep travelers from bringing in invasive species like Didymo. Chile did not move rapidly. Regional authorities hope it's not too late to restore the reputation of Patagonia's rivers as the most pristine on Earth. **–PATRICIO SEGURA**

Patricio Segura is a freelance journalist in Coyhaique, Chile.

Published by AAAS

ScienceNOW

From *Science's* Online Daily News Site

Some Don't Like It Hot

As oceans continue to warm and acidify, the survival of the tiny floating young of marine mollusks (*Haliotis coccoradiata*) and sea urchins (*Heliocidaris erythrogramma*) looks bleak, researchers report online in the *Proceedings of Royal Society B.* Maria Byrne of the University of Sydney in Australia and colleagues found that young mollusks maturing in slightly warmer and more acidic seawater couldn't calcify their shells and formed amorphous blobs (picture, top right). Most died after only a 2°C rise in temperature. Sea urchins fared better but formed far fewer spines if the water was 4°C warmer (bottom right). http://scim.ag/warm-waters

You Could Have Fooled Me
The "placebo effect" may work even if patients know they are taking fake pills, a new clinical trial suggests. Ted Kaptchuk of Harvard Medical School in Boston and colleagues gave either a placebo or no pill to 80 people with irritable bowel syndrome (IBS). All subjects were told that placebos contain no active ingredient but can have a powerful effect because the body responds to them "like Pavlov's dogs" to a bell. Three weeks later, those on the pills reported significant improvement, comparable to that seen in trials of real IBS drugs, the team reports online in *PLoS ONE.* http://scim.ag/placebo-effect

The Eyes Have It
How do we judge whether a face is that of a living person or an inanimate object? Christine Looser and Thalia Wheatley of Dartmouth College had student volunteers look at pictures of human and doll faces, blended together to various degrees using software, and decide which ones were alive. Nearly all participants looked at the eyes more than the mouth, nose, or skin, suggesting that we rely on the eyes to judge whether a face has a mind behind it, the pair reports online in *Psychological Science*. http://scim.ag/lively-eyes

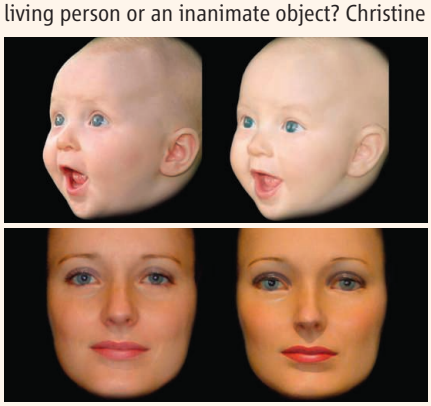

Doll face. Researchers used morphed faces to test how humans decide whether a face is alive.

Finger Points to New Type of Human
By sequencing DNA from an ancient finger bone, researchers have confirmed the discovery of a new type of human that lived in the Altai Mountains in southern Siberia more than 30,000 years ago. The Denisovans, named after the Denisova cave in which the bone was found, lived at roughly the same time modern humans and Neandertals roamed the region but were more closely related to Neandertals. Before going extinct, they bred with modern humans; people from New Guinea and nearby islands appear to have inherited between 4% and 6% of their DNA from the Denisovans, lead author Svante Pääbo and scientists at the Max Planck Institute for Evolutionary Anthropology in Leipzig, Germany, report online in *Nature*. http://scim.ag/new-human

Read the full postings, comments, and more at **http://news.sciencemag.org/sciencenow**.

CREDITS (TOP TO BOTTOM): EUNICE WONG AND HANNAH SHEPPARD-BRENNAND/UNIVERSITY OF SYDNEY; CHRISTINE E. LOOSER/DARTMOUTH COLLEGE

ScienceInsider

From the *Science* Policy Blog

Brazil will pay more than €250 million over a decade to **join the European Southern Observatory (ESO)**, becoming the first member from outside Europe. The agreement boosts Brazil's effort to strengthen its domestic science programs by joining big international projects such as ESO's cluster of telescopes in Chile. http://scim.ag/brazil-joins-ESO

White House science adviser John Holdren sat down recently with *Science*Insider to talk about the joys of **working for a president who "gets it"** on science and the frustrations of never having enough time to plan ahead despite working 16-hour days. "I still find it more exhilarating than exhausting," he says. http://scim.ag/jholdren

The French medical system is in turmoil over the failure of the government to **restrict or ban a diabetes drug** called benfluorex that was widely prescribed as a weight-loss drug. A top official acknowledged "serious failures" in France's drug licensing system. Parliament has launched its own investigation. http://scim.ag/drug_scandal

A new world of **U.S. Environmental Protection Agency regulations regarding greenhouse gas emissions** opened on 2 January. *Science*Insider provided a primer, with one post explaining the basic structure of the rules and a second analyzing the legal challenges facing the agency. http://scim.ag/EPA_regs_primer1 and http://scim.ag/EPA-regs-primer2

An attempt to spur U.S. innovation died on the last day of the lame-duck Congress, as the House of Representatives failed to take up a Senate-passed bill that would have enlarged and broadened two long-running **federal research programs that help high-tech start-ups**. The SBIR and STTR programs are due to expire at the end of the month. http://scim.ag/sbir-bill-falters

Dozens of U.K. scientists have urged the government to **maintain its commitment to forensic science** despite its decision to close the Forensic Science Service. http://scim.ag/fss-letter

For more science policy news, visit **http://news.sciencemag.org/scienceinsider**.

Published by AAAS

Was North Africa The Launch Pad For Modern Human Migrations?

A growing number of researchers suspect that long-neglected North Africa was the original home of the modern humans who first trekked out of the continent

LAST YEAR, ARCHAEOLOGISTS EXCAVATING at the Grotte des Contrebandiers (Smuggler's Cave) on Morocco's Atlantic coast unearthed a rare prize: the skull and partial skeleton of a 7- or 8-year-old child. The fossils, dated to 108,000 years ago, appear to belong to an early member of our species, although study of them has just begun.

But one feature stands out already: "It has huge teeth," says Harold Dibble of the University of Pennsylvania, co-leader of the dig team. That's a feature the child shares not only with other hominin fossils found across North Africa but also with some of the first modern humans to leave Africa. And so the new fossil may contain clues to an enduring mystery in human origins research: Just where in Africa did the modern humans who first colonized the rest of the world come from? "It's a very exciting specimen," says anthropologist Jean-Jacques Hublin of the Max Planck Institute for Evolutionary Anthropology in Leipzig, Germany.

Old youngster. This fossil child had big teeth.

For Hublin, who was born in Algeria, the Contrebandiers child adds to growing evidence that North Africa was likely a major source of the modern humans who first left humanity's homeland and spread into Europe and Asia as early as 130,000 years ago. "If you look at a map and think how modern humans would have moved out, you would logically look at North Africa," he says.

Nevertheless, until very recently, most researchers studying the origins of *Homo sapiens* looked elsewhere, focusing instead on the fossils of East Africa and the sophisticated tools and ornaments of famed South African sites such as Blombos Cave (*Science*, 16 April 2004, p. 369). Few scientists thought that much of evolutionary significance had gone on in North Africa, or that the region's big-toothed, somewhat archaic-looking hominins might be closely related to the ancestors of many living people. "We've left North Africa off the map for so long, and now it deserves to be there," says paleoanthropologist Chris Stringer of the Natural History Museum in London.

Indeed, a flurry of research has now put the region firmly on the map of human evolution. Thanks to new excavations and more accurate dating, North Africa now boasts unequivocal signs of modern human behavior as early as anywhere else in the world, including South Africa. Climate reconstructions and fossil studies now suggest that the region was more hospitable during key periods than once thought. The data suggest that the Sahara Desert was a land of lakes and rivers about 130,000 years ago, when moderns first left Africa for sites in what is today Israel. And new studies of hominin fossils suggest some strong resemblances—and possible evolutionary connections—

CREDITS: HAROLD DIBBLE

Published by AAAS

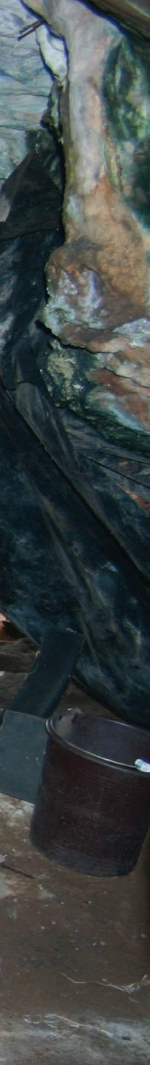

Digging for our roots. Modern humans occupied many North African sites, like this one at Contrebandiers, Morocco.

between North African specimens and fossils representing migrations out of Africa between 130,000 and 40,000 years ago.

This barrage of new evidence is reported in recent papers and in two new edited volumes (see Additional Reading below). Human evolution researchers working in other parts of Africa are taking notice. The new studies are "long overdue," says anthropologist Stanley Ambrose of the University of Illinois, Urbana-Champaign, who works in East Africa. They "show that North Africans may be responsible" for both early and later *H. sapiens* migrations out of Africa. Adds archaeologist Curtis Marean of Arizona State University, Tempe, "If I were not working in South Africa, I would probably be in North Africa."

But a key question, Marean and other researchers say, is whether modern humans in North Africa were foremost among the migrants that eventually left Africa, or whether those populations represented an evolutionary cul-de-sac that was left behind when humans from other parts of the continent began moving into Asia and Europe. The evidence that North Africa was a population pool for migrations to Eurasia is not yet conclusive, says anthropologist Gerhard Weber of the University of Vienna. Marean is also cautious for now but says the new work should provide "some good answers in the future."

Old tools, new dates

Given what researchers already know about modern human evolution, the long neglect of North Africa might seem surprising. Most anthropologists think that our species, *H. sapiens*, first evolved in sub-Saharan Africa about 200,000 years ago and began migrating out of Africa between 70,000 and 50,000 years ago, eventually colonizing the globe. And although the expansion has often been considered a single migration, many researchers are beginning to suspect that moderns left Africa in two or more waves.

Some of these early migrants may have gone east, across the Red Sea and along the southern coast of Arabia. But the earliest known modern human fossils outside Africa suggest a northern route, perhaps through the Nile Valley: Modern human skulls and other bones discovered in the early 20th century in the Skhul and Qafzeh caves in Israel are now dated to between 100,000 and 130,000 years ago, although researchers debate whether these early colonizers traveled any farther at that early date (*Science*, 9 October 2009, p. 224).

Online
sciencemag.org
Podcast interview with author Michael Balter.

Despite this early connection to the Middle East, not so long ago most experts thought that modern humans occupied North Africa itself relatively late. The earliest known modern human fossils were from East Africa: Skulls and bones found near Kenya's Omo River by Richard Leakey and others are now dated to 195,000 years ago, and skulls found at Herto in Ethiopia clock in at about 160,000 years old. Then, in recent years, Hublin, Stringer, and others convinced most anthropologists that a 160,000-year-old skull from Jebel Irhoud in Morocco was that of an archaic modern human and not a Neandertal, as previously thought. But that skull was considered an anomaly, perhaps representing a population that got trapped north of the Sahara and then died out.

This picture of North African hominins as Johnny-come-latelies was reinforced by assumptions about the dates of characteristic stone tools in the region. Called Aterian after their discovery in 1917 at the site of Bir el Ater in eastern Algeria, the tools include triangular objects that some suggested were used as arrowheads or spear points (see photo, p. 23). At least 100 Aterian sites have now been uncovered across North Africa, including in what is now the Sahara Desert. But when archaeologists radiocarbon-dated these sites, they tended to throw out any results older than 40,000 years, says archaeologist Elena Garcea of the University of Cassino in Italy, because such dates were at the limit of the radiocarbon technique and considered unreliable (*Science*, 15 September 2006, p. 1560). "In the past, the Aterian was thought to be relatively late and not terribly exciting, … a sideline or a dead end," says archaeologist Nick Barton of the University of Oxford in the United Kingdom.

By 1998, however, it began to look like archaeologists might be throwing away the

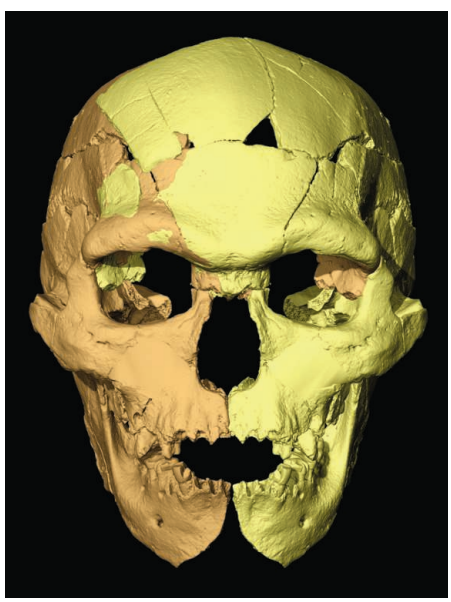

O pioneers. Early modern humans like this one from Dar es-Soltan (computer reconstruction, *right*) may have spread across North Africa and into Eurasia.

North African hominin sites

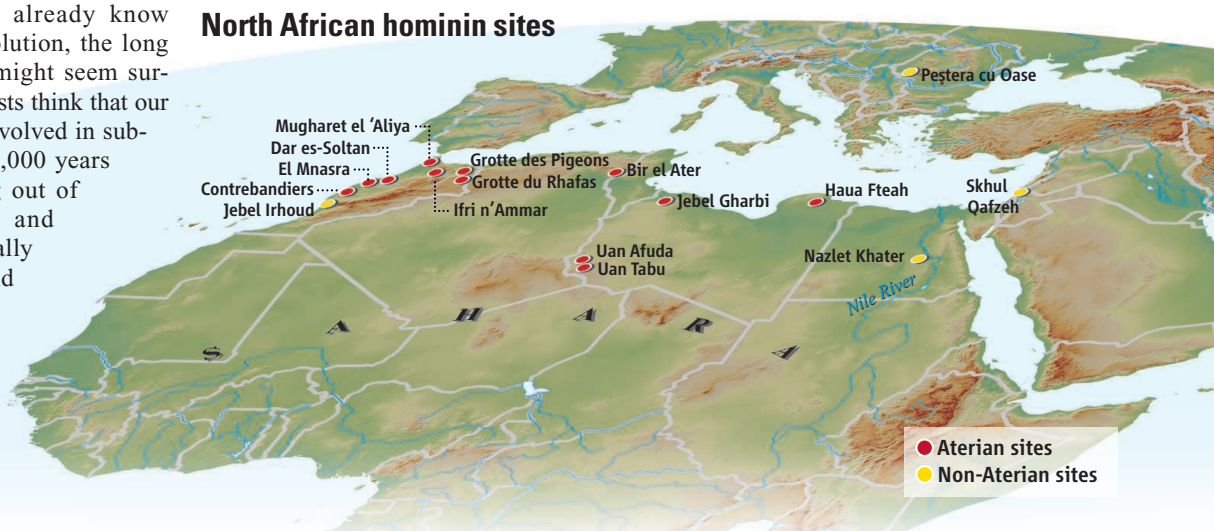

CREDIT: RECONSTRUCTION BY HUBLIN AND NEUBAUER

Published by AAAS

wrong dates. That year, researchers used the new techniques of optically stimulated luminescence (OSL) and thermoluminescence (TL) to date Aterian sites in Libya back to 70,000 years, and soon afterward similar dates using these and other methods were found at other Aterian sites in the region.

During the past 2 years, the dates have gotten even older. In 2009, Barton and Abdeljalil Bouzouggar of the National Institute of Archaeological and Heritage Sciences in Rabat reported OSL dates of at least 110,000 years from the Aterian site of Dar es-Soltan in Morocco; and in a new volume edited by Garcea, the team reports similarly old dates from three other Moroccan caves. Then in September, TL dates of about 145,000 years were reported for Ifri n'Ammar in Morocco. "The Aterian goes back at least 145,000 years," Stringer says. "That's an incredible length of time."

Those early dates are coupled with a growing realization that the Aterians were just as behaviorally sophisticated as modern humans in other parts of Africa. In addition to their skillfully made tools, they made personal ornaments—a key sign of modern, symbolic behavior—from shell beads 82,000 years ago at Morocco's Grotte des Pigeons (Pigeon Cave). That's somewhat earlier than when the same genus of shells, *Nassarius*, was used to make beads at Blombos Cave thousands of kilometers away in South Africa 75,000 years ago. *Nassarius* beads show up at Qafzeh in Israel even earlier, at least 100,000 years ago (*Science*, 23 June 2006, p. 1785). Researchers are now studying 108,000-year-old perforated *Nassarius* shells from Contrebandiers to determine whether they, too, were used as personal ornaments.

All this implies that the Aterian was not a sideshow but a "[cultural] package that may be linked with the emergence of modern human behavior," says Barton. That's not direct evidence that the Aterians were the source of out-of-Africa migrations, but it suggests that they met an important prerequisite: Rather than being a small, isolated population unlikely to go on the move, they apparently were part of extensive social networks that used ornaments to signal the identities of different groups that were in contact with one another, perhaps across long distances (*Science*, 9 April, p. 164).

This is in contrast to recent genetic research, which has suggested that the humans who dispersed to Europe, Asia, and Australia by 50,000 years ago originated in sub-Saharan Africa (*Science*, 1 May 2009, p. 575). But Hublin argues that such studies, which are based on the genetic diversity of humans today, might not capture past patterns. For example, some of the Aterians in the Sahara area—along with their genes—may have moved east or south when the Sahara became hotter and drier after 60,000 years ago.

Leading geneticists support the idea that some of the populations that live south of the Sahara today may have Aterian roots. "This is entirely plausible," says Sarah Tishkoff of the University of Pennsylvania. "We can only study populations present today, and their present-day distribution probably doesn't reflect where they originated from tens of thousands of years ago."

Facing the past. The Max Planck's Jean-Jacques Hublin sees similarities between the Aterians and the first modern humans to leave Africa.

Rain over the Sahara

Today, no sensible hominin would think of trying to cross the Sahara Desert. This vast landscape of sand dunes, rocky plains, and plateaus covers 5 million square kilometers from the Atlantic Ocean in the west to the Red Sea in the east. The Sahara overall receives less than 8 centimeters of rain each year, and the driest parts might not see rain for years on end. But during key periods in human prehistory, new data from multiple sources suggest, at least parts of the Sahara featured lakes, rivers, and trees.

Scientists are now working to correlate the cyclical greening of the Sahara with archaeological signs of human occupations. For example, satellite radar imaging has revealed a system of more than 800 kilometers of channels, some more than 5 kilometers wide, buried under the eastern Sahara sands. A 2008 study of 120,000-year-old snail shells suggests that these are river corridors, which could have supported human migrations (http://scim.ag/wetsahara). And trees increased markedly 120,000 and 50,000 years ago, according to work published last year on isotopes from plant leaves in a marine core off the coast of northwest Africa.

Other recent work suggests that Libya, Chad, Tunisia, and Egypt were dotted with huge "megalakes" about 120,000 years ago; about 10% of Libya might have been underwater around that time, concludes geographer Nick Drake of King's College London. These wet phases lasted for thousands of years.

"One of the wettest times was around 120,000 to 130,000 years ago," says geologist Jennifer Smith of Washington University in St. Louis (WUSTL). That's about when modern humans first left Africa and are found in the Israeli caves of Skhul and Qafzeh.

A wet Sahara between 100,000 and 130,000 years ago may also help explain how shell bead ornaments ended up in both North and South Africa some tens of

European connection? Some features, such as the molars, of these 40,000-year-old specimens from Romania resemble those of earlier North African hominins.

Published by AAAS

"We've left North Africa off the map for so long, and now it deserves to be there."

—CHRIS STRINGER, THE NATURAL HISTORY MUSEUM IN LONDON

thousands of years later, says Hublin, if far-flung populations were in touch across the continent. "If you look before 100,000 years ago, North Africa was very much connected to the rest of Africa," he says, adding that fossils of sub-Saharan animals such as rhinos, giraffes, and hippos have been found at North African sites. "We had a network of early modern populations all over Africa, sometimes connected and sometimes separated."

Yet despite some evidence, for example from the tree study, that parts of the Sahara continued to experience wet periods as late as 50,000 years ago, the climate data suggest that the Sahara had greatly expanded by that time. Indeed, Garcea says, no Aterian sites are found in the Sahara after about 60,000 years ago, although the Aterian continues until about 40,000 years ago all along Africa's northern Mediterranean coast.

Bones tell a new tale

Did the Aterians themselves die out, or did they live on to join the exodus out of Africa? The bones they left behind offer some tantalizing clues. The Aterians were kind to human evolution researchers: They left not only ample artifacts but also one of Africa's best collections of modern human fossils. Now new analyses of Aterian faces and teeth suggest that at key times, populations across North Africa and the Middle East were "relatively closely related," says paleoanthropologist Katerina Harvati of the University of Tübingen in Germany. For example, in a paper in an upcoming volume co-edited by Hublin, Harvati and Hublin compared an Aterian skull with those of other early hominins. They analyzed the facial features of a partial skull found at Dar es-Soltan—now dated to about 80,000 years ago—using the three-dimensional coordinates of 19 facial landmarks. The Dar es-Soltan skull most closely resembled two 100,000-year-old skulls from Qafzeh as well as the 160,000-year-old Jebel Irhoud skull; it showed much less affinity with Neandertal skulls or with younger modern humans from any continent.

In a second paper, Hublin, along with dental experts Shara Bailey of New York University and Tanya Smith of Harvard University, compared the size and shape of more than 50 hominin teeth from Aterian sites with more than 200 teeth from Neandertals as well as modern humans from several continents. The Aterian teeth, which have very large molars and a distinctive pattern of cusps, clustered most closely with those from Qafzeh and Skhul. And they also strikingly resembled those of the earliest known modern humans in Europe: a cranium and mandible, dated to about 40,000 years ago, from the site of Peştera cu Oase in Romania.

Signs of sophistication. The Aterians made personal ornaments (*above*) and advanced stone tools (*below*).

Earlier, other researchers had also found resemblances—such as the robust shape of the lower jaw and forward-facing cheekbones—between Oase and a 40,000-year-old skull from the site of Nazlet Khater in Egypt, providing another potential North African link to the earliest Europeans. "There are indeed some affinities between Oase and Nazlet Khater," says anthropologist Hélène Rougier of California State University, Northridge, who worked on some of these studies, although she notes that the contemporaneous skulls differ in other traits.

The big teeth "certainly potentially link the Aterians with Oase," says the Natural History Museum's Stringer, making the Aterians candidates for the ancestors of later Europeans.

But to nail down those evolutionary relationships, Stringer says, "we need good samples from northeast Africa," because most Aterian fossils are from Morocco in northwest Africa. "The people in Morocco could have been marginal." He adds that the early Oase skull from Romania might not have been closely related to the modern humans who later colonized the rest of western Europe and left the famed Aurignacian and Gravettian cultures; those cultures could represent a later wave of more gracile, smaller-toothed *H. sapiens*.

Other researchers remain even more skeptical. Paleoanthropologist Erik Trinkaus of WUSTL, who has extensively studied the Oase fossils and thinks they represent admixture between Neandertals and moderns, rejects any close connection between them and the Aterians. He sees "some superficial resemblances in terms of large molars" between Oase and Aterian specimens but few other similarities. In fact, he thinks the Aterians weren't fully modern humans but "archaics" living in an isolated corner of Africa who were an evolutionary dead end. North Africa was "just another cul-de-sac," he says.

But that view of the Aterians is rejected by many other anthropologists. The emerging evidence, Hublin and others say, suggests that at the critical time, prehistoric North Africans enjoyed the right climate, engaged in the right symbolic behavior, and possessed the right anatomy to be leading candidates for the ancestors of at least some of the *H. sapiens* who left Africa. So for a growing number of researchers, North Africa is a very promising place to look. Says Dibble: "We have exactly the kind of thing everyone has been searching for, right here." **–MICHAEL BALTER**

Additional Reading:

E. A. A. Garcea, Ed., *South-Eastern Mediterranean Peoples Between 130,000 and 10,000 Years Ago* (Oxbow Books, 2010).

J.-J. Hublin and S. McPherron, Eds., *Modern Origins: A North African Perspective* (Springer, in press).

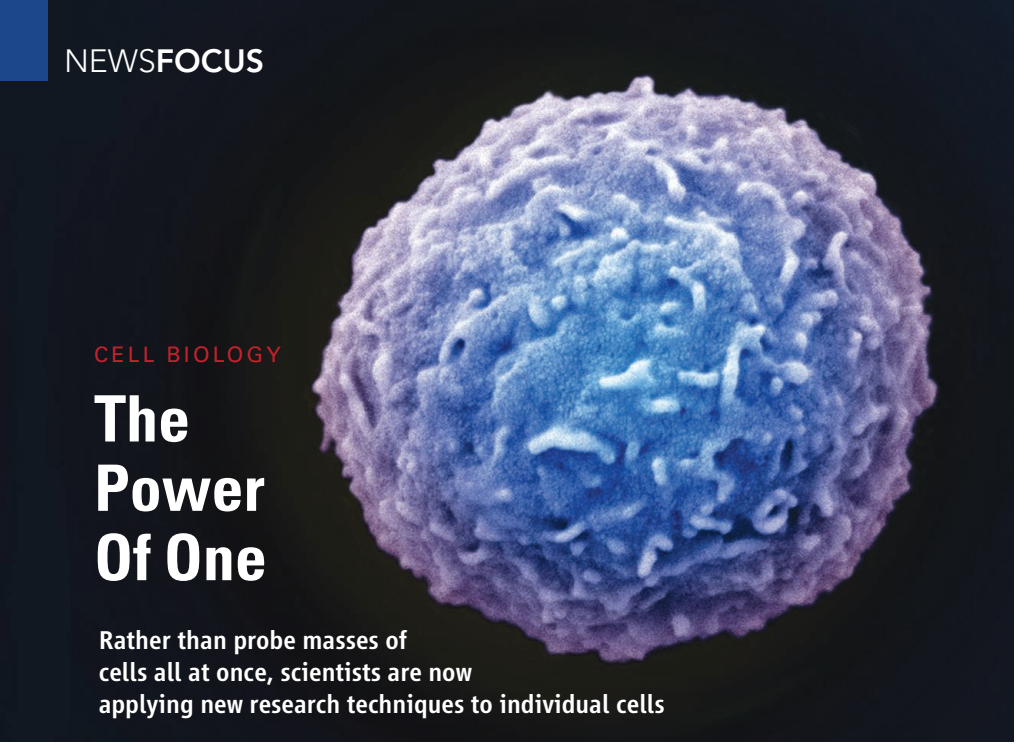

CELL BIOLOGY

The Power Of One

Rather than probe masses of cells all at once, scientists are now applying new research techniques to individual cells

Small sample size. Researchers are exploring new ways of investigating individual cells such as this human white blood cell.

1) Measure out a heaping portion of cells.
2) Grind until thoroughly mixed.
3) Analyze.

Cellular studies still pretty much stick to this traditional recipe, whether the goal is probing bacterial metabolism, following differentiation of stem cells, or tabulating gene activity in tumors. But mashing up a multitude of cells—one common method of studying gene expression typically requires more than 10,000—obliterates key differences between cells, researchers have come to realize. "If you take an average of a large number of cells, you get an average answer," says analytical chemist Renato Zenobi of the Swiss Federal Institute of Technology in Zurich.

That's why more and more scientists are opting for the alternative approach of taking the measure of individual cells. Although much of this work is in its early stages, "there is an increasingly diverse set of examples where single-cell studies have provided qualitative insights that couldn't be obtained from population-level studies," says biophysicist Michael Elowitz of the California Institute of Technology in Pasadena.

Scientists have already recorded the most accurate measurements of how much an individual cell weighs and gauged how much oxygen one requires. They've flagged specific cancer cells resistant to chemotherapy and developed ways to pinpoint rare, disease-causing bacteria among swarms of harmless microbes. Developmental biologists have tallied gene activity as a fertilized egg starts its course of division and specialization, work that might help clarify the factors that spur a cell in the embryo to become one tissue and its seemingly identical next-door neighbor to become something else. And Elowitz and other researchers have spelled out how individual cells not only cope with but actually benefit from "noise," random fluctuations in their internal and external conditions.

Of course, scientists have paid attention to single cells ever since the first microscopes were invented. What's changed is that researchers are now applying to individual cells the powerful techniques, including genome sequencing, mass spectrometry, and gene expression analysis, that formerly required batches of cells. "Real biological tissues are complex, and if you want to dissect that complexity and heterogeneity, you have to have tools to do it at the single-cell level," says biophysicist Stephen Quake of Stanford University in Palo Alto, California.

Good technique

Single-cell research tools range from old standbys to cutting-edge inventions (see sidebar for a sample of methods). Many of them allow researchers to get into what Quake calls "production mode," analyzing large numbers of individual cells in parallel or over a short period of time. The technology he calls "absolutely central" to the surge in single-cell research is microfluidics, which uses miniaturized networks of channels, valves, pumps, and chambers to control microscopic quantities of liquid. So-called lab-on-a-chip devices combine microfluidic circuits and can perform several analytical steps.

An example of how microfluidics can elucidate single-cell behavior comes from Quake, his Stanford colleague Markus Covert, and their colleagues. Last July in *Nature*, the

Single-Cell Tech Primer

Microfluidics is the hot technique in the single-cell field (see main text). However, it's just one of the methods that are enabling researchers to delve into individual cells.

• Gene Expression

Many modern gene-expression studies apply the mingled contents of thousands of cells to devices called microarrays that look like glass slides or microchips. But with microfluidic chips, researchers can make the same measurements on one cell. Take the gene-expression chips from California-based Fluidigm, a company co-founded by Stephen Quake of Stanford University in Palo Alto, California. The devices isolate samples from individual cells and mix them with the chemicals necessary for quantitative polymerase chain reaction, a technique that determines gene activity by measuring how much messenger RNA a gene makes. The company's most powerful version allows researchers to simultaneously gauge the activity of 96 genes in 96 individual cells, churning through a batch in about 4 hours.

Another new technology, known as RNA-seq, provides an alternative to microfluidic chips for measuring gene activity in one cell. An offshoot of next-generation genome sequencing, the procedure involves converting a cell's mRNA molecules back into short strands of DNA, sequencing those DNA fragments, and then matching them up with the gene that originally spawned the mRNAs. Last May in *Cell Stem Cell*, molecular geneticist M. Azim Surani of the University of Cambridge in the United Kingdom and colleagues reported one of the first studies to apply the RNA-seq technique to single cells, revealing the expression of 385 genes in individual embryonic stem cells. Fans of RNA-seq emphasize that it can measure more genes at once than can microfluidic chips. Meanwhile, chip devotees tout their method's superior speed.

• Flow Cytometry

A classic technique, flow cytometry sifts and counts cells based

CREDIT: ANNE WESTON/CANCER RESEARCH UK/VISUALS UNLIMITED, INC.

Published by AAAS

team reported using a microfluidic chip to dose individual cells with different concentrations of tumor necrosis factor α (TNF-α), a protein that can trigger inflammation and cell suicide. Previous work on cells en masse suggested that they respond to a range of TNF-α concentrations. But the researchers found that sensitivity to TNF-α varied from cell to cell—a result that might help clarify how the body fine-tunes TNF-α's effects.

Single-cell techniques also allow researchers to ferret out rare troublemakers such as *Escherichia coli* bacteria of the O157:H7 strain. Just a handful of the malignant microbes in undercooked hamburger could be enough to cause fatal food poisoning, so detection methods need high sensitivity. Last year, biophysical chemist Richard Mathies of the University of California (UC), Berkeley, and colleagues revealed a strategy that can finger a single cell of the lethal strain from among as many as 100,000 normal *E. coli*. The key step in their method, which the researchers described in *Analytical Chemistry*, involves a microfluidic circuit that creates tiny, uniform oil droplets in which DNA sequences from normal and lethal bacteria are copied.

Predicting which patients will benefit from cancer treatment could be another use of single-cell methods. Immunologist Garry Nolan of Stanford and colleagues have profiled individual cancer cells with phosphospecific flow cytometry, a technique for determining whether proteins have undergone certain chemical modifications that can change cell behavior. For cancers such as acute myeloid leukemia and lymphoma, Nolan and colleagues showed that some abnormal cells contain patterns of protein modifications indicating resistance to chemotherapy. Based on these patterns, "you could pick out patients who would respond to chemo and [those] who wouldn't," he says.

Gone genome fishing

Microbial ecologists and microbiologists are looking to single-cell techniques for help with their culture problem. More than 99% of microbial species remain enigmatic because they refuse to grow under lab conditions and scientists can't obtain enough of the microbes' DNA to sequence their genomes. To fill in the gaps, researchers have turned to metagenomics (*Science*, 30 March 2007, p. 1781), trawling environments such as the open ocean and the human colon for any microbial DNA and then sequencing it to identify genes. Such an analysis can reveal the metabolic capabilities of an entire microbial community, and in a few cases researchers have been able to piece together an unculturable bacterium's genome from the jumble of DNA fragments. But it's usually impossible to pin down which genes belong to a specific microbe. That means researchers can't determine which species perform which ecological roles or reconstruct their evolution, notes microbial ecologist Ramunas Stepanauskas of the Bigelow Laboratory for Ocean Sciences in West Boothbay Harbor, Maine.

In 2001, however, genome biologist Roger Lasken, now at the J. Craig Venter Institute in Rockville, Maryland, and colleagues unveiled a method called multiple displacement amplification (MDA) that can expand the minute amount of DNA in a single bacterial cell by

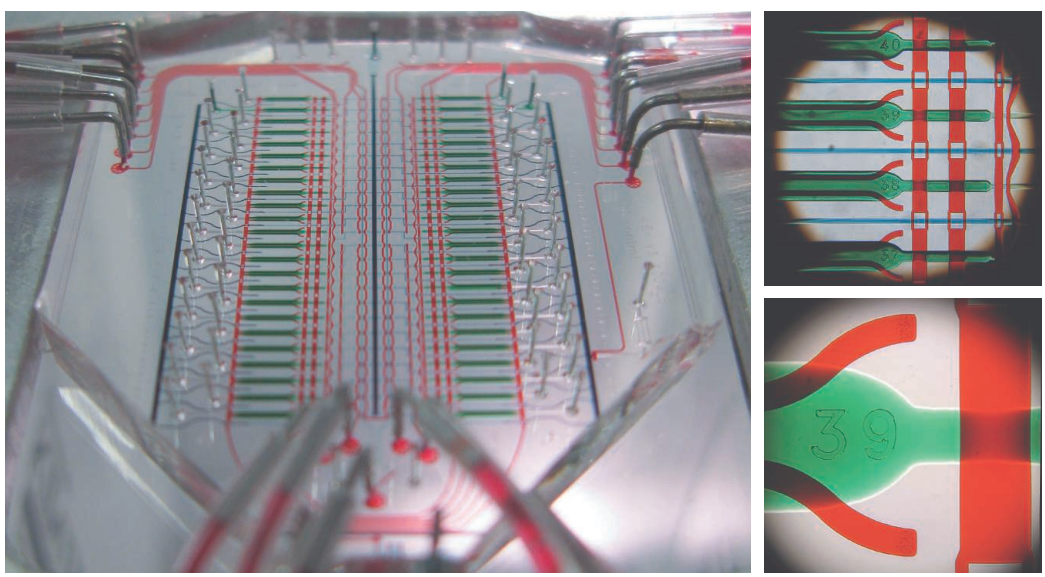

Dynamic fluids. With microfluidic chips like this one, researchers can sort single cells, copy their DNA, measure their gene activity, and perform other kinds of analysis.

CREDITS: PAUL C. BLAINEY/STEPHEN R. QUAKE GROUP/STANFORD MICROFLUIDICS FOUNDRY

on characteristics such as the presence of certain proteins on their surface. Researchers use it today for single-cell work because it can handle large numbers of cells quickly. Garry Nolan of Stanford and colleagues have turned to phosphospecific flow cytometry, a version that detects whether some of a cell's signaling proteins have been tagged with phosphate groups, which are chemical switches that can turn the proteins on or off. Measuring the phosphorylation status of the proteins in a circuit that controls a particular cellular function provides an indication of a cell's status: how other cells have influenced it and how it might respond in the future.

Along with more accurate cancer prognoses, potential uses of phosphospecific flow cytometry include drug screening, Nolan says. The technique is even more powerful when combined with mass spectrometry, he notes. In phosphospecific flow cytometry, the small number of fluorescent tags limits researchers to measuring about 15 of a cell's phosphorylated proteins. But a new instrument developed by DVS Sciences in Canada uses different isotopes of elements such as lanthanum as labels and mass spectrometry to detect the tags, hiking the number of proteins researchers can monitor to approximately 100. "This is not your grandmother's flow cytometry," Nolan says.

• Mass Spectrometry

Mass spectrometry alone might also provide insights into individual cells. Renato Zenobi's lab at the Swiss Federal Institute of Technology in Zurich, for example, is one of several taking advantage of the method to tally the products of biochemical reactions one cell at a time. The cellular concentrations of metabolic compounds such as ATP, the molecule cells use to store energy, are well within the sensitivity of mass spectrometry, he says. The trick now, adds Zenobi, is figuring out what questions biologists can answer by performing mass spectrometry on an individual cell. "We need to show a really hot application of the data, and that will convince" more researchers that adopting it is a good idea.

–M.L.

Published by AAAS

a billion times, thus providing enough material for sequencing. "The great excitement is that we have access to this whole world of bacteria that's been hidden," Lasken says.

His group provided the first glimpse into this world in 2005, sequencing an uncultured microbe that they dug out of the soil. Genomes from previously furtive bacteria have been trickling in ever since.

Four years ago, Quake and colleagues announced that they had used the technique on microbes from a dark and mysterious environment: the human mouth. The researchers scraped the teeming gunk from the gum line of a volunteer who hadn't brushed his teeth for 5 days. Then the scientists sequenced the genome of an unknown bacterium they sifted from the samples with a microfluidic chip. And in 2009, Stepanauskas and colleagues added genome sequences for two unidentified bacteria they'd fished from the Gulf of Maine. Stepanauskas says that thanks to MDA, he expects a flood of genomes for unculturable microbes in the next few years.

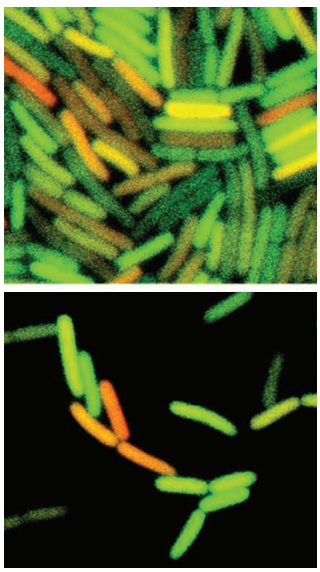

Microbial rainbow. Although these bacteria are genetically identical, random fluctuations in gene expression turn them different colors.

MDA can't capture the entire genome; typically the coverage falls between 40% and 90%, says Lasken. But that's enough to furnish a wealth of information about an organism's way of life, says Stepanauskas: "Even if we only recover 50% of the genome of groups that are driving the biogeochemistry of the planet, that's great."

Going their own way

Other researchers are using single-cell techniques to pinpoint molecular events in the embryo, probing the key time when cells begin to specialize and follow disparate developmental paths. "It's always been a goal for developmental biologists to understand, at the single-cell level, what decisions are being made" as this process unfolds, says molecular developmental biologist Paul Robson of the Genome Institute of Singapore. However, researchers didn't have the tools to detect changes in individual cells, he notes.

Now they do. Robson and colleagues, for example, used a microfluidic chip to track the activity of 48 genes as a single-celled zygote morphed into a 64-cell blastocyst, which harbors three cell types. The study revealed surprising behavior by transcription factors, proteins that latch onto DNA to flip genes on or off. Researchers had assumed that differentiation would involve activation of previously silent transcription factors, which would then nudge the cell in a new direction. But as Robson and colleagues reported last year in *Developmental Cell*, mouse embryonic cells appear to differentiate at least partly by subtraction: Transcription factors expressed throughout the embryo switch off in a cell starting down a particular developmental path.

Researchers can use such single-cell techniques to study other embryonic stages, Robson says: "We can capture cell fate decisions anywhere in development." This work might provide insight into how birth defects originate. And by identifying factors that hasten or hinder cell differentiation, such studies might also improve researchers' ability to nurture embryonic stem cells and to guide their development into the desired tissues.

Vive la différence

Single-cell research has also prodded scientists to rethink their ideas of how cells control and coordinate actions. We tend to imagine cells as governed by clockwork circuits of genes and proteins, which keep neighboring cells performing in sync like musicians in an orchestra. But evidence that began to accumulate in the late 1950s has shown that cellular variables such as gene activity fluctuate randomly. The supposedly clockwork networks are riddled with what researchers call noise.

When it's making a protein, for example, a cell typically doesn't pour out a steady stream of the molecule. Instead, it blurts out pulses of the protein at irregular intervals. Such molecular vagaries create differences between even genetically identical cells in a uniform tissue. The discovery of this variability "opens up the question, how do cells do anything, [if] it's so noisy?" says molecular biologist Jeff Hasty of UC San Diego.

In many cases, recent studies suggest, cells capitalize on such noise to guide their development, coordinate gene activity, and perform other tasks. "Heterogeneity is useful, not just a nuisance," says molecular cell biologist Michael White of the University of Liverpool in the United Kingdom.

A study of single cells by White and colleagues, published in 2010 in the *Proceedings of the National Academy of Sciences*, provides an example. The researchers tracked how individual mouse or human cells manage NF-κB, which flits in and out of a cell's nucleus, turning on genes that spur inflammation when it's inside. Two closely related proteins shut down NF-κB, but cells stagger production of the two inhibitors. White's group tweaked the production delay in individual cells and found that the delay's natural length is fine-tuned to accentuate differences in NF-κB activity between cells, thus increasing the amount of noise. "I suggest that the system is optimized to make the cells as asynchronous as possible," White says. By keeping neighboring cells out of step, the strategy might prevent release of a large, potentially harmful burst of inflammation-triggering molecules.

Even development, which seems so orderly, might rely on noise. Elowitz and colleagues have probed that possibility by dissecting differentiation in the microbe *Bacillus subtilis*. Although the changes a single bacterium undergoes are a far cry from the development of a plant or an animal, the simplicity of bacteria can provide insights into the more complex cases, researchers say. When a bacterium such as *B. subtilis* is stressed out, for example, it can gain the ability to absorb DNA from its surroundings—an altered state called competence that might boost its genetic variation. In studies of individual *B. subtilis* cells over the past few years, Elowitz's group has concluded that random fluctuations within a two-gene network control whether one of the bacteria becomes competent. Similar noisy circuits, says Elowitz, "may apply to differentiation in more complex systems," such as in biofilms that comprise multiple kinds of bacteria or in the development of multicellular animals.

The spotlight on a cell's internal noise is a direct result of the ability to study one cell at a time rather than masses of them. And researchers predict that the best is yet to come for single-cell studies, as they hone an expanding repertoire of techniques and apply them to new questions. "I think this will be one of the great new areas where advancing bioanalytical technologies combine with cell biology," Mathies says.

–MITCH LESLIE

CREDIT: M. B. ELOWITZ *ET AL.*, *SCIENCE* **297** (16 AUGUST 2002)

NATIONAL SCIENCE FOUNDATION

Face-to-face, almost. An alternative way to bring scientists together for confidential reviews.

Meeting for Peer Review at A Resort That's Virtually Free

More than 19,000 scientists travel to NSF headquarters each year to take part in grant evaluation panels. Could their avatars do the job as well?

The view from the terrace is stunning. Sunlight glimmers across a wind-riffled ocean right to the horizon. Over the past year, William Sims Bainbridge, a sociologist and program director at the U.S. National Science Foundation (NSF), has invited scientists here to take part in grant-review panels. "We usually work over there," he says, walking to a ring of stools. "This is Vannevar Bush, our patron saint," he says, admiring a framed portrait of the computer scientist who helped create NSF in 1950. Bainbridge rubs his hands together, and a floating cube the size of a refrigerator box grows out of thin air. It rotates, each face covered with scientific plots and data. "Let's teleport upstairs so I can show you around." He vanishes.

That was Bainbridge's avatar, of course, and the glimmering ocean nothing more than code in the online world of Second Life. Bainbridge helped build this virtual scientific resort for NSF as an experiment. Can the hard work of grant review be done without face-to-face meetings? With budgets tightening, scientific organizations like NSF are exploring ways to reduce the number of their physical meetings. Proponents see it as a win-win scenario, saving not only time and money but also carbon emissions. Whether the technology is up to the task is another matter.

Over the past year, more than 19,000 scientists traveled to NSF headquarters in Arlington, Virginia, to take part in traditional review panels. Most of them worked for two solid days, huddled in groups of six to 10, carefully reading, discussing, and scoring dozens of research proposals competing for over $6 billion in grants. It's the scientific equivalent of jury duty. NSF covers expenses, but the small honorarium—typically $500—hardly covers a scientist's time, especially considering the days lost to travel. But how else can NSF evaluate the merits of all those proposals?

The U.S. National Institutes of Health (NIH) has an equally heavy load. Over the past year, 17,000 reviewers evaluated 61,000 proposals competing for more than $15 billion in NIH grants. But nearly 20% of those scientists never met face to face, relying instead on combinations of phone and video conferencing, says Antonio Scarpa, director of the NIH Center for Scientific Review. Starting this year, NIH has been testing a technology called Cisco TelePresence, a videoconferencing system used by the military and large corporations. Strategically placed screens, speakers, and microphones make it seem as though remote participants are sitting around the same table. "It is so convincing that people reach for coffee cups that are not really there," says Scarpa. Although the system is expensive—NIH declined to cite a number because they are currently negotiating the price—Scarpa predicts that it will eventually reduce the cost of face-to-face meetings "by one-third."

Although very few scientists currently have access to a Cisco TelePresence station, anyone can log in to Second Life with a laptop. Since March 2009, six grant-review panels have convened on NSF's island in Second Life, known as IISLand. "Real-world panelists are provided with some resources," says Bainbridge. "So it was felt appropriate to provide them with the cost of a decent set of virtual clothes." Once the scientists had created avatars, they each received 1000 Linden dollars—which cost NSF $4—to shop in Second Life's virtual stores. (They also received a $240 honorarium of real money per day.)

Aside from those virtual quirks, the format of the meetings followed a traditional schedule, and all of the work was completed on time. Bainbridge estimates that switching to virtual review can save as much as $10,000 per panel. NSF pays $3600 in rent per year to Linden Labs, the company that operates Second Life, he says, so "just one normal-sized panel pays for the island more than twice over."

Not everyone liked it. "The work got done," says a cognitive scientist who took part in a Second Life panel in April, "but as soon as the computer turns off, you're gone. I much prefer the pain of going somewhere, hanging out, and having meals together." But virtual meetings are better than videoconferencing, he notes, because "at least you can sit around in your pajamas."

Other scientists say that the advantages of virtual and video meetings are too good to pass up. "Is what is missing about physical presence relevant at all to making scientific recommendations? In my experience, it is not," says Douglas Fisher, a computer scientist at Vanderbilt University in Nashville, Tennessee, who has taken part in other virtual meetings. "The real impediment to change is discomfort" with the virtual environment. That may be less of an issue for a younger generation of scientists accustomed to avatars in online gaming worlds. Then again, says Bainbridge, "I just turned 70. So age is no barrier."

NSF is now evaluating the Second Life panels to decide whether to expand the program. Eventually, Bainbridge calls it "plausible" that as much as 50% of grant review could be done in virtual worlds.

–JOHN BOHANNON

CREDITS: WILLIAM SIMS BAINBRIDGE/NSF

Published by AAAS

LETTERS

edited by Jennifer Sills

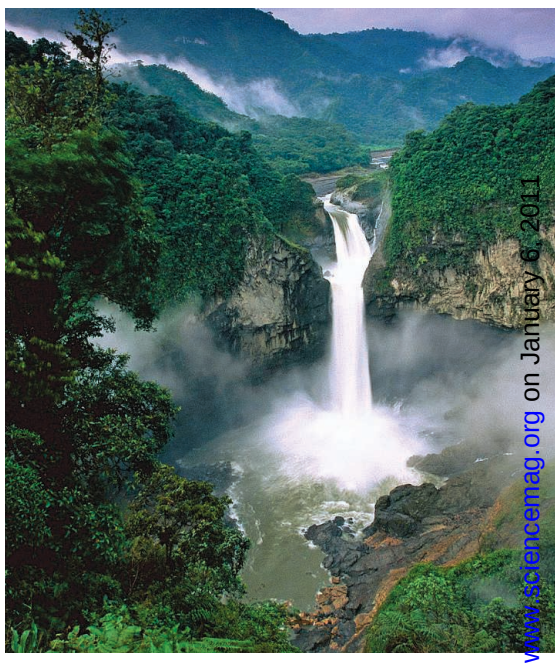

Fight for Yasuni Far from Finished

AS A SCIENTIST WITH EXPERIENCE IN WESTERN AMAZONIA SINCE 1979, INCLUDING 16 YEARS monitoring oil impacts in Yasuni, I appreciate the publicity that E. Marx's News Focus story ("The fight for Yasuni," 26 November 2010, p. 1170) brings to the issue of conserving the biodiversity in this Ecuadorian forest. However, when Marx writes that we're "on the verge of winning" the battle, I simply must differ.

Undoubtedly, gathering and sharing hard data from Yasuni over the past two decades have substantially strengthened arguments for its conservation. Nonetheless, filling the trust fund with enough contributions to compensate Ecuador for the oil fields that will not be built in Yasuni is a daunting challenge. After 3 years of worldwide campaigning for the Yasuni-ITT Initiative, we received contributions of just US$100,000 in the first 4 months after its launch—this sum represents a mere 1/1000th of the first year's requirement. Each and every day for the next year, we need to receive nearly US$300,000 if we are to reach our goal of US$100 million by December 2011. More dauntingly, the second year requires 3 times that amount—US$300 million—and the Initiative calls for that amount to be repeated annually for another 11 years. Complacency or a premature "mission accomplished" won't suffice.

KELLY SWING

Tiputini Biodiversity Station, University of San Francisco de Quito, Quito, Ecuador. E-mail: kswing@usfq.edu.ec

Publish and Flourish

IN THEIR LETTER "BATTLING THE PAPER GLUT" (17 September 2010, p. 1466), D. Siegel and P. Baveye lament that the academic community continues to enforce a "publish or perish" policy that is bad for science.

Siegel and Baveye suggest that high publication output may be correlated with low quality. Yet objective measures of quantity and quality of publications in science indicate that the best authors are usually the ones who publish the most (*1*).

Siegel and Baveye further claim that scientists who publish prolifically are trying to pad their resumés (in a "salami slicing" approach), but publishing one's lifetime work all at once would be of very limited use to the scientific community. It can be argued that the "least publishable unit" is a valuable scientific tool that facilitates data management, provides rapid dissemination of information, and stimulates integration of research efforts (*2*).

Siegel and Baveye go on to argue that the "paper glut" is responsible for a perceived deluge of publications and, consequently, for our inability to keep up with the literature. Yet, half a century ago, Derek Price found that publications in progressive sciences develop exponentially and have been doing so since at least the early 1900s (*3*). This trend indicates that scientists have felt overwhelmed by the scientific literature since long before the "publish or perish" policy took hold in the 1950s.

It is perhaps symptomatic that the letter was titled "Battling the paper glut." Most of us who are actively involved in science today do not worry about a hypothetical paper glut, for the simple reason that we store scientific documents electronically, not on paper. In the electronic age, the claim can be made that a manuscript is suitable for publication if it is technically sound and that the importance of any particular article should be determined after publication by the readership. This is the claim made by *PLoS ONE*, whose explosive success in scientific publishing is an indication that the contemporary scientific community endorses the claim (*4*).

With a rigorous peer-review system, competent scientists can publish and will flourish; incompetent scientists cannot publish and will perish. In the end, science wins.

ROBERTO REFINETTI

Circadian Rhythm Laboratory, University of South Carolina, Walterboro, SC 29488, USA. E-mail: refinetti@sc.edu

References

1. D. K. Simonton, *Scientific Genius: A Psychology of Science* (Cambridge Univ. Press, New York, 1988).
2. R. Refinetti, *FASEB J.* **4**, 128 (1990).
3. D. J. S. Price, *Little Science, Big Science, and Beyond* (Columbia Univ. Press, New York, 1963).
4. J. Kaiser, *Science* **329**, 896 (2010).

Indian Science: Steps to Excellence

THE NEWS OF THE WEEK STORY "INDIA'S vision: From scientific pipsqueak to powerhouse" (P. Bagla, 1 October 2010, p. 23) highlights a number of steps that India could undertake to increase its scientific output to a level on par with developed countries. We disagree with the implication that the

Indian government is not bolstering scientific research. In addition to luring excellent nonresident Indian scientists back to the country, the government has recently opened several high-quality research institutions (such as the Indian Institutes of Science Education and Research) and established additional campuses of the Indian Institutes of Technology. The number of Ph.D. and postdoctoral fellowships has doubled over the past 5 years (*1*–*3*).

However, Bagla overlooked two important explanations of India's underachievement. First, the reservation system, based on the caste system, downgrades the importance of merit and quality when it comes to the appointment and promotion of faculty members. Moreover, tenured faculty positions in Indian universities are safe until retirement irrespective of research output. The disconnect between achievement and advancement curbs students' enthusiasm for the research career and leads many of the best scientists to pursue opportunities in western countries. Second, other than the central institutions of excellence, most Indian universities have not traditionally focused on research but rather on producing graduates for industry. The brightest students are attracted to professional courses leading to the lucrative job market, further shrinking the student base needed for basic science research.

To revolutionize science in India, the reservation-based selection process of students and faculty should be abolished, and scientists should be promoted and given salary incentives based on their research quality. Without these initiatives, although it may be possible to meet the target of 30,000 science Ph.D.'s per year by 2025, the quality of student work and that of India's overall research effort will still be lacking.

JAGADEESH BAYRY,[1,2]* SRINI V. KAVERI,[1,2] PETER FOLLETTE[3]

[1]INSERM U 872, Centre de Recherche des Cordeliers, Université Pierre et Marie Curie and Université Paris Descartes, 15 rue de l'Ecole de Médicine, Paris 75006, France. [2]International Associated Laboratory, INSERM, France; and Indian Council of Medical Research, India. [3]Bases, Corpus, Langage (UMR 6039), Institute of Developmental Biology and Cancer (UMR 6543), Université de Nice–Sophia Antipolis, Parc Valrose, 06108 Nice, Cedex 2, France. *To whom correspondence should be addressed. E-mail: jagadeesh.bayry@crc.jussieu.fr

References

1. University Grant commission, "Annual Report 2005-2006" (Bahadur Shah Zafar Marg, New Delhi, 110-002, India), p. 95; www.ugc.ac.in/pub/annualreport/annualreport_0506.pdf.
2. C. Chauhan, "Researchers to get money equal to IAS entrants," *Hindustan Times*, 18 August 2009.
3. Ministry of Science and Technology, Department of Science and Technology, Government of India, "Office memorandum A.20020/11/97-IFD" (31 March 2010); http://mnre.gov.in/r&d/rnd-gerpf-a7.pdf.

Culture and Biodiversity Losses Linked

IN THEIR REVIEW "BIODIVERSITY CONSERvation: Challenges beyond 2010" (10 September 2010, p. 1298), M. R. W. Rands *et al*. do not sufficiently emphasize the connection between the biodiversity crisis and threats facing indigenous communities. The United Nations' recent "State of the World's Indigenous Peoples" report highlights the threat of extinction looming over traditional customs and knowledge around the world (*1*). According to the report, indigenous communities "make up about one-third of the world's 900 million extremely poor rural people," whose livelihoods are intimately tied to regional ecology (*1*). Traditional culture loss and biodiversity loss share several important drivers, such as urbanization and exposure to globalized commercialization (*2*).

Preserving traditional ecological knowledge and know-how can abet conservation research and practice. Community inclusion has yielded data on the identification and distribution of new and previously described species (*3*–*5*) and has also contributed to natural resource assessments (*6*). Furthermore, given access to basic technological resources such as GPS and participatory mapping, local peoples have effectively contributed to and enforced conservation policies (*7*). These dynamics between indigenous communities and biodiversity loss, and the challenges and opportunities therein, merit more rigorous consideration in conservation planning.

TONG WU AND MICHAEL ANTHONY PETRIELLO

School of Forestry, Northern Arizona University, Flagstaff, AZ 86011, USA.

*To whom correspondence should be addressed. E-mail: tong.wu@nau.edu

CORRECTIONS AND CLARIFICATIONS

Research Articles: "Integrative analysis of the *Caenorhabditis elegans* genome by the modENCODE Project" by M. B. Gerstein *et al*. (24 December 2010, p. 1775). There were two errors in the reference list. The first author of reference 15 should be W. C. Spencer. The periodical in reference 57 should be *Genome Biology*.

Books *et al*.: "Inventive constructions using biobricks" by V. Vinson (17 December 2010, p. 1629). The word "biobrick" was incorrectly used as a noun. The word "biobrick" is an adjective trademarked by the public-benefit BioBricks Foundation (BBF) that defines a brand of standard biological parts.

Books *et al*.: Browsings (10 December 2010, p. 1482). The title of Richard Evan Schwartz's book is "You Can Count on Monsters: The First 100 Numbers and Their Characters."

Books *et al*.: "Shades of gray in DNA drama" by B. Juncosa (3 December 2010, p. 1322). The second sentence in the last paragraph should have concluded "her contributions to the human understanding of life's hereditary material are difficult to overstate."

Reports: "A magnetized jet from a massive protostar" by C. Carrasco-González *et al*. (26 November 2010, p. 1209). The scale bars were mistakenly omitted from Fig. 1. The correct figure is shown here.

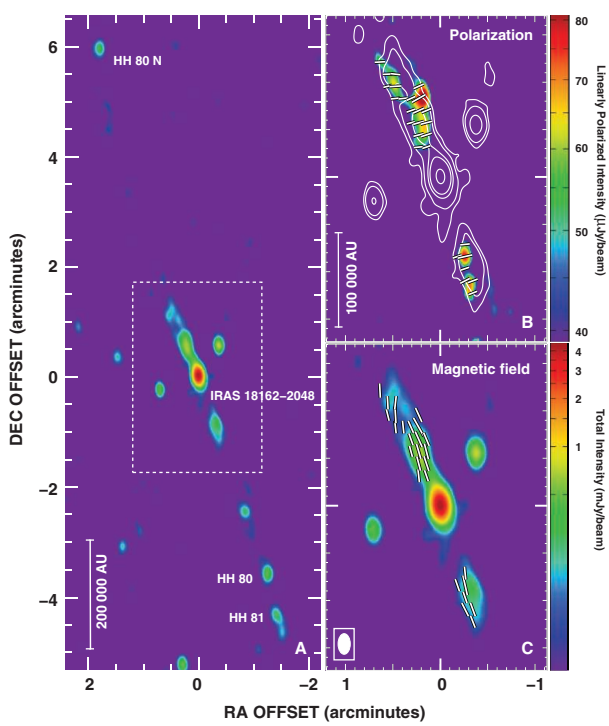

Reports: "A *Vibrio* effector protein is an inositol phosphatase and disrupts host cell membrane integrity" by C. A. Broberg *et al*. (24 September 2010, p. 1660). The legend for Fig. 3, E and F, incorrectly referred to 2xFYVE domain instead of PH(PLCd1)-GFP. The legend should read: "Quantitation of (**E**) blebbing or (**F**) GFP at the membrane in Hela cells transfected with PH(PLCd1)-GFP and empty vector, VPA0450, or VPA0450-H356A."

Published by AAAS

References
1. United Nations, "State of the World's Indigenous Peoples" (United Nations, New York, 2009).
2. Worldwatch Institute, "State of the World 2010" (Worldwatch Institute, Washington, DC, 2010).
3. S. I. FitzGibbon, D. N. Jones, *Wildlife Res*. **33**, 233 (2006).
4. C. A. Garcia, G. Lescuyer, *Biodiversity Conserv*. **17**, 1303 (2008).
5. T. Kadoya, I. S. Hiroshi, R. Kikucki, S. Suda, I. Washitani, *Biol. Conserv*. **142**, 1011 (2009).
6. C. E. Roa Garcia, S. Brown, *J. Environ. Manage*. **90**, 3040 (2009).
7. M. K. McCall, P. A. Minang, *Geograph. J*. **171**, 340 (2005).

Response

WE COMPLETELY AGREE WITH WU AND Petriello that a connection exists between the biodiversity crisis and threats to indigenous communities. Indeed, there are remarkable parallels between the geographic pattern of threats to biodiversity and threats to indigenous languages (*1*). Although this geographic congruence was not the subject of our Review, we did touch on the argument that indigenous knowledge, action, and involvement can help conservation.

The world's governments have also recognized this link through the newly adopted Strategic Plan of the Convention on Biological Diversity (*2*). Target 18 of the plan specifies that by 2020, "the traditional knowledge, innovations and practices of indigenous and local communities relevant for the conservation and sustainable use of biodiversity, and their customary use of biological resources, are respected," in ways that have "the full and effective participation of indigenous and local communities, at all relevant levels." We support this objective but note that this target presents a considerable practical and political challenge, given the marginalized status and impoverishment of indigenous and local communities. Greater involvement of local communities will be essential if conservation efforts are to succeed in making substantial and sustainable progress in tackling biodiversity loss.

MICHAEL R. W. RANDS,[1]* WILLIAM M. ADAMS,[2] LEON BENNUN,[3] STUART H. M. BUTCHART,[3] ANDREW CLEMENTS,[4] DAVID COOMES,[5] ABIGAIL ENTWISTLE,[6] IAN HODGE,[7] VALERIE KAPOS,[8,9,10] JÖRN P. W. SCHARLEMANN,[8] WILLIAM J. SUTHERLAND,[10] BHASKAR VIRA[2]

[1]Cambridge Conservation Initiative, Judge Business School, University of Cambridge, Cambridge CB2 1AG, UK. [2]Department of Geography, University of Cambridge, Cambridge CB2 3EN, UK. [3]BirdLife International, Wellbrook Court, Cambridge CB3 0NA, UK. [4]British Trust for Ornithology, The Nunnery, Thetford, Norfolk IP24 2PU, UK. [5]Department of Plant Sciences, University of Cambridge, Cambridge CB2 3EA, UK. [6]Fauna and Flora International, Jupiter House, Cambridge CB1 2JD, UK. [7]Department of Land Economy, University of Cambridge, Cambridge CB3 9EP, UK. [8]United Nations Environment Programme World Conservation Monitoring Centre, 219 Huntingdon Road, Cambridge CB3 0DL, UK. [9]Cambridge Conservation Forum, c/o Department of Zoology, University of Cambridge, Cambridge CB2 3EJ, UK. [10]Conservation Science Group, Department of Zoology, University of Cambridge, Cambridge CB2 3EJ, UK.

*To whom correspondence should be addressed. E-mail: mr494@cam.ac.uk

References
1. W. J. Sutherland, *Nature* **423**, 276 (2003).
2. Convention on Biological Diversity, Strategic Plan for Biodiversity 2011–2020 (www.cbd.int/nagoya/outcomes).

Letters to the Editor

Letters (~300 words) discuss material published in *Science* in the past 3 months or matters of general interest. Letters are not acknowledged upon receipt. Whether published in full or in part, Letters are subject to editing for clarity and space. Letters submitted, published, or posted elsewhere, in print or online, will be disqualified. To submit a Letter, go to www.submit2science.org.

Published by AAAS

LETTERS

edited by Jennifer Sills

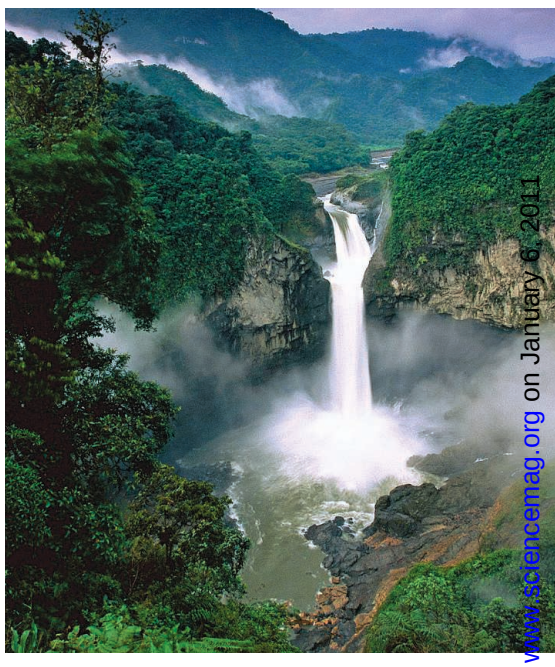

Fight for Yasuni Far from Finished

AS A SCIENTIST WITH EXPERIENCE IN WESTERN AMAZONIA SINCE 1979, INCLUDING 16 YEARS monitoring oil impacts in Yasuni, I appreciate the publicity that E. Marx's News Focus story ("The fight for Yasuni," 26 November 2010, p. 1170) brings to the issue of conserving the biodiversity in this Ecuadorian forest. However, when Marx writes that we're "on the verge of winning" the battle, I simply must differ.

Undoubtedly, gathering and sharing hard data from Yasuni over the past two decades have substantially strengthened arguments for its conservation. Nonetheless, filling the trust fund with enough contributions to compensate Ecuador for the oil fields that will not be built in Yasuni is a daunting challenge. After 3 years of worldwide campaigning for the Yasuni-ITT Initiative, we received contributions of just US$100,000 in the first 4 months after its launch—this sum represents a mere 1/1000th of the first year's requirement. Each and every day for the next year, we need to receive nearly US$300,000 if we are to reach our goal of US$100 million by December 2011. More dauntingly, the second year requires 3 times that amount—US$300 million—and the Initiative calls for that amount to be repeated annually for another 11 years. Complacency or a premature "mission accomplished" won't suffice.

KELLY SWING

Tiputini Biodiversity Station, University of San Francisco de Quito, Quito, Ecuador. E-mail: kswing@usfq.edu.ec

Publish and Flourish

IN THEIR LETTER "BATTLING THE PAPER GLUT" (17 September 2010, p. 1466), D. Siegel and P. Baveye lament that the academic community continues to enforce a "publish or perish" policy that is bad for science.

Siegel and Baveye suggest that high publication output may be correlated with low quality. Yet objective measures of quantity and quality of publications in science indicate that the best authors are usually the ones who publish the most (*1*).

Siegel and Baveye further claim that scientists who publish prolifically are trying to pad their resumés (in a "salami slicing" approach), but publishing one's lifetime work all at once would be of very limited use to the scientific community. It can be argued that the "least publishable unit" is a valuable scientific tool that facilitates data management, provides rapid dissemination of information, and stimulates integration of research efforts (*2*).

Siegel and Baveye go on to argue that the "paper glut" is responsible for a perceived deluge of publications and, consequently, for our inability to keep up with the literature. Yet, half a century ago, Derek Price found that publications in progressive sciences develop exponentially and have been doing so since at least the early 1900s (*3*). This trend indicates that scientists have felt overwhelmed by the scientific literature since long before the "publish or perish" policy took hold in the 1950s.

It is perhaps symptomatic that the letter was titled "Battling the paper glut." Most of us who are actively involved in science today do not worry about a hypothetical paper glut, for the simple reason that we store scientific documents electronically, not on paper. In the electronic age, the claim can be made that a manuscript is suitable for publication if it is technically sound and that the importance of any particular article should be determined after publication by the readership. This is the claim made by *PLoS ONE*, whose explosive success in scientific publishing is an indication that the contemporary scientific community endorses the claim (*4*).

With a rigorous peer-review system, competent scientists can publish and will flourish; incompetent scientists cannot publish and will perish. In the end, science wins.

ROBERTO REFINETTI

Circadian Rhythm Laboratory, University of South Carolina, Walterboro, SC 29488, USA. E-mail: refinetti@sc.edu

References

1. D. K. Simonton, *Scientific Genius: A Psychology of Science* (Cambridge Univ. Press, New York, 1988).
2. R. Refinetti, *FASEB J.* **4**, 128 (1990).
3. D. J. S. Price, *Little Science, Big Science, and Beyond* (Columbia Univ. Press, New York, 1963).
4. J. Kaiser, *Science* **329**, 896 (2010).

Indian Science: Steps to Excellence

THE NEWS OF THE WEEK STORY "INDIA'S vision: From scientific pipsqueak to powerhouse" (P. Bagla, 1 October 2010, p. 23) highlights a number of steps that India could undertake to increase its scientific output to a level on par with developed countries. We disagree with the implication that the

Indian government is not bolstering scientific research. In addition to luring excellent nonresident Indian scientists back to the country, the government has recently opened several high-quality research institutions (such as the Indian Institutes of Science Education and Research) and established additional campuses of the Indian Institutes of Technology. The number of Ph.D. and postdoctoral fellowships has doubled over the past 5 years (*1*–*3*).

However, Bagla overlooked two important explanations of India's underachievement. First, the reservation system, based on the caste system, downgrades the importance of merit and quality when it comes to the appointment and promotion of faculty members. Moreover, tenured faculty positions in Indian universities are safe until retirement irrespective of research output. The disconnect between achievement and advancement curbs students' enthusiasm for the research career and leads many of the best scientists to pursue opportunities in western countries. Second, other than the central institutions of excellence, most Indian universities have not traditionally focused on research but rather on producing graduates for industry. The brightest students are attracted to professional courses leading to the lucrative job market, further shrinking the student base needed for basic science research.

To revolutionize science in India, the reservation-based selection process of students and faculty should be abolished, and scientists should be promoted and given salary incentives based on their research quality. Without these initiatives, although it may be possible to meet the target of 30,000 science Ph.D.'s per year by 2025, the quality of student work and that of India's overall research effort will still be lacking.

JAGADEESH BAYRY,[1,2]* SRINI V. KAVERI,[1,2] PETER FOLLETTE[3]

[1]INSERM U 872, Centre de Recherche des Cordeliers, Université Pierre et Marie Curie and Université Paris Descartes, 15 rue de l'Ecole de Médicine, Paris 75006, France. [2]International Associated Laboratory, INSERM, France; and Indian Council of Medical Research, India. [3]Bases, Corpus, Langage (UMR 6039), Institute of Developmental Biology and Cancer (UMR 6543), Université de Nice–Sophia Antipolis, Parc Valrose, 06108 Nice, Cedex 2, France. *To whom correspondence should be addressed. E-mail: jagadeesh.bayry@crc.jussieu.fr

References

1. University Grant commission, "Annual Report 2005-2006" (Bahadur Shah Zafar Marg, New Delhi, 110-002, India), p. 95; www.ugc.ac.in/pub/annualreport/annualreport_0506.pdf.
2. C. Chauhan, "Researchers to get money equal to IAS entrants," *Hindustan Times*, 18 August 2009.
3. Ministry of Science and Technology, Department of Science and Technology, Government of India, "Office memorandum A.20020/11/97-IFD" (31 March 2010); http://mnre.gov.in/r&d/rnd-gerpf-a7.pdf.

Culture and Biodiversity Losses Linked

IN THEIR REVIEW "BIODIVERSITY CONSERvation: Challenges beyond 2010" (10 September 2010, p. 1298), M. R. W. Rands *et al*. do not sufficiently emphasize the connection between the biodiversity crisis and threats facing indigenous communities. The United Nations' recent "State of the World's Indigenous Peoples" report highlights the threat of extinction looming over traditional customs and knowledge around the world (*1*). According to the report, indigenous communities "make up about one-third of the world's 900 million extremely poor rural people," whose livelihoods are intimately tied to regional ecology (*1*). Traditional culture loss and biodiversity loss share several important drivers, such as urbanization and exposure to globalized commercialization (*2*).

Preserving traditional ecological knowledge and know-how can abet conservation research and practice. Community inclusion has yielded data on the identification and distribution of new and previously described species (*3*–*5*) and has also contributed to natural resource assessments (*6*). Furthermore, given access to basic technological resources such as GPS and participatory mapping, local peoples have effectively contributed to and enforced conservation policies (*7*). These dynamics between indigenous communities and biodiversity loss, and the challenges and opportunities therein, merit more rigorous consideration in conservation planning.

TONG WU AND MICHAEL ANTHONY PETRIELLO

School of Forestry, Northern Arizona University, Flagstaff, AZ 86011, USA.

*To whom correspondence should be addressed. E-mail: tong.wu@nau.edu

CORRECTIONS AND CLARIFICATIONS

Research Articles: "Integrative analysis of the *Caenorhabditis elegans* genome by the modENCODE Project" by M. B. Gerstein *et al*. (24 December 2010, p. 1775). There were two errors in the reference list. The first author of reference 15 should be W. C. Spencer. The periodical in reference 57 should be *Genome Biology*.

Books *et al*.: "Inventive constructions using biobricks" by V. Vinson (17 December 2010, p. 1629). The word "biobrick" was incorrectly used as a noun. The word "biobrick" is an adjective trademarked by the public-benefit BioBricks Foundation (BBF) that defines a brand of standard biological parts.

Books *et al*.: Browsings (10 December 2010, p. 1482). The title of Richard Evan Schwartz's book is "You Can Count on Monsters: The First 100 Numbers and Their Characters."

Books *et al*.: "Shades of gray in DNA drama" by B. Juncosa (3 December 2010, p. 1322). The second sentence in the last paragraph should have concluded "her contributions to the human understanding of life's hereditary material are difficult to overstate."

Reports: "A magnetized jet from a massive protostar" by C. Carrasco-González *et al*. (26 November 2010, p. 1209). The scale bars were mistakenly omitted from Fig. 1. The correct figure is shown here.

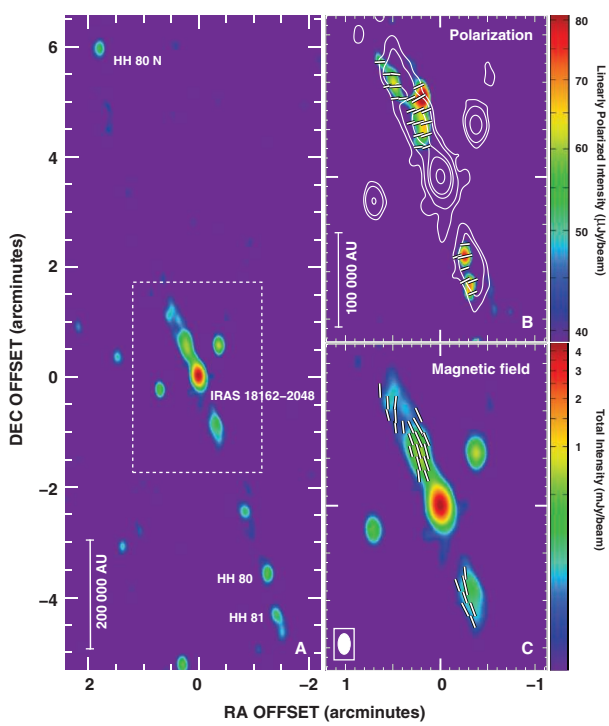

Reports: "A *Vibrio* effector protein is an inositol phosphatase and disrupts host cell membrane integrity" by C. A. Broberg *et al*. (24 September 2010, p. 1660). The legend for Fig. 3, E and F, incorrectly referred to 2xFYVE domain instead of PH(PLCd1)-GFP. The legend should read: "Quantitation of (**E**) blebbing or (**F**) GFP at the membrane in Hela cells transfected with PH(PLCd1)-GFP and empty vector, VPA0450, or VPA0450-H356A."

Published by AAAS

References
1. United Nations, "State of the World's Indigenous Peoples" (United Nations, New York, 2009).
2. Worldwatch Institute, "State of the World 2010" (Worldwatch Institute, Washington, DC, 2010).
3. S. I. FitzGibbon, D. N. Jones, *Wildlife Res*. **33**, 233 (2006).
4. C. A. Garcia, G. Lescuyer, *Biodiversity Conserv*. **17**, 1303 (2008).
5. T. Kadoya, I. S. Hiroshi, R. Kikucki, S. Suda, I. Washitani, *Biol. Conserv*. **142**, 1011 (2009).
6. C. E. Roa Garcia, S. Brown, *J. Environ. Manage*. **90**, 3040 (2009).
7. M. K. McCall, P. A. Minang, *Geograph. J*. **171**, 340 (2005).

Response

WE COMPLETELY AGREE WITH WU AND Petriello that a connection exists between the biodiversity crisis and threats to indigenous communities. Indeed, there are remarkable parallels between the geographic pattern of threats to biodiversity and threats to indigenous languages (*1*). Although this geographic congruence was not the subject of our Review, we did touch on the argument that indigenous knowledge, action, and involvement can help conservation.

The world's governments have also recognized this link through the newly adopted Strategic Plan of the Convention on Biological Diversity (*2*). Target 18 of the plan specifies that by 2020, "the traditional knowledge, innovations and practices of indigenous and local communities relevant for the conservation and sustainable use of biodiversity, and their customary use of biological resources, are respected," in ways that have "the full and effective participation of indigenous and local communities, at all relevant levels." We support this objective but note that this target presents a considerable practical and political challenge, given the marginalized status and impoverishment of indigenous and local communities. Greater involvement of local communities will be essential if conservation efforts are to succeed in making substantial and sustainable progress in tackling biodiversity loss.

MICHAEL R. W. RANDS,[1]* WILLIAM M. ADAMS,[2] LEON BENNUN,[3] STUART H. M. BUTCHART,[3] ANDREW CLEMENTS,[4] DAVID COOMES,[5] ABIGAIL ENTWISTLE,[6] IAN HODGE,[7] VALERIE KAPOS,[8,9,10] JÖRN P. W. SCHARLEMANN,[8] WILLIAM J. SUTHERLAND,[10] BHASKAR VIRA[2]

[1]Cambridge Conservation Initiative, Judge Business School, University of Cambridge, Cambridge CB2 1AG, UK. [2]Department of Geography, University of Cambridge, Cambridge CB2 3EN, UK. [3]BirdLife International, Wellbrook Court, Cambridge CB3 0NA, UK. [4]British Trust for Ornithology, The Nunnery, Thetford, Norfolk IP24 2PU, UK. [5]Department of Plant Sciences, University of Cambridge, Cambridge CB2 3EA, UK. [6]Fauna and Flora International, Jupiter House, Cambridge CB1 2JD, UK. [7]Department of Land Economy, University of Cambridge, Cambridge CB3 9EP, UK. [8]United Nations Environment Programme World Conservation Monitoring Centre, 219 Huntingdon Road, Cambridge CB3 0DL, UK. [9]Cambridge Conservation Forum, c/o Department of Zoology, University of Cambridge, Cambridge CB2 3EJ, UK. [10]Conservation Science Group, Department of Zoology, University of Cambridge, Cambridge CB2 3EJ, UK.

*To whom correspondence should be addressed. E-mail: mr494@cam.ac.uk

References
1. W. J. Sutherland, *Nature* **423**, 276 (2003).
2. Convention on Biological Diversity, Strategic Plan for Biodiversity 2011–2020 (www.cbd.int/nagoya/outcomes).

Letters to the Editor

Letters (~300 words) discuss material published in *Science* in the past 3 months or matters of general interest. Letters are not acknowledged upon receipt. Whether published in full or in part, Letters are subject to editing for clarity and space. Letters submitted, published, or posted elsewhere, in print or online, will be disqualified. To submit a Letter, go to www.submit2science.org.

Published by AAAS

MOLECULAR BIOLOGY

Surely You're Joking, Mr. Brenner

Ronald H. A. Plasterk

It was the fall of 1986, at the Medical Research Council's Laboratory of Molecular Biology (LMB), in Cambridge, England. As people gathered in the crowded seminar room, I (fresh from the Netherlands, a young postdoc with John Sulston) ended up sitting next to the institute director, Sydney Brenner. Looking around and seeing the joint heads of the Division of Cell Biology walk in, Brenner remarked: "Look, there comes the gang of two. Or, as I like to think of them, the gang of one-and-a-half." Young as I was, I thought this comment witty but that making it aloud was probably not an ideal way to lead an institute. In Errol Friedberg's *Sydney Brenner: A Biography*, we read that looking back, Brenner considered his decision to become LMB director "the biggest mistake of his life."

Friedberg (a pathologist at the University of Texas Southwestern Medical Center at Dallas) offers a wonderful overview of the life of one of the most interesting scientists living today. The book takes readers through Brenner's youth in a Jewish family in South Africa, his studies there and in England, and a busy 1954 visit to the United States. After a couple of years teaching back in South Africa, Brenner began his long stay at Cambridge, where he teamed up with another great mind of biology, Francis Crick. The author finds the right tone for discussing Brenner's scientific thoughts and discoveries: his descriptions of the science are basic enough that nonbiologists will understand the essence but not simplified too far.

Friedberg's biography includes echoes of Horace Freeland Judson's classic account of the birth of molecular biology, *The Eighth Day of Creation* (*1*). Indeed the story of the modern field's origins to a large extent consists of the stories of the circle of people (including Fred Sanger, Jim Watson, and Seymour Benzer) in which Brenner carried out his research. Another reason for the similarity may be that Judson, too, drew heavily on interviews, many with Brenner—and Brenner gives wonderful interviews.

One dramatic episode recounted in the book is the quarrel between Brenner and John Sulston, with whom he would later share the 2002 Nobel Prize in Medicine, awarded for their *Caenorhabditis elegans* research. Looking back, both regret their quarrel and the fact that it never really got resolved. Anybody working around the two at the time noticed the tension, but one never asked what was at the base of it and neither volunteered to tell. Thirty years later, we learn that Brenner, after having left the *C. elegans* genome project entirely in the hands of Sulston, had given an interview in *New Scientist* (*2*) in which he said he was mapping the worm genome, without mentioning contributions from Sulston and Alan Coulson. Sulston and Coulson sent an angry letter to *New Scientist*: "We would like to clarify … [that] the nematode genome is not being mapped in Sydney Brenner's laboratory … as would have been clear had the authorship and journal been cited for the published figure" (*3*). Brenner later commented: "When people behave that way I don't have time to deal with them. I simply move on. I have too much to do—and life is too short to be caught up in this sort of thing."

Sydney Brenner
A Biography
by Errol C. Friedberg
Cold Spring Harbor Laboratory Press, Cold Spring Harbor, NY, 2010. 379 pp. $39. ISBN 9780879699475.

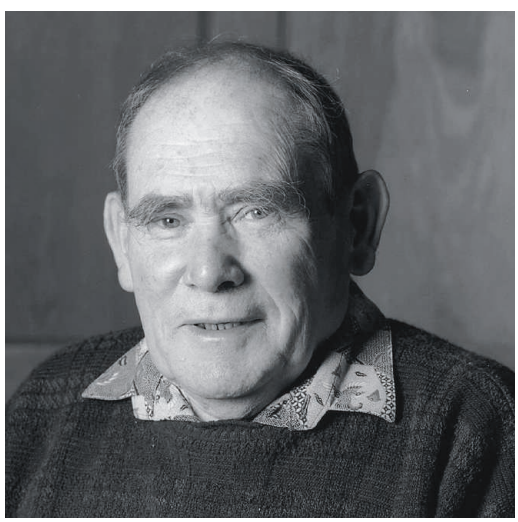

Here, as in other places, the biography remains somewhat superficial. Having chosen to describe Brenner's life as a train of scientific thoughts, Friedberg ignores the psychology. Reading 300 pages does not bring us truly close to the person Brenner. Who is he really? From *Double Helix* (*4*), it is clear that Watson was inspired by his friendly rivalry with Crick. Brenner shared a room with Crick for 22 years; how did they get along? Did Brenner indeed not care about the animosity with Sulston? And what explains what Robert Horvitz (the third person sharing that 2002 Nobel Prize) describes as Brenner's "darker side"?

Brenner has the mind and the life history to be the Richard Feynman of biology. He is a genius, the symbol for an entire field of research. Like Feynman, he has to his name long lists of one-liners that are constantly quoted by others in the field. Two from the book: "Theories should be treated like mistresses. One should never fall in love with them and they should be discarded when the pleasure they provide is over." And, on a colleague: "Why sit at home and be miserable, when you can come into the laboratory and work—and be miserable?" Like Feynman, Brenner is witty and has won a Nobel Prize. But most important for a legend, Brenner, like Feynman, has this wonderful superiority complex, which results in irreverence, disdain for authority, and allergy to pomposity. This is what young starting scientists love.

Three years ago I gave my son, then in high school, a copy of *"Surely You're Joking, Mr. Feynman!"* (*5*). He read it but did not say much and two years later registered for university study in psychology. After his first year, however, he switched to physics. This is, of course, a no-control experiment, so we will never know if Feynman's enticing "cult book" played a role. Concise and entertaining, Friedberg's *Sydney Brenner* is a must-read for anyone interested in the history of molecular biology. It is not, however, the sort of account that could attract floods of young people to the field. That still unwritten book will need to get closer to the demon in Brenner.

The reviewer is at the House of Representatives, Postbox 20018, 2500 EA The Hague, Netherlands. E-mail: plasterk@tiscali.nl

References

1. H. F. Judson, *The Eighth Day of Creation: Makers of the Revolution in Biology* (Simon and Schuster, New York, 1979); reviewed in (*6*).
2. G. Vines, *New Sci.* **5**, 10 (1987).
3. J. Sulston, A. Coulson, S. Brenner, *New Sci.* **19**, 64 (1987).
4. J. D. Watson, *The Double Helix: A Personal Account of the Discovery of the Structure of DNA* (Atheneum, New York, 1968).
5. R. P. Feynman, R. Leighton, *"Surely You're Joking, Mr. Feynman!" Adventures of a Curious Character*, E. Hutchings, Ed. (Norton, New York, 1985).
6. E. J. Yoxen, *Science* **205**, 1119 (1979).

10.1126/science.1199528

HISTORY OF SCIENCE

Commerce at the Helm?

Steven Shapin

At some point over the past 30 or 40 years, it is widely said, university research ceased being valued "for its own sake" and began to be assessed for its contribution to concrete external goals. The label attached to this change varies. If you don't like the new order of things, you may tend to call it "commercialization" or, if you're really critical, "commodification." If you do approve, you are less likely to have a fixed name for it, most likely just celebrating the increasing integration of the academy into the hard-headed values of civic life. University administrators are often enthusiastic about the new "relevance," seeing ways to raise funds, monetize scholarship, and encourage research that can more readily attract money; to objectively assess academic merit and "rationalize" appointments and promotions; and to display the concrete value of the university's activities to politicians and businesspeople constitutionally skeptical of what they take to be ivory tower pointlessness. The celebrants tend not to write books about these things, partly because that isn't the sort of thing they do and partly because they don't feel they have to. The future seems to be going their way.

The despair and the criticism have mainly come from a handful of journalists and, internally, from the humanities, the social sciences, and especially from scholars studying social aspects of science and technology, warning that scientific integrity is being disastrously undermined. In recent years, the most vigorous American expressions of alarm include books by Sheldon Krimsky, Derek Bok, and Jennifer Washburn (*1*–*3*), and Philip Mirowski's (almost certainly very critical) *Science-Mart* will soon be released (*4*).

The contributors to Hans Radder's collection *The Commodification of Academic Research* work in the despairing and critical parts of the academy. The overwhelming majority here are philosophers or ethicists, lightly leavened with social scientists. (Oddly, no historian was apparently invited to describe and interpret a historical process.) The result is an uneven, and sometimes empirically thin, performance, one in which several of the parts satisfy more than the whole in which they are embedded. There are chapters on intellectual property and technology transfer, the nature of scientific "norms" and the effect of commercial interests on them, the specific influence of pharmaceutical companies on scientific research agendas, recommended ways to minimize corrosive effects of commercialization on intellectual quality, the problematic place of intellectual "justification" within commercially orientated science, and the notion of commodification in theoretical critiques of capitalism.

The assemblage is awkward for a number of reasons, one of which is highlighted by the editor's introduction, where Radder (a philosopher of science at the Free University of Amsterdam) struggles to find a definite sense of what sorts of processes commodification reliably and coherently designates. Now largely shorn of its associations with Marxist theory, the root sensibility of commodification as used in this volume seems nevertheless to retain much of the original notion—conferring economic value on things that were not previously thought of in econometric terms. The editor and his contributors find the term useful, but they won't be constrained by any stable definition. Since the 1980s, Western universities have, the editor says, been substantially changed by the forces of commodification, but within a few pages he warns against any simplistic understanding of what commodification is and, specifically, against equating commodification with commercialization. Commodification may, indeed, include making scientific inquiry wholly or partly subservient to commercial goals and metrics. But, he notes, it may also encompass tendencies as diverse as the administratively imposed "rationalization" of academic departments, corporate sponsorship of research and professorial chairs, universities' own attempts to raise revenue through patenting and licensing, attempts to quantify scientific quality and impact, and a "publish-or-perish" academic culture—not all of which have any clear connection with economic metrics and each of which may proceed from distinct causes.

The Commodification of Academic Research
Science and the Modern University
Hans Radder, Ed.
University of Pittsburgh Press, Pittsburgh, 2010. 360 pp. $50. ISBN 9780822943969.

The less-impressive contributions to this volume criticize more than they seek to understand. The better ones take a nuanced approach to the identity of the problem and its causes. Here the chapter by sociologist Daniel Lee Kleinman stands out, not least for the writer's interest in the deeper historical background and for his skepticism about direct commercial influences as causes of what's been happening in the modern university. Kleinman directs attention away from what commerce has done to the university and toward what the university has willingly done to itself. He does not deny that academic scholarship, including science, proceeds within an increasingly econometric framework, but he doubts that corporate influence is its direct cause. For all its visibility, only 7% of U.S. academic research is now funded by industry. The alignment of scientific work with commercial concerns can also arise from patterns internal to modern science—scientists' investments in disciplinary models, theories, and instrumental resources—and from researchers' uncoerced desire to do work interesting to a range of potential funding sources.

It is evident, Kleinman accepts, that many aspects of university culture have come closely to resemble corporate culture, but direct influence does not seem to be a pertinent and powerful explanation. Despite pervasive myths of an ivory tower past, universities have always served their social masters and have always molded their internal cultures to those of the powers surrounding and sustaining them. They have never done so completely, but neither have they ever been as contemplatively disengaged as legend implies. Our whole society has become shot through with econometric sensibilities and corporate patterns of organization. Why ever should we expect universities to be much different? It's a good question, meriting a considered and informed answer. We've heard from the humanists and the social scientists; it's time to hear a lot more from the natural scientists and engineers. If the inhabitants of the modern research university cannot collectively agree that they want to push back, then the further alignment of research and teaching with econometric sensibilities is likely to be the future.

References

1. S. Krimsky, *Science in the Private Interest: Has the Lure of Profits Corrupted Biomedical Research?* (Rowman and Littlefield, Lanham, MD, 2003).
2. D. Bok, *Universities in the Marketplace: The Commercialization of Higher Education* (Princeton Univ. Press, Princeton, NJ, 2003).
3. J. Washburn, *University, Inc.: The Corporate Corruption of American Higher Education* (Basic, New York, 2005).
4. P. Mirowski, *Science-Mart: Privatizing American Science* (Harvard Univ. Press, Cambridge, MA, February 2011).

The reviewer is at the Department of the History of Science, Harvard University, Cambridge, MA 02138, USA. E-mail: shapin@fas.harvard.edu

10.1126/science.1198434

ETHICS

Bad Science Used to Support Torture and Human Experimentation

Despite prior U.S. recognition of "enhanced interrogation" techniques as torture, science was misrepresented to support their use.

Vincent Iacopino,[1,2,3]* Scott A. Allen,[1,4]* Allen S. Keller[5,6]

In the wake of the September 11, 2001, attacks, the U.S. government authorized "enhanced interrogation" techniques (EITs) (i.e., prolonged sleep, sensory deprivation, forced nudity, and painful body positions) that were routinely applied to detainees in U.S. custody in at least three theaters of operation and an unknown number of secret "black sites" operated by the Central Intelligence Agency (CIA). They did this despite the fact that each EIT was considered torture by the United Nations (*1*), and the United States recognized them as such in its reports on human rights practices (*2*). Although legal sources and trained interrogation experts warned of the unreliability and questionable legality of coerced confessions (*3*), EITs were authorized by the CIA in January 2003 (*4*) and the Department of Defense (DoD) in April 2003 (*3*).

U.S. torture and the complicity of scientists and health professionals were enabled in part by the Department of Justice's (DOJ's) revised definition of torture in the Bybee memo (*5*), which raised the physical and mental pain thresholds for torture (*6*). Critically, mental pain or suffering was defined as "significant psychological harm of significant duration, e.g., lasting for months or even years" (*6*). Even if these thresholds were exceeded, infliction of severe physical pain and severe and prolonged mental pain had to be the interrogator's "precise objective" to constitute torture. The Bybee language of "specific intent" (*7*) undermined any meaningful definition of torture for medical personnel charged with recognizing it.

Science Used to Justify Torture

After being used by the Chinese and North Koreans to extract false confessions from U.S. soldiers during the Korean War, these EIT methods were included in the survival, evasion, resistance, and escape (SERE) training of U.S. soldiers to resist torture if captured by an enemy (*3*). Studies on U.S.

military personnel undergoing SERE training before September 11 were cited to justify the EITs as "safe, legal and effective" (*8*). SERE medical personnel advised DoD that "if there are any long-term negative psychological effects of [U.S. Air Force Resistance Training], they are certainly minimal" (*3*). But the SERE studies did not include any long-term psychological measures [such as detailed in (*9*)], depending instead on acute monitoring, which limited use of these studies in informing assessments of mental pain or suffering, particularly with respect to Bybee's significant-duration standards. The studies also demonstrated marked increases in stress hormone levels and measures of psychological stress and dissociation symptoms (96% of subjects), a symptom of posttraumatic stress disorder (*8*). Moreover, the studies were conducted on subjects who were exposed to only limited forms of EITs, provided their consent for the study, and were able to stop their participation at any time (*8*)—all conditions that may limit studies' usefulness in informing use of EITs in actual detainee interrogations.

Given prior U.S. recognition of each EIT method as torture (*2*) and literature on the harmful physical, psychological, and social health consequences associated with such abuse (*1*, *8*, *9*), one would expect that a "good faith" effort to ensure safe, legal, and effective interrogations would include effective medical assessments (*9*) of possible torture. This was not the case. Although declassified documents refer to psychological evaluations of detainees (*10*, *11*), such assessments of detainees made available as a result of Freedom of Information Act litigation consist primarily of identification of psychological vulnerabilities, without any assessment of possible physical or mental harm (*4*, *10*). The CIA's "Draft OMS [Office of Medical Services] Guidelines on Medical and Psychological Support to Detainee Interrogations" [Appendix F (*4*)] do not contain guidelines for any form of psychological assessment, not even those assessments used in the SERE studies (*4*).

In 2005, the DOJ's Bradbury memos referred to research findings to justify EIT practices on detainees (*8*, *11*). The research findings are not publicly available, thus there is insufficient information to judge scientific merit, but they appear to constitute unethical, illegal human-subject research conducted on detainees without their consent (*8*). For example, the memo justifies certain EIT practices to be used in combination by referring to cursory psychological observations during interrogations by OMS personnel when EITs were applied to 25 detainees (*8*). Such psychological assessments are not consistent with standards for assessing torture (*9*). Rather, the studies appear to have served the predetermined conclusion that EITs were safe, legal, and effective because they were used to justify EITs without assessing legally relevant, long-term psychological harm as defined by Bybee. The studies also failed to recognize decades of scientific literature on the harmful physical, psychological, and social health consequences of EITs and other forms of torture (*1*, *8*, *9*).

Science, Ethics, and the Government

Because the "science" referred to in the Bradbury memos appears to have neglected long-term psychological harm, and given

[1]Physicians for Human Rights, Cambridge, MA 02138, USA. [2]University of Minnesota Medical School, Minneapolis, MN 55455, USA. [3]Human Rights Center, University of California, Berkeley, Berkeley, CA 94720, USA. [4]Alpert Medical School, Brown University, Providence, RI 02912, USA. [5]Bellevue/NYU Program for Survivors of Torture, New York, NY 10016, USA. [6]Center for Health and Human Rights, Division of General Internal Medicine, Department of Medicine, New York University School of Medicine, New York, NY 10016, USA.

*These authors contributed equally to this work. †Author for correspondence. E-mail: docallen1@me.com

Published by AAAS

concerns about how the Bybee memo may make it difficult or impossible to assess mental pain or suffering, doubts may be raised about whether any actual science was conducted. But in terms of standards of human-subjects research, such systematic medical monitoring of detainee enhanced interrogations and the collection of generalizable medical knowledge do indeed constitute research. Such research, although unethical and illegal, was not only instrumental in the authorization and implementation of torture, it also facilitated complicity of health professionals and scientists in criminal acts of torture that they were responsible for recognizing. The health professionals who were charged with ensuring detainees' safety were instead, in light of Bybee's specific intent language and unmeasured states of mental pain or suffering, calibrating the harm inflicted upon them.

Any scientist or clinician should know that intentional infliction of harm without consent of and/or direct benefit to the individual cannot be construed as "ensuring safety" and that complicity in torture and ill treatment, including by military personnel, can never be justified (*12*). As the Declaration of Tokyo states, "the physician's fundamental role is to alleviate the distress of his or her fellow men, and no motive whether personal, collective or political shall prevail against this higher purpose" (*12*).

It seems highly unlikely that a monitoring clinician would not be able to recognize severe physical and mental pain caused by EITs. Detainees who have been evaluated by independent forensic medical experts using international standards for the medical documentation of torture (*9*) have consistently demonstrated evidence of torture (*13*). Also, there is evidence in official detainee medical records that medical doctors and mental health personnel assigned to the DoD neglected and/or concealed medical evidence of intentional harm (*13*).

Policy-makers, scientists, and clinicians who may have rationalized torture and human experimentation in the name of "national security," regardless of their intent, may have made a grave miscalculation. Not only is torture always immoral and illegal, it may undermine security, for example, if policies and actions are based on information of questionable reliability elicited by confession during torture. The consequences of this can be profound. For example, Ibn al-Shaykh al-Libi, a Libyan paramilitary trainer for Al-Qaeda, was interrogated by U.S. forces in 2001. Under pain of torture in Egypt, he confessed to knowledge of weapons of mass destruction (WMD) in Iraq. Although such WMDs were never found, this statement was a key influence on the U.S. decision to invade Iraq (*14*).

Conclusion and Recommendations

The science used to justify torture was bad because it repeatedly failed to assess important long-term physical and mental health outcomes, even though Bybee definitions explicitly referred to long-term impacts, and thus appears to have been inappropriately used to justify a predetermined conclusion that torture could be safe, legal, and effective. The science was also bad because it violated the most basic tenet of medical ethics and scientific inquiry—*primum non nocere*—first, do no harm. Scientists and health professionals must hold themselves to the highest professional standards of commitment to the human rights and dignity of the people whose lives they have the privilege of serving. To that end, we make the following recommendations.

Independence and accountability:

- Independence from the security chain of command for all government scientists, particularly those working in national security settings, and for forensic evaluators of alleged abuse in custody.
- Military medical personnel compliance with all civilian medical ethics standards.
- Independent and thorough investigation of the role of health professionals in torture and unethical human experimentation.
- Accountability measures, including punitive sanctions, such as federal and state regulations, should link licensing to compliance with the Nuremberg Code, the Geneva Conventions, the Common Rule (*15*), and the United Nations Convention Against Torture.

Peer review and monitoring:

- Monitoring of government health professionals in national security settings by peers from outside of the security chain of command.
- Documentation and reporting of torture and other human rights violations in accordance with international standards (*9*).
- Appeals and protective mechanisms for third parties who document/report abuses.

Training and education:

- Compulsory training for government scientists and health professionals, particularly those in national security settings, including professional ethics, human rights standards, and medical documentation of torture and ill treatment in accordance with international standards (*9*).

Governmental accountability:

- Independent investigation of all officials involved in the authorization and implementation of possible torture and unethical human experimentation. This includes investigation of all relevant classified information.
- Punitive sanctions in accordance with the law.

References and Notes

1. S. Allen *et al.*, *Leave No Marks: Enhanced Interrogation Techniques and the Risk of Criminality* (Physicians for Human Rights, Cambridge, MA, and Human Rights First, New York, 2007); http://physiciansforhumanrights.org/library/documents/reports/leave-no-marks.pdf.
2. Human Rights Watch, Appendix: U.S. Criticisms of Mistreatment and Torture Practices in *"Enduring Freedom": Abuses by U.S. Forces in Afghanistan* (Human Rights Watch, New York, 2004); www.hrw.org/reports/2004/afghanistan0304/7.htm.
3. Committee on Armed Services U.S. Senate (SASC), *Inquiry into the Treatment of Detainees* (SASC Publication, Washington, DC, 2008); http://armed-services.senate.gov/pubs.htm.
4. Office of Inspector General, Central Intelligence Agency, *Counterterrorism Detention and Interrogations, Special Review* (CIA Inspector General Publication, Washington, DC, 2004); www.gwu.edu/~nsarchiv/torture_archive/20040507.pdf.
5. J. Bybee, Assistant Attorney General, Office of Legal Counsel, DOJ, memorandum for A. Gonzales. Counsel to the President, 1 August 2002; www.washingtonpost.com/wp-srv/nation/documents/dojinterrogationmemo20020801.pdf.
6. Physical pain: "equivalent in intensity to the pain accompanying serious physical injury, such as organ failure, impairment of bodily function, or even death; …." (*5*).
7. The Bybee memo stated that in order "for a defendant to have acted with specific intent, he must expressly intend to achieve the forbidden act." Under that interpretation, to violate the law, a person must expressly intend to commit torture and the memo stated that "knowledge alone that a particular result is certain to occur does not constitute specific intent" (*5*).
8. N. Raymond *et al.*, *Experiments in Torture: Evidence of Human Subject Research and Experimentation in the "Enhanced" Interrogation Program* (Physicians for Human Rights, Cambridge, MA, 2010); http://phrtorturepapers.org/?dl_id=9.
9. V. Iacopino *et al.*, *The Istanbul Protocol: Manual on the Effective Investigation and Documentation of Torture and Other Cruel, Inhuman, and Degrading Treatment or Punishment* (United Nations Publications HR/P/PT/8, Office of the High Commissioner for Human Rights, New York and Geneva, 2001); www.ohchr.org/Documents/Publications/training8Rev1en.pdf.
10. JTF-GTMO BSCT (Joint Task Force–Guantanamo Bay, Cuba, Behavioral Science Consultation Team), DoD, *Standard Operating Procedures*, 2002, 2004, and 2005; www.americantorture.com/documents/gitmo/05.pdf.
11. S. G. Bradbury, Central Intelligence Agency, memoranda, 10 May 2005; www.aclu.org/accountability/olc.html.
12. World Medical Association, *Declaration of Tokyo* (World Medical Association, Ferney-Voltaire, France, 1975); www.wma.net/en/30publications/10policies/c18/index.html.
13. F. Hashemian *et al.*, *Broken Laws, Broken Lives: Medical Evidence of Torture by U.S. Personnel and Its Impact* (Physicians for Human Rights, Cambridge, MA, 2008); http://brokenlives.info/?page_id=69.
14. Select Committee on Intelligence, U.S. Senate, *Postwar Findings About Iraq's WMD Programs and Links to Terrorism and How They Compare with Prewar Assessments* (Select Committee on Intelligence, Washington, DC, 2006); http://intelligence.senate.gov/phaseiiaccuracy.pdf.
15. 45 Code of Federal Regulations (C.F.R.) §46.102(d), 2005.

10.1126/science.1194437

PLANT SCIENCE

When Vernalization Makes Sense

A noncoding RNA molecule is required for plants to become competent to flower after a period of cold.

Franziska Turck and George Coupland

Many plants flower in the spring after exposure to low winter temperatures to ensure reproductive success and maximize seed production. This response to cold, called vernalization, overcomes a block that prevents premature flowering in autumn. The molecular mechanisms underlying vernalization are fascinating because they must induce flowering only after a plant has been exposed to cold for several weeks, but not after short exposures characteristic of autumn, and must allow flowering to proceed stably after temperatures rise in spring (see the figure). On page 76 in this issue, Heo and Sung (*1*) describe how a temporal cascade of RNA transcripts generated from a single genomic locus regulates this response.

In the model plant species *Arabidopsis thaliana*, the *FLOWERING LOCUS C* (*FLC*) gene is the major target of vernalizaton (*2*, *3*). *FLC* encodes a transcription factor that blocks flowering before winter by repressing key genes required for flowering (*4*). Expression of *FLC* messenger RNA (mRNA) gradually decreases during the first phase of vernalization, and this becomes irreversible in the second phase, so that abundance remains low when plants are exposed to higher temperatures in spring. These phases are tightly controlled by changes in the chromatin structure of *FLC* (*5*, *6*). In *A. thaliana*, many mutations in chromatin regulators affect flowering time primarily by influencing the expression of *FLC* (*7*).

During cell differentiation in animals, chromatin changes mediated by Polycomb group (PcG) proteins ensure that gene repression is maintained throughout subsequent cell divisions. In *A. thaliana*, some mutations that impair PcG proteins affect the stable repression of *FLC* after vernalization (*8*, *9*). However, these mutants behave similarly to wild-type plants when *FLC* expression is decreased during the first phase of vernalization. The recent discovery of an antisense transcript called *COOLAIR* that is expressed from a promoter located in the 3′-flanking (noncoding) region of the *FLC* gene suggested that this could be involved in repression of *FLC* expression during the first phase of vernalization (*10*). Now, Heo and Sung describe how another noncoding transcript called *COLDAIR* links decreased *FLC* expression to the maintenance of its repression by PcG protein complexes. *COLDAIR* is also encoded at the *FLC* locus, but is a sense RNA.

Before vernalization, *FLC* produces abundant mRNA in the sense orientation that encodes the FLC protein, thereby repressing flowering. Chilling gradually increases the expression of *COOLAIR*, a noncoding antisense transcript that corresponds to the entire *FLC* locus and is partially spliced (*10*). Heo and Sung observed that *COOLAIR* expression rises during the first phase of vernalization, before *FLC* mRNA markedly decreases. As *COOLAIR* reaches its peak of expression, the amount of *FLC* mRNA starts to fall and transcription of *COLDAIR* is initiated. This sense transcript and its promoter are encoded in the first *FLC* intron. Activation of transcription from the *COLDAIR* promoter is induced by cold independently of the promoter's genomic context. Nevertheless, earlier in vernalization, *COOLAIR* might gradually create a favorable chromatin structure that facilitates the expression of *COLDAIR*. Conceptually, this would provide a threshold for inducing *COLDAIR* transcription that helps explain why repression of *FLC* only occurs after extended exposure to low temperatures.

The right time. *Arabidopsis thaliana* is induced to flower in response to seasonal cues such as winter chilling. Shown are mature plants flowering in spring after exposure to winter temperatures.

CREDIT: ROBERT VIDEKI/DORONICUM KFT./BUGWOOD.ORG

Heo and Sung further show that *COLDAIR* transcripts are bound by PcG protein complexes. Whether PcG proteins recognize the secondary structure or specific *COLDAIR* sequences remains unclear. The PcG protein CURLY LEAF, which is required for stable *FLC* repression (*11*), binds to *COLDAIR* RNA, but Heo and Sung show that other proteins are required to ensure specificity of this interaction. Presumably during or after its transcription, *COLDAIR* remains associated with the *FLC* locus long enough to recruit a vernalization-specific PcG protein complex that initiates chromatin changes required for stable *FLC* repression. The PcG protein complex sets a repressive signal by methylating the amino-terminal tails of histone H3 at the locus. This modification is then specifically recognized by a second PcG protein complex that is required for stable *FLC* repression. As soon as the different PcG complexes have been recruited, the noncoding transcripts seem no longer to be necessary for *FLC* repression. By the end of vernalization none of the transcripts–*COOLAIR*, *COLDAIR*, or *FLC* mRNA–are expressed to an appreciable extent.

In animals, long intergenic noncoding transcripts (lincRNAs) orchestrate the repression of neighboring genomic regions, similarly to what is described by Heo and Sung for *COLDAIR*. The most prominent example is the lincRNA *HOTAIR* that regulates the developmentally crucial *HOX* gene cluster in mammals (*12*). So far, functional lincRNAs have not been discovered in plants, but perhaps intronic noncoding transcripts (incRNAs) substitute for them.

In addition to the noncoding RNAs, the vernalization-specific PcG complexes responsible for modifying the chromatin at *FLC* are altered during vernalization by the attachment of accessory proteins (*9*, *11*). The mRNA expression of one such protein, VIN3, is increased during the second phase of vernalization. Heo and Sung show that the abundance of *VIN3* mRNA during vernalization increases after *COLDAIR* levels subside. However, *VIN3* is part of a small gene family, and other members of the gene family might compensate for the lack of VIN3 in the earlier stages of vernalization.

It remains unclear how transcription of *COOLAIR* and later *COLDAIR* are induced

Max Planck Institute for Plant Breeding Research, Carl von Linn Weg 10, Cologne, 50829 Germany. E-mail: coupland@mpipz.mpg.de

Published by AAAS

during cold. Both transcripts are generated by promoters that respond gradually to cold independently of their genomic context. Surprisingly, none of the many mutations in *A. thaliana* that alter the response of *FLC* to vernalization affect classical transcription factors responsible for the expression of any of these transcripts. Therefore, the mechanism by which the expression of *COLDAIR*, *COOLAIR*, and *VIN3* transcripts are induced by cold is unknown. One possibility is that the chromatin structure of *FLC* per se is sensitive to temperature (*13*). Also, the stable repression of *FLC* is altered during evolution, so that in perennial relatives of *A. thaliana*, *FLC* orthologs are repressed during vernalization but their expression is restored after the return to higher temperatures (*14*, *15*). It is not yet known which part of the mechanism that stably represses *FLC* in *A. thaliana* is altered during evolution. There are also other important loci involved in flowering that are regulated by proteins related to the PcG complex. Determining whether these genes feature incRNAs that recruit PcG complexes to specific targets awaits further study.

References

1. J. B. Heo, S. Sung, *Science* **331**, 76 (2011).
2. S. D. Michaels, R. M. Amasino, *Plant Cell* **11**, 949 (1999).
3. C. C. Sheldon, D. T. Rouse, E. J. Finnegan, W. J. Peacock, E. S. Dennis, *Proc. Natl. Acad. Sci. U.S.A.* **97**, 3753 (2000).
4. I. Searle *et al.*, *Genes Dev.* **20**, 898 (2006).
5. R. Bastow *et al.*, *Nature* **427**, 164 (2004).
6. S. Sung, R. M. Amasino, *Nature* **427**, 159 (2004).
7. D. H. Kim, M. R. Doyle, S. Sung, R. M. Amasino, *Annu. Rev. Cell Dev. Biol.* **25**, 277 (2009).
8. A. R. Gendall, Y. Y. Levy, A. Wilson, C. Dean, *Cell* **107**, 525 (2001).
9. F. De Lucia, P. Crevillen, A. M. Jones, T. Greb, C. Dean, *Proc. Natl. Acad. Sci. U.S.A.* **105**, 16831 (2008).
10. S. Swiezewski, F. Liu, A. Magusin, C. Dean, *Nature* **462**, 799 (2009).
11. C. C. Wood *et al.*, *Proc. Natl. Acad. Sci. U.S.A.* **103**, 14631 (2006).
12. J. L. Rinn *et al.*, *Cell* **129**, 1311 (2007).
13. S. V. Kumar, P. A. Wigge, *Cell* **140**, 136 (2010).
14. S. Aikawa, M. J. Kobayashi, A. Satake, K. K. Shimizu, H. Kudoh, *Proc. Natl. Acad. Sci. U.S.A.* **107**, 11632 (2010).
15. R. Wang *et al.*, *Nature* **459**, 423 (2009).

10.1126/science.1200786

PALEONTOLOGY

The Feeding Habits of Ammonites

Synchrotron x-ray observations of ammonite fossils reveal the diet of Cretaceous organisms.

Kazushige Tanabe

Ammonites, a group of cephalopods with external shells, were among the most abundant marine invertebrates in Earth's history. Because of their rich fossil record and rapid morphological evolution, paleontologists have used ammonite fossils to date the age of rock strata (biochronology) and to correlate the ages of ammonite-bearing strata across wide regions. Ammonites as biological entities, however, are poorly understood, largely owing to the absence of a direct living counterpart. Their feeding and dietary habits, for example, have been unclear. On page 70 of this issue, however, Kruta *et al.* (*1*) offer some insight into how—and what—one Late Cretaceous ammonite ate. It is the first study to use synchrotron x-ray microtomographic techniques to investigate the paleobiology of ammonites.

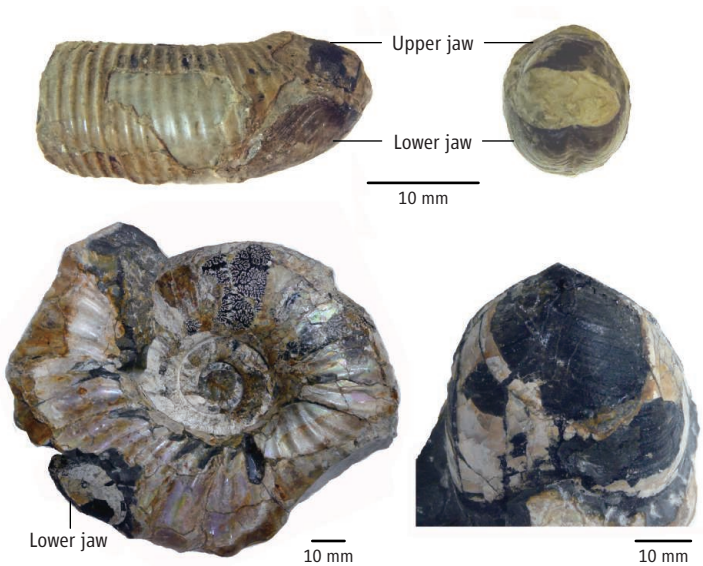

Feeding apparatus. Two ammonites from the Late Cretaceous rocks of Hokkaido, Japan, with a jaw apparatus in situ within the body chamber. (**Top**) *Polytoychoceras* sp. with Baculites-like lower and upper jaws. Right lateral (left) and frontal (right) views. (**Bottom**) *Anaudryceras limatum* (a lytoceratid) with a Nautilus-like lower jaw. Lateral view of the shell (left) and frontal view of the lower jaw (right).

Studies of living cephalopods have shown that feeding apparatuses are made mainly of a chitin-protein complex (*2*) and consist of upper and lower jaws and a radula (a tooth-containing ribbon that has been compared to a tongue) (*3*, *4*). They are accommodated within a globular organ, called the buccal mass, in the proximal (front) portion of the digestive system and have a specialized function of feeding on prey with the aid of the surrounding muscular system (*4*). Fossilized remains of jaws and a radula are occasionally preserved within the body chambers of ammonites whose taxonomic relationships are known (*4*, *5*). Only exceptionally preserved fossils, however, show how feeding apparatuses are associated with the ammonite's prey and shell (*5*).

Kruta *et al.* present evidence of jaws, a radula, and possible food remains within the buccal mass region of a Late Cretaceous ammonite in the genus *Baculites*. The authors succeeded in obtaining clear three-dimensional images of the jaws and radula. They also identified the remains of isopods (a type of crustacean) and the larval shell of a bottom-dwelling (benthic) gastropod in the buccal mass region of the digestive system, and interpreted them as the ammonite's prey. This interpretation is supported by evidence that the isopod and gastropod remains are restricted to the buccal mass region. Because currently living isopods live in the water column as zooplankton (*6*), Kruta *et al.* reasonably concluded that *Baculites* also lived in the water column and fed on small zooplankton.

This diet of *Baculites* appears to be intimately reflected in their jaw and radular structures. The lower jaw is characterized by the presence of a pair of calcareous plates (known as the aptychus) separated by a median slit, which covers the underlying chitinous layer and lacks a sharp rostral tip. In contrast, this sharp tip is present in the lower jaws of

Department of Earth and Planetary Science, University of Tokyo, Tokyo 113-0033, Japan. E-mail: tanabe@eps.s.u-tokyo.ac.jp

during cold. Both transcripts are generated by promoters that respond gradually to cold independently of their genomic context. Surprisingly, none of the many mutations in *A. thaliana* that alter the response of *FLC* to vernalization affect classical transcription factors responsible for the expression of any of these transcripts. Therefore, the mechanism by which the expression of *COLDAIR*, *COOLAIR*, and *VIN3* transcripts are induced by cold is unknown. One possibility is that the chromatin structure of *FLC* per se is sensitive to temperature (*13*). Also, the stable repression of *FLC* is altered during evolution, so that in perennial relatives of *A. thaliana*, *FLC* orthologs are repressed during vernalization but their expression is restored after the return to higher temperatures (*14*, *15*). It is not yet known which part of the mechanism that stably represses *FLC* in *A. thaliana* is altered during evolution. There are also other important loci involved in flowering that are regulated by proteins related to the PcG complex. Determining whether these genes feature incRNAs that recruit PcG complexes to specific targets awaits further study.

References

1. J. B. Heo, S. Sung, *Science* **331**, 76 (2011).
2. S. D. Michaels, R. M. Amasino, *Plant Cell* **11**, 949 (1999).
3. C. C. Sheldon, D. T. Rouse, E. J. Finnegan, W. J. Peacock, E. S. Dennis, *Proc. Natl. Acad. Sci. U.S.A.* **97**, 3753 (2000).
4. I. Searle *et al.*, *Genes Dev.* **20**, 898 (2006).
5. R. Bastow *et al.*, *Nature* **427**, 164 (2004).
6. S. Sung, R. M. Amasino, *Nature* **427**, 159 (2004).
7. D. H. Kim, M. R. Doyle, S. Sung, R. M. Amasino, *Annu. Rev. Cell Dev. Biol.* **25**, 277 (2009).
8. A. R. Gendall, Y. Y. Levy, A. Wilson, C. Dean, *Cell* **107**, 525 (2001).
9. F. De Lucia, P. Crevillen, A. M. Jones, T. Greb, C. Dean, *Proc. Natl. Acad. Sci. U.S.A.* **105**, 16831 (2008).
10. S. Swiezewski, F. Liu, A. Magusin, C. Dean, *Nature* **462**, 799 (2009).
11. C. C. Wood *et al.*, *Proc. Natl. Acad. Sci. U.S.A.* **103**, 14631 (2006).
12. J. L. Rinn *et al.*, *Cell* **129**, 1311 (2007).
13. S. V. Kumar, P. A. Wigge, *Cell* **140**, 136 (2010).
14. S. Aikawa, M. J. Kobayashi, A. Satake, K. K. Shimizu, H. Kudoh, *Proc. Natl. Acad. Sci. U.S.A.* **107**, 11632 (2010).
15. R. Wang *et al.*, *Nature* **459**, 423 (2009).

10.1126/science.1200786

PALEONTOLOGY

The Feeding Habits of Ammonites

Synchrotron x-ray observations of ammonite fossils reveal the diet of Cretaceous organisms.

Kazushige Tanabe

Ammonites, a group of cephalopods with external shells, were among the most abundant marine invertebrates in Earth's history. Because of their rich fossil record and rapid morphological evolution, paleontologists have used ammonite fossils to date the age of rock strata (biochronology) and to correlate the ages of ammonite-bearing strata across wide regions. Ammonites as biological entities, however, are poorly understood, largely owing to the absence of a direct living counterpart. Their feeding and dietary habits, for example, have been unclear. On page 70 of this issue, however, Kruta *et al.* (*1*) offer some insight into how—and what—one Late Cretaceous ammonite ate. It is the first study to use synchrotron x-ray microtomographic techniques to investigate the paleobiology of ammonites.

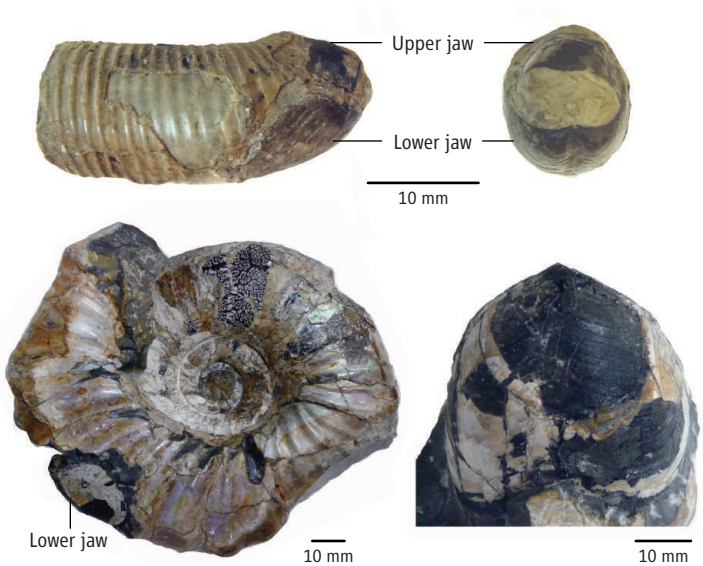

Feeding apparatus. Two ammonites from the Late Cretaceous rocks of Hokkaido, Japan, with a jaw apparatus in situ within the body chamber. (**Top**) *Polytoychoceras* sp. with Baculites-like lower and upper jaws. Right lateral (left) and frontal (right) views. (**Bottom**) *Anaudryceras limatum* (a lytoceratid) with a Nautilus-like lower jaw. Lateral view of the shell (left) and frontal view of the lower jaw (right).

Studies of living cephalopods have shown that feeding apparatuses are made mainly of a chitin-protein complex (*2*) and consist of upper and lower jaws and a radula (a tooth-containing ribbon that has been compared to a tongue) (*3*, *4*). They are accommodated within a globular organ, called the buccal mass, in the proximal (front) portion of the digestive system and have a specialized function of feeding on prey with the aid of the surrounding muscular system (*4*). Fossilized remains of jaws and a radula are occasionally preserved within the body chambers of ammonites whose taxonomic relationships are known (*4*, *5*). Only exceptionally preserved fossils, however, show how feeding apparatuses are associated with the ammonite's prey and shell (*5*).

Kruta *et al.* present evidence of jaws, a radula, and possible food remains within the buccal mass region of a Late Cretaceous ammonite in the genus *Baculites*. The authors succeeded in obtaining clear three-dimensional images of the jaws and radula. They also identified the remains of isopods (a type of crustacean) and the larval shell of a bottom-dwelling (benthic) gastropod in the buccal mass region of the digestive system, and interpreted them as the ammonite's prey. This interpretation is supported by evidence that the isopod and gastropod remains are restricted to the buccal mass region. Because currently living isopods live in the water column as zooplankton (*6*), Kruta *et al.* reasonably concluded that *Baculites* also lived in the water column and fed on small zooplankton.

This diet of *Baculites* appears to be intimately reflected in their jaw and radular structures. The lower jaw is characterized by the presence of a pair of calcareous plates (known as the aptychus) separated by a median slit, which covers the underlying chitinous layer and lacks a sharp rostral tip. In contrast, this sharp tip is present in the lower jaws of

Department of Earth and Planetary Science, University of Tokyo, Tokyo 113-0033, Japan. E-mail: tanabe@eps.s.u-tokyo.ac.jp

modern nautilids and coleoids (*4*). The upper jaw is much smaller than the lower jaw, and the radula is characterized by small, multicuspidate rachidian teeth, with tall saberlike marginal teeth; this is similar to the radula of the Early Cretaceous ammonite *Aconeceras*, which has a comparable jaw structure (*7*). On the basis of features of the lower and upper jaws and the shape of the radular teeth, Kruta *et al*. concluded that these ammonites did not have the ability to capture large prey and cut it into small pieces.

Jaws of ammonites have been documented in 43 genera (*5*, *8*). The upper jaw is similar among different genera and consists of a pair of widely open inner lamellae (platelike structures) and a short reduced outer lamella. The lower jaws, in contrast, show remarkable variation in their overall shape, structure, and degree of development of an outer calcareous element. In particular, the lower jaws of lytoceratid and phylloceratid ammonites (see the figure) are similar to those of modern and fossil nautilids in their overall shape and structure, as well as the presence of a thick anterior calcareous tip with denticles. The similarity in overall lower jaw structures between these ammonites and nautilids has been interpreted as convergent adaptation to a scavenging-predatory mode of feeding (*9*).

Ammonites survived for about 340 million years, from the Early Devonian to the end of the Cretaceous (*10*). They became extinct at the end of the Cretaceous (65.5 million years ago), and the timing is coincident with an abrupt decline in several groups of plankton (*11*). Kruta *et al*. proposed that the collapse of the marine food web at that time contributed to the extinction of aptychus-type lower jaw–bearing ammonites, which depended on plankton as a food source. However, phylloceratid and lytoceratid ammonites, possibly with a modern nautilus-like mode of feeding, also became extinct simultaneously. The reason that all ammonites became extinct at the end of the Cretaceous, and that nautilids survived after the end-Cretaceous mass extinction event, is still not understood. A plausible hypothesis for the terminal extinction of ammonites is related to their early life history. Newly hatched Mesozoic ammonites had shells that ranged in size from 0.5 to 1.8 mm, which is much smaller than those of modern and fossil nautilids (*12*, *13*). This evidence strongly suggests that ammonites laid a large number of small eggs and that newly hatched juveniles ate small plankton. The abrupt decline of plankton at the end of the Cretaceous would have greatly affected the survival of newly hatched ammonites, as well as adults that relied on plankton as a food source. This hypothesis should be verified by future studies of well-preserved fossil material by means of new analytical techniques.

References

1. I. Kruta *et al*., *Science* **331**, 70 (2011).
2. S. Hunt, M. Nixon, *Comp. Biochem. Physiol.* **68B**, 535 (1981).
3. M. Nixon, in *The Mollusca,* vol. 12, M. R. Clarke, E. R. Trueman, Eds. (Academic Press, London, 1988), pp. 103–122.
4. K. Tanabe, Y. Fukuda, in *Functional Morphology of the Invertebrate Skeleton*, E. Savazzi, Ed. (Wiley, London, 1999), pp. 245–262.
5. U. Lehmann, *The Ammonites: Their Life and Their World* (Cambridge Univ. Press, Cambridge, 1981).
6. A. L. Alldredge, J. M. King, *Mar. Biol.* **84**, 253 (1985).
7. L. A. Doguzhaeva, H. Mutvei, *Palaeontographica* **223A**, 167 (1992).
8. K. Tanabe, N. H. Landman, *Abh. Geol. B* **A57**, 157 (2002).
9. K. Tanabe, Y. Fukuda, Y. Kanie, U. Lehmann, *Lethaia* **13**, 157 (1980).
10. M. R. House, in *The Ammonoidea: Environment, Ecology, and Evolutionary Change*, M. R. House, Ed. (Clarendon Press, Oxford, 1993), pp. 13–34.
11. B. T. Huber, K. G. MacLeod, R. D. Norris, in *Catastrophic Events and Mass Extinction: Impacts and Beyond*, C. Koeberl, K. G. MacLeod, Eds. (Geological Society of America, Boulder, CO, 2002), pp. 277–289.
12. N. H. Landman *et al*., in *Ammonoid Paleobiology*, N. H. Landman *et al*., Eds. (Plenum, New York, 1996), pp. 343–405.
13. N. H. Landman, in *Cephalopods: Present and Past*, J. Kullmann, J. Wiedmann, Eds. (Schweizerbart'sche Verlag, Stuttgart, 1988), pp. 215–228.

10.1126/science.1201002

ATMOSPHERIC SCIENCE

Getting a Better Estimate of an Atmospheric Radical

Better measures of how global levels of OH vary from year to year will improve climate science.

I. S. A. Isaksen[1,2] and S. B. Dalsøren[2]

The hydroxyl radical (OH) is an oxidizing molecule that has a major impact on the distribution and concentrations of pollutants and greenhouse gases in Earth's atmosphere. It is the most common oxidant in the troposphere, the lowest portion of the atmosphere. Understanding OH variability is important to evaluating human impacts on the atmosphere and climate. Measuring global OH distribution and variability, however, has been difficult, in part because the molecule has a lifetime of less than one second. On page 67 of this issue, Montzka *et al*. (*1*) use an indirect method to present a global estimate of OH's interannual variability that is consistent with past model-based estimates (*2*–*5*). This could be an important step toward understanding OH's role in the atmosphere, including its role in influencing concentrations of methane (CH_4), a gas important in considerations of global warming.

Directly measuring OH provides information only about local concentrations. To obtain a global view, researchers have either created models based on what is known about photochemical reaction rates in the atmosphere or drawn indirect estimates of global OH by measuring gases that are removed from the atmosphere through reactions with OH. One such gas is methyl chloroform (MCF), a solvent that was once widely used in the dry-cleaning and manufacturing industries but is now being phased out owing to the threat it poses to Earth's protective ozone layer. In the troposphere, MCF has a chemical lifetime of about 5 years. That is long enough to obtain average global MCF concentrations from a limited number of tropospheric measurement sites. Long-term data from these sites show a sharp decline in MCF abundance in the atmosphere, consistent with the phase-out of MCF production. Atmospheric MCF is eliminated through reactions with OH, and researchers can use the known rate of these reactions to calculate global OH concentrations that are consistent with the observed levels.

Montzka *et al*. analyzed MCF observations for the period 1998 to 2007. They obtained a global mean OH interannual variability (IAV) of 2.3 ± 1.5% for this period, with no clear trend. This implies that global OH has been rather stable. In contrast, previous studies that used MCF data from the 1980s and 1990s showed larger interannual variability (~10% to 20%) in global average OH (*6*, *7*). Montzka *et al*. argue that the

[1]Department of Geosciences, University of Oslo, 0316 Oslo, Norway. [2]CICERO, Centre for International Climate and Environmental Research-Oslo, 0349 Oslo, Norway. E-mail: i.s.a.isaksen@geo.uio.no

modern nautilids and coleoids (*4*). The upper jaw is much smaller than the lower jaw, and the radula is characterized by small, multicuspidate rachidian teeth, with tall saberlike marginal teeth; this is similar to the radula of the Early Cretaceous ammonite *Aconeceras*, which has a comparable jaw structure (*7*). On the basis of features of the lower and upper jaws and the shape of the radular teeth, Kruta *et al*. concluded that these ammonites did not have the ability to capture large prey and cut it into small pieces.

Jaws of ammonites have been documented in 43 genera (*5*, *8*). The upper jaw is similar among different genera and consists of a pair of widely open inner lamellae (platelike structures) and a short reduced outer lamella. The lower jaws, in contrast, show remarkable variation in their overall shape, structure, and degree of development of an outer calcareous element. In particular, the lower jaws of lytoceratid and phylloceratid ammonites (see the figure) are similar to those of modern and fossil nautilids in their overall shape and structure, as well as the presence of a thick anterior calcareous tip with denticles. The similarity in overall lower jaw structures between these ammonites and nautilids has been interpreted as convergent adaptation to a scavenging-predatory mode of feeding (*9*).

Ammonites survived for about 340 million years, from the Early Devonian to the end of the Cretaceous (*10*). They became extinct at the end of the Cretaceous (65.5 million years ago), and the timing is coincident with an abrupt decline in several groups of plankton (*11*). Kruta *et al*. proposed that the collapse of the marine food web at that time contributed to the extinction of aptychus-type lower jaw–bearing ammonites, which depended on plankton as a food source. However, phylloceratid and lytoceratid ammonites, possibly with a modern nautilus-like mode of feeding, also became extinct simultaneously. The reason that all ammonites became extinct at the end of the Cretaceous, and that nautilids survived after the end-Cretaceous mass extinction event, is still not understood. A plausible hypothesis for the terminal extinction of ammonites is related to their early life history. Newly hatched Mesozoic ammonites had shells that ranged in size from 0.5 to 1.8 mm, which is much smaller than those of modern and fossil nautilids (*12*, *13*). This evidence strongly suggests that ammonites laid a large number of small eggs and that newly hatched juveniles ate small plankton. The abrupt decline of plankton at the end of the Cretaceous would have greatly affected the survival of newly hatched ammonites, as well as adults that relied on plankton as a food source. This hypothesis should be verified by future studies of well-preserved fossil material by means of new analytical techniques.

References

1. I. Kruta *et al*., *Science* **331**, 70 (2011).
2. S. Hunt, M. Nixon, *Comp. Biochem. Physiol.* **68B**, 535 (1981).
3. M. Nixon, in *The Mollusca,* vol. 12, M. R. Clarke, E. R. Trueman, Eds. (Academic Press, London, 1988), pp. 103–122.
4. K. Tanabe, Y. Fukuda, in *Functional Morphology of the Invertebrate Skeleton*, E. Savazzi, Ed. (Wiley, London, 1999), pp. 245–262.
5. U. Lehmann, *The Ammonites: Their Life and Their World* (Cambridge Univ. Press, Cambridge, 1981).
6. A. L. Alldredge, J. M. King, *Mar. Biol.* **84**, 253 (1985).
7. L. A. Doguzhaeva, H. Mutvei, *Palaeontographica* **223A**, 167 (1992).
8. K. Tanabe, N. H. Landman, *Abh. Geol. B* **A57**, 157 (2002).
9. K. Tanabe, Y. Fukuda, Y. Kanie, U. Lehmann, *Lethaia* **13**, 157 (1980).
10. M. R. House, in *The Ammonoidea: Environment, Ecology, and Evolutionary Change*, M. R. House, Ed. (Clarendon Press, Oxford, 1993), pp. 13–34.
11. B. T. Huber, K. G. MacLeod, R. D. Norris, in *Catastrophic Events and Mass Extinction: Impacts and Beyond*, C. Koeberl, K. G. MacLeod, Eds. (Geological Society of America, Boulder, CO, 2002), pp. 277–289.
12. N. H. Landman *et al*., in *Ammonoid Paleobiology*, N. H. Landman *et al*., Eds. (Plenum, New York, 1996), pp. 343–405.
13. N. H. Landman, in *Cephalopods: Present and Past*, J. Kullmann, J. Wiedmann, Eds. (Schweizerbart'sche Verlag, Stuttgart, 1988), pp. 215–228.

10.1126/science.1201002

ATMOSPHERIC SCIENCE

Getting a Better Estimate of an Atmospheric Radical

Better measures of how global levels of OH vary from year to year will improve climate science.

I. S. A. Isaksen[1,2] and S. B. Dalsøren[2]

The hydroxyl radical (OH) is an oxidizing molecule that has a major impact on the distribution and concentrations of pollutants and greenhouse gases in Earth's atmosphere. It is the most common oxidant in the troposphere, the lowest portion of the atmosphere. Understanding OH variability is important to evaluating human impacts on the atmosphere and climate. Measuring global OH distribution and variability, however, has been difficult, in part because the molecule has a lifetime of less than one second. On page 67 of this issue, Montzka *et al*. (*1*) use an indirect method to present a global estimate of OH's interannual variability that is consistent with past model-based estimates (*2*–*5*). This could be an important step toward understanding OH's role in the atmosphere, including its role in influencing concentrations of methane (CH_4), a gas important in considerations of global warming.

Directly measuring OH provides information only about local concentrations. To obtain a global view, researchers have either created models based on what is known about photochemical reaction rates in the atmosphere or drawn indirect estimates of global OH by measuring gases that are removed from the atmosphere through reactions with OH. One such gas is methyl chloroform (MCF), a solvent that was once widely used in the dry-cleaning and manufacturing industries but is now being phased out owing to the threat it poses to Earth's protective ozone layer. In the troposphere, MCF has a chemical lifetime of about 5 years. That is long enough to obtain average global MCF concentrations from a limited number of tropospheric measurement sites. Long-term data from these sites show a sharp decline in MCF abundance in the atmosphere, consistent with the phase-out of MCF production. Atmospheric MCF is eliminated through reactions with OH, and researchers can use the known rate of these reactions to calculate global OH concentrations that are consistent with the observed levels.

Montzka *et al*. analyzed MCF observations for the period 1998 to 2007. They obtained a global mean OH interannual variability (IAV) of 2.3 ± 1.5% for this period, with no clear trend. This implies that global OH has been rather stable. In contrast, previous studies that used MCF data from the 1980s and 1990s showed larger interannual variability (~10% to 20%) in global average OH (*6*, *7*). Montzka *et al*. argue that the

[1]Department of Geosciences, University of Oslo, 0316 Oslo, Norway. [2]CICERO, Centre for International Climate and Environmental Research-Oslo, 0349 Oslo, Norway. E-mail: i.s.a.isaksen@geo.uio.no

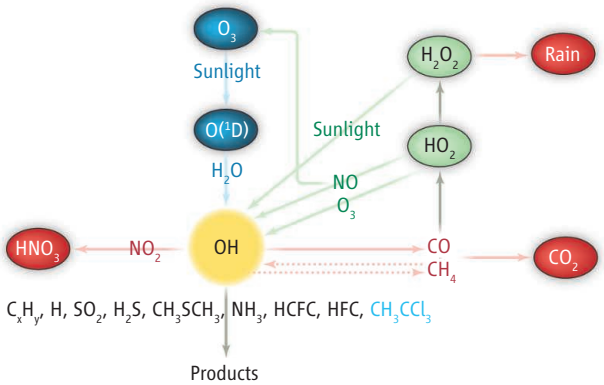

Radical role. In the troposphere, the hydroxyl radical (OH) is involved in reactions that affect pollutants and greenhouse gases. Reactions result in OH production (blue), recycling (green), or loss (red). For CO and the greenhouse gas CH_4, a feedback loop (dashed red arrows) enhances the OH loss. OH also destroys pollutants and greenhouse gases (gray), with OH levels remaining relatively unchanged. MCF (CH_3CCl_3, light blue) is destroyed through reactions with OH.

difference is not due to reduced variability during the last decade; rather, the phase-out of MCF resulted in less uncertainty in estimates of the MCF emissions that affect derived OH variability. In addition, the error attributed to using relatively few observation sites to estimate global averaged MCF has become smaller. The differences in MCF concentration gradients between measurement sites are now one-fourth the size of those in the 1980s and early 1990s. Montzka *et al*. also found a small OH IAV when they analyzed several other gases primarily oxidized by OH.

OH is involved in tropospheric oxidation processes (see the figure) that influence pollutants and greenhouse gases, including nitrogen dioxide (NO_2), carbon monoxide (CO), sulfur dioxide (SO_2), ozone (O_3), hydrochlorofluorocarbons (HCFCs), and CH_4. These reactions drive three major processes. First, in "source reactions," O_3 molecules are broken down by photons and interact with water vapor to form OH. Second, in "loss reactions," OH is removed, although some recycling of OH can occur. In reactions with CO and CH_4, there is also a feedback loop that enhances the loss of OH. Finally, there are reactions in which OH destroys pollutants and greenhouse gases, with OH levels remaining relatively unchanged.

Of particular interest is the role that OH may play in the recent trends and year-to-year variation of CH_4 (*8*, *9*). Changes in methane may originate either from changes in emissions or from changes in its rate of loss, mainly through reactions with OH. To understand the role played by OH variability, however, it is extremely important to know whether OH IAV is just a few percent, as indicated by Montzka *et al*. and by model studies (*2*–*5*), or is up to 10% or 20%, as indicated by past analyses (*6*, *7*), including studies that measured carbon isotopes (^{14}CO) (*10*). There are considerable uncertainties in the models, and they can vary by a factor of 2 in the calculated lifetime of methane because of reaction with OH (*11*, *12*). Although the accuracy of the MCF and ^{14}CO methods has been questioned (*13*, *14*), the much larger IAV in past MCF and ^{14}CO studies prompted discussion of the lack of a theoretical understanding of the OH budget. Now, Montzka *et al*.'s findings support several past model studies (*2*–*5*) and indicate that global OH is quite stable. It could be that increased OH formation by nitrogen oxides (*5*) compensated for depletion of OH by reactive carbon gases.

In the future, human-induced pollution and climate change could lead to substantial changes in the OH budget if they alter some of the central processes that involve OH. To better understand these issues, investigators need models that have higher resolution, include interactive coupling with biospheric processes and climate change, and draw on improved emission inventories. Observational networks of pollutants and climate compounds should include more stations to get better global coverage, and funding is required to secure long-term data series. As the concentration of MCF approaches zero, perhaps the most useful tool for estimating global OH will disappear. The possibility of producing and releasing dedicated "tracer" gases (*2*) to replace MCF should be investigated.

References

1. S. Montzka *et al*., *Science* **331**, 67 (2011).
2. J. Lelieveld *et al*., *Atmos. Environ.* **40**, 5741 (2006).
3. F. Dentener *et al*., *J. Geophys. Res.* **108** (D15), 4442 (2003).
4. B. Duncan, J. Logan, *Atmos. Chem. Phys.* **8**, 7389 (2008).
5. S. B. Dalsøren, I. S. A. Isaksen, *Geophys. Res. Lett.* **33**, L23811 (2006).
6. P. Bousquet, D. A. Hauglustaine, P. Peylin, C. Carouge, P. Ciais, *Atmos. Chem. Phys.* **5**, 2635 (2005).
7. R. G. Prinn *et al*., *Geophys. Res. Lett.* **32**, L07809 (2005).
8. M. Rigby *et al*., *Geophys. Res. Lett.* **35**, L22805 (2008).
9. E. J. Dlugokencky *et al*., *Geophys. Res. Lett.* **36**, L18803 (2009).
10. M. R. Manning, D. C. Lowe, R. C. Moss, G. E. Bodeker, W. Allan, *Nature* **436**, 1001 (2005).
11. D. T. Shindell *et al*., *J. Geophys. Res.* **111** (D19), D19306 (2006).
12. P. Hoor *et al*., *Atmos. Chem. Phys.* **9**, 3113 (2009).
13. M. Krol, J. Lelieveld, *J. Geophys. Res.* **108** (D3), 4125 (2003).
14. M. Krol *et al*., *Atmos. Chem. Phys.* **8**, 5033 (2008).

10.1126/science.1199773

CELL BIOLOGY

Formin Tip Tracking

Thomas D. Pollard

A simple protein machine tracks the tip of a growing actin filament.

Eukaryotic cells, including those of humans, depend on filaments of actin protein for their physical integrity and movements. Formins are a class of proteins that regulate actin assembly, producing filaments that participate in cell division, cell migration, and intracellular transport, among other cellular processes (*1*). Although many proteins have been identified that regulate actin, we need to better understand their modes of action at the molecular level. Technical advances, such as single-molecule imaging in real time with purified proteins and in live cells, are extending this knowledge. On page 80 of this issue, Mizuno *et al*. (*2*) present a method for visualizing the rotational movement of actin filaments as they grow from immobilized formin proteins. The study confirms that actin elongation is coupled to rotation motion of the filament, and provides clues about how formins might transmit actin-generated force to other cellular structures.

Formin proteins exist as dimers through the interaction of their homology 2 (FH2) domain. The dimer of FH2 domains initiates the polymerization of a new actin filament and then remains bound to the fast-growing end (known as the barbed end) of the filament as it elongates (*3*, *4*). Remarkably, as each new actin molecule associates with the filament, the formin dimer moves reliably onto a new elongated end (see the figure). Through thousands of cycles of actin sub-

Departments of Molecular, Cellular and Developmental Biology, Molecular Biophysics and Biochemistry, and Cell Biology, Yale University, New Haven, CT 06520, USA. E-mail: thomas.pollard@yale.edu

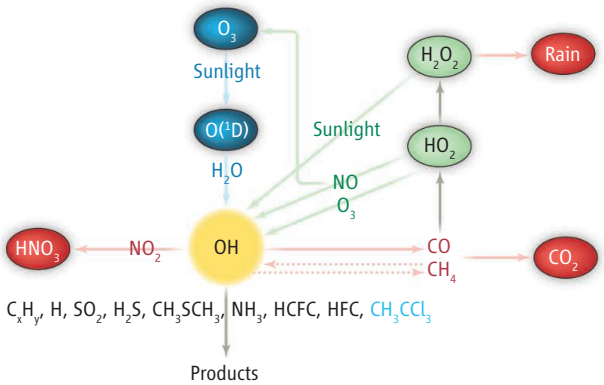

Radical role. In the troposphere, the hydroxyl radical (OH) is involved in reactions that affect pollutants and greenhouse gases. Reactions result in OH production (blue), recycling (green), or loss (red). For CO and the greenhouse gas CH_4, a feedback loop (dashed red arrows) enhances the OH loss. OH also destroys pollutants and greenhouse gases (gray), with OH levels remaining relatively unchanged. MCF (CH_3CCl_3, light blue) is destroyed through reactions with OH.

difference is not due to reduced variability during the last decade; rather, the phase-out of MCF resulted in less uncertainty in estimates of the MCF emissions that affect derived OH variability. In addition, the error attributed to using relatively few observation sites to estimate global averaged MCF has become smaller. The differences in MCF concentration gradients between measurement sites are now one-fourth the size of those in the 1980s and early 1990s. Montzka *et al*. also found a small OH IAV when they analyzed several other gases primarily oxidized by OH.

OH is involved in tropospheric oxidation processes (see the figure) that influence pollutants and greenhouse gases, including nitrogen dioxide (NO_2), carbon monoxide (CO), sulfur dioxide (SO_2), ozone (O_3), hydrochlorofluorocarbons (HCFCs), and CH_4. These reactions drive three major processes. First, in "source reactions," O_3 molecules are broken down by photons and interact with water vapor to form OH. Second, in "loss reactions," OH is removed, although some recycling of OH can occur. In reactions with CO and CH_4, there is also a feedback loop that enhances the loss of OH. Finally, there are reactions in which OH destroys pollutants and greenhouse gases, with OH levels remaining relatively unchanged.

Of particular interest is the role that OH may play in the recent trends and year-to-year variation of CH_4 (*8*, *9*). Changes in methane may originate either from changes in emissions or from changes in its rate of loss, mainly through reactions with OH. To understand the role played by OH variability, however, it is extremely important to know whether OH IAV is just a few percent, as indicated by Montzka *et al*. and by model studies (*2*–*5*), or is up to 10% or 20%, as indicated by past analyses (*6*, *7*), including studies that measured carbon isotopes (^{14}CO) (*10*). There are considerable uncertainties in the models, and they can vary by a factor of 2 in the calculated lifetime of methane because of reaction with OH (*11*, *12*). Although the accuracy of the MCF and ^{14}CO methods has been questioned (*13*, *14*), the much larger IAV in past MCF and ^{14}CO studies prompted discussion of the lack of a theoretical understanding of the OH budget. Now, Montzka *et al*.'s findings support several past model studies (*2*–*5*) and indicate that global OH is quite stable. It could be that increased OH formation by nitrogen oxides (*5*) compensated for depletion of OH by reactive carbon gases.

In the future, human-induced pollution and climate change could lead to substantial changes in the OH budget if they alter some of the central processes that involve OH. To better understand these issues, investigators need models that have higher resolution, include interactive coupling with biospheric processes and climate change, and draw on improved emission inventories. Observational networks of pollutants and climate compounds should include more stations to get better global coverage, and funding is required to secure long-term data series. As the concentration of MCF approaches zero, perhaps the most useful tool for estimating global OH will disappear. The possibility of producing and releasing dedicated "tracer" gases (*2*) to replace MCF should be investigated.

References

1. S. Montzka *et al*., *Science* **331**, 67 (2011).
2. J. Lelieveld *et al*., *Atmos. Environ.* **40**, 5741 (2006).
3. F. Dentener *et al*., *J. Geophys. Res.* **108** (D15), 4442 (2003).
4. B. Duncan, J. Logan, *Atmos. Chem. Phys.* **8**, 7389 (2008).
5. S. B. Dalsøren, I. S. A. Isaksen, *Geophys. Res. Lett.* **33**, L23811 (2006).
6. P. Bousquet, D. A. Hauglustaine, P. Peylin, C. Carouge, P. Ciais, *Atmos. Chem. Phys.* **5**, 2635 (2005).
7. R. G. Prinn *et al*., *Geophys. Res. Lett.* **32**, L07809 (2005).
8. M. Rigby *et al*., *Geophys. Res. Lett.* **35**, L22805 (2008).
9. E. J. Dlugokencky *et al*., *Geophys. Res. Lett.* **36**, L18803 (2009).
10. M. R. Manning, D. C. Lowe, R. C. Moss, G. E. Bodeker, W. Allan, *Nature* **436**, 1001 (2005).
11. D. T. Shindell *et al*., *J. Geophys. Res.* **111** (D19), D19306 (2006).
12. P. Hoor *et al*., *Atmos. Chem. Phys.* **9**, 3113 (2009).
13. M. Krol, J. Lelieveld, *J. Geophys. Res.* **108** (D3), 4125 (2003).
14. M. Krol *et al*., *Atmos. Chem. Phys.* **8**, 5033 (2008).

10.1126/science.1199773

CELL BIOLOGY

Formin Tip Tracking

Thomas D. Pollard

A simple protein machine tracks the tip of a growing actin filament.

Eukaryotic cells, including those of humans, depend on filaments of actin protein for their physical integrity and movements. Formins are a class of proteins that regulate actin assembly, producing filaments that participate in cell division, cell migration, and intracellular transport, among other cellular processes (*1*). Although many proteins have been identified that regulate actin, we need to better understand their modes of action at the molecular level. Technical advances, such as single-molecule imaging in real time with purified proteins and in live cells, are extending this knowledge. On page 80 of this issue, Mizuno *et al*. (*2*) present a method for visualizing the rotational movement of actin filaments as they grow from immobilized formin proteins. The study confirms that actin elongation is coupled to rotation motion of the filament, and provides clues about how formins might transmit actin-generated force to other cellular structures.

Formin proteins exist as dimers through the interaction of their homology 2 (FH2) domain. The dimer of FH2 domains initiates the polymerization of a new actin filament and then remains bound to the fast-growing end (known as the barbed end) of the filament as it elongates (*3*, *4*). Remarkably, as each new actin molecule associates with the filament, the formin dimer moves reliably onto a new elongated end (see the figure). Through thousands of cycles of actin sub-

Departments of Molecular, Cellular and Developmental Biology, Molecular Biophysics and Biochemistry, and Cell Biology, Yale University, New Haven, CT 06520, USA. E-mail: thomas.pollard@yale.edu

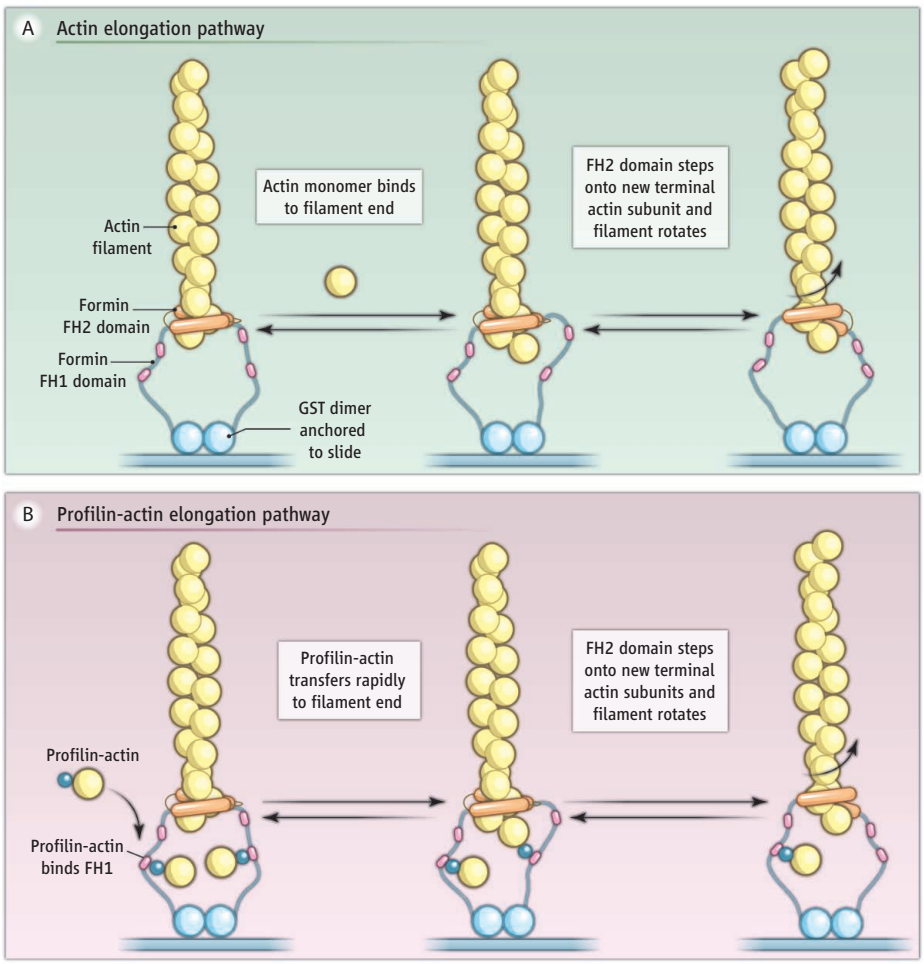

Actin filament enlongation. (**A**) Actin can be added to the end of a filament from the bulk phase. (**B**) A profilin-actin complex can bind to one of multiple sites (purple) in the flexible FH1 domain of formin and then transfer rapidly onto the end of the filament. In both cases, the dimeric FH2 domain of formin steps reliably onto the new actin subunit. When formin is anchored (*2*), the filament rotates as the FH2 domain tracks along the elongating helical filament. GST, glutathione *S*-transferase.

unit addition, formin never fails to step forward and never falls off the end of the filament. Consequently, a formin anchored to a structure in the cell can send out an actin filament to explore the surrounding cytoplasm. In one well-studied example in budding yeast, these filaments grow at a rate of 100 subunits per second, or 0.27 μm/s (*5*).

Because actin subunits in a filament are arranged in a helix, and given specific interactions between the donut-shaped dimer of formin FH2 domains with the end of the filament (*6*), one expects the formin to follow a helical path as the polymer grows. According to this view, if the filament were anchored, the formin would rotate, or if the formin were anchored, the filament would rotate. However, when the distal end of a filament and the formin on the growing end were both attached to a glass microscope slide, actin polymerization produced enough force to buckle the filament but, contrary to expectations, the doubly tethered filament did not twist into a supercoil, as expected if the formin tracked along the growing helix (*7*). Two hypotheses were proposed to explain this "rotation paradox" (*8*): Torque might cause the formin to slip around the end of the filament, or the connection of the formin to the slide might rotate.

Mizuno *et al*. observed an actin filament growing from a formin that was attached to a microscope slide by antibody molecules. Their innovation was to label just a few of the actin molecules in the filament with a fluorescent dye and to observe the filaments with polarized light. By exciting the dye molecules with polarized light and observing the emitted fluorescence through a polarizer, only those subunits in the filament with a favorably oriented dye were visible. The authors observed that the fluorescence appeared and disappeared every time the filament underwent half a rotation, showing that the filament rotates relative to the immobilized formin on the end, exactly as predicted if the formin tracks along the growing helical polymer. Mizuno *et al*. also confirmed that the filament does not rotate when both the growing end (with the formin) and the distal end of the filament are immobilized. This supports the idea that the slippage is between the formin and the slide, but does not rule out slippage between the formin and the filament.

In addition to initiating filament formation and tracking processively on the fast-growing end, formins also allow actin polymers to break the diffusion speed limit as they polymerize. Biophysical experiments established long ago that the rate of elongation is determined by the frequency of collisions of diffusing actin molecules with the end of the filament, with about 2% of the collisions resulting in incorporation of a new subunit into the filament. Remarkably, the FH1 domain of a formin allows filaments to grow at rates that exceed this diffusion limit by a factor of 2 to 5 (*9*). The flexible FH1 domain is positioned next to the FH2 domain and, like a tentacle, binds to the protein profilin, which brings along a molecule of actin. Binding of profilin-actin to the FH1 domain is rate-limiting because the actin subunit is transferred very rapidly onto the end of the filament. These reactions provide more sites for diffusion to provide subunits to grow the filament. Mizuno *et al*. show that filaments elongating by the FH1-profilin pathway rotate as they track the actin filament helix.

Mizuno *et al*. use their new assay to confirm that hydrolysis of adenosine 5′-triphosphate (ATP) bound to actin is not required for formins to mediate elongation of actin filaments, but they find that the nucleotide bound to the actin subunits influences both polymerization and depolymerization. After assembly, each actin subunit quickly hydrolyzes its bound ATP to ADP (adenosine 5′-diphosphate) and phosphate, followed by slow dissociation of the phosphate. Mizuno *et al*. show that formin-mediated elongation reactions are reversible. The FH2 domain tracks along the actin helix of shortening filaments of ADP-actin subunits and profilin promotes this process, but not if the γ-phosphate of ATP remains bound to the subunits. Thus, in principle, a shortening actin filament might be able to produce force on a processively associated formin and any attached cargo.

Formidable challenges remain. One for the biophysicists is to characterize the mechanics that allow formin FH2 domains to track processively on the end of a grow-

Published by AAAS

ing filament. Another is to determine how bundles of cross-linked filaments elongate from formin attached to cellular structures. Formins have well-established distinct roles in fungi (*3*), but cell biologists must sort out the overlapping functions of more than a dozen formins in human cells.

References

1. T. D. Pollard, J. A. Cooper, *Science* **326**, 1208 (2009).
2. H. Mizuno *et al.*, *Science* **331**, 80 (2011).
3. B. L. Goode, M. J. Eck, *Annu. Rev. Biochem.* **76**, 593 (2007).
4. A. Paul, T. D. Pollard, *Cell Motil. Cytoskeleton* **66**, 606 (2009).
5. H. C. Yang, L. A. Pon, *Proc. Natl. Acad. Sci. U.S.A.* **99**, 751 (2002).
6. T. Otomo *et al.*, *Nature* **433**, 488 (2005).
7. D. R. Kovar, T. D. Pollard, *Proc. Natl. Acad. Sci. U.S.A.* **101**, 14725 (2004).
8. T. Shemesh, T. Otomo, M. K. Rosen, A. D. Bershadsky, M. M. Kozlov, *J. Cell Biol.* **170**, 889 (2005).
9. D. R. Kovar, E. S. Harris, R. Mahaffy, H. N. Higgs, T. D. Pollard, *Cell* **124**, 423 (2006).

10.1126/science.1200773

PHYSICS

More Intense, Shorter Pulses

Large-scale laser facilities may also provide the ultimate source of ultrashort laser pulses.

Gerard Mourou[1] and Toshiki Tajima[2]

A few years ago, a new type of large-scale laser infrastructure specifically conceived to produce the highest peak power and focused intensity was announced: the Extreme Light Infrastructure, ELI (*1*), designed to be the first exawatt-class (10^{18} W) laser. This gargantuan power will be obtained by cramming a kilojoule of energy into a pulse only 10 fs in duration. Analysis of the history of laser development reveals that the pulse duration and intensity of lasers (or derived coherent radiation bursts) are linearly related over more than 18 orders of magnitude (see the figure). This observation leads us to the conclusion that the shortest coherent pulse should come from such a large-sized laser. If zeptosecond and perhaps yoctosecond pulses can be produced using kilojoule-megajoule systems, it would open a route to time-resolved nuclear physics exploration and the possibility of peeking into the nucleus interior in the same way that chemical reactions or atoms can be probed today.

The motivation underpinning the push toward such extreme power (*2*) is not only ultrahigh laser intensity and the associated field that could be attained, but also the prospect of producing exceedingly short bursts of energetic radiation and particles. Since the first laser demonstrated by Maiman in 1960 (*3*) that operated with kilowatt-scale peak powers and internal intensity in the kW cm^{-2} range with an overall pulse duration in the microsecond regime, the continual developments in laser design have produced peak intensities exceeding 1 TW cm^{-2} with pulses 10 fs or shorter (*4*–*6*). At this point, the pulse bandwidth for the broadest bandwidth amplifying material, Ti:sapphire.

Shorter pulses need to acquire a broader spectrum before they can be recompressed. This is accomplished in a gas-filled hollow fiber (*7*) that can achieve the single-wavelength limit of 2.6 fs for 800 nm. To go to even shorter than one light period, higher frequencies must be generated. This is done by high harmonic generation (*8*) in a gas jet. The laser intensity is increased by focusing the compressed pulse beam after the fiber and the compressor. A fraction of the harmonic spectrum is selected to produce pulses down to 0.08 fs (*9*).

If we want to obtain even shorter pulses, we need to resort to even higher intensities, leave the nonlinear bound electron regime, and enter the high-energy relativistic regime, which is greater than 10^{18} W cm^{-2} for a wavelength of 1 μm. In this relativistic regime, the strength of the laser field propels the electrons to such high speeds that their "mass" changes as they oscillate. A laser pulse producing this intensity will make the target surface electrons oscillate in and out at relativistic velocity. As a consequence, any light hitting this oscillating mirror is modulated periodically, resulting in the generation of high harmonics (*10*, *11*). Relativistic high harmonic generation gives the prospect of a much broader

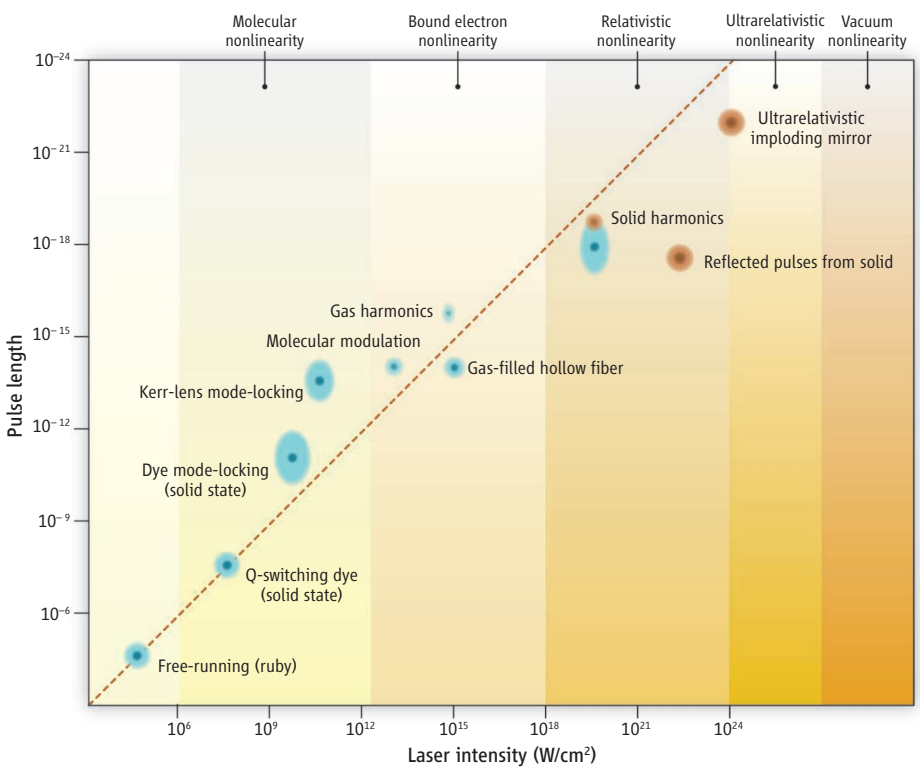

Shorter, more intense. An inverse linear dependence exists over 18 orders of magnitude between the pulse duration of coherent light emission and the laser intensity. These entries encompass different underlying physical regimes that exhibit molecular, bound atomic electron, relativistic plasma, ultrarelativistic, and vacuum nonlinearities. Blue patches represent experimental data; red patches denote simulation or theory.

[1]Institut Lumiere Extreme, ENSTA, Chemin de la Huniere, 91128 Palaiseau, France. [2]Faculty of Physics, Ludwig-Maximillians-Universität München, 85748 Garching, Germany. E-mail: gerardmourou@gmail.com

ing filament. Another is to determine how bundles of cross-linked filaments elongate from formin attached to cellular structures. Formins have well-established distinct roles in fungi (*3*), but cell biologists must sort out the overlapping functions of more than a dozen formins in human cells.

References

1. T. D. Pollard, J. A. Cooper, *Science* **326**, 1208 (2009).
2. H. Mizuno *et al.*, *Science* **331**, 80 (2011).
3. B. L. Goode, M. J. Eck, *Annu. Rev. Biochem.* **76**, 593 (2007).
4. A. Paul, T. D. Pollard, *Cell Motil. Cytoskeleton* **66**, 606 (2009).
5. H. C. Yang, L. A. Pon, *Proc. Natl. Acad. Sci. U.S.A.* **99**, 751 (2002).
6. T. Otomo *et al.*, *Nature* **433**, 488 (2005).
7. D. R. Kovar, T. D. Pollard, *Proc. Natl. Acad. Sci. U.S.A.* **101**, 14725 (2004).
8. T. Shemesh, T. Otomo, M. K. Rosen, A. D. Bershadsky, M. M. Kozlov, *J. Cell Biol.* **170**, 889 (2005).
9. D. R. Kovar, E. S. Harris, R. Mahaffy, H. N. Higgs, T. D. Pollard, *Cell* **124**, 423 (2006).

10.1126/science.1200773

PHYSICS

More Intense, Shorter Pulses

Large-scale laser facilities may also provide the ultimate source of ultrashort laser pulses.

Gerard Mourou[1] and Toshiki Tajima[2]

A few years ago, a new type of large-scale laser infrastructure specifically conceived to produce the highest peak power and focused intensity was announced: the Extreme Light Infrastructure, ELI (*1*), designed to be the first exawatt-class (10^{18} W) laser. This gargantuan power will be obtained by cramming a kilojoule of energy into a pulse only 10 fs in duration. Analysis of the history of laser development reveals that the pulse duration and intensity of lasers (or derived coherent radiation bursts) are linearly related over more than 18 orders of magnitude (see the figure). This observation leads us to the conclusion that the shortest coherent pulse should come from such a large-sized laser. If zeptosecond and perhaps yoctosecond pulses can be produced using kilojoule-megajoule systems, it would open a route to time-resolved nuclear physics exploration and the possibility of peeking into the nucleus interior in the same way that chemical reactions or atoms can be probed today.

The motivation underpinning the push toward such extreme power (*2*) is not only ultrahigh laser intensity and the associated field that could be attained, but also the prospect of producing exceedingly short bursts of energetic radiation and particles. Since the first laser demonstrated by Maiman in 1960 (*3*) that operated with kilowatt-scale peak powers and internal intensity in the kW cm^{-2} range with an overall pulse duration in the microsecond regime, the continual developments in laser design have produced peak intensities exceeding 1 TW cm^{-2} with pulses 10 fs or shorter (*4*–*6*). At this point, the pulse bandwidth for the broadest bandwidth amplifying material, Ti:sapphire.

Shorter pulses need to acquire a broader spectrum before they can be recompressed. This is accomplished in a gas-filled hollow fiber (*7*) that can achieve the single-wavelength limit of 2.6 fs for 800 nm. To go to even shorter than one light period, higher frequencies must be generated. This is done by high harmonic generation (*8*) in a gas jet. The laser intensity is increased by focusing the compressed pulse beam after the fiber and the compressor. A fraction of the harmonic spectrum is selected to produce pulses down to 0.08 fs (*9*).

If we want to obtain even shorter pulses, we need to resort to even higher intensities, leave the nonlinear bound electron regime, and enter the high-energy relativistic regime, which is greater than 10^{18} W cm^{-2} for a wavelength of 1 μm. In this relativistic regime, the strength of the laser field propels the electrons to such high speeds that their "mass" changes as they oscillate. A laser pulse producing this intensity will make the target surface electrons oscillate in and out at relativistic velocity. As a consequence, any light hitting this oscillating mirror is modulated periodically, resulting in the generation of high harmonics (*10*, *11*). Relativistic high harmonic generation gives the prospect of a much broader

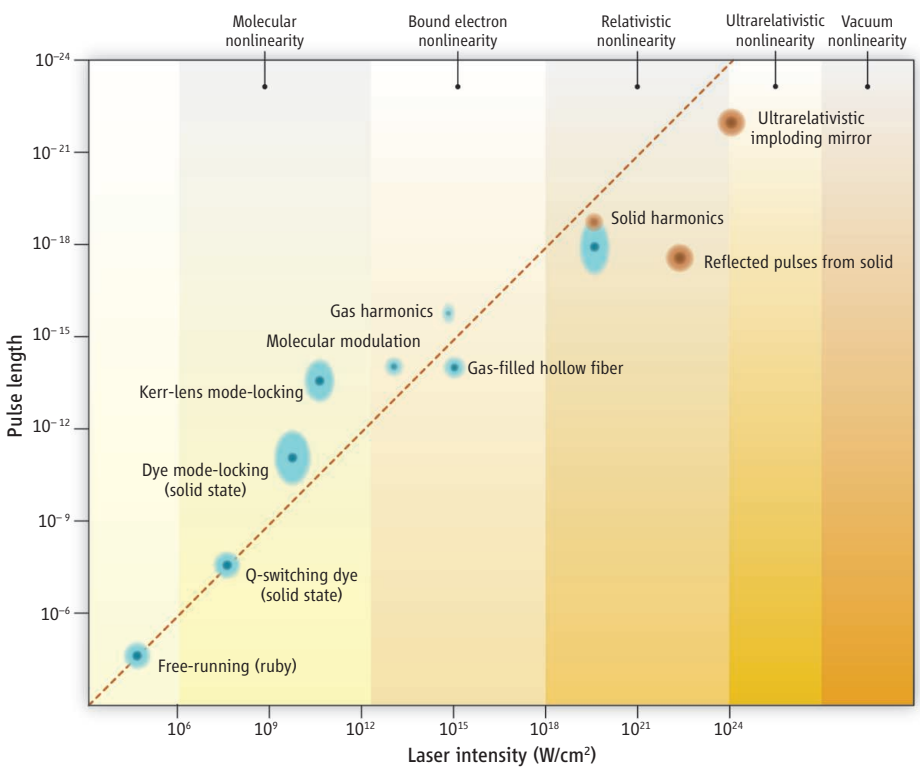

Shorter, more intense. An inverse linear dependence exists over 18 orders of magnitude between the pulse duration of coherent light emission and the laser intensity. These entries encompass different underlying physical regimes that exhibit molecular, bound atomic electron, relativistic plasma, ultrarelativistic, and vacuum nonlinearities. Blue patches represent experimental data; red patches denote simulation or theory.

[1]Institut Lumiere Extreme, ENSTA, Chemin de la Huniere, 91128 Palaiseau, France. [2]Faculty of Physics, Ludwig-Maximillians-Universität München, 85748 Garching, Germany. E-mail: gerardmourou@gmail.com

harmonic spectrum, and this has been experimentally verified (*12*) using the long pulse duration (300 fs) of the Vulcan laser at the 3200th harmonic order.

In a related scheme based on a pulse of a few cycles (*13*), the relativistic mirror ceases to be planar and deforms because of the indentation created by the focused laser beam. As it moves, simulation shows that it simultaneously compresses the pulses but also scatters them in specific directions. This technique may lead to an elegant method for both compressing and isolating individual attosecond pulses. For intensities on the order of 10^{22} W cm^{-2}, the compressed pulse could be on the order of only a few attoseconds. Such short, intense pulses could provide a way to produce beams of x-rays or even γ-rays by scattering the pulses off of bunches of free electrons. A similar concept called the "relativistic flying mirror" has been advocated and demonstrated (*14*), using a thin sheet of accelerated electrons. Reflection from this relativistic mirror leads to a high efficiency and pulse compression.

When one wishes to go to the γ-ray regime, the mirror that compresses the laser into γ rays must be of extremely high density (~10^{27} cm^{-3}) so that the laser may be coherently reflected into γ photons. One possibility is to use a combination of the relativistic flying mirror with the implosion of this flying mirror so that its density may be enhanced by a factor of 10 in each dimension (thus by a factor of 1000 in its density). This may be achieved by a large energy pulse (~1 MJ) at the ultrarelativistic intensity of 10^{24} W cm^{-2} on a partial shell of a concave spherical target. This imploding ultrarelativistic flying mirror (*15*) would be capable of coherently backscattering an injected 10-keV coherent x-ray pulse into a coherent γ-ray pulse with a duration of 100 ys (10^{-22} s).

We know that matter exhibits nonlinearities when irradiated with a strong enough laser; the manifested nonlinearities vary depending on the strength of the "bending" field (and thus the intensity). The stronger we bend the constituent matter, the more rigid the bending force we need to exert; the more rigid the force is, the higher the restoring frequency (or the shorter the time scale) is. The nonlinearities of matter may vary, but this response is universal, ranging over molecular, atomic, plasma electronic, ionic, and even vacuum nonlinearities.

The observed correlation between laser pulse intensity and duration over 18 orders of magnitude provides an invaluable guide for the development of future laser systems for ultra-intense and short-pulse experiments. Most notably, the correlation shows that the shortest coherent pulse in the zeptosecond-yoctosecond regime should be produced by the largest lasers such as ELI, the National Ignition Facility, and the Laser Mégajoule facility under construction in France, if they are reconfigured (*16*) as femtosecond pulse systems.

References and Notes

1. Extreme Light Infrastructure European Project (www.extreme-light-infrastructure.eu).
2. G. A. Mourou, T. Tajima, S. V. Bulanov, *Rev. Mod. Phys.* **78**, 309 (2006).
3. T. H. Maiman, *Nature* **187**, 493 (1960).
4. A. Stingl, M. Lenzner, Ch. Spielmann, F. Krausz, R. Szipocs, *Opt. Lett.* **20**, 602 (1995).
5. D. H. Sutter *et al.*, *Appl. Phys. B* **70**, S5 (2000).
6. R. Ell *et al.*, *Opt. Lett.* **26**, 373 (2001).
7. M. Nisoli, S. De Silvestri, O. Svelto, *Appl. Phys. Lett.* **68**, 2793 (1996).
8. P. Antoine, A. L'Huillier, M. Lewenstein, *Phys. Rev. Lett.* **77**, 1234 (1996).
9. E. Goulielmakis *et al.*, *Science* **320**, 1614 (2008).
10. S. V. Bulanov, N. M. Naumova, F. Pegoraro, *Phys. Plasmas* **1**, 745 (1994).
11. G. D. Tsakiris, K. Eidmann, J. Meyer-ter-Vehn, F. Krausz, *N. J. Phys.* **8**, 19 (2006).
12. B. Dromey *et al.*, *Nat. Phys.* **2**, 456 (2006).
13. N. M. Naumova, J. A. Nees, I. V. Sokolov, B. Hou, G. Mourou, *Phys. Rev. Lett.* **92**, 063902 (2004).
14. S. V. Bulanov, T. Esirkepov, T. Tajima, *Phys. Rev. Lett.* **91**, 085001 (2003).
15. T. Esirkepov, M. Borghesi, S. V. Bulanov, G. Mourou, T. Tajima, *Phys. Rev. Lett.* **92**, 175003 (2004).
16. T. Tajima, G. A. Mourou, *Phys. Rev. Spec. Top. Accel. Beams* **5**, 031301 (2002).

17. We thank J. Nees, N. Naumova, E. Moses, and N. Artemiev, F. Krauz, as well as D. Verwaerde and C. L. Labaune, for fruitful discussions. T.T. was supported in part by the Blaise Pascal Foundation and by Deutsche Forschungsgemeinschaft Cluster of Excellence MAP (Munich Centre for Advanced Photonics). G.M. is supported by the École Polytechnique, the CNRS, ENSTA, and ELI 212105.

10.1126/science.1200292

CHEMISTRY

The Chlorine Dilemma

David L. Sedlak[1] and Urs von Gunten[2,3]

Chorination of drinking water and municipal wastewater can create toxic chemical by-products, but alternatives pose their own set of hazards.

Chlorine disinfection has been instrumental in the provision of safe drinking water, but the use of chlorine has a dark side: In addition to inactivating waterborne pathogens, chlorine reacts with natural organic matter to produce a variety of toxic disinfection by-products (DBPs). Regulatory guidelines were established in the United States for DBPs, such as chloroform, shortly after they were discovered in chlorinated drinking water in the mid-1970s, and the discovery of a potential link between DBPs and increased rates of miscarriages and bladder cancer led to more stringent regulations and substantial changes in the operation of water treatment systems during the past decade (*1*). These concerns and the risks associated with storing chlorine gas have recently led many drinking-water and wastewater treatment plants to discontinue the use of chlorine disinfection (see the figure). A series of recent studies suggest that some of these changes have had unintended consequences that pose risks to public health and the environment.

Chlorine DBPs can be controlled in drinking-water systems by more effective removal of natural organic matter—the main precursors of DBPs—through physical-chemical treatment processes such as enhanced coagulation and activated carbon filtration. Although these approaches are effective and pose no known health risks, they are generally the most expensive way of minimizing DBP formation. As a result, many utilities worldwide have opted for the less expensive approach of using chloramine. This less reactive form of chlorine is produced by adding excess ammonia to water before addition of chlorine.

One unexpected consequence of this substitution has been the production of a different set of toxic DBPs. Most notably, carcinogenic nitrosamines such as *N*-nitrosodimethylamine (NDMA) are produced when chloramines react with nitrogen-containing organic compounds (*2*). Formation of NDMA was first recognized at advanced water reclamation plants where chloramine was being used to disinfect sewage effluent before its passage through mem-

[1]Department of Civil and Environmental Engineering, University of California, Berkeley, CA 94720, USA. [2]Eawag, Swiss Federal Institute of Aquatic Science and Technology, Dübendorf 8600, Switzerland. [3]Civil and Environmental Engineering, École Polytechnique Fédérale de Lausanne-EPFL, Lausanne, Switzerland. E-mail: sedlak@berkeley.edu (D.L.S.); vongunten@eawag.ch (U.v.G.)

harmonic spectrum, and this has been experimentally verified (*12*) using the long pulse duration (300 fs) of the Vulcan laser at the 3200th harmonic order.

In a related scheme based on a pulse of a few cycles (*13*), the relativistic mirror ceases to be planar and deforms because of the indentation created by the focused laser beam. As it moves, simulation shows that it simultaneously compresses the pulses but also scatters them in specific directions. This technique may lead to an elegant method for both compressing and isolating individual attosecond pulses. For intensities on the order of 10^{22} W cm^{-2}, the compressed pulse could be on the order of only a few attoseconds. Such short, intense pulses could provide a way to produce beams of x-rays or even γ-rays by scattering the pulses off of bunches of free electrons. A similar concept called the "relativistic flying mirror" has been advocated and demonstrated (*14*), using a thin sheet of accelerated electrons. Reflection from this relativistic mirror leads to a high efficiency and pulse compression.

When one wishes to go to the γ-ray regime, the mirror that compresses the laser into γ rays must be of extremely high density (~10^{27} cm^{-3}) so that the laser may be coherently reflected into γ photons. One possibility is to use a combination of the relativistic flying mirror with the implosion of this flying mirror so that its density may be enhanced by a factor of 10 in each dimension (thus by a factor of 1000 in its density). This may be achieved by a large energy pulse (~1 MJ) at the ultrarelativistic intensity of 10^{24} W cm^{-2} on a partial shell of a concave spherical target. This imploding ultrarelativistic flying mirror (*15*) would be capable of coherently backscattering an injected 10-keV coherent x-ray pulse into a coherent γ-ray pulse with a duration of 100 ys (10^{-22} s).

We know that matter exhibits nonlinearities when irradiated with a strong enough laser; the manifested nonlinearities vary depending on the strength of the "bending" field (and thus the intensity). The stronger we bend the constituent matter, the more rigid the bending force we need to exert; the more rigid the force is, the higher the restoring frequency (or the shorter the time scale) is. The nonlinearities of matter may vary, but this response is universal, ranging over molecular, atomic, plasma electronic, ionic, and even vacuum nonlinearities.

The observed correlation between laser pulse intensity and duration over 18 orders of magnitude provides an invaluable guide for the development of future laser systems for ultra-intense and short-pulse experiments. Most notably, the correlation shows that the shortest coherent pulse in the zeptosecond-yoctosecond regime should be produced by the largest lasers such as ELI, the National Ignition Facility, and the Laser Mégajoule facility under construction in France, if they are reconfigured (*16*) as femtosecond pulse systems.

References and Notes

1. Extreme Light Infrastructure European Project (www.extreme-light-infrastructure.eu).
2. G. A. Mourou, T. Tajima, S. V. Bulanov, *Rev. Mod. Phys.* **78**, 309 (2006).
3. T. H. Maiman, *Nature* **187**, 493 (1960).
4. A. Stingl, M. Lenzner, Ch. Spielmann, F. Krausz, R. Szipocs, *Opt. Lett.* **20**, 602 (1995).
5. D. H. Sutter *et al.*, *Appl. Phys. B* **70**, S5 (2000).
6. R. Ell *et al.*, *Opt. Lett.* **26**, 373 (2001).
7. M. Nisoli, S. De Silvestri, O. Svelto, *Appl. Phys. Lett.* **68**, 2793 (1996).
8. P. Antoine, A. L'Huillier, M. Lewenstein, *Phys. Rev. Lett.* **77**, 1234 (1996).
9. E. Goulielmakis *et al.*, *Science* **320**, 1614 (2008).
10. S. V. Bulanov, N. M. Naumova, F. Pegoraro, *Phys. Plasmas* **1**, 745 (1994).
11. G. D. Tsakiris, K. Eidmann, J. Meyer-ter-Vehn, F. Krausz, *N. J. Phys.* **8**, 19 (2006).
12. B. Dromey *et al.*, *Nat. Phys.* **2**, 456 (2006).
13. N. M. Naumova, J. A. Nees, I. V. Sokolov, B. Hou, G. Mourou, *Phys. Rev. Lett.* **92**, 063902 (2004).
14. S. V. Bulanov, T. Esirkepov, T. Tajima, *Phys. Rev. Lett.* **91**, 085001 (2003).
15. T. Esirkepov, M. Borghesi, S. V. Bulanov, G. Mourou, T. Tajima, *Phys. Rev. Lett.* **92**, 175003 (2004).
16. T. Tajima, G. A. Mourou, *Phys. Rev. Spec. Top. Accel. Beams* **5**, 031301 (2002).

17. We thank J. Nees, N. Naumova, E. Moses, and N. Artemiev, F. Krauz, as well as D. Verwaerde and C. L. Labaune, for fruitful discussions. T.T. was supported in part by the Blaise Pascal Foundation and by Deutsche Forschungsgemeinschaft Cluster of Excellence MAP (Munich Centre for Advanced Photonics). G.M. is supported by the École Polytechnique, the CNRS, ENSTA, and ELI 212105.

10.1126/science.1200292

CHEMISTRY

The Chlorine Dilemma

David L. Sedlak[1] and Urs von Gunten[2,3]

Chorination of drinking water and municipal wastewater can create toxic chemical by-products, but alternatives pose their own set of hazards.

Chlorine disinfection has been instrumental in the provision of safe drinking water, but the use of chlorine has a dark side: In addition to inactivating waterborne pathogens, chlorine reacts with natural organic matter to produce a variety of toxic disinfection by-products (DBPs). Regulatory guidelines were established in the United States for DBPs, such as chloroform, shortly after they were discovered in chlorinated drinking water in the mid-1970s, and the discovery of a potential link between DBPs and increased rates of miscarriages and bladder cancer led to more stringent regulations and substantial changes in the operation of water treatment systems during the past decade (*1*). These concerns and the risks associated with storing chlorine gas have recently led many drinking-water and wastewater treatment plants to discontinue the use of chlorine disinfection (see the figure). A series of recent studies suggest that some of these changes have had unintended consequences that pose risks to public health and the environment.

Chlorine DBPs can be controlled in drinking-water systems by more effective removal of natural organic matter—the main precursors of DBPs—through physical-chemical treatment processes such as enhanced coagulation and activated carbon filtration. Although these approaches are effective and pose no known health risks, they are generally the most expensive way of minimizing DBP formation. As a result, many utilities worldwide have opted for the less expensive approach of using chloramine. This less reactive form of chlorine is produced by adding excess ammonia to water before addition of chlorine.

One unexpected consequence of this substitution has been the production of a different set of toxic DBPs. Most notably, carcinogenic nitrosamines such as *N*-nitrosodimethylamine (NDMA) are produced when chloramines react with nitrogen-containing organic compounds (*2*). Formation of NDMA was first recognized at advanced water reclamation plants where chloramine was being used to disinfect sewage effluent before its passage through mem-

[1]Department of Civil and Environmental Engineering, University of California, Berkeley, CA 94720, USA. [2]Eawag, Swiss Federal Institute of Aquatic Science and Technology, Dübendorf 8600, Switzerland. [3]Civil and Environmental Engineering, École Polytechnique Fédérale de Lausanne-EPFL, Lausanne, Switzerland. E-mail: sedlak@berkeley.edu (D.L.S.); vongunten@eawag.ch (U.v.G.)

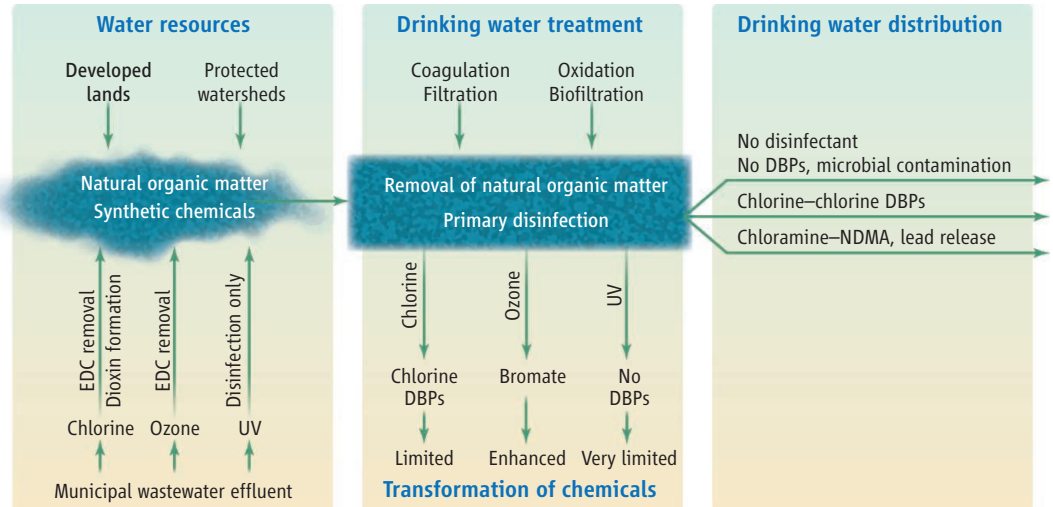

More than just water after water treatment. A schematic of water purification processes for drinking water and municipal wastewater. Water resources may contain not only microorganisms but also natural and synthetic compounds; the latter include endocrine-disrupting compounds (EDCs) that may or may not have been removed during wastewater treatment. After removal of natural organic matter, some disinfection processes can lead to unwanted reactions of dissolved compounds. Chlorination can create chlorine disinfection by-products (DBPs), and ozonation can introduce bromate or aldehydes. Further reaction in the drinking-water distribution system can increase concentrations of DBPs after chlorination, and chloramine use can cause increased release of lead from plumbing and can lead to formation of nitrosamines.

branes. Subsequently, NDMA and other nitrosamines have been detected in drinking-water treatment systems where chloramine reacts with the synthetic polymers used for water softening and flocculation (*3*).

In addition to forming carcinogenic nitrosamines, the switch from chlorine to chloramine has also been implicated in elevated levels of lead recently observed in drinking water and human blood in Washington, DC, and other cities (*4*). In these drinking-water distribution systems, the leaching of lead from pipes had been inhibited for many decades by the presence of chlorine, which had created a coating of sparingly soluble lead oxide (PbO_2), a Pb(IV) compound, on the surface of the pipes. After chlorine was replaced by chloramine, which is not as strong an oxidant, the coatings were reduced to Pb(II)-containing minerals, which are more soluble, thereby releasing higher concentrations of lead into the drinking water (*5*).

Several recently published studies have also uncovered unexpected findings related to the reactions of chlorine with synthetic chemicals now commonly found in surface water and groundwater, such as pharmaceuticals, personal care products, and polar pesticides. Many of these compounds contain electron-rich phenolic and amine moieties that are transformed during chlorine disinfection through electrophilic substitution (*6*). For example, chlorination of the phenolic compound triclosan, an antimicrobial widely used in soaps, leads to chlorination of the aromatic ring. The ring then undergoes cleavage reactions and releases chloroform and related trihalomethanes (*7*). In surface waters downstream of sewage treatment plants, where wastewater is disinfected with chlorine, the ring-chlorinated triclosan derivatives undergo photochemical transformation to form di-, tri-, and tetrachlorinated dioxins that accumulate in downstream sediments (*8*).

The production of potentially toxic compounds by chlorine disinfection can be problematic, but transformation reactions occurring during chlorination also can be beneficial. For example, endocrine-disrupting compounds (EDCs) in wastewater effluent that enters natural waterways have been implicated in the feminization of fish. The EDCs most often responsible for fish feminization—17β-estradiol, 17α-ethinylestradiol, estrone, and nonylphenol (*9*)—are transformed during chlorine disinfection through reactions with phenolic moieties (*10*). The estrogen receptor has high specificity, so the products of these reactions are much less estrogenic than the parent compounds (*11*, *12*). Other compounds in wastewater effluent that pose potential risks to aquatic ecosystems, including antibiotics and β-blockers, also are transformed to less reactive products during chlorine disinfection (*6*). Because of concerns associated with chlorine DBPs and potential hazards associated with handling of chlorine gas, many wastewater utilities are now switching to ultraviolet (UV) disinfection systems that leave these biologically active compounds unchanged. This switch has resulted in the loss of the beneficial side effect of chlorine's reactivity with electron-rich organic compounds.

Recognition of these unexpected consequences of the shift away from chlorine disinfection raises new challenges with respect to the operation of drinking-water and wastewater treatment plants. For drinking-water treatment plants with aging distribution systems, chlorine plays an important role in controlling microbial growth and preventing the release of lead. Research is needed into more effective methods of removing DBP precursors and applying disinfectants other than chlorine (such as UV light and ozone) at the drinking-water treatment plant. Such advances could lower the concentrations of DBPs enough to make it possible to continue to add some chlorine as a residual disinfectant. For treatment plants with newer or better-maintained drinking-water distribution systems, research may help to identify ways of more effectively operating water distribution systems without residual disinfectants. To avoid the formation of chlorine DBPs when wastewater is disinfected (while still disinfecting water and removing EDCs), a disinfectant with oxidizing capacity may be useful. Ozone appears to meet these needs, provided that the challenges associated with ozone DBPs, such as bromate and low-molecular-weight aldehydes, are effectively addressed.

References

1. Federal Register (U.S. Government Printing Office, Washington, DC, 1998), vol. 40, pp. 69390–69476.
2. W. A. Mitch, D. L. Sedlak, *Environ. Sci. Technol.* **36**, 588 (2002).
3. S. H. Park *et al.*, *Environ. Sci. Technol.* **43**, 1360 (2009).
4. M. Edwards, A. Dudi, *J. Am. Water Works Assoc.* **96**, 69 (2004).
5. H. Z. Liu, G. V. Korshin, J. F. Ferguson, *Environ. Sci. Technol.* **43**, 3278 (2009).
6. M. Deborde, U. von Gunten, *Water Res.* **42**, 13 (2008).
7. K. L. Rule, V. R. Ebbett, P. J. Vikesland, *Environ. Sci. Technol.* **39**, 3176 (2005).
8. J. M. Buth *et al.*, *Environ. Sci. Technol.* **44**, 4545 (2010).
9. J. P. Sumpter, A. C. Johnson, R. J. Williams, A. Kortenkamp, M. Scholze, *Environ. Sci. Technol.* **40**, 5478 (2006).
10. M. Deborde, S. Rabouan, H. Gallard, B. Legube, *Environ. Sci. Technol.* **38**, 5577 (2004).
11. B. C. Lee *et al.*, *Water Res.* **38**, 733 (2004).
12. Y. Lee, B. I. Escher, U. von Gunten, *Environ. Sci. Technol.* **42**, 6333 (2008).

10.1126/science.1196397

Published by AAAS

Innate or Adaptive Immunity? The Example of Natural Killer Cells

Eric Vivier,[1,2,3,4]*† David H. Raulet,[5]† Alessandro Moretta,[6]† Michael A. Caligiuri,[7]† Laurence Zitvogel,[8]† Lewis L. Lanier,[9]† Wayne M. Yokoyama,[10]† Sophie Ugolini[1,2,3]*†

Natural killer (NK) cells were originally defined as effector lymphocytes of innate immunity endowed with constitutive cytolytic functions. More recently, a more nuanced view of NK cells has emerged. NK cells are now recognized to express a repertoire of activating and inhibitory receptors that is calibrated to ensure self-tolerance while allowing efficacy against assaults such as viral infection and tumor development. Moreover, NK cells do not react in an invariant manner but rather adapt to their environment. Finally, recent studies have unveiled that NK cells can also mount a form of antigen-specific immunologic memory. NK cells thus exert sophisticated biological functions that are attributes of both innate and adaptive immunity, blurring the functional borders between these two arms of the immune response.

The immune system is classically divided into innate and adaptive immunity. The distinctive features of innate immunity commonly refer to a broadly distributed variety of myeloid and lymphoid cells that can exert rapid effector function through a limited repertoire of germline-encoded receptors. In contrast, adaptive immunity in mammals is characterized by two types of lymphocytes, T and B cells, clonally expressing a large repertoire of antigen receptors that are produced by site-specific somatic recombination, that is, T cell receptor (TCR) and antibody/B cell receptor (BCR). Functionally, naive T and B cells encounter antigens in specialized lymphoid organs and undergo a process of cell division and maturation before exerting their effector function. Natural killer (NK) cells represent a subgroup of white blood cells. Since their identification in 1975 (*1*, *2*), NK cells have been classified as lymphocytes on the basis of their morphology, their expression of many lymphoid markers, and their origin from the common lymphoid progenitor cell in the bone marrow. NK cells, however, are generally considered to be components of innate immune defense because they lack antigen-specific cell surface receptors. In addition, despite the extreme rarity of convincing cases of selective NK cell deficiency in humans (Online Mendelian Inheritance in Man database 609981) (*3*), NK cells have been shown in humans and mice to participate in the early control against virus infection, especially herpesvirus infection (*4*), and in tumor immunosurveillance (*5*). The lack of gross abnormalities in X-linked severe combined immunodeficiency (SCID-X1) patients who have undergone hematopoietic stem cell transplantation (HSCT) or *IL2RG* gene therapy, but remain unexpectedly NK cell deficient, has supported the possibility that NK cells might exert redundant function (*6*). However, the presence of NK cells in nonhuman mammals and NK cell orthologs in other vertebrates argues for their importance (*7*). Notably, NK cells are peculiar in their capacity to invade the uterus, where they have been shown to contribute to the development of the embryo (*8*). These data prompt speculation that the role of NK cells during reproduction has contributed to their selection.

How Do NK Cells Contribute to Immunity?

NK cells were originally described as cytolytic effector lymphocytes, which, unlike cytotoxic T

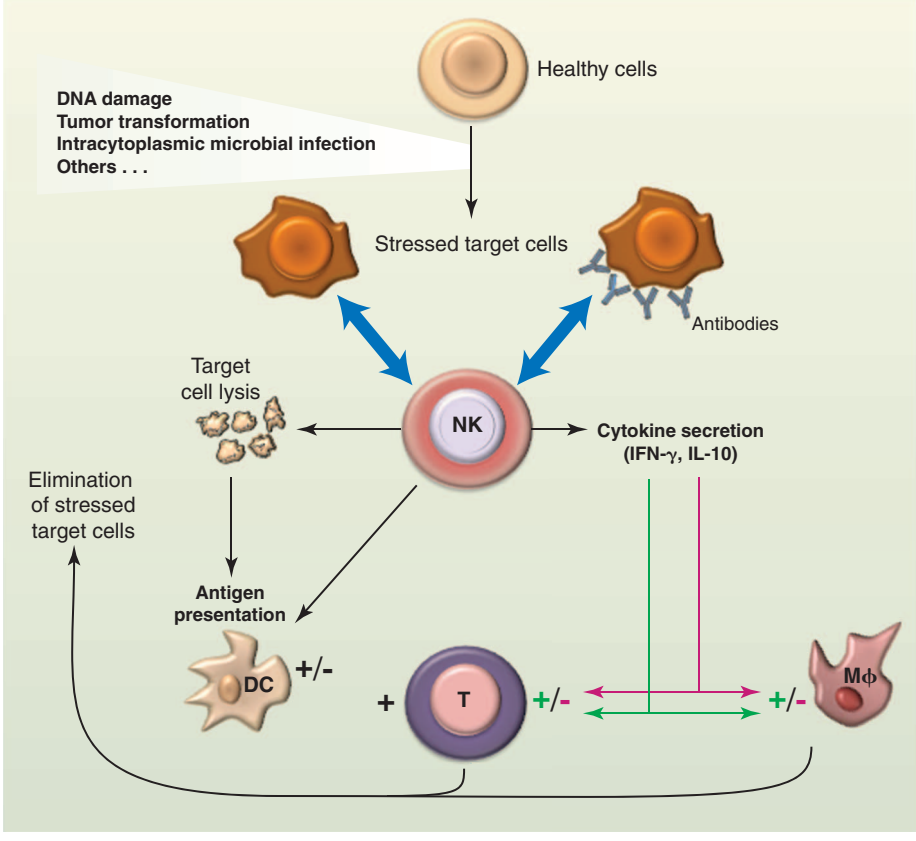

Fig. 1. The biological functions of NK cells. NK cells can recognize a variety of stressed cells in the absence or in the presence of antibodies (blue arrows). NK cell activation triggered by this recognition can lead to the lysis of the target cell and to the production of various cytokines and chemokines depending on the nature of the stimulation. Whereas NK cells are biased to produce IFN-γ in many conditions, there are situations of chronic or systemic inflammation that promote IL-10 secretion. NK can also cross-talk with DC in many different ways, including the NK cell killing of immature DC and the promotion of DC maturation by NK cell–derived IFN-γ and TNF-α, which leads to enhanced antigen presentation to T cells. Through these biological activities, NK cells participate in the shaping of the subsequent immune response; in the depicted example, NK cells boost or dampen macrophage and T cell responses through IFN-γ (green arrows) or IL-10 secretion (red arrows), respectively.

[1]Centre d'Immunologie de Marseille-Luminy (CIML), Université de la Méditerranée UM 631, Campus de Luminy, 13288 Marseille, France. [2]INSERM UMR-S 631, Marseille, France. [3]CNRS, UMR6102, Marseille, France. [4]Assistance Publique des Hôpitaux de Marseille, Hôpital de la Conception, Marseille, France. [5]Department of Molecular and Cell Biology and Cancer Research Laboratory, University of California, Berkeley, Berkeley, CA 94720–3200, USA. [6]Department of Experimental Medicine and Centre of Excellence for Biomedical Research (CEBR), University of Genova, Italy. [7]The Ohio State University Comprehensive Cancer Center, The James Cancer Hospital and Solove Research Institute, Columbus, OH 43220, USA. [8]U1015 INSERM, Institut Gustave Roussy, 94805 Villejuif, France. [9]Department of Microbiology and Immunology and the Cancer Research Institute, University of California San Francisco, San Francisco, CA 94143–0414, USA. [10]Howard Hughes Medical Institute, Rheumatology Division, Campus Box 8045, Washington University School of Medicine, 660 South Euclid Avenue, St. Louis, MO 63110, USA.

*To whom correspondence should be addressed. E-mail: vivier@ciml.univ-mrs.fr (E.V.); ugolini@ciml.univ-mrs.fr (S.U.)
†All authors contributed equally to this work.

cells, can directly induce the death of tumor cells and virus-infected cells in the absence of specific immunization; hence their name. Subsequently, NK cells have been recognized as major producers of cytokines such as interferon-γ (IFN-γ) in many physiological and pathological conditions. NK cells also produce an array of other cytokines, both proinflammatory and immunosuppressive, such as tumor necrosis factor–α (TNF-α) and interleukin (IL)–10, respectively, and growth factors such as GM-CSF (granulocyte macrophage colony-stimulating factor), G-CSF (granulocyte colony-stimulating factor), and IL-3. NK cells also secrete many chemokines, including CCL2 (MCP-1), CCL3 (MIP1-α), CCL4 (MIP1-β), CCL5 (RANTES), XCL1 (lymphotactin), and CXCL8 (IL-8) (*9*). Whereas the biological function of the growth factors secreted by NK cells remains to be clarified, their secretion of chemokines is key to their colocalization with other hematopoietic cells such as dendritic cells (DC) in areas of inflammation (*10*). Furthermore, the production of IFN-γ by NK cells helps to shape T cell responses in lymph nodes, possibly by a direct interaction between naïve T cells and NK cells migrating to secondary lymphoid compartments from inflamed peripheral tissues and by an indirect effect on DC (*11*) (Fig. 1). NK cell–mediated killing of target cells also impacts T cell responses, possibly by decreasing the antigenic load (*12*) and/or because target cell debris might promote antigen cross-presentation to $CD8^+$ cytotoxic T cells (*13*) (Fig. 1). Although NK cells can positively (*12*, *13*) or negatively (*14*) influence host T and B cell immunity, depending on the nature of the antigenic challenge, the emerging notion is that NK cells are not only cytolytic effector cells against microbe-infected cells or tumor cells. Rather, NK cell–mediated cytotoxicity and cytokine production impact DC, macrophages, and neutrophils (*10*) and endow NK cells with regulatory function affecting subsequent antigen-specific T and B cell responses. Conversely, the "natural" effector function of NK cells has been revisited. NK cells require priming by various factors, such as IL-15 presented by DC (*15*) or macrophages (*16*), IL-12 (*17*) or IL-18 (*18*), to achieve their full effector potential, highlighting the intimate regulatory interactions between NK cells and other components of the immune response. Thus, NK cells, like T and B cells, participate in the immunity in many different ways and undergo a process of functional maturation to fulfill these functions.

How Are NK Cells Regulated?

NK cells are equipped with an array of receptors that can either stimulate NK cell reactivity (activating receptors) or dampen NK cell reactivity (inhibitory receptors) (*19*, *20*). Activating receptors include receptors that interact with soluble ligands such as cytokines and receptors that interact with cell surface molecules (Fig. 2). Cytokine receptors that are coupled to the common gamma chain (γc), such as IL-15R, IL-2R, and IL-21R, are involved in NK cell development and effector function. In particular, IL-15 is required for the maturation and survival of NK cells, consistent with the absence of circulating NK cells in SCID-X1 patients and in mice lacking IL-15 or IL-15R components (*21*). Cytokine receptors that are linked to the adapter protein MyD88 are also important for NK cell maturation, namely IL-1R in humans (*22*) and IL-18R in the mouse (*18*).

NK cells exert their biological functions by various means. NK cells can kill a variety of target cells, including virus-infected cells and tumors, in the absence of antibody. In the case of viruses, the mouse Ly49H activating receptor recognizes a cytomegalovirus-encoded ligand (m157) (*23*, *24*), and NKp46 has been reported to interact with hemagglutinins derived from influenza and parainfluenza viruses (*25*). NK cells are also able to detect antibody-coated cells through the FcγRIIIA (CD16) cell surface receptor and to exert antibody-dependent cell cytotoxicity (ADCC) and cytokine production. CD16 is coupled to the CD3ζ and FcRγ signal transduction polypeptides bearing intracytoplasmic immunoreceptor tyrosine-based activation motifs (ITAMs). The natural cytotoxicity receptors (NKp46/NCR1, NKp44/NCR2, and NKp30/NCR3) are also potent activation receptors linked to the ITAM-bearing CD3ζ, FcRγ, or DAP12 molecules (*26*). In mice, the NK1.1 (Nkrp1c) molecule on $CD3^-$ cells has been a useful marker for NK cells, but its expression is confined to only certain strains of mice. NKp46 appears to be the most specific NK cell marker across mammalian species, although discrete subsets of T cells also express it (*27*). Accumulating data in humans and mice also indicate that NCR^+ cells ($NKp46^+$ in the mouse, $NKp46^+NKp44^+$ in humans) that produce IL-22, a cytokine noted to be important in mucosal immunity, are found in gut-associated mucosal tissue. In contrast to bona fide NK cells, these $NCR^+IL\text{-}22^+$ mucosal cells express the transcription factor RORγt, are not cytotoxic, do not secrete IFN-γ, and are not dependent on IL-15 for their development (*28*, *29*). $NCR^+IL\text{-}22^+$ are thus clearly distinct from the conventional NK cell subsets and likely derive from a different lineage that could be related to the lymphoid tissue inducer (LTi) cells involved in the formation of lymphoid tissue (*28*, *29*). In contrast to the ITAM-coupled antigen-specific TCR and BCR whose absence leads to a complete block in T and B cell development, respectively, NK cells still develop in the absence of ITAM-bearing molecules (*30*). These results highlight the redundancy of NK cell developmental pathways and may explain the robustness of this lymphoid cell compartment in most cases of immune deficiencies.

A feature of several NK cell activating receptors resides in their capacity to detect self molecules induced in conditions of cellular stress (*31*). This is the case for NKG2D, which interacts with various ligands that are expressed at low

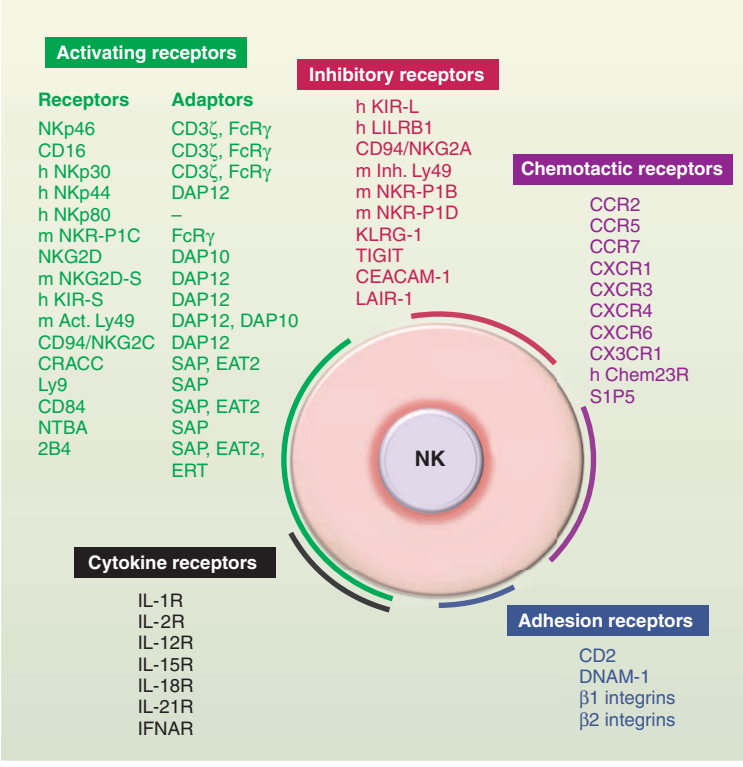

Fig. 2. NK cell receptors. NK cells express many cell surface receptors that can be grouped into activating (green), inhibitory (red), adhesion (blue), cytokine (black) and chemotactic receptors (purple). In addition to MHC class I–specific receptors, other NK cell inhibitory receptors specific for non-MHC ligands also regulate NK cell reactivity (*78*). Adaptor molecules involved in the signaling cascade downstream of the engagement of activating receptors (green) are also indicated. The list of cell surface molecules involved in the regulation of mouse and human NK cell function is not exhaustive. Unless indicated (h, human; m, mouse), receptors are conserved in both species.

levels in most tissues but are overexpressed upon initiation of cellular distress, for example, after initiation of the DNA damage response (*32*). This is also the case for B7-H6, a ligand for NKp30 that has not been detected in healthy cells but is expressed on certain tumor cells (*33*).

Pioneering work showed that NK cells can detect the lack of major histocompatibility complex (MHC) class I ("missing self"), a situation that can occur when cells are perturbed by viral infection or cellular transformation (*34*). This "missing self" recognition is explained by the NK cell surface expression of a variety of MHC class I–specific inhibitory receptors that include killer cell immunoglobulin-like receptors (KIRs) in humans, lectin-like Ly49 molecules in mice, and CD94/NKG2A heterodimers in both species (*35*, *36*). These MHC class I receptors belong to the large family of inhibitory receptors that mediate their function by signaling through intracytoplasmic immunoreceptor tyrosine-based inhibition motifs (ITIMs) (*19*). Thus, NK cells spare healthy cells that express self-MHC class I molecules and low amounts of stress-induced self molecules, whereas they selectively kill target cells "in distress" that down-regulate MHC class I molecules and/or up-regulate stress-induced self molecules such as NKG2D ligands (Fig. 3) (*32*).

Why Aren't NK Cells Self-Reactive?

Like T cells and B cells, NK cells have the potential for autoreactivity even though NK receptor genes do not undergo somatic diversification. This is because some NK cells lack inhibitory receptors that bind to the MHC class I molecules of the host (*37*, *38*) or they express activating receptors that recognize self ligands, including MHC molecules (*39*–*41*). These patterns of expression arise because the array of receptors that individual NK cells come to express during development is largely random, and the MHC ligands recognized by these receptors are inherited independently of the receptor genes (*42*). Therefore, some NK cells may express activating receptors for a self ligand, yet fail to express inhibitory receptors for self-MHC molecules.

To avoid autoreactivity, an education system exists whereby such NK cells acquire self-tolerance. The potentially autoreactive NK cells are not generally clonally deleted but instead acquire a state of hyporesponsiveness to stimulation through various activating receptors. Thus, in normal mice (*38*) or humans (*43*), a fraction of NK cells lack inhibitory receptors for self-MHC, and these NK cells are unresponsive to self cells (Fig. 4A). A related situation applies in mice or humans that lack MHC class I molecules, where NK cells exist in normal numbers but fail to exert detectable autoimmunity or to kill MHC class I–deficient autologous cells in vivo or in vitro (*44*–*46*) (Fig. 4B). In both cases, the NK cells not only are unresponsive to self cells but also exhibit reduced responses to various other stimuli, including MHC class I–deficient tumor cells or cross-linking antibodies specific for activating receptors (*37*, *38*, *43*, *44*, *47*). By comparison, by an MHC-dependent education process described as licensing by some investigators, the NK cells that express receptors for self MHC in normal animals or humans exhibit greater responsiveness to stimulation, but their effector function against neighboring normal cells is inhibited by engagement of the MHC-specific inhibitory receptors (*37*, *38*, *48*). Whether NK responsiveness is actively induced by encounters with cells expressing MHC ligands for these NK cells (called "arming"), or hyporesponsiveness is actively induced by encounters with normal cells that lack MHC ligands and at the same time express stimulatory ligands for these NK cells (called "disarming," or energy), or both, remain unsettled issues (*48*). The molecular mechanisms that govern responsiveness are also not established, except that it is clear that changes in responsiveness are not correlated with changes in the expression of the known activating receptors (*37*, *38*, *43*, *44*, *47*, *49*).

Experimental evidence for NK cell education in an MHC-independent scenario has been obtained using mice engineered to express ligands for activating receptors such as NKG2D (Fig. 4C) or Ly49H (*50*, *51*) (Fig. 4D). The NK cells in these mice are tolerant to expressed ligand but retain expression of the corresponding receptor. Similarly, in humans, NK cells expressing the KIR2DS1 activating receptor specific for the human lymphocyte antigen (HLA)–C2 allotype are functional only when derived from C1/C2 or C1/C1 donors but hyporesponsive in donors homozygous for C2 (*52*). This suggests that in the presence of high levels of activating ligands, a negative tuning effect may occur (*53*) (Fig. 4E).

It is possible that some of the mechanisms that confer tolerance in mice with constitutive expression of activating ligands are the same as those that operate when NK cells lack inhibitory receptors for self-MHC. One possible mechanism for the impaired responsiveness of NK cells that are not inhibited by MHC molecules is the induction of an anergic state, as can occur in autoreactive T cells and B cells. Another is a failure of these NK cells to undergo terminal functional

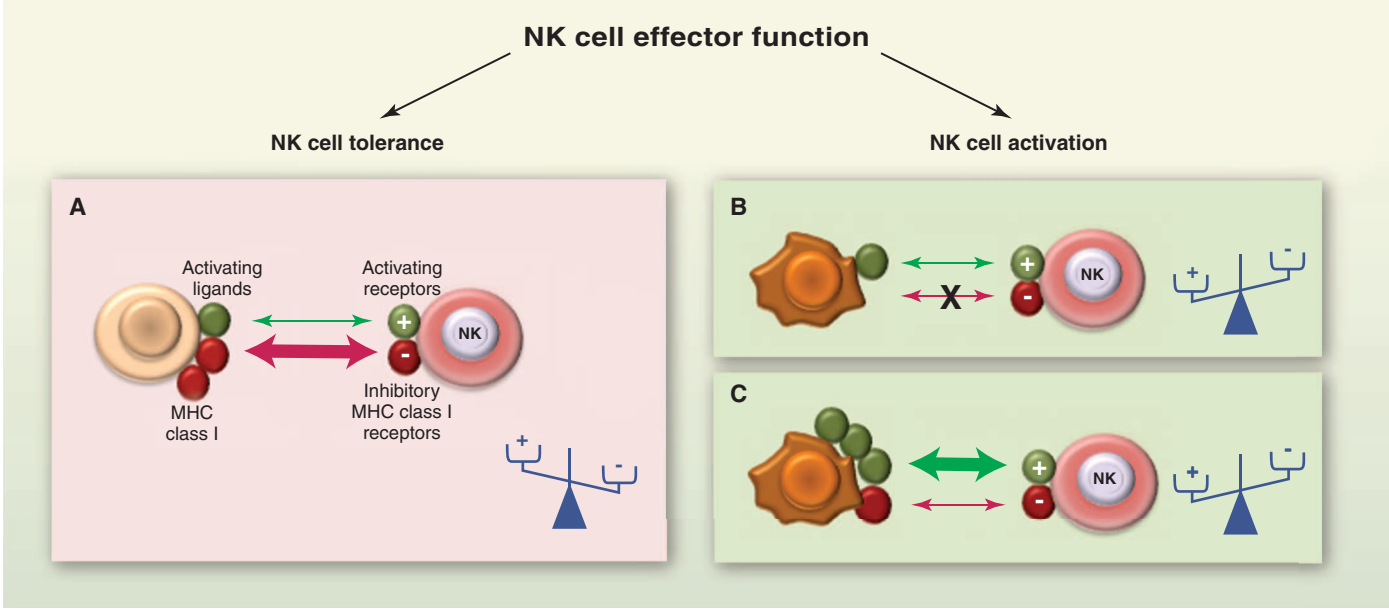

Fig. 3. The dynamic regulation of NK cell effector function. NK cells sense the density of various cell surface molecules expressed at the surface of interacting cells. The integration of these distinct signals dictates the quality and the intensity of the NK cell response. NK cells spare healthy cells that express self-MHC class I molecules and low amounts of stress-induced self molecules (**A**), whereas they selectively kill target cells "in distress" that down-regulate MHC class I molecules (**B**) or up-regulate stress-induced self molecules (**C**). +, activating receptors; –, inhibitory receptors.

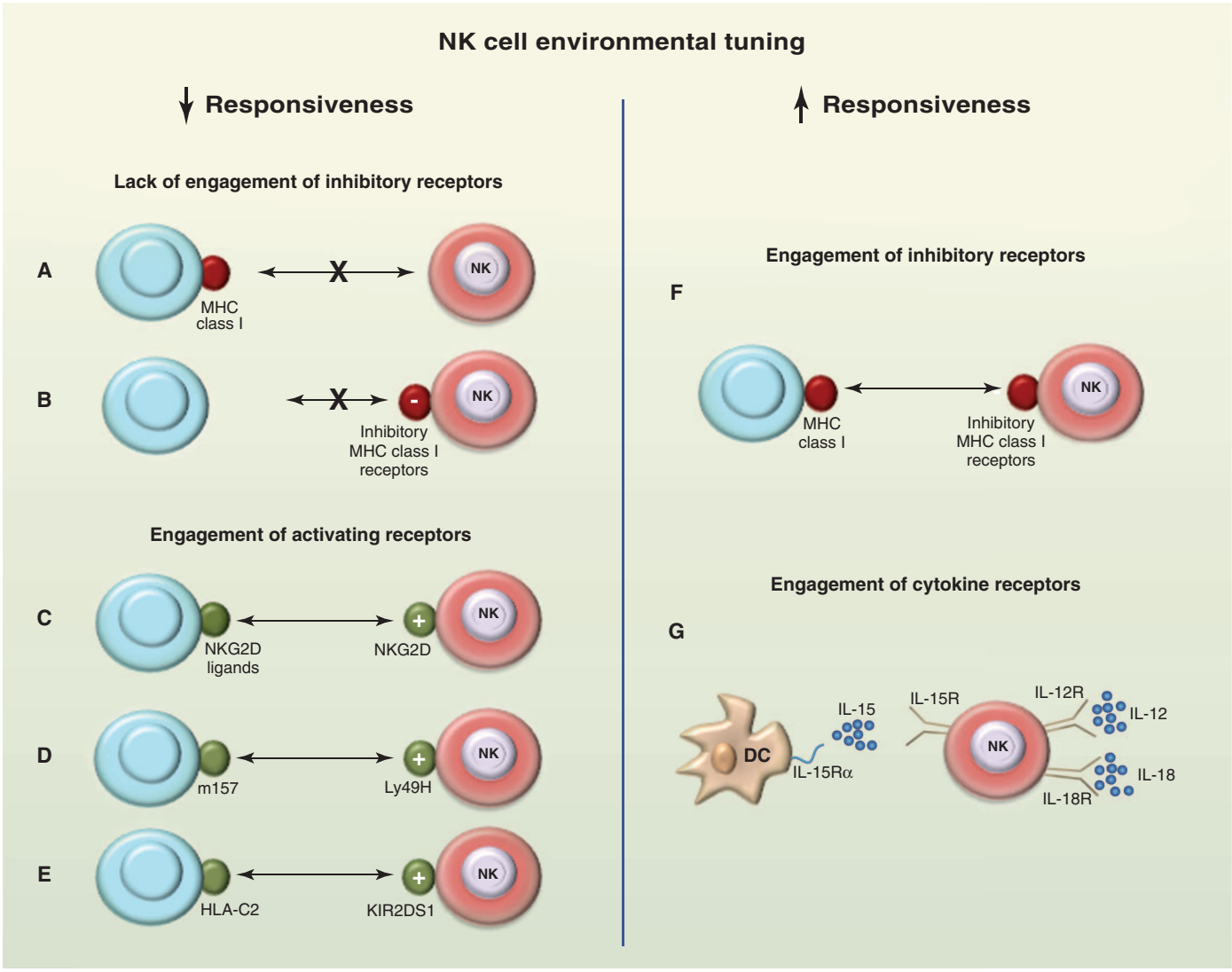

Fig. 4. NK cell tuning. Experimental conditions in which NK cells have been shown to adapt to their environment are schematized. In the absence of detection of MHC class I, such as when NK cells lack cognate MHC class I receptors (**A**) or in MHC class I–deficient hosts (**B**), NK cells are hyporesponsive at steady state. NK cells are rendered "anergic" by the chronic engagement of various activating receptors such as NKG2D (**C**), Ly49H in the mouse (**D**), or KIR2DS1 in humans (**E**). NK cells can be educated by MHC class I molecules via their cognate inhibitory receptors in trans (**F**) or in cis (not depicted) and primed by cytokines (**G**).

maturation, which may depend on interactions between MHC and inhibitory receptors on NK cells. Other possibilities include the function of inhibitory receptors for non-MHC ligands or the action of suppressor cells, but these are unlikely to fully account for these outcomes.

Whatever the mechanism (or mechanisms), it must account for the existence of intermediate states of responsiveness. NK cells vary in the number and affinity of inhibitory receptors specific for self-MHC, and the functional response of NK cells to activating stimuli was shown to increase commensurately with the number of different inhibitory receptors for self-MHC that the NK cells expressed (*53*, *54*). Despite exhibiting greater responsiveness, NK cells with more inhibitory receptors are not autoreactive, because interactions of their inhibitory receptors with MHC class I molecules on normal cells inhibits their activity. Thus, NK cells appear to be "tuned" such that the greater effector cell inhibition that accompanies the expression of more inhibitory receptors is balanced by a greater potential responsiveness of the NK cells.

Several findings suggest that the responsiveness of mature NK cells is not fixed but may adapt to a changing environment in vivo. In the absence of infection or other disease, transfer of mature NK cells to mice with no MHC ligands led to a reduced responsiveness of the NK cells, indicating that encounters with cells lacking self-MHC, which would normally stimulate these cells, instead drive them into a hyporesponsive state (*55*). Conversely, transfer of NK cells from MHC-deficient mice to MHC class I^+ mice resulted in increased responsiveness, specifically of those NK cells with an inhibitory receptor specific for MHC molecules in the new host, indicating that the inhibitory interaction is instrumental in increasing NK responsiveness (*55*, *56*). Hence, persistent stimulation without inhibition results in NK cell hyporesponsiveness, whereas persistent stimulation coupled with commensurate inhibition results in NK cell responsiveness. These results suggest that NK cell tuning might occur throughout the lifetime of the NK cell under steady-state conditions. In infected animals, however, hyporesponsive NK cells are converted to a higher state of responsiveness. In fact, NK cells lacking self-MHC–specific inhibitory receptors play a more important role than other NK cells in protective responses to mouse cytomegalovirus infections (*57*), probably reflecting an increased responsiveness associated with infection coupled with the absence of inhibitory receptor interactions. Taken together, these findings suggest that in steady-state conditions, NK cell tuning enables those NK cells with inhibitory receptors for self-MHC to rapidly eliminate MHC class I–deficient cells that arise in the environment, whereas NK

cells with fewer such receptors can be mobilized by inflammatory signals that accompany pathogen infections (*38*, *48*).

Can NK Cell Reactivity Be Manipulated in Anticancer Treatments?

The dissection of NK cell reactivity has unveiled the basis of the recognition of tumor cells by NK cells. In mice, NK cells reject tumors that lack MHC class I expression or overexpress NKG2D ligands or costimulatory signals, a phenomenon facilitating T cell–mediated antitumor immunity. NK cells protect the host against methylcholanthrene-induced sarcomas and against B cell lymphoma arising in mice lacking perforin and β2 microglobulin (a component of MHC class I) (*58*). In humans, the major receptors responsible for tumor recognition by NK cells are NKp46, NKp30, NKp44, DNAM1, and NKG2D. The NK cell-mediated lysis of tumor cells involves several such receptors, depending on the malignancy. The target cell ligands recognized by some receptors have been identified, such as MICA/B and the ULBPs for NKG2D, PVR and Nectin-2 for DNAM-1, and B7-H6 for NKp30, which are primarily expressed or up-regulated on cells after activation, proliferation, or cellular transformation (*31*).

Several lines of evidence indicate that NK cells or their receptors have a role in immunosurveillance of spontaneous tumors, including in humans. Indeed, tumors have evolved mechanisms to escape NK cell control such as the shedding of soluble NKG2D ligands that function as decoys for the activating NKG2D receptor on NK cells, a phenomenon correlating with poor prognosis in human melanoma and prostate cancer (*58*). Mice deficient in NKG2D exhibited a higher incidence or greater severity of tumors in transgenic models of cancer (*59*). Furthermore, studies with mice deficient in DNAM-1, NKp46, or NKG2D demonstrate that in the presence of NK cells, tumors alter their expression of ligands (*60*, *61*). In addition, an 11-year follow-up survey revealed that low NK lytic activity is associated with cancer risk (*62*).

This knowledge has prompted efforts to harness NK cell functions for an improved management of cancer patients. The seminal observation was the demonstration in humans that the success of T cell–depleted HSCT for the treatment of leukemia patients is much greater when the recipient lacks one HLA haplotype compared with the donor marrow and donor NK cells are present in the bone marrow cell infusion (*63*). This outcome can be attributed to "missing-self" recognition by a subset of donor alloreactive NK cells of the recipient's tumor cells (*64*). These alloreactive NK cells, which express KIRs that do not recognize MHC molecules in the recipient, persist for several years and attack the recipient's leukemic cells (graft versus leukemia reaction) but fail to cause the generalized graft-versus-host disease that alloreactive T cells can cause (*65*, *66*). These NK cells have been shown also to promote engraftment and prevent graft-versus-host disease due to their ability to kill recipient antigen-presenting cells (*63*). On the basis of the education and tuning phenomena, these alloreactive NK cells would be expected to be hyporesponsive. Potentially, the infusion of large numbers of $CD34^+$ cells provides a hematopoietic microenvironment predominantly of donor type in which the process of NK cell education and tuning would be similar to that occurring in the donor and result in generation of NK cells displaying alloreactivity against leukemic blasts. Recently, an alternative to manipulating NK cell–mediated "missing self" recognition has been set up, using the infusion of human monoclonal antibodies to KIR in cancer patients (*67*). These protocols are being tested in phase II clinical trials in acute myeloid leukemia and multiple myeloma. Finally, production of clinical-grade human NK cells has proven feasible, safe, and promising (*65*, *68*), and combinations of adoptive NK cell transfer with therapeutic monoclonal antibodies are being conducted. NK cell–based therapy should benefit from a better knowledge of NK cell biodistribution and homing in vivo, identification of ligands for some activating receptors, and NK-specific immunosuppressive and immunomodulatory mechanisms. Additional studies on the role of NK cell education and KIR mismatch may also provide optimal strategies for exploiting NK cells in antitumor therapies. Moreover, genetic epidemiologic studies have shown that the expression of certain KIRs and MHC class I polymorphisms are linked to resistance to several microbes, such as human immunodeficiency virus type 1 (HIV-1) and hepatitis C, or to susceptibility to various autoimmune or inflammatory syndromes (*69*). As KIR can also be expressed by T cell subsets, the direct relevance of some of these data to NK cell biology remains to be firmly established. Nevertheless, these studies prompt us to extend the design of NK cell–based therapies to other disease conditions than cancer, such as infections and inflammation.

Do NK Cells Remember?

Immunological memory is a hallmark of adaptive immunity and is characterized by the long-term persistence of memory cells that rapidly undergo clonal expansion and present enhanced effector functions in response to secondary challenge. Although recent findings have shown a form of immunological memory in lower organisms that are reported to lack adaptive immunity (*70*), the innate immune system has been commonly considered to lack the capacity for immunological memory. Moreover, in the case of mature NK cells, their half-life has been estimated to be 17 days in steady-state conditions (*71*). Therefore, recent findings that at least some mature NK cells or their progeny can be long-lived and that NK cells can mount a robust recall response are quite striking.

The first evidence for NK cell memory was observed in a model of hapten-induced contact hypersensitivity in recombination activating gene–2 (Rag-2)–deficient mice, which lack T and B cells but possess NK cells (*72*). Hapten-induced contact hypersensitivity (CHS) was previously thought to be mediated only by $CD4^+$ T cells after priming mice with a chemical hapten. Unexpectedly, this NK cell–mediated CHS response in Rag-2–deficient mice could be detected for at least a month after chemical priming, and the response was hapten-specific. These "memory" NK cells were unexpectedly found to reside only in the liver, but not in the spleen, and were marked by high levels of expression of cell surface Thy1 (*72*) and CXCR6 (*73*). A hapten-specific CHS response was observed in mice receiving an adoptive transfer of liver NK cells from hapten-primed mice. Although blocking the NKG2D receptor on the NK cells inhibited the CHS, the receptor responsible for hapten-specific recognition has not been identified (*72*, *73*).

NK cell memory has also been demonstrated in viral infections. In C57BL/6 mice, the activating Ly49H receptor recognizes the mouse cytomegalovirus (MCMV) m157 glycoprotein that is displayed on the cell surface of infected cells, resulting in NK cell–mediated control of the infection (*23*, *24*). After infection with MCMV, these $Ly49H^+$ NK cells undergo preferential expansion (*74*). In experiments in which genetically marked, mature $Ly49H^+$ NK cells were adoptively transferred into recipients infected with MCMV, the $Ly49H^+$ NK cell population underwent contraction after control of the virus, but memory NK cells could be detected in the recipient more than a month later (*75*). Similar to memory T lymphocytes, upon restimulation these memory NK cells demonstrated enhanced cytolytic function and cytokine production compared with "naïve" NK cells and were more efficient at protecting MCMV-susceptible neonatal mice against infection (*75*). Memory NK cells isolated from the first host can be adoptively transferred to a second and even a third recipient and undergo subsequent rounds of proliferation in response to MCMV infection (*75*). At about 2 months after the initial infection with MCMV, memory NK cells could be detected in essentially all tissues and organs, including spleen, lymph nodes, liver, lung, and kidney (*75*). Although there is as yet no unique marker of memory, these long-lived MCMV-expanded NK cells stably express high levels of KLRG1, an inhibitory receptor that recognizes cadherins. Recently, memory NK cells have been described in mice after exposure to influenza, vesicular stomatitis virus (VSV), or HIV-1 (*73*), although a virus-specific NK receptor for these pathogens has not been identified.

In addition, recent studies have demonstrated that NK cells activated with cytokines in vitro and adoptively transferred into naïve recipients can also persist for at least a month and have an enhanced ability to produce cytokines upon restimulation (*76*). These findings suggest that, once activated, mature NK cells may acquire stable, heritable properties that influence their be-

havior during subsequent infections. Thus, NK cells appear to remember their past, a trait conventionally only considered possible for the adaptive immune system. The emerging evidence for immunological memory and the capacity for self-renewal of mature cells in the NK cell lineage raises many questions: Can NK cells expanded in response to one pathogen provide enhanced protection against other unrelated pathogens, given that NK cells possess multiple activating receptors rather than a single, dominant antigen receptor like B and T cells? Is it possible to vaccinate NK cells for enhanced host defense? What receptor systems provide for hapten-specific recognition by NK cells? What epigenetic alterations account for the longevity and enhanced effector functions demonstrated by memory NK cells? Can NK cells, like T cells, differentiate into functionally distinct subsets with regulatory roles in shaping the magnitude and nature of the immune response to different pathogens? Is memory confined to a certain subset of NK cells, as suggested by their apparent localizing in the liver as observed in some experimental systems?

Innate or Adaptive Immunity?

In addition to the above questions that they raise, recent advances in NK cell biology have thus shown that NK cells have attributes of both innate and adaptive immunity. These findings also lead to the speculation that the shared innate and adaptive features are likely not unique to NK cells. Along this line, macrophages rapidly phagocytose CD47-deficient erythrocytes, because the inhibitory macrophage receptor SIRP1α is no longer engaged by CD47, but macrophages from CD47-deficient mice do not phagocytose CD47-deficient erythrocytes (*77*), suggesting that macrophages have adapted to the absence of CD47 in their environment. Therefore, macrophages might undergo a process of education through the interaction of the ITIM-bearing SIRP1α with its cognate CD47 ligand, reminiscent of NK cell education through MHC class I–specific receptor engagement. Thus, notions originally restricted to T and B cells, such as diverse receptor repertoires, education, and memory, which now apply to NK cells, prompt investigation into whether other innate immune cells show similar properties. Therefore, defining "innate" as having germline-encoded receptors versus "adaptive" as having rearranged receptors appears sufficient to distinguish these two arms of immunity.

References and Notes

1. R. B. Herberman, M. E. Nunn, D. H. Lavrin, *Int. J. Cancer* **16**, 216 (1975).
2. R. Kiessling, E. Klein, H. Wigzell, *Eur. J. Immunol.* **5**, 112 (1975).
3. C. Eidenschenk *et al.*, *Am. J. Hum. Genet.* **78**, 721 (2006).
4. S. H. Lee, T. Miyagi, C. A. Biron, *Trends Immunol.* **28**, 252 (2007).
5. M. J. Smyth, Y. Hayakawa, K. Takeda, H. Yagita, *Nat. Rev. Cancer* **2**, 850 (2002).
6. A. Fischer, *Immunity* **27**, 835 (2007).
7. C. A. Jansen *et al.*, *Dev. Comp. Immunol.* **34**, 759 (2010).
8. A. Moffett-King, *Nat. Rev. Immunol.* **2**, 656 (2002).
9. T. Walzer, M. Dalod, S. H. Robbins, L. Zitvogel, E. Vivier, *Blood* **106**, 2252 (2005).
10. A. Moretta *et al.*, *Trends Immunol.* **26**, 668 (2005).
11. A. Martín-Fontecha *et al.*, *Nat. Immunol.* **5**, 1260 (2004).
12. S. H. Robbins *et al.*, *PLoS Pathog.* **3**, e123 (2007).
13. P. Krebs *et al.*, *Blood* **113**, 6593 (2009).
14. D. M. Andrews *et al.*, *J. Exp. Med.* **207**, 1333 (2010).
15. M. Lucas, W. Schachterle, K. Oberle, P. Aichele, A. Diefenbach, *Immunity* **26**, 503 (2007).
16. E. Mortier *et al.*, *Immunity* **31**, 811 (2009).
17. S. Guia *et al.*, *Blood* **111**, 5008 (2008).
18. J. Chaix *et al.*, *J. Immunol.* **181**, 1627 (2008).
19. E. Vivier, J. A. Nunès, F. Vély, *Science* **306**, 1517 (2004).
20. Y. T. Bryceson, M. E. March, H. G. Ljunggren, E. O. Long, *Immunol. Rev.* **214**, 73 (2006).
21. M. A. Caligiuri, *Blood* **112**, 461 (2008).
22. T. Hughes *et al.*, *Immunity* **32**, 803 (2010).
23. H. Arase, E. S. Mocarski, A. E. Campbell, A. B. Hill, L. L. Lanier, *Science* **296**, 1323 (2002).
24. H. R. Smith *et al.*, *Proc. Natl. Acad. Sci. U.S.A.* **99**, 8826 (2002).
25. O. Mandelboim *et al.*, *Nature* **409**, 1055 (2001).
26. A. Moretta *et al.*, *Annu. Rev. Immunol.* **19**, 197 (2001).
27. T. Walzer *et al.*, *Proc. Natl. Acad. Sci. U.S.A.* **104**, 3384 (2007).
28. E. Vivier, H. Spits, T. Cupedo, *Nat. Rev. Immunol.* **9**, 229 (2009).
29. H. Veiga-Fernandes, D. Kioussis, M. Coles, *J. Exp. Med.* **207**, 269 (2010).
30. S. Chiesa *et al.*, *Blood* **107**, 2364 (2006).
31. C. Bottino, R. Castriconi, L. Moretta, A. Moretta, *Trends Immunol.* **26**, 221 (2005).
32. D. H. Raulet, N. Guerra, *Nat. Rev. Immunol.* **9**, 568 (2009).
33. C. S. Brandt *et al.*, *J. Exp. Med.* **206**, 1495 (2009).
34. K. Kärre, H. G. Ljunggren, G. Piontek, R. Kiessling, *Nature* **319**, 675 (1986).
35. F. M. Karlhofer, R. K. Ribaudo, W. M. Yokoyama, *Nature* **358**, 66 (1992).
36. A. Moretta *et al.*, *Annu. Rev. Immunol.* **14**, 619 (1996).
37. N. C. Fernandez *et al.*, *Blood* **105**, 4416 (2005).
38. S. Kim *et al.*, *Nature* **436**, 709 (2005).
39. L. L. Lanier, *Annu. Rev. Immunol.* **23**, 225 (2005).
40. A. Moretta *et al.*, *J. Exp. Med.* **182**, 875 (1995).
41. C. A. Stewart *et al.*, *Proc. Natl. Acad. Sci. U.S.A.* **102**, 13224 (2005).
42. P. Parham, *Nat. Rev. Immunol.* **5**, 201 (2005).
43. N. Anfossi *et al.*, *Immunity* **25**, 331 (2006).
44. N.-S. Liao, M. Bix, M. Zijlstra, R. Jaenisch, D. Raulet, *Science* **253**, 199 (1991).
45. P. Höglund *et al.*, *Eur. J. Immunol.* **28**, 370 (1998).
46. J. Zimmer *et al.*, *J. Exp. Med.* **187**, 117 (1998).
47. S. Cooley *et al.*, *Blood* **110**, 578 (2007).
48. D. H. Raulet, R. E. Vance, *Nat. Rev. Immunol.* **6**, 520 (2006).
49. P. Höglund, P. Brodin, *Nat. Rev. Immunol.* **10**, 724 (2010).
50. S. K. Tripathy *et al.*, *J. Exp. Med.* **205**, 1829 (2008).
51. J. C. Sun, L. L. Lanier, *J. Exp. Med.* **205**, 1819 (2008).
52. C. Fauriat, M. A. Ivarsson, H. G. Ljunggren, K. J. Malmberg, J. Michaëlsson, *Blood* **115**, 1166 (2010).
53. P. Brodin, K. Kärre, P. Höglund, *Trends Immunol.* **30**, 143 (2009).
54. N. T. Joncker, N. C. Fernandez, E. Treiner, E. Vivier, D. H. Raulet, *J. Immunol.* **182**, 4572 (2009).
55. N. T. Joncker, N. Shifrin, F. Delebecque, D. H. Raulet, *J. Exp. Med.* **207**, 2065 (2010).
56. J. M. Elliott, J. A. Wahle, W. M. Yokoyama, *J. Exp. Med.* **207**, 2073 (2010).
57. M. T. Orr, W. J. Murphy, L. L. Lanier, *Nat. Immunol.* **11**, 321 (2010).
58. M. Terme, E. Ullrich, N. F. Delahaye, N. Chaput, L. Zitvogel, *Nat. Immunol.* **9**, 486 (2008).
59. N. Guerra *et al.*, *Immunity* **28**, 571 (2008).
60. A. Iguchi-Manaka *et al.*, *J. Exp. Med.* **205**, 2959 (2008).
61. M. Elboim *et al.*, *J. Immunol.* **184**, 5637 (2010).
62. K. Imai, S. Matsuyama, S. Miyake, K. Suga, K. Nakachi, *Lancet* **356**, 1795 (2000).
63. L. Ruggeri *et al.*, *Science* **295**, 2097 (2002).
64. P. Parham, K. L. McQueen, *Nat. Rev. Immunol.* **3**, 108 (2003).
65. H. G. Ljunggren, K. J. Malmberg, *Nat. Rev. Immunol.* **7**, 329 (2007).
66. D. Pende *et al.*, *Blood* **113**, 3119 (2009).
67. F. Romagné *et al.*, *Blood* **114**, 2667 (2009).
68. J. S. Miller *et al.*, *Blood* **105**, 3051 (2005).
69. S. I. Khakoo, M. Carrington, *Immunol. Rev.* **214**, 186 (2006).
70. J. Kurtz, *Trends Immunol.* **26**, 186 (2005).
71. A. M. Jamieson, P. Isnard, J. R. Dorfman, M. C. Coles, D. H. Raulet, *J. Immunol.* **172**, 864 (2004).
72. J. G. O'Leary, M. Goodarzi, D. L. Drayton, U. H. von Andrian, *Nat. Immunol.* **7**, 507 (2006).
73. S. Paust *et al.*, *Nat. Immunol.* **11**, 1127 (2010).
74. A. O. Dokun *et al.*, *Nat. Immunol.* **2**, 951 (2001).
75. J. C. Sun, J. N. Beilke, L. L. Lanier, *Nature* **457**, 557 (2009).
76. M. A. Cooper *et al.*, *Proc. Natl. Acad. Sci. U.S.A.* **106**, 1915 (2009).
77. H. Wang *et al.*, *Proc. Natl. Acad. Sci. U.S.A.* **104**, 13744 (2007).
78. V. Kumar, M. E. McNerney, *Nat. Rev. Immunol.* **5**, 363 (2005).

79. The authors apologize for not having been able to quote all relevant papers due to space limitations and thank C. Beziers-Lafosse (CIML) for excellent graphic assistance as well as members of their laboratories for help and discussions. E.V. and S.U. are supported by grants from the Agence Nationale de la Recherche (ANR), Ligue Nationale Contre le Cancer (Equipe Labellisée "La Ligue"), Fondation Del Duca, and institutional grants from INSERM, CNRS, and Université de la Méditerranée to the CIML. E.V. is a scholar from the Institut Universitaire de France and is a cofounder and shareholder of Innate-Pharma. D.H.R. is supported by NIH grants AI035021, AI039642, and CA093678 and is a scientific board member and shareholder of Innate-Pharma. A.M. is supported by grants awarded by Associazione Italiana per la Ricerca sul Cancro (AIRC), Ministero dell'Istruzione, dell'Università e della Ricerca, and a Special Project from the AIRC and is a cofounder and shareholder of Innate-Pharma. M.A.C. is supported by U.S. National Cancer Institute grants CA16058, CA95426, and CA68458. L.Z. is supported by Institut National du Cancer, ANR, Ligue Nationale Contre le Cancer (Equipe Labellisée "La Ligue"), and INFLARE EU grants. L.L.L. is an American Cancer Society professor and is supported by NIH grants AI068129, CA095137, and AI066897 and is a consultant for Novo Nordisk and SBI Biotech Co., Ltd. W.M.Y. is supported by the Howard Hughes Medical Institute and NIH grants AI33903, AI34385, AI51345, and AI5716.

10.1126/science.1198687

Freshwater Methane Emissions Offset the Continental Carbon Sink

David Bastviken,[1]* Lars J. Tranvik,[2] John A. Downing,[3] Patrick M. Crill,[4] Alex Enrich-Prast[5]

A cornerstone of our understanding of the contemporary global carbon cycle is that the terrestrial land surface is an important greenhouse gas (GHG) sink (*1*, *2*). The global land sink is estimated to be 2.6 ± 1.7 Pg of C $year^{-1}$ (variability ± range, excluding C emissions because of deforestation) (*1*). Lakes, impoundments, and rivers are parts of the terrestrial landscape, but they have not yet been included in the terrestrial GHG balance (*3*, *4*). Available data suggest, however, that freshwaters can be substantial sources of CO_2 (*3*, *5*) and CH_4 (*6*). Over time, soil carbon reaches freshwaters by lateral hydrological transport, where it can meet several fates, including burial in sediments, further transport to the sea, or evasion to the atmosphere as CO_2 or CH_4 (*7*). CH_4 emissions may be small in terms of carbon, but CH_4 is a more potent GHG than CO_2 over century time scales. This study indicates that global CH_4 emissions expressed as CO_2 equivalents correspond to at least 25% of the estimated terrestrial GHG sink.

CH_4 can be emitted from freshwaters through several different pathways, including ebullition (bubble flux from sediments), diffusive flux, and plant-mediated transport through emergent aquatic plants (*6*). Additional pathways may be important for hydroelectric reservoirs, such as emissions upon passage through turbines and downstream of reservoirs (*8*, *9*). We compiled CH_4 emission estimates from 474 freshwater ecosystems for which the emission pathways were clearly defined (Table 1) (*10*).

By using recent data on the area and distribution of inland waters (*11*, *12*), we estimate the total CH_4 emission from freshwaters to be 103 Tg of CH_4 $year^{-1}$ (Table 1). Expressed as CO_2 equivalents (eq), this corresponds to 0.65 Pg of C (CO_2 eq) $year^{-1}$ or 25% of the estimated land GHG sink, assuming that 1 kg of CH_4 corresponds to 25 kg of CO_2 over a 100-year period (*13*). Ebullition and plant flux, which are both poorly represented in the data set, dominate the other flux pathways that have been studied more frequently (Table 1). Ebullition is most likely to be underestimated because it is episodic and not representatively captured by the usual short-term measurements (*6*). Accordingly, our global estimate of freshwater CH_4 emissions is probably conservative. For further discussion of the results, see supporting online material (SOM) text.

This study indicates that CH_4 emissions from freshwaters can substantially affect the global land GHG sink estimate. Moreover, proper consideration of ebullition and plant-mediated emission will most likely result in increased future estimates of CH_4 emission. Combining the present CH_4 emission estimate of 0.65 Pg of C (CO_2 eq) $year^{-1}$ with the most recent estimate of freshwater CO_2 emissions, 1.4 Pg of C (CO_2 eq) $year^{-1}$ (*5*)—together corresponding to 79% of the estimated land GHG sink—it becomes clear that freshwaters are an important component of the continental GHG balance. Accordingly, the terrestrial GHG sink may be smaller than currently believed, and data on GHG release from inland waters are needed in future revision of net continental GHG fluxes.

Table 1. Freshwater CH_4 emissions (Emiss., in Tg CH_4 $year^{-1}$) estimated from average areal estimates (flux m^{-2} $year^{-1}$) times the areal estimates for different latitudes (*10*). Total open water is the sum of open water fluxes, that is, ebullition, diffusive flux, and flux when CH_4 stored in the water column is emitted upon lake overturn (Stored). *n* and CV (%) denote the sample size (number of systems) and the coefficient of variation. Note the small sample size for many large emission values. The total sums of the yearly fluxes are expressed in Tg CH_4. Lake and river areas are from (*11*); reservoir areas, from (*12*). Plant fluxes (plant-mediated emission) are according to (*10*).

Latitude	Fluxes												Area (km^2)
	Total open water			Ebullition			Diffusive			Stored			
	Emiss.	*n*	CV	Emiss.	*n*	CV	Emiss.	*n*	CV	Emiss.	*n*	CV	
Lakes													
>66°	6.8	17	72	6.4	17	74	0.7	60	37				288,318
>54°–66°	6.6	5	155	9.1	9	60	1.1	271	185	0.1	217	2649	1,533,084
25°–54°	31.6	15	127	15.8	15	177	4.8	33	277	3.7	36	125	1,330,264
<24°	26.6	29	51	22.2	28	54	3.1	29	97	21.3	1		585,536*
Reservoirs													
>66°	0.2†												35,289
>54°–66°	1.0	24	176	1.8	2	140	0.2	4	93				161,352
25°–54°	0.7‡												116,922
<24°	18.1	11	87										186,437
Rivers													
>66°	0.1	1											38,895
>54°–66°	0.2†												80,009
25°–54°	0.3	20	302										61,867
<24°	0.9‡												176,856
Sum open water	93.1	116		55.3	71		9.9	397		25.1	254		
Plant flux	10.2												
Sum all	103.3												

*Likely underestimated. For comparison, the mean flooded areas for the major South American savanna wetlands and the lowland Amazon (below 500 m above sea level) are 115,620 km^2 and 750,000 km^2, respectively (*14*). †Estimated assuming similar emissions per area unit at latitudes >54°. ‡Estimated assuming similar emissions per area unit at latitudes from 0° to 54°.

References and Notes

1. K. L. Denman *et al.*, in *Climate Change 2007: The Physical Science Basis*, S. Solomon *et al.*, Eds. (Cambridge Univ. Press, New York, 2007), chap. 7.
2. S. Luyssaert *et al.*, *Nature* **455**, 213 (2008).
3. T. J. Battin *et al.*, *Nat. Geosci.* **2**, 598 (2009).
4. J. J. Cole *et al.*, *Ecosystems* **10**, 171 (2007).
5. L. J. Tranvik *et al.*, *Limnol. Oceanogr.* **54**, 2298 (2009).
6. D. Bastviken, J. J. Cole, M. L. Pace, L. J. Tranvik, *Global Biogeochem. Cycles* **18**, GB4009 (2004).
7. G. Benoy, K. Cash, E. McCauley, F. Wrona, *Environ. Rev.* **15**, 175 (2007).
8. F. Guérin *et al.*, *Geophys. Res. Lett.* **33**, L21407 (2006).
9. A. Kemenes, B. R. Forsberg, J. M. Melack, *Geophys. Res. Lett.* **34**, L12809 (2007).
10. Materials and methods are available as supporting material on *Science* Online.
11. J. A. Downing, C. Duarte, in *Encyclopedia of Inland Waters*, G. E. Likens, Ed. (Elsevier, Oxford, 2009), vol. 1.
12. International Commission on Large Dams, *The Dams Newsletter*, issue no. 5 (May 2006), p. 2; www.icold-cigb.net/images/PDF-multilangue/newsletter5.pdf.
13. P. Forster *et al.*, in *Climate Change 2007: The Physical Science Basis*, S. Solomon *et al.*, Eds. (Cambridge Univ. Press, New York, 2007), chap. 2.
14. J. M. Melack *et al.*, *Glob. Change Biol.* **10**, 530 (2004).

15. We thank J. Cole, N. Than Duc, and H. Marotta for valuable input. This study was supported by the Swedish Research Council (VR) and the Swedish Research Council for Environment, Agricultural Sciences, and Spatial Planning (Formas). Analyses of global surface water area come from the ITAC (Integrating the Terrestrial and Aquatic Carbon Cycle) Working Group supported by the National Center for Ecological Analysis and Synthesis, a center funded by NSF (grant DEB-94-21535), the University of California at Santa Barbara, and the state of California.

Supporting Online Material

www.sciencemag.org/cgi/content/full/331/6013/50/DC1
Materials and Methods
SOM Text
References

23 August 2010; accepted 19 November 2010
10.1126/science.1196808

[1]Department of Thematic Studies–Water and Environmental Studies, Linköping University, SE-58183 Linköping, Sweden. [2]Department of Limnology, Evolutionary Biology Centre, Uppsala University, SE-75236 Uppsala, Sweden. [3]Department of Ecology, Evolution, and Organismal Biology, Iowa State University, Ames, IA 50011, USA. [4]Department of Geological Sciences, Stockholm University, SE-10691 Stockholm, Sweden. [5]Department of Ecology, University Federal of Rio de Janeiro, 68020 Rio de Janeiro, Brazil.

*To whom correspondence should be addressed. E-mail: david.bastviken@liu.se

Biscrolling Nanotube Sheets and Functional Guests into Yarns

Márcio D. Lima, Shaoli Fang, Xavier Lepró, Chihye Lewis, Raquel Ovalle-Robles, Javier Carretero-González, Elizabeth Castillo-Martínez, Mikhail E. Kozlov, Jiyoung Oh, Neema Rawat, Carter S. Haines, Mohammad H. Haque, Vaishnavi Aare, Stephanie Stoughton, Anvar A. Zakhidov, Ray H. Baughman*

Multifunctional applications of textiles have been limited by the inability to spin important materials into yarns. Generically applicable methods are demonstrated for producing weavable yarns comprising up to 95 weight percent of otherwise unspinnable particulate or nanofiber powders that remain highly functional. Scrolled 50-nanometer-thick carbon nanotube sheets confine these powders in the galleries of irregular scroll sacks whose observed complex structures are related to twist-dependent extension of Archimedean spirals, Fermat spirals, or spiral pairs into scrolls. The strength and electronic connectivity of a small weight fraction of scrolled carbon nanotube sheet enables yarn weaving, sewing, knotting, braiding, and charge collection. This technology is used to make yarns of superconductors, lithium-ion battery materials, graphene ribbons, catalytic nanofibers for fuel cells, and titanium dioxide for photocatalysis.

Powders of particles or nanofibers are well-known additives for introducing new and improved functionality into yarns, and the importance of this area motivates new advances (*1*–*3*). Current methods use additive dispersion in a fiber matrix or incorporation on fiber surfaces, but problems remain: (i) powder loading levels are typically low, (ii) nanoparticle and nanofiber functionality can degrade when processing decreases accessible surface area, and (iii) powders on yarn surfaces can lack durability. Powders are rarely spinnable into yarns without changing basic structure; a notable exception is solution (*4*, *5*) and solid-state spun (*6*–*12*) carbon nanotubes (CNTs). Strong, weavable multifunctional yarns could be seamlessly integrated into intelligent clothing, structural textiles, and woven electrodes that are flexible, durable, and hierarchically engineered in porosity by yarn weaving, thereby providing advantages over conventional multifunctional film and bulk composites. Our goal is to spin porous multifunctional yarns in which a low concentration of strong host enables weavability, flexibility, and durability, while a high guest concentration adds functions such as energy storage, harvesting, and conversion.

Fabrication of biscrolled yarns. Our approach involves twist-based spinning of CNT sheets (the host) that are overlaid with a layer of up to 99 weight percent (wt %) of one or more other functional materials (the guest). We will scroll guest-host bilayers into a biscrolled yarn in which a minor CNT sheet concentration confines guest powders in down to nanometer-scale proximity in scroll galleries. The composition of biscrolled yarns is denoted X% guest@host$_{i,j}$, where X is the wt % of guest in the yarn and subscripts i and j denote the number of host sheet stacks under and over the guest layer, respectively.

Unless otherwise noted, the host sheets were drawn from carbon multiwalled nanotube (MWNT) forests grown by chemical vapor deposition (CVD). The forest height was typically ~350 μm, and the nanotubes had an outer diameter of ~9 nm and contained ~6 walls. Forest-drawn CNT sheets (*7*) were overlaid with the guest and then twist-spun using methods that, in some cases, are like those for making pure CNT yarns (*6*–*12*). The as-drawn CNT sheets have remarkable structure and properties (*6*, *7*, *13*) that are useful for making biscrolled yarns. Although these sheets are aerogels having a carbon network density (~1.5 mg/cm^3) close to that of air and an areal density of only about 1 to 3 μg/cm^2, they have a high specific strength (i.e., strength normalized by density) of up to 144 MPa cm^3/g (*7*). Densification decreases sheet thickness to as low as 50 nm and increases nanotube direction sheet specific strength to 560 MPa cm^3/g, compared with ~125 MPa cm^3/g for the Mylar and Kapton used for ultralight air vehicles (*7*). Using an approximate density of 0.8 g/cm^3 for the densified sheet, the unnormalized strengths for the nanotube sheet and the Mylar and Kapton are 450 MPa and 175 MPa.

Biscrolling begins with fabrication of a guest/host stack by depositing guest material onto (i) a

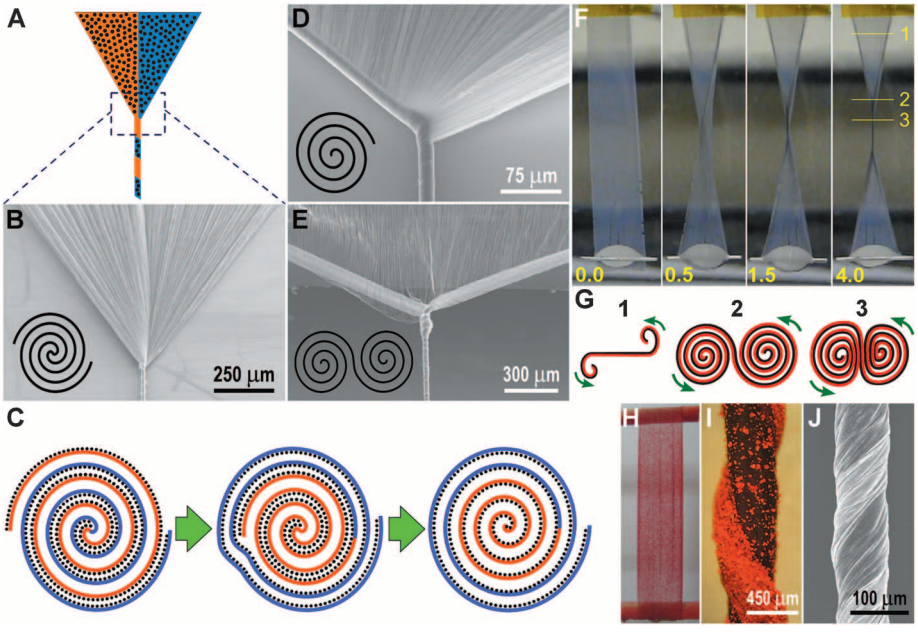

Fig. 1. (**A**) Illustration of biscrolling by twist insertion in a spinning wedge, where black dots represent guest particles. (**B**) SEM micrograph of Fermat-type twist insertion during spinning from a MWNT forest. The inset illustrates a Fermat scroll. (**C**) Illustration of evolution from a Fermat scroll to an Archimedean scroll. (**D** and **E**) SEM images of guest-free spinning wedges showing Archimedean (D) and dual Archimedean (E) scrolls, which are illustrated in the insets. (**F**) Sequential photographs of liquid-state twist insertion in a 1-cm-wide MWNT sheet that is coated with filtration-deposited 92 wt % boron nitride nanotube guest. The number of inserted turns is shown at the bottom of each photograph. (**G**) Illustration of the expected cross sections at the positions marked in (F). (**H** and **I**) Photographs of a 1-cm-wide, bilayered stack fabricated by electrostatic deposition of a commercial red paint powder on a single MWNT sheet (H) and a biscrolled yarn made by dry-state twist insertion in a stack of eight MWNT sheets that was similarly electrostatically coated with this dry red paint (I) (*14*). (**J**) SEM image of a 70% Ti@MWNT$_{2,0}$ biscrolled yarn produced by symmetrically inserting twist in a rectangular bilayer sheet that is rigidly supported in a liquid bath. The Ti guest was deposited by electron beam evaporation.

The Alan G. MacDiarmid NanoTech Institute, University of Texas at Dallas, Richardson, TX 75083, USA.

*To whom correspondence should be addressed: E-mail: ray.baughman@utdallas.edu

CNT sheet wedge directly produced by twist-based spinning from a forest (Fig. 1, A, B, and D) or (ii) forest-drawn CNT sheets (Fig. 1, E and F) (*14*). Guest deposition onto a CNT web using an electrostatic powder coating gun is fast and controllable due to attraction between charged guest particles and the oppositely charged web (Fig. 1, H and I) (*14*). Other liquid-free guest deposition processes include electron beam evaporation (Fig. 1J), sputtering, and aerosol filtration (Fig. 2, E and F) (*14*). Liquid-based guest deposition also works, like using a MWNT sheet stack as a filter to capture liquid-dispersed, CVD-synthesized (*15*) boron nitride (BN) nanotubes (Fig. 1F), electrophoretic deposition, and ink-jet printing (*14*). Ink-jet printing of guest can be used for even a single self-supported MWNT sheet having 1 $\mu g/cm^2$ areal density and enables patterned depositions of guest—thereby producing engineered variation in guest composition along the yarn length and diameter (movie S3). In the liquid filtration method, MWNT sheets are placed on a filter membrane; liquid-dispersed particles/nanofibers are deposited on the nanotube sheets by filtration; the resulting bilayer guest/host stack on the filter membrane is cut into a strip, attached to end supports, and mounted in a liquid bath, where the filter membrane is dissolved so that twist can be inserted (Fig. 1F and fig. S3) (*14*).

The process for biscrolled yarn fabrication ends with twisting a bilayer guest/sheet stack to make yarn. The amount of inserted twist was typically selected so that the yarn bias angle (the angle between yarn direction and the orientation direction of helically wrapped nanotubes on the outer yarn surface) was between about 30° and 45° (*14*). Although use of such large twist angles does not maximize tensile strength for guest-free yarn, it provides high compressive forces that are useful for confining guest powders in biscrolled yarns.

Biscrolling can be easily extended from CNT host to electrically insulating hosts such as SiO_2 and Si_3N_4 nanotubes (*14*). Individual CNTs and CNT bundles in free-standing, forest-drawn MWNT sheets were conformally coated with from 4-nm- to 18-nm-thick SiO_2 or Si_3N_4 by plasma-enhanced CVD. Both ceramic-coated CNT sheets and derived ceramic nanotube sheets, with CNT cores oxidatively removed, were twist-spun to make yarns (fig. S5D), and both can be overlaid with other functional materials to enable the spinning of biscrolled yarns (*14*). Figure 3, A and B, shows a Si_3N_4NT@$MWNT_{0,2}$ biscrolled yarn made by twist-based spinning a stack of Si_3N_4NT sheets and solid-state-drawn MWNT sheets. Conformally coating MWNTs in MWNT sheets with ~18-nm thickness of Si_3N_4 does not appreciably affect the in-plane sheet conductance or the conductance of derived twisted yarns.

Structure development and transitions for scrolled and biscrolled yarn. Can we find ways to dramatically modify yarn structure, so that future efforts can optimize yarn properties by structure manipulation? Toward this goal, we have discovered that fundamentally different nanotube yarn structures are produced by changing spinning conditions and resulting parameters (such as end constraints, stress asymmetry during spinning, spinning-wedge base width, and "wedge angle," the total apex angle where the wedge converges to yarn) (*14*). The observed structures (Figs. 1 and 2) are related to Archimedean and Fermat spirals and more complicated interconnected spirals. Accordingly, ignoring the radial dependence of interlayer spacings, we name structures observed for biscrolled and guest-free yarns as Archimedean, Fermat, and dual Archimedean scrolls. "Archimedean" means that a sheet edge is buried deep in a scroll, and "dual Archimedean" means that sheet edges are buried in different interconnected scrolls, like in two dimensions for a Cornu spiral (Fig. 1, E and G) (*16*).

In Fermat biscrolling (or Fermat scrolling for a guest-free yarn), the twist process starts from the center of a symmetric spinning wedge, as shown in Fig. 1, A and B. The edges of the spinning wedge wrap (i.e., scroll) in opposite directions around the thereby formed scroll core (Fig. 1B and fig. S2A), so that both wedge edges are exterior in the final yarn. Asymmetry in the stress applied to opposite sides of the spinning wedge can displace the core of the Fermat scroll from the center of the spinning wedge, so that one edge of the spinning wedge twists on top of the other, thereby burying this latter edge in an unbalanced Fermat scroll, as illustrated in Fig. 1C. If the scroll core is moved to a wedge edge (Fig. 1D and fig. S2B), scroll unbalancing is complete and an Archimedean scroll results. Because they have similar geometry, we approximate a highly unbalanced Fermat scroll by an Archimedean scroll and a largely balanced Fermat scroll as a Fermat scroll. Like a hanging curtain that is bunched at the bottom to form a wedge, use of a large wedge angle introduces pleats for Fermat scrolling and asymmetric Archimedean scrolling (Fig. 1, B and D, and fig. S2B) because of the need to incorporate the base width in a wedge width that decreases as the wedge apex is approached (*14*).

Spinning a rectangular sheet strip under constant load is more complicated than continuous spinning from a forest-derived wedge, for which we have observed only formation of single Fermat scrolls, single Archimedean scrolls, and intermediate states between these extremes. Twist of a rectangular sheet starts with sheet folding that is origami-like, except that plastic sheet deformation occurs. This folding repeats during subsequent rotations to form a new system of folds until two spinning wedges are obtained. Subsequently, for symmetric twisting, two interconnected Archimedean scrolls form for each spinning wedge, which are centered on the folds located at wedge edges (Fig. 1F and movie S1). These Archimedean scrolls are ultimately twisted together as in two-ply yarn (Fig. 1, F, G, I, and J). Because the guest is exterior to the MWNT sheet for one scroll and interior for the second, the barber-pole–like structure of Fig. 1, I and J, arises

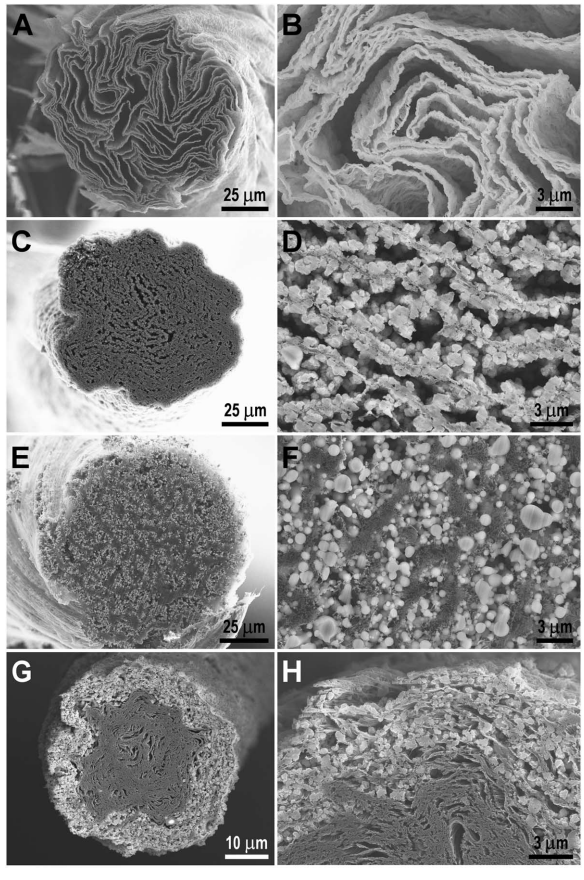

Fig. 2. SEM images of the cross sections of biscrolled yarns. (**A** and **B**) 70% Ti@$MWNT_{2,0}$ yarn fabricated by guest deposition using electron beam evaporation (25 nm Ti) and symmetrical twist insertion in liquid. (**C** and **D**) 93% TiO_2@$MWNT_{2,1}$ yarn made by filtration-based guest deposition and symmetrical twist in liquid. (**E** and **F**) TiO_2@$MWNT_{2,0}$ yarn made by aerosol-based guest deposition and twist insertion in air. (**G** and **H**) TiO_2@$MWNT_{2,1}$ yarn made by patterned filtration-based guest deposition on MWNT sheets and asymmetrical twist insertion in liquid. The patterned deposition was limited to a strip along the sheet's edge spanning 15% of its width.

in the final yarn. Conversely, applying sufficiently asymmetric loads to opposite sides of the bilayered sheet (by using nonparallel supporting rods) produces a single Archimedean scroll (*14*), with either the host or guest side of the bilayer exterior to the yarn.

The absence of observed Fermat scrolling for twisting a short rectangular sheet strip or bilayer stack between rigid supports (in either liquid or air) and the absence of observed formation of two interconnected Archimedean scrolls during continuous spinning from a forest wedge can be attributed to change from a rigid end support to one that enables partial relief of twist-generated strain. In fact, if we symmetrically twist a rectangular sheet strip that is rigidly supported at one end and connected to a nanotube forest at the opposite end, the generated spinning wedge on the forest end shows Fermat scrolling and the spinning wedge attached to the rigid support shows formation of dual Archimedean scrolls.

Scanning electron microscopy (SEM) images of the cross sections obtained by cutting biscrolled yarns with a focused Ga ion beam reveals the gallery structure that confines the guest (Fig. 2). The biscrolled yarns in Fig. 2, A to F, result from twisting a rectangular sheet stack between rigid supports, and in each case the macroscopically observed twist process is dual Archimedean. This interpretation is supported by the barber-pole–type structure of Fig. 1J for the biscrolled yarn of Fig. 2, A and B. If we coat only 15% of the sheet with guest (adjacent to one sheet edge) and asymmetrically apply twist so that formation of a single Archimedean scroll is macroscopically observed, the yarn structure of Fig. 2, G and H, results. As expected for a single Archimedean scroll that starts from the guest-free side of the wedge, an inner core of scrolled guest-free nanotube sheet is surrounded by an outer sheath having guest particles in host galleries. Figure 3, A and B, show lateral and cross-sectional views for a biscrolled yarn obtained by dry-state twist insertion in a rectangular stack consisting of MWNT sheets on top of Si_3N_4 nanotube (Si_3N_4NT) sheets (*14*).

Biscrolled yarns made by all-dry processing can have low densities and high void volume fraction (F_{void}, exterior to the nanotube bundles and guest), which enable SEM imaging of particles deep inside the yarn (Fig. 3C for TiO_2@$MWNT_{1,0}$). The guest particles interfere with twist-based densification, and dry processing avoids densification caused by liquid surface tension. For instance, the density of dry-processed 50% TiO_2@$MWNT_{1,0}$ yarn is only 0.19 g/cm^3 (F_{void} = 0.91), compared with 0.8 g/cm^3 (F_{void} = 0.42) for guest-free, dry-spun MWNT yarn and 0.7 g/cm^3 (F_{void} = 0.79) for liquid-state processed 93% TiO_2@$MWNT_{2,1}$ yarn (Fig. 2, C and D) (*14*). Despite the very low density and high void volume fraction for 50% TiO_2@$MWNT_{1,0}$ yarn, the specific strength for this dry-state fabricated yarn is ~200 MPa cm^3/g (Fig. 4A).

Why are the galleries of host and guest so complicated and irregular (Fig. 2, A to H) when the images in Fig. 1 clearly show scrolling and biscrolling processes that are structurally related to three-dimensionally extended Fermat, Archimedean, or dual Archimedean spiral geometries? One reason is that scroll cores formed during the initial stages of biscrolling have low density, and yarn densification during the final stages of twist insertion involves layer buckling and plastic deformation. Another reason is that yarn densification by joining pleat sidewalls can look in yarn cross-section like layer branching and termination. Origami-like folding of a rectangular sheet during wedge formation increases complexity, as does the collapse of dual Archimedean spirals as they are plied together (Fig. 1, G, I, and J). Structural irregularity also results from layer buckling and yarn shape distortion due to surface-tension–induced yarn densification during wet-state processing and variations in the size and shapes of large-diameter guest particles.

Processability and strength of biscrolled yarns. Even when a very small amount of CNT host mechanically confines an otherwise unbonded powder guest, biscrolled yarns can be knotted and sewn, as indicated by the images in Fig. 3, D to F. Experiments also show that a biscrolled yarn containing 93 wt % TiO_2 can be attached to a textile and washed in an ordinary washing machine without measurable (>2 wt %) loss of the guest or change in the strength (~50 MPa cm^3/g) of the biscrolled yarn (*14*).

We use two types of specific strength to describe mechanical properties: "specific strength" and "MWNT specific strength," which correspond to the breaking force divided by the total linear yarn density and the linear density of the MWNTs in the yarn, respectively. Specific strengths can be more reliable than usual strength measurements, because errors in yarn cross-sectional area are avoided. Figure 4A results for TiO_2 particles deposited from an aerosol (*14*) (movie S2) show that the yarn specific strength decreases approximately linearly with increasing wt % TiO_2, reaching 120 MPa cm^3/g for 76% TiO_2@MWNT. This strength retention and the ability of the host nanotubes to confine guest nanoparticles results from long MWNT lengths and the known (*7*) self-weaving within CNT sheets.

Applications potential of multifunctional biscrolled yarns. Superconducting yarn was obtained by biscrolling a mixture of magnesium and boron powders as guest on MWNT sheets (*14*). One percent CNT host held 99 wt % of these precursors during twist insertion and harsh chemical treatment, despite the large B and Mg particle diameters (~40 μm) compared with the ~50-nm thickness for densified MWNT sheet. Yarn stability during conversion of this guest to superconducting MgB_2 by exposure to highly corrosive Mg vapor (750°C for 30 min in Ar) indicates the ability of the MWNT host to confine the guest in chemical and thermal environments where most materials degrade. Four-probe electrical conductivity measurements (Fig. 4B) show that the biscrolled yarn becomes superconducting at the expected critical temperature (39 K) for MgB_2 (*17*). This method for making superconducting yarn avoids the more than 30 drawing steps needed to produce millimeter-diameter, iron-clad superconducting wires from

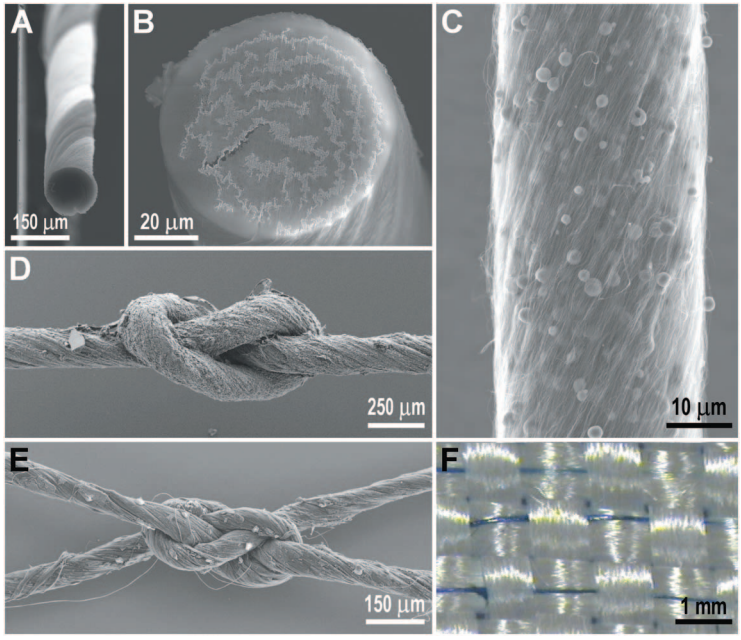

Fig. 3. (**A** and **B**) SEM images of Si_3N_4NT@$MWNT_{0,2}$ biscrolled yarn that was twist-spun in air. The brighter areas correspond to MWNTs. (**C**) SEM image of TiO_2@$MWNT_{1,0}$ yarn made by aerosol-based guest deposition and twist insertion in air. (**D**) SEM image of overhand knot in 95% $LiFePO_4$@$MWNT_{3,3}$ yarn. (**E**) SEM image of carrick bend knot between two 88% SiO_2@$MWNT_{3,0}$ yarns. (**F**) Photograph of 85% TiO_2@$MWNT_{3,0}$ yarn that has been hand sewn into Kevlar (DuPont) textile.

Mg/B/MWNT precursor using the powder-in-tube method (*18*).

Biscrolled yarns containing up to 98 wt % graphene oxide nanoribbons in 2 wt % MWNT host were made and then converted to graphene nanoribbon yarn by reducing the graphene oxide nanoribbons (*14*). The graphene oxide nanoribbons were synthesized by minor modification of Tour's method (*19*), which involves longitudinally unzipping MWNTs in an oxidizing mixture of $KMnO_4$ in aqueous H_2SO_4 (*14*). The specific strength of biscrolled yarn containing 70 wt % of unoriented graphene oxide nanoribbons reached 95 MPa cm^3/g, which is higher than for graphene oxide sheets (68 MPa cm^3/g) (*20*). Conversion of the graphene oxide nanoribbon guest to graphene nanoribbons by thermal annealing the yarn (900°C in 5% H_2 in argon) did not appreciably change specific strength, although yarn weight decreased by 57 wt %. The high reported Li^+ storage capacity of graphene oxide nanoribbons (*21*) suggests that biscrolled graphene nanoribbon yarns may be used as weavable anodes for flexible Li-ion batteries.

The performance of biscrolled yarns as flexible battery cathodes was evaluated by using $LiFePO_4$ as guest, which is an inexpensive, environmentally friendly, high-performance Li-ion battery cathode material (*22*, *23*). Charge collection from this high-rate, high-capacity redox material is an important problem because of its low electronic conductivity, and the nanoscale proximity between highly conducting MWNT host and the $LiFePO_4$ in biscrolled yarns should provide a solution to this problem that minimizes total electrode weight.

A biscrolled yarn with 98.5 wt % $LiFePO_4$ guest exhibited an unexpectedly high gravimetric electrical conductivity of 8 S cm^2/g (*14*). The corresponding gravimetric conductivity based on the mass/length ratio of host MWNT (~530 S cm^2/g) is within experimental error of that for a twist-spun MWNT yarn that does not contain guest (410 S cm^2/g), indicating that guest inclusion does not degrade electrical transport by the host MWNTs. This high gravimetric electrical conductivity means biscrolled yarn cathodes do not require the commonly used aluminum current collector, conducting additive, and binding agent that can increase electrode weight over 30%.

The electrode results of Fig. 4C are for a 100-μm-diameter biscrolled yarn containing 95 wt % $LiFePO_4$ guest, which is weavable and knottable (Fig. 3D) despite this massive powder concentration (*14*). Based on total electrode weight, reversible charge storage capabilities of 115 mAh/g at C/3 rate and 99 mAh/g at 1C were obtained, where a C/3 rate is the discharge rate needed to release one-third of the theoretical storage capacity of $LiFePo_4$ (170 mAh/g) in 1 hour. An impressive capacity of 146 mAh/g at 1C rate (based on $LiFePO_4$ weight) has been reported for a $LiFePO_4$/MWNT/binder composite sheet (*24*), which reduces to 105 mAh/g when based on estimated total electrode weight (including a likely 20 wt % Al foil current collector, such as those found in commercial $LiFePO_4$ batteries). Using Li metal as the anode and the total cathode weight to provide normalization for energy and power densities, energy storage densities of 379 Wh/kg and 135 Wh/kg resulted for power densities of 180 W/kg and 4590 W/kg, respectively. By plying together such a biscrolled yarn cathode and biscrolled yarn anode (e.g., graphene nanoribbon guest), a Li-ion battery that is a single two-ply yarn could be made, such as those demonstrated for supercapacitors using solution-spun CNT yarns (*25*).

Because catalytic oxygen reduction is crucial for fuel cells and metal-air batteries, and the cost of noble metal catalysts is a major problem, we next investigated whether nitrogen-doped MWNT (N_xMWNT) guest in biscrolled yarns can provide this catalysis. Although N_xMWNT is known to be a promising oxygen-reduction catalyst (*26*–*29*), the question is, "Can this catalytic activity be retained in a biscrolled yarn that is weavable into a strong, flexible cathode?" Evidence for catalytic activity was obtained by comparing the cyclic voltammetry of 91% MWNT@MWNT and 90% N_xMWNT@MWNT biscrolled yarns that were identically fabricated except for replacing undoped MWNT guest with N_xMWNT. The N-doped MWNTs (N/C ~ 0.03) were prepared using a floating catalyst method and purified to remove iron catalyst (*14*, *30*). Figure 4D shows that the onset potential for oxygen reduction by N_xMWNT@MWNT shifts by ~0.3 V with respect to that for MWNT@MWNT. The same shift in onset potential was observed for the bilayer sheet stack that was precursor to the N_xMWNT@MWNT yarn, indicating that biscrolling is not interfering with catalytic activity.

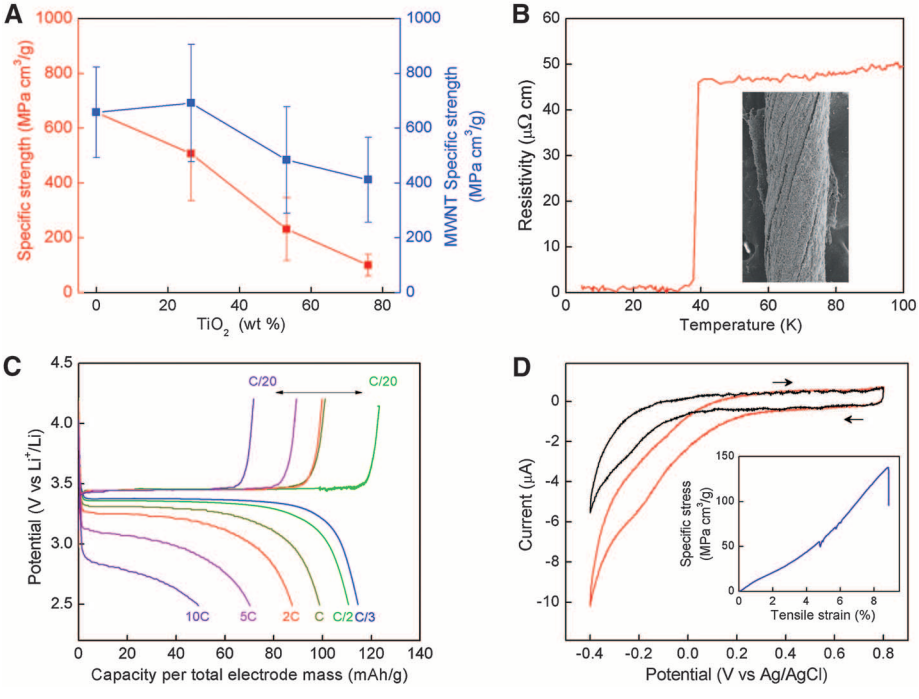

Fig. 4. (**A**) Specific strength and MWNT specific strength of TiO_2@$MWNT_{2,0}$ yarn as a function of TiO_2 loading, showing ±1 SD error bars (for $N \geq 4$ per data point). The biscrolled yarn was made by deposition of TiO_2 from a chemically produced aerosol and dry-state twist insertion into a rectangular bilayer sheet. (**B**) Electrical resistivity versus temperature for superconducting MgB_2@$MWNT_{2,1}$ yarn, showing T_c = 39 K. (Inset) SEM image of the 170-μm-diameter yarn. (**C**) Galvanostatic charge-discharge curves versus charge level (per total weight of electrode) for a 95% $LiFePO_4$@$MWNT_{4,6}$ yarn using different discharge rates. (**D**) Cyclic voltammetry at 5 mV/s for a 90% N_xMWNT@$MWNT_{1,0}$ yarn (red curve) and 91% MWNT@$MWNT_{1,0}$ yarn (black curve) in oxygen-saturated 0.5 M H_2SO_4, showing a voltage shift in the onset for oxygen reduction due to catalysis by the N-doped MWNTs. (Inset) Specific stress versus tensile strain for 70% N_xMWNT@$MWNT_{1,2}$ yarn.

Summary. We show that a minute amount of MWNT host web enables twist-based spinning of yarn from diverse powders and nanofibers, while maintaining guest functionality. The mechanical properties of these webs enables weavability, knottability, and durability for biscrolled yarns containing up to at least 95 wt % guest, which can result in applications for wearable electronic textiles and for strong woven electrodes of batteries and fuel cells. Using patterned deposition for bilayer stacks, TiO_2 guest can be located in the sheath of a biscrolled yarn, thereby optimizing light absorption for such applications as self-cleaning textiles and Graetzel solar cells. The ability to make biscrolled yarns having Fermat, Archimedean, and dual Archimedean scroll geometries can be exploited to optimize yarn properties. The demonstrated use of CNT sheets as removable templates for making spinnable sheets of other nanotubes extends biscrolling to new hosts and provides a route to other types of nanotube yarns.

References and Notes

1. D. Li, Y. Xia, *Adv. Mater.* **16**, 1151 (2004).
2. H. Ye, H. Lam, N. Titchenal, Y. Gogotsi, F. Ko, *Appl. Phys. Lett.* **85**, 1775 (2004).
3. M. J. Uddin *et al.*, *J. Photochem. Photobiol. Chem.* **199**, 64 (2008).
4. B. Vigolo *et al.*, *Science* **290**, 1331 (2000).
5. M. E. Kozlov *et al.*, *Adv. Mater.* **17**, 614 (2005).
6. M. Zhang, K. R. Atkinson, R. H. Baughman, *Science* **306**, 1358 (2004).
7. M. Zhang *et al.*, *Science* **309**, 1215 (2005).
8. X. Zhang *et al.*, *Adv. Mater.* **18**, 1505 (2006).
9. Q. Li *et al.*, *Adv. Mater.* **18**, 3160 (2006).
10. X. Zhang *et al.*, *Small* **3**, 244 (2007).
11. L. Xiao *et al.*, *Appl. Phys. Lett.* **92**, 153108 (2008).
12. Y. Nakayama, *Jpn. J. Appl. Phys.* **47**, 8149 (2008).
13. A. E. Aliev *et al.*, *Science* **323**, 1575 (2009).
14. Materials and methods are available as supporting material on *Science* Online.
15. D. Golberg, Y. Bando, C. Tang, C. Zhi, *Adv. Mater.* **19**, 2413 (2007).
16. V. M. Castaño, *Jpn. J. Appl. Phys.* **44**, 5009 (2005).
17. J. Nagamatsu, N. Nakagawa, T. Muranaka, Y. Zenitani, J. Akimitsu, *Nature* **410**, 63 (2001).
18. S. X. Dou *et al.*, *Adv. Mater.* **18**, 785 (2006).
19. D. V. Kosynkin *et al.*, *Nature* **458**, 872 (2009).
20. D. A. Dikin *et al.*, *Nature* **448**, 457 (2007).
21. T. Bhardwaj, A. Antic, B. Pavan, V. Barone, B. D. Fahlman, *J. Am. Chem. Soc.* **132**, 12556 (2010).
22. A. K. Padhi, K. S. Nanjundaswamy, J. B. Goodenough, *J. Electrochem. Soc.* **144**, 1188 (1997).
23. J. Chen, M. S. Whittingham, *Electrochem. Commun.* **8**, 855 (2006).
24. X. Li, F. Kang, X. Bai, W. Shen, *Electrochem. Commun.* **9**, 663 (2007).
25. A. B. Dalton *et al.*, *Nature* **423**, 703 (2003).
26. K. Gong, F. Du, Z. Xia, M. Durstock, L. Dai, *Science* **323**, 760 (2009).
27. S. Kundu *et al.*, *J. Phys. Chem. C* **113**, 14302 (2009).
28. S. Maldonado, K. J. Stevenson, *J. Phys. Chem. B* **109**, 4707 (2005).
29. Y. Shao, J. Sui, G. Yin, Y. Gao, *Appl. Catal. B* **79**, 89 (2008).
30. M. Terrones, R. Kamalakaran, T. Seeger, M. Rühle, *Chem. Commun. (Camb.)* **23**, 2335 (2000).

31. We thank A. L. Elias and M. Terrones for N-doped MWNTs; D. Goldberg and Y. Bando for boron nitride nanotubes; E. J. Kneeland, A. E. Nabinger, S. Y. Yoon, and M. J. de Andrade for help with experiments; and A. E. Aliev and D. M. Rogers for useful comments. Supported by Air Force Grant AOARD-10-4067, Air Force Office of Scientific Research grants FA9550-09-1-0384 and FA9550-09-1-0537, Office of Naval Research Multidisciplinary University Research Initiative grant N00014-08-1-0654, NSF grant DMI-0609115, and Robert A. Welch Foundation grant AT-0029. Some of the authors have filed patent application PCT/US2010/36378 (27 May 2010).

Supporting Online Material

www.sciencemag.org/cgi/content/full/331/6013/51/DC1
Materials and Methods
Figs. S1 to S7
References
Movies S1 to S3

2 August 2010; accepted 26 November 2010
10.1126/science.1195912

The Origins of Hot Plasma in the Solar Corona

B. De Pontieu,[1]* S. W. McIntosh,[2] M. Carlsson,[3] V. H. Hansteen,[3,1] T. D. Tarbell,[1] P. Boerner,[1] J. Martinez-Sykora,[1,3] C. J. Schrijver,[1] A. M. Title[1]

The Sun's outer atmosphere, or corona, is heated to millions of degrees, considerably hotter than its surface or photosphere. Explanations for this enigma typically invoke the deposition in the corona of nonthermal energy generated by magnetoconvection. However, the coronal heating mechanism remains unknown. We used observations from the Solar Dynamics Observatory and the Hinode solar physics mission to reveal a ubiquitous coronal mass supply in which chromospheric plasma in fountainlike jets or spicules is accelerated upward into the corona, with much of the plasma heated to temperatures between ~0.02 and 0.1 million kelvin (MK) and a small but sufficient fraction to temperatures above 1 MK. These observations provide constraints on the coronal heating mechanism(s) and highlight the importance of the interface region between photosphere and corona.

A wide variety of theoretical models to explain the heating of the solar corona have been proposed since the discovery in the corona of emission from ions that are formed at temperatures of several million kelvin (MK) (*1*). These models range from energy deposition through the damping of magnetohydrodynamic waves, to nanoflares (*2*) that arise when the magnetic field is stressed (via reconnection) (*3*). Despite decades of effort to determine which mechanism dominates, the lack of detailed observations of the fundamental heating process has hampered progress. Instead, most efforts have focused on statistical approaches that study the dependence of the heating mechanism on magnetic field strength, loop length, or plasma density (*4*), or that are based on assumptions about unresolved individual heating events (*5*).

Spicules are phenomena that have held particular promise as discrete coronal heating events (*6*, *7*). The chromospheric mass flux that these jets propel to coronal heights is estimated to be two orders of magnitude larger than the mass flux of the solar wind (*8*). Although they have been observed in a variety of chromospheric and transition region (TR) lines (*9*, *10*), a coronal counterpart has not been observed. As a result, a role for spicules in coronal heating has been dismissed as unlikely (*8*). On the other hand, recent observations have revealed a new type of spicule that is shorter-lived (~100 s) and more dynamic (~50 to 100 km/s) than its classical counterpart (*10*, *11*). Recently, a spatiotemporal correlation between chromospheric brightness changes, suggestively linked to these "type II" spicules, and coronal upflows of 50 to 100 km/s, deduced from spectral line asymmetries of coronal lines at the footpoints of loops, was found (*12*). This statistical relationship suggests that the chromospheric jets may play a substantial role in providing the corona with hot plasma, but a detailed one-to-one correlation between spicules and their coronal counterparts has remained elusive (*10*, *11*, *13*).

We exploited the recent detection of the disk counterpart of type II spicules: rapid blueshifted events (RBEs), which are observed in chromospheric lines such as Hα 6563 Å (*14*, *15*). Observations suggest evidence for acceleration and heating along their long axis before they rapidly fade out of the chromospheric passbands, which may indicate heating to TR temperatures (*15*). We used coordinated observations of RBEs in the blue wing of Hα (–0.868 Å or –41 km/s) with the Narrowband Filter Imager of the Solar Optical Telescope (SOT) (*17*) onboard the Hinode solar physics mission (*16*), and found direct evidence of a strong correlation of RBEs with short-lived brightenings in a wide range of TR and coronal passbands observed with the Atmospheric Imaging Assembly (AIA) onboard the recently launched Solar Dynamics Observatory (SDO). Using an automated detection code, we found 2434 RBEs occurring in the active-region plage footpoints of coronal loops during a 1-hour-long time series (*18*) on 25 April 2010 (Fig. 1 and fig. S1).

RBEs form rapidly and often recur in the same position (Fig. 2). They become visible as an absorbing feature in the upper chromospheric Hα line that is blueshifted by 40 to 60 km/s along the line of sight (*18*). A little bit later, brightenings occur in the vicinity of the leading edge of the RBE in the He II 304 Å, Fe IX 171 Å, and Fe XIV 211 Å AIA passbands (Fig. 2). These passbands are dominated by lines from ions that are formed at temperatures of 0.1, 0.8, and 2 MK, respectively (*18*). The extreme ultraviolet emission moves at velocities similar to those of the leading end of the RBE, although the emission in He II 304 Å (and sometimes Fe IX 171 Å) often,

[1]Lockheed Martin Solar and Astrophysics Laboratory, 3251 Hanover Street, Organization ADBS, Building 252, Palo Alto, CA 94304, USA. [2]High Altitude Observatory, National Center for Atmospheric Research, Post Office Box 3000, Boulder, CO 80307, USA. [3]Institute of Theoretical Astrophysics, University of Oslo, Post Office Box 1029 Blindern, 0315 Oslo, Norway.

*To whom correspondence should be addressed. E-mail: bdp@lmsal.com

References and Notes

1. D. Li, Y. Xia, *Adv. Mater.* **16**, 1151 (2004).
2. H. Ye, H. Lam, N. Titchenal, Y. Gogotsi, F. Ko, *Appl. Phys. Lett.* **85**, 1775 (2004).
3. M. J. Uddin *et al.*, *J. Photochem. Photobiol. Chem.* **199**, 64 (2008).
4. B. Vigolo *et al.*, *Science* **290**, 1331 (2000).
5. M. E. Kozlov *et al.*, *Adv. Mater.* **17**, 614 (2005).
6. M. Zhang, K. R. Atkinson, R. H. Baughman, *Science* **306**, 1358 (2004).
7. M. Zhang *et al.*, *Science* **309**, 1215 (2005).
8. X. Zhang *et al.*, *Adv. Mater.* **18**, 1505 (2006).
9. Q. Li *et al.*, *Adv. Mater.* **18**, 3160 (2006).
10. X. Zhang *et al.*, *Small* **3**, 244 (2007).
11. L. Xiao *et al.*, *Appl. Phys. Lett.* **92**, 153108 (2008).
12. Y. Nakayama, *Jpn. J. Appl. Phys.* **47**, 8149 (2008).
13. A. E. Aliev *et al.*, *Science* **323**, 1575 (2009).
14. Materials and methods are available as supporting material on *Science* Online.
15. D. Golberg, Y. Bando, C. Tang, C. Zhi, *Adv. Mater.* **19**, 2413 (2007).
16. V. M. Castaño, *Jpn. J. Appl. Phys.* **44**, 5009 (2005).
17. J. Nagamatsu, N. Nakagawa, T. Muranaka, Y. Zenitani, J. Akimitsu, *Nature* **410**, 63 (2001).
18. S. X. Dou *et al.*, *Adv. Mater.* **18**, 785 (2006).
19. D. V. Kosynkin *et al.*, *Nature* **458**, 872 (2009).
20. D. A. Dikin *et al.*, *Nature* **448**, 457 (2007).
21. T. Bhardwaj, A. Antic, B. Pavan, V. Barone, B. D. Fahlman, *J. Am. Chem. Soc.* **132**, 12556 (2010).
22. A. K. Padhi, K. S. Nanjundaswamy, J. B. Goodenough, *J. Electrochem. Soc.* **144**, 1188 (1997).
23. J. Chen, M. S. Whittingham, *Electrochem. Commun.* **8**, 855 (2006).
24. X. Li, F. Kang, X. Bai, W. Shen, *Electrochem. Commun.* **9**, 663 (2007).
25. A. B. Dalton *et al.*, *Nature* **423**, 703 (2003).
26. K. Gong, F. Du, Z. Xia, M. Durstock, L. Dai, *Science* **323**, 760 (2009).
27. S. Kundu *et al.*, *J. Phys. Chem. C* **113**, 14302 (2009).
28. S. Maldonado, K. J. Stevenson, *J. Phys. Chem. B* **109**, 4707 (2005).
29. Y. Shao, J. Sui, G. Yin, Y. Gao, *Appl. Catal. B* **79**, 89 (2008).
30. M. Terrones, R. Kamalakaran, T. Seeger, M. Rühle, *Chem. Commun. (Camb.)* **23**, 2335 (2000).

31. We thank A. L. Elias and M. Terrones for N-doped MWNTs; D. Goldberg and Y. Bando for boron nitride nanotubes; E. J. Kneeland, A. E. Nabinger, S. Y. Yoon, and M. J. de Andrade for help with experiments; and A. E. Aliev and D. M. Rogers for useful comments. Supported by Air Force Grant AOARD-10-4067, Air Force Office of Scientific Research grants FA9550-09-1-0384 and FA9550-09-1-0537, Office of Naval Research Multidisciplinary University Research Initiative grant N00014-08-1-0654, NSF grant DMI-0609115, and Robert A. Welch Foundation grant AT-0029. Some of the authors have filed patent application PCT/US2010/36378 (27 May 2010).

Supporting Online Material

www.sciencemag.org/cgi/content/full/331/6013/51/DC1
Materials and Methods
Figs. S1 to S7
References
Movies S1 to S3

2 August 2010; accepted 26 November 2010
10.1126/science.1195912

The Origins of Hot Plasma in the Solar Corona

B. De Pontieu,[1]* S. W. McIntosh,[2] M. Carlsson,[3] V. H. Hansteen,[3,1] T. D. Tarbell,[1] P. Boerner,[1] J. Martinez-Sykora,[1,3] C. J. Schrijver,[1] A. M. Title[1]

The Sun's outer atmosphere, or corona, is heated to millions of degrees, considerably hotter than its surface or photosphere. Explanations for this enigma typically invoke the deposition in the corona of nonthermal energy generated by magnetoconvection. However, the coronal heating mechanism remains unknown. We used observations from the Solar Dynamics Observatory and the Hinode solar physics mission to reveal a ubiquitous coronal mass supply in which chromospheric plasma in fountainlike jets or spicules is accelerated upward into the corona, with much of the plasma heated to temperatures between ~0.02 and 0.1 million kelvin (MK) and a small but sufficient fraction to temperatures above 1 MK. These observations provide constraints on the coronal heating mechanism(s) and highlight the importance of the interface region between photosphere and corona.

A wide variety of theoretical models to explain the heating of the solar corona have been proposed since the discovery in the corona of emission from ions that are formed at temperatures of several million kelvin (MK) (*1*). These models range from energy deposition through the damping of magnetohydrodynamic waves, to nanoflares (*2*) that arise when the magnetic field is stressed (via reconnection) (*3*). Despite decades of effort to determine which mechanism dominates, the lack of detailed observations of the fundamental heating process has hampered progress. Instead, most efforts have focused on statistical approaches that study the dependence of the heating mechanism on magnetic field strength, loop length, or plasma density (*4*), or that are based on assumptions about unresolved individual heating events (*5*).

Spicules are phenomena that have held particular promise as discrete coronal heating events (*6*, *7*). The chromospheric mass flux that these jets propel to coronal heights is estimated to be two orders of magnitude larger than the mass flux of the solar wind (*8*). Although they have been observed in a variety of chromospheric and transition region (TR) lines (*9*, *10*), a coronal counterpart has not been observed. As a result, a role for spicules in coronal heating has been dismissed as unlikely (*8*). On the other hand, recent observations have revealed a new type of spicule that is shorter-lived (~100 s) and more dynamic (~50 to 100 km/s) than its classical counterpart (*10*, *11*). Recently, a spatiotemporal correlation between chromospheric brightness changes, suggestively linked to these "type II" spicules, and coronal upflows of 50 to 100 km/s, deduced from spectral line asymmetries of coronal lines at the footpoints of loops, was found (*12*). This statistical relationship suggests that the chromospheric jets may play a substantial role in providing the corona with hot plasma, but a detailed one-to-one correlation between spicules and their coronal counterparts has remained elusive (*10*, *11*, *13*).

We exploited the recent detection of the disk counterpart of type II spicules: rapid blueshifted events (RBEs), which are observed in chromospheric lines such as Hα 6563 Å (*14*, *15*). Observations suggest evidence for acceleration and heating along their long axis before they rapidly fade out of the chromospheric passbands, which may indicate heating to TR temperatures (*15*). We used coordinated observations of RBEs in the blue wing of Hα (–0.868 Å or –41 km/s) with the Narrowband Filter Imager of the Solar Optical Telescope (SOT) (*17*) onboard the Hinode solar physics mission (*16*), and found direct evidence of a strong correlation of RBEs with short-lived brightenings in a wide range of TR and coronal passbands observed with the Atmospheric Imaging Assembly (AIA) onboard the recently launched Solar Dynamics Observatory (SDO). Using an automated detection code, we found 2434 RBEs occurring in the active-region plage footpoints of coronal loops during a 1-hour-long time series (*18*) on 25 April 2010 (Fig. 1 and fig. S1).

RBEs form rapidly and often recur in the same position (Fig. 2). They become visible as an absorbing feature in the upper chromospheric Hα line that is blueshifted by 40 to 60 km/s along the line of sight (*18*). A little bit later, brightenings occur in the vicinity of the leading edge of the RBE in the He II 304 Å, Fe IX 171 Å, and Fe XIV 211 Å AIA passbands (Fig. 2). These passbands are dominated by lines from ions that are formed at temperatures of 0.1, 0.8, and 2 MK, respectively (*18*). The extreme ultraviolet emission moves at velocities similar to those of the leading end of the RBE, although the emission in He II 304 Å (and sometimes Fe IX 171 Å) often,

[1]Lockheed Martin Solar and Astrophysics Laboratory, 3251 Hanover Street, Organization ADBS, Building 252, Palo Alto, CA 94304, USA. [2]High Altitude Observatory, National Center for Atmospheric Research, Post Office Box 3000, Boulder, CO 80307, USA. [3]Institute of Theoretical Astrophysics, University of Oslo, Post Office Box 1029 Blindern, 0315 Oslo, Norway.

*To whom correspondence should be addressed. E-mail: bdp@lmsal.com

sometimes with a short delay, fills in along the whole length of the RBE, usually after the RBE disappears out of the chromospheric passband (movies S2 to S7). Space-time plots show that the apparent velocity of the chromospheric, TR, and coronal signals is similar, with typical velocities on the order of 50 to 100 km/s (Fig. 2 and fig. S2).

The location of the hot plasma with respect to the chromospheric RBE varies substantially as a function of temperature *T*, with a clear displacement of the hottest emission toward locations ahead of the leading edge of the RBE (in a vertical geometry this would be "upward from the RBE"). The hotter Fe XIV emission often occurs over a larger spatial range than the other TR and coronal lines, usually protruding ahead of the RBE for a few megameters (Mm) (fig. S2 and movies S4 and S5). This may be caused by the effects of thermal conduction, which is much more efficient at Fe XIV temperatures, given its temperature dependence ($T^{3.5}$). Thermal conduction is clearly not the only cause for the "upward" extension of the coronal emission associated with RBEs: The presence of strong line-of-sight Doppler velocities in the chromosphere, and the compatible apparent velocities of the coronal brightenings moving along with the RBEs, show that the apparent motion of the coronal brightenings is associated with strong mass flows on the order of 50 to 100 km/s. This is confirmed by the presence (in regions with RBE activity) of blueward asymmetries (*18*) in the Si VII 275 Å spectral line profiles from the Extreme Ultraviolet Imaging Spectrometer (EIS) (*19*) onboard Hinode (Fig. 1). Such asymmetries have been linked to a faint secondary component of strongly upflowing (50 to 100 km/s) coronal plasma (*12*, *20*).

The heating of plasma to coronal temperatures in association with spicules is ubiquitous: We find evidence for a similar process in active regions, in the quiet Sun, and in coronal holes (figs. S3 to S5). In particular, chromospheric spicules (observed with Hinode's SOT in Ca II H 3968 Å) at the limb in coronal holes are intimately linked to the formation of features at TR and coronal temperatures (Fig. 3). The spicules show strong apparent upward motions on the order of 50 100 km/s before rapidly fading out of the chromospheric passband (movies S8 and S9). Using coaligned AIA images, we find that the fading of chromospheric spicules is directly linked

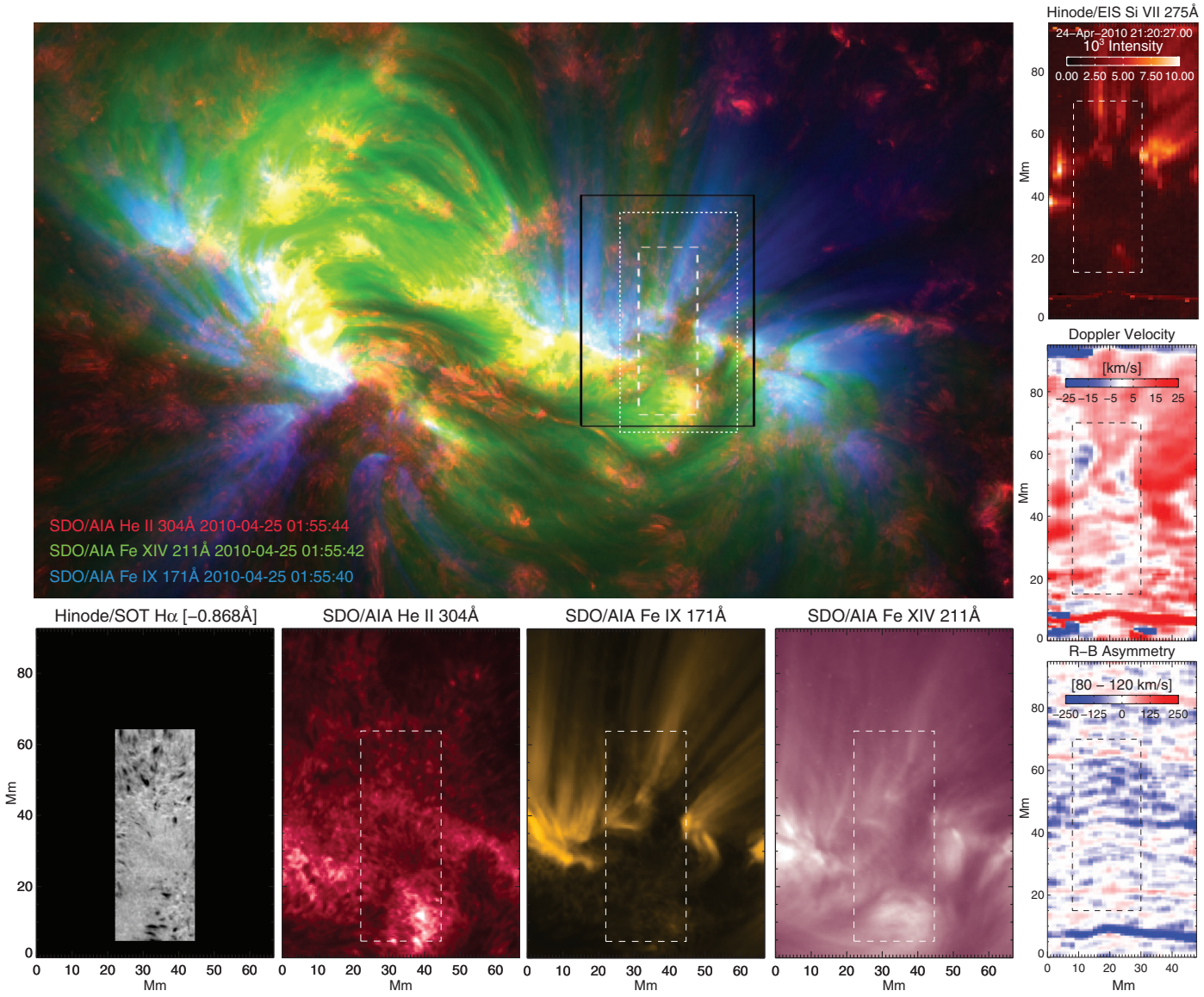

Fig. 1. The chromosphere, TR, and corona of the active region studied on 25 April 2010 (see fig. S1 and movies S1 to S3). (**Upper panel**) A composite layering with He II 304 Å (red, 0.1 MK), Fe XIV 211 Å (green, 2 MK), and Fe IX 171 Å (blue, 0.8 MK) images from AIA. (**Bottom row**) RBEs in Hα –0.868 Å (lower left) throughout the SOT field of view (white/black dashed lines in other panels), and AIA images for the region of interest (solid black line in top panel). (**Right column**) Si VII 275 Å EIS spectral raster (outlined by dotted line in top left panel) taken a few hours before with intensity (top), Doppler shift (middle), and blueward asymmetries at velocities of 80 to 120 km/s (bottom).

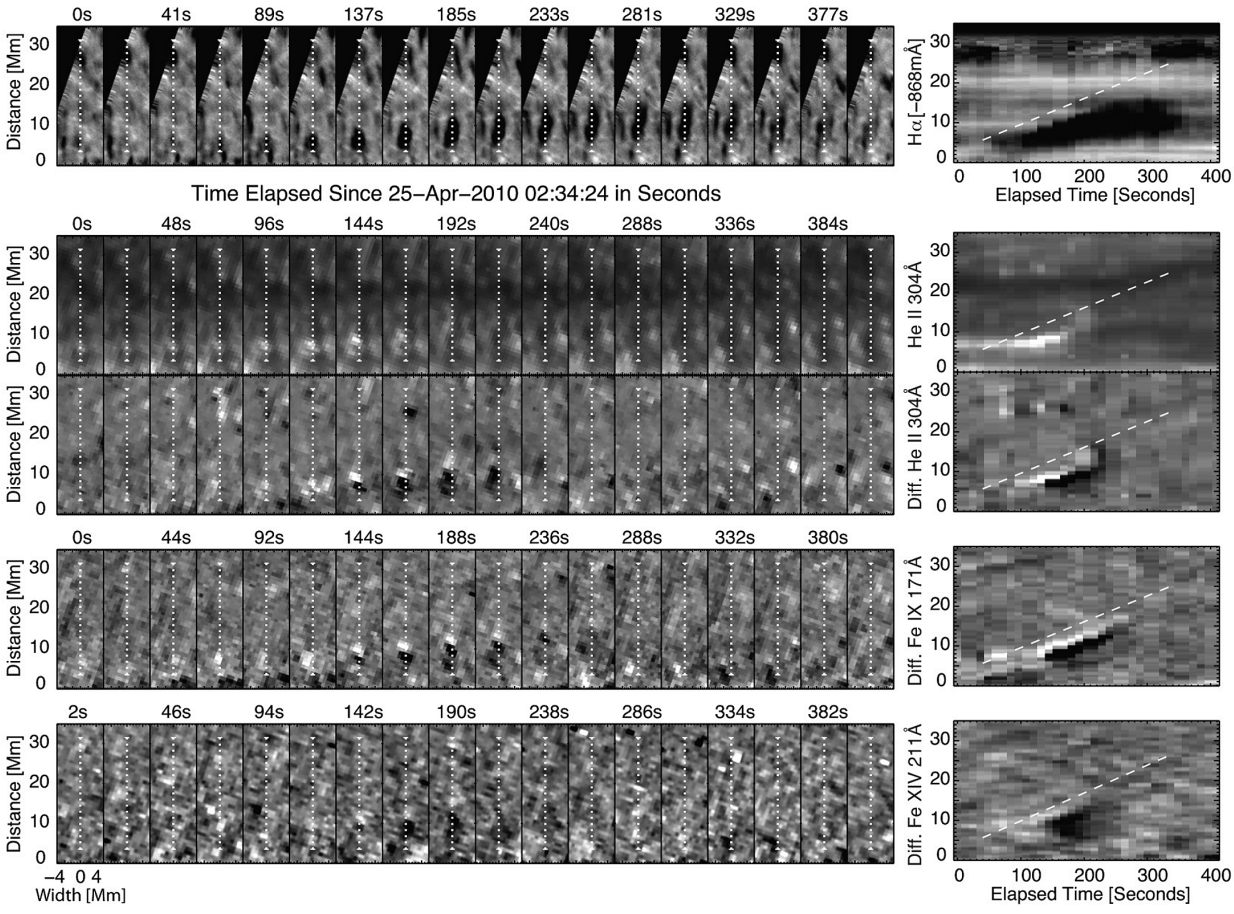

Fig. 2. Typical dynamic and thermal evolution of a succession of RBEs. (**Left panels, top to bottom**) The temporal evolution of Hα –0.868 Å, He II 304 Å intensity, and the running time-difference time series (*18*) (32 s) for He II 304 Å, Fe IX 171 Å, and Fe XIV 211 Å. (**Right panels, top to bottom**) Space-time plots along the axis of the RBE (dotted white lines) for the same passbands, with a dashed guideline to illustrate speeds of 70 km/s. See fig. S2 for another example and movies S2 to S7.

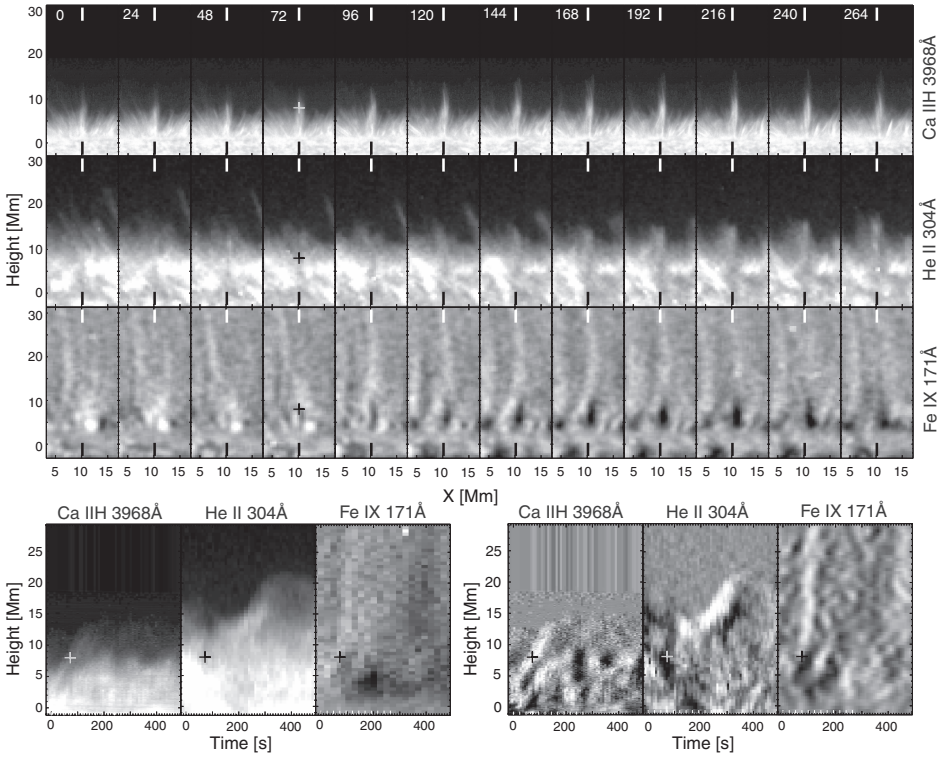

Fig. 3. Typical dynamic and thermal evolution of type II spicules at the coronal hole limb on 27 April 2010. The top panels show, from top to bottom, the temporal evolution of a succession of type II spicules visible as jetlike features in Ca II H 3968 Å and He II 304 Å, and as absorbing features at the bottom and streaklike brightenings at the spicule tops in Fe IX 171 Å. Space-time plots along the line connecting the black and white short lines (at top and bottom of top panels) for the intensity (lower left panels; for the 171 Å panel, the time average has been subtracted) and the running time difference (40 s, lower right panels) show rapid upflows and fading at heights below 15 Mm (marked by crosses in the lower panels) for Ca II, followed by parabolic paths up to heights of 20 to 25 Mm for He II 304 Å and upward-propagating disturbances in Fe IX 171 Å (visible in running time-difference panels). A detailed, annotated description of the sequence of events in this figure is available as movie S8. See also figs. S4 and S5 and movie S9.

to the formation of spicular features in He II 304 Å (~0.1 MK). These TR spicules appear with a time delay of around 10 to 20 s, reach much larger heights (~10 to 20 Mm), and typically fall back to the surface within a matter of several minutes, following a parabolic path (Fig. 3 and fig. S5). Despite the enormous line-of-sight superposition at the limb, we often also observe a coronal counterpart of chromospheric/TR spicules (Fig. 3 and fig. S5) in the Fe IX 171 Å images. At the bottom, this takes the form of a dark feature that corresponds to the bright Ca II H feature (movie S8), likely from continuum absorption from neutral hydrogen and helium (*21*). During the later stages, the dark feature disappears (likely because heating reduces the amount of neutral hydrogen and helium), and bright coronal counterparts propagate upward into the coronal hole with similar velocities as the apparent motions of the chromospheric spicules (fig. S5). These coronal counterparts appear to be related to the propagating disturbances in coronal holes that have previously been interpreted as waves (*22*) and more recently linked to upflows (*23*, *24*).

Our observations support a scenario in which chromospheric plasma is propelled upward with speeds of ~50 to 100 km/s, with the bulk of the mass rapidly heated to TR temperatures (~0.02 to 0.1 MK), after which it returns to the surface (invisible to chromospheric passbands). Directly associated with these jets, plasma is heated to coronal temperatures of at least 1 to 2 MK, at the bottom during the initial stages, and both along and toward the top of the chromospheric feature later on. The coronal counterparts of the jets are seen to rapidly propagate upward, likely as a result of strong upflows and/or thermal conduction or waves. Based on the ubiquity of these events and the observed coronal intensities, we estimate that these events carry a mass flux density of 1.5×10^{-9} g/cm^2/s and an energy flux density of $\sim 2 \times 10^6$ erg/cm^2/s into the corona (*25*). This is of the order that is required to sustain the energy lost from the active-region corona (*26*). Given the conservative nature of our estimate, these events are likely to play a substantial role in the coronal energy balance.

Although early models have implicated the heating of chromospheric spicules in the coronal heating problem (*6*), the detailed thermal and spatiotemporal evolution we observed is not compatible with any of the well-established models for coronal heating: None of those predict such strong upflows (driven from below) at chromospheric temperatures (*2*, *27*). These models typically assume energy deposition in the corona, which leads to heating and evaporation of plasma from the chromospheric mass reservoir, driven by thermal conduction from above. Recent advanced numerical models do predict heating rates per particle that reach their maximum in the upper chromosphere (*28*, *29*), which is compatible with our observations. Some analytical models also suggest that dissipation of current sheets resulting from the shuffling of ubiquitous mixed-polarity fields on small scales can provide coronal heating at low heights (*30*). However, there are currently no models for what drives and heats the observed jets (*31*). These first detailed observations of individual coronal heating events highlight the importance of the chromosphere and magnetohydrodynamic/plasma physics approaches for a better understanding of heating in the solar atmosphere.

References and Notes

1. B. Edlen, *Z. Astrophysik* **22**, 30 (1942).
2. J. A. Klimchuk, *Sol. Phys.* **234**, 41 (2006).
3. E. N. Parker, *Geophys. Astrophys. Fluid Dyn.* **50**, 229 (1990).
4. C. J. Schrijver, A. W. Sandman, M. J. Aschwanden, M. L. DeRosa, *Astrophys. J.* **615**, 512 (2004).
5. M. J. Aschwanden, R. Nightingale, P. Boerner, *Astrophys. J.* **656**, 577 (2007).
6. G. W. Pneuman, R. A. Kopp, *Sol. Phys.* **57**, 49 (1978).
7. R. G. Athay, T. E. Holzer, *Astrophys. J.* **255**, 743 (1982).
8. G. L. Withbroe, *Astrophys. J.* **267**, 825 (1983).
9. K. P. Dere, J.-D. F. Bartoe, G. E. Brueckner, *Sol. Phys.* **123**, 41 (1989).
10. R. Rutten, *ASP Conf. Ser.* **354**, 276 (2006)
11. B. De Pontieu *et al.*, *Pub. Astron. Soc. Jpn.* **59**, 655 (2007).
12. B. De Pontieu, S. W. McIntosh, V. H. Hansteen, C. J. Schrijver, *Astrophys. J.* **701**, L1 (2009).
13. J. Mariska, *Solar Transition Region* (Cambridge Astrophysics Series, vol. 23, Cambridge Univ. Press, New York, 1992).
14. Ø. Langangen *et al.*, *Astrophys. J.* **679**, L167 (2008).
15. L. Rouppe van der Voort, J. Leenaarts, B. de Pontieu, M. Carlsson, G. Vissers, *Astrophys. J.* **705**, 272 (2009).
16. T. Kosugi *et al.*, *Sol. Phys.* **243**, 3 (2007).
17. S. Tsuneta *et al.*, *Sol. Phys.* **249**, 167 (2008).
18. See materials and methods in the supporting online material (SOM) on *Science* Online.
19. J. L. Culhane *et al.*, *Sol. Phys.* **243**, 19 (2007).
20. H. Hara *et al.*, *Astrophys. J.* **678**, L67 (2008).
21. U. Anzer, P. Heinzel, *Astrophys. J.* **622**, 714 (2005).
22. D. Banerjee *et al.*, *Astron. Astrophys.* **499**, 29 (2009).
23. S. W. McIntosh, B. De Pontieu, *Astrophys. J.* **707**, 524 (2009).
24. S.W. McIntosh *et al.*, *Astron. Astrophys.* **510**, 2 (2010).
25. See SOM discussion.
26. E. R. Priest, *Solar Magnetohydrodynamics* (D. Reidel Publishing, Dordrecht, Netherlands, 1982).
27. S. Patsourakos, J. A. Klimchuk, *Astrophys. J.* **647**, 1452 (2006).
28. B. V. Gudiksen, A. Nordlund, *Astrophys. J.* **618**, 1031 (2005).
29. V. H. Hansteen, H. Hara, B. De Pontieu, M. Carlsson, *Astrophys. J.* **718**, 1070 (2010).
30. E. Priest, J. Heyvaerts, A. Title, *Astrophys. J.* **576**, 533 (2002).
31. A. Sterling, *Sol. Phys.* **196**, 79 (2000).

32. This work is supported by NASA grants NNX08AL22G and NNX08BA99G (to B.D.P. and S.W.M.), NASA contracts NNM07AA01C (Hinode) and NNG04EA00C (AIA), and the Research Council of Norway (M.C. and V.H.H.). The National Center for Atmospheric Research is sponsored by NSF. Hinode is a Japanese mission developed by the Institute of Space and Astronautical Science/Japan Aerospace Exploration Agency, with the National Astronomical Observatory of Japan as domestic partner and NASA and Science and Technology Facilities Council (UK) as international partners. It is operated in cooperation with the European Space Agency and the Norwegian Space Centre (Norway).

Supporting Online Material

www.sciencemag.org/cgi/content/full/331/6013/55/DC1
Materials and Methods
SOM Text
Figs. S1 to S5
References
Movies S1 to S9

13 September 2010; accepted 2 December 2010
10.1126/science.1197738

Universal Quantum Viscosity in a Unitary Fermi Gas

C. Cao,[1] E. Elliott,[1] J. Joseph,[1] H. Wu,[1] J. Petricka,[2] T. Schäfer,[3] J. E. Thomas[1]*

A Fermi gas of atoms with resonant interactions is predicted to obey universal hydrodynamics, in which the shear viscosity and other transport coefficients are universal functions of the density and temperature. At low temperatures, the viscosity has a universal quantum scale $\hbar n$, where n is the density and $\hbar$ is Planck's constant h divided by 2π, whereas at high temperatures the natural scale is $p_T^3/\hbar^2$, where p_T is the thermal momentum. We used breathing mode damping to measure the shear viscosity at low temperature. At high temperature T, we used anisotropic expansion of the cloud to find the viscosity, which exhibits precise $T^{3/2}$ scaling. In both experiments, universal hydrodynamic equations including friction and heating were used to extract the viscosity. We estimate the ratio of the shear viscosity to the entropy density and compare it with that of a perfect fluid.

Ultracold, strongly interacting Fermi gases are of broad interest because they provide a tunable tabletop paradigm for strongly interacting systems, ranging from high-temperature superconductors to nuclear matter. First observed in 2002, quantum degenerate, strongly interacting Fermi gases are being widely studied (*1*–*4*). To obtain strong interactions (characterized by a divergent s-wave scattering length), a bias magnetic field is used to tune the gas to a broad collisional (Feshbach) resonance, for which the range of the collision potential is small compared with the interparticle spacing. In this so-called unitary regime, the properties of the gas are universal functions of the density n and temperature T. The universal behavior of the equilibrium thermodynamic properties has been studied in detail (*5*–*11*), whereas the measurement of universal transport coefficients presents new challenges.

[1]Department of Physics, Duke University, Durham, NC 27708, USA. [2]Department of Physics, Gustavus Adolphus College, Saint Peter, MN 56082, USA. [3]Department of Physics, North Carolina State University, Raleigh, NC 27695, USA.

*To whom correspondence should be addressed. E-mail: jet@phy.duke.edu

to the formation of spicular features in He II 304 Å (~0.1 MK). These TR spicules appear with a time delay of around 10 to 20 s, reach much larger heights (~10 to 20 Mm), and typically fall back to the surface within a matter of several minutes, following a parabolic path (Fig. 3 and fig. S5). Despite the enormous line-of-sight superposition at the limb, we often also observe a coronal counterpart of chromospheric/TR spicules (Fig. 3 and fig. S5) in the Fe IX 171 Å images. At the bottom, this takes the form of a dark feature that corresponds to the bright Ca II H feature (movie S8), likely from continuum absorption from neutral hydrogen and helium (*21*). During the later stages, the dark feature disappears (likely because heating reduces the amount of neutral hydrogen and helium), and bright coronal counterparts propagate upward into the coronal hole with similar velocities as the apparent motions of the chromospheric spicules (fig. S5). These coronal counterparts appear to be related to the propagating disturbances in coronal holes that have previously been interpreted as waves (*22*) and more recently linked to upflows (*23*, *24*).

Our observations support a scenario in which chromospheric plasma is propelled upward with speeds of ~50 to 100 km/s, with the bulk of the mass rapidly heated to TR temperatures (~0.02 to 0.1 MK), after which it returns to the surface (invisible to chromospheric passbands). Directly associated with these jets, plasma is heated to coronal temperatures of at least 1 to 2 MK, at the bottom during the initial stages, and both along and toward the top of the chromospheric feature later on. The coronal counterparts of the jets are seen to rapidly propagate upward, likely as a result of strong upflows and/or thermal conduction or waves. Based on the ubiquity of these events and the observed coronal intensities, we estimate that these events carry a mass flux density of 1.5×10^{-9} g/cm^2/s and an energy flux density of $\sim 2 \times 10^6$ erg/cm^2/s into the corona (*25*). This is of the order that is required to sustain the energy lost from the active-region corona (*26*). Given the conservative nature of our estimate, these events are likely to play a substantial role in the coronal energy balance.

Although early models have implicated the heating of chromospheric spicules in the coronal heating problem (*6*), the detailed thermal and spatiotemporal evolution we observed is not compatible with any of the well-established models for coronal heating: None of those predict such strong upflows (driven from below) at chromospheric temperatures (*2*, *27*). These models typically assume energy deposition in the corona, which leads to heating and evaporation of plasma from the chromospheric mass reservoir, driven by thermal conduction from above. Recent advanced numerical models do predict heating rates per particle that reach their maximum in the upper chromosphere (*28*, *29*), which is compatible with our observations. Some analytical models also suggest that dissipation of current sheets resulting from the shuffling of ubiquitous mixed-polarity fields on small scales can provide coronal heating at low heights (*30*). However, there are currently no models for what drives and heats the observed jets (*31*). These first detailed observations of individual coronal heating events highlight the importance of the chromosphere and magnetohydrodynamic/plasma physics approaches for a better understanding of heating in the solar atmosphere.

References and Notes

1. B. Edlen, *Z. Astrophysik* **22**, 30 (1942).
2. J. A. Klimchuk, *Sol. Phys.* **234**, 41 (2006).
3. E. N. Parker, *Geophys. Astrophys. Fluid Dyn.* **50**, 229 (1990).
4. C. J. Schrijver, A. W. Sandman, M. J. Aschwanden, M. L. DeRosa, *Astrophys. J.* **615**, 512 (2004).
5. M. J. Aschwanden, R. Nightingale, P. Boerner, *Astrophys. J.* **656**, 577 (2007).
6. G. W. Pneuman, R. A. Kopp, *Sol. Phys.* **57**, 49 (1978).
7. R. G. Athay, T. E. Holzer, *Astrophys. J.* **255**, 743 (1982).
8. G. L. Withbroe, *Astrophys. J.* **267**, 825 (1983).
9. K. P. Dere, J.-D. F. Bartoe, G. E. Brueckner, *Sol. Phys.* **123**, 41 (1989).
10. R. Rutten, *ASP Conf. Ser.* **354**, 276 (2006)
11. B. De Pontieu *et al.*, *Pub. Astron. Soc. Jpn.* **59**, 655 (2007).
12. B. De Pontieu, S. W. McIntosh, V. H. Hansteen, C. J. Schrijver, *Astrophys. J.* **701**, L1 (2009).
13. J. Mariska, *Solar Transition Region* (Cambridge Astrophysics Series, vol. 23, Cambridge Univ. Press, New York, 1992).
14. Ø. Langangen *et al.*, *Astrophys. J.* **679**, L167 (2008).
15. L. Rouppe van der Voort, J. Leenaarts, B. de Pontieu, M. Carlsson, G. Vissers, *Astrophys. J.* **705**, 272 (2009).
16. T. Kosugi *et al.*, *Sol. Phys.* **243**, 3 (2007).
17. S. Tsuneta *et al.*, *Sol. Phys.* **249**, 167 (2008).
18. See materials and methods in the supporting online material (SOM) on *Science* Online.
19. J. L. Culhane *et al.*, *Sol. Phys.* **243**, 19 (2007).
20. H. Hara *et al.*, *Astrophys. J.* **678**, L67 (2008).
21. U. Anzer, P. Heinzel, *Astrophys. J.* **622**, 714 (2005).
22. D. Banerjee *et al.*, *Astron. Astrophys.* **499**, 29 (2009).
23. S. W. McIntosh, B. De Pontieu, *Astrophys. J.* **707**, 524 (2009).
24. S.W. McIntosh *et al.*, *Astron. Astrophys.* **510**, 2 (2010).
25. See SOM discussion.
26. E. R. Priest, *Solar Magnetohydrodynamics* (D. Reidel Publishing, Dordrecht, Netherlands, 1982).
27. S. Patsourakos, J. A. Klimchuk, *Astrophys. J.* **647**, 1452 (2006).
28. B. V. Gudiksen, A. Nordlund, *Astrophys. J.* **618**, 1031 (2005).
29. V. H. Hansteen, H. Hara, B. De Pontieu, M. Carlsson, *Astrophys. J.* **718**, 1070 (2010).
30. E. Priest, J. Heyvaerts, A. Title, *Astrophys. J.* **576**, 533 (2002).
31. A. Sterling, *Sol. Phys.* **196**, 79 (2000).

32. This work is supported by NASA grants NNX08AL22G and NNX08BA99G (to B.D.P. and S.W.M.), NASA contracts NNM07AA01C (Hinode) and NNG04EA00C (AIA), and the Research Council of Norway (M.C. and V.H.H.). The National Center for Atmospheric Research is sponsored by NSF. Hinode is a Japanese mission developed by the Institute of Space and Astronautical Science/Japan Aerospace Exploration Agency, with the National Astronomical Observatory of Japan as domestic partner and NASA and Science and Technology Facilities Council (UK) as international partners. It is operated in cooperation with the European Space Agency and the Norwegian Space Centre (Norway).

Supporting Online Material

www.sciencemag.org/cgi/content/full/331/6013/55/DC1
Materials and Methods
SOM Text
Figs. S1 to S5
References
Movies S1 to S9

13 September 2010; accepted 2 December 2010
10.1126/science.1197738

Universal Quantum Viscosity in a Unitary Fermi Gas

C. Cao,[1] E. Elliott,[1] J. Joseph,[1] H. Wu,[1] J. Petricka,[2] T. Schäfer,[3] J. E. Thomas[1]*

A Fermi gas of atoms with resonant interactions is predicted to obey universal hydrodynamics, in which the shear viscosity and other transport coefficients are universal functions of the density and temperature. At low temperatures, the viscosity has a universal quantum scale $\hbar n$, where n is the density and $\hbar$ is Planck's constant h divided by 2π, whereas at high temperatures the natural scale is $p_T^3/\hbar^2$, where p_T is the thermal momentum. We used breathing mode damping to measure the shear viscosity at low temperature. At high temperature T, we used anisotropic expansion of the cloud to find the viscosity, which exhibits precise $T^{3/2}$ scaling. In both experiments, universal hydrodynamic equations including friction and heating were used to extract the viscosity. We estimate the ratio of the shear viscosity to the entropy density and compare it with that of a perfect fluid.

Ultracold, strongly interacting Fermi gases are of broad interest because they provide a tunable tabletop paradigm for strongly interacting systems, ranging from high-temperature superconductors to nuclear matter. First observed in 2002, quantum degenerate, strongly interacting Fermi gases are being widely studied (*1*–*4*). To obtain strong interactions (characterized by a divergent s-wave scattering length), a bias magnetic field is used to tune the gas to a broad collisional (Feshbach) resonance, for which the range of the collision potential is small compared with the interparticle spacing. In this so-called unitary regime, the properties of the gas are universal functions of the density n and temperature T. The universal behavior of the equilibrium thermodynamic properties has been studied in detail (*5*–*11*), whereas the measurement of universal transport coefficients presents new challenges.

[1]Department of Physics, Duke University, Durham, NC 27708, USA. [2]Department of Physics, Gustavus Adolphus College, Saint Peter, MN 56082, USA. [3]Department of Physics, North Carolina State University, Raleigh, NC 27695, USA.

*To whom correspondence should be addressed. E-mail: jet@phy.duke.edu

The measurement of the viscosity is of particular interest in the context of a recent conjecture, derived using string theory methods, that defines a perfect normal fluid (*12*). An example of a nearly perfect fluid is the quark-gluon plasma produced in gold ion collisions, which exhibits almost perfect frictionless flow and is thought to be a good approximation to the state of matter that existed microseconds after the Big Bang (*13*). The conjecture states that the ratio of the shear viscosity η to the entropy density s has a universal minimum, $\eta/s \geq \hbar/(4\pi k_B)$, where $\hbar$ is Planck's constant h divided by 2π and k_B is the Boltzmann constant. This ratio is experimentally accessible in a trapped unitary Fermi gas, in which the entropy has been measured both globally (*6*, *9*) and locally (*10*, *11*) and the viscosity can be determined from hydrodynamic experiments (*14*–*17*), so that the predicted minimum ratio can be directly compared with that from Fermi gas experiments (*16*, *17*).

In a Fermi gas, the η/s ratio for the normal fluid is expected to reach a minimum just above the superfluid transition temperature (*16*). This can be understood by using dimensional analysis. Shear viscosity has units of momentum per area. For a unitary gas, the natural momentum is the relative momentum $\hbar k$ of a colliding pair of particles, whereas the natural area is the resonant s-wave collision cross section, $4\pi/k^2$ (*18*). Thus, $\eta \propto \hbar k^3$. At temperatures well below the Fermi temperature at which degeneracy occurs, the Fermi momentum sets the scale so that $k \cong 1/L$, where L is the interparticle spacing. Then, $\eta \propto \hbar/L^3$, and $\eta \propto \hbar n$. For a normal fluid above the critical temperature, the scale of entropy density $s \cong n k_B$, so that $\eta/s \cong \hbar/k_B$. For much higher temperatures above the Fermi temperature, one expects that $\hbar k$ is comparable with the thermal momentum $p_T = \sqrt{2mk_BT}$, giving the scale $\eta \propto p_T^3/\hbar^2 \propto T^{3/2}/\hbar^2$.

To properly measure the shear viscosity with high precision over a wide temperature range, we used universal hydrodynamic equations, which contain both the friction force and the heating rate, to extract the viscosity from two experiments, one for each of two temperature ranges. For measurement at high temperatures, we observed the expansion dynamics of a unitary Fermi gas after release from a deep optical trap and demonstrated the predicted universal $T^{3/2}$ temperature scaling. For measurement at low temperatures, we used the damping rate of the radial breathing mode, using the raw cloud profiles from our previous work (*19*). The smooth joining of the data from the two measurement methods when heating is included (*20*), and the discontinuity of the data when heating is excluded, demonstrates the importance of including the heating as well as the friction force in the universal hydrodynamic analysis.

The experiments employ a 50-50 mixture of the two lowest hyperfine states of ^{6}Li, which was magnetically tuned to a broad Feshbach resonance and cooled by means of evaporation in the optical trap. The initial energy per particle E is measured from the trapped cloud profile (*20*).

In the high-temperature regime, the total energy of the gas E is larger than $2E_F$, well above the critical energy $E_c < 0.8E_F$ for the superfluid transition (*9*–*11*). In this case, the density profile is well fit by a Gaussian, $n(x,y,z,t) = n_0(t) \exp(-x^2/\sigma_x^2 - y^2/\sigma_y^2 - z^2/\sigma_z^2)$, where $\sigma_i(t)$ is a time-dependent width, $n_0(t) = N/(\pi^{3/2}\sigma_x\sigma_y\sigma_z)$ is the central density, and N is the total number of atoms.

The aspect ratio $\sigma_x(t)/\sigma_z(t)$ was measured as a function of time after release so as to characterize the hydrodynamics, for different energies E between $2.3E_F$ and $4.6E_F$ (Fig. 1). We also took expansion data at one low-energy point $E = 0.6E_F$, where the viscosity is small as compared with that obtained at higher temperatures and the density profile is approximately a zero-temperature Thomas-Fermi distribution. The black curve in Fig. 1 shows the fit for zero viscosity and no free parameters. To obtain a high signal-to-background ratio, we measured the aspect ratio only up to 1.4. For comparison, the green dashed curve in Fig. 1 shows the prediction for a ballistic gas.

We determined the shear viscosity η by using a hydrodynamic description of the velocity field $\mathbf{v}(\mathbf{x},t)$ in terms of the scalar pressure and the shear viscosity pressure tensor,

$$m(\partial_t + \mathbf{v} \cdot \nabla)v_i = f_i + \sum_j \frac{\partial_j(\eta\,\sigma_{ij})}{n} \qquad (1)$$

where $\mathbf{f} = -\nabla P/n$ is the force per particle arising from the scalar pressure P and m is the atom mass. For a unitary gas, the bulk viscosity is predicted to vanish in the normal fluid (*21*, *22*), so we did not include it in the analysis for the expansion. The second term on the right describes the friction forces arising from the shear viscos-

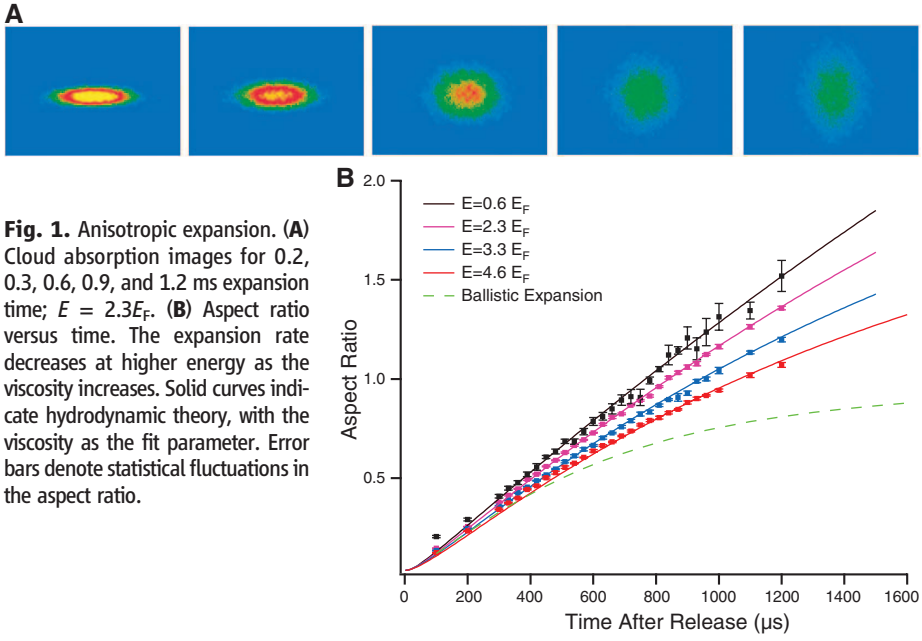

Fig. 1. Anisotropic expansion. (**A**) Cloud absorption images for 0.2, 0.3, 0.6, 0.9, and 1.2 ms expansion time; $E = 2.3E_F$. (**B**) Aspect ratio versus time. The expansion rate decreases at higher energy as the viscosity increases. Solid curves indicate hydrodynamic theory, with the viscosity as the fit parameter. Error bars denote statistical fluctuations in the aspect ratio.

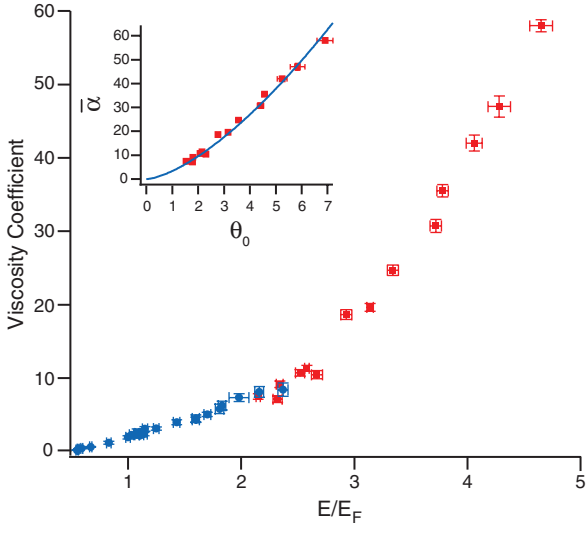

Fig. 2. Trap-averaged viscosity coefficient $\bar{\alpha} = \int d^3\mathbf{x}\, \eta/(\hbar N)$ versus initial energy per atom. Blue circles indicate breathing-mode measurements; red squares indicate anisotropic expansion measurements. Bars denote statistical error arising from the uncertainty in E and the cloud dimensions. (**Inset**) $\bar{\alpha}$ versus reduced temperature θ_0 at the trap center before release of the cloud. The blue curve shows the fit $\alpha_0 = \alpha_{3/2}\,\theta_0^{3/2}$, demonstrating the predicted universal high-temperature scaling. Bars denote statistical error arising from the uncertainty in θ_0 and $\bar{\alpha}$. A 3% systematic uncertainty in E_F and 7% in θ_0 arises from the systematic uncertainty in the absolute atom number (*20*).

ity, where $\sigma_{ij} = \partial v_i/\partial x_j + \partial v_j/\partial x_i - 2\delta_{ij}\nabla \cdot \mathbf{v}/3$ is symmetric and traceless.

For a unitary gas, the evolution equation for the pressure takes a simple form because $P = 2\mathcal{E}/3$ (*23*, *24*), where $\mathcal{E}$ is the local energy density (sum of the kinetic and interaction energy). Then, energy conservation and Eq. 1 implies $(\partial_t + \mathbf{v} \cdot \nabla + 5\nabla \cdot \mathbf{v}/3)P = 2 \cdot \dot{q}/3$. Here, the heating rate per unit volume times $\dot{q} = \eta\sigma_{ij}^2/2$ arises from friction from the relative motion of neighboring volume elements. To express this in terms of the force per particle (f_i), we differentiated this equation for P with respect to x_i and used the continuity equation for the density to obtain

$$\left(\partial_t + \mathbf{v} \cdot \nabla + \frac{2}{3}\nabla \cdot \mathbf{v}\right) f_i + \sum_j (\partial_i v_j) f_j - \frac{5}{3}(\partial_i \nabla \cdot \mathbf{v})\frac{P}{n} = -\frac{2}{3}\frac{\partial_i \dot{q}}{n} \quad (2)$$

Force balance in the trapping potential $U_{trap}(\mathbf{x})$, just before release of the cloud, determines the initial condition $f_i(0) = \partial_i U_{trap}(\mathbf{x})$.

These hydrodynamic equations include both the force and the heating arising from viscosity. The solution is greatly simplified when the cloud is released from a deep, nearly harmonic trapping potential U_{trap} because $f_i(0)$ is then linear in the spatial coordinate. If we neglect viscosity, the force per particle and hence the velocity field remain linear functions of the spatial coordinates as the cloud expands. Thus, $\partial_i(\nabla \cdot \mathbf{v}) = 0$, and the pressure P does not appear in Eq. 2. Through numerical integration (*25*), we found that nonlinearities in the velocity field are very small, even if the viscosity is not zero, because dissipative forces tend to restore a linear flow profile. Hence, the evolution Eqs. 1 and 2 are only weakly dependent on the precise initial spatial profile of P and independent of the detailed thermodynamic properties.

We therefore assumed that the velocity field is exactly linear in the spatial coordinates. We took $f_i = a_i(t)x_i$ and $\sigma_i(t) = b_i(t)\sigma_i(0)$; the density changes by a scale transformation (*26*), where current conservation then requires $v_i = x_i \dot{b}_i(t)/b_i(t)$.

In general, the viscosity takes the universal form $\eta = \alpha(\theta)\hbar n$, where θ is the local reduced temperature and $\eta \to 0$ in the low-density region of the cloud (*20*, *27*). Using the measured trap frequencies, and Eqs. 1 and 2, the aspect ratio data are fit to determine the trap-averaged viscosity parameter, $\bar{\alpha} = (1/N\hbar)\int d^3\mathbf{x}\ \eta(\mathbf{x},t)$, which arises naturally independent of the spatial profile of and is equivalent to assuming η. Because θ has a zero convective derivative everywhere (in the zeroth-order adiabatic approximation) and the number of atoms in a volume element is conserved along a stream tube, $\bar{\alpha}$ is a constant that can be compared with predictions for the trapped cloud before release.

As shown in Fig. 1, the expansion data are very well fit over the range of energies studied, using $\bar{\alpha}$ as the only free parameter. We found that the friction force produces a curvature that matches the aspect ratio–versus-time data, whereas the indirect effect of heating is important in increasing the outward force, which increases the fitted $\bar{\alpha}$ by a factor of ≅2, as compared with that obtained when heating is omitted (*20*).

For measurements at low temperatures, where the viscosity is small, we determined $\bar{\alpha}$ from the damping rate of the radial breathing mode (*19*). For the breathing mode, the cloud radii change by a scale transformation of the form $b_i = 1 + \dot{\varepsilon}_i$, with $\varepsilon_i << 1$, and the heating rate in Eq. 2 is $\propto \dot{\varepsilon}_i^2$, which is negligible. Hence, the force per particle evolves adiabatically. Adding the trapping force to Eq. 1, one obtains the damping rate $1/\tau = \hbar\,\bar{\alpha}/(3m\langle x^2\rangle)$ (*20*, *28*).

The fitted viscosity coefficients $\bar{\alpha}$ for the entire energy range are shown in Fig. 2, which can be used to test predictions (*29*–*31*). Despite the large values of $\bar{\alpha}$ at the higher energies, the viscosity causes only a moderate perturbation to the adiabatic expansion, as shown by the expansion data and the fits in Fig. 1. The breathing mode data and expansion data smoothly join, provided that the heating rate is included in the analysis. In contrast, omitting the heating rate produces a discontinuity between the high- and low-temperature viscosity data (*20*). The agreement between these very different measurements when heating is included shows that hydrodynamics in the universal regime is well described by Eqs. 1 and 2.

To test the prediction of the $T^{3/2}$ temperature scaling in the high-temperature regime, we assumed that η relaxes to the equilibrium value in the center of the trap but vanishes in the low-density region so that $\bar{\alpha}$ is well defined. This behavior is predicted by kinetic theory (*27*). We expect that $\bar{\alpha} \cong \alpha_0$, where $\eta_0 = \alpha_0\,\hbar\,n_0$ is the viscosity at the trap center before release. At high temperatures (*15*),

$$\alpha_0 = \alpha_{3/2}\,\theta_0^{3/2} \quad (3)$$

where $\alpha_{3/2}$ is a universal coefficient. Because θ has a zero convective derivative everywhere (in the zeroth-order adiabatic approximation), θ_0 at the trap center has a zero time derivative, and α_0 is therefore constant, as is $\bar{\alpha}$.

The inset in Fig. 2 shows the high-temperature (expansion) data for $\bar{\alpha}$ versus the initial reduced temperature at the trap center, θ_0. Here, $\theta_0 = T_0/T_F(n_0) = (T_0/T_{FI})(n_I/n_0)^{2/3}$. The local Fermi temperature $T_F(n_0) = \hbar^2(3\pi^2 n_0)^{2/3}/(2mk_B)$, and $T_{FI} = E_F/k_B = T_F(n_I)$ is the ideal gas Fermi temperature at the trap center. n_I is the ideal gas central density for a zero-temperature Thomas-Fermi distribution. We used $(n_I/n_0)^{2/3} = 4(\sigma^2{}_z/\sigma^2{}_{Fz})/\pi^{1/3}$ and obtained the initial T_0/T_{FI} from the cloud profile (*20*).

The excellent fit of Eq. 3 to the data (Fig. 2, inset) demonstrates that at high temperature, the viscosity coefficient very well obeys the $\theta_0^{3/2}$ scaling, which is in agreement with predictions (*15*). Eq. 3 predicts that α_0 scales nearly as E^3 because $\theta_0 \propto T_0/n_0^{2/3} \propto E^2$. This explains the factor of ≅10 increase in the viscosity coefficients as the initial energy is increased from $E = 2.3E_F$ to $E = 4.6E_F$.

A precise comparison between the viscosity data and theory requires calculation of the trap-average $\bar{\alpha}$ from the local shear viscosity, where the relation is tightly constrained by the observed $T^{3/2}$ scaling. Our simple approximation $\bar{\alpha} \cong \alpha_0$ yields $\alpha_{3/2} = 3.4(0.03)$, where 0.03 is the statistical error from the fit. A better estimate based on a relaxation model (*29*) shows that $\bar{\alpha} = 1.3\,\alpha_0$ at high T, yielding $\alpha_{3/2} = 2.6$. At sufficiently high temperature, the mean free path becomes longer than the interparticle spacing because the unitary collision cross section decreases with increasing energy. In this limit, a two-body Boltzmann equation description of the viscosity is valid. For a Fermi gas in a 50-50 mixture of two spin states, a variational calculation (*15*) yields $\alpha_{3/2} = 45\pi^{3/2}/(64\sqrt{2}) = 2.77$, which is in reasonable agreement with the fitted values.

Lastly, Fig. 3 shows an estimate of the ratio of $\eta/s = \alpha\hbar n/s = (\hbar/k_B)\alpha/(s/nk_B) \cong (\hbar/k_B)\,\bar{\alpha}/S$, where S is the average entropy per particle of the trapped gas in units of k_B. We obtain S in the low-

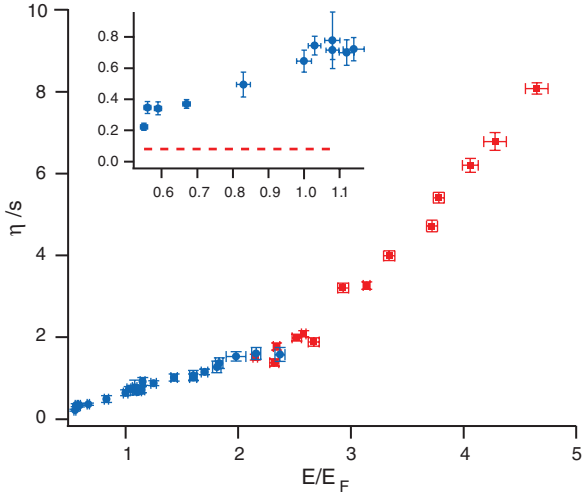

Fig. 3. Estimated ratio of the shear viscosity to the entropy density. Blue circles indicate breathing-mode measurements; red squares indicate anisotropic expansion measurements. **(Inset)** The red dashed line denotes the string theory limit. Bars denote statistical error arising from the uncertainty in E, $\bar{\alpha}$, and S (*20*).

temperature regime from (*9*), which joins smoothly to the second virial coefficient approximation for S in the high-temperature regime (*20*). The Fig. 3 inset shows the low-temperature behavior, which is about five times the string theory limit (Fig. 3, inset, red dashed line) near the critical energy $E_c/E_F = 0.7–0.8$ (*9*, *20*). The apparent decrease of the η/s ratio as the energy approaches the ground state $0.48E_F$ (*9*) does not require that the local ratio $\rightarrow 0$ as $T \rightarrow 0$ because contributions from the cloud edges significantly increase S as compared with the local s at the center.

References and Notes

1. K. M. O'Hara, S. L. Hemmer, M. E. Gehm, S. R. Granade, J. E. Thomas, *Science* **298**, 2179 (2002).
2. S. Giorgini, L. P. Pitaevskii, S. Stringari, *Rev. Mod. Phys.* **80**, 1215 (2008).
3. I. Bloch, J. Dalibard, W. Zwerger, *Rev. Mod. Phys.* **80**, 885 (2008).
4. W. Ketterle, M. W. Zwierlein, "Making, probing and understanding ultracold Fermi gases," in *Ultracold Fermi Gases, Proceedings of the International School of Physics "Enrico Fermi,"* Course CLXIV, Varenna, 20 to 30 June 2006 (IOS Press, Amsterdam, 2008).
5. J. Kinast *et al.*, *Science* **307**, 1296 (2005).
6. L. Luo, B. Clancy, J. Joseph, J. Kinast, J. E. Thomas, *Phys. Rev. Lett.* **98**, 080402 (2007).
7. J. T. Stewart, J. P. Gaebler, C. A. Regal, D. S. Jin, *Phys. Rev. Lett.* (2006).
8. H. Hu, P. D. Drummond, X.-J. Liu, *Nat. Phys.* **3**, 469 (2007).
9. L. Luo, J. E. Thomas, *J. Low Temp. Phys.* **154**, 1 (2009).
10. M. Horikoshi, S. Nakajima, M. Ueda, T. Mukaiyama, *Science* **327**, 442 (2010).
11. S. Nascimbène, N. Navon, K. J. Jiang, F. Chevy, C. Salomon, *Nature* **463**, 1057 (2010).
12. P. K. Kovtun, D. T. Son, A. O. Starinets, *Phys. Rev. Lett.* **94**, 111601 (2005).
13. L. P. Csernai, J. I. Kapusta, L. D. McLerran, *Phys. Rev. Lett.* **97**, 152303 (2006).
14. B. A. Gelman, E. V. Shuryak, I. Zahed, *Phys. Rev. A* **72**, 043601 (2005).
15. G. M. Bruun, H. Smith, *Phys. Rev. A* **75**, 043612 (2007).
16. T. Schäfer, *Phys. Rev. A* **76**, 063618 (2007).
17. A. Turlapov *et al.*, *J. Low Temp. Phys.* **150**, 567 (2008).
18. The experiments were performed far from p-wave Feshbach resonances. The relevant threshold energy for p-wave scattering was then comparable with the barrier height. Using the known C_6 coefficients, the barrier height for ^{40}K is 280 μK, whereas for ^{6}Li the barrier height is 8 mK. Hence, for temperatures in the μK range as used in the experiments, p-wave scattering is negligible, and s-wave scattering dominates.
19. J. Kinast, A. Turlapov, J. E. Thomas, *Phys. Rev. Lett.* **94**, 170404 (2005).
20. Materials and methods are available as supporting material on *Science* Online.
21. D. T. Son, *Phys. Rev. Lett.* **98**, 020604 (2007).
22. M. A. Escobedo, M. Mannarelli, C. Manuel, *Phys Rev. A*, http://arxiv.org/abs/0904.3023v2.
23. T.-L. Ho, *Phys. Rev. Lett.* **92**, 090402 (2004).
24. J. E. Thomas, J. Kinast, A. Turlapov, *Phys. Rev. Lett.* **95**, 120402 (2005).
25. T. Schäfer, http://arxiv.org/abs/1008.3876v1.
26. C. Menotti, P. Pedri, S. Stringari, *Phys. Rev. Lett.* **89**, 250402 (2002).
27. P. Massignan, G. M. Bruun, H. Smith, *Phys. Rev. A* **71**, 033607 (2005).
28. We give the damping rate $1/\tau$ for a cylindrically symmetric cigar-shaped trap. For $\delta \equiv (\omega_x - \omega_y)/\sqrt{\omega_x\omega_y} << 1$, with ω_x,ω_y the transverse trap frequencies, $1/\tau$ contains an additional factor $1 - \delta$.
29. H. Guo, D. Wulin, C.-C. Chien, K. Levin, http://arxiv.org/abs/1008.0423v3.
30. E. Taylor, M. Randeria, *Phys. Rev. A* **81**, 053610 (2010).
31. T. Enss, R. Haussmann, W. Zwerger, http://dx.doi.org/10.1016/j.aop.2010.10.002.
32. T. Scäfer, C. Chafin, http://arxiv.org/abs/0912.4236v3.

33. This research is supported by the Physics Divisions of NSF, the Army Research Office, the Air Force Office Office of Sponsored Research, and the Division of Materials Science and Engineering, the Office of Basic Energy Sciences, Office of Science, U.S. Department of Energy. J.E.T. and T.S. thank the ExtreMe Matter Institute (EMMI) for hospitality.

Supporting Online Material

www.sciencemag.org/cgi/content/full/science.1195219/DC1
Materials and Methods
Figs. S1 and S2
References

16 July 2010; accepted 24 November 2010
Published online 9 December 2010;
10.1126/science.1195219

Time-Resolved Holography with Photoelectrons

Y. Huismans,[1]* A. Rouzée,[1,2] A. Gijsbertsen,[1] J. H. Jungmann,[1] A. S. Smolkowska,[1] P. S. W. M. Logman,[1] F. Lépine,[3] C. Cauchy,[3] S. Zamith,[4] T. Marchenko,[5] J. M. Bakker,[6] G. Berden,[6] B. Redlich,[6] A. F. G. van der Meer,[6] H. G. Muller,[1] W. Vermin,[7] K. J. Schafer,[8] M. Spanner,[9] M. Yu. Ivanov,[10] O. Smirnova,[2] D. Bauer,[11] S. V. Popruzhenko,[12] M. J. J. Vrakking[1,2]*

Ionization is the dominant response of atoms and molecules to intense laser fields and is at the basis of several important techniques, such as the generation of attosecond pulses that allow the measurement of electron motion in real time. We present experiments in which metastable xenon atoms were ionized with intense 7-micrometer laser pulses from a free-electron laser. Holographic structures were observed that record underlying electron dynamics on a sublaser-cycle time scale, enabling photoelectron spectroscopy with a time resolution of almost two orders of magnitude higher than the duration of the ionizing pulse.

After a strong laser field ionizes an atom or molecule, the liberated electron is accelerated by the oscillatory laser electric field and driven back toward the ion (*1*). Electron-ion recollision leads to the emission of extreme ultraviolet (XUV) radiation, with a duration that approaches the atomic unit of time (24.2 as) (*2*, *3*) and encodes detailed structural and dynamical information about the atomic or molecular medium used (*4*–*7*). Alternatively, the returning electron may elastically or inelastically scatter (*8*, *9*). These processes benefit from the 10^{11} A/cm^2 electron recollision current incident on the target ion, exceeding current densities used in transmission electron microscopes (*10*). The laser-driven electron motion is fully coherent, allowing one to put into practice the concept of holography (*11*) and to extend it to electron-ion collisions involving laser-ionized and -driven photoelectrons (*9*, *12*, *13*). We show how under suitably chosen experimental conditions, a hologram can be recorded that encodes temporal and spatial information both about the ion (the "target") and the recollision electron (the "source"), opening the way to a new type of ultrafast photoelectron spectroscopy of electron and nuclear dynamics in molecules.

Key to holographic electron imaging is the observation of an interference pattern between a reference wave, which is emitted from the source and does not interact with the target, and a signal wave, which scatters off the target and encodes its structure. The encoded information is stored when the signal wave interferes with the reference wave on a detector. A simple analysis borrowed from ray optics (Fig. 1A) shows that because of path length differences, a phase difference $\Delta\varphi = (k - k_z)z_0$ (where k is the total momentum, k_z is the momentum in the z direction, and z_0 is the distance to the scattering center) arises between the reference and scattered waves, resulting in the pattern shown in Fig. 1B.

To record a clear holographic picture, it is desirable that the reference wave not be influenced by the positively charged target and, therefore, that the electron source is located at some distance from the target, z_0. A suitable way to

[1]FOM Institute AMOLF, Science Park 113, 1098 XG Amsterdam, Netherlands. [2]Max-Born-Institut, Max Born Straße 2A, D-12489 Berlin, Germany. [3]Université Lyon I, CNRS, Laboratoire de Spectrométrie Ionique et Moléculaire, UMR 5579, Bâtiment. Kastler, 43, Boulevard du 11 Novembre 1918, F69622 Villeurbanne Cedex, France. [4]Laboratoire Collisions, Agrégats, Réactivité, Institut de Recherche sur les Systèmes Atomiques et Moléculaires Complexes, UPS, Université de Toulouse and UMR 5589 CNRS, 31062 Toulouse, France. [5]Université Pierre et Marie Curie Université Paris 6, CNRS, UMR 7614, Laboratoire de Chimie Physique-Matière et Rayonnement, 11 rue Pierre et Marie Curie, F-75005 Paris, France. [6]FOM-Institute for Plasma Physics Rijnhuizen, Edisonbaan 14, 3439 MN Nieuwegein, Netherlands. [7]SARA Computing and Networking Services, Science Park 121, 1098 XG Amsterdam, Netherlands. [8]Department of Physics and Astronomy, Louisiana State University (LSU), Baton Rouge, Louisiana 70803–4001, USA. [9]National Research Council of Canada, Ottawa, Ontario K1A 0R6, Canada. [10]Department of Physics, Imperial College, London SW7 2BW, UK. [11]Institut für Physik, Universität Rostock, 18051 Rostock, Germany. [12]Moscow Engineering Physics Institute, National Research Nuclear University, Kashirskoe Shosse 31, Moscow, 115409, Russia.

*To whom correspondence should be addressed. E-mail: huismans@amolf.nl (Y.H.); marc.vrakking@mbi.berlin.de (M.J.J.V.)

temperature regime from (*9*), which joins smoothly to the second virial coefficient approximation for S in the high-temperature regime (*20*). The Fig. 3 inset shows the low-temperature behavior, which is about five times the string theory limit (Fig. 3, inset, red dashed line) near the critical energy $E_c/E_F = 0.7–0.8$ (*9*, *20*). The apparent decrease of the η/s ratio as the energy approaches the ground state $0.48E_F$ (*9*) does not require that the local ratio $\rightarrow 0$ as $T \rightarrow 0$ because contributions from the cloud edges significantly increase S as compared with the local s at the center.

References and Notes

1. K. M. O'Hara, S. L. Hemmer, M. E. Gehm, S. R. Granade, J. E. Thomas, *Science* **298**, 2179 (2002).
2. S. Giorgini, L. P. Pitaevskii, S. Stringari, *Rev. Mod. Phys.* **80**, 1215 (2008).
3. I. Bloch, J. Dalibard, W. Zwerger, *Rev. Mod. Phys.* **80**, 885 (2008).
4. W. Ketterle, M. W. Zwierlein, "Making, probing and understanding ultracold Fermi gases," in *Ultracold Fermi Gases, Proceedings of the International School of Physics "Enrico Fermi,"* Course CLXIV, Varenna, 20 to 30 June 2006 (IOS Press, Amsterdam, 2008).
5. J. Kinast *et al*., *Science* **307**, 1296 (2005).
6. L. Luo, B. Clancy, J. Joseph, J. Kinast, J. E. Thomas, *Phys. Rev. Lett.* **98**, 080402 (2007).
7. J. T. Stewart, J. P. Gaebler, C. A. Regal, D. S. Jin, *Phys. Rev. Lett.* (2006).
8. H. Hu, P. D. Drummond, X.-J. Liu, *Nat. Phys.* **3**, 469 (2007).
9. L. Luo, J. E. Thomas, *J. Low Temp. Phys.* **154**, 1 (2009).
10. M. Horikoshi, S. Nakajima, M. Ueda, T. Mukaiyama, *Science* **327**, 442 (2010).
11. S. Nascimbène, N. Navon, K. J. Jiang, F. Chevy, C. Salomon, *Nature* **463**, 1057 (2010).
12. P. K. Kovtun, D. T. Son, A. O. Starinets, *Phys. Rev. Lett.* **94**, 111601 (2005).
13. L. P. Csernai, J. I. Kapusta, L. D. McLerran, *Phys. Rev. Lett.* **97**, 152303 (2006).
14. B. A. Gelman, E. V. Shuryak, I. Zahed, *Phys. Rev. A* **72**, 043601 (2005).
15. G. M. Bruun, H. Smith, *Phys. Rev. A* **75**, 043612 (2007).
16. T. Schäfer, *Phys. Rev. A* **76**, 063618 (2007).
17. A. Turlapov *et al*., *J. Low Temp. Phys.* **150**, 567 (2008).
18. The experiments were performed far from p-wave Feshbach resonances. The relevant threshold energy for p-wave scattering was then comparable with the barrier height. Using the known C_6 coefficients, the barrier height for ^{40}K is 280 μK, whereas for ^{6}Li the barrier height is 8 mK. Hence, for temperatures in the μK range as used in the experiments, p-wave scattering is negligible, and s-wave scattering dominates.
19. J. Kinast, A. Turlapov, J. E. Thomas, *Phys. Rev. Lett.* **94**, 170404 (2005).
20. Materials and methods are available as supporting material on *Science* Online.
21. D. T. Son, *Phys. Rev. Lett.* **98**, 020604 (2007).
22. M. A. Escobedo, M. Mannarelli, C. Manuel, *Phys Rev. A*, http://arxiv.org/abs/0904.3023v2.
23. T.-L. Ho, *Phys. Rev. Lett.* **92**, 090402 (2004).
24. J. E. Thomas, J. Kinast, A. Turlapov, *Phys. Rev. Lett.* **95**, 120402 (2005).
25. T. Schäfer, http://arxiv.org/abs/1008.3876v1.
26. C. Menotti, P. Pedri, S. Stringari, *Phys. Rev. Lett.* **89**, 250402 (2002).
27. P. Massignan, G. M. Bruun, H. Smith, *Phys. Rev. A* **71**, 033607 (2005).
28. We give the damping rate $1/\tau$ for a cylindrically symmetric cigar-shaped trap. For $\delta \equiv (\omega_x - \omega_y)/\sqrt{\omega_x\omega_y} << 1$, with ω_x,ω_y the transverse trap frequencies, $1/\tau$ contains an additional factor $1 - \delta$.
29. H. Guo, D. Wulin, C.-C. Chien, K. Levin, http://arxiv.org/abs/1008.0423v3.
30. E. Taylor, M. Randeria, *Phys. Rev. A* **81**, 053610 (2010).
31. T. Enss, R. Haussmann, W. Zwerger, http://dx.doi.org/10.1016/j.aop.2010.10.002.
32. T. Scäfer, C. Chafin, http://arxiv.org/abs/0912.4236v3.

33. This research is supported by the Physics Divisions of NSF, the Army Research Office, the Air Force Office Office of Sponsored Research, and the Division of Materials Science and Engineering, the Office of Basic Energy Sciences, Office of Science, U.S. Department of Energy. J.E.T. and T.S. thank the ExtreMe Matter Institute (EMMI) for hospitality.

Supporting Online Material

www.sciencemag.org/cgi/content/full/science.1195219/DC1
Materials and Methods
Figs. S1 and S2
References

16 July 2010; accepted 24 November 2010
Published online 9 December 2010;
10.1126/science.1195219

Time-Resolved Holography with Photoelectrons

Y. Huismans,[1]* A. Rouzée,[1,2] A. Gijsbertsen,[1] J. H. Jungmann,[1] A. S. Smolkowska,[1] P. S. W. M. Logman,[1] F. Lépine,[3] C. Cauchy,[3] S. Zamith,[4] T. Marchenko,[5] J. M. Bakker,[6] G. Berden,[6] B. Redlich,[6] A. F. G. van der Meer,[6] H. G. Muller,[1] W. Vermin,[7] K. J. Schafer,[8] M. Spanner,[9] M. Yu. Ivanov,[10] O. Smirnova,[2] D. Bauer,[11] S. V. Popruzhenko,[12] M. J. J. Vrakking[1,2]*

Ionization is the dominant response of atoms and molecules to intense laser fields and is at the basis of several important techniques, such as the generation of attosecond pulses that allow the measurement of electron motion in real time. We present experiments in which metastable xenon atoms were ionized with intense 7-micrometer laser pulses from a free-electron laser. Holographic structures were observed that record underlying electron dynamics on a sublaser-cycle time scale, enabling photoelectron spectroscopy with a time resolution of almost two orders of magnitude higher than the duration of the ionizing pulse.

After a strong laser field ionizes an atom or molecule, the liberated electron is accelerated by the oscillatory laser electric field and driven back toward the ion (*1*). Electron-ion recollision leads to the emission of extreme ultraviolet (XUV) radiation, with a duration that approaches the atomic unit of time (24.2 as) (*2*, *3*) and encodes detailed structural and dynamical information about the atomic or molecular medium used (*4*–*7*). Alternatively, the returning electron may elastically or inelastically scatter (*8*, *9*). These processes benefit from the 10^{11} A/cm^2 electron recollision current incident on the target ion, exceeding current densities used in transmission electron microscopes (*10*). The laser-driven electron motion is fully coherent, allowing one to put into practice the concept of holography (*11*) and to extend it to electron-ion collisions involving laser-ionized and -driven photoelectrons (*9*, *12*, *13*). We show how under suitably chosen experimental conditions, a hologram can be recorded that encodes temporal and spatial information both about the ion (the "target") and the recollision electron (the "source"), opening the way to a new type of ultrafast photoelectron spectroscopy of electron and nuclear dynamics in molecules.

Key to holographic electron imaging is the observation of an interference pattern between a reference wave, which is emitted from the source and does not interact with the target, and a signal wave, which scatters off the target and encodes its structure. The encoded information is stored when the signal wave interferes with the reference wave on a detector. A simple analysis borrowed from ray optics (Fig. 1A) shows that because of path length differences, a phase difference $\Delta\varphi = (k - k_z)z_0$ (where k is the total momentum, k_z is the momentum in the z direction, and z_0 is the distance to the scattering center) arises between the reference and scattered waves, resulting in the pattern shown in Fig. 1B.

To record a clear holographic picture, it is desirable that the reference wave not be influenced by the positively charged target and, therefore, that the electron source is located at some distance from the target, z_0. A suitable way to

[1]FOM Institute AMOLF, Science Park 113, 1098 XG Amsterdam, Netherlands. [2]Max-Born-Institut, Max Born Straße 2A, D-12489 Berlin, Germany. [3]Université Lyon I, CNRS, Laboratoire de Spectrométrie Ionique et Moléculaire, UMR 5579, Bâtiment. Kastler, 43, Boulevard du 11 Novembre 1918, F69622 Villeurbanne Cedex, France. [4]Laboratoire Collisions, Agrégats, Réactivité, Institut de Recherche sur les Systèmes Atomiques et Moléculaires Complexes, UPS, Université de Toulouse and UMR 5589 CNRS, 31062 Toulouse, France. [5]Université Pierre et Marie Curie Université Paris 6, CNRS, UMR 7614, Laboratoire de Chimie Physique-Matière et Rayonnement, 11 rue Pierre et Marie Curie, F-75005 Paris, France. [6]FOM-Institute for Plasma Physics Rijnhuizen, Edisonbaan 14, 3439 MN Nieuwegein, Netherlands. [7]SARA Computing and Networking Services, Science Park 121, 1098 XG Amsterdam, Netherlands. [8]Department of Physics and Astronomy, Louisiana State University (LSU), Baton Rouge, Louisiana 70803–4001, USA. [9]National Research Council of Canada, Ottawa, Ontario K1A 0R6, Canada. [10]Department of Physics, Imperial College, London SW7 2BW, UK. [11]Institut für Physik, Universität Rostock, 18051 Rostock, Germany. [12]Moscow Engineering Physics Institute, National Research Nuclear University, Kashirskoe Shosse 31, Moscow, 115409, Russia.

*To whom correspondence should be addressed. E-mail: huismans@amolf.nl (Y.H.); marc.vrakking@mbi.berlin.de (M.J.J.V.)

accomplish this is tunnel ionization in a strong low-frequency laser field, in which the electron tunnels through a barrier created by the laser field and appears at some distance from the ion.

In the presence of the laser field, the electronic wave function can be written as

$$\psi = \psi_{signal} + \psi_{ref} \quad (1)$$

where ψ_{signal} represents a signal wave packet that oscillates in the laser field and scatters off the target and ψ_{ref} represents a reference wave packet, which only experiences the laser field and does not interact with the target (*14*). To calculate the interference pattern produced by these two terms, we used an extension of the strong field approximation (SFA), which includes the laser field fully and the electron-ion scattering in the first Born approximation (*15*, *16*). The result of the calculation (fig. S3A) (*14*) predicts that in a strong laser field, the holographic fringes remain visible and that the phase difference between the signal and the reference wave packets is

$$\Delta\varphi \approx p_r^2(t_C - t_0^{ref})/2 \quad (2)$$

Here, p_r is the momentum perpendicular to the laser polarization axis, t_C is the time when the signal wave packet scatters off the ion, and t_0^{ref} is the moment of birth of the reference wave packet. Thus, the hologram can be viewed as a pump-probe experiment on the femtosecond-to–sub-femtosecond time scale (fig. S3, B and C), which can encode changes in the scattering potential between t_0^{ref} and t_C, as well as changes in the ionization rate between t_0^{ref} and t_0^{signal}, which is the time of birth of the signal wave packet (*14*). The signal and reference wave packets that produce the holographic pattern originate from the same quarter cycle; thus, subcycle time resolution is encoded, even when long pulses are used.

A crucial aspect in our holographic imaging approach is the existence of a large electron oscillation amplitude of $\alpha >> 1$ Å and a large average oscillation energy $U_p >> \hbar\omega_{laser}$, where ω_{laser} is the laser frequency and $\hbar$ is Planck's constant h divided by 2π. In experiments with 800 nm radiation, these requirements lead to high laser intensities ($I \sim 10^{14}$ W/cm^2) that can only be applied to ground-state atoms and molecules with a large ionization potential. To make recollision-based imaging possible at lower intensities, the laser wavelength λ_{laser} must be increased because both α and U_p scale as λ_{laser}^2.

To demonstrate the strong-field electron holography experimentally, metastable (6 s) xenon atoms were ionized with 7-μm mid-infrared (mid-IR) radiation from the FELICE (Free Electron Laser for Intra-Cavity Experiments) beamline at the Free Electron Laser for Infrared Experiments (FELIX) facility (fig. S1) (*14*, *17*). The use of a large λ_{laser} in combination with a modest ionization potential (IP = 3.8 eV) allowed the preparation of electron wave packets born at large $z_0 = IP/F_{laser}$, where F_{laser} is the laser field strength, displaying a large excursion α_0, without the need for a very high laser intensity (7×10^{11} W/cm^2), and remaining in the tunneling regime $\left[\gamma = \left(\frac{\omega_{laser}}{F_{laser}}\right)\sqrt{2IP} < 1\right]$. Angle-resolved photoelectron spectra were recorded with a velocity map imaging spectrometer (VMI) (*18*) integrated into the FELICE laser cavity. The metastable xenon atoms were exposed to a train of 5000 mid-IR laser pulses separated by 1 ns.

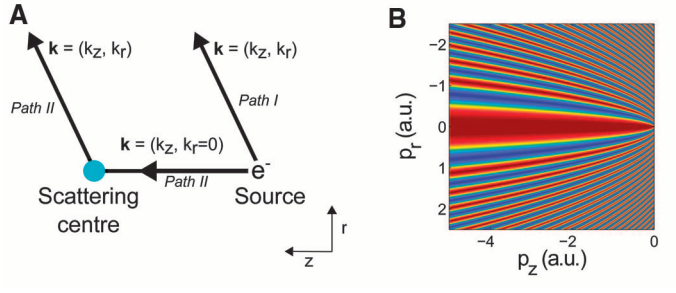

Fig. 1. (**A**) Diagram illustrating the concept of electron holography. Two interfering paths with the same final momentum $\mathbf{k} = (k_z,k_r)$ are indicated. Path I is a reference wave, leaving the source with momentum $\mathbf{k} = (k_z,k_r)$. Path II is a signal wave, incident on the target with $k_r = 0$, $k_z = k = |\mathbf{k}|$ and scattering into $\mathbf{k} = (k_z,k_r)$. The phase difference $\Delta\varphi = (k - k_z)z_0$ that follows from the path length differences leads to interference fringes ~cos[$(k - k_z)z_0$]. (**B**) Interference pattern generated by a Gaussian wave packet released at a distance z_0 = 50 atomic units (a.u.) from a scattering center, with no laser field present. A hologram is created as a result of interference between a scattering-signal wave packet and a direct-reference wave packet.

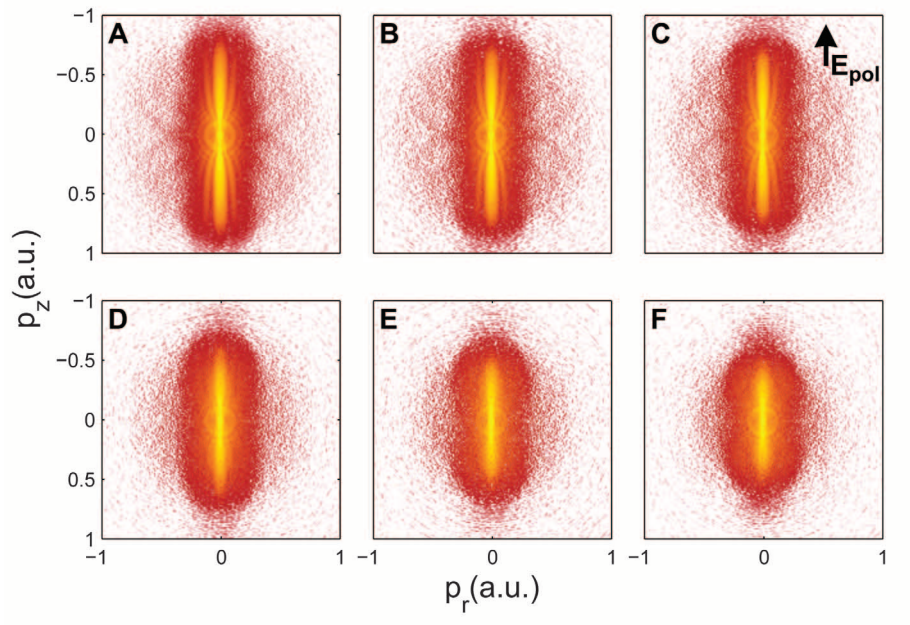

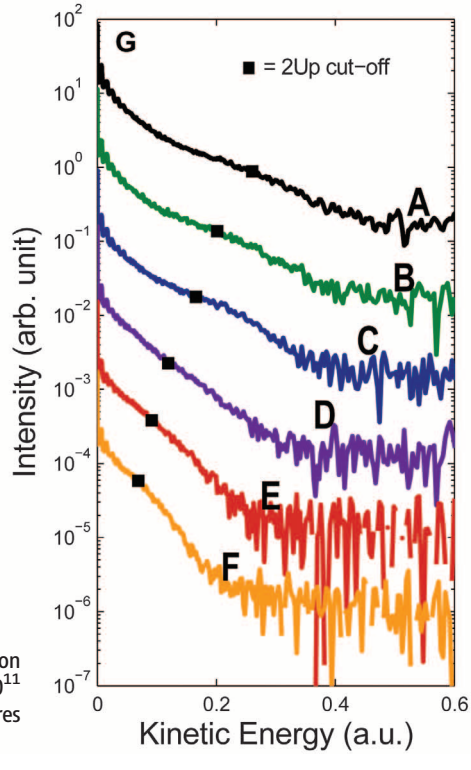

Fig. 2. Intensity dependence of measured velocity map images and the corresponding photoelectron kinetic energy distributions. (**A**) 7.1 × 10^{11} W/cm^2; (**B**) 5.5 × 10^{11} W/cm^2; (**C**) 4.5 × 10^{11} W/cm^2; (**D**) 3.2 × 10^{11} W/cm^2; (**E**) 2.5 × 10^{11} W/cm^2; and (**F**) 1.9 × 10^{11} W/cm^2. (**G**) Angle-integrated photoelectron spectra. Squares indicate the energy that corresponds to the classical $2U_p$ cutoff energy.

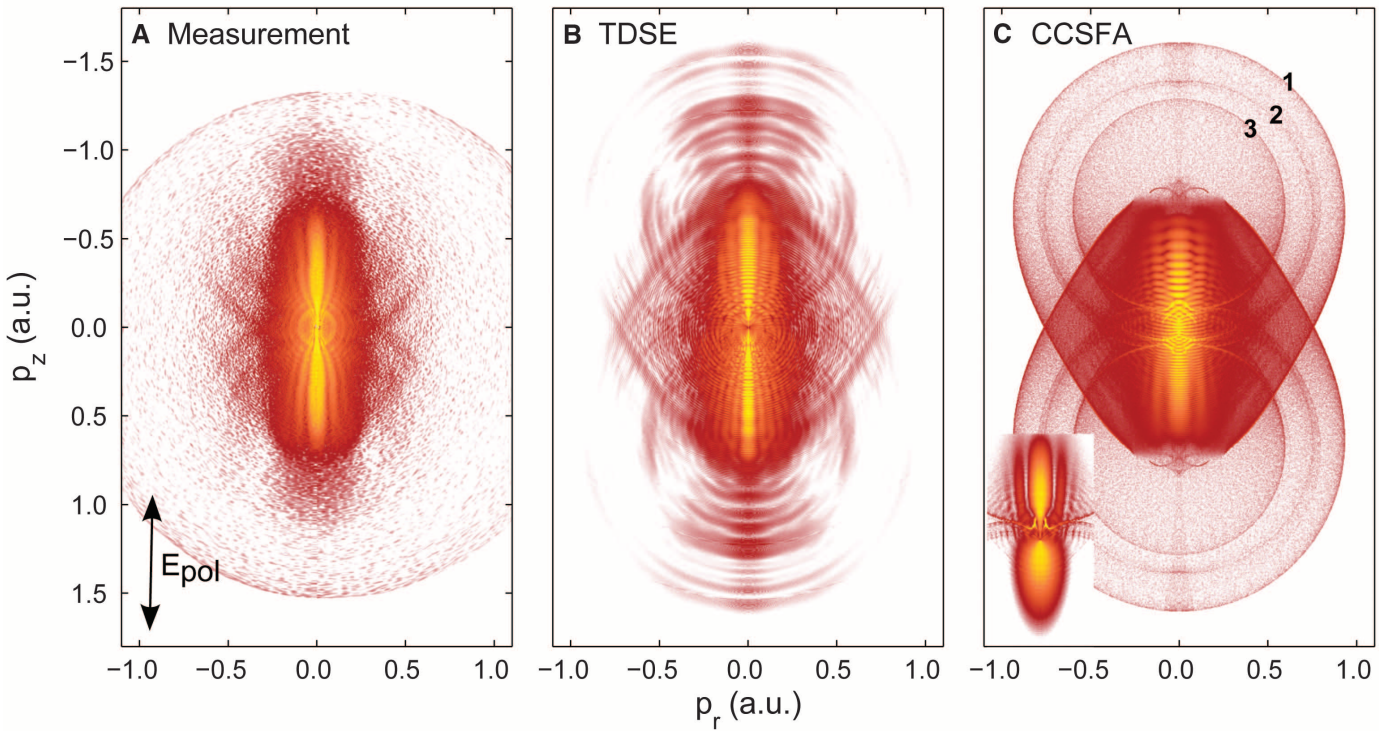

Fig. 3. Comparison of an experimental two-dimensional photo-electron velocity map image with calculations (CCSFA and TDSE). (**A**) Four-hour-long measurement of the ionization of metastable xenon under conditions similar to those used in the measurements shown in Fig. 2A. (**B**) TDSE calculation for ionization of argon (5 *s*) (*IP* = 0.14 a.u., four-cycle flat-top 7-μm pulse, peak field strength of 0.0045 a.u.). (**C**) CCSFA calculation for ionization of a model hydrogenic atom (*IP* = 0.14 a.u., λ_{laser} = 7 μm, peak field strength of 0.0045 a.u.). (Inset) CCSFA single half-cycle calculation, illustrating that the side-lobes are due to an interference between two trajectories that leave the atom within the same half-cycle.

Varying the position of the experimental apparatus along the laser propagation axis allowed the peak intensity to be tuned by approximately a factor of five. Figure 2, A to F, shows a dominant electron emission along the laser polarization axis, with a high-energy cutoff (Fig. 2G) that agrees well with the classical expectation $E_{cutoff} = F_{laser}^2/2\omega_{laser}^2$. In Fig. 3A, "side-lobes" are observed that extend from low to high momentum and run parallel to the laser polarization axis for high momenta. These side-lobes qualitatively agree with the patterns calculated in fig. S3A and result from a holographic interference. Additionally, a number of weaker transverse structures extend sideways approximately orthogonal to the laser polarization. Neither of these structures should be confused with the so-called side-lobes, "wings," or "rings" caused by backscattered electrons that were observed in higher-order above-threshold ionization (*19*, *20*), nor are they related to the interferences observed in recent experiments on ionization of helium by a few-cycle pulse (*21*).

The experimental observation of holographic interferences is confirmed through full time-dependent Schrödinger equation (TDSE) calculations, which show the same fringe pattern (Fig. 3B) (*22*). The fringe spacing agrees with the experiment and is reduced compared with the SFA-based calculation (fig. S3A), in which the long-range Coulomb potential was neglected.

Insight into the role of the Coulomb potential was gained by performing semiclassical calculations with the Coulomb-corrected strong-field approximation (CCSFA) (*14*) (*23*). In these calculations, complex quantum trajectories are calculated that, after tunneling, include the Coulomb interaction of the electron in the classically allowed region. The spectrum is calculated by summing contributions from different trajectories, including their phases (*14*). The results (Fig.

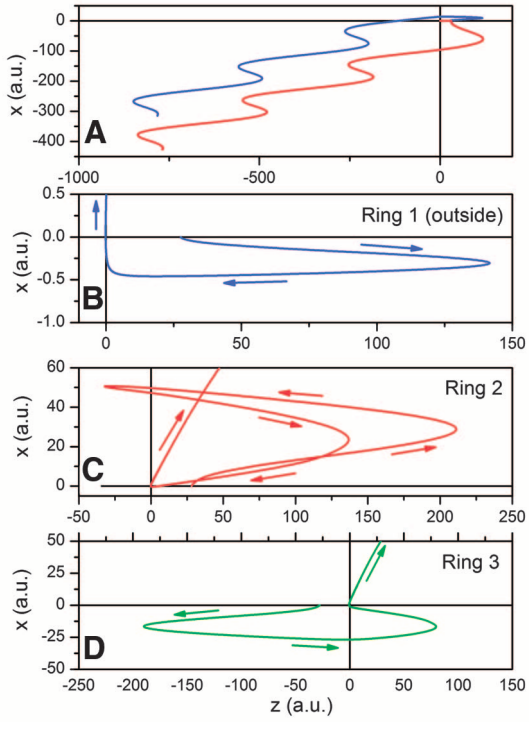

Fig. 4. (**A**) Two trajectories that lead to the formation of electrons with a final momentum of $p_r = -0.01$ a.u. and $p_z = -0.46$ a.u. The red trajectory corresponds to an electron that only weakly interacts with the ionic core. The blue trajectory corresponds to an electron that strongly interacts with the ionic core and that undergoes Coulomb focusing. (**B** to **D**) Recollision trajectories, illustrating the occurrence of a recollision at the first (ring 1), second (ring 3), or third (ring 2) opportunity. The highest kinetic energy of electrons on ring 1 is 1.289 a.u. (10.75 U_p).

3C) quantitatively reproduce the main features discussed above. Inspection of the trajectories responsible for the side-lobes shows that these trajectories can indeed be considered as a reference and scattered wave packet, creating a hologram (Fig. 4A).

The efficiency of electron-ion recollision drops dramatically with increasing λ_{laser} because of spreading of the wave packet between ionization and recollision. Still, a clear hologram can be observed at 7 μm. Two effects make this possible. First, the hologram results from a heterodyne experiment, in which a weaker signal is mixed with a stronger signal. Second, to create a clear reference a large-impact parameter is needed in order to limit the interaction with the Coulomb field. For large λ_{laser}, a small p_r already leads to large-impact parameters because of the long excursion time between ionization and recollision.

Inspection of the electron trajectories contributing to the transverse structures (Fig. 3) reveals that they are due to recollision events in which the scattering does not occur on the first opportunity but on the second or third (*20*, *24*, *25*). Typical examples of these trajectories are shown in Fig. 4, B to D. One, respectively two glancing electron-ion collisions can be observed before the real recollision takes place. Usually, these rare events do not leave an imprint on the photoelectron spectrum. However, the combination of a long laser wavelength and Coulomb focusing (*24*) increases the probability because a small deviation introduced by the Coulomb potential can be sufficient to focus the returning wave packet onto the ion.

In our model study on the ionization of metastable xenon, we have experimentally shown the possibility to record holographic structures. Furthermore, our theoretical exploration shows that the hologram stores spatial and temporal information about the core- and electron dynamics. This offers opportunities to extend strong-field holography to more complicated systems and to use it to time-resolve electron-dynamics. As revealed in recent experiments (*6*, *26*), electron-ion recollision phenomena encode hole dynamics that occur in ions during the first few femtoseconds after strong-field ionization. When properly implemented with the use of a long-wavelength-driving laser, photo-electron holography appears especially well suited for studying this type of dynamics, in particular in molecules with a low binding energy that cannot easily be studied by other means.

References and Notes

1. P. B. Corkum, *Phys. Rev. Lett.* **71**, 1994 (1993).
2. F. Krausz, M. Y. Ivanov, *Rev. Mod. Phys.* **81**, 163 (2009).
3. M. F. Kling, M. J. J. Vrakking, *Annu. Rev. Phys. Chem.* **59**, 463 (2008).
4. J. Itatani *et al.*, *Nature* **432**, 867 (2004).
5. D. Shafir, Y. Mairesse, D. M. Villeneuve, P. B. Corkum, N. Dudovich, *Nat. Phys.* **5**, 412 (2009).
6. O. Smirnova *et al.*, *Nature* **460**, 972 (2009).
7. S. Baker *et al.*, *Science* **312**, 424 (2006).
8. M. Meckel *et al.*, *Science* **320**, 1478 (2008).
9. M. Spanner, O. Smirnova, P. B. Corkum, M. Y. Ivanov, *J. Phys. At. Mol. Opt. Phys.* **37**, L243 (2004).
10. H. Niikura *et al.*, *Nature* **417**, 917 (2002).
11. D. Gabor, *Nobel Lectures, Physics 1971-1980* (World Scientific, Singapore, 1992).
12. G. G. Paulus *et al.*, *Phys. Rev. Lett.* **84**, 3791 (2000).
13. J. Mauritsson *et al.*, *Phys. Rev. Lett.* **100**, 073003 (2008).
14. Materials and methods are available as supporting material on *Science* Online.
15. W. Becker, A. Lohr, M. Kleber, *J. Phys. At. Mol. Opt. Phys.* **27**, L325 (1994).
16. M. Lewenstein, K. C. Kulander, K. J. Schafer, P. H. Bucksbaum, *Phys. Rev. A* **51**, 1495 (1995).
17. J. M. Bakker *et al.*, *J. Chem. Phys.* **132**, 074305 (2010).
18. A. T. J. B. Eppink, D. H. Parker, *Rev. Sci. Instrum.* **68**, 3477 (1997).
19. B. R. Yang *et al.*, *Phys. Rev. Lett.* **71**, 3770 (1993).
20. G. G. Paulus, W. Becker, W. Nicklich, H. Walther, *J. Phys. At. Mol. Opt. Phys.* **27**, L703 (1994).
21. R. Gopal *et al.*, *Phys. Rev. Lett.* **103**, 053001 (2009).
22. H. G. Muller, *Laser Phys.* **9**, 138 (1999).
23. S. V. Popruzhenko, D. Bauer, *J. Mod. Opt.* **55**, 2573 (2008).
24. T. Brabec, M. Y. Ivanov, P. B. Corkum, *Phys. Rev. A* **54**, R2551 (1996).
25. G. L. Yudin, M. Y. Ivanov, *Phys. Rev. A* **63**, 033404 (2001).
26. Y. Mairesse *et al.*, *Phys. Rev. Lett.* **104**, 213601 (2010).

27. We acknowledge R. Kemper, H. Schoenmaker, A. de Snaijer, I. Cerjak, and the staff at the FELIX facility for their great technical assistance. This work is part of the research program of FOM, which is financially supported by the Nederlandse organisatie voor Wetenschappelijk Onderzoek (NWO). K.J.S. is supported by NSF grant PHY-0701372 and the Ball Professorship at LSU. M.Y.I. is supported by Science and Innovation grant EP/E036112/1 of the Engineering and Physical Sciences Research Council. O.S. acknowledges a Leibniz SAW award.

Supporting Online Material

www.sciencemag.org/cgi/content/full/science.1198450/DC1
Materials and Methods
SOM Text
Figs. S1 to S5
References

29 September 2010; accepted 7 December 2010
Published online 6 December 2010;
10.1126/science.1198450

Spin Crossover in Ferropericlase at High Pressure: A Seismologically Transparent Transition?

Daniele Antonangeli,[1,2]* Julien Siebert,[1,2] Chantel M. Aracne,[2] Daniel L. Farber,[2,3] A. Bosak,[4] M. Hoesch,[4] M. Krisch,[4] Frederick J. Ryerson,[2] Guillaume Fiquet,[1] James Badro[1,2]

Seismic discontinuities in Earth typically arise from structural, chemical, or temperature variations with increasing depth. The pressure-induced iron spin state transition in the lower mantle may influence seismic wave velocities by changing the elasticity of iron-bearing minerals, but no seismological evidence of an anomaly exists. Inelastic x-ray scattering measurements on $(Mg_{0.83}Fe_{0.17})O$-ferropericlase at pressures across the spin transition show effects limited to the only shear moduli of the elastic tensor. This explains the absence of deviation in the aggregate seismic velocities and, thus, the lack of a one-dimensional seismic signature of the spin crossover. The spin state transition does, however, influence shear anisotropy of ferropericlase and should contribute to the seismic shear wave anisotropy of the lower mantle.

The characterization of pressure- and temperature-induced transformations in mantle minerals and their connection to seismic discontinuities aid in the understanding of Earth's interior. In this sense, the series of phase transformations that occurs in olivine—which with increasing pressure first transforms to wadsleyite, then to ringwoodite, and then breaks down into ferropericlase and perovskite—is emblematic. These phase changes are accompanied by density and sound-velocity variations that are responsible for the main seismic discontinuities in the upper mantle (*1*).

In contrast, the recently discovered iron spin-state transition—where compression favors the electron spin pairing, with the system changing from a high-spin to a low-spin state—in both ferropericlase (*2*) and perovskite (*3*), the two main phases of the lower mantle, does not clearly relate to any seismic signature, although effects on mantle density and seismic wave velocity have been anticipated (*4*–*8*). In ferropericlase, the spin transition occurs without structural changes (*4*, *9*), but experimental (*10*) and theoretical (*11*) studies suggest large softening of all the elastic moduli and, consequently, a major decrease in the aggregate sound velocities. Thus, at pressure and temperature conditions of the lower mantle, such an effect should be associated to a broad seismic anomaly (*12*) that, conversely, is not observed (*13*, *14*).

Here we present inelastic x-ray scattering (IXS) measurements on $(Mg_{0.83}Fe_{0.17})O$-ferropericlase across the spin transition and up to 70 GPa (*15*). We obtained the complete elastic tensor (that is,

[1]Institut de Minéralogie et de Physique des Milieux Condensés, UMR CNRS 7590, Institut de Physique du Globe de Paris, Université Pierre et Marie Curie, Université Paris Diderot, 75005 Paris, France. [2]Lawrence Livermore National Laboratory, Livermore, CA 94550, USA. [3]Department of Earth and Planetary Sciences, University of California, Santa Cruz, Santa Cruz, CA, 95064, USA. [4]European Synchrotron Radiation Facility, BP 220, 38043 Grenoble Cedex, France.

*To whom correspondence should be addressed. E-mail: daniele.antonangeli@impmc.upmc.fr

3C) quantitatively reproduce the main features discussed above. Inspection of the trajectories responsible for the side-lobes shows that these trajectories can indeed be considered as a reference and scattered wave packet, creating a hologram (Fig. 4A).

The efficiency of electron-ion recollision drops dramatically with increasing λ_{laser} because of spreading of the wave packet between ionization and recollision. Still, a clear hologram can be observed at 7 μm. Two effects make this possible. First, the hologram results from a heterodyne experiment, in which a weaker signal is mixed with a stronger signal. Second, to create a clear reference a large-impact parameter is needed in order to limit the interaction with the Coulomb field. For large λ_{laser}, a small p_r already leads to large-impact parameters because of the long excursion time between ionization and recollision.

Inspection of the electron trajectories contributing to the transverse structures (Fig. 3) reveals that they are due to recollision events in which the scattering does not occur on the first opportunity but on the second or third (*20*, *24*, *25*). Typical examples of these trajectories are shown in Fig. 4, B to D. One, respectively two glancing electron-ion collisions can be observed before the real recollision takes place. Usually, these rare events do not leave an imprint on the photoelectron spectrum. However, the combination of a long laser wavelength and Coulomb focusing (*24*) increases the probability because a small deviation introduced by the Coulomb potential can be sufficient to focus the returning wave packet onto the ion.

In our model study on the ionization of metastable xenon, we have experimentally shown the possibility to record holographic structures. Furthermore, our theoretical exploration shows that the hologram stores spatial and temporal information about the core- and electron dynamics. This offers opportunities to extend strong-field holography to more complicated systems and to use it to time-resolve electron-dynamics. As revealed in recent experiments (*6*, *26*), electron-ion recollision phenomena encode hole dynamics that occur in ions during the first few femtoseconds after strong-field ionization. When properly implemented with the use of a long-wavelength-driving laser, photo-electron holography appears especially well suited for studying this type of dynamics, in particular in molecules with a low binding energy that cannot easily be studied by other means.

References and Notes

1. P. B. Corkum, *Phys. Rev. Lett.* **71**, 1994 (1993).
2. F. Krausz, M. Y. Ivanov, *Rev. Mod. Phys.* **81**, 163 (2009).
3. M. F. Kling, M. J. J. Vrakking, *Annu. Rev. Phys. Chem.* **59**, 463 (2008).
4. J. Itatani *et al.*, *Nature* **432**, 867 (2004).
5. D. Shafir, Y. Mairesse, D. M. Villeneuve, P. B. Corkum, N. Dudovich, *Nat. Phys.* **5**, 412 (2009).
6. O. Smirnova *et al.*, *Nature* **460**, 972 (2009).
7. S. Baker *et al.*, *Science* **312**, 424 (2006).
8. M. Meckel *et al.*, *Science* **320**, 1478 (2008).
9. M. Spanner, O. Smirnova, P. B. Corkum, M. Y. Ivanov, *J. Phys. At. Mol. Opt. Phys.* **37**, L243 (2004).
10. H. Niikura *et al.*, *Nature* **417**, 917 (2002).
11. D. Gabor, *Nobel Lectures, Physics 1971-1980* (World Scientific, Singapore, 1992).
12. G. G. Paulus *et al.*, *Phys. Rev. Lett.* **84**, 3791 (2000).
13. J. Mauritsson *et al.*, *Phys. Rev. Lett.* **100**, 073003 (2008).
14. Materials and methods are available as supporting material on *Science* Online.
15. W. Becker, A. Lohr, M. Kleber, *J. Phys. At. Mol. Opt. Phys.* **27**, L325 (1994).
16. M. Lewenstein, K. C. Kulander, K. J. Schafer, P. H. Bucksbaum, *Phys. Rev. A* **51**, 1495 (1995).
17. J. M. Bakker *et al.*, *J. Chem. Phys.* **132**, 074305 (2010).
18. A. T. J. B. Eppink, D. H. Parker, *Rev. Sci. Instrum.* **68**, 3477 (1997).
19. B. R. Yang *et al.*, *Phys. Rev. Lett.* **71**, 3770 (1993).
20. G. G. Paulus, W. Becker, W. Nicklich, H. Walther, *J. Phys. At. Mol. Opt. Phys.* **27**, L703 (1994).
21. R. Gopal *et al.*, *Phys. Rev. Lett.* **103**, 053001 (2009).
22. H. G. Muller, *Laser Phys.* **9**, 138 (1999).
23. S. V. Popruzhenko, D. Bauer, *J. Mod. Opt.* **55**, 2573 (2008).
24. T. Brabec, M. Y. Ivanov, P. B. Corkum, *Phys. Rev. A* **54**, R2551 (1996).
25. G. L. Yudin, M. Y. Ivanov, *Phys. Rev. A* **63**, 033404 (2001).
26. Y. Mairesse *et al.*, *Phys. Rev. Lett.* **104**, 213601 (2010).

27. We acknowledge R. Kemper, H. Schoenmaker, A. de Snaijer, I. Cerjak, and the staff at the FELIX facility for their great technical assistance. This work is part of the research program of FOM, which is financially supported by the Nederlandse organisatie voor Wetenschappelijk Onderzoek (NWO). K.J.S. is supported by NSF grant PHY-0701372 and the Ball Professorship at LSU. M.Y.I. is supported by Science and Innovation grant EP/E036112/1 of the Engineering and Physical Sciences Research Council. O.S. acknowledges a Leibniz SAW award.

Supporting Online Material

www.sciencemag.org/cgi/content/full/science.1198450/DC1
Materials and Methods
SOM Text
Figs. S1 to S5
References

29 September 2010; accepted 7 December 2010
Published online 6 December 2010;
10.1126/science.1198450

Spin Crossover in Ferropericlase at High Pressure: A Seismologically Transparent Transition?

Daniele Antonangeli,[1,2]* Julien Siebert,[1,2] Chantel M. Aracne,[2] Daniel L. Farber,[2,3] A. Bosak,[4] M. Hoesch,[4] M. Krisch,[4] Frederick J. Ryerson,[2] Guillaume Fiquet,[1] James Badro[1,2]

Seismic discontinuities in Earth typically arise from structural, chemical, or temperature variations with increasing depth. The pressure-induced iron spin state transition in the lower mantle may influence seismic wave velocities by changing the elasticity of iron-bearing minerals, but no seismological evidence of an anomaly exists. Inelastic x-ray scattering measurements on $(Mg_{0.83}Fe_{0.17})O$-ferropericlase at pressures across the spin transition show effects limited to the only shear moduli of the elastic tensor. This explains the absence of deviation in the aggregate seismic velocities and, thus, the lack of a one-dimensional seismic signature of the spin crossover. The spin state transition does, however, influence shear anisotropy of ferropericlase and should contribute to the seismic shear wave anisotropy of the lower mantle.

The characterization of pressure- and temperature-induced transformations in mantle minerals and their connection to seismic discontinuities aid in the understanding of Earth's interior. In this sense, the series of phase transformations that occurs in olivine—which with increasing pressure first transforms to wadsleyite, then to ringwoodite, and then breaks down into ferropericlase and perovskite—is emblematic. These phase changes are accompanied by density and sound-velocity variations that are responsible for the main seismic discontinuities in the upper mantle (*1*).

In contrast, the recently discovered iron spin-state transition—where compression favors the electron spin pairing, with the system changing from a high-spin to a low-spin state—in both ferropericlase (*2*) and perovskite (*3*), the two main phases of the lower mantle, does not clearly relate to any seismic signature, although effects on mantle density and seismic wave velocity have been anticipated (*4*–*8*). In ferropericlase, the spin transition occurs without structural changes (*4*, *9*), but experimental (*10*) and theoretical (*11*) studies suggest large softening of all the elastic moduli and, consequently, a major decrease in the aggregate sound velocities. Thus, at pressure and temperature conditions of the lower mantle, such an effect should be associated to a broad seismic anomaly (*12*) that, conversely, is not observed (*13*, *14*).

Here we present inelastic x-ray scattering (IXS) measurements on $(Mg_{0.83}Fe_{0.17})O$-ferropericlase across the spin transition and up to 70 GPa (*15*). We obtained the complete elastic tensor (that is,

[1]Institut de Minéralogie et de Physique des Milieux Condensés, UMR CNRS 7590, Institut de Physique du Globe de Paris, Université Pierre et Marie Curie, Université Paris Diderot, 75005 Paris, France. [2]Lawrence Livermore National Laboratory, Livermore, CA 94550, USA. [3]Department of Earth and Planetary Sciences, University of California, Santa Cruz, Santa Cruz, CA, 95064, USA. [4]European Synchrotron Radiation Facility, BP 220, 38043 Grenoble Cedex, France.

*To whom correspondence should be addressed. E-mail: daniele.antonangeli@impmc.upmc.fr

all of the independent moduli that linearly relate stress and strain) and derived the aggregate sound velocities, the aggregate elastic moduli, and the shear anisotropy at corresponding depth. IXS has proven to be a useful technique for the high-pressure and high-temperature study of elasticity and sound velocities of powders (*16*–*18*) and single crystals (*19*, *20*). In particular, IXS allows all of the independent elements of the elastic tensor to be directly determined from the initial slope of the phonon dispersion of selected longitudinal acoustic (LA) and transverse acoustic (TA) modes, without any external input or a priori model (*15*). Thus, IXS overcomes the limitations of previously used surface-sensitive techniques [such as impulsive stimulated light scattering (ISLS) (*8*, *21*)] that require a complex data inversion, involving modeling of the sound waves at the interfaces and input of external parameters to obtain bulk properties. Brillouin measurements, which also directly provide sound velocities, were limited in the case of ferropericlase to the only shear velocities and the longitudinal moduli computed after input of the (independently measured) bulk modulus (*22*). IXS allows for the in situ determination of sample density (*15*), which is an important parameter in the mixed-spin region. Furthermore, whereas Brillouin scattering is restricted to transparent samples (*22*–*24*), IXS is not. Thus, we have been able to investigate high–iron-content ferropericlase [17 mole percent (mol %) Fe], which is more relevant to the lower mantle than that used in recent work (*8*, *22*–*24*).

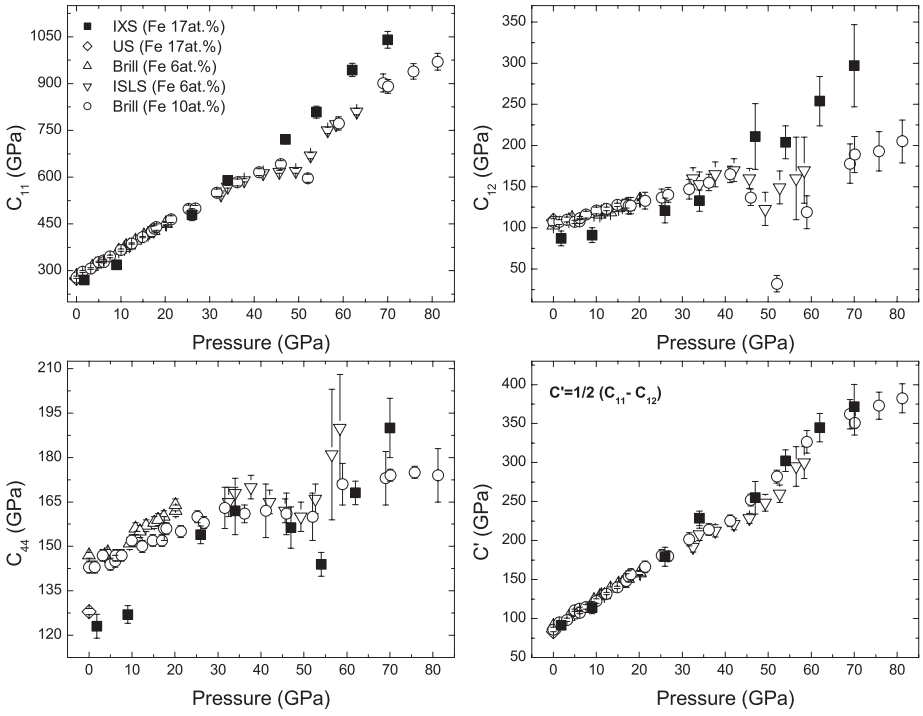

Fig. 1. Pressure evolution of the single-crystal elastic moduli of $(Mg_{1-x},Fe_x)O$-ferropericlase (table S1) (*15*). Solid squares, IXS data for $x = 0.17$ (this work); open diamonds, ambient pressure ultrasonic determinations for $x = 0.17$ (*26*); open triangles, Brillouin measurements for $x = 0.06$ (*23*); open inverted triangles, ISLS results for $x = 0.06$ (*10*); open circles, Brillouin determinations for $x = 0.10$ (*22*). Error bars account for the uncertainties on the measured velocities and densities (*15*). at. %, atomic percent.

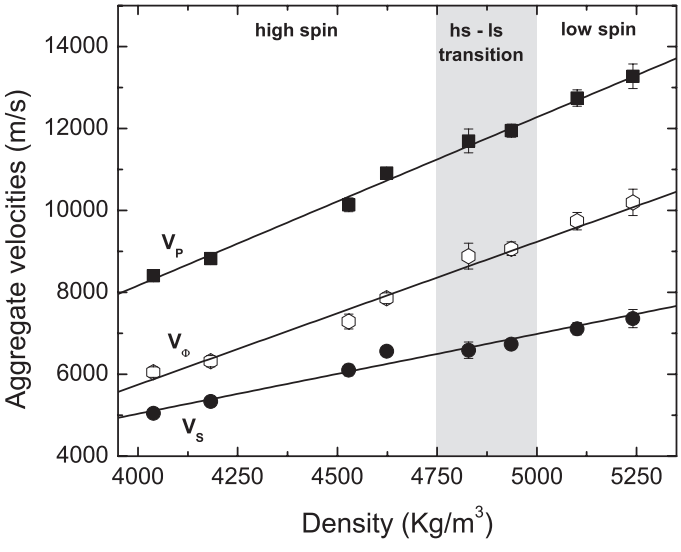

Fig. 2. Density evolution of the aggregate sound velocities (Voigt-Reuss-Hill average) (*15*). Solid squares, compressional sound velocity (V_P); solid circles, shear sound velocity (V_S); open hexagons, bulk sound velocity ($V_\Phi = \sqrt{K/\rho}$). The lines are linear fits to the experimental data. The density range corresponding to the spin-transition zone (4750 to 5000 kg/m^3) is shaded. Error bars on the aggregate velocities come from the propagation of the uncertainties on the elastic moduli and the difference between the Voigt and Reuss average (*15*).

Up to ~40 GPa, all the elastic moduli exhibit a monotonic increase with pressure (Fig. 1 and table S1), as is expected with compression. In the 40–to–60-GPa pressure range, where the spin transition occurs (*2*, *4*, *25*), we observe a distinct softening of C_{44} and a small variation in C_{12}, whereas C_{11} retains a continuous trend. Above 60 GPa, the usual monotonic increase with pressure is observed for all of the moduli, albeit with a larger pressure derivative. The back extrapolations of our results to ambient pressure are within a few percent of the ultrasonic determinations for the same composition (*26*). However, if we compare our high-pressure measurements with ISLS (*10*) and Brillouin (*22*, *24*) data obtained on samples with lower iron content, we observe qualitative agreement for C_{44} and $C' = 1/2(C_{11} - C_{12})$, which display softening in the pressure range of the spin transition for all methods (quantitative differences are at least partially due to differences in iron concentration), but disagreement for C_{12} and C_{11}. Whereas both optical studies (*8*, *22*) report a large softening of C_{11} in the 40–to–60-GPa range, the direct determination of C_{11} by IXS [via sound velocity measurements of the LA[100] mode (*15*)] does not show any anomaly (Fig. 1). To support our findings, we stress that in other systems where pressure-induced, spin-pairing transitions occur (such as the extensively investigated Fe-, Co-, and Mn-Invar alloys), these transitions are commonly accompanied by much larger effects on the shear elastic moduli than on the longitudinal moduli (*27*, *28*).

From the measured single-crystalline C_{ij}, we computed the aggregate elastic properties bulk and shear moduli, as well as the compressional (V_P) and shear (V_S) sound velocities by straightforward averaging [see (*15*)]. The values we obtain for the bulk and shear moduli compare favorably with the ambient-pressure ultrasonic determination (*26*) and with the values obtained by x-ray diffraction (*4*) for both the low-spin and the high-spin state (figs. S3 and S4).

A direct consequence of the lack of softening of C_{11} and of the moderate effect on C_{12} is the absence of any sizable deviation from a linear density evolution of the aggregate V_P and V_S (Fig. 2). In contrast to recent claims (*8*, *11*, *22*),

neither V_P nor V_S show an anomaly due to the spin-pairing transition.

With respect to Earth's lower mantle, recent optical (*8*, *22*) and theoretical (*11*) studies proposed that an anomalous (albeit smooth) softening of the aggregate elastic properties (especially the bulk modulus K and the bulk velocity $V_\Phi = \sqrt{K/\rho}$, where ρ is density) should occur at depth. The range over which this takes place has been suggested to extend from 1000 to 1500 km, based on room-temperature results (*8*), and from 1300 to 1800 km, when including high-temperature effects (*22*), such as those along a mantle geotherm (*11*). Our study provides an explanation for the lack of a seismic signature (*13*, *14*) associated with the spin crossover in the lower mantle.

The high-spin–to–low-spin transition does, however, have an effect on the single-crystal elasticity of ferropericlase (when not smeared due to averaging over many grains as in an ideally random aggregate). The relative magnitude of the shear elastic moduli C_{44} and C' (corresponding to the sound velocity of the $TA[110]_{<001>}$ and $TA[110]_{<-110>}$ modes, respectively) evolves with pressure (Fig. 3). At ambient and low pressures, $C_{44} > C'$, but the pressure derivative of C' is larger than that of C_{44}, so that the two intersect around 16 to 17 GPa. At higher pressures, the sign of shear anisotropy is reversed. This behavior is in good agreement with results of Brillouin spectroscopy on samples with 10 mol % Fe (*24*). Above 60 GPa, in the low-spin phase, the pressure derivative of the two shear moduli is almost the same. Accordingly, the pressure evolution of the shear anisotropy, defined as $A = 2(C' - C_{44})/(C' + C_{44})$, is very different for the high- and low-spin ferropericlase (see inset of Fig. 3): A increases linearly with pressure in the high-spin phase, whereas it remains almost constant (or slightly decreases) in the low-spin phase. Thus, we suggest that a seismically detectable signature of the spin transition in the lower mantle may be found in the shear anisotropy. Because ferropericlase is much weaker than perovskite, it can accommodate most of the strain (*29*) and develop strong texture (*30*). Our measurements indicate a very large shear anisotropy, ~70% at 70 GPa for ferropericlase with a Fe content of 17 mol %, a value very close to that measured for ferropericlase with 10 mol % Fe (*24*) and at least 50% larger than the shear anisotropy of MgO (*24*). Such a considerable anisotropy, in conjunction with lattice-preferred orientation, supports the notion that ferropericlase is the main phase responsible for the seismic shear anisotropy of the lower mantle (*24*). Therefore, the different shear anisotropy behavior of high- and low-spin ferropericlase should be considered together with temperature and chemical variations to interpret local seismic heterogeneity.

Finally, the values of V_P and V_S for $(Mg_{0.83}Fe_{0.17})O$-ferropericlase at 70 GPa (13300 ± 300 m/s and 7360 ± 220 m/s, respectively) are very close to the measured V_S (*31*) and computed V_P and V_S (*32*, *33*) values for $MgSiO_3$-perovskite at the same pressure. Because both Fe and Al are expected to lower the aggregate velocities of perovskite (*33*, *34*), our results suggest that the velocities of the two major phases of the lower mantle might become comparable (if not ferropericlase faster than perovskite) in the lowermost 1000 to 1200 km of the lower mantle. This could challenge current compositional models of the lowermost mantle based on an extrapolation of lower-pressure elasticity data. However, direct high-pressure, high-temperature measurements on both ferropericlase and perovskite (with relevant major-element compositions) are required to confirm these conjectures.

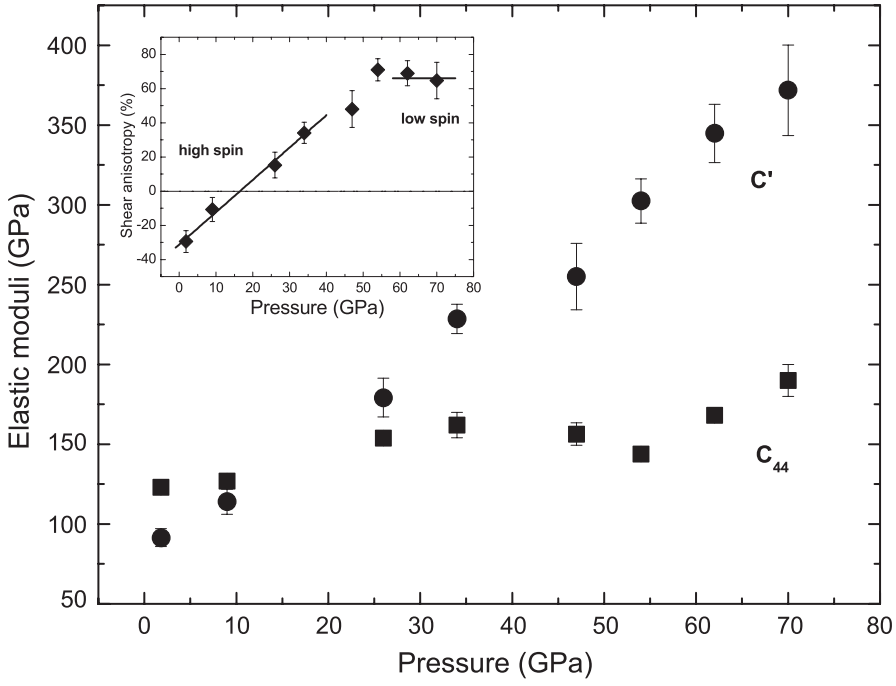

Fig. 3. Comparison of the pressure evolution of C_{44} (squares) and C' (circles), corresponding to the two different polarizations of the shear mode in the diagonal plane of a cubic lattice. (**Inset**) Shear anisotropy as a function of pressure. The lines are guides for the eye. Error bars account for the uncertainties on the measured velocities and densities (*15*).

References and Notes

1. J.-P. Poirier, *Introduction to the Physics of the Earth's Interior* (Cambridge Univ. Press, Cambridge, 2000).
2. J. Badro *et al.*, *Science* **300**, 789 (2003); 10.1126/science.1081311.
3. J. Badro *et al.*, *Science* **305**, 383 (2004).
4. J.-F. Lin *et al.*, *Nature* **436**, 377 (2005).
5. J.-F. Lin *et al.*, *Geophys. Res. Lett.* **33**, L22304 (2006).
6. J.-F. Lin *et al.*, *Geophys. Res. Lett.* **34**, L09301 (2007).
7. S. Speziale *et al.*, *J. Geophys. Res.* **112**, B10212 (2007).
8. K. Catalli *et al.*, *Earth Planet. Sci. Lett.* **289**, 68 (2010).
9. Y. Fei *et al.*, *Geophys. Res. Lett.* **34**, L17307 (2007).
10. J. C. Crowhurst, J. M. Brown, A. F. Goncharov, S. D. Jacobsen, *Science* **319**, 451 (2008).
11. R. M. Wentzcovitch *et al.*, *Proc. Natl. Acad. Sci. U.S.A.* **106**, 8447 (2009).
12. J.-F. Lin *et al.*, *Science* **317**, 1740 (2007).
13. G. Masters, *Eos Trans. AGU* **89** (53), Fall Meet. Suppl., abstr. MR23A-04 (2008).
14. F. Cammarano, H. Marquardt, S. Speziale, P. J. Tackley, *Geophys. Res. Lett.* **37**, L03308 (2010).
15. Materials and methods are available as supporting material on *Science* Online.
16. D. Antonangeli *et al.*, *Earth Planet. Sci. Lett.* **225**, 243 (2004).
17. D. Antonangeli *et al.*, *Phys. Rev. B* **72**, 134303 (2005).
18. D. Antonangeli *et al.*, *Earth Planet. Sci. Lett.* **295**, 292 (2010).
19. D. Antonangeli *et al.*, *Phys. Rev. Lett.* **93**, 215505 (2004).
20. D. Antonangeli, M. Krisch, D. L. Farber, D. G. Ruddle, G. Fiquet, *Phys. Rev. Lett.* **100**, 085501 (2008).
21. J. C. Crowhurst *et al.*, *Appl. Phys. Lett.* **89**, 111920 (2006).
22. H. Marquardt, S. Speziale, H. J. Reichmann, D. J. Frost, F. R. Schilling, *Earth Planet. Sci. Lett.* **287**, 345 (2009).
23. J. M. Jackson *et al.*, *J. Geophys. Res.* **111**, B09203 (2006).
24. H. Marquardt *et al.*, *Science* **324**, 224 (2009).
25. A. F. Goncharov, V. V. Struzhkin, S. D. Jacobsen, *Science* **312**, 1205 (2006).
26. S. D. Jacobsen *et al.*, *J. Geophys. Res.* **107**, 2037 (2002).
27. F. Decremps, L. Nataf, *Phys. Rev. Lett.* **92**, 157204 (2004).
28. L. Nataf, F. Decremps, M. Gauthier, G. Syfosse, *Ultrasonics* **44** (suppl. 1), e555 (2006).
29. K. Madi, S. Forest, P. Cordier, M. Boussuge, *Earth Planet. Sci. Lett.* **237**, 223 (2005).
30. C. E. Tommaseo, J. Devine, S. Merkel, S. Speziale, H. K. Wenk, *Phys. Chem. Miner.* **33**, 84 (2006).
31. M. Murakami, S. Sinogeikin, H. Hellwig, J. Bass, J. Li, *Earth Planet. Sci. Lett.* **256**, 47 (2007).
32. A. R. Oganov, J. P. Brodholt, G. D. Price, *Earth Planet. Sci. Lett.* **184**, 555 (2001).
33. B. Kiefer, L. Stixrude, R. M. Wentzcovitch, *Geophys. Res. Lett.* **29**, 1539 (2002).

34. J. M. Jackson, J. Zhang, J. Shu, S. V. Sinogeikin, J. D. Bass, *Geophys. Res. Lett.* **32**, L21305 (2005).

35. We thank F. Occelli, G. Le Marchand, P. Munsch, P. Bouvier, M. Hanfland, M. Mezouar, and A. L. Auzende for experimental help. This work was performed under the auspices of the U.S. Department of Energy and Lawrence Livermore National Laboratory under contract DE-AC52-07NA27344 and was supported by the Office of Basic Energy Sciences–Geosciences Research Program (F.J.R.). D.A., J.B., and J.S. acknowledge financial support from the European Research Council (ERC) under the European Community's Seventh Framework Programme (FP7/2007-2013)/ERC grant agreement no. 207467. This work was supported by the French National Research Agency grant no. ANR-07-BLAN-0124-01 and ERC grant agreement no. 207467.

Supporting Online Material
www.sciencemag.org/cgi/content/full/331/6013/64/DC1
Materials and Methods
Figs. S1 to S4
Table S1
References and Notes

28 September 2010; accepted 6 December 2010
10.1126/science.1198429

Small Interannual Variability of Global Atmospheric Hydroxyl

S. A. Montzka,[1]* M. Krol,[2,3] E. Dlugokencky,[1] B. Hall,[1] P. Jöckel,[4]† J. Lelieveld[4,5]

The oxidizing capacity of the global atmosphere is largely determined by hydroxyl (OH) radicals and is diagnosed by analyzing methyl chloroform (CH_3CCl_3) measurements. Previously, large year-to-year changes in global mean OH concentrations have been inferred from such measurements, suggesting that the atmospheric oxidizing capacity is sensitive to perturbations by widespread air pollution and natural influences. We show how the interannual variability in OH has been more precisely estimated from CH_3CCl_3 measurements since 1998, when atmospheric gradients of CH_3CCl_3 had diminished as a result of the Montreal Protocol. We infer a small interannual OH variability as a result, indicating that global OH is generally well buffered against perturbations. This small variability is consistent with measurements of methane and other trace gases oxidized primarily by OH, as well as global photochemical model calculations.

The hydroxyl radical (OH) is the primary oxidant for many non-CO_2 greenhouse gases, several stratospheric ozone-depleting substances and their substitutes, and hazardous air pollutants. It is also central to atmospheric photochemistry and the regulation of tropospheric ozone, and thus controls the influence of chemically reduced trace gases on climate, the stratospheric ozone layer, and air quality (*1*–*4*). The interannual variability (IAV) in OH concentrations ([OH]) on large spatial scales provides insight into the stability of the atmospheric oxidation capacity and its sensitivity to human-induced and natural perturbations. However, a consistent, predictive understanding of the net response of [OH] on broad scales to such perturbations is lacking. For example, a range of negative [OH] feedbacks is calculated from changes in atmospheric methane abundance (*3*, *5*–*7*).

Theory suggests that the sensitivity of [OH] to environmental changes depends on the relative importance of primary and secondary (recycling) OH formation pathways (*7*). The balance between primary OH formation initiated by ultraviolet light and formation by recycling is determined by atmospheric abundances and distributions of NO_x, H_2O, O_3, CO, and CH_4, as well as other parameters (*3*, *8*), many of which are highly variable in space and time and are relatively poorly characterized on global scales and in model calculations. As a result, calculated sensitivities of global [OH] to IAV in the chemical and physical makeup of the atmosphere have yet to be adequately tested.

Although OH can be measured directly on local scales, these results cannot characterize the integrated response of global mean [OH] to the many processes that control its formation and loss. Instead, indirect techniques are used in which [OH] is derived from observations of OH-oxidized trace gases such as CH_3CCl_3 and ^{14}CO (*9*–*19*). However, these approaches can suggest a very different sensitivity of [OH] to variations in the atmospheric environment than is derived in atmospheric models (*20*). Year-to-year changes in global [OH] as high as 20 to 25% have been derived from analyses of CH_3CCl_3 observations between 1980 and 2003, and these analyses imply a mean IAV of 7 to 9% (*16*, *17*). Chemistry transport models calculate a global [OH] variability of only 1 to 2%, but these models do not currently include variability in all factors influencing [OH] (*20*–*23*). Variations in [OH] of up to 20% have been estimated from ^{14}CO, although only over a few months and on semihemispheric spatial scales (*19*).

Global mean [OH] can be estimated from atmospheric observations of a trace gas whose predominant sink is reaction with OH from mass balance considerations by equating the rate of change in the global burden (dG/dt) to the difference between the global emission rate (E) and loss. Solving for the pseudo–first-order rate constant for loss (k_G), which is proportional to [OH], gives

$$[\mathrm{OH}] \propto k_G = \frac{E}{G} - \frac{dG/dt}{G} \qquad (1)$$

where G is the global burden estimated from surface measurements. Although CH_3CCl_3 losses (and k_G) are dominated by OH oxidation according to $k(T) \times [\mathrm{OH}]$, they include stratospheric photolysis, hydrolysis in surface waters, and other processes. Global mean [OH] derived in this

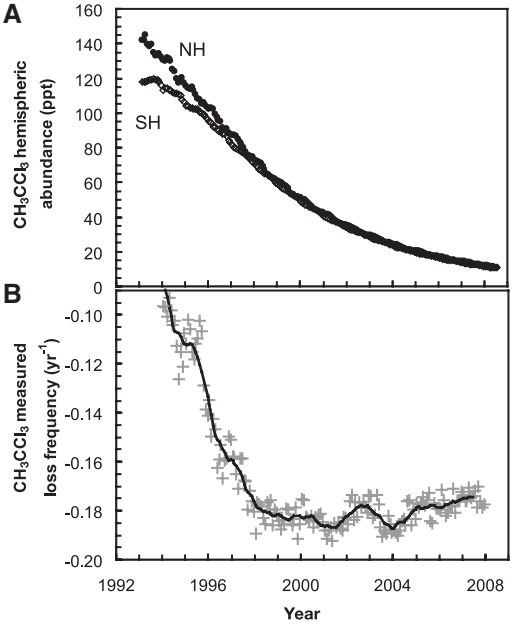

Fig. 1. (**A**) Observed hemispheric monthly mean mixing ratios of CH_3CCl_3 [update of (*14*)]. NH and SH denote Northern and Southern Hemispheres, respectively. (**B**) Exponential loss frequencies for CH_3CCl_3 derived from global surface means. Gray points are independent estimates derived from monthly means 12 months apart [e.g., $\ln(G_{\mathrm{Jan.\ 2007}}/G_{\mathrm{Jan.\ 2006}})$] plotted at the midpoint of this interval; the black line is the 12-month running mean.

[1]NOAA Earth System Research Laboratory, Boulder, CO 80305, USA. [2]Institute for Marine and Atmospheric Research Utrecht, University of Utrecht, 3584 CC Utrecht, Netherlands. [3]Meteorology and Air Quality Group, Wageningen University, 6708 PB Wageningen, Netherlands. [4]Department of Atmospheric Chemistry, Max Planck Institute for Chemistry, D-55128 Mainz, Germany. [5]Cyprus Institute, Nicosia 1645, Cyprus.

*To whom correspondence should be addressed. E-mail: stephen.a.montzka@noaa.gov

†Present address: Deutsches Zentrum für Luft- und Raumfahrt, Institut für Physik der Atmosphäre, Oberpfaffenhofen, D-82234 Wessling, Germany.

34. J. M. Jackson, J. Zhang, J. Shu, S. V. Sinogeikin, J. D. Bass, *Geophys. Res. Lett.* **32**, L21305 (2005).

35. We thank F. Occelli, G. Le Marchand, P. Munsch, P. Bouvier, M. Hanfland, M. Mezouar, and A. L. Auzende for experimental help. This work was performed under the auspices of the U.S. Department of Energy and Lawrence Livermore National Laboratory under contract DE-AC52-07NA27344 and was supported by the Office of Basic Energy Sciences–Geosciences Research Program (F.J.R.). D.A., J.B., and J.S. acknowledge financial support from the European Research Council (ERC) under the European Community's Seventh Framework Programme (FP7/2007-2013)/ERC grant agreement no. 207467. This work was supported by the French National Research Agency grant no. ANR-07-BLAN-0124-01 and ERC grant agreement no. 207467.

Supporting Online Material
www.sciencemag.org/cgi/content/full/331/6013/64/DC1
Materials and Methods
Figs. S1 to S4
Table S1
References and Notes

28 September 2010; accepted 6 December 2010
10.1126/science.1198429

Small Interannual Variability of Global Atmospheric Hydroxyl

S. A. Montzka,[1]* M. Krol,[2,3] E. Dlugokencky,[1] B. Hall,[1] P. Jöckel,[4]† J. Lelieveld[4,5]

The oxidizing capacity of the global atmosphere is largely determined by hydroxyl (OH) radicals and is diagnosed by analyzing methyl chloroform (CH_3CCl_3) measurements. Previously, large year-to-year changes in global mean OH concentrations have been inferred from such measurements, suggesting that the atmospheric oxidizing capacity is sensitive to perturbations by widespread air pollution and natural influences. We show how the interannual variability in OH has been more precisely estimated from CH_3CCl_3 measurements since 1998, when atmospheric gradients of CH_3CCl_3 had diminished as a result of the Montreal Protocol. We infer a small interannual OH variability as a result, indicating that global OH is generally well buffered against perturbations. This small variability is consistent with measurements of methane and other trace gases oxidized primarily by OH, as well as global photochemical model calculations.

The hydroxyl radical (OH) is the primary oxidant for many non-CO_2 greenhouse gases, several stratospheric ozone-depleting substances and their substitutes, and hazardous air pollutants. It is also central to atmospheric photochemistry and the regulation of tropospheric ozone, and thus controls the influence of chemically reduced trace gases on climate, the stratospheric ozone layer, and air quality (*1*–*4*). The interannual variability (IAV) in OH concentrations ([OH]) on large spatial scales provides insight into the stability of the atmospheric oxidation capacity and its sensitivity to human-induced and natural perturbations. However, a consistent, predictive understanding of the net response of [OH] on broad scales to such perturbations is lacking. For example, a range of negative [OH] feedbacks is calculated from changes in atmospheric methane abundance (*3*, *5*–*7*).

Theory suggests that the sensitivity of [OH] to environmental changes depends on the relative importance of primary and secondary (recycling) OH formation pathways (*7*). The balance between primary OH formation initiated by ultraviolet light and formation by recycling is determined by atmospheric abundances and distributions of NO_x, H_2O, O_3, CO, and CH_4, as well as other parameters (*3*, *8*), many of which are highly variable in space and time and are relatively poorly characterized on global scales and in model calculations. As a result, calculated sensitivities of global [OH] to IAV in the chemical and physical makeup of the atmosphere have yet to be adequately tested.

Although OH can be measured directly on local scales, these results cannot characterize the integrated response of global mean [OH] to the many processes that control its formation and loss. Instead, indirect techniques are used in which [OH] is derived from observations of OH-oxidized trace gases such as CH_3CCl_3 and ^{14}CO (*9*–*19*). However, these approaches can suggest a very different sensitivity of [OH] to variations in the atmospheric environment than is derived in atmospheric models (*20*). Year-to-year changes in global [OH] as high as 20 to 25% have been derived from analyses of CH_3CCl_3 observations between 1980 and 2003, and these analyses imply a mean IAV of 7 to 9% (*16*, *17*). Chemistry transport models calculate a global [OH] variability of only 1 to 2%, but these models do not currently include variability in all factors influencing [OH] (*20*–*23*). Variations in [OH] of up to 20% have been estimated from ^{14}CO, although only over a few months and on semihemispheric spatial scales (*19*).

Global mean [OH] can be estimated from atmospheric observations of a trace gas whose predominant sink is reaction with OH from mass balance considerations by equating the rate of change in the global burden (dG/dt) to the difference between the global emission rate (E) and loss. Solving for the pseudo–first-order rate constant for loss (k_G), which is proportional to [OH], gives

$$[\mathrm{OH}] \propto k_G = \frac{E}{G} - \frac{dG/dt}{G} \qquad (1)$$

where G is the global burden estimated from surface measurements. Although CH_3CCl_3 losses (and k_G) are dominated by OH oxidation according to $k(T) \times [\mathrm{OH}]$, they include stratospheric photolysis, hydrolysis in surface waters, and other processes. Global mean [OH] derived in this

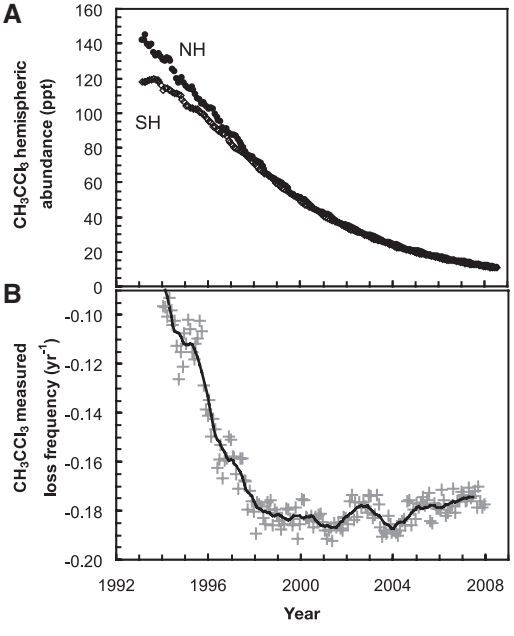

Fig. 1. (**A**) Observed hemispheric monthly mean mixing ratios of CH_3CCl_3 [update of (*14*)]. NH and SH denote Northern and Southern Hemispheres, respectively. (**B**) Exponential loss frequencies for CH_3CCl_3 derived from global surface means. Gray points are independent estimates derived from monthly means 12 months apart [e.g., $\ln(G_{\mathrm{Jan.\ 2007}}/G_{\mathrm{Jan.\ 2006}})$] plotted at the midpoint of this interval; the black line is the 12-month running mean.

[1]NOAA Earth System Research Laboratory, Boulder, CO 80305, USA. [2]Institute for Marine and Atmospheric Research Utrecht, University of Utrecht, 3584 CC Utrecht, Netherlands. [3]Meteorology and Air Quality Group, Wageningen University, 6708 PB Wageningen, Netherlands. [4]Department of Atmospheric Chemistry, Max Planck Institute for Chemistry, D-55128 Mainz, Germany. [5]Cyprus Institute, Nicosia 1645, Cyprus.

*To whom correspondence should be addressed. E-mail: stephen.a.montzka@noaa.gov

†Present address: Deutsches Zentrum für Luft- und Raumfahrt, Institut für Physik der Atmosphäre, Oberpfaffenhofen, D-82234 Wessling, Germany.

way is implicitly weighted by the trace-gas loss frequency (or inverse lifetime, τ^{-1}). To account for non-OH losses that are assumed constant over interannual periods, anomalies in [OH] are augmented depending on the magnitude of OH oxidation relative to other losses (*24*).

We derived variability in [OH] during the period 1998–2007 from CH_3CCl_3 observations made from paired-flask samples collected approximately weekly at nine remote sites across the globe (*14*, *24*). We concentrate on this decade because it followed a rapid CH_3CCl_3 emission decline owing to the revised and amended Montreal Protocol on Substances that Deplete the Ozone Layer. By 1998, yearly emissions of CH_3CCl_3 had diminished to become only a small fraction of the amount of CH_3CCl_3 annually removed by OH (fig. S1). Furthermore, uncertainties associated with estimating the global burden of CH_3CCl_3 and its rate of change have also diminished (*14*). Under these conditions, the pseudo–first-order loss of CH_3CCl_3, and therefore global [OH], is more directly reflected in an observable quantity: the measured decline of CH_3CCl_3 mixing ratios in the background atmosphere.

The rapid decline in CH_3CCl_3 emissions during the mid-1990s led to a nearly constant exponential decay in global atmospheric CH_3CCl_3 mixing ratios of -0.181 ± 0.005 year^{-1} during the period 1998–2007 (Fig. 1). From these observations, we derive a mean IAV in global [OH] of $2.3 \pm 1.5\%$ during 1998–2007 (Fig. 2). Unlike the period before 1998, when the variability implied for [OH] depended strongly on the magnitude and uncertainty in emissions (*16*), the variability in [OH] derived since then is insensitive to the emissions chosen (*24*). This IAV is less than the mean variability calculated for OH since 1997 with CH_3CCl_3 observations from an independent sampling network (*25*).

An IAV for [OH] of $2.3 \pm 1.5\%$ during 1998–2007 is much smaller than the pre-1995 mean variability of ~7 to 9% (up to 25%) derived previously (*16*, *17*). We suggest that this difference arises because of reduced uncertainties in the analysis of CH_3CCl_3 data during 1998–2007 rather than a substantial reduction in the variability of atmospheric oxidizing capacity after 1997. IAV in [OH] is more accurately determined since 1998 because uncertainties in both E/G and $(dG/dt)/G$ have become smaller as CH_3CCl_3 emissions declined rapidly in response to the Montreal Protocol phase-out of CH_3CCl_3 production (*14*) (fig. S1). During the 1980s, E/G was 120% of k_G; from 1990 to 1998, E/G was decreasing by 10 to 50% per year. For these periods, estimates of [OH] variability are highly sensitive to small errors in poorly constrained CH_3CCl_3 emissions: We estimate that a small shift (±0.25 year) in the timing of emissions during 1990–1998 as production rapidly declined would cause a ±8% change in the annual mean [OH] derived for these years. Since 1998, however, E/G has been a rather small and constant fraction (~10%) of the derived k_G (fig. S1). Although emissions and their interannual changes remain uncertain, their influence on estimates of k_G since 1998 has been substantially reduced.

Uncertainty in $(dG/dt)/G$ for CH_3CCl_3 is also reduced since 1998 because its atmospheric gradients have diminished substantially in response to near-zero emissions. Annual mean mixing ratio gradients between remote stations were as much as 30 to 40% of the global mean in the 1980s (*17*)

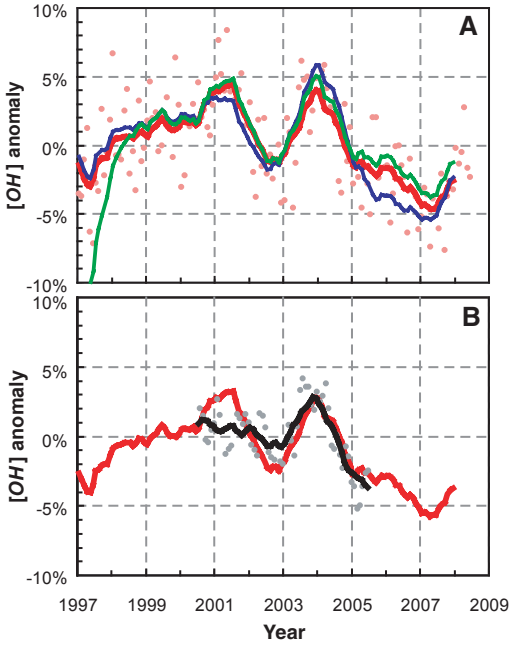

Fig. 2. Anomalies in global [OH] derived from NOAA CH_3CCl_3 data with different modeling approaches and emissions. (**A**) [OH] anomalies inferred from measured global surface means of CH_3CCl_3 and a box model (see text and Eq. 1) incorporating three different emission histories: emissions through 2000 (*17*) then declining exponentially thereafter at –20% year^{-1} (red line); those same emissions updated after 2002 with (*25*) (blue line); and zero emissions (green line). Anomalies are relative to mean [OH] during 1998–2007. Points represent an [OH] anomaly derived from two monthly means 12 months apart and exponentially declining emissions after 2000 (see above); smoothed lines are 12-month running means. (**B**) [OH] anomalies derived from a high-resolution 3D inversion of the NOAA flask data (points and black line) (*18*) and exponentially declining emissions. Modeled anomalies determined for yearly intervals centered about each month during 2000–2005 (gray points) are smoothed over 12-month periods (black line) to allow a consistent comparison with box model results. The red line is repeated from the top panel but is calculated relative to mean [OH] during 2000–2005 to be consistent with the modeled period.

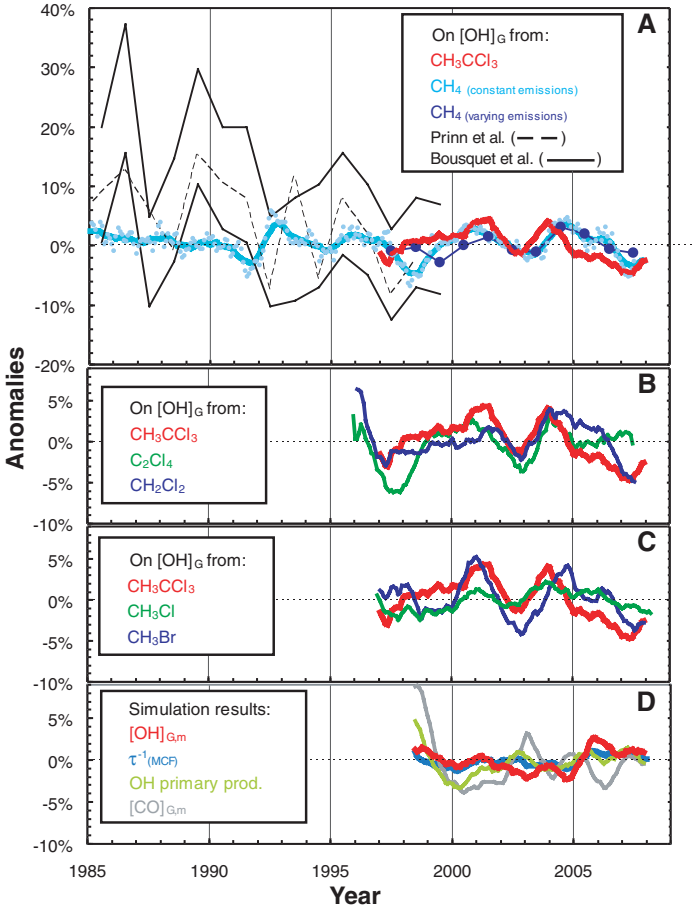

Fig. 3. Anomalies in [OH] inferred from trace gas data and calculated in a global model simulation. (**A**) Anomalies inferred from NOAA CH_3CCl_3 data [red line from Fig. 2; also in (B) and (C)]; from global CH_4 data with constant or varying emissions; from Bousquet *et al.* (*16*) (range includes internal and external uncertainties); and from Prinn *et al.* (*17*). Anomalies are relative to estimates after 1997. (**B** and **C**) [OH] anomalies inferred from NOAA measurements of multiple trace gases [see text and (*24*)]. (**D**) Model simulated [OH] anomalies weighted by mass ($[OH]_{G,m}$) or expressed as the CH_3CCl_3 loss frequency ($\tau^{-1}_{(MCF)}$). Simulated anomalies in OH primary production ($O^1D + H_2O$) and CO weighted by mass ($[CO]_{G,m}$) are also shown (*24*, *30*).

compared to ~7% since 1998 (*14*). Diminished gradients result in improved estimates of [OH] variability because of reduced errors in estimating the global CH_3CCl_3 burden (G) and its rate of change (dG/dt) from measurements at a small number of sampling sites (fig. S2).

Our box model approach and previous calculations (*17*) have shortcomings that could affect conclusions regarding [OH] in the presence of large CH_3CCl_3 emissions (*26*). To investigate these influences during a period when CH_3CCl_3 emissions and atmospheric mixing ratio gradients are reduced and transport-related errors are therefore minimized, we derived [OH] variability with a three-dimensional inversion technique that includes interannually varying meteorology (*18*). In this approach, the monthly global [OH] during 2000–2005 is optimized by minimizing the differences between modeled and observed CH_3CCl_3 (*24*). Results for 2000 to 2005 are highly consistent with the box model analysis and suggest an annual mean [OH] IAV of 2.3 ± 1.2% (Fig. 2B). Thus, in the absence of substantial CH_3CCl_3 emissions, a similar year-to-year variability magnitude in mean [OH] is calculated with different methods from measurements of CH_3CCl_3.

A reliable estimate of [OH] variability must be consistent with observations of other trace gases oxidized by OH. We derived estimates of [OH] variability by applying Eq. 1 to global CH_4 observations from an independent sampling network (*24*, *27*). A mean IAV for [OH] of 2.1 ± 1.8% is implied during 1985–2008, assuming constant CH_4 emissions (Fig. 3A). This estimate is likely an upper limit, however, because methane emissions vary on interannual time scales. When interannual changes in CH_4 emissions from biomass burning and wetlands during 1998–2007 are included (*24*, *28*, *29*), an IAV for [OH] of 1.8 ± 1.2% is inferred for this period, which is less than the variability in [OH] of 2.9 ± 1.9% derived for 1998–2007 assuming constant methane emissions (Fig. 3A).

Our analysis of methane allows three important conclusions. First, when emissions variations of methane are considered, implied global [OH] variability is reduced. This is consistent with the anticorrelation expected between methane and [OH], all other things being constant (*3*). It is unlikely that global annual CH_4 emissions varied coherently with [OH] during the 1980s and 1990s by up to the 25% needed to mask large OH changes implied from CH_3CCl_3 analyses for these years. Second, the IAV in global [OH] implied from methane has been quite constant at about 2% over 25 years, a period during which global anthropogenic emissions of gases that affect OH varied substantially. Hence, a substantial reduction in [OH] variability as inferred from an analysis of CH_3CCl_3 observations before and after 1997 seems unlikely. Third, the global [OH] variability implied from methane is consistent with that implied from CH_3CCl_3 only after 1997. This confirms that the reduced uncertainties associated with estimating [OH] variability from CH_3CCl_3 after 1997 allow a more accurate diagnosis of global [OH] variations during this period.

We applied this same methodology to observations of additional gases oxidized primarily by OH (CH_3Cl, CH_3Br, C_2Cl_4, and CH_2Cl_2). Although interannual variations in emissions of these chemicals are poorly characterized, they arise from a variety of natural and anthropogenic processes. As a result, consistent variability in atmospheric abundances of these compounds implies changes in oxidation by the OH radical. By accounting for multiyear changes in trace-gas emissions with smoothed fits to observed global mixing ratios and, for the methyl halides, annual variations in biomass burning and industrial emission (table S1 and figs. S3 and S4), we derived variations in annual [OH] needed to account for the trace-gas residual mixing ratio variations. The results for these four gases imply IAV in global [OH] of 1 to 3% since the late 1990s (Fig. 3, B and C), consistent with the small [OH] variability derived from CH_3CCl_3 and CH_4.

These results also suggest that the timings of [OH] variations derived with these four additional trace gases are similar to those derived from methane and CH_3CCl_3 (Fig. 3, A to C). [OH] values derived for 1997–1999, 2002–2003, and 2006–2007 are consistently lower than those derived during 2000–2001 and 2004–2005 for all of the trace gases considered. Less consistency is derived for 1997–1998, but during this period variations implied from CH_4, CH_3Cl, and CH_3Br depend strongly on uncertain emission magnitudes from enhanced biomass burning, likely associated with the strong El Niño then (Fig. 3, A and C, and fig. S4).

A theory-based estimate of [OH] variability was also derived with an atmospheric chemistry general circulation model for 1998 to June 2008 in which assimilated observed meteorology was used (*24*, *30*). In this model, [OH] is calculated from a suite of chemical and physical parameters that vary over time and space with consideration of IAV in water vapor, photolysis rates, and biomass burning (Fig. 3D and figs. S5 and S6). Although the detailed variations implied from our trace-gas observations are not well reproduced in the model simulation, a low IAV in global tropospheric [OH] of 0.9 ± 0.8% is calculated (weighted by mass or the CH_3CCl_3 loss frequency), consistent with the [OH] variations derived from the trace-gas data, which are likely to be upper limits (*24*). This small [OH] variability is derived even though simulated variabilities for primary OH production and mixing ratios of CO, a strong sink for tropospheric OH (*3*), are calculated to be substantially larger. A small variability (<2%) was also suggested for annual mean [OH] from independent model simulations of the period 1979–2001 (*21*–*23*).

These observationally derived results substantially clarify our understanding of the sensitivity of Earth's atmospheric oxidizing capacity to environmental perturbations. Both observations and model calculations demonstrate that global mean [OH] is well buffered on interannual time scales, consistent with both primary and secondary OH formation pathways and atmospheric oxidant transport playing important roles in maintaining its global abundance. The improved understanding of this fundamental atmospheric property thus enables more reliable projections of trace-gas climate forcing and atmospheric oxidizing capacity given expected changes in future anthropogenic emissions.

References and Notes

1. H. Levy 2nd, *Science* **173**, 141 (1971).
2. J. A. Logan, M. J. Prather, S. C. Wofsy, M. B. McElroy, *J. Geophys. Res.* **86**, 7210 (1981).
3. C. M. Spivakovsky *et al.*, *J. Geophys. Res.* **105**, 8931 (2000).
4. P. Forster *et al.*, in *Climate Change 2007: The Physical Science Basis. Contribution of Working Group I to the Fourth Assessment Report of the Intergovernmental Panel on Climate Change*, S. Solomon *et al.*, Eds. (Cambridge Univ. Press, Cambridge, 2007), pp. 129–234.
5. Y. Wang, D. J. Jacob, *J. Geophys. Res.* **103**, 31123 (1998).
6. D. Ehhalt *et al.*, in *Climate Change 2001, The Scientific Basis*, J. T. Houghton *et al.*, Eds. (Cambridge Univ. Press, New York, 2001), pp. 239–287.
7. J. Lelieveld, F. J. Dentener, W. Peters, M. C. Krol, *Atmos. Chem. Phys.* **4**, 2337 (2004).
8. J. Lelieveld *et al.*, *Nature* **452**, 737 (2008).
9. B. Weinstock, H. Niki, *Science* **176**, 290 (1972).
10. H. B. Singh, *Geophys. Res. Lett.* **4**, 453 (1977).
11. J. E. Lovelock, *Nature* **267**, 32 (1977).
12. C. A. M. Brenninkmeijer *et al.*, *Nature* **356**, 50 (1992).
13. J. E. Mak, C. A. M. Brenninkmeijer, M. R. Manning, *Geophys. Res. Lett.* **19**, 1467 (1992).
14. S. A. Montzka *et al.*, *Science* **288**, 500 (2000).
15. P. Jöckel, C. A. M. Brenninkmeijer, M. G. Lawrence, A. B. M. Jeuken, P. F. J. van Velthoven, *J. Geophys. Res.* **107**, 4446 (2002).
16. P. Bousquet, D. A. Hauglustaine, P. Peylin, C. Carouge, P. Ciais, *Atmos. Chem. Phys.* **5**, 2635 (2005).
17. R. G. Prinn *et al.*, *Geophys. Res. Lett.* **32**, L07809 (2005).
18. M. C. Krol *et al.*, *Atmos. Chem. Phys.* **8**, 5033 (2008).
19. M. R. Manning, D. C. Lowe, R. C. Moss, G. E. Bodeker, W. Allan, *Nature* **436**, 1001 (2005).
20. J. Lelieveld *et al.*, *Atmos. Environ.* **40**, 5741 (2006).
21. F. Dentener *et al.*, *J. Geophys. Res.* **108**, 4442 (2003).
22. B. Duncan, J. Logan, *Atmos. Chem. Phys.* **8**, 7389 (2008).
23. S. B. Dalsøren, I. S. A. Isaksen, *Geophys. Res. Lett.* **33**, L23811 (2006).
24. See supporting material on *Science* Online.
25. M. Rigby *et al.*, *Geophys. Res. Lett.* **35**, L22805 (2008).
26. M. Krol, J. Lelieveld, *J. Geophys. Res.* **108**, 4125 (2003).
27. E. J. Dlugokencky *et al.*, *Geophys. Res. Lett.* **36**, L18803 (2009).
28. G. R. van der Werf *et al.*, *Atmos. Chem. Phys.* **6**, 3423 (2006).
29. B. P. Walter, M. Heimann, E. Matthews, *J. Geophys. Res.* **106**, 34189 (2001).
30. P. Jöckel *et al.*, *Atmos. Chem. Phys.* **6**, 5067 (2006).

31. We thank C. Siso, B. Miller, L. Miller, D. Mondeel, L. Bruhwiler, P. Novelli, B. Weatherhead, J. W. Elkins, J. H. Butler, station personnel involved with sampling flasks, C. M. Spivakovsky, R. G. Prinn, and other AGAGE scientists, P. Bergamaschi, and J.-F. Meirink. Supported in part by the Atmospheric Composition and Climate Program of NOAA's Climate Program Office and by the Stichting Nationale Computerfaciliteiten (National Computing Facilities Foundation).

Supporting Online Material

www.sciencemag.org/cgi/content/full/331/6013/67/DC1
Materials and Methods
SOM Text
Figs. S1 to S6
Table S1
References

10.1126/science.1197640

The Role of Ammonites in the Mesozoic Marine Food Web Revealed by Jaw Preservation

Isabelle Kruta,[1]* Neil Landman,[2] Isabelle Rouget,[3] Fabrizio Cecca,[3] Paul Tafforeau[4]

Ammonites are prominent in macroevolutionary studies because of their abundance and diversity in the fossil record, but their paleobiology and position in the marine food web are not well understood due to the lack of preserved soft tissue. We present three-dimensional reconstructions of the buccal apparatus in the Mesozoic ammonite *Baculites* with the use of synchrotron x-ray microtomography. Buccal mass morphology, combined with the coexistence of food remains found in the buccal mass, suggests that these ammonites fed on plankton. This diet may have extended to all aptychophoran ammonites, which share the same buccal mass morphology. Understanding the role of these ammonites in the Mesozoic food web provides insights into their radiation in the Early Jurassic, as well as their extinction at the end of the Cretaceous/early Paleogene.

Ammonites were externally shelled cephalopods that lived from the Early Devonian [407 million years ago (Ma)] to the end of the Cretaceous (65.5 Ma) and commonly occur in the fossil record. They are widely used in biostratigraphy to subdivide geologic time. Ammonites are one of the most diverse fossil groups in marine environments; their ecology, however, is poorly understood (*1*, *2*). The modern nautilus generally serves as a model to reconstruct their mode of life, but phylogenetic studies suggest that coleoids are better models (*3*). Information about their diet is based on examination of the buccal mass—consisting of the upper jaw, lower jaw, and radula—that is occasionally preserved inside the body chamber. Jaws have been documented in 43 genera of ammonites (*4*, *5*), but radulae are observed in only 9 genera (*6*, *7*) because their discovery depends on accidental breaks or fortuitous exposure by weathering. In addition, traditional techniques used to study radulae (polished serial sections) do not usually reveal sufficient detail for comparative analysis.

Here, we report phase-contrast synchrotron x-ray microtomographic three-dimensional (3D) reconstructions of the buccal masses of three fossil specimens of *Baculites* sp., one of the few ammonite genera that persisted up to and perhaps even across the Cretaceous-Paleogene boundary (*8*). In addition, we document a larval shell of a gastropod and three fragments of crustaceans that are preserved inside the jaw in one specimen. The specimens were discovered in the Upper Cretaceous Pierre Shale, Belle Fourche, South Dakota, USA (*9*).

As in other members of the aptychophoran group of ammonites (*10*), the lower jaw of *Baculites* is relatively large, with a slit along the midline and a blunt anterior margin (Fig. 1, A to C). The two halves of the lower jaw are covered with a pair of calcareous plates (known as the aptychus). The upper jaw of *Baculites* is evident in these reconstructions (Fig. 1C, fig. S1, and movie S1); it is less than one-half the length of the lower jaw and is relatively thin (140 μm thick at the anterior margin), indicating that the original chitin may have been poorly tanned and slightly flexible.

All three specimens of *Baculites* contain a radula (figs. S2 to S4). In American Museum of Natural History (AMNH) specimen numbers 55901 and 66267, the teeth are preserved close to their original life position (Fig. 1, D and E, and movie S1). Although they were originally solid

[1]UMR-CNRS 7207, Département Histoire de la Terre, Muséum National d'Histoire Naturelle, 47 rue Cuvier 75231 Paris Cedex 05, France. [2]Division of Paleontology (Invertebrates), American Museum of Natural History, Central Park West at 79th Street, New York, NY, USA. [3]UMR-CNRS 7207, Université Pierre et Marie Curie - Paris 6, 4-Place Jussieu, case 104, 75252 Paris Cedex 05, France. [4]European Synchrotron Radiation Facility (ESRF), BP 220, 6 rue Jules Horowitz, 38043 Grenoble Cedex, France.

*To whom correspondence should be addressed. E-mail: kruta@mnhn.fr

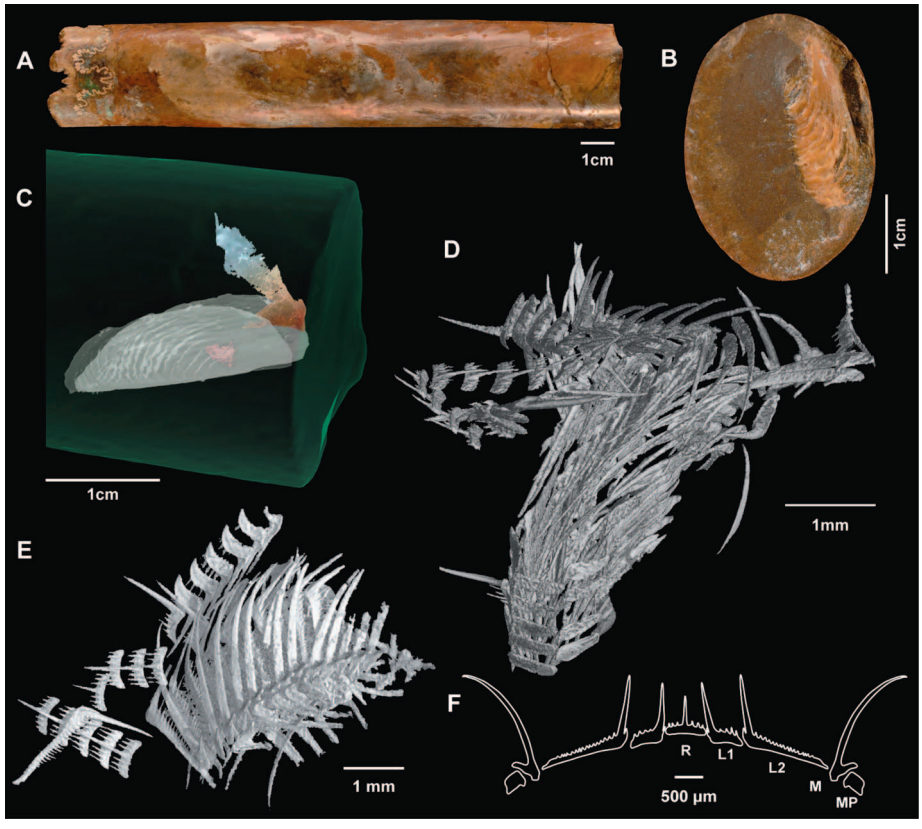

Fig. 1. Exceptionally preserved radula in ammonites from the Upper Cretaceous (Belle Fourche, South Dakota, USA). (**A**) Shell of *Baculites* sp. (AMNH 55901). Only a portion of the body chamber and phragmocone is preserved. (**B**) Aperture of the shell with one of the valves of the lower jaw (aptychus) exposed on the right side. (**C**) Virtual reconstruction of the buccal mass based on a composite of two specimens (AMNH 55901 and AMNH 66253). Green, shell; white, valves of the lower jaw; color gradation from yellow to brown, upper jaw; red, radula. The upper jaw has been enlarged to compensate for the size difference between the two specimens. (**D** and **E**) 3D virtual extraction of the radula of *Baculites* sp. as it appears inside the ammonite (in situ) [(D) AMNH 55901; (E) AMNH 66267]. (**F**) Sketch of the radula of *Baculites* sp. R, rachidian tooth; L1, first lateral tooth; L2, second lateral tooth; M, marginal tooth; MP, marginal plate.

structures, the radular teeth are hollow or infilled with material similar in composition to that of the matrix (but of different density). In analogy with modern cephalopods, they may have been composed of chitin, with possibly some degree of mineralization (*11*). As in all cephalopod radula, the teeth and marginal plates in each transverse row repeat those in the preceding and succeeding rows (Fig. 2A) (*11*). In AMNH 55901, the radula forms a U-shaped structure, possibly reflecting its original shape in the radular canal (Fig. 2B and movie S1). If the radula were unfolded, it would be ~6 mm wide and ~7 mm long.

Each radular row consists of nine elements, including seven teeth and two marginal plates, thus corresponding to the definition of the Angusteradulata (ammonoids plus octopus, cuttlefish, and squid) (Fig. 2A) (*12*). Four elements appear on each side of the central rachidian tooth. The teeth vary in shape, and they are multicuspidate and comblike (*11*). The cusps of the rachidian tooth are narrow and sharp and decrease in height with increasing distance from the central cone (Fig. 2C, fig. S5, and table S1). Each lateral tooth (L1 and L2) bears a single small cusp on the inner side of a prominent cone that is ~1 mm high and multiple cusps on the outer side, decreasing in height toward the margin: four on the first lateral tooth (L1) and 17 on the second lateral tooth (L2) (Fig. 2D). The marginal tooth is unicuspate (Fig. 2E), 1.6 mm high, curved, and sabrelike. The marginal plates are small and flat. High-resolution scans with voxel (volumetric pixel) size of 1.4 μm reveal a carena running from the tip of the highest cone to its base on the second lateral tooth (fig. S2). These radulae are similar to a previously reported structure in the same species of *Baculites*, but most of the teeth in this previously reported specimen were not visible, precluding any detailed reconstruction of the radula (*7*).

The jaws in *Baculites* are similar to those in other aptychophoran ammonites. Comparison of the radula in *Baculites* with that of previously described ammonites is limited because of the low degree of resolution available in older studies. However, the radula reported in other aptychophoran ammonites also appears to consist of small, delicate teeth with a tall, sabrelike marginal tooth [e.g., *Aconeceras* (*13*)].

The morphology of the jaws and radula in ammonites, and mollusks in general, is related to diet (*14*); therefore, the study of these structures can help clarify the feeding habits and ecology of these animals. However, the buccal mass of aptychophoran ammonites has no equivalent among modern cephalopods, and its function has been debated for the past 150 years. Several of the features of the lower jaw—such as its blunt anterior margin, the presence of a slit rather than a thickening along the midline, and the very large size relative to the upper jaw—are incompatible with biting and tearing large prey (*12*). In contrast, the buccal apparatus in modern nautilus consists of a beaklike jaw with robust radular teeth (*11*), which is consistent with the scavenging mode of life of these animals (*15*). Similarly, in most modern coleoids such as squid and cuttlefish, which bite and tear large prey, the apical end of the jaw is very sharp, and the radular teeth are robust. There are only three examples of a buccal apparatus in modern cephalopod species that superficially resemble that in *Baculites*. In mesobathypelagic octopods such as Bolitaenidae, the lower jaw ends in a finely toothed, blunt anterior margin, the upper jaw is weakly tanned, and the radula is multicuspidate (ctenoglossan) (*16*). The diet of *Japetella diaphana* and *Bolitaena pygmea* consists of copepods, krill, and other small organisms (*17*). In *Argonauta argo*, the buccal apparatus also superficially resembles that in *Baculites* (weakly tanned upper and lower jaws, absence of a sharp beak); it feeds on heteropods and pteropods. Outside of cephalopods, the radula in *Baculites* most closely resembles that in heteropod mollusks (multicuspidate, with sabrelike marginal teeth); they feed on plankton and gelatinous prey (*18*).

These comparisons suggest that the buccal apparatus in *Baculites*, as well as in other aptychophoran ammonites in general, is an adaptation for capturing and eating small organisms in the water column. This is consistent with rare finds of ammonite stomach contents, most of which consist of small organisms, such as tiny crustaceans and juvenile ammonites (*12*, *19*). In addition, the radular teeth in *Baculites* do not show a progressive loss of cusps, which has been observed in modern cephalopods where the radula is used as an abrasive device (*20*).

Lending further support to this hypothesis are the remains of several small organisms preserved inside the buccal mass in AMNH 66253 (Fig. 3). Three fragments of crustaceans 5.0, 3.0, and 1.6 mm in length are present between the two valves of the aptychus (figs. S7 and S8). The anterior portion of the body is missing in two fragments, whereas the third fragment consists of a cephalon with two pereonites (fig. S7). The ventral part and appendages are not well preserved. The fragment of the cephalon matches the posterior part of the fragment near the radula, indicating that the two pieces belong to the same individual. The overall morphology of these specimens suggests that they are isopods, one of which is an adult and the other a juvenile. They probably belong to the family Cirolanidae and were capable of swimming. However, the fragmentary nature of the material does not permit a more precise determination. A small gastropod 975 μm long is present near the radula and upper jaw. It appears to be a planktotrophic larva of a benthic gastropod (fig. S9).

The presence of these organisms in the buccal mass could be explained as the result of predation

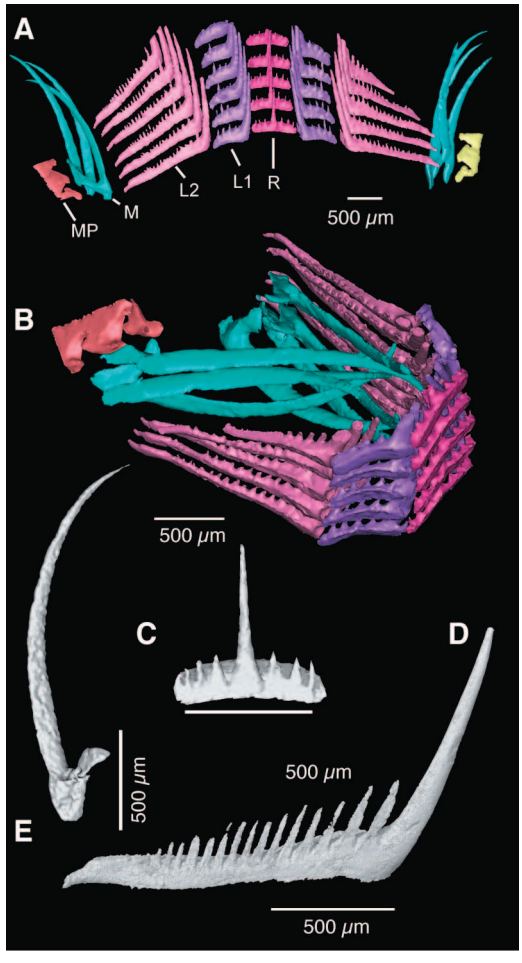

Fig. 2. Morphology of the radula and teeth in *Baculites* sp. (**A**) Virtual reconstruction of the radula in *Baculites* sp. (AMNH 55901) as if unfolded. Rows of teeth are repeated all along the length of the radula. Blue, marginal teeth; light pink, second lateral teeth; purple, first lateral teeth; dark pink, rachidian teeth; yellow, marginal plates. (**B**) Part of the radula of *Baculites* sp. (AMNH 55901). The radula is folded, as it may have appeared in the tube-shaped radular canal. (**C**) Adoral view of the rachidian tooth. (**D**) Lateral view of the second lateral tooth, center of the ribbon on the right-hand side. (**E**) Lateral view of the marginal tooth.

by the ammonite, scavenging of the buccal mass by the isopods, or a hydrodynamic accumulation of postmortem debris (or any combination of the three). We favor the first interpretation. The fact that all of the fossils occur in the buccal mass and not in the rest of the body chamber provides evidence against their interpretation as a hydrodynamic accumulation. The gastropod may have been living in the plankton and was eaten by the ammonite. The fragments of crustaceans are broken in half, and the remains of their soft tissues are preserved inside, suggesting that they were bitten off by the ammonite jaw. Today, marine isopods live on the sea floor or in the water column just above the bottom [demersal zooplankton (*21*)] and are eaten by modern cephalopods, especially juveniles in which the jaw is not yet sufficiently well developed (stiff) to bite harder prey (*22*).

Thus, the morphology of the jaws and radula in *Baculites* and the presence of possible prey remains inside the buccal mass suggest that these ammonites fed on small organisms in the water column, rather than capturing and eating large prey on the ocean bottom, as exemplified by living nautilus. The aptychophoran ammonites represent a diverse clade in the Jurassic and Cretaceous, consisting of hundreds to thousands of species (*23*, *24*) [e.g., aptychophoran ammonites represented a large portion of the Ammonoidea in the Cretaceous (*24*)]. They include species with a variety of shell shapes, ranging from closely coiled to straight, as in *Baculites*. These species may have exhibited different hydrodynamic properties (*25*) and lived in different habitats (for instance, different depths in the water column) (*1*). However, the similarity in their buccal apparatus suggests that all of them followed the same feeding habit.

The unique role of these ammonites in the marine food web may have influenced Earth system processes during the Jurassic and Cretaceous (for example, processing of particulate organic matter and its transport to the sea floor). The appearance of this feeding strategy may have led to the radiation of the aptychophoran ammonites in the Early Jurassic and Cretaceous, possibly in conjunction with the radiation of new groups of plankton (*26*, *27*). However, this diet may have ultimately contributed to the extinction of the ammonites. The end of the Cretaceous was marked by an abrupt decline in several groups of plankton (*28*). The ammonites, which may have depended on these animals for food, eventually became extinct, whereas closely related groups such as the nautilids, which relied on other food sources, survived and even flourished in the succeeding era (*29*).

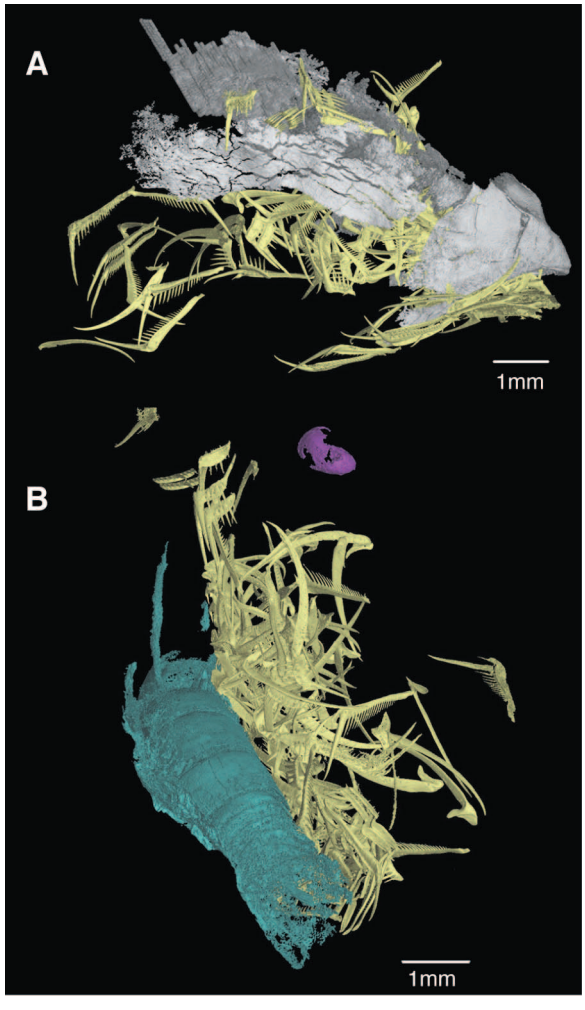

Fig. 3. Upper jaw, radula, and associated crustaceans (AMNH 66253). (**A**) Lateral view of the upper jaw (gray); anterior margin on the left. The radular teeth (yellow) are enclosed by the upper jaw. (**B**) Dorsal view of the crustacean (isopod) showing the segments. Posterior part of the crustacean on the bottom right; radular tooth, yellow; gastropod larval shell, pink; isopod, blue.

References and Notes

1. G. E. G. Westermann, in *Ammonoid Paleobiology*, N. H. Landman, K. Tanabe, R. A. Davis, Eds. (Plenum Press, New York, 1996), pp. 607–707.
2. D. Korn, C. Klug, in *Cephalopods Present and Past: New Insights and Fresh Perspectives*, N. H. Landman, R. A. Davis, R. H. Mapes, Eds. (Springer, New York, 2007), pp. 57–85.
3. D. K. Jacobs, N. H. Landman, *Lethaia* **26**, 101 (1993).
4. K. Tanabe, Y. Fukuda, in *Functional Morphology of the Invertebrate Skeleton*, E. Savazzi, Ed. (Wiley, London, 1999), pp. 245–262.
5. K. Tanabe, N. H. Landman, *Abh. Geol. B. A* **57**, 157 (2002).
6. W. J. Kennedy, N. H. Landman, W. A. Cobban, N. L. Larson, *Abh. Geol. B. A* **57**, 113 (2002).
7. N. H. Landman, N. L. Larson, W. A. Cobban, in *Cephalopods Present and Past: New Insights and Fresh Perspectives*, N. H. Landman, R. A. Davis, R. H. Mapes, Eds. (Springer, New York, 2007), pp. 257–298.
8. M. Machalski, C. Heinberg, *Bull. Geol. Soc. Den.* **52**, 97 (2005).
9. Materials and methods are available as supporting material on *Science* Online.
10. T. Engeser, H. Keupp, *Lethaia* **35**, 79 (2002).
11. M. Nixon, *J. Zool. (London)* **236**, 73 (1995).
12. U. Lehmann, *The Ammonites: Their Life and Their World* (Cambridge Univ. Press, Cambridge, 1981).
13. L. A. Doguzhaeva, H. Mutvei, *Palaeontogr. Abt. A* **223**, 167 (1992).
14. G. Owen, in *Physiology of Mollusca Vol. 2*, K. M. Wilbur, C. M. Yonge, Eds. (Academic Press, New York, 1966), pp. 1–52.
15. P. D. Ward, *The Natural History of Nautilus* (Allen & Unwin, Boston, 1987).
16. S. Thore, *Dana Report* **33**, 1 (1949).
17. M. Nixon, J. Z. Young, *The Brains and Lives of Cephalopods* (Oxford Univ. Press, Oxford, 2003).
18. C. M. Lalli, R. W. Gilmer, *Pelagic Snails: The Biology of Holoplanktonic Gastropod Molluscs* (Stanford Univ. Press, Stanford, CA, 1989).
19. M. Jäger, R. Fraaye, *Paleontology* **40**, 557 (1997).
20. N. W. Runham, C. J. Bailey, M. Carr, C. A. Evans, S. Malhalm, *Sci. Mar.* **61** (suppl. 2), 67 (1997).
21. A. L. Alldredge, J. M. King, *Mar. Biol.* **84**, 253 (1985).
22. J. J. Castro, V. Hernández-Garcia, *Sci. Mar. Barcelona* **59**, 347 (1995).
23. W. J. Arkell, B. Kummel, C. W. Wright, in *Treatise on Invertebrate Paleontology. Pt. L, Mollusca 4*, R. C. Moore, Ed. (Geological Society of America and Univ. of Kansas Press, Boulder, CO, Lawrence, KS, 1957), pp. L 80–L 465.
24. C. W. Wright, J. H. Callomon, M. K. Howarth, in *Treatise on Invertebrate Paleontology. Pt. L, Mollusca 4* (revised), R. L. Kaesler, Ed. (Geological Society of America and Univ. of Kansas Press, Boulder, CO, Lawrence, KS, 1996), pp. 1–362.
25. D. K. Jacobs, J. A. Chamberlain, in *Ammonoid Paleobiology*, N. H Landman, K. Tanabe, R. A. Davis, Eds. (Plenum Press, New York, 1996), pp. 169–224.
26. F. Cecca, *C. R. Acad. Sci. Paris Sér. II* **325**, 629 (1997).
27. S. Rigby, C. V. Milsom, *Annu. Rev. Ecol. Syst.* **31**, 293 (2000).
28. B. T. Huber, K. G. MacLeod, R. D. Norris, in *Catastrophic Events and Mass Extinctions: Impacts and Beyond*, C. Koeberl, K. G. MacLeod, Eds. (Geological Society of America, Boulder, CO, 2002), pp. 277–289.
29. A. K. Miller, *Evolution* **3**, 231 (1949).

30. This work was supported by ESRF, UMR CNRS 7207, its 3D platform, and the Annette Kade Fellowship (AMNH). P. Janvier and C. Klug reviewed an earlier draft of the manuscript; A. Lethiers helped produce the figures and movie; N. Larson and K. Cochran helped in field work; and D. Defaye, N. Bruce, R. Feldmann, and K. Bandel helped in the identification of non-ammonite material. Data are available at the ESRF database http://paleo.esrf.eu.

Supporting Online Material

www.sciencemag.org/cgi/content/full/331/6013/70/DC1
Materials and Methods
Figs. S1 to S9
Table S1
References
Movie S1

7 October 2010; accepted 18 November 2010
10.1126/science.1198793

Developmental Plasticity in Sexual Roles of Butterfly Species Drives Mutual Sexual Ornamentation

Kathleen L. Prudic,[1,2]* Cheonha Jeon,[3] Hui Cao,[4] Antónia Monteiro[1,5]*

Current explanations for why sexual ornaments are found in both sexes include genetic correlation, same sex competition, and mutual mate choice. In this study, we report developmental plasticity in mating behavior as induced by temperature during development in the butterfly *Bicyclus anynana.* Males and females reciprocally change their sexual roles depending on their larval rearing temperatures. This switch is correlated with a change in mating benefits to females and costs to males. The discrete seasonal environments, wet season and dry season, are known to produce the two developmental forms and as a consequence impose alternating, symmetrical patterns of sexual selection, one season on male ornaments, the following season on female ornaments. Thus, reciprocal selection through time may result in mutual sexual ornamentation.

Morphology and behavior can be developmentally plastic and change in response to environmental variation experienced during ontology (*1*). Butterflies often exhibit seasonal polyphenism in wing coloration, a form of developmental plasticity triggered by certain environmental cues experienced during critical ontogenetic periods in larval and pupal development (*2*, *3*). To what extent rearing environment also influences adult butterfly behavior is largely unknown. We investigated both courtship and mate preference in the developmentally plastic African butterfly, *Bicyclus anynana*. This species is known to have multiple generations per year and to display two different developmental forms, wet season and dry season (WS and DS) (Fig. 1). In nature, these two forms are separated temporally and are adapted to their respective seasons (*4*). The WS form has large eyespots and a conspicuous transversal band on the ventral wings (Fig. 1A), whereas the DS form has reduced eyespots and cryptic, uniform ground coloration on the ventral wings (*5*) (Fig. 1B). These wing patterns are determined primarily by larval rearing temperature, not genetic differences (*5*). Females are known to mate multiply, and the DS females delay laying eggs until the end of the dry season, whereas the WS form will lay eggs immediately after mating (*6*).

The dorsal forewing eyespots, unlike ventral eyespots, show little size variation with larval rearing temperatures (*7*) (Fig. 1, C to F) and are the WS male sexual ornament (*8*). WS males actively court WS females, and these females prefer males with intact dorsal eyespots, specifically the presence of the white, ultraviolet (UV)-reflective center often called the pupil (*8*). These same ornaments are also present on females. We investigated whether dorsal eyespot pupils are signals in courtship and mate preference used by both sexes and by both developmental forms. We reared the two forms simultaneously in the lab and assessed both male and female courtship behavior among and between forms. We then measured mate response toward individuals with intact versus manipulated dorsal eyespots among and between forms.

We conducted courtship observations using a two-by-two factorial design (sex by developmental form). Courtship in *B. anynana* is highly ritualized (*9*, *10*). It involves the courter displaying the dorsal eyespots to the receiver by rapidly opening and closing its wings in front of the eyes of the receiver (*9*). We found DS females courted either male form more often than WS females courted males [analysis of variance (ANOVA) $F_{1,19} = 3.69$, $P = 0.018$; no sex by form interaction] (Fig. 2A). Developmental form also affected male courtship; WS males courted females more often than DS males courted females ($F_{1,19} = 9.04$, $P = 0.0012$; no sex by form interaction) (Fig. 2B). Within developmental forms, we found that WS males courted more than WS females ($F_{1,19} = 9.23$, $P = 0.001$) (Fig. 2), whereas DS females courted more than DS males ($F_{1,19} = 5.10$, $P = 0.004$) (Fig. 2). There is a developmental shift in the intensity of courtship behavior displayed by each sex, irrespective of the developmental form of the receiver.

To test the effect of developmental plasticity on mate preference, we manipulated the sexual ornaments of each sex in turn and evaluated mate preference in each form. We eliminated the dorsal eyespot pupils, the white, UV-reflective centers, by concealing them with paint (*8*, *10*). Consistent with previous work (*8*), we found WS females preferred to mate with males with intact dorsal eyespot pupils ($F_{1,19} = 5.27$, $P = 0.003$) (Fig. 3A). However, DS females showed no preference

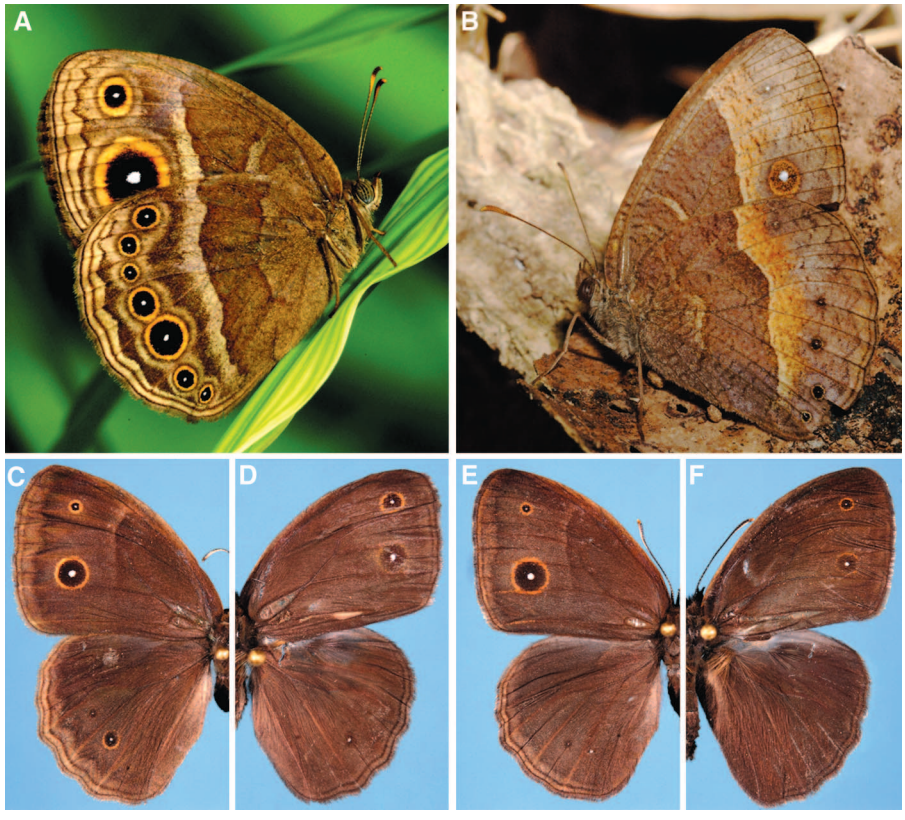

Fig. 1. Wet and dry seasonal forms of *B. anynana*. (**A**) WS ventral female, (**B**) DS ventral female, (**C**) WS dorsal female, (**D**) WS dorsal male, (**E**) DS dorsal female, (**F**) DS dorsal male. Note the difference in degree of plasticity between ventral and dorsal surfaces. Dorsal forewing eyespots (the sexual ornament) are not plastic compared with ventral eyespots.

[1]Ecology and Evolutionary Biology, Yale University, 165 Prospect Street, New Haven, CT 06511, USA. [2]Yale Institute for Biospheric Studies, Yale University, 165 Prospect Street, New Haven, CT 06511, USA. [3]Electrical Engineering, Yale University, New Haven, CT 06511, USA. [4]Applied Physics and Physics, Yale University, New Haven, CT 06511, USA. [5]Assistant Curator of Entomology, Peabody Museum of Natural History, Yale University, 165 Prospect Street, New Haven, CT 06511, USA.

*To whom correspondence should be addressed. E-mail: Kathleen.prudic@yale.edu (K.L.P.); antonia.monteiro@yale.edu (A.M)

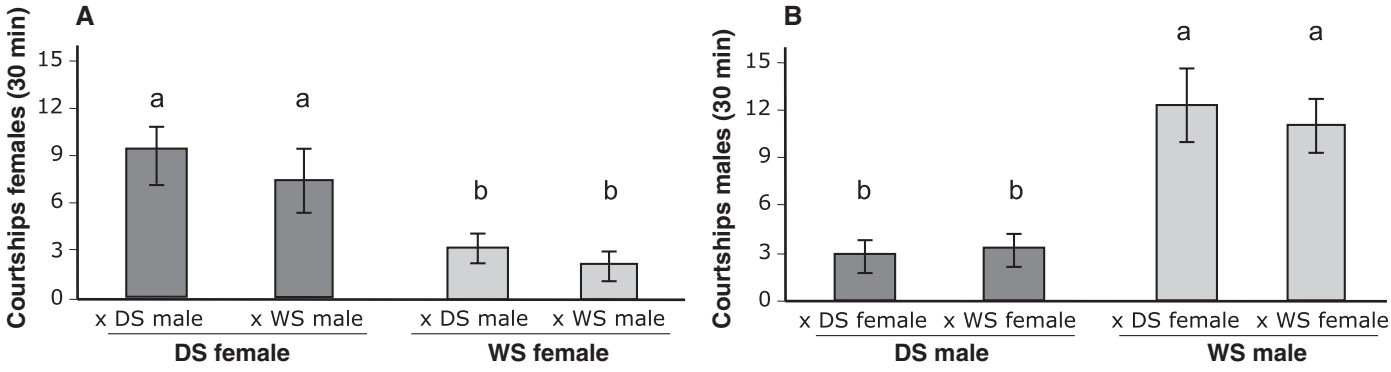

Fig. 2. Courtship behavior of DS and WS *B. anynana*. (**A**) Female behavior and (**B**) male behavior. Shade denotes the developmental form of the courter, not whom they courted: medium gray for dry season, light gray for wet season. Different letters above graphs represent significant differences. Error bars represent 95% CI of means.

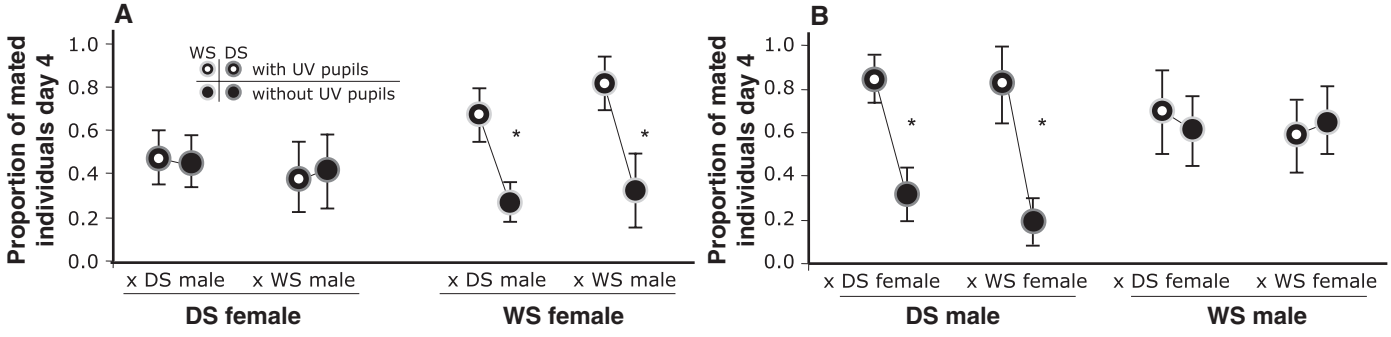

Fig. 3. Mate choice relative to presence or absence of intact dorsal eyespots in both developmental forms. (**A**) Female preference and (**B**) male preference. Shade denotes the developmental form of the discriminating sex: medium gray for dry season and light gray for wet season. Eyespot shape denotes UV pupil intact on the manipulated sex, and solid shape denotes UV pupil blocked with paint on the manipulated sex. Asterisks (*) indicate significant differences. Error bars represent 95% CI of means.

between males with or without pupils ($F_{1,19}$ = 0.41, P = 0.690) (Fig. 3A). In the male choice experiments, we found DS males preferred to mate with females with intact pupils ($F_{1,19}$ = 4.93, P = 0.006) (Fig. 3B), but WS males showed no preference ($F_{1,19}$ = 0.41, P = 0.170) (Fig. 3B). Each developmental form was of similar genetic stock, and all individuals experienced the same environmental cues during the behavior experiments. Thus, early temperature differences during larvae and/or pupal development cause the switch in courtship and mate preference behavior.

Dorsal eyespot pupils are thought to be consistent in UV reflectance and size between sexes and seasonal forms, representing monomorphic ornaments (*7*). Our detailed measurements of these small wing pattern elements indicated that there is both a UV reflectance and size difference between DS and WS forms. WS males have greater UV reflectance than DS males [DS males = 47% with 4% confidence interval (CI), WS males = 58% with 6% CI, $F_{1,19}$ = 9.63, P = 0.006], whereas DS females have greater UV reflectance than WS females (DS females = 56% with 4% CI, WS females = 50% with 3% CI, $F_{1,19}$ = 4.67, P = 0.044). Pupil size is also larger in WS males relative to DS males, both in absolute size and relative to wing size (DS males = 0.056 mm^2 with 0.02 mm^2 CI, WS males = 0.111 mm^2 with 0.05 mm^2 CI, $F_{1,19}$ = 4.93, P = 0.006), but pupil size differences were not observed in females (DS females = 0.310 mm^2 with 0.05 mm^2 CI, WS females = 0.310 mm^2 with 0.04 mm^2 CI, $F_{1,19}$ = 0.35, P = 0.563). Thus, the dorsal eyespots pupils in *B. anynana* are cryptic, seasonally dimorphic sexual ornaments.

This developmental polyphenism in mating behavior and sexual ornaments should be caused by a corresponding shift in the relative costs and benefits of mating. Because mating in insects is often associated with female fitness benefits via the transfer of a spermatophore or some other nuptial gift (*11*, *12*), we investigated changes in the direct benefit to females between mating with WS and DS males. The relative effects of mating on male and female longevity were measured as the number of days until death in the absence of all adult resources except water (*10*). Both WS and DS female longevity (DS female $F_{1,35}$ = 24.54, P = 0.0001; WS female $F_{1,35}$ = 22.71, P = 0.0001) and number of eggs laid (DS female $F_{1,23}$ = 18.98, P = 0.0001; WS female $F_{1,23}$ = 3.18, P = 0.052) increased when females mated with a DS male (Fig. 4A) (Fig. 4C). However, female longevity did not differ between unmated females and those that mated with a WS male (DS female $F_{1,35}$ = 1.39, P = 0.157; WS female $F_{1,35}$ = 0.19, P = 0.762) (Fig. 4A). Conversely, DS male longevity was negatively affected by mating, whereas WS male longevity was not (DS male $F_{1,35}$ = 18.22, P = 0.001; WS male $F_{1,35}$ = 2.11, P = 0.132) (Fig. 4B). These results suggest that females can increase their longevity by soliciting copulations and receiving a more beneficial nuptial gift from DS males. DS females may be actively seeking mating opportunities and the resultant male nuptial gifts, as seen in other butterfly species (*13*, *14*). The number of copulations may limit female survival and subsequent probability of reproduction, and females may compete for mates in the dry season. We found no obvious preliminary difference in spermatophore size between WS and DS males, so additional research is necessary to elucidate the underlying mechanism promoting female longevity. Although we did not measure costs to males of multiple matings, it is possible that these costs could accumulate and affect subsequent mating opportunities. This hypothesis is bolstered by two findings in WS males: As the number of matings increase, (i) smaller spermataphores are produced (*15*), and (ii) less sperm is transferred (*16*).

We have shown that courtship, mate preference, and ornament UV reflectance in *B. anynana* changes reciprocally with developmental temperature, suggesting that seasonal temperature variation in the field drives a complex polyphenism in mating behavior and morphology. Compared with congeners, *B. anynana* is not obviously sexually dimorphic (*17*). We found that the seem-

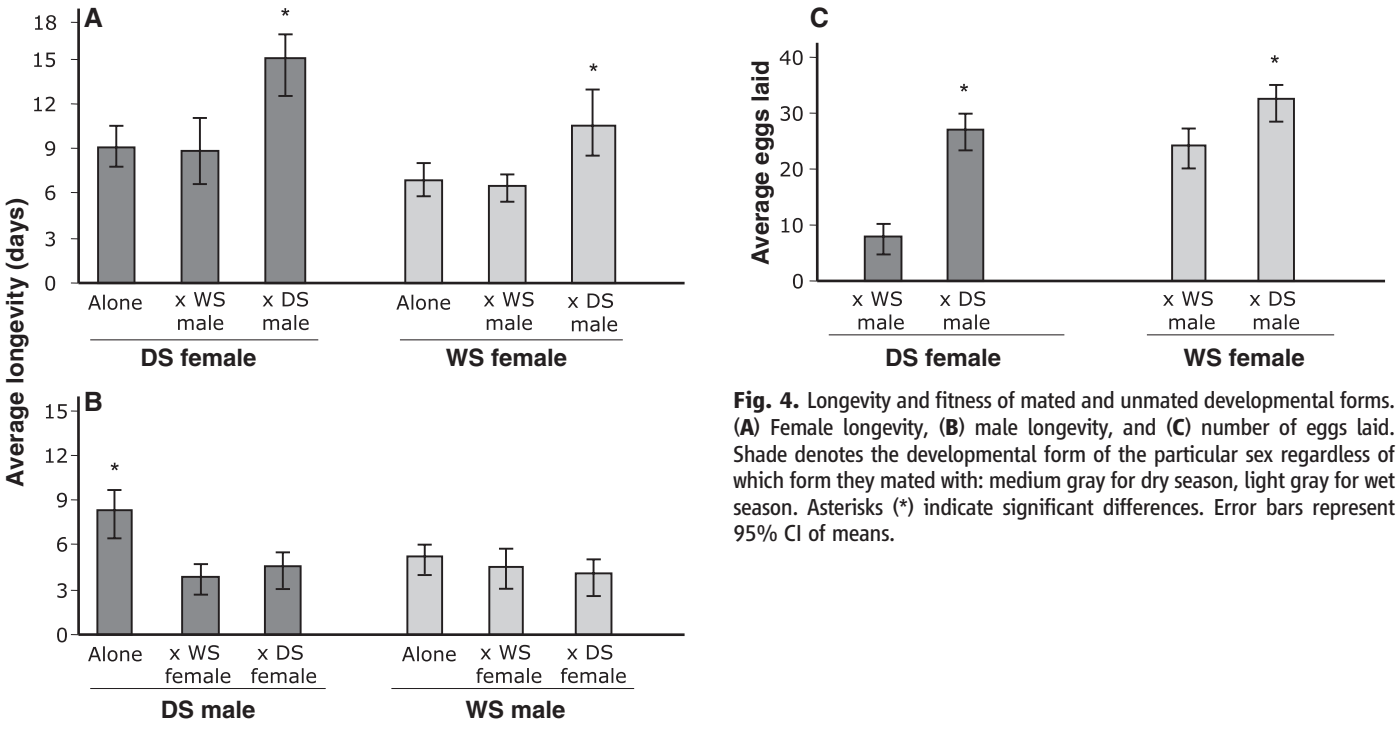

Fig. 4. Longevity and fitness of mated and unmated developmental forms. (**A**) Female longevity, (**B**) male longevity, and (**C**) number of eggs laid. Shade denotes the developmental form of the particular sex regardless of which form they mated with: medium gray for dry season, light gray for wet season. Asterisks (*) indicate significant differences. Error bars represent 95% CI of means.

ingly monomorphic wing pattern is actually seasonally dimorphic and is likely being maintained by the alternating sexual roles of males and females across seasons. The morphological differences between the sexual ornaments are cryptic to humans because the signal is in the UV range. It is possible that genetic correlations across sexes prevent the complete removal of eyespot pupils in the season where they are not being used in sexual display. Alternatively, dorsal eyespot pupils may play an additional role in predator-prey interactions beneficial to both sexes.

Previous work on vertebrates demonstrates that both males and females may simultaneously use their ornaments in making mating decisions (*18*) and that mate preference can change through adult life (*19*, *20*). Similarly, other insect studies have shown seasonal changes in mating behavior within adult individuals based on changes in environmental conditions (*21*, *22*). When adult resources are limiting in tettigonid bushcrickets, males become the choosier sex, whereas females initiate courtship more and compete more with each other for mating opportunities (*20*–*23*). These behaviors are not fixed during development as seen in *B. anynana*; instead, they can change in adults with the introduction of more food resources (*21*). Furthermore, the sexual ornament in bushcricket mate signaling is currently not known or not important in this mating system, although female size is a factor in mate preference (*22*, *23*). In other butterfly species, there are examples of seasonal changes in mate preference in one sex (*24*, *25*), but our study demonstrates a complete switch in mating behavior between the sexes.

Our study reveals another mechanism by which sexual ornaments may be maintained in both sexes beyond genetic correlation (*26*), same sex competition (*27*), or mutual mate choice (*28*). Like certain morphological traits, courtship behavior and mate preference is seasonally plastic in *B. anynana*. This developmental control of mating behavior in different environments may be a generalized phenomenon, especially in insects. Many insect species have multiple generations per year and consistent seasonal differences in form between generations (*29*). These seasonal forms can have profound differences in wing pattern, mating behavior, and nuptial gifts (*29*–*31*). In these situations, developmental plasticity in sexual roles may help explain the evolution of both male and female ornaments. Adult mating behavior encoded during early ontology may be common in insects that have short reproductive periods relative to the length of the season and predictable environmental fluctuations. Seasonal developmental polyphenism in mating behavior would allow adults to immediately perform the correct behavior for a particular season with minimal learning costs. Thus, the complete reversal observed in *B. anynana* adds to our current understanding of environmentally induced sexual role reversal and suggests a dynamic mechanism promoting the evolution and maintenance of sexual ornaments in both males and females.

References and Notes

1. M.-J. West-Eberhard, *Developmental Plasticity and Evolution* (Oxford Univ. Press, New York, 2003).
2. H. F. Nijhout, *Bioscience* **49**, 181 (1999).
3. R. E. Kooi, P. M. Brakefield, *J. Insect Physiol.* **45**, 201 (1999).
4. P. M. Brakefield, W. A. Frankino, in *Phenotypic Plasticity of Insects: Mechanisms and Consequences*, D. W. Whitman, T. N. Ananthakrishnan, Eds. (Science Publishers, Enfield, NH, 2008), pp. 121–152.
5. P. M. Brakefield, V. Mazzotta, *J. Evol. Biol.* **8**, 559 (1995).
6. P. M. Brakefield, N. Reitsma, *Ecol. Entomol.* **16**, 291 (1991).
7. P. M. Brakefield, F. Kesbeke, P. B. Koch, *Am. Nat.* **152**, 853 (1998).
8. K. A. Robertson, A. Monteiro, *Proc. Biol. Sci.* **272**, 1541 (2005).
9. C. M. Nieberding *et al.*, *PLoS One* **3**, e2751 (2008).
10. Materials and methods are available as supporting material on *Science* Online.
11. L. W. Simmons, *Nature* **358**, 61 (1992).
12. B. Karlsson, *Ecology* **79**, 2931 (1998).
13. C. L. Boggs, *Am. Nat.* **136**, 598 (1990).
14. A. Kaitala, C. Wiklund, *Behav. Ecol. Sociobiol.* **35**, 385 (1994).
15. F. Molleman, B. J. Zwaan, P. M. Brakefield, *Behav. Ecol. Sociobiol.* **56**, 404 (2004).
16. Z. Lewis, N. Wedell, *J. Insect Behav.* **20**, 201 (2007).
17. J. C. Oliver, K. A. Robertson, A. Monteiro, *Proc. Biol. Sci.* **276**, 2369 (2009).
18. A. Berglund, M. S. Wideo, G. Rosenqvist, *Behav. Ecol.* **16**, 649 (2005).
19. A. M. Billing, G. Rosenqvist, A. Berglund, *Behav. Ecol.* **18**, 535 (2007).
20. A. S. Chaine, B. E. Lyon, *Science* **319**, 459 (2008).
21. D. T. Gwynne, L. W. Simmons, *Nature* **346**, 172 (1990).
22. M. G. Ritchie, D. Sunter, L. R. Hockham, *J. Insect Biol.* **11**, 481 (1998).
23. D. T. Gwynne, *Evolution* **38**, 1011 (1984).
24. M. Friberg, C. Wiklund, *Behav. Ecol.* **18**, 758 (2007).
25. Y. Obara, G. Ozawa, Y. Fukano, K. Watanabe, T. Satoh, *Zoolog. Sci.* **25**, 1 (2008).
26. R. Lande, *Evolution* **34**, 292 (1980).
27. T. H. Clutton-Brock, *Science* **318**, 1882 (2007).
28. N. R. LeBas, *Trends Ecol. Evol.* **21**, 170 (2006).
29. A. M. Shapiro, *Evol. Biol.* **9**, 259 (1976).
30. J. G. Kingsolver, *Evolution* **49**, 932 (1995).
31. C. Wiklund, B.-S. Tullberg, *Anim. Behav.* **68**, 621 (2004).

32. Visual recordings of *O. anynana* courtship displays are available online at www.youtube.com/watch?v=_1AjNkJuyX0. We thank A. Alonzo, H. Kindsvater, J. Oliver, D. Papaj, E. Snell-Rood, A. Stoehr, and three anonymous reviewers for comments and R. Rak and C. Bolick for rearing host plants. Funding was provided by the American Association of University Women and Yale Institute of Biospheric Studies to K.L.P., Yale University to A.M., and the Yale NSF-MRSEC (DMR-0520495) to H.C.

Supporting Online Material

www.sciencemag.org/cgi/content/full/331/6013/73/DC1
Materials and Methods
References

30 August 2010; accepted 11 November 2010
10.1126/science.1197114

Vernalization-Mediated Epigenetic Silencing by a Long Intronic Noncoding RNA

Jae Bok Heo[1] and Sibum Sung[1]*

Vernalization is an environmentally-induced epigenetic switch in which winter cold triggers epigenetic silencing of floral repressors and thus provides competence to flower in spring. In *Arabidopsis*, winter cold triggers enrichment of tri-methylated histone H3 Lys^{27} at chromatin of the floral repressor, *FLOWERING LOCUS C* (*FLC*), and results in epigenetically stable repression of *FLC*. This epigenetic change is mediated by an evolutionarily conserved repressive complex, polycomb repressive complex 2 (PRC2). Here, we show that a long intronic noncoding RNA [termed COLD ASSISTED INTRONIC NONCODING RNA (COLDAIR)] is required for the vernalization-mediated epigenetic repression of *FLC*. COLDAIR physically associates with a component of PRC2 and targets PRC2 to *FLC*. Our results show that COLDAIR is required for establishing stable repressive chromatin at *FLC* through its interaction with PRC2.

Developmental fates of cells are determined by innate genetic programs and interactions with their environments. A major environmental cue that plants sense to monitor seasonal change is winter cold, as exemplified by vernalization (*1*). Vernalization is the process by which certain plants acquire competence to flower rapidly in spring by sensing prolonged exposure to winter cold (*1*). In *Arabidopsis*, the stability of the vernalized state results from the stable repression of a potent floral repressor, *FLOWERING LOCUS C* (*FLC*) (*2*). A prolonged exposure to cold induces a plant homeo domain (PHD) finger–containing protein, VERNALIZATION INSENSITIVE 3 (VIN3) (*3*), and VIN3 becomes associated with an evolutionarily conserved repressive complex, polycomb repressive complex 2 (PRC2) (*4*, *5*). PRC2 mediates histone H3 Lys^{27} trimethylation (H3K27me3) through its core component, a histone methyltransferase, Enhancer of Zeste [E(z)] (*2*, *6*). During and after vernalization, PRC2 occupancy at *FLC* increases and correlates with an increased level of H3K27me3 at *FLC* chromatin, which is required for the stable maintenance of *FLC* repression (*2*, *5*, *7*, *8*). In *Arabidopsis*, there are three homologs of E(z). These include CURLY LEAF (CLF), SWINGER (SWN), and MEDEA, which are involved in several developmental programs in *Arabidopsis* (*6*). However, the molecular determinants for the increased recruitment of PRC2 and subsequent establishment of H3K27me3-enriched repressive chromatin at *FLC* by vernalization are not known. We identified a long intronic, noncoding transcript that plays role in the vernalization-mediated epigenetic silencing of *FLC* through the recruitment of PRC2 to *FLC* locus.

Several long noncoding RNAs (ncRNAs) have been shown to target repressive histone-modifying activities and epigenetically silence transcription through a molecular interaction with specific chromatin domains (*9*, *10*). Notably, PRC2-mediated silencing includes the interaction with such ncRNAs (*11*, *12*). A group of related antisense ncRNAs (termed COOLAIR) from *FLC* have been proposed to be involved in vernalization-mediated *FLC* repression (*13*). However, the importance of COOLAIR in the vernalization process has yet to be demonstrated. We independently hypothesized that long ncRNAs may play a role in vernalization-mediated repression of *FLC*, and we identified a candidate ncRNA from *FLC* that is distinct from COOLAIR and that we have designated COLD ASSISTED INTRONIC NONCODING RNA (COLDAIR) (Fig. 1A and fig S1A). We found COLDAIR by using a "tiling" reverse transcription polymerase chain reaction (RT-PCR) approach with more than 100 pairs of oligonucleotide primers to cover the entire *FLC* genomic region during the course of vernalization (Fig. 1A). From this tiling RT-PCR approach, we observed a contiguous batch of RT-PCR products from the first intron of *FLC* that transiently appear during the cold exposure (Fig. 1, A and B).

Unlike COOLAIR, COLDAIR is in the sense direction relative to *FLC* mRNA transcription (Fig. 1A and fig. S1B). COLDAIR contains a 5′ cap structure (fig. S1C), but we did not observe significant levels of COLDAIR in a polyadenylate[poly(A)]-rich fraction of RNA (fig.S1D), suggesting that COLDAIR is not likely to be polyadenylated. Thus, the 3′ ends of COLDAIR were determined by a tiling 5′ rapid amplification of cDNA ends RT-PCR approach (fig S1F). The approximate size of COLDAIR is 1100 bases long (fig. S1, A, F, and G).

The increased level of COLDAIR was observed only during cold exposure with the maximum expression at 20 days of cold, and COLDAIR levels returned to the prevernalized level after more than 30 days of cold (Fig. 1B and fig S2). This transient induction of COLDAIR during cold exposure is similar to that observed for COOLAIR (*13*); however, the induction of COOLAIR peaked at 10 days of cold exposure, earlier than the COLDAIR peak (Fig. 1B).

Deletion of the vernalization response element (VRE) in the first intron of *FLC* impairs vernalization-mediated *FLC* repression without compromising the floral repressor function of *FLC* (*14*). The transcription start site of COLDAIR is within the VRE region (Fig. 1A). To test whether the 5′ region of the VRE (excluding the COLDAIR transcribed region) is sufficient to mediate cold-inducible transcription, we generated transgenic lines in which luciferase is driven by 109 base pairs (bp) of the VRE 5′ region (Fig. 1C). We observed strong luciferase expression after 20 days of cold treatment in multiple transgenic lines (Fig. 1, C and D), confirming the presence of a cryptic promoter in VRE. In addition, luciferase expression remained robust as long as plants were kept in cold (Fig. 1, C and D). Endogenous COLDAIR was induced by ~10 to 20 days of cold (Fig. 1, B and D). However, after 20 days, *FLC* becomes repressed through chromatin changes, and thus COLDAIR promoter regions would become inaccessible to the transcription machinery. Consistent with this interpretation, COLDAIR was expressed well beyond 20 days of cold in *vin3-like 1* (*vil1*)/*vernalization 5* (*vrn5*) and *vernalization 1* (*vrn1*) mutants in which *FLC* repression by vernalization is impaired (fig. S3).

A group of long ncRNAs is transcribed by RNA polymerase V (RNAPV) together with RNA polymerase IV (RNAPIV) to mediate the silencing of constitutively silenced loci in *Arabidopsis* (*15*, *16*). This class of ncRNAs also has a 5′ cap but lacks a 3′ poly(A) tail similar to COLDAIR. However, neither RNAPIV nor RNAPV appears to be involved in the transcription of COLDAIR (fig. S4). Instead, we observed that, although the enrichment of RNA polymerase II (RNAPII) diminished at the *FLC* promoter as plants were exposed to cold, the enrichment of RNAPII at the COLDAIR promoter region transiently increased when expression of COLDAIR peaked at 20 days of cold (Fig. 1E). Thus, it is likely that RNAPII is responsible for the transcription of COLDAIR.

The PRC2 complex, including E(z), interacts with ncRNAs in vitro and in vivo (*11*, *17*). We tested for direct interactions between COLDAIR and the protein components of PRC2 {CURLY LEAF (CLF) and SWINGER (SWN) [E(z) homologs] and VERNALIZATION 2 (VRN2) [Su(z)12 homolog]} recombinant proteins by using in vitro RNA binding assays (Fig. 2, A and B, and fig. S5A). Both E(z) homologs, CLF and SWN, bound to COLDAIR in vitro through the CXC domain (Fig. 2, A and C). However, recombinant CLF protein also bound to antisense COLDAIR (fig. S5B), suggesting non–sequence-specific binding. The non–sequence-specific binding to single-stranded nucleotides (including RNA) by E(z) has been reported previously (*18*). To address the specificity of the interaction between COLDAIR and native CLF protein, we used nuclear extracts prepared from *GFP::CLF*-tagged transgenic lines (where GFP is green fluorescent protein)

[1]Section of Molecular Cell and Developmental Biology and Institute for Cellular and Molecular Biology, the University of Texas at Austin, TX 78712, USA.

*To whom correspondence should be addressed. E-mail: sbsung@mail.utexas.edu

(*8*) to perform RNA binding assay. Unlike that observed for recombinant CLF proteins, we detected the CLF association only with the sense strand of COLDAIR (Fig. 2D), confirming the specific interaction of COLDAIR with native PRC2.

We also addressed the specific in vivo association of COLDAIR with PRC2 during the course of vernalization by RNA immunoprecipitation (RIP) assays using the *GFP::CLF*-tagged lines (Fig. 2E). Indeed, we retrieved COLDAIR from precipitates during the course of vernalization (Fig. 2E). We observed the strongest association of COLDAIR with CLF when COLDAIR expression was maximal at 20 days of cold. However, this is not due to the expression level of COLDAIR, because we normalized fold enrichments to reflect RNA populations in input material (*19*). Thus, there is an increased association of COLDAIR with PRC2 specifically during the cold exposure. We also examined the enrichment of COOLAIR from the RIP assays and did not observe any significant enrichment of COOLAIR (Fig. 2E). Thus, COLDAIR, but not COOLAIR, interacts with PRC2.

To address the biological function of COLDAIR, we used RNA interference (RNAi) to knock down expression of COLDAIR in the *GFP::CLF* line (Fig. 3). Many of the RNAi-expressing transgenic lines showed late flowering after vernalization (Fig. 3A), suggesting that COLDAIR knockdown compromises the vernalization response. We chose two representative COLDAIR knockdown lines for further analysis. COLDAIR knockdown lines have greatly reduced levels of COLDAIR during the course of vernalization compared with those of the parental line (fig. S6). Parental lines showed accelerated flowering, whereas COLDAIR knockdown lines exhibited late flowering after vernalization treatment (Fig. 3, A and B). The reduced vernalization responses observed in COLDAIR knockdown lines are consistent with levels of *FLC* expression during the course of vernalization (Fig. 3C).

Repression of *FLC* was still observed in COLDAIR knockdown lines during the cold exposure (Fig. 3C). However, after plants were returned to a warm growth temperature, *FLC* repression was not maintained (Fig. 3C), indicating that COLDAIR is required to establish a silenced state that is stable. The transient repression of *FLC* in the COLDAIR knockdown lines is similar to that observed in mutations in other components of PRC2 and in other genes that are required for the stable maintenance of repressed *FLC* by vernalization (*4*, *14*, *20*, *21*).

After longer vernalization, COLDAIR knockdown lines showed substantially earlier flowering than nonvernalized plants (Fig. 3B), although the level of *FLC* was significantly higher (Fig. 3, C and D). Other *FLC*-related floral repressor genes, including *FLOWERING LOCUS M* (*FLM*)/*MADS AFFECTING FLOWERING* (*MAF1*), *MAF2,* and *MAF3*, are also repressed in response to vernalization (*22*). In COLDAIR knockdown lines, repression of *FLM/MAF1*, *MAF2*, and *MAF3* by vernalization still occured as in the parental lines (Fig. 3D), and thus it is likely that repression of these *FLC*-related genes causes the earlier flowering in COLDAIR knockdown lines after longer vernalization. This also indicates that COLDAIR knockdown specifically affects *FLC* expression but not expression of these *FLC*-related genes.

COLDAIR knockdown lines exhibited much later flowering than the parental line without vernalization (Fig. 3, A and B), consistent with higher levels of *FLC* expression in COLDAIR knockdown lines before vernalization treatment (Fig. 3, B and C). It has been reported that levels of *FLC* mRNA expression increase in *clf* mutants, consistent with the findings that *FLC* chromatin has a basal level of PRC2 occupancy before vernalization (*8*, *23*). However, late flowering is not observed in *clf* mutants because the loss of *CLF* also causes the derepression of floral activators, such as *FLOWERING LOCUS T* (*FT*) and *AGAMOUS* (*AG*), resulting in early flowering (*23*). The delay in flowering observed in COLDAIR knockdown lines before vernalization further confirms that COLDAIR is necessary for the activity of PRC2 to be directed to *FLC* chromatin.

As noted above, there is a basal level of CLF occupancy at *FLC* before vernalization, and the level of occupancy increases after vernalization

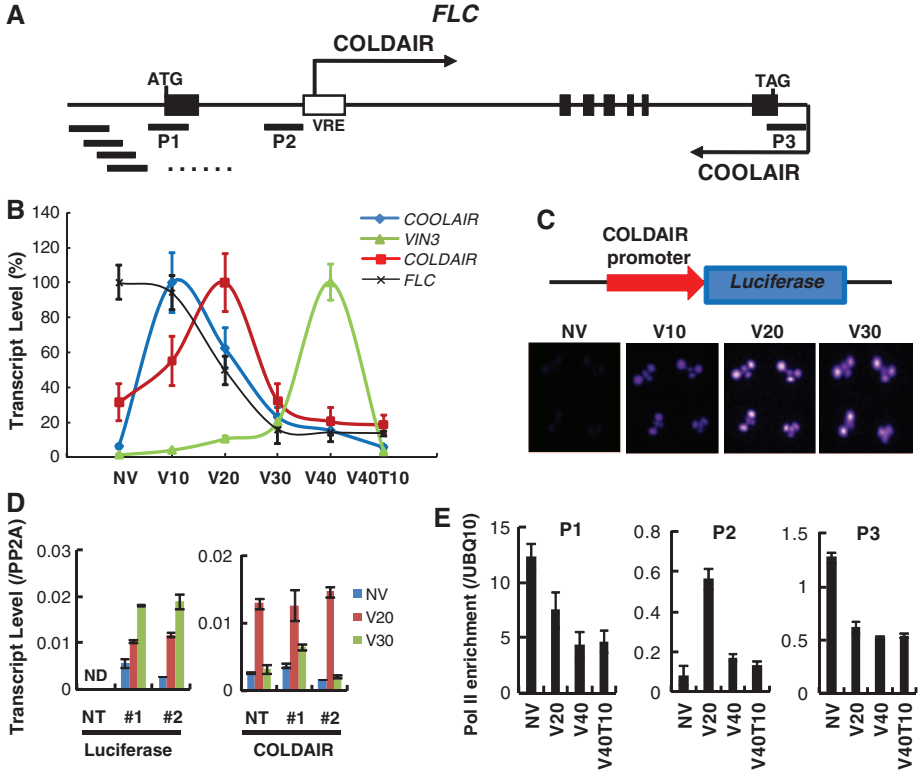

Fig. 1. COLDAIR, an intronic long ncRNA of the *FLC*. (**A**) Schematic representation of transcription start sites for COLDAIR and COOLAIR and the location of VRE at the *FLC* genomic region. (**B**) Transcript expression patterns of COOLAIR, COLDAIR, *VIN3*, and *FLC* during the course of vernalization. Relative levels of mRNA expressions were calculated compared with those of the control, *PP2A*. Maximum expression for each gene is set as 100%, and relative levels are shown. Mean ± SD of quantitative RT-PCR data are shown (n = 3). NV, nonvernalized. V10, 10 days of vernalization treatment. V20, 20 days of vernalization treatment. V30, 30 days of vernalization treatment. (**C**) Luciferase expression in COLDAIR-promoter::*Luciferase* transgenic lines during the course of vernalization. (**D**) Expression patterns of luciferase (left) and COLDAIR (right) transcripts in two stable representative COLDAIR-promoter::*Luciferase* transgenic lines (1 and 2) and nontransgenic line (NT). Mean ± SD of quantitative RT-PCR data compared with the control, *PP2A*, are shown (n = 3). ND, not detectable. (**E**) Transient increase in RNAPII occupancy at the COLDAIR promoter region. Chromatin immunoprecipitation (ChIP) using RNAPII antibody (8WG16). Relative occupancies of RNAPII at *FLC* regions were calculated by comparison to occupancy of RNAPII at the *UBQ10* promoter region. Relative locations of P1 to P3 are shown in (A). Mean ± SD of quantitative ChIP-PCR data are shown (n = 3). V40, 40 days of vernalization treatment; V40T10, 40 days of vernalization treatment followed by 10 days of normal growth temperature.

(Fig. 4, B) (*5*). In COLDAIR knockdown lines, the enrichment of CLF at *FLC* chromatin was greatly reduced (Fig. 4B). The relative enrichment of CLF at *FLC* chromatin was lower before vernalization, and the increased enrichment of CLF by vernalization was not observed in COLDAIR knockdown lines (Fig. 4B). This is consistent with elevated levels of *FLC* transcripts in COLDAIR knockdown lines during the course of vernalization, showing that COLDAIR is necessary for the recruitment of CLF to *FLC* chromatin.

Consistent with the increased occupancy of CLF at *FLC* chromatin, the levels of H3K27me3 also increased at *FLC* chromatin as a result of vernalization (Fig. 4C) (*7*, *8*, *24*, *25*). In COLDAIR knockdown lines, however, cold-mediated H3K27me3 enrichment was largely impaired (Fig. 4C). In addition, vernalization results in the stable reduction of the levels of histone H3 Lys^4 trimethylation (H3K4me3), a histone mark associated with active chromatin, at *FLC* chromatin (Fig. 4 D) (*14*). In COLDAIR knockdown lines, the levels of H3K4me3 at *FLC* chromatin

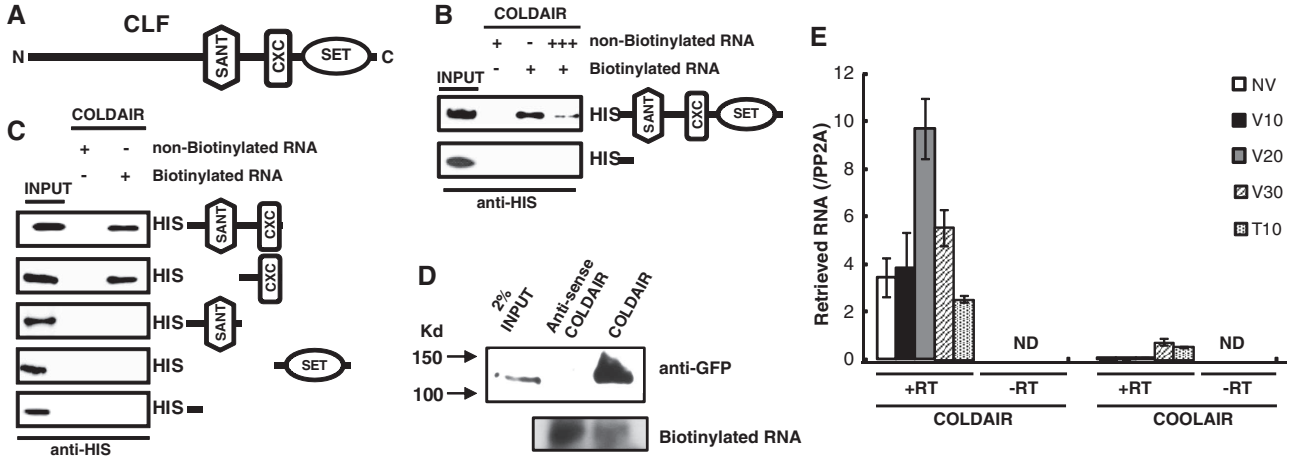

Fig. 2. COLDAIR associates with PRC2 during the cold exposure. (**A**) Domain structure of CLF protein. (**B**) In vitro transcribed (IVT) biotinylated COLDAIR RNA retrieves recombinant CLF protein. (**C**) In vitro RNA binding assays using domains of CLF in isolation. IVT biotinylated COLDAIR RNA retrieves CXC domain. (**D**) IVT COLDAIR RNA retrieves CLF-containing PRC2 from nuclear extracts. (**E**) CLF immunoprecipitation retrieves COLDAIR RNA but not COOLAIR RNA during the course of vernalization. Data (mean ± SD of quantitative PCR; $n = 3$) are relative to the background level of RNA precipitation (*PP2A*). +RT, with reverse transcription of precipitates. −RT, without reverse transcription of precipitates. T10, 30 days of vernalization treatment followed by 10 days of normal growth temperature.

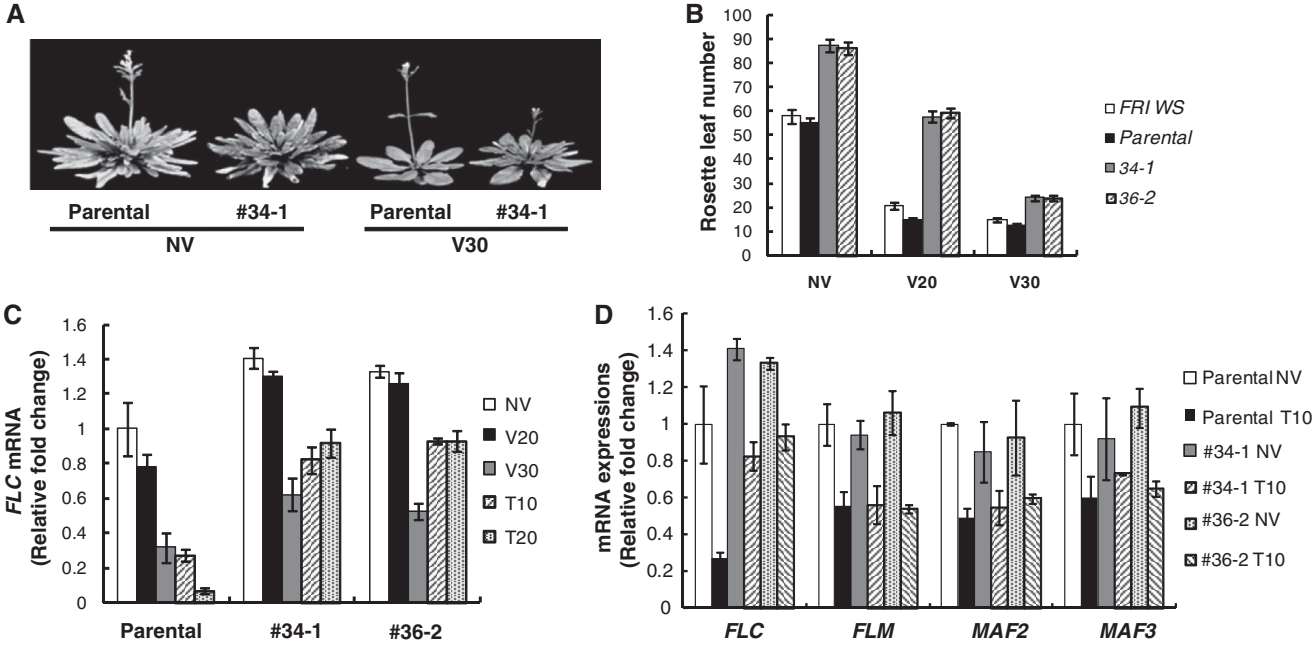

Fig. 3. COLDAIR is required for proper repression of *FLC* during the course of vernalization. (**A**) Flowering behaviors of the parental line and a representative COLDAIR knockdown line. (**B**) Flowering times are determined by the rosette leaf number at the timing of flowerings of *FRI* in Ws, the parental line, and two representative COLDAIR knockdown lines (34-1, 36-2). (**C**) Changes in *FLC* mRNA during the course of vernalization in the parental line and two representative COLDAIR knockdown lines. Data (fold change; mean ± SD of quantitative RT-PCR; $n = 3$) are relative to the *FLC* mRNA level in the parental line before vernalization. T20, 30 days of vernalization treatment followed by 20 days of normal growth temperature. (**D**) Changes in *FLC*, *FLM*, *MAF2*, and *MAF3* mRNA during the course of vernalization in the parental line and two representative COLDAIR knockdown lines. Data (fold change; mean ± SD of quantitative RT-PCR; $n = 3$) are relative to the *FLC*, *FLM*, *MAF2*, and *MAF3* mRNA levels in the parental line before vernalization.

transiently decreases when plants are kept in cold but return to the prevernalized levels once plants are returned to a warm temperature (Fig. 4D). The transient reduction in the level of H3K4me3 at *FLC* chromatin is also observed in vernalization mutants that are involved in the maintenance of the repression (*14*). Thus, the intronic ncRNA COLDAIR mainly plays a role in the recruitment of PRC2 to *FLC* chromatin to establish the stable silencing of *FLC* by vernalization (fig. S7).

Transiently increased interaction between COLDAIR and PRC2 during vernalizing cold suggests that COLDAIR mainly acts to recruit PRC2 to *FLC* during the cold (fig. S7). It remains to be determined whether COLDAIR participates in maintaining the PRC2 association with *FLC* after vernalization treatment. Alternatively, formation of the PHD-PRC2 complex may contribute to the maintenance after the cold (fig. S7).

In animals, a long intergenic noncoding RNA, HOTAIR, is transcribed from *HOXC* locus and targets PRC2 to silence *HOXD* and other loci (*11*, *12*). We observed a similar interaction of a long ncRNA with PRC2 in plants, suggesting that the interaction of long ncRNA with PRC2 appears to be an evolutionarily conserved mechanism. Unlike HOTAIR, COLDAIR is transcribed from an intron of the target gene itself, *FLC*. *FLC* harbors a cryptic promoter for COLDAIR ncRNA within its first intron, and this promoter becomes active when *FLC* is being repressed. Deep RNA sequencing efforts have revealed transcripts that originated from intergenic regions as well as from previously known intronic regions in eukaryotes (*26*–*28*). Although some intronic transcripts represent alternative splicing forms (*28*), our identification of an intronic long ncRNA that plays a regulatory role in gene repression suggests that intronic transcripts can function as a part of targeting mechanisms for transcriptional regulatory machineries in eukaryotes.

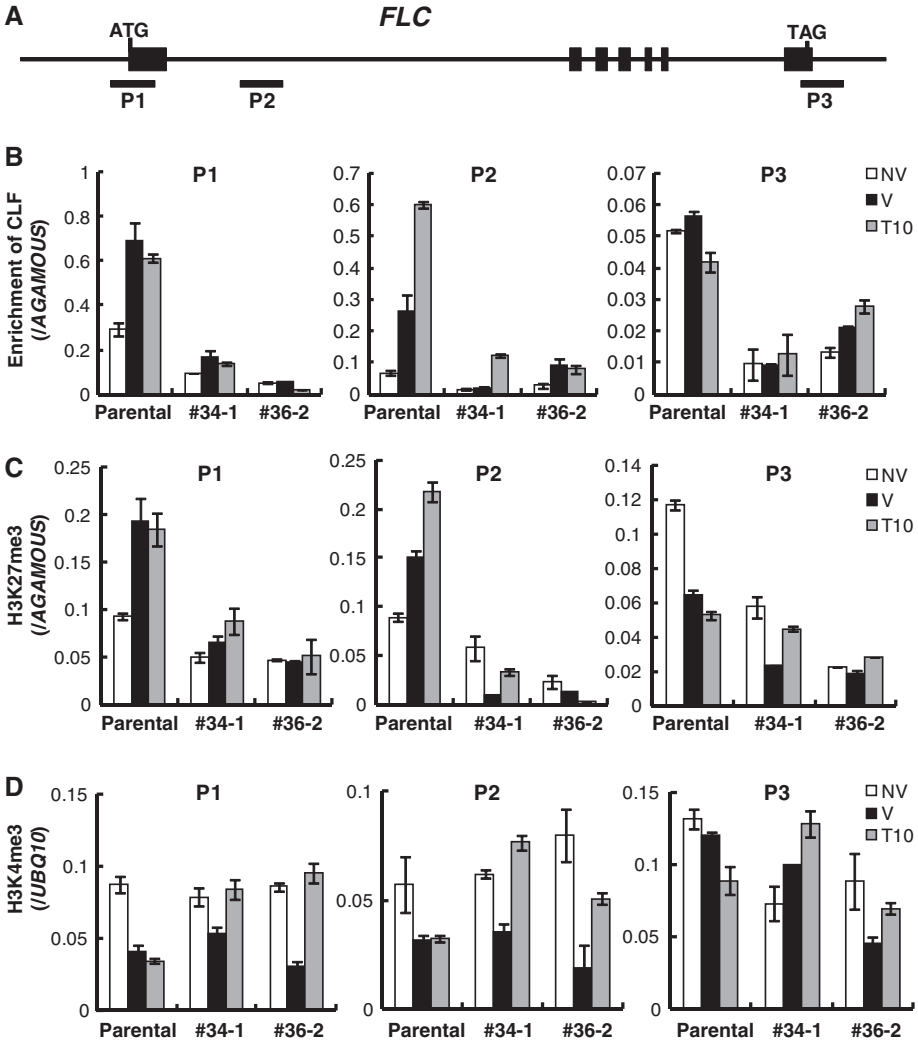

Fig. 4. Dynamic changes at *FLC* chromatin during the course of vernalization. (**A**) Schematic representation of the *FLC* genomic region. Relative positions of primer sets used for ChIP assays are shown (P1 to P3). (**B**) Changes in occupancy of CLF at *FLC* chromatin during the course of vernalization. (**C**) Changes in enrichment of H3K27me3 at *FLC* chromatin during the course of vernalization. (**D**) Changes in enrichment of H3K4me3 at *FLC* chromatin during the course of vernalization. Data (mean ± SD of quantitative ChIP-PCR; $n = 3$) is relative to the occupancy of CLF at *AGAMOUS* chromatin (B), the level of H3K27me3 enrichment at *AGAMOUS* chromatin (C), and the level of H3K4me3 enrichment at *UBQ10* chromatin (D).

References and Notes

1. A. Lang, in *Physiology of Flower Initiation*: *Encyclopedia of Plant Physiology*, W. Ruhland, Ed. (Springer-Verlag, Berlin, 1965), pp. 1371–1536.
2. D. H. Kim, M. R. Doyle, S. Sung, R. M. Amasino, *Annu. Rev. Cell Dev. Biol.* **25**, 277 (2009).
3. S. Sung, R. M. Amasino, *Nature* **427**, 159 (2004).
4. C. C. Wood *et al.*, *Proc. Natl. Acad. Sci. U.S.A.* **103**, 14631 (2006).
5. F. De Lucia, P. Crevillen, A. M. Jones, T. Greb, C. Dean, *Proc. Natl. Acad. Sci. U.S.A.* **105**, 16831 (2008).
6. T. F. Hsieh, O. Hakim, N. Ohad, R. L. Fischer, *Trends Plant Sci.* **8**, 439 (2003).
7. M. R. Doyle, R. M. Amasino, *Plant Physiol.* **151**, 1688 (2009).
8. D. Schubert *et al.*, *EMBO J.* **25**, 4638 (2006).
9. C. P. Ponting, P. L. Oliver, W. Reik, *Cell* **136**, 629 (2009).
10. J. T. Lee, *Genes Dev.* **23**, 1831 (2009).
11. J. L. Rinn *et al.*, *Cell* **129**, 1311 (2007).
12. M. C. Tsai *et al.*, *Science* **329**, 689 (2010); 10.1126/science.1192002.
13. S. Swiezewski, F. Liu, A. Magusin, C. Dean, *Nature* **462**, 799 (2009).
14. S. Sung *et al.*, *Nat. Genet.* **38**, 706 (2006).
15. A. T. Wierzbicki, J. R. Haag, C. S. Pikaard, *Cell* **135**, 635 (2008).
16. C. S. Pikaard, J. R. Haag, T. Ream, A. T. Wierzbicki, *Trends Plant Sci.* **13**, 390 (2008).
17. J. Zhao, B. K. Sun, J. A. Erwin, J. J. Song, J. T. Lee, *Science* **322**, 750 (2008).
18. W. A. Krajewski, T. Nakamura, A. Mazo, E. Canaani, *Mol. Cell. Biol.* **25**, 1891 (2005).
19. Materials and methods are available as supporting material on *Science* Online.
20. A. R. Gendall, Y. Y. Levy, A. Wilson, C. Dean, *Cell* **107**, 525 (2001).
21. J. S. Mylne *et al.*, *Proc. Natl. Acad. Sci. U.S.A.* **103**, 5012 (2006).
22. C. C. Sheldon, E. Jean Finnegan, W. James Peacock, E. S. Dennis, *Plant J.* **59**, 488 (2009).
23. D. Jiang, Y. Wang, Y. Wang, Y. He, *PLoS One* **3**, e3404 (2008).
24. S. Sung, R. J. Schmitz, R. M. Amasino, *Genes Dev.* **20**, 3244 (2006).
25. T. Greb *et al.*, *Curr. Biol.* **17**, 73 (2007).
26. R. Louro, A. S. Smirnova, S. Verjovski-Almeida, *Genomics* **93**, 291 (2009).
27. P. Khaitovich *et al.*, *PLoS Genet.* **2**, e171 (2006).
28. H. van Bakel, C. Nislow, B. J. Blencowe, T. R. Hughes, *PLoS Biol.* **8**, e1000371 (2010).

29. We thank the members of Sung lab and E. Huq for helpful discussions, C. Pikaard for RNAPIV and RNAPV mutant seeds, and J. Goodrich for *GFP::CLF* seeds. S.S. thanks R. Amasino for encouragement and mentoring on the vernalization study. This work was supported by the start-up funds from the University of Texas at Austin and in part by the NSF to S.S.

Supporting Online Material

www.sciencemag.org/cgi/content/full/science.1197349/DC1
Materials and Methods
Figs. S1 to S7
Table S1
References

3 September 2010; accepted 16 November 2010
Published online 2 December 2010;
10.1126/science.1197349

Rotational Movement of the Formin mDia1 Along the Double Helical Strand of an Actin Filament

Hiroaki Mizuno,[1] Chiharu Higashida,[2]* Yunfeng Yuan,[2] Toshimasa Ishizaki,[2] Shuh Narumiya,[2] Naoki Watanabe[1]†

Formin homology proteins (formins) elongate actin filaments (F-actin) by continuously associating with filament tips, potentially harnessing actin-generated pushing forces. During this processive elongation, formins are predicted to rotate along the axis of the double helical F-actin structure (referred to here as helical rotation), although this has not yet been definitively shown. We demonstrated helical rotation of the formin mDia1 by single-molecule fluorescence polarization (FL_P). FL_P of labeled F-actin, both elongating and depolymerizing from immobilized mDia1, oscillated with a periodicity corresponding to that of the F-actin long-pitch helix, and this was not altered by actin-bound nucleotides or the actin-binding protein profilin. Thus, helical rotation is an intrinsic property of formins. To harness pushing forces from growing F-actin, formins must be anchored flexibly to cell structures.

Actin polymerization is regulated by factors such as Rho family guanosine triphosphatases (GTPases) and actin nucleators, and can rapidly remodel the cortical cytoskeleton and generate force for cell edge protrusion (*1*). Formin proteins are the major actin nucleators and function in diverse processes such as cell migration, polarity formation, and cytokinesis (*2*, *3*). Formins share the conserved formin homology 1 and 2 domains (FH1 and FH2, respectively), where FH2 enhances F-actin nucleation. FH2 remains associated with the growing barbed end of F-actin and processively elongates the assembling actin filament (*4*, *5*). FH1 binds the G-actin–binding protein profilin, and this interaction facilitates great enhancement of adenosine 5′-triphosphate (ATP)–actin assembly at the FH2-bound filament tip (*6*). FH2 forms a ring-shaped dimer that binds around the barbed end of F-actin (*7*). The subunits in actin filaments form two strands arranged in a right-handed, long-pitch double helix (*8*). If FH2 tracks processively along the long-pitch helix as the filament elongates, FH2 will rotate on the barbed end of the filament.

Several studies have reported functions of formins that might involve organelle transport, such as regulation of endosome motility by hDia2C (*9*) and transport of meiotic chromatin by Formin-2 (*10*). Anchoring growing actin ends to the cell cortex is another possible function of formins. In animal cells, Rho GTPase and its effector, the formin protein mDia1, induce the formation of actin stress fibers (*11*, *12*). The truncated FH1-FH2 mutant of mDia1 processively moves over several tens of micrometers at a speed of 2 μm/s in cells (*4*). However, among wild-type mDia1 visualized as single molecules, processively moving mDia1 constitutes a minor population (4.3%), and half of mDia1 (47.5%) is stationary (*13*). Yeast formins for3p and Bni1p are thought to processively assemble actin cables while remaining at the cell tip (*14*, *15*). In vitro, actin polymerization from an immobilized formin produces a pushing force in the piconewton range (*16*). However, it has not been established that formins can transmit force produced by actin polymerization for the movement of cellular structures. It is thus important to elucidate how the actin polymerization force acts on formins.

We analyzed the rotational movement of F-actin assembled by recombinant FH1-FH2 domains of mDia1 [amino acids 543 to 1192, glutathione *S*-transferase (GST)–mDia1ΔN3] (*17*) using fluorescence polarization of single dye molecules on the filament (*18*). GST-mDia1ΔN3, the presumptive structure of which is a dimer harboring GST-GST and FH2-FH2 interactions, was immobilized on a glass surface within protein aggregates formed by antibodies to GST and secondary antibodies (*4*). We observed F-actin, which contains tetramethylrhodamine-labeled actin (TMR-actin) at a low density. The emission moment of fluorescence polarization on TMR-F-actin lies at an angle of 45° to the filament axis (*18*). Thus, the orientation of TMR-actin in a diagonally aligned filament can be monitored by separating the fluorescence into vertically (FL_V) and horizontally (FL_H) polarized components (Fig. 1).

Under normal actin elongation conditions with ATP–monomeric actin (G-actin; 0.5 μM), the intensities of FL_V and FL_H alternated periodically (Fig. 2, A and C, and movie S1). The fluorescent spot moved directionally (Fig. 2B), and the fluorescence polarization [$FL_P = (FL_V - FL_H)/(FL_V + FL_H)$] of the spot alternated over a long distance (Fig. 2D). The periodic alternation in FL_P was not observed when processive actin elongation was arrested (fig. S1). Analysis of the spot displacement yielded 36.1 ± 0.33 nm (mean ± SEM) per inversion between FL_V and FL_H, which corresponds to the half-pitch length of the F-actin long-pitch helix (Fig. 2E). These results indicate that mDia1 undergoes helical rotation during processive filament elongation.

Previous studies concluded that formins slip around the filament like a bearing when both the formin and the distal end of the filament are anchored to the slide (*16*, *19*). Kovar and Pollard (*16*) observed that F-actin elongating from Bni1p(FH1-FH2) nonspecifically adsorbed on glass did not form a supercoil when the pointed end of the filament was fixed. However, they left it uncertain whether slippage occurs between FH2 and the glass surface (*3*, *6*). We hypothesized that when helical rotation is faithfully coupled to elongation, the buckling frequency should be lower when FH2 is immobilized tightly than loosely. We therefore compared the F-actin buckling frequency obtained by the previous immobilization method for FH2 (*16*) with that obtained by our method. When a portion of F-actin was trapped through the interaction between biotinylated actin and streptavidin-coated glass, the buckling fre-

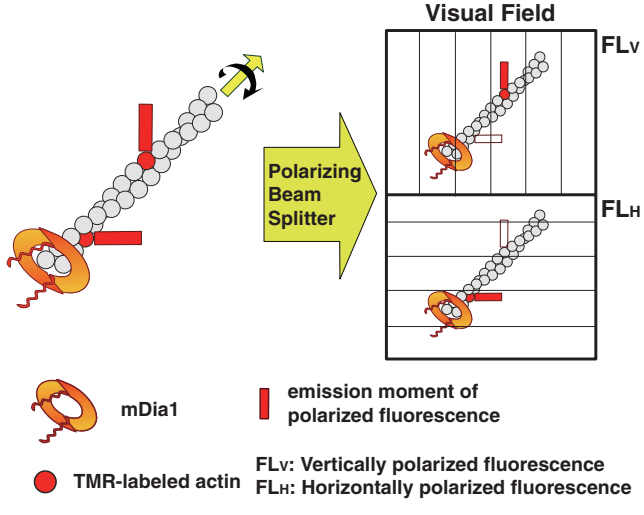

Fig. 1. Detection of the polarized fluorescence from single-molecule tetramethylrhodamine (TMR) on growing actin filaments. F-actin was nucleated by mDia1 and TMR-G-actin (1.5%). TMR emits polarized fluorescence at an angle of 45° to the filament axis (*18*). When the filament lies diagonally, the orientation of TMR-actin subunits can be monitored by separating the fluorescence into vertically (FL_V) and horizontally (FL_H) polarized components with a polarizing beam splitter.

[1]Laboratory of Single-Molecule Cell Biology, Tohoku University Graduate School of Life Sciences, 6-3 Aoba, Aramaki-Aza, Aoba-ku, Sendai, Miyagi 980-8578, Japan. [2]Department of Pharmacology, Kyoto University Faculty of Medicine, Yoshida Konoe-cho, Sakyo-ku, Kyoto 606-8501, Japan.

*Present address: Department of Biophysical Genetics, Kanazawa University Graduate School of Medical Science, 13-1 Takaramachi, Kanazawa 920-8640, Japan.

†To whom correspondence should be addressed. E-mail: nwatanabe@m.tohoku.ac.jp

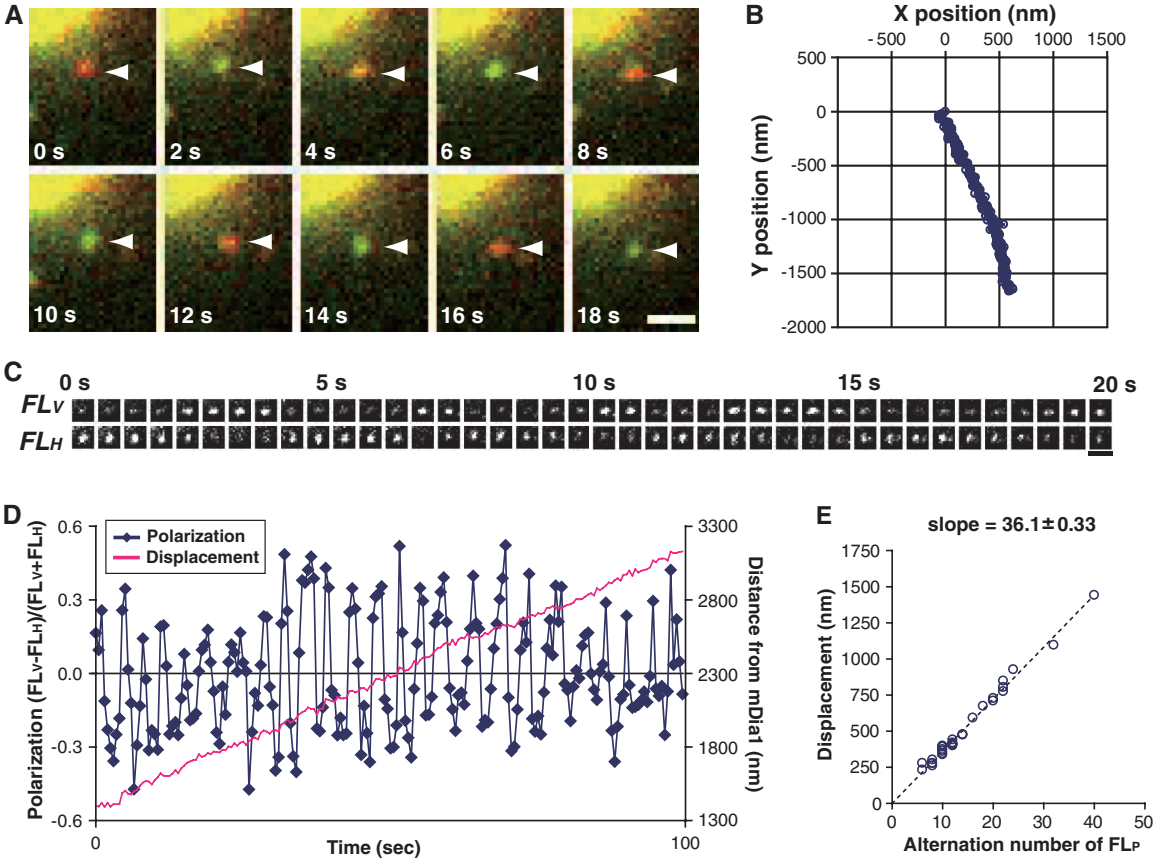

Fig. 2. Helical rotation of ATP-F-actin growing from immobilized mDia1. F-actin was nucleated by incubating 1 μM TMR-ATP-G-actin (1.5%) with protein aggregates containing GST-mDia1FH1-FH2 (mDia1ΔN3) adsorbed on a glass surface. After 1 min, free TMR-G-actin was washed out, and the elongation of F-actin was observed in the presence of 0.5 μM unlabeled ATP-G-actin. (**A**) Merged images of FL_V (red) and FL_H (green) from TMR-actin at 2-s intervals. The alternation between the intensity of FL_V and FL_H of the spot (arrowheads) is apparent. (**B** and **C**) Displacement (B) and time-lapse images of FL_V and FL_H at 0.5-s intervals (C) of the spot in (A). (**D**) Fluorescence polarization (FL_P) (blue) and distance from mDia1ΔN3 aggregates (pink) of the spot in (A). (**E**) Distance per half-rotation of ATP-F-actin (mean ± SEM; 19 independent experiments, n = 28 spots, total 428 alternations). Scale bars (A and C), 1 μm.

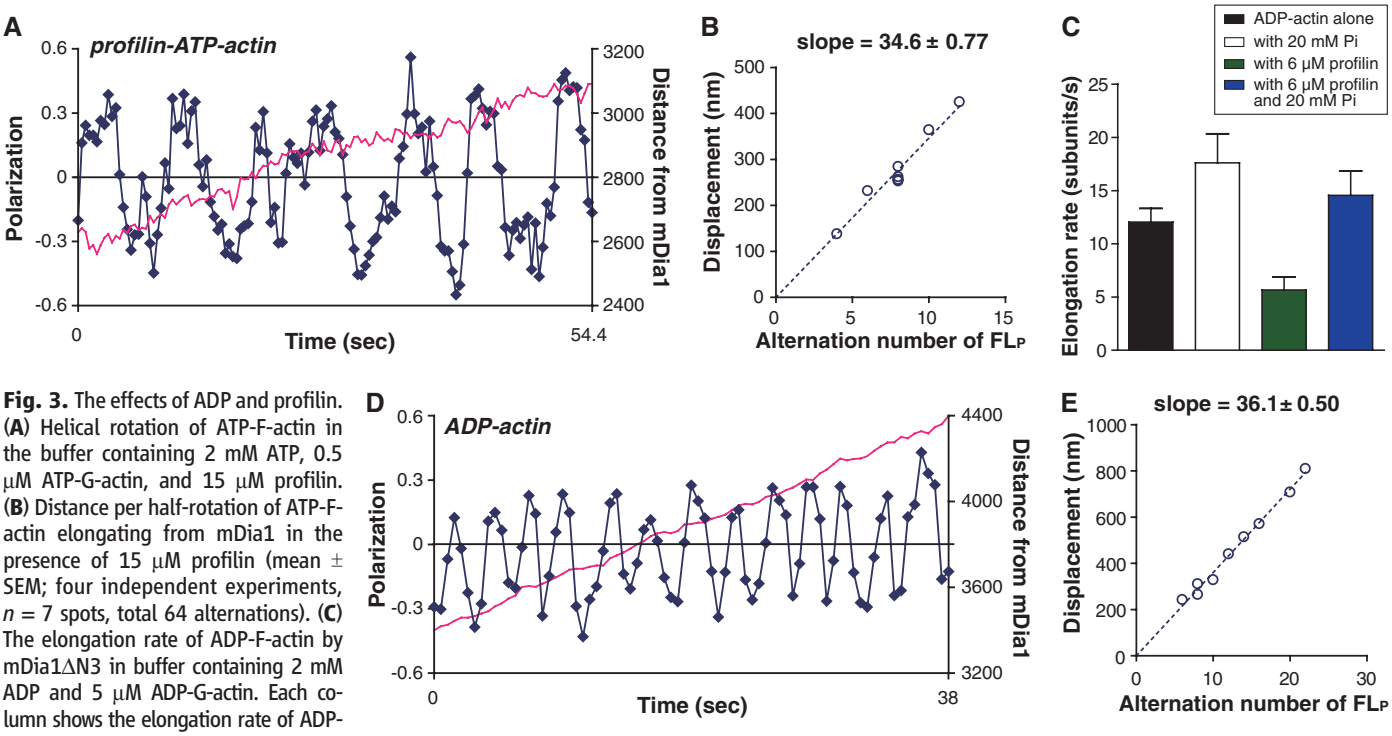

Fig. 3. The effects of ADP and profilin. (**A**) Helical rotation of ATP-F-actin in the buffer containing 2 mM ATP, 0.5 μM ATP-G-actin, and 15 μM profilin. (**B**) Distance per half-rotation of ATP-F-actin elongating from mDia1 in the presence of 15 μM profilin (mean ± SEM; four independent experiments, n = 7 spots, total 64 alternations). (**C**) The elongation rate of ADP-F-actin by mDia1ΔN3 in buffer containing 2 mM ADP and 5 μM ADP-G-actin. Each column shows the elongation rate of ADP-G-actin alone (black), ADP-G-actin with 20 mM P_i (white), ADP-G-actin with 6 μM profilin (green), and ADP-G-actin with 6 μM profilin and 20 mM P_i (blue). Error bars indicate SD (n = 20 to 25 filaments for each condition). (**D**) Helical rotation of ADP-actin elongating from mDia1ΔN3 with 5 μM ADP-G-actin alone. (**E**) Distance per half-rotation (mean ± SEM) of ADP-actin elongating from mDia1 (four independent experiments, n = 9 spots, total 116 alternations).

quency with mDia1-antibody aggregates was smaller than that with mDia1 nonspecifically adsorbed to the glass surface (fig. S2). During buckled actin elongation, we did not observe periodic alternation of FL_P (fig. S3 and movie S2). We also verified helical rotation of F-actin elongating from Bni1p(FH1-FH2) (fig. S4 and movie S3). The different buckling frequencies resulting from different immobilization methods of FH2 indicate that torsional stress can be relaxed through slippage between FH2 and the glass surface in both the previous experiments by Kovar and Pollard (*16*) and the present study. We believe that formins undergo helical rotation faithfully along the long-pitch helix, although our data do not exclude the possibility that FH2 might rotate like a bearing under strong torsional stress.

Profilin promotes ATP-actin elongation at the FH1-FH2 bound barbed end, which could affect the actin polymerization force. We therefore examined whether helical rotation is retained in the presence of profilin. Consistent with a previous report (*6*), the addition of 6 μM profilin accelerated mDia1-mediated actin elongation in the presence of 1 μM ATP-G-actin from 7.8 to 48 subunits s^{-1}. To reduce the elongation rate for FL_P detection, we needed to use 15 μM profilin and 0.5 μM actin. Under this condition, actin elongation is suppressed because free profilin competes with the profilin-actin complex for binding to FH1 (*6*). We detected a periodic alternation of FL_P on processively elongating F-actin in the presence of profilin (Fig. 3A and movie S4). The distance per half-rotation was 34.6 ± 0.77 nm (mean ± SEM) (Fig. 3B). Thus, the interaction between FH1 and profilin does not interfere with the helical rotation of FH2.

We next tested whether ADP-G-actin supports helical rotation. Although profilin accelerates elongation of ATP-actin, its effect on ADP-actin remains controversial. Repeatedly, mDia1-mediated elongation of ADP-actin has been shown to be slow with ADP-G-actin alone (~36% of that without mDia1) (*6*) and almost negligible in the presence of profilin (*20*). Because prolonged depletion of ATP during preparation of ADP-G-actin may deteriorate the conformation of assembled F-actin (*21*), we carefully prepared ADP-G-actin. In addition, ATP hydrolysis may be involved in the aging process of F-actin (*22*). Recent studies (*23*) reported that transiently (~2 min) after polymerization, actin forms filaments, which structurally deviated from the Holmes model (*24*). Taking advantage of our system, we also investigated the effect of nucleotides on the helical twist of assembling actin filaments.

ADP-G-actin alone processively elongated mDia1-nucleated F-actin (Fig. 3C). The addition of profilin decreased the elongation rate by 53% (Fig. 3C). These data differ from those reported in a previous study (*6*), in which profilin accelerated the elongation of ADP-actin at the mDia1FH1-FH2–bound barbed end. This discrepancy arises from the difference in the elongation rate without profilin. Our data do not favor the view that profilin accelerates mDia1-associated actin elongation regardless of the actin-bound nucleotides (*6*) (see below).

F-actin rotated periodically during elongation from immobilized mDia1 with ADP-G-actin (Fig. 3D and movie S5). Thus, helical rotation proceeds without ATP hydrolysis. We did not detect any change in the distance per half-rotation with ADP-actin (Fig. 3E) and ATP-actin (Fig. 2E).

Our data also revealed that profilin lowers the ADP-actin elongation rate not by capping, as previously concluded (*20*), but by enhancing the off-rate of actin at the barbed end. Direct observations show that profilin promotes processive depolymerization of the formin-bound barbed end (Fig. 4A). Profilin enhanced the processive depolymerization rate of the mDia1-bound barbed end from 1.4 to 11.6 s^{-1}. This enhancement was observed at a lower concentration of profilin than that required for the promotion of depolymerization of the free barbed end (*25*), which was also found in a previous observation of bulk filament disassembly (*20*). FH1 and profilin thus accelerate both ATP-actin elongation and ADP-actin depolymerization. The ADP-F-actin rotates as it shortens in the presence of 20 μM profilin (Fig. 4B and movie S6). The distance between the spot and the barbed end decreased by 36.8 nm per half-rotation (Fig. 4C).

Inorganic phosphate (P_i) decreases the off-rate of ADP-F-actin at the free barbed end (*26*). P_i also blocks the binding of F-actin and ADF/cofilin (*27*), which increases the filament twist (*28*). We therefore examined the effect of P_i on the processive elongation and twist of mDia1-nucleated ADP-actin. We found that P_i abolished the profilin-

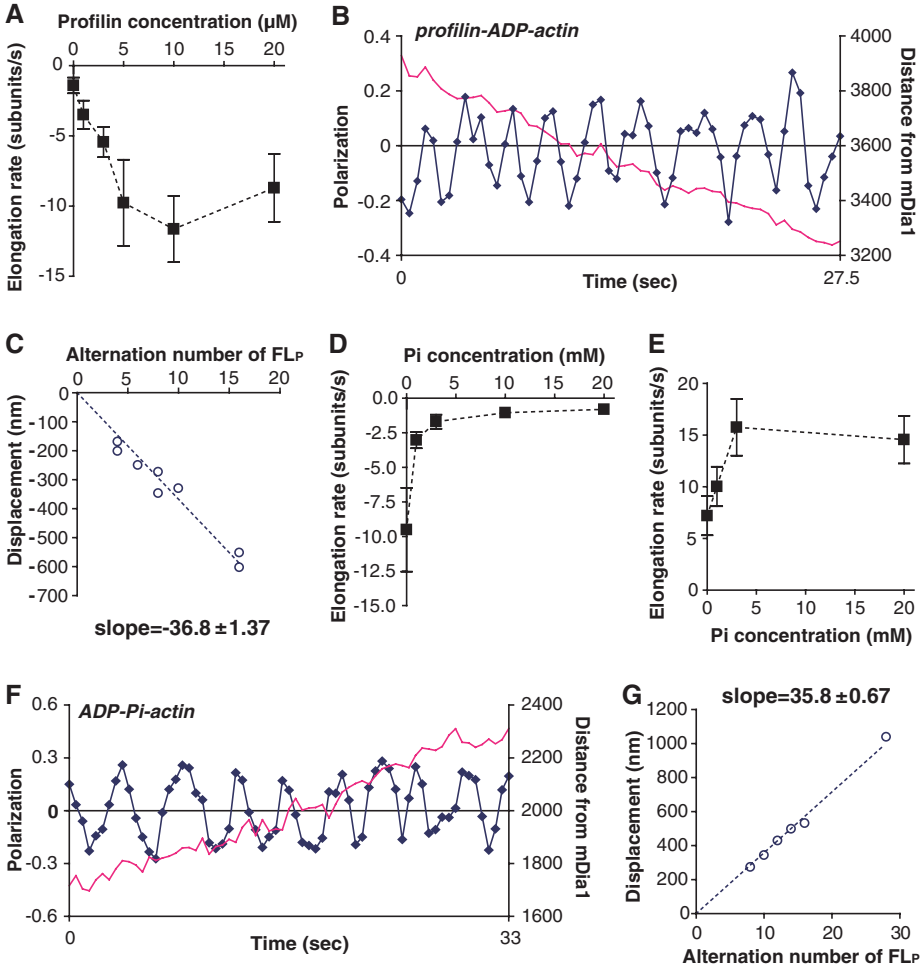

Fig. 4. Effects of profilin and inorganic phosphate (P_i) on elongation, depolymerization, and helical rotation of mDia1ΔN3. (**A**) The dose-dependent effect of profilin on depolymerization of ADP-F-actin bound to mDia1ΔN3. (**B**) Helical rotation of ADP-F-actin during profilin-accelerated depolymerization at the mDia1ΔN3-bound barbed end. Depolymerization of ADP-F-actin was induced by perfusion of a buffer containing 2 mM ADP and 20 μM profilin. (**C**) Distance per half-rotation (mean ± SEM) of ADP-F-actin bound to mDia1 during depolymerization with 20 μM profilin (three independent experiments, n = 8 spots, total 72 alternations). (**D**) The dose-dependent effect of P_i on profilin (5 μM)–enhanced depolymerization of ADP-F-actin bound to mDia1ΔN3 at pH 7.0. (**E**) The dose-dependent effect of P_i on mDia1ΔN3-mediated elongation of ADP-actin (5 μM) in the presence of 5 μM profilin. (**F**) Helical rotation of ADP-F-actin elongating from mDia1ΔN3 in the presence of 5 mM P_i. (**G**) Distance per half-rotation (mean ± SEM) of ADP-F-actin elongating from mDia1 in the presence of 5 mM P_i (three independent experiments, n = 6 spots, total 88 alternations).

enhanced actin depolymerization at the mDia1-bound barbed end. This inhibition occurs in the submillimolar range of P_i, which is two orders of magnitude lower than the dissociation constant of P_i and G-actin (*26*). Thus, binding of P_i to F-actin inhibits profilin-induced depolymerization (Fig. 4E).

ADP-G-actin (5 μM) elongated mDia1-bound F-actin faster in the presence of 20 mM P_i than in its absence (Fig. 3C). This effect of P_i was more prominent in the presence of profilin than in its absence (Fig. 3C). The decrease in the actin off-rate (Fig. 4D) corresponds well with the increase in the ADP-actin elongation rate by 3 to 20 mM P_i (Fig. 4E). We thus suggest that P_i cancels the inhibitory effect of profilin on ADP-actin elongation (Fig. 3C) by abolishing the enhanced barbed end off-rate. The discrepancy of the effect of 1 mM P_i on depolymerization and assembly (Fig. 4, D, and E) is because slow dissociation of P_i prebound to a fraction of the ADP-F-actin subunits [dissociation constant (K_d) ≈1.5 mM] may limit terminal subunit dissociation during depolymerization (*26*), but not dissociation of assembling ADP-actin, which is mostly free from P_i. Profilin thus allows processive elongation of the FH1-FH2–bound barbed end regardless of the actin-bound nucleotide, but attenuates ADP-actin elongation by increasing the barbed end off-rate. Our results urge reconsideration of the ATP-specific acceleration mechanism for formin-associated actin elongation.

Helical rotation of mDia1 was observed during processive ADP-actin elongation in the presence of P_i (Fig. 4F and movie S7). The distance per half-rotation was 35.8 nm (Fig. 4G).

Our data demonstrate continuous rotation of mDia1-bound filaments during both elongation and depolymerization. The distance per half-rotation of F-actin is in the range of 34.6 to 36.8 nm regardless of the actin-bound nucleotide and presence of P_i and profilin (Figs. 2 to 4). These findings indicate that helical rotation of FH2 is an intrinsic property derived from the helical structure of F-actin. Cellular actin filaments are highly cross-linked as evidenced by single-molecule observations showing movement of actin subunits with no change in their relative positions (*29*). Therefore, formins must rotate in the cell. The rotation speed of for3p at the cell tip and processively moving mDia1 can reach 250 and 1700 rpm, respectively. If anchoring the growing end of F-actin is the function of formins, the link between formins and cellular structures must be flexible. Alternatively, formin-mediated actin elongation may be regulated by torsional stress in F-actin.

Conversely, formins might modulate the stability of F-actin by helical rotation. Torsional stress induces destabilization of the filament (*30*). Cofilin, the major actin depolymerizing factor, twists the strand of F-actin, which is thought to contribute to actin disassembly (*28*). Our data have opened up the possibility that actin elongation and remodeling could be regulated by axial torsion in the filament. Our findings should help elucidate the actin turnover mechanism regulated by formins in the cell.

References and Notes

1. N. Watanabe, *Proc. Jpn. Acad. Ser. B Phys. Biol. Sci.* **86**, 62 (2010).
2. M. Evangelista, S. Zigmond, C. Boone, *J. Cell Sci.* **116**, 2603 (2003).
3. B. L. Goode, M. J. Eck, *Annu. Rev. Biochem.* **76**, 593 (2007).
4. C. Higashida *et al.*, *Science* **303**, 2007 (2004).
5. M. Pring, M. Evangelista, C. Boone, C. Yang, S. H. Zigmond, *Biochemistry* **42**, 486 (2003).
6. D. R. Kovar, E. S. Harris, R. Mahaffy, H. N. Higgs, T. D. Pollard, *Cell* **124**, 423 (2006).
7. T. Otomo *et al.*, *Nature* **433**, 488 (2005).
8. K. C. Holmes, *Nature* **457**, 389 (2009).
9. S. Gasman, Y. Kalaidzidis, M. Zerial, *Nat. Cell Biol.* **5**, 195 (2003).
10. B. Leader *et al.*, *Nat. Cell Biol.* **4**, 921 (2002).
11. A. J. Ridley, A. Hall, *Cell* **70**, 389 (1992).
12. N. Watanabe, T. Kato, A. Fujita, T. Ishizaki, S. Narumiya, *Nat. Cell Biol.* **1**, 136 (1999).
13. C. Higashida *et al.*, *J. Cell Sci.* **121**, 3403 (2008).
14. S. M. Buttery, S. Yoshida, D. Pellman, *Mol. Biol. Cell* **18**, 1826 (2007).
15. S. G. Martin, F. Chang, *Curr. Biol.* **16**, 1161 (2006).
16. D. R. Kovar, T. D. Pollard, *Proc. Natl. Acad. Sci. U.S.A.* **101**, 14725 (2004).
17. Materials and methods are available as supporting material on *Science* Online.
18. I. Sase, H. Miyata, S. Ishiwata, K. Kinosita Jr., *Proc. Natl. Acad. Sci. U.S.A.* **94**, 5646 (1997).
19. T. Shemesh, T. Otomo, M. K. Rosen, A. D. Bershadsky, M. M. Kozlov, *J. Cell Biol.* **170**, 889 (2005).
20. S. Romero *et al.*, *J. Biol. Chem.* **282**, 8435 (2007).
21. T. D. Pollard, I. Goldberg, W. H. Schwarz, *J. Biol. Chem.* **267**, 20339 (1992).
22. H. Y. Kueh, T. J. Mitchison, *Science* **325**, 960 (2009).
23. A. Orlova *et al.*, *Proc. Natl. Acad. Sci. U.S.A.* **101**, 17664 (2004).
24. K. C. Holmes, D. Popp, W. Gebhard, W. Kabsch, *Nature* **347**, 44 (1990).
25. M. R. Bubb, E. G. Yarmola, B. G. Gibson, F. S. Southwick, *J. Biol. Chem.* **278**, 24629 (2003).
26. I. Fujiwara, D. Vavylonis, T. D. Pollard, *Proc. Natl. Acad. Sci. U.S.A.* **104**, 8827 (2007).
27. L. Blanchoin, T. D. Pollard, *J. Biol. Chem.* **274**, 15538 (1999).
28. A. McGough, B. Pope, W. Chiu, A. Weeds, *J. Cell Biol.* **138**, 771 (1997).
29. N. Watanabe, T. J. Mitchison, *Science* **295**, 1083 (2002).
30. Y. Tsuda, H. Yasutake, A. Ishijima, T. Yanagida, *Proc. Natl. Acad. Sci. U.S.A.* **93**, 12937 (1996).

31. We thank H. Honda for rabbit muscle acetone powder and T. M. Watanabe for customizing the G-track software. This work was supported by Grants-in-Aid from the Ministry of Education, Culture, Sports, Science and Technology of Japan (MEXT) and grants from the Uehara Memorial Foundation (N.W.) and the Human Frontier Science Program (N.W.).

Supporting Online Material

www.sciencemag.org/cgi/content/full/science.1197692/DC1
Materials and Methods
Figs. S1 to S4
References
Movies S1 to S9

13 September 2010; accepted 16 November 2010
Published online 9 December 2010;
10.1126/science.1197692

Spontaneous Cortical Activity Reveals Hallmarks of an Optimal Internal Model of the Environment

Pietro Berkes,[1]† Gergő Orbán,[1,2,3] Máté Lengyel,[3]* József Fiser[1,4,5]*

The brain maintains internal models of its environment to interpret sensory inputs and to prepare actions. Although behavioral studies have demonstrated that these internal models are optimally adapted to the statistics of the environment, the neural underpinning of this adaptation is unknown. Using a Bayesian model of sensory cortical processing, we related stimulus-evoked and spontaneous neural activities to inferences and prior expectations in an internal model and predicted that they should match if the model is statistically optimal. To test this prediction, we analyzed visual cortical activity of awake ferrets during development. Similarity between spontaneous and evoked activities increased with age and was specific to responses evoked by natural scenes. This demonstrates the progressive adaptation of internal models to the statistics of natural stimuli at the neural level.

Our percepts rely on an internal model of the environment, relating physical processes of the world to inputs received by our senses, and thus their veracity critically hinges upon how well this internal model is adapted to the statistical properties of the environment. For example, internal models in vision are used to extract the features, such as low-level oriented edges or high-level objects, that gave rise to the retinal image (*1*). This requires that the internal model is adapted to the cooccurrence statistics of visual features in the environment and the way they jointly determine natural images. Several aspects of perception (*2*, *3*), motor control (*4*), decision making (*5*, *6*), and higher cognitive reasoning (*7*, *8*) are governed by such statistically optimal internal

[1]Volen National Center for Complex Systems, Brandeis University, Waltham, MA 02454, USA. [2]Department of Biophysics, Research Institute for Particle and Nuclear Physics, Hungarian Academy of Sciences, H-1121 Budapest, Hungary. [3]Computational and Biological Learning Lab, Department of Engineering, University of Cambridge, Cambridge CB2 1PZ, UK. [4]Department of Psychology and the Neuroscience Program, Brandeis University, Waltham, MA 02454, USA. [5]Collegium Budapest Institute for Advanced Study, Szentháromság utca 2, Budapest H-1014, Hungary.

*These authors contributed equally to this work.
†To whom correspondence should be addressed. E-mail: berkes@brandeis.edu

enhanced actin depolymerization at the mDia1-bound barbed end. This inhibition occurs in the submillimolar range of P_i, which is two orders of magnitude lower than the dissociation constant of P_i and G-actin (*26*). Thus, binding of P_i to F-actin inhibits profilin-induced depolymerization (Fig. 4E).

ADP-G-actin (5 μM) elongated mDia1-bound F-actin faster in the presence of 20 mM P_i than in its absence (Fig. 3C). This effect of P_i was more prominent in the presence of profilin than in its absence (Fig. 3C). The decrease in the actin off-rate (Fig. 4D) corresponds well with the increase in the ADP-actin elongation rate by 3 to 20 mM P_i (Fig. 4E). We thus suggest that P_i cancels the inhibitory effect of profilin on ADP-actin elongation (Fig. 3C) by abolishing the enhanced barbed end off-rate. The discrepancy of the effect of 1 mM P_i on depolymerization and assembly (Fig. 4, D, and E) is because slow dissociation of P_i prebound to a fraction of the ADP-F-actin subunits [dissociation constant (K_d) ≈1.5 mM] may limit terminal subunit dissociation during depolymerization (*26*), but not dissociation of assembling ADP-actin, which is mostly free from P_i. Profilin thus allows processive elongation of the FH1-FH2–bound barbed end regardless of the actin-bound nucleotide, but attenuates ADP-actin elongation by increasing the barbed end off-rate. Our results urge reconsideration of the ATP-specific acceleration mechanism for formin-associated actin elongation.

Helical rotation of mDia1 was observed during processive ADP-actin elongation in the presence of P_i (Fig. 4F and movie S7). The distance per half-rotation was 35.8 nm (Fig. 4G).

Our data demonstrate continuous rotation of mDia1-bound filaments during both elongation and depolymerization. The distance per half-rotation of F-actin is in the range of 34.6 to 36.8 nm regardless of the actin-bound nucleotide and presence of P_i and profilin (Figs. 2 to 4). These findings indicate that helical rotation of FH2 is an intrinsic property derived from the helical structure of F-actin. Cellular actin filaments are highly cross-linked as evidenced by single-molecule observations showing movement of actin subunits with no change in their relative positions (*29*). Therefore, formins must rotate in the cell. The rotation speed of for3p at the cell tip and processively moving mDia1 can reach 250 and 1700 rpm, respectively. If anchoring the growing end of F-actin is the function of formins, the link between formins and cellular structures must be flexible. Alternatively, formin-mediated actin elongation may be regulated by torsional stress in F-actin.

Conversely, formins might modulate the stability of F-actin by helical rotation. Torsional stress induces destabilization of the filament (*30*). Cofilin, the major actin depolymerizing factor, twists the strand of F-actin, which is thought to contribute to actin disassembly (*28*). Our data have opened up the possibility that actin elongation and remodeling could be regulated by axial torsion in the filament. Our findings should help elucidate the actin turnover mechanism regulated by formins in the cell.

References and Notes

1. N. Watanabe, *Proc. Jpn. Acad. Ser. B Phys. Biol. Sci.* **86**, 62 (2010).
2. M. Evangelista, S. Zigmond, C. Boone, *J. Cell Sci.* **116**, 2603 (2003).
3. B. L. Goode, M. J. Eck, *Annu. Rev. Biochem.* **76**, 593 (2007).
4. C. Higashida *et al.*, *Science* **303**, 2007 (2004).
5. M. Pring, M. Evangelista, C. Boone, C. Yang, S. H. Zigmond, *Biochemistry* **42**, 486 (2003).
6. D. R. Kovar, E. S. Harris, R. Mahaffy, H. N. Higgs, T. D. Pollard, *Cell* **124**, 423 (2006).
7. T. Otomo *et al.*, *Nature* **433**, 488 (2005).
8. K. C. Holmes, *Nature* **457**, 389 (2009).
9. S. Gasman, Y. Kalaidzidis, M. Zerial, *Nat. Cell Biol.* **5**, 195 (2003).
10. B. Leader *et al.*, *Nat. Cell Biol.* **4**, 921 (2002).
11. A. J. Ridley, A. Hall, *Cell* **70**, 389 (1992).
12. N. Watanabe, T. Kato, A. Fujita, T. Ishizaki, S. Narumiya, *Nat. Cell Biol.* **1**, 136 (1999).
13. C. Higashida *et al.*, *J. Cell Sci.* **121**, 3403 (2008).
14. S. M. Buttery, S. Yoshida, D. Pellman, *Mol. Biol. Cell* **18**, 1826 (2007).
15. S. G. Martin, F. Chang, *Curr. Biol.* **16**, 1161 (2006).
16. D. R. Kovar, T. D. Pollard, *Proc. Natl. Acad. Sci. U.S.A.* **101**, 14725 (2004).
17. Materials and methods are available as supporting material on *Science* Online.
18. I. Sase, H. Miyata, S. Ishiwata, K. Kinosita Jr., *Proc. Natl. Acad. Sci. U.S.A.* **94**, 5646 (1997).
19. T. Shemesh, T. Otomo, M. K. Rosen, A. D. Bershadsky, M. M. Kozlov, *J. Cell Biol.* **170**, 889 (2005).
20. S. Romero *et al.*, *J. Biol. Chem.* **282**, 8435 (2007).
21. T. D. Pollard, I. Goldberg, W. H. Schwarz, *J. Biol. Chem.* **267**, 20339 (1992).
22. H. Y. Kueh, T. J. Mitchison, *Science* **325**, 960 (2009).
23. A. Orlova *et al.*, *Proc. Natl. Acad. Sci. U.S.A.* **101**, 17664 (2004).
24. K. C. Holmes, D. Popp, W. Gebhard, W. Kabsch, *Nature* **347**, 44 (1990).
25. M. R. Bubb, E. G. Yarmola, B. G. Gibson, F. S. Southwick, *J. Biol. Chem.* **278**, 24629 (2003).
26. I. Fujiwara, D. Vavylonis, T. D. Pollard, *Proc. Natl. Acad. Sci. U.S.A.* **104**, 8827 (2007).
27. L. Blanchoin, T. D. Pollard, *J. Biol. Chem.* **274**, 15538 (1999).
28. A. McGough, B. Pope, W. Chiu, A. Weeds, *J. Cell Biol.* **138**, 771 (1997).
29. N. Watanabe, T. J. Mitchison, *Science* **295**, 1083 (2002).
30. Y. Tsuda, H. Yasutake, A. Ishijima, T. Yanagida, *Proc. Natl. Acad. Sci. U.S.A.* **93**, 12937 (1996).

31. We thank H. Honda for rabbit muscle acetone powder and T. M. Watanabe for customizing the G-track software. This work was supported by Grants-in-Aid from the Ministry of Education, Culture, Sports, Science and Technology of Japan (MEXT) and grants from the Uehara Memorial Foundation (N.W.) and the Human Frontier Science Program (N.W.).

Supporting Online Material

www.sciencemag.org/cgi/content/full/science.1197692/DC1
Materials and Methods
Figs. S1 to S4
References
Movies S1 to S9

13 September 2010; accepted 16 November 2010
Published online 9 December 2010;
10.1126/science.1197692

Spontaneous Cortical Activity Reveals Hallmarks of an Optimal Internal Model of the Environment

Pietro Berkes,[1]† Gergő Orbán,[1,2,3] Máté Lengyel,[3]* József Fiser[1,4,5]*

The brain maintains internal models of its environment to interpret sensory inputs and to prepare actions. Although behavioral studies have demonstrated that these internal models are optimally adapted to the statistics of the environment, the neural underpinning of this adaptation is unknown. Using a Bayesian model of sensory cortical processing, we related stimulus-evoked and spontaneous neural activities to inferences and prior expectations in an internal model and predicted that they should match if the model is statistically optimal. To test this prediction, we analyzed visual cortical activity of awake ferrets during development. Similarity between spontaneous and evoked activities increased with age and was specific to responses evoked by natural scenes. This demonstrates the progressive adaptation of internal models to the statistics of natural stimuli at the neural level.

Our percepts rely on an internal model of the environment, relating physical processes of the world to inputs received by our senses, and thus their veracity critically hinges upon how well this internal model is adapted to the statistical properties of the environment. For example, internal models in vision are used to extract the features, such as low-level oriented edges or high-level objects, that gave rise to the retinal image (*1*). This requires that the internal model is adapted to the cooccurrence statistics of visual features in the environment and the way they jointly determine natural images. Several aspects of perception (*2*, *3*), motor control (*4*), decision making (*5*, *6*), and higher cognitive reasoning (*7*, *8*) are governed by such statistically optimal internal

[1]Volen National Center for Complex Systems, Brandeis University, Waltham, MA 02454, USA. [2]Department of Biophysics, Research Institute for Particle and Nuclear Physics, Hungarian Academy of Sciences, H-1121 Budapest, Hungary. [3]Computational and Biological Learning Lab, Department of Engineering, University of Cambridge, Cambridge CB2 1PZ, UK. [4]Department of Psychology and the Neuroscience Program, Brandeis University, Waltham, MA 02454, USA. [5]Collegium Budapest Institute for Advanced Study, Szentháromság utca 2, Budapest H-1014, Hungary.

*These authors contributed equally to this work.
†To whom correspondence should be addressed. E-mail: berkes@brandeis.edu

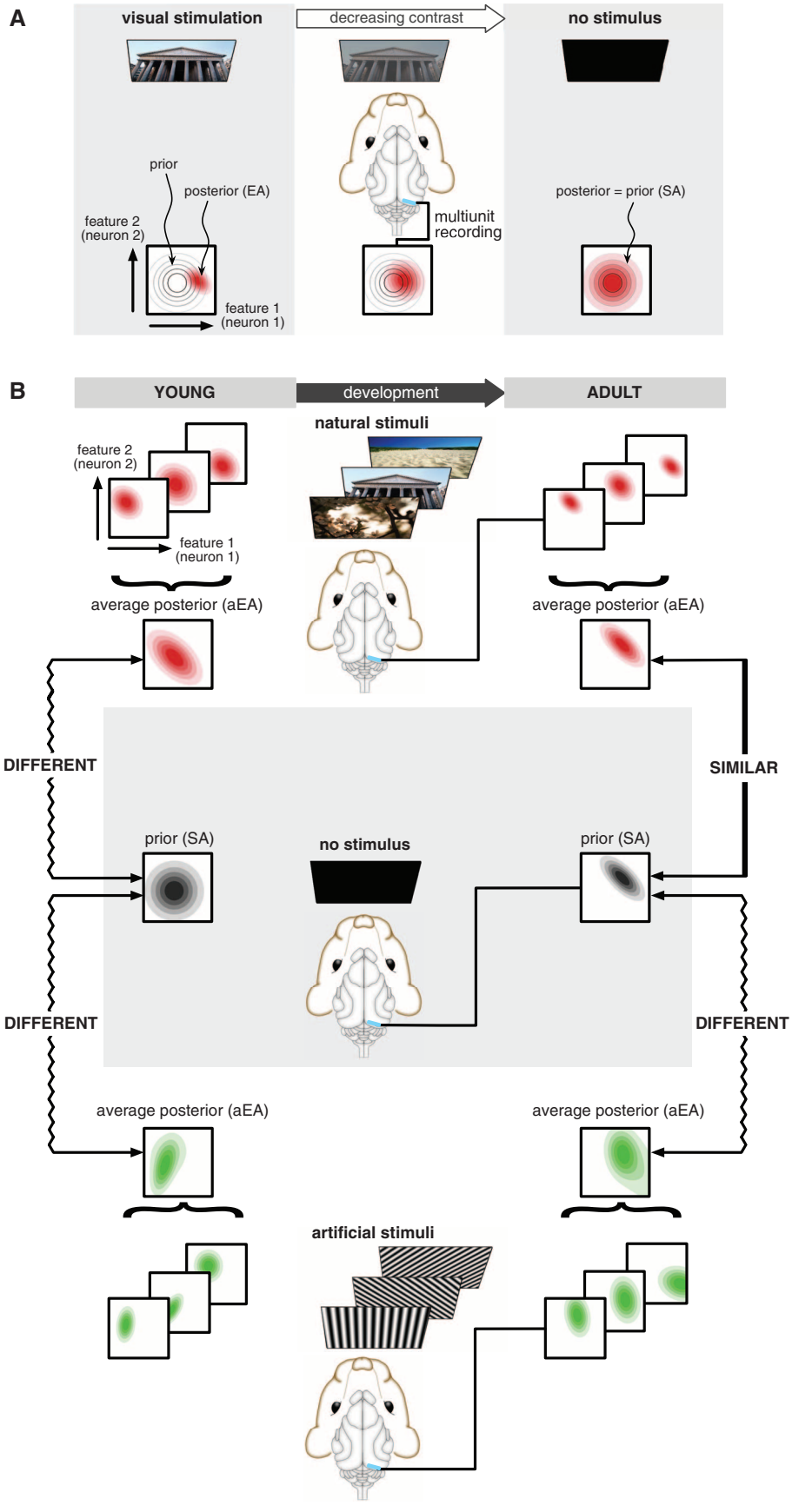

Fig. 1. Assessing the statistical optimality of the internal model in the visual cortex. (**A**) The posterior distribution represented by EA (bottom, red-filled contours show pairwise activity distributions) in response to a visual stimulus (top) is increasingly dominated by the prior distribution (bottom, gray contours) as brightness or contrast is decreased from maximum (left) to lower levels (center). In the absence of stimulation (right), the posterior converges to the prior, and thus, SA recorded in darkness represents this prior. (**B**) Multiunit activity recorded in V1 of awake, freely viewing ferrets either receiving no stimulus (middle) or viewing natural (top) or artificial stimuli (bottom) is used to construct neural activity distributions in young and adult animals. Under natural and artificial stimuli conditions, EA distributions represent distributions of visual features (red and green panels) inferred from particular stimuli. Average EA distributions (aEA) evoked by different stimuli ensembles are compared with the distribution of SA recorded in darkness (black panels), representing the prior expectations about visual features. Quantifying the dissimilarity between the SA distribution and the aEA distribution reveals the level of statistical adaptation of the internal model to the stimulus ensemble. The internal model of young animals (left) is expected to show little adaptation to the natural environment and thus aEA for natural (and also for artificial) scenes should be different from SA. Adult animals (right) are expected to be adapted to natural scenes and thus to exhibit a high degree of similarity between SA and natural stimuli–aEA, but not between SA and artificial stimuli–aEA.

models. Yet identifying the neural correlates of optimal internal models has remained a challenge (see supporting online text).

We addressed this problem by relating evoked and spontaneous neural activity (EA and SA, respectively) (*9*) to two key aspects of Bayesian computations performed with the internal model (Fig. 1A). The first key aspect is that a statistically optimal internal model needs to represent its inferences as a probability distribution, the Bayesian posterior $P(\text{features}|\text{input, model})$ (*2*, *10*) describing the inferred probability that a particular combination of features may underlie the input. Thus, under the general assumption that the visual cortex implements such an optimal internal model, EA should represent the posterior probability distribution for a given input image (*2*, *11*, *12*), and SA should represent the posterior distribution elicited by a blank stimulus. The second key aspect of a statistically optimal internal model, under only mild assumptions about its structure, is that the posterior represented by SA converges to the prior distribution, which describes prior expectations about the frequency with which any given combination of features may occur in the environment, $P(\text{features}|\text{model})$. This is because as the brightness or contrast of the visual stimulus is decreased, inferences about the features present in the input will be increasingly dominated by these prior expectations (for a formal derivation, see supporting online text). This effect has been demonstrated in behavioral studies (*3*, *13*), and it is also consistent with data on neural responses in the primary visual cortex (V1) (*14*). Relating EA and SA to the posterior and prior distributions provides a complete, data-driven characterization of the internal model without making strong theoretical assumptions about its precise nature.

Crucially, this interpretation of the EA and SA distributions allowed us to assess statistical optimality of the internal model with respect to an ensemble of visual inputs, $P(\text{input})$, using a standard benchmark of the optimality of statistical models (Fig. 1B) (*15*). A statistical model of visual inputs that is optimally adapted to a stimulus ensemble must have prior expectations that match the actual frequency with which it encounters different visual features in that ensemble (*16*). The degree of mismatch can be quantified as the divergence between the average posterior and the prior:

$$\text{Div}[\langle P(\text{features}|\text{iput, model})\rangle_{P(\text{input})} \parallel P(\text{features}|\text{model})] \quad (1)$$

where the angular brackets indicate averaging over the stimulus ensemble. A well-calibrated model will predict correctly the frequency of feature combinations in actual visual scenes, leading to a divergence close to zero. However, if the model is not adapted, or it is adapted to a different stimulus ensemble from the actual test ensemble, then a large divergence is expected. As we identified EA and SA with the posterior and prior distributions of the internal model, the statistical optimality of neural responses with respect to a stimulus ensemble can be quantified by applying Eq. 1 to neural data, i.e., by computing the divergence between the average distribution of multineural EA (aEA), collected in response to stimuli sampled from the stimulus ensemble, and the distribution of SA (*17*) (Fig. 2A).

Because the internal model of the visual cortex needs to be adapted to the statistical properties of natural scenes, Eq. 1 should yield a low divergence between aEA for natural scenes and SA in the mature visual system. We therefore measured the population activity within the visual cortex of awake, freely viewing ferrets in response to natural-scene movies (aEA) and in darkness (SA) at four different developmental stages: after eye opening at postnatal day 29 (P29) to P30, after the maturation of orientation tuning and long-range horizontal connections at P44 to P45 (*18*), and in two groups of mature animals at P83 to P90 and P129 to P151

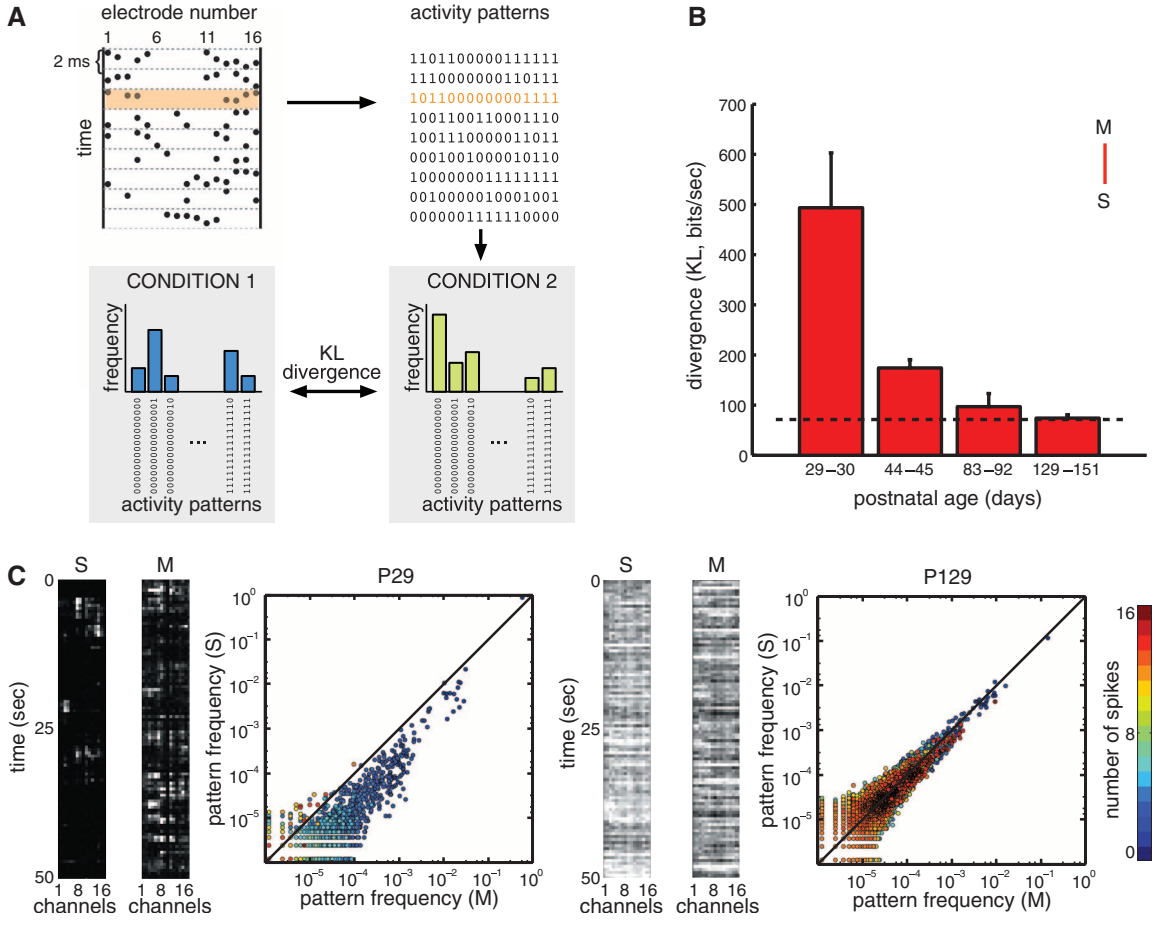

Fig. 2. Improving match between aEA and SA over development. (**A**) Spikes were recorded on 16 electrodes, divided into discrete 2-ms bins, and converted to binary strings, so that each string described the activity pattern of cells at a given time point (top). For each condition, the histogram of activity patterns was constructed, and different histograms were compared by measuring their divergence (bottom). (**B**) Divergence between the distributions of activity patterns in movie-aEA (M) and SA (S), as a function of age (red bars). As a reference, the dashed line shows the average of the within-condition baselines computed with within-condition data split into two halves (fig. S1). (**C**) Frequency of occurrence of activity patterns under SA (S, *y* axis) versus movie-aEA (M, *x* axis) in a young (left) and adult (right) animal. Each dot represents one of the 2^{16} = 65,536 possible binary activity patterns; color code indicates number of spikes. Black line shows equality. The panels at the left of the plots show examples of neural activity on the 16 electrodes in representative SA and movie-aEA trials for the same animals. Error bars on all figures represent SEM.

(n = 16 animals in total, table S1). The divergence between aEA and SA decreased with age (Fig. 2, B and C, Spearman's $\rho = -0.70$, $P < 0.004$), and the two distributions were not significantly different in mature animals (fig. S1, P83 to P90: $m = 5.74$, $P = 0.11$; P129 to P151: $m = 2.03$, $P = 0.25$).

What aspects of aEA and SA are responsible for their improving match with age? Redundancy reduction, one prominent assumption regarding neural coding (*19*), would predict that neurons behave as sparse (*20*, *21*) and uncorrelated information channels (*22*). To assess the importance of correlations between the activities of different neurons, we constructed surrogate distributions for aEA and SA that preserved single-neuron firing rates but otherwise assumed that neurons fired independently (*17*). Thus, any divergence between a real and a surrogate distribution must be due to correlated neural activities of second (*23*) or higher order. By computing this divergence, we found that the activity of neurons in both aEA and SA became increasingly correlated (Fig. 3A, Spearman's $\rho = 0.73$, $P < 0.002$ for both curves) and increasingly nonsparse with age (fig. S2), which argues against redundancy reduction. Moreover, these increasing correlations were important for the match between aEA and SA because the surrogate SA did not converge to the true aEA (Fig. 3B, Spearman's $\rho = 0.34$, $P = 0.22$), excluding the possibility that the decreasing divergence between aEA and SA

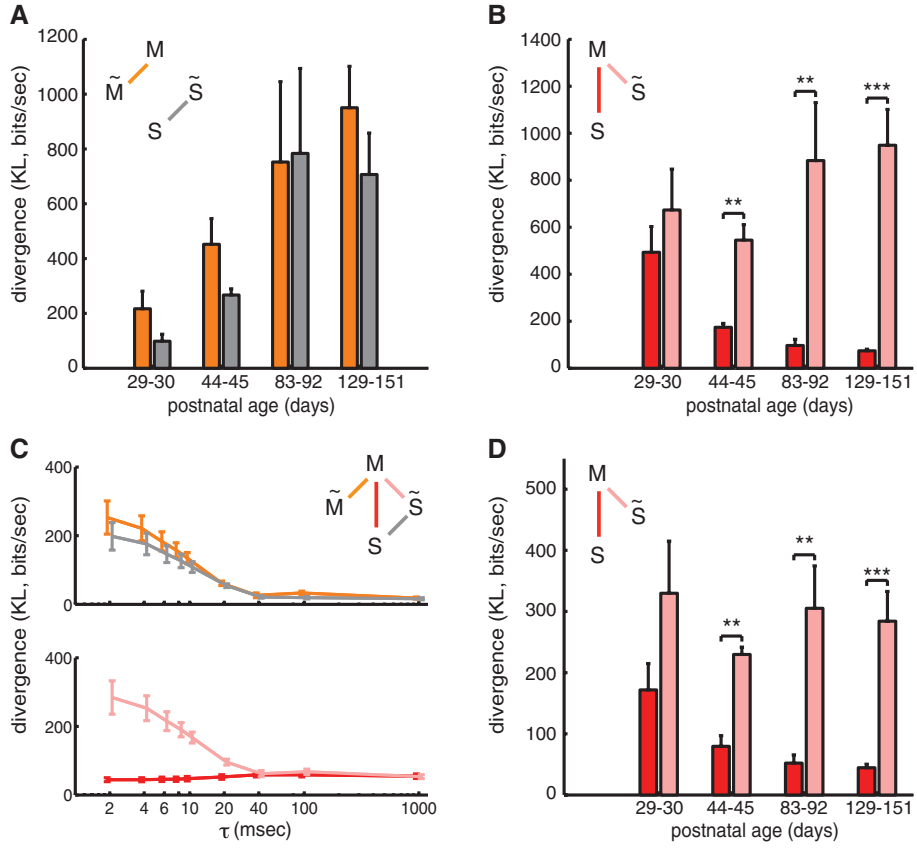

Fig. 3. Contribution of spatial and temporal correlations to the match between aEA and SA. (**A** and **B**) The role of spatial correlations was quantified by the divergence between the measured distributions of neural activity patterns, movie-aEA (M) and SA (S), and the surrogate versions of the same distributions ($\tilde{M}$ and $\tilde{S}$), in which correlations between channels were removed, while the firing rates were kept intact (*17*). (A) The divergence between the measured and surrogate distributions increased significantly over age for both movie-aEA (orange) and SA (gray). (B) Enhanced match between movie-aEA and SA over development (red, compare Fig. 2B) disappeared when spatial correlations were removed from SA (pink). (**C** and **D**) Divergence of transition probability distributions between measured neural activity patterns and their surrogate versions, in which temporal correlations were removed, while firing rates and spatial correlations were kept intact (*17*). (C) Temporal correlations in adult animals (P129 to P151) as a function of the time interval, τ. Within-condition divergences (top) show that temporal correlations decreased with time lag in both movie-aEA (orange) and SA (gray). Across-condition comparison (bottom) of the divergence of aEA from the measured SA (red) and from the surrogate SA (pink) shows that temporal correlations in the two conditions were matched up to time intervals when they decayed to zero. (D) Temporal correlations at the shortest time interval (τ = 2 ms) as a function of age. The match of transition probabilities between movie-aEA and SA improved (red). Removing temporal correlations from SA eliminated this match (pink). In all figures, *$P < 0.05$, **$P < 0.01$, ***$P < 0.001$, m test (*17*).

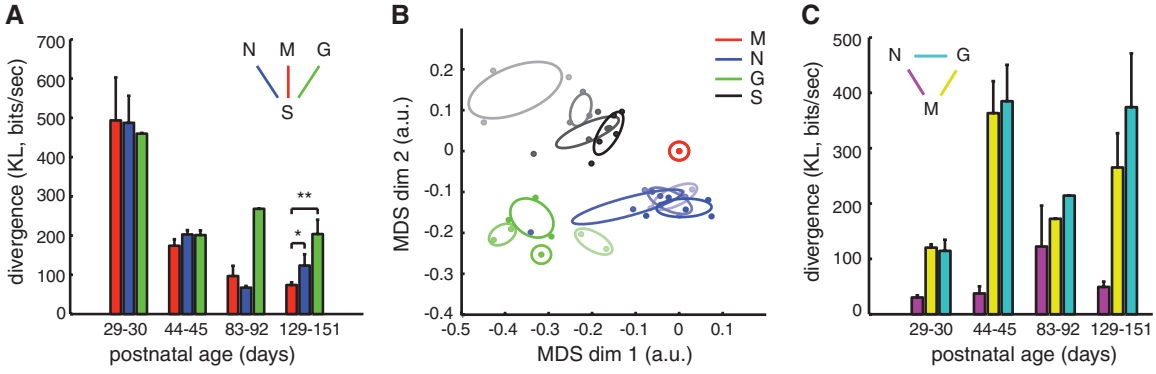

Fig. 4. Similarity between aEA and SA is specific to natural scenes. (**A**) Divergence between neural activity patterns evoked by different stimulus ensembles (movie-aEA: red, M; noise-aEA: blue, N; gratings-aEA: green, G) and those observed in SA. In adult animals, SA was significantly more similar to movie-aEA than noise-aEA or gratings-aEA. (**B**) Two-dimensional projection of all neural activity distributions. Each dot represents one activity distribution in a different animal, colors indicate stimulus ensembles (movie-aEA: red, M; noise-aEA: blue, N; gratings-aEA: green, G; SA: black, S), intensity indicates age group (in order of increasing intensity: P29 to P30, P44 to P45, P83 to P92, and P129 to P151), ellipses delineate distributions belonging to the same age group. Positions of dots were computed by multidimensional scaling (MDS) to be maximally consistent with pairwise divergences between distributions. Movie-aEAs were defined to be at the origin. For young animals (faintest colors), SA was significantly dissimilar from all aEA distributions. In the course of development, SA moved closer to all aEAs; but by P129 to P151, SA was significantly more similar to movie-aEA than artificial stimuli–aEAs, as quantified in (A). (**C**) Divergences measured directly between different aEA distributions (noise-aEA and movie-aEA: magenta, gratings-aEA and movie-aEA: yellow, gratings-aEA and noise-aEA: cyan) showed no decrease in the specificity of the responses to different stimulus ensembles.

could be accounted for by changes in the firing rates of neurons alone.

An appropriate model of the visual environment should also capture its temporal dynamics. Therefore, we extended our analysis beyond the purely spatial domain to the temporal domain. We measured the probability of transitioning between any two patterns in a wide range of temporal delays for all conditions and tested the strength and match of temporal correlations by using surrogate distributions as was done in the spatial domain (*17*). The activity of neurons showed strong temporal correlations up to ~20 ms in both aEA and SA in adult animals (Fig. 3C). A strong prediction of the hypothesis that V1 neural activity reflects a statistically optimal internal model is that these transition probabilities should also be matched between aEA, when V1 processes temporally strongly structured visual input, and SA, when no visual stimulus is provided. Indeed, we found that the match between transition probabilities in aEA and SA significantly improved with age (Fig. 3D, Spearman's $\rho = -0.72$, $P < 0.003$), such that in adult animals the temporal correlations were matched up to delays when they decayed to zero (Fig. 3C).

If the internal model reflected in V1 activity is tuned specifically to the natural visual environment, then the match between aEA and SA should also be specific to using a natural image ensemble for eliciting aEA, and other, "artificial" stimulus ensembles should yield higher divergences between aEA and SA for mature animals. To test this prediction, aEA was collected with two other types of stimulus classes: drifting sinusoid gratings at different orientations and frequencies, as well as dynamic binary block noise that was updated at frame rate (*17*). Indeed, although in young animals there was no significant difference between the degree of match of SA and aEA, in the oldest age group SA was significantly better matched to neural activity evoked by natural images than that evoked by the two artificial stimulus ensembles (Fig. 4, A and B, movie versus noise: $m = 16.47$, $P < 0.05$; movie versus grating: $m = 943.07$, $P < 0.002$). Furthermore, the divergence between different aEA distributions did not decrease significantly with age (Fig. 4, B and C, movie versus noise: $\rho = 0.19$, $P = 0.49$, movie versus grating: $\rho = 0.5$, $P = 0.21$, noise versus grating: $\rho = 0.67$, $P = 0.07$), which ruled out the possibility that the decreasing divergence between aEA and SA was due to a general decoupling of V1 from sensory input (see also fig. S3).

Our results suggest that V1 implements an internal model that is adapted gradually during development to the statistical structure of the natural visual environment and that SA reflects prior expectations of this internal model. Although these findings do not address the degree to which statistical adaptation in the cortex is driven by visual experience or by developmental programs, they set useful constraints for both dynamical (*24*) and functional models (*12*) of sensory processing. We expect our approach to extend to other brain areas and to provide a general, quantitative way to test future proposals for computational strategies used by the cortex.

References and Notes

1. D. Kersten, P. Mamassian, A. Yuille, *Annu. Rev. Psychol.* **55**, 271 (2004).
2. J. Fiser, P. Berkes, G. Orbán, M. Lengyel, *Trends Cogn. Sci.* **14**, 119 (2010).
3. Y. Weiss, E. P. Simoncelli, E. H. Adelson, *Nat. Neurosci.* **5**, 598 (2002).
4. D. M. Wolpert, Z. Ghahramani, M. I. Jordan, *Science* **269**, 1880 (1995).
5. A. C. Courville, N. D. Daw, D. S. Touretzky, *Trends Cogn. Sci.* **10**, 294 (2006).
6. J. Trommershäuser, L. T. Maloney, M. S. Landy, *Trends Cogn. Sci.* **12**, 291 (2008).
7. A. P. Blaisdell, K. Sawa, K. J. Leising, M. R. Waldmann, *Science* **311**, 1020 (2006).
8. D. Sobel, J. B. Tenenbaum, A. Gopnik, *Cogn. Sci.* **28**, 303 (2004).
9. Unlike traditional neural data analysis methods (*15*), which require averaging responses over trials using the same stimulus, here the term EA refers to the whole distribution of evoked neural activity patterns in response to a stimulus.
10. E. T. Jaynes, *Probability Theory: The Logic of Science* (Cambridge Univ. Press, Cambridge, 2003).
11. P. O. Hoyer, A. Hyvarinen, *Adv. Neural Inf. Process Syst.* **16**, 293 (2003).
12. W. J. Ma, J. M. Beck, P. E. Latham, A. Pouget, *Nat. Neurosci.* **9**, 1432 (2006).
13. A. A. Stocker, E. P. Simoncelli, *Nat. Neurosci.* **9**, 578 (2006).
14. I. Nauhaus, L. Busse, M. Carandini, D. L. Ringach, *Nat. Neurosci.* **12**, 70 (2009).
15. P. Dayan, L. F. Abbott, *Theoretical Neuroscience* (MIT Press, Cambridge, MA, 1999).
16. Y. W. Teh, M. Welling, S. Osindero, G. E. Hinton, *J. Mach. Learn. Res.* **4**, 1235 (2004).
17. Materials and methods are available as supporting material on *Science* Online.
18. F. Sengpiel, P. C. Kind, *Curr. Biol.* **12**, R818 (2002).
19. H. B. Barlow, in *Sensory Communication* (MIT Press, Cambridge, MA, 1961), pp. 217–234.
20. B. A. Olshausen, D. J. Field, *Nature* **381**, 607 (1996).
21. Y. Karklin, M. S. Lewicki, *Nature* **457**, 83 (2009).
22. A. J. Bell, T. J. Sejnowski, *Vision Res.* **37**, 3327 (1997).
23. E. Schneidman, M. J. Berry 2nd, R. Segev, W. Bialek, *Nature* **440**, 1007 (2006).
24. J. A. Goldberg, U. Rokni, H. Sompolinsky, *Neuron* **42**, 489 (2004).

25. We thank D. Wolpert and D. Katz for suggestions on the manuscript, C. Chiu and M. Weliky for help with the data collection, and D. Lisitsyn for technical help. This work was supported by the Swartz Foundation (J.F., G.O., and P.B.), the Swiss National Science Foundation (P.B.), an EU-FP7 Marie Curie Intra-European Fellowship (G.O.), the Wellcome Trust (M.L.), and NIH (J.F.).

Supporting Online Material

www.sciencemag.org/cgi/content/full/331/6013/83/DC1
Materials and Methods
SOM Text
Figs. S1 to S4
Tables S1 and S2
References

30 July 2010; accepted 29 November 2010
10.1126/science.1195870

Electrical Synapses Control Hippocampal Contributions to Fear Learning and Memory

Stephanie Bissiere, Moriel Zelikowsky, Ravikumar Ponnusamy, Nathan S. Jacobs, Hugh T. Blair, Michael S. Fanselow*

The role of electrical synapses in synchronizing neuronal assemblies in the adult mammalian brain is well documented. However, their role in learning and memory processes remains unclear. By combining Pavlovian fear conditioning, activity-dependent immediate early gene expression, and in vivo electrophysiology, we discovered that blocking neuronal gap junctions within the dorsal hippocampus impaired context-dependent fear learning, memory, and extinction. Theta rhythms in freely moving rats were also disrupted. Our results show that gap junction–mediated neuronal transmission is a prominent feature underlying emotional memories.

Unlike chemical synapses, the role of electrical synapses in fear learning and memory remains largely unknown (*1*–*3*). In the adult mammalian brain, gap junctions formed by connexin 36 (Cx36) couple γ-aminobutyric acid–releasing (GABAergic) interneurons that participate in the generation of synchronized oscillations (*2*–*4*). Cx36 expression has been localized within the amygdala-hippocampus-cortical axis (*4*, *5*), and disrupted hippocampal and cortical oscillations have been reported in Cx36 knockout mice (*6*, *7*). Electrical synapses undergo posttranslational modifications and activity-dependent plasticity similar to chemical synapses (*8*, *9*). Thus, we hypothesized that electrical synapses may be important for the formation and maintenance of fear behaviors and memories.

Rats received intraperitoneal injections of the general gap junction blocker carbenoxolone (Cbx) (*10*, *11*) or the selective Cx36 blocker mefloquine (Meflo) (*12*) and were fear-conditioned using three pairings of a neutral tone (conditional stimulus, CS) with an aversive footshock (uncon-

Department of Psychology, University of California, Los Angeles, CA 90095, USA.

*To whom correspondence should be addressed. E-mail: fanselow@psych.ucla.edu

could be accounted for by changes in the firing rates of neurons alone.

An appropriate model of the visual environment should also capture its temporal dynamics. Therefore, we extended our analysis beyond the purely spatial domain to the temporal domain. We measured the probability of transitioning between any two patterns in a wide range of temporal delays for all conditions and tested the strength and match of temporal correlations by using surrogate distributions as was done in the spatial domain (*17*). The activity of neurons showed strong temporal correlations up to ~20 ms in both aEA and SA in adult animals (Fig. 3C). A strong prediction of the hypothesis that V1 neural activity reflects a statistically optimal internal model is that these transition probabilities should also be matched between aEA, when V1 processes temporally strongly structured visual input, and SA, when no visual stimulus is provided. Indeed, we found that the match between transition probabilities in aEA and SA significantly improved with age (Fig. 3D, Spearman's $\rho = -0.72$, $P < 0.003$), such that in adult animals the temporal correlations were matched up to delays when they decayed to zero (Fig. 3C).

If the internal model reflected in V1 activity is tuned specifically to the natural visual environment, then the match between aEA and SA should also be specific to using a natural image ensemble for eliciting aEA, and other, "artificial" stimulus ensembles should yield higher divergences between aEA and SA for mature animals. To test this prediction, aEA was collected with two other types of stimulus classes: drifting sinusoid gratings at different orientations and frequencies, as well as dynamic binary block noise that was updated at frame rate (*17*). Indeed, although in young animals there was no significant difference between the degree of match of SA and aEA, in the oldest age group SA was significantly better matched to neural activity evoked by natural images than that evoked by the two artificial stimulus ensembles (Fig. 4, A and B, movie versus noise: $m = 16.47$, $P < 0.05$; movie versus grating: $m = 943.07$, $P < 0.002$). Furthermore, the divergence between different aEA distributions did not decrease significantly with age (Fig. 4, B and C, movie versus noise: $\rho = 0.19$, $P = 0.49$, movie versus grating: $\rho = 0.5$, $P = 0.21$, noise versus grating: $\rho = 0.67$, $P = 0.07$), which ruled out the possibility that the decreasing divergence between aEA and SA was due to a general decoupling of V1 from sensory input (see also fig. S3).

Our results suggest that V1 implements an internal model that is adapted gradually during development to the statistical structure of the natural visual environment and that SA reflects prior expectations of this internal model. Although these findings do not address the degree to which statistical adaptation in the cortex is driven by visual experience or by developmental programs, they set useful constraints for both dynamical (*24*) and functional models (*12*) of sensory processing. We expect our approach to extend to other brain areas and to provide a general, quantitative way to test future proposals for computational strategies used by the cortex.

References and Notes

1. D. Kersten, P. Mamassian, A. Yuille, *Annu. Rev. Psychol.* **55**, 271 (2004).
2. J. Fiser, P. Berkes, G. Orbán, M. Lengyel, *Trends Cogn. Sci.* **14**, 119 (2010).
3. Y. Weiss, E. P. Simoncelli, E. H. Adelson, *Nat. Neurosci.* **5**, 598 (2002).
4. D. M. Wolpert, Z. Ghahramani, M. I. Jordan, *Science* **269**, 1880 (1995).
5. A. C. Courville, N. D. Daw, D. S. Touretzky, *Trends Cogn. Sci.* **10**, 294 (2006).
6. J. Trommershäuser, L. T. Maloney, M. S. Landy, *Trends Cogn. Sci.* **12**, 291 (2008).
7. A. P. Blaisdell, K. Sawa, K. J. Leising, M. R. Waldmann, *Science* **311**, 1020 (2006).
8. D. Sobel, J. B. Tenenbaum, A. Gopnik, *Cogn. Sci.* **28**, 303 (2004).
9. Unlike traditional neural data analysis methods (*15*), which require averaging responses over trials using the same stimulus, here the term EA refers to the whole distribution of evoked neural activity patterns in response to a stimulus.
10. E. T. Jaynes, *Probability Theory: The Logic of Science* (Cambridge Univ. Press, Cambridge, 2003).
11. P. O. Hoyer, A. Hyvarinen, *Adv. Neural Inf. Process Syst.* **16**, 293 (2003).
12. W. J. Ma, J. M. Beck, P. E. Latham, A. Pouget, *Nat. Neurosci.* **9**, 1432 (2006).
13. A. A. Stocker, E. P. Simoncelli, *Nat. Neurosci.* **9**, 578 (2006).
14. I. Nauhaus, L. Busse, M. Carandini, D. L. Ringach, *Nat. Neurosci.* **12**, 70 (2009).
15. P. Dayan, L. F. Abbott, *Theoretical Neuroscience* (MIT Press, Cambridge, MA, 1999).
16. Y. W. Teh, M. Welling, S. Osindero, G. E. Hinton, *J. Mach. Learn. Res.* **4**, 1235 (2004).
17. Materials and methods are available as supporting material on *Science* Online.
18. F. Sengpiel, P. C. Kind, *Curr. Biol.* **12**, R818 (2002).
19. H. B. Barlow, in *Sensory Communication* (MIT Press, Cambridge, MA, 1961), pp. 217–234.
20. B. A. Olshausen, D. J. Field, *Nature* **381**, 607 (1996).
21. Y. Karklin, M. S. Lewicki, *Nature* **457**, 83 (2009).
22. A. J. Bell, T. J. Sejnowski, *Vision Res.* **37**, 3327 (1997).
23. E. Schneidman, M. J. Berry 2nd, R. Segev, W. Bialek, *Nature* **440**, 1007 (2006).
24. J. A. Goldberg, U. Rokni, H. Sompolinsky, *Neuron* **42**, 489 (2004).

25. We thank D. Wolpert and D. Katz for suggestions on the manuscript, C. Chiu and M. Weliky for help with the data collection, and D. Lisitsyn for technical help. This work was supported by the Swartz Foundation (J.F., G.O., and P.B.), the Swiss National Science Foundation (P.B.), an EU-FP7 Marie Curie Intra-European Fellowship (G.O.), the Wellcome Trust (M.L.), and NIH (J.F.).

Supporting Online Material

www.sciencemag.org/cgi/content/full/331/6013/83/DC1
Materials and Methods
SOM Text
Figs. S1 to S4
Tables S1 and S2
References

30 July 2010; accepted 29 November 2010
10.1126/science.1195870

Electrical Synapses Control Hippocampal Contributions to Fear Learning and Memory

Stephanie Bissiere, Moriel Zelikowsky, Ravikumar Ponnusamy, Nathan S. Jacobs, Hugh T. Blair, Michael S. Fanselow*

The role of electrical synapses in synchronizing neuronal assemblies in the adult mammalian brain is well documented. However, their role in learning and memory processes remains unclear. By combining Pavlovian fear conditioning, activity-dependent immediate early gene expression, and in vivo electrophysiology, we discovered that blocking neuronal gap junctions within the dorsal hippocampus impaired context-dependent fear learning, memory, and extinction. Theta rhythms in freely moving rats were also disrupted. Our results show that gap junction–mediated neuronal transmission is a prominent feature underlying emotional memories.

Unlike chemical synapses, the role of electrical synapses in fear learning and memory remains largely unknown (*1*–*3*). In the adult mammalian brain, gap junctions formed by connexin 36 (Cx36) couple γ-aminobutyric acid–releasing (GABAergic) interneurons that participate in the generation of synchronized oscillations (*2*–*4*). Cx36 expression has been localized within the amygdala-hippocampus-cortical axis (*4*, *5*), and disrupted hippocampal and cortical oscillations have been reported in Cx36 knockout mice (*6*, *7*). Electrical synapses undergo posttranslational modifications and activity-dependent plasticity similar to chemical synapses (*8*, *9*). Thus, we hypothesized that electrical synapses may be important for the formation and maintenance of fear behaviors and memories.

Rats received intraperitoneal injections of the general gap junction blocker carbenoxolone (Cbx) (*10*, *11*) or the selective Cx36 blocker mefloquine (Meflo) (*12*) and were fear-conditioned using three pairings of a neutral tone (conditional stimulus, CS) with an aversive footshock (uncon-

Department of Psychology, University of California, Los Angeles, CA 90095, USA.

*To whom correspondence should be addressed. E-mail: fanselow@psych.ucla.edu

ditional stimulus, US) (Fig. 1, A and B). All animals exhibited equal levels of freezing when tested 24 hours later for their tone fear memories (Fig. 1C). However, both drugs significantly reduced context fear ($F_{2,34}$ = 31.1, P < 0.0001; Bonferroni corrected post hoc tests at P < 0.05 indicated that both drugs were different from vehicle but not from each other) (Fig. 1D). During training, all rats froze similarly during tone presentations and the intertrial interval, indicating that the drugs did not interfere with short-term memory or the ability to freeze [3 (drug) × 3 (trial) analysis of variance (ANOVA) for freezing during tone: trial, $F_{2,82}$ = 133.2, P < 0.0001; drug, $F_{2,82}$ = 1.82, n.s.; interaction, $F_{4,82}$ = 1.19, n.s.] (Fig. 1B; see fig. S1 for intertrial interval). Locomotor activity and shock reactivity were identical in all groups, ruling out indirect effects on sensorimotor processes (figs. S2 and S3). To determine whether the drugs affected acquisition, consolidation, or expression of context fear, we injected Cbx and Meflo posttraining, pretest, or both pretraining and pretest (Fig. 1E). Posttraining injections of Cbx and Meflo attenuated later context fear expression (one-way ANOVA, $F_{2,25}$ = 9.78, P < 0.001) (Fig. 1G). Pretest manipulations did not affect fear expression (Fig. 1G), indicating that once context memories were consolidated, they became resistant to disruption of electrical communication. The deficit seen in the pretraining group was maintained in the pretraining and pretest group, ruling out a state-dependent effect (Fig. 1G).

Because the drugs prevented context fear learning, tone fear may have been acquired in a context-independent manner and thus might be more susceptible to extinction (*13*). Rats were fear-conditioned as previously described and were given 2 days of extinction training in a novel context (Fig. 1F). On extinction day 1, all groups initially exhibited similar tone fear responses (Fig. 1H). However, 40 tones across two extinction days were required for the vehicle group to fully extinguish, whereas in the drug groups, one session was sufficient to induce an accelerated decrease in freezing [3 (drug) × 4 (trial block) ANOVA; drug, $F_{2,140}$ = 10.86, P = 0.0002; block, $F_{4,140}$ = 75.15, P < 0.0001; interaction, $F_{8,140}$ = 6.291, P < 0.0001] (Fig. 1H). When tested for extinction memory on extinction day 2, freezing in the Cbx and Meflo groups had already reached baseline levels (percent time spent freezing, average of the first four tone presentations: Cbx, 21.6 ± 6.1; Meflo, 18.5 ± 4.9; vehicle, 66.7 ± 7.4; P < 0.0001) (Fig. 1H).

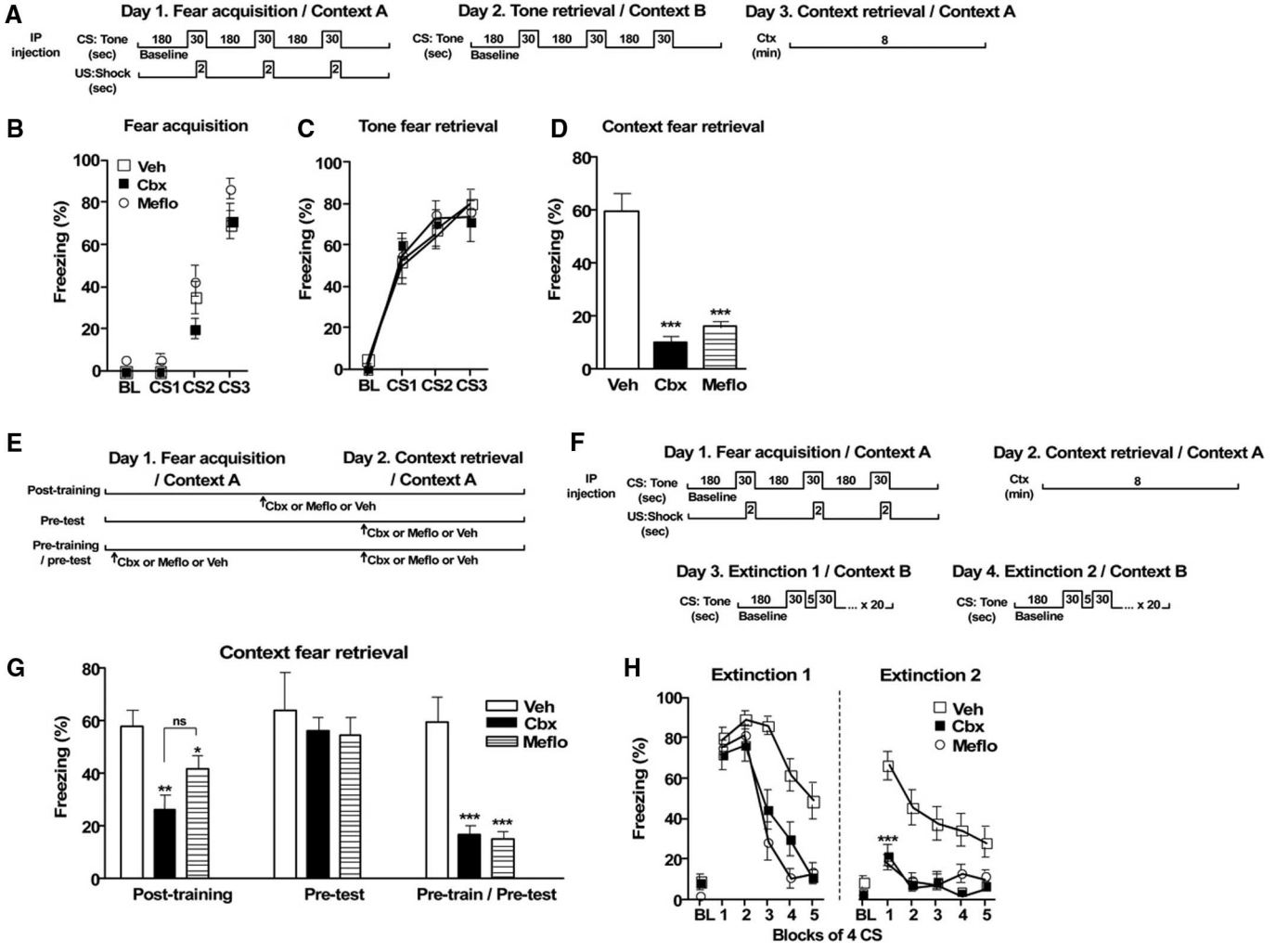

Fig. 1. Systemic blockade of gap junctions impairs context-dependent memories and accelerates extinction. (**A**) Experimental design. (**B**) Fear acquisition [vehicle (Veh), n = 20; Cbx, n = 13; Meflo, n = 11]. (**C**) Tone fear memory was intact in all groups (Veh, n = 14; Cbx, n = 13; Meflo, n = 11). (**D**) Context fear retrieval was impaired in the drug groups (Veh, n = 14; Cbx, n = 13; Meflo, n = 11). (**E**) Experimental design for posttraining, pretraining, and dual pretraining and pretest injections. (**F**) Posttraining injections of Cbx and Meflo impaired consolidation of context fear memories (Veh, n = 10; Cbx, n = 10; Meflo, n = 8). Pretesting injections did not affect context fear retrieval (Veh, n = 12; Cbx, n = 8; Meflo, n = 6). Dual pretraining and pretesting injections showed no drug state dependency (Veh, n = 10; Cbx, n = 6; Meflo, n = 6). (**G**) Experimental design for extinction experiment. (**H**) Cbx and Meflo groups exhibited rapid reduction in freezing on days 1 and 2 (Veh, n = 15; Cbx, n = 13; Meflo, n = 10). Between-group differences: *P < 0.05, **P < 0.01, ***P < 0.001; n.s., not significant. Results are presented as means ± SEM. BL, baseline; CS, conditional stimulus; Ctx, context; US, unconditional stimulus. Contexts A and B refer to two different conditioning chambers.

Given that extinction is context-dependent, it is possible that the accelerated loss of tone fear resulted from impaired contextual learning and that the drugs' effects were mediated by the dorsal hippocampus (DH) (*14*). Thus, we blocked gap junctions specifically in the DH with Cbx, Meflo, and the mimetic connexin peptides GAP27 and GAP36 (*15*) (Fig. 2), which were injected at both pretraining and posttraining to ensure blockade during acquisition and consolidation. Similar to systemic injections, DH microinfusions reduced context fear memories ($F_{4,51} = 17.14$, $P < 0.0001$) (Fig. 2, A and B) and accelerated extinction [5 (drug) × 4 (trial block) ANOVA; drug, $F_{4,172} = 10.74$, $P = 0.0001$; block, $F_{4,172} = 121.7$, $P < 0.0001$; interaction, $F_{16,172} = 4.35$, $P < 0.0001$] (Fig. 2C). Post hoc tests revealed a significant reduction in context fear and facilitated extinction in all drug groups, with no differences between peptides and blockers (Fig. 2, B and C). When animals were reconditioned to a white noise in a novel context and tested for context fear the next day, all groups exhibited similar amounts of context freezing (fig. S5), ruling out permanent DH damage from the infusion.

Because fear renewal is also susceptible to DH manipulations (*16*), we hypothesized that contextual information encoded in the presence of gap junction blockers and the subsequent enhancement of extinction might prevent renewal of fear. As predicted, fear renewal measured in the original context was compromised in the drug and peptide groups ($F_{4,37} = 8.82$, $P < 0.0001$) (Fig. 2, A and D). To distinguish between an effect on contextual encoding proper and encoding in the presence of an aversive experience, we used the immediate shock deficit paradigm (*17*, *18*). Cbx or GAP36 infused before a shock-free preexposure session abolished the preexposure's ability to rescue the immediate shock deficit ($F_{3,20} = 9.8$, $P < 0.0001$) (Fig. 2, E and F).

If electrical synapses in the DH are required to form and consolidate contextual representations, then rats may not recognize a context previously explored under blockade of gap junctions and treat that environment as novel. We thus examined c-fos expression as an indication of context familiarity (*19*, *20*). Rats exposed to the testing context for the first time served as a novel environment control ("1st expo" group). In both the CA1 and CA3 regions of the hippocampus, c-fos expression was higher in the vehicle group than in the home cage controls (HC) but was lower than in animals placed in the context for the first time (1st expo, Fig. 3). However, in rats initially trained under Cbx, c-fos expression was similar to the 1st expo but higher than the vehicle and HC groups (one-way ANOVA on vehicle, CBX, 1st expo, and HC, per region: CA1, $F_{3,12} = 65.96$, $P < 0.0001$; CA3, $F_{3,12} = 31.84$, $P < 0.0001$) (Fig. 3). The 1st expo group did not receive any aversive experience in that context; this suggests that rats in the Cbx group, when reintroduced to the training context, exhibited neuronal activity similar to a first-time contextual exposure. Contrasting results were found in the basolateral amygdala (BLA), the site where context-shock associations are formed (*21*) ($F_{3,13} = 38.64$, $P < 0.0001$). Post hoc tests indicated reduced c-fos expression in both the Cbx and 1st expo groups relative to the vehicle group. There were no differences between the Cbx and 1st expo groups. However, the Cbx group showed higher c-fos

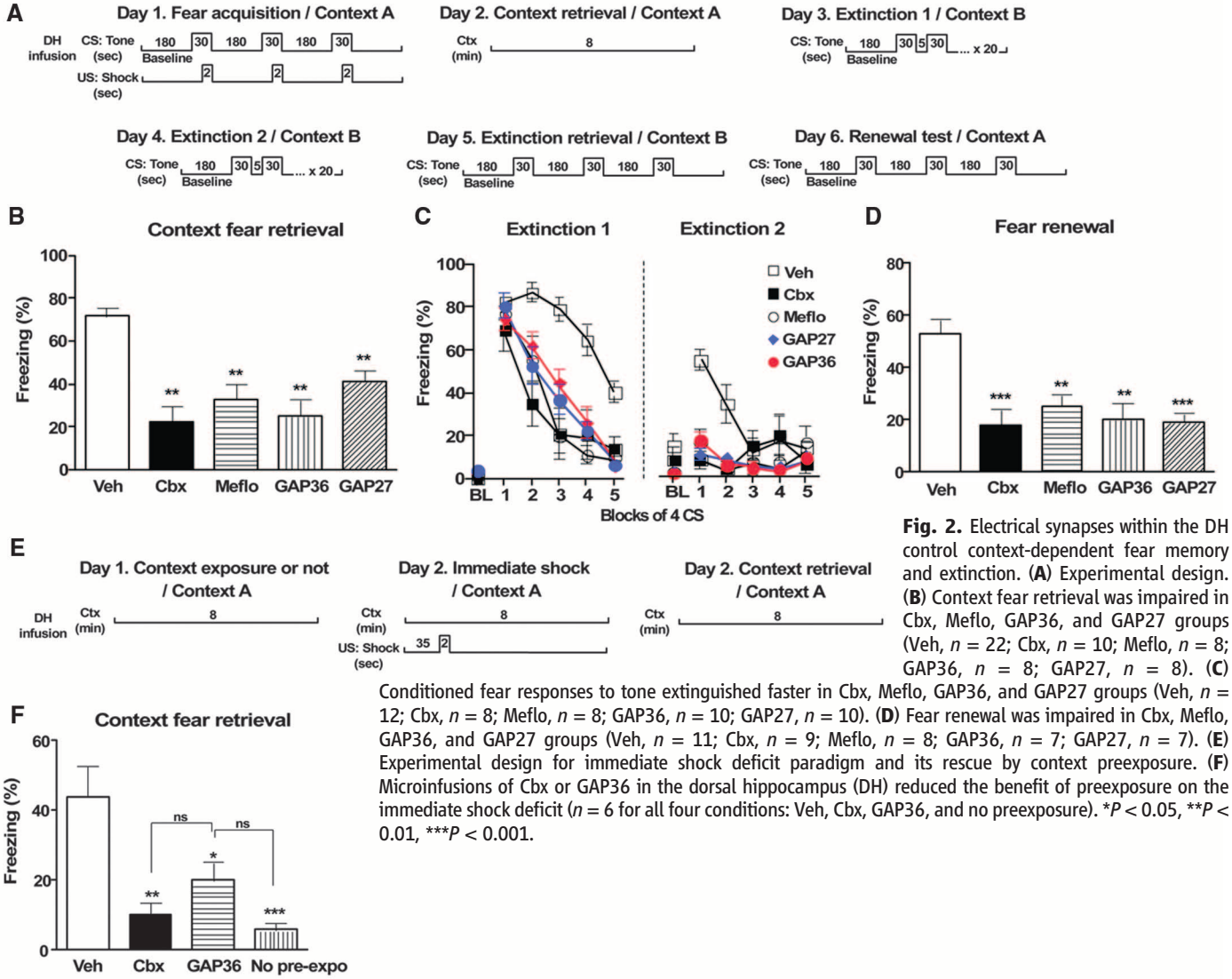

Fig. 2. Electrical synapses within the DH control context-dependent fear memory and extinction. (**A**) Experimental design. (**B**) Context fear retrieval was impaired in Cbx, Meflo, GAP36, and GAP27 groups (Veh, $n = 22$; Cbx, $n = 10$; Meflo, $n = 8$; GAP36, $n = 8$; GAP27, $n = 8$). (**C**) Conditioned fear responses to tone extinguished faster in Cbx, Meflo, GAP36, and GAP27 groups (Veh, $n = 12$; Cbx, $n = 8$; Meflo, $n = 8$; GAP36, $n = 10$; GAP27, $n = 10$). (**D**) Fear renewal was impaired in Cbx, Meflo, GAP36, and GAP27 groups (Veh, $n = 11$; Cbx, $n = 9$; Meflo, $n = 8$; GAP36, $n = 7$; GAP27, $n = 7$). (**E**) Experimental design for immediate shock deficit paradigm and its rescue by context preexposure. (**F**) Microinfusions of Cbx or GAP36 in the dorsal hippocampus (DH) reduced the benefit of preexposure on the immediate shock deficit ($n = 6$ for all four conditions: Veh, Cbx, GAP36, and no preexposure). *$P < 0.05$, **$P < 0.01$, ***$P < 0.001$.

expression relative to HC rats, whereas the 1st expo group did not. To distinguish the effects of blocking electrical synapses on contextual encoding versus context-shock associations, we repeated the experiment with shock-free context exposure (fig. S7). Again, c-fos expression was higher in both the Cbx and 1st expo groups in the CA1 and CA3 regions relative to the vehicle group (one-way ANOVA on Veh, CBX, and 1st expo, per region: CA1, $F_{2,9} = 6.49$, $P < 0.0001$; CA3, $F_{2,9} = 5.90$, $P < 0.05$) (fig. S7), confirming an effect on the context encoding.

GABAergic interneurons expressing Cx36 in the DH and medial septum drive hippocampal theta rhythms previously linked to investigatory behaviors (*22*–*25*). We recorded theta electroencephalograms (EEGs) from the CA1 of freely moving rats after Cbx intracerebroventricular (icv) infusions, which reproduced the behavioral effects on contextual memories (fig. S8). Cbx specifically disrupted theta oscillations (Fig. 4, A and B). A 3 (speed) × 2 (Cbx, pre versus post) ANOVA revealed that blocking electrical synapses attenuated the power of theta rhythms (main effect of Cbx: $F_{1,5} = 25.6$, $P < 0.005$) (Fig. 4C) but did not disrupt the normal positive correlation between theta power and running speed (main effect of speed: $F_{2,10} = 5.78$, $P < 0.05$; speed × Cbx interaction: $F_{2,10} = 0.08$, n.s.). Theta rhythm frequency was also increased after Cbx ($F_{1,3} = 11.54$, $P < 0.05$) (Fig. 4D), but the normal positive correlation between theta frequency and running speed was unaffected (main effect of speed: $F_{2,6} = 5.54$, $P < 0.05$; speed × Cbx interaction: $F_{2,6} = 0.98$, n.s.). Cbx had no effect on time spent running ($F_{1,5} = 0.17$, n.s.) or on mean running speed recorded at each frequency (Fig. 4D). Vehicle infusions did not affect theta power ($F_{1,5} = 5.25$, n.s.) or frequency ($F_{1,5} = 0.03$, n.s.).

Our c-fos analyses (Fig. 3), the immediate shock deficit experiment, and the disruption of theta rhythms during novel exploration (Fig. 4) all suggest that blocking DH gap junctions disrupts contextual encoding and thereby prevents contextual fear learning (Figs. 1 and 2). Considering that place cells fire in relation to the theta cycle (*24*), disrupting theta may abolish the temporal code for that location. Furthermore, blocking gap junctions in the DH before or during the consolidation of aversive experiences may disrupt theta-band synchronization within the amygdalohippocampal network required for the consolidation of fear memories (*26*).

Pretraining blockade of gap junctions in the DH spared tone-shock learning but rendered tone fear memories more prone to extinction and impaired renewal (Fig. 2). This suggests that extinction learning was facilitated by a lack of contextualization of the tone-shock memory. Our findings not only provide new evidence for a functional role for electrical synapses in mechanisms underlying fear learning

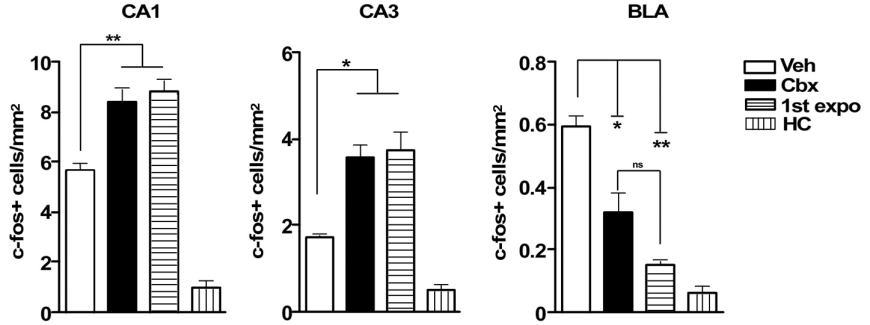

Fig. 3. Blocking of pretraining at gap junctions affects c-fos expression within the amygdalohippocampal network, as shown by quantification of c-fos expression in CA1, CA3, and BLA. *$P < 0.05$, **$P < 0.01$.

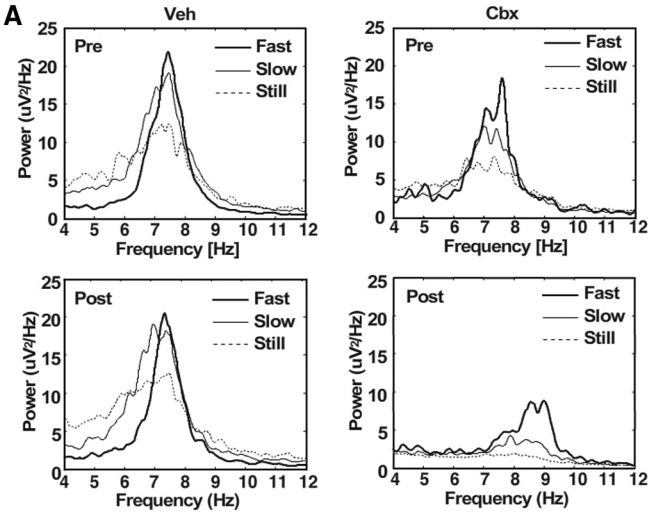

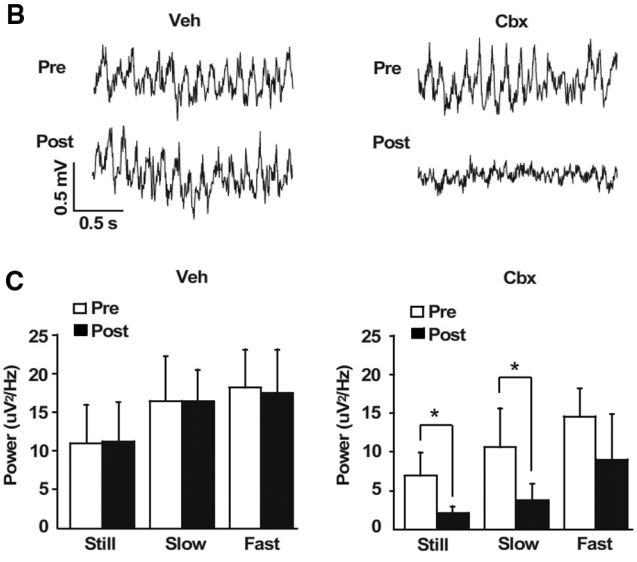

Fig. 4. Blocking gap junctions alters hippocampal theta EEG. (**A**) Averaged power spectra of hippocampal EEG in the theta band (4 to 12 Hz). (**B**) Representative example of EEG traces. (**C**) Height of peak theta power was reduced by icv microinfusions. (**D**) Central frequency of peak theta (*y* axis) as a function of icv CBX or Veh infusions and running speed ($n = 6$). *$P < 0.05$, **$P < 0.01$, †$P < 0.1$ (trend).

and memory in the adult mammalian brain, but may also point toward new therapeutic avenues for the treatment of trauma and anxiety disorders.

References and Notes

1. M. V. Bennett, R. S. Zukin, *Neuron* **41**, 495 (2004).
2. G. Buzsáki, *Neuron* **31**, 342 (2001).
3. B. W. Connors, M. A. Long, *Annu. Rev. Neurosci.* **27**, 393 (2004).
4. D. F. Condorelli, N. Belluardo, A. Trovato-Salinaro, G. Mudò, *Brain Res. Brain Res. Rev.* **32**, 72 (2000).
5. J. F. Muller, F. Mascagni, A. J. McDonald, *J. Neurosci.* **25**, 7366 (2005).
6. D. L. Buhl, K. D. Harris, S. G. Hormuzdi, H. Monyer, G. Buzsáki, *J. Neurosci.* **23**, 1013 (2003).
7. C. Frisch *et al.*, *Behav. Brain Res.* **157**, 177 (2005).
8. C. Alev *et al.*, *Proc. Natl. Acad. Sci. U.S.A.* **105**, 20964 (2008).
9. C. E. Landisman *et al.*, *J. Neurosci.* **22**, 1002 (2002).
10. D. G. Placantonakis, A. A. Bukovsky, S. A. Aicher, H. P. Kiem, J. P. Welsh, *J. Neurosci.* **26**, 5008 (2006).
11. R. J. Thompson, N. Zhou, B. A. MacVicar, *Science* **312**, 924 (2006).
12. S. J. Cruikshank *et al.*, *Proc. Natl. Acad. Sci. U.S.A.* **101**, 12364 (2004).
13. J. J. Quinn, H. M. Wied, Q. D. Ma, M. R. Tinsley, M. S. Fanselow, *Hippocampus* **18**, 640 (2008).
14. S. Maren, G. J. Quirk, *Nat. Rev. Neurosci.* **5**, 844 (2004).
15. W. H. Evans, L. Leybaert, *Cell Commun. Adhes.* **14**, 265 (2007).
16. M. E. Bouton, R. F. Westbrook, K. A. Corcoran, S. Maren, *Biol. Psychiatry* **60**, 352 (2006).
17. M. S. Fanselow, *Behav. Brain Res.* **110**, 73 (2000).
18. D. L. Stote, M. S. Fanselow, *Behav. Neurosci.* **118**, 253 (2004).
19. A. Sheth, S. Berretta, N. Lange, H. Eichenbaum, *Hippocampus* **18**, 169 (2008).
20. A. Vazdarjanova, J. F. Guzowski, *J. Neurosci.* **24**, 6489 (2004).
21. M. S. Fanselow, J. E. LeDoux, *Neuron* **23**, 229 (1999).
22. G. Buzsáki, *Neuron* **33**, 325 (2002).
23. G. Buzsáki, *Hippocampus* **15**, 827 (2005).
24. J. J. Kim *et al.*, *Proc. Natl. Acad. Sci. U.S.A.* **104**, 18297 (2007).
25. T. F. Freund, M. Antal, *Nature* **336**, 170 (1988).
26. T. Seidenbecher, T. R. Laxmi, O. Stork, H. C. Pape, *Science* **301**, 846 (2003).

27. Supported by NIMH grant RO1-MH62122 and P01NS35985 (M.S.F.), Swiss National Fund grant PA00A-115367 (S.B.), and NIMH grant RO1-MH079511 (H.T.B.).

Supporting Online Material

www.sciencemag.org/cgi/content/full/331/6013/87/DC1
Materials and Methods
Figs. S1 to S8
References

15 June 2010; accepted 25 November 2010
10.1126/science.1193785

Structure of Precursor-Bound NifEN: A Nitrogenase FeMo Cofactor Maturase/Insertase

Jens T. Kaiser,[1]* Yilin Hu,[2]* Jared A. Wiig,[2] Douglas C. Rees,[1,3]† Markus W. Ribbe[2]†

NifEN plays an essential role in the biosynthesis of the nitrogenase iron-molybdenum (FeMo) cofactor (M cluster). It is an $\alpha_2\beta_2$ tetramer that is homologous to the catalytic molybdenum-iron (MoFe) protein (NifDK) component of nitrogenase. NifEN serves as a scaffold for the conversion of an iron-only precursor to a matured form of the M cluster before delivering the latter to its target location within NifDK. Here, we present the structure of the precursor-bound NifEN of *Azotobacter vinelandii* at 2.6 angstrom resolution. From a structural comparison of NifEN with des-M-cluster NifDK and holo NifDK, we propose similar pathways of cluster insertion for the homologous NifEN and NifDK proteins.

Nitrogenase is a complex metalloenzyme that catalyzes a key step in the global nitrogen cycle: the reduction of atmospheric dinitrogen to bioavailable ammonia. The Mo-dependent nitrogenase is a two-component system, in which the Fe protein (NifH) mediates the adenosine triphosphate–dependent transfer of electrons to the catalytic MoFe protein (NifDK) during substrate turnover (*1*). The MoFe protein is an $\alpha_2\beta_2$ tetramer that contains two unusual metalloclusters per αβ dimer, the P cluster and the M cluster. The P cluster is an [8Fe-7S] cluster at the α/β-subunit interface, coordinated by three Cys ligands from the α subunit and three Cys ligands from the β subunit. The M cluster (or FeMo cofactor) is a [Mo-7Fe-9S-X-homocitrate] cluster (where X = C, N, or O) located within the α subunit, coordinated by a His ligand at the Mo end and a Cys ligand at the opposite Fe atom, with a Lys residue binding to the homocitrate entity (*2*, *3*). During catalysis, the P cluster is thought to mediate the electron flow from the Fe protein to the M cluster, where substrate reduction occurs.

NifEN is an essential player in M-cluster biosynthesis (*4*–*6*). It presumably receives a precursor form of the M cluster from NifB and hosts the conversion of this precursor to a mature M cluster before delivering the latter to the MoFe protein (*4*, *5*). A role for NifEN in FeMo cofactor biosynthesis was initially hypothesized based on a considerable degree of similarity between the primary sequences of NifEN and MoFe protein, suggesting that NifEN may contain P- and M-like clusters (*6*). Subsequently, the NifEN-associated clusters were identified through the biochemical and spectroscopic analyses of three forms of NifEN. The first, apo NifEN, is free of any cofactor species and contains a [4Fe-4S] cluster in place of the [8Fe-7S] P cluster (*7*). The second, NifEN, contains, in addition to the [4Fe-4S] cluster, an all-iron precursor that closely resembles the Fe/S core of the M cluster (*8*). The third, holo NifEN, contains a mature M cluster and the [4Fe-4S] cluster (*9*). NifEN could be readily converted to holo NifEN by Fe protein-mediated insertion of Mo and homocitrate into the precursor (*10*), and holo NifEN could directly serve as a cofactor donor for the apo MoFe protein (*11*). These observations not only establish the role of NifEN in cofactor biosynthesis but also illustrate the dynamic nature of the cofactor site in NifEN during the assembly process. However, the mechanistic details of the biosynthetic events on NifEN have remained unclear without structural information on this protein. In this study, the structure of the precursor-bound NifEN of *Azotobacter vinelandii* has been solved to 2.6 Å resolution (*12*). From a structural comparison of NifEN with des-M-cluster MoFe protein (apo NifDK) (*11*) and holo MoFe protein (NifDK) (*2*, *3*), we propose similar pathways of cluster insertion for the homologous NifEN and NifDK proteins.

The crystal structure determination of NifEN is summarized in tables S1 and S2. Like the $\alpha_2\beta_2$-tetrameric NifDK, NifEN consists of a pair of αβ dimers that are related by a molecular twofold rotation axis (Fig. 1A). The α and β subunits of NifEN, like those of NifDK and apo NifDK, are composed of three domains each—αI, αII, and αIII, and βI, βII, and βIII, respectively. All domains of NifEN, as for NifDK and apo NifDK, are organized around a common core of a four-stranded, parallel β sheet flanked with α helices and additional β strands (*13*). Moreover, NifEN contains two types of clusters that correspond to the P and M clusters in NifDK: one, termed the O cluster, is a [4Fe-4S] cluster that is coordinated by $Cys^{\alpha37}$, $Cys^{\alpha62}$, $Cys^{\alpha124}$, and $Cys^{\beta44}$ at the same site in the α/β-subunit interface as the P cluster; the other, termed the L cluster, is an iron-only precursor form of the M cluster that is at least ligated by $Cys^{\alpha25}$ at one end (Fig. 1B) (*14*). Although the electron density is not sufficiently well resolved to unambiguously establish the structure of the L cluster, the shape and extent of the density is compatible with the core geometry of the M cluster and, therefore, consistent with the previously proposed 8Fe model (*8*) of this M-cluster precursor (Fig. 1B).

Strikingly, although the L and M clusters are both positioned at the junction between the αI,

[1]Division of Chemistry and Chemical Engineering, California Institute of Technology, Mail Code 114-96, Pasadena, CA 91125, USA. [2]Department of Molecular Biology and Biochemistry, University of California, Irvine, CA 92697–3900, USA. [3]Howard Hughes Medical Institute, California Institute of Technology, Mail Code 114-96, Pasadena, CA 91125, USA.

*These authors contributed equally to this work.
†To whom correspondence should be addressed. E-mail: dcrees@caltech.edu (D.C.R.); mribbe@uci.edu (M.W.R.)

and memory in the adult mammalian brain, but may also point toward new therapeutic avenues for the treatment of trauma and anxiety disorders.

References and Notes

1. M. V. Bennett, R. S. Zukin, *Neuron* **41**, 495 (2004).
2. G. Buzsáki, *Neuron* **31**, 342 (2001).
3. B. W. Connors, M. A. Long, *Annu. Rev. Neurosci.* **27**, 393 (2004).
4. D. F. Condorelli, N. Belluardo, A. Trovato-Salinaro, G. Mudò, *Brain Res. Brain Res. Rev.* **32**, 72 (2000).
5. J. F. Muller, F. Mascagni, A. J. McDonald, *J. Neurosci.* **25**, 7366 (2005).
6. D. L. Buhl, K. D. Harris, S. G. Hormuzdi, H. Monyer, G. Buzsáki, *J. Neurosci.* **23**, 1013 (2003).
7. C. Frisch *et al.*, *Behav. Brain Res.* **157**, 177 (2005).
8. C. Alev *et al.*, *Proc. Natl. Acad. Sci. U.S.A.* **105**, 20964 (2008).
9. C. E. Landisman *et al.*, *J. Neurosci.* **22**, 1002 (2002).
10. D. G. Placantonakis, A. A. Bukovsky, S. A. Aicher, H. P. Kiem, J. P. Welsh, *J. Neurosci.* **26**, 5008 (2006).
11. R. J. Thompson, N. Zhou, B. A. MacVicar, *Science* **312**, 924 (2006).
12. S. J. Cruikshank *et al.*, *Proc. Natl. Acad. Sci. U.S.A.* **101**, 12364 (2004).
13. J. J. Quinn, H. M. Wied, Q. D. Ma, M. R. Tinsley, M. S. Fanselow, *Hippocampus* **18**, 640 (2008).
14. S. Maren, G. J. Quirk, *Nat. Rev. Neurosci.* **5**, 844 (2004).
15. W. H. Evans, L. Leybaert, *Cell Commun. Adhes.* **14**, 265 (2007).
16. M. E. Bouton, R. F. Westbrook, K. A. Corcoran, S. Maren, *Biol. Psychiatry* **60**, 352 (2006).
17. M. S. Fanselow, *Behav. Brain Res.* **110**, 73 (2000).
18. D. L. Stote, M. S. Fanselow, *Behav. Neurosci.* **118**, 253 (2004).
19. A. Sheth, S. Berretta, N. Lange, H. Eichenbaum, *Hippocampus* **18**, 169 (2008).
20. A. Vazdarjanova, J. F. Guzowski, *J. Neurosci.* **24**, 6489 (2004).
21. M. S. Fanselow, J. E. LeDoux, *Neuron* **23**, 229 (1999).
22. G. Buzsáki, *Neuron* **33**, 325 (2002).
23. G. Buzsáki, *Hippocampus* **15**, 827 (2005).
24. J. J. Kim *et al.*, *Proc. Natl. Acad. Sci. U.S.A.* **104**, 18297 (2007).
25. T. F. Freund, M. Antal, *Nature* **336**, 170 (1988).
26. T. Seidenbecher, T. R. Laxmi, O. Stork, H. C. Pape, *Science* **301**, 846 (2003).

27. Supported by NIMH grant RO1-MH62122 and P01NS35985 (M.S.F.), Swiss National Fund grant PA00A-115367 (S.B.), and NIMH grant RO1-MH079511 (H.T.B.).

Supporting Online Material

www.sciencemag.org/cgi/content/full/331/6013/87/DC1
Materials and Methods
Figs. S1 to S8
References

15 June 2010; accepted 25 November 2010
10.1126/science.1193785

Structure of Precursor-Bound NifEN: A Nitrogenase FeMo Cofactor Maturase/Insertase

Jens T. Kaiser,[1]* Yilin Hu,[2]* Jared A. Wiig,[2] Douglas C. Rees,[1,3]† Markus W. Ribbe[2]†

NifEN plays an essential role in the biosynthesis of the nitrogenase iron-molybdenum (FeMo) cofactor (M cluster). It is an $\alpha_2\beta_2$ tetramer that is homologous to the catalytic molybdenum-iron (MoFe) protein (NifDK) component of nitrogenase. NifEN serves as a scaffold for the conversion of an iron-only precursor to a matured form of the M cluster before delivering the latter to its target location within NifDK. Here, we present the structure of the precursor-bound NifEN of *Azotobacter vinelandii* at 2.6 angstrom resolution. From a structural comparison of NifEN with des-M-cluster NifDK and holo NifDK, we propose similar pathways of cluster insertion for the homologous NifEN and NifDK proteins.

Nitrogenase is a complex metalloenzyme that catalyzes a key step in the global nitrogen cycle: the reduction of atmospheric dinitrogen to bioavailable ammonia. The Mo-dependent nitrogenase is a two-component system, in which the Fe protein (NifH) mediates the adenosine triphosphate–dependent transfer of electrons to the catalytic MoFe protein (NifDK) during substrate turnover (*1*). The MoFe protein is an $\alpha_2\beta_2$ tetramer that contains two unusual metalloclusters per αβ dimer, the P cluster and the M cluster. The P cluster is an [8Fe-7S] cluster at the α/β-subunit interface, coordinated by three Cys ligands from the α subunit and three Cys ligands from the β subunit. The M cluster (or FeMo cofactor) is a [Mo-7Fe-9S-X-homocitrate] cluster (where X = C, N, or O) located within the α subunit, coordinated by a His ligand at the Mo end and a Cys ligand at the opposite Fe atom, with a Lys residue binding to the homocitrate entity (*2*, *3*). During catalysis, the P cluster is thought to mediate the electron flow from the Fe protein to the M cluster, where substrate reduction occurs.

NifEN is an essential player in M-cluster biosynthesis (*4*–*6*). It presumably receives a precursor form of the M cluster from NifB and hosts the conversion of this precursor to a mature M cluster before delivering the latter to the MoFe protein (*4*, *5*). A role for NifEN in FeMo cofactor biosynthesis was initially hypothesized based on a considerable degree of similarity between the primary sequences of NifEN and MoFe protein, suggesting that NifEN may contain P- and M-like clusters (*6*). Subsequently, the NifEN-associated clusters were identified through the biochemical and spectroscopic analyses of three forms of NifEN. The first, apo NifEN, is free of any cofactor species and contains a [4Fe-4S] cluster in place of the [8Fe-7S] P cluster (*7*). The second, NifEN, contains, in addition to the [4Fe-4S] cluster, an all-iron precursor that closely resembles the Fe/S core of the M cluster (*8*). The third, holo NifEN, contains a mature M cluster and the [4Fe-4S] cluster (*9*). NifEN could be readily converted to holo NifEN by Fe protein-mediated insertion of Mo and homocitrate into the precursor (*10*), and holo NifEN could directly serve as a cofactor donor for the apo MoFe protein (*11*). These observations not only establish the role of NifEN in cofactor biosynthesis but also illustrate the dynamic nature of the cofactor site in NifEN during the assembly process. However, the mechanistic details of the biosynthetic events on NifEN have remained unclear without structural information on this protein. In this study, the structure of the precursor-bound NifEN of *Azotobacter vinelandii* has been solved to 2.6 Å resolution (*12*). From a structural comparison of NifEN with des-M-cluster MoFe protein (apo NifDK) (*11*) and holo MoFe protein (NifDK) (*2*, *3*), we propose similar pathways of cluster insertion for the homologous NifEN and NifDK proteins.

The crystal structure determination of NifEN is summarized in tables S1 and S2. Like the $\alpha_2\beta_2$-tetrameric NifDK, NifEN consists of a pair of αβ dimers that are related by a molecular twofold rotation axis (Fig. 1A). The α and β subunits of NifEN, like those of NifDK and apo NifDK, are composed of three domains each—αI, αII, and αIII, and βI, βII, and βIII, respectively. All domains of NifEN, as for NifDK and apo NifDK, are organized around a common core of a four-stranded, parallel β sheet flanked with α helices and additional β strands (*13*). Moreover, NifEN contains two types of clusters that correspond to the P and M clusters in NifDK: one, termed the O cluster, is a [4Fe-4S] cluster that is coordinated by $Cys^{\alpha37}$, $Cys^{\alpha62}$, $Cys^{\alpha124}$, and $Cys^{\beta44}$ at the same site in the α/β-subunit interface as the P cluster; the other, termed the L cluster, is an iron-only precursor form of the M cluster that is at least ligated by $Cys^{\alpha25}$ at one end (Fig. 1B) (*14*). Although the electron density is not sufficiently well resolved to unambiguously establish the structure of the L cluster, the shape and extent of the density is compatible with the core geometry of the M cluster and, therefore, consistent with the previously proposed 8Fe model (*8*) of this M-cluster precursor (Fig. 1B).

Strikingly, although the L and M clusters are both positioned at the junction between the αI,

[1]Division of Chemistry and Chemical Engineering, California Institute of Technology, Mail Code 114-96, Pasadena, CA 91125, USA. [2]Department of Molecular Biology and Biochemistry, University of California, Irvine, CA 92697–3900, USA. [3]Howard Hughes Medical Institute, California Institute of Technology, Mail Code 114-96, Pasadena, CA 91125, USA.

*These authors contributed equally to this work.
†To whom correspondence should be addressed. E-mail: dcrees@caltech.edu (D.C.R.); mribbe@uci.edu (M.W.R.)

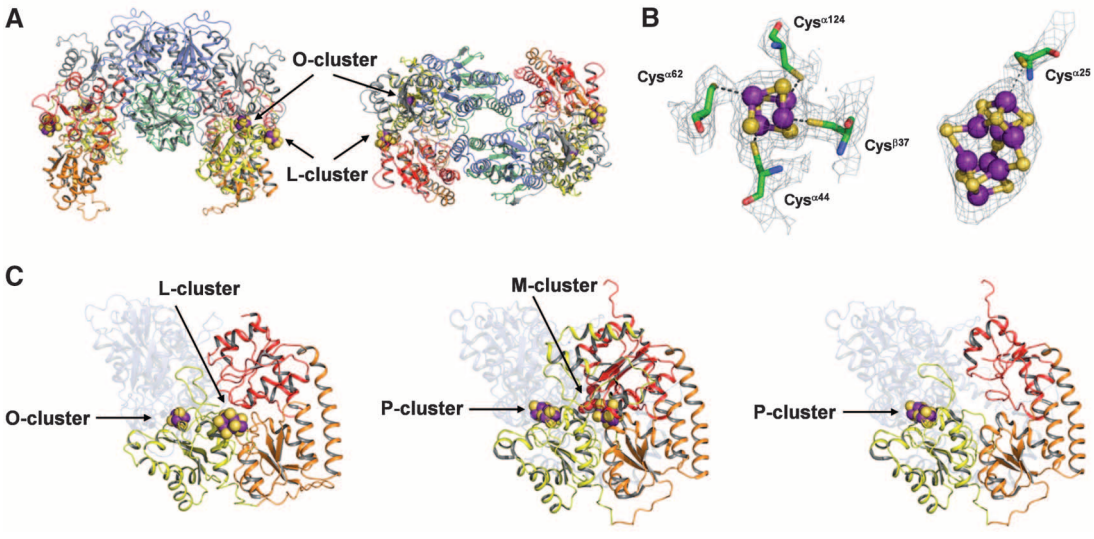

Fig. 1. (**A**) The structure of the NifEN tetramer with the molecular twofold axis oriented vertically (left) and along the viewing direction (right). The domains of the α subunits are colored yellow (αI), orange (αII), and red (αIII); and the domains of β subunits are colored gray (βI), blue (βII), and green (βIII). The L cluster (precursor of M cluster) and O cluster ([4Fe-4S] cluster) are illustrated as space-filling models, with atoms colored as follows: Fe, purple; S, yellow. (**B**) Structures and ligands of O cluster (left) and L cluster (right) overlaid with electron density maps. Both clusters are illustrated as ball-and-stick models, whereas the ligands are shown in stick presentation. Additional L-cluster ligands may be present (*14*). The atoms are colored as follows: Fe, purple; S, yellow; O, red; C, green; N, blue. The structure of L cluster overlaid with anomalous difference electron density map is shown in fig. S1. (**C**) Structures of the αβ pairs of NifEN (left), NifDK (middle, PDB entry 1M1N), and apo NifDK (right, PDB entry 1L5H). The α subunits are presented in the foreground, and the β subunits are rendered transparent in the background. The domains of the subunits in all three proteins are colored as in (A). All clusters are illustrated as space-filling models, with atoms colored as follows: Fe, purple; S, yellow; O, red; C, gray. The Mo atom and the interstitial ligand of the M cluster are not visible.

αII, and αIII domains of their respective proteins, the L cluster of NifEN is nearly surface exposed, possibly shielded from solvent by only a small stretch of disordered polypeptide between residues α14 and α24. In contrast, the M cluster of NifDK occupies a buried site ~10 Å below the surface of the protein (*2*). Given the homology between NifEN and NifDK, it is possible that, after maturation, the M cluster is inserted into a site in NifEN that is analogous to its binding site in NifDK. Notably, the α subunit of NifEN assumes a conformation that is more "open" than that of NifDK (presumably corresponding to holo NifEN) yet less "open" than that of apo NifDK (presumably corresponding to apo NifEN), suggesting that the α subunit undergoes major structural rearrangements upon the maturation of the L cluster on NifEN (Fig. 1C). Consistent with this proposal, a comparison of the molecular surfaces of these proteins reveals the presence of a positively charged funnel in apo NifDK, which is closed in NifDK containing a buried M cluster (fig. S2). There is a similar accumulation of positive charges on the surface of NifEN; however, an insertion funnel could not be clearly defined, perhaps due to a partial closure of the entrance by docking of the L cluster (fig. S2). In contrast, the β subunits of the three proteins are similar in structure, except for the presence of an extended loop and an extra helix-turn-helix structure in the holo and apo NifDK (fig. S3).

The αI and αII domains of apo NifDK do not show notable C_α deviations from those of NifDK, except for a short loop (α49 to α52) that follows a disordered region (α1 to α48) at the N terminus of the protein (fig. S4A, top, and Fig. 2A, left). A similar loop (α24 to α27) at the N terminus of NifEN aligns more closely with the corresponding region in NifDK (fig. S4A, bottom, and Fig. 2A, right).

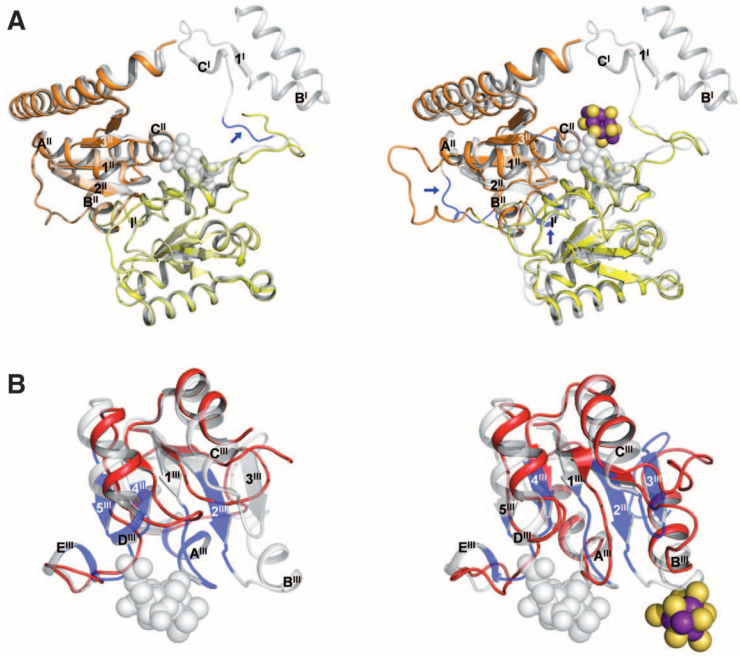

Fig. 2. (**A**) Superposition of αI and αII domains of apo NifDK and NifDK (left) and those of NifEN and NifDK (right). The domains of apo NifDK and NifEN are color coded as in Fig. 1. NifDK is shown in gray (transparent). Regions with substantial shifts in C_α positions are colored blue and indicated by arrows, and the secondary structural elements of these regions are labeled according to those in fig. S4A. The L cluster is illustrated as in Fig. 1. The M cluster is shown as a space-filling model in gray (transparent). PyMOL was used to prepare the figure (*19*). (**B**) Superposition of the αIII domains of apo NifDK and NifDK (left) and those of NifEN and NifDK (right). Apo NifDK and NifEN are colored red; NifDK is shown in gray (transparent). Regions with substantial shifts in C_α positions are colored blue. The secondary structural elements are labeled according to those shown in fig. S4A. The L cluster is illustrated as in Fig. 1. The M cluster is shown as a space-filling model in gray (transparent). PyMOL was used to prepare the figure (*19*).

Cys$^{\alpha 25}$, which ligates one of the terminal Fe atoms of the L cluster, is located near the end of this loop. Thus, this loop is likely oriented by docking of the L cluster on Cys$^{\alpha 25}$. Apart from this feature, NifEN contains an extra sequence (α187 to α192), which forms a larger external loop between the αI (α helix I^I) and αII (β strand 1^{II}) domains (fig. S4A and Fig. 2A). At the site that would contain a buried M

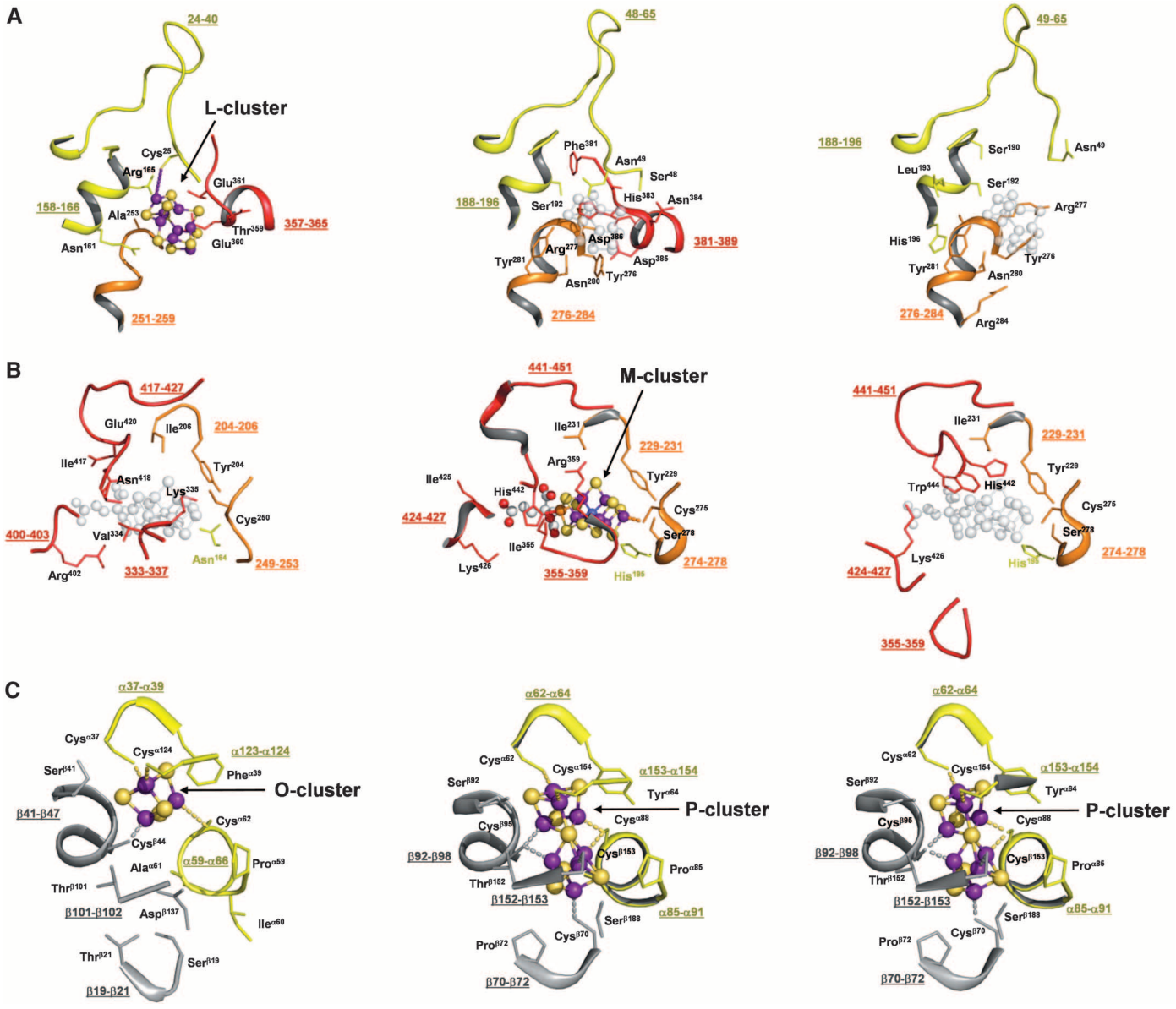

Fig. 3. Close-up of the protein environment surrounding the L cluster (**A**), M cluster (**B**), and O/P cluster (**C**) of NifEN (left), NifDK (middle), and apo NifDK (right), respectively. Shown are parts of the backbones (with numbers of residues underlined) and some side-chain residues in the close vicinity of the clusters. The domains of the α and β subunits are colored as in Fig. 1A. All clusters are illustrated as ball-and-stick models, with atoms colored as follows: Fe, purple; S, yellow; O, red; C, gray; Mo, orange; X, blue. The superimposed positions of the L cluster in NifDK and apo NifDK [(A), middle and right], and of the M cluster in NifEN and apo NifDK [(B), left and right], are indicated in gray (transparent). PyMOL was used to prepare the figure (*19*).

cluster in NifDK, the area surrounding the potential $Cys^{\alpha250}$ ligand (α248 to α252) features an α helix (C^{II}) that is shorter toward the N terminus, with an extended loop in its place that could add flexibility to the dynamic M-cluster site in NifEN (fig. S4A and Fig. 2A).

The αIII domain of apo NifDK shows substantial C_α deviations from that of NifDK in four distinct areas: a "lid loop" (α353 to α364), a disordered region (α381 to α407), and regions surrounding the homocitrate anchor (α421 to α428) and the histidine ligand (α436 to α446) of the M cluster (fig. S4B, top). By comparison, the αIII domain of NifEN shows C_α deviations from NifDK that are reminiscent of, yet much less substantial than, those of apo NifDK from NifDK (fig. S4B, bottom). The β-strands (1^{III}, 2^{III}, and 4^{III}) and α-helices (A^{III}, C^{III}, and D^{III}) of apo NifDK are considerably shortened and displaced from those of NifDK (Fig. 2B, left). These changes result in a major relocation of the lid loop and the adjacent (disordered) region in apo NifDK, which completely opens up the M-cluster site for cluster insertion (*11*). The same β-strands (1^{III}, 2^{III}, and 4^{III}) and α-helices (A^{III}, C^{III}, and D^{III}) in NifEN are shorter than those in NifDK; however, they are more extended and less displaced than those in apo NifDK, resulting in a conformation of NifEN intermediate between those of apo and holo NifDK (Fig. 2B, right). The changes of these structural elements, along with the structuring of α helix B^{III}, lead to the formation of an ordered, yet partially closed, M-cluster site in NifEN (Fig. 2B, right). In particular, the downwardly bent β-strand 1^{III} anchors the lid loop in a position close to that in NifDK, whereas β-strand 2^{III}, together with α helix B^{III}, extend toward the L cluster at the surface of the protein (Fig. 2B, right). Two β-strands (3^{III} and 5^{III}) and one α helix (E^{III}) are missing from the structures of both NifEN and apo NifDK (Fig. 2B). The presence of irregular loops in places of β-strand 3^{III} (which "hinges" the α helix B^{III} at the L-cluster site) and β strand 5^{III}/α helix E^{III} (which flank the Asn ligand at the M-cluster site) may

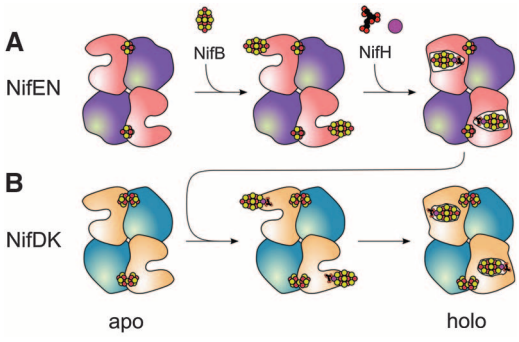

Fig. 4. Schematic presentation of the proposed biosynthesis events that occur on NifEN (**A**) and NifDK (**B**). (A) After the synthesis of an O-cluster–containing, yet L-cluster–deficient, apo NifEN (left), the L cluster is delivered from NifB to the entrance of the cluster insertion funnel in NifEN (middle). Subsequently, the Fe protein (NifH) inserts Mo and homocitrate into the L cluster, resulting in a matured form of the M cluster that is transferred to its binding site in NifEN (right). (B) NifDK first appears as a P-cluster–containing, yet M-cluster–deficient, apo form (left). The mature M cluster is then transferred from NifEN to the entrance of the cluster insertion funnel in NifDK upon direct protein-protein interactions (middle). Subsequently, the M cluster is inserted into its binding site in NifDK, leading to the formation of holo NifDK (right). The proposed biosynthetic events on NifEN parallel those on NifDK, which is consistent with the close similarities between the overall structure and the cluster topology of the two proteins. The presence of O cluster ([4Fe-4S]) and P cluster ([8Fe-7S]) in apo NifEN and apo NifDK, respectively, may further imply an evolutionary connection between the two proteins. It can be hypothesized that the P-cluster site evolved from the O-cluster site upon the acquisition of missing ligands, thereby accommodating a second [4Fe-4S] cluster at this site for the subsequent coupling of two [4Fe-4S] modules into a mature P cluster (*20*).

contribute to the conformational flexibility of the polypeptides surrounding the L- and M-cluster sites of NifEN, which could facilitate the transfer of the cluster from the L-cluster site to the M-cluster site upon maturation.

A closer examination of the L- and M-cluster sites in the three proteins provides additional insights into the pathway of M-cluster assembly. In all cases, an "L-cluster site" can be identified at the surface of the structure, located directly above the M-cluster site within the protein. The "L-cluster site" in apo NifDK is wide open, with a disordered region (α381 to α389) and a loop (α49 to α65) adjacent to $Cys^{\alpha45}$ shifted away from those in holo NifDK (Fig. 3A and fig. S5A). The corresponding regions in NifEN (α357 to α365 and α24 to α40) are ordered, suggesting a concerted action between the two regions upon the ligation of the L cluster to $Cys^{\alpha25}$ at the tip of the loop. The arrangement of the L-cluster site in NifEN is similar to that of the "L-cluster site" in NifDK; however, NifDK contains amino acids with bulky side chains (e.g., $Phe^{\alpha381}$, $His^{\alpha383}$, and $Tyr^{\alpha276}$) that close up the M-cluster site (located below the "L-cluster site"), whereas NifEN contains amino acids with small side chains (e.g., $Ala^{\alpha253}$ and $Ser^{\alpha251}$) that may provide the cluster with more freedom to move between the L and M sites during cluster assembly and delivery. A similar pattern is observed when the M-cluster sites of the three proteins are compared (Fig. 3B and fig. S5B). The M-cluster site of apo NifDK is opened by a substantial displacement of the lid loop (α355 to α359), whereas the corresponding loop in NifEN (α333 to α337) is positioned similarly to that in NifDK. Likewise, the likely ligands ($Asn^{\alpha418}$ and $Cys^{\alpha250}$) and homocitrate anchor ($Arg^{\alpha402}$) of the M cluster in NifEN occupy positions that are similar to those of the M cluster ($His^{\alpha442}$, $Cys^{\alpha275}$, and $Lys^{\alpha426}$) in NifDK. Despite these similarities, $Tyr^{\alpha444}$, which switches positions with $His^{\alpha442}$ and locks the M cluster in place in NifDK through its bulky side chain (*4*), is not present in NifEN. This could facilitate the eventual release of the cluster from the M-cluster site of NifEN and its subsequent delivery to the homologous M-cluster site in NifDK. In contrast, the O-cluster site in NifEN assumes a nearly identical conformation to the P-cluster sites in apo and holo NifDK, except for the presence of an incomplete complement of Cys ligands that only accommodates a [4Fe-4S] cluster (Fig. 3C).

Similar pathways of cluster insertion can be proposed for NifEN and NifDK on the basis of these structural analyses (Fig. 4). It involves the formation of an apo protein that contains an open cluster insertion funnel, the docking of the cluster at (or near) the entrance of the funnel, and the subsequent insertion of the cluster into the funnel. In the case of NifEN, the L cluster is delivered from NifB to the surface of apo NifEN, where it is poised to be transformed into a mature M cluster upon the insertion of Mo and homocitrate by NifH (Fig. 4A). The M cluster is then relocated from the surface to the binding site within NifEN. Interactions between NifEN and NifDK may cause conformational changes that release the M cluster and facilitate its movement back to the surface of NifEN. Subsequently, the M cluster is transferred to and incorporated into NifDK in a manner similar to the insertion of M cluster into NifEN; only the M cluster is securely locked at its binding site in this case (Fig. 4B). The coordination of the various cluster intermediates to cysteines located in loops ($Cys^{\alpha25}$ of NifEN and, potentially, the corresponding $Cys^{\alpha45}$ of NifDK) may serve to tether and facilitate efficient intermolecular transfer of these species without their escaping to the surrounding environment. Mechanistic parallels in this respect are evident between the functions of NifEN and metallochaperones for copper and other transition metals (*15*).

The presence of similar insertion funnels in these homologous proteins is further supported by the recently solved crystal structure of protochlorophyllide reductase (BchNB) (*16*, *17*). Responsible for the reduction of a specific double bond of protochlorophyllide (Pchlide), BchNB is an $\alpha_2\beta_2$ tetramer that assumes a conformation highly homologous to those of NifEN and NifDK (fig. S6). Moreover, it contains one [4Fe-4S] cluster and one Pchlide at locations similar to those of the O/P clusters and L/M clusters in NifEN and NifDK. Interestingly, based on their locations in the respective homologous proteins, the L cluster, M cluster, and Pchlide can be sequentially placed along the insertion funnel in apo NifDK (fig. S7). This observation supports the hypothesis that a common ancestral protein—which appears to have adapted to accommodate different ligands—gave rise to all of these homologous proteins (*18*).

References and Notes

1. B. K. Burgess, D. J. Lowe, *Chem. Rev.* **96**, 2983 (1996).
2. J. Kim, D. C. Rees, *Nature* **360**, 553 (1992).
3. O. Einsle *et al.*, *Science* **297**, 1696 (2002).
4. Y. Hu, A. W. Fay, C. C. Lee, J. Yoshizawa, M. W. Ribbe, *Biochemistry* **47**, 3973 (2008).
5. G. Schwarz, R. R. Mendel, M. W. Ribbe, *Nature* **460**, 839 (2009).
6. P. C. Dos Santos, D. R. Dean, Y. Hu, M. W. Ribbe, *Chem. Rev.* **104**, 1159 (2004).
7. Y. Hu, A. W. Fay, M. W. Ribbe, *Proc. Natl. Acad. Sci. U.S.A.* **102**, 3236 (2005).
8. M. C. Corbett *et al.*, *Proc. Natl. Acad. Sci. U.S.A.* **103**, 1238 (2006).
9. Y. Hu *et al.*, *Proc. Natl. Acad. Sci. U.S.A.* **103**, 17119 (2006).
10. Y. Hu *et al.*, *Proc. Natl. Acad. Sci. U.S.A.* **103**, 17125 (2006).
11. B. Schmid *et al.*, *Science* **296**, 352 (2002).
12. Materials and methods are available as supporting material on *Science* Online.
13. D. C. Rees, J. B. Howard, *Curr. Opin. Chem. Biol.* **4**, 559 (2000).
14. The electron density around the L cluster suggests that the cluster may be coordinated by more than one ligand to NifEN. However, because this region is largely disordered, it is difficult to accurately assign ligand(s) other than $Cys^{\alpha25}$.
15. Z. Ma, F. E. Jacobsen, D. P. Giedroc, *Chem. Rev.* **109**, 4644 (2009).
16. N. Muraki *et al.*, *Nature* **465**, 110 (2010).
17. M. J. Bröcker *et al.*, *J. Biol. Chem.* **285**, 27336 (2010).
18. J. Raymond, J. L. Siefert, C. R. Staples, R. E. Blankenship, *Mol. Biol. Evol.* **21**, 541 (2004).
19. PyMOL, www.pymol.org.
20. C. C. Lee *et al.*, *Proc. Natl. Acad. Sci. U.S.A.* **106**, 18474 (2009).
21. This work was supported by NIH grants GM-67626 (M.W.R.) and GM-45162 (D.C.R.) D.C.R. is an investigator of the Howard Hughes Medical Institute. We acknowledge the Gordon and Betty Moore Foundation for support of the Molecular Observatory at California Institute of Technology. Operations at the Stanford Synchrotron Radiation Lightsource are supported by the U.S. Department of Energy and NIH. The coordinates and structure factors have been deposited with the Protein Data Bank (PDB), accession number 3PDI.

Supporting Online Material

www.sciencemag.org/cgi/content/full/331/6013/91/DC1
Materials and Methods
Figs. S1 to S7
Tables S1 and S2
References

25 August 2010; accepted 5 November 2010
10.1126/science.1196954

MASS SPECTROMETER

The LCMS-8030 combines the power of triple quadrupole mass spectrometry with unmatched speed to provide the ideal complement to its UHPLC systems. The LCMS-8030 features ultrafast multiple reaction monitoring transitions, enabling data acquisition with up to 500 different channels per second. The improvements to the electronics provide ultrafast mass spectrum measurement speeds of 15,000 µ/sec without sacrificing sensitivity or resolution, and ultrafast polarity switching (15 msec) for the most information without signal deterioration. Patented UFsweeper technology accelerates ions out of the collision cell by forming a pseudo-potential surface. The result is high-efficiency collision-induced dissociation and ultrafast ion transport, reducing the sensitivity losses and cross talk observed on other systems. The LCMS-8030's robust design allows maximum uptime, resulting in a system that can handle most complex matrices. Maintenance of the desolvation line without breaking vacuum minimizes instrument downtime.

Shimadzu Scientific Instruments, Inc.

For info: 800-477-1227 | www.ssi.shimadzu.com

PROTEOGLYCAN KIT

Glycosaminoglycans (GAGs) are polysaccharides consisting of repeated dimers. All but hyaluronic acid possess sulfate bases and exist in living organisms in the form of proteoglycans. The new Sulfated GAG Quantitation Kit allows easy quantification of sulfated GAGs in tissues such as cartilage, cultured chondrocytes, and chondrocyte culture solution. Based on a colorimetric determination method using 1,9-dimethylmethylene blue, the new kit is capable of measuring amounts in the 2.5 to 80 µg/mL range within a wide standard curve. Provided in a standard 96-well plate format that can be stored for up to one year, the kit facilitates simple, simultaneous processing of multiple samples. Additionally, a selection of new standards for a broad range of glycobiology and glycoanalysis has been launched, including oversulfated chondroitin sulfate, dermatan sulfate, hyaluronic acid from porcine skin, and heparan sulfate from porcine mucosa.

AMS Biotechnology

For info: +44-1235-828200 | www.amsbio.com

GLYCAN/GLYCOPEPTIDE DATA ANALYSIS

SimGlycan is a high throughput glycan and glycopeptide structure elucidation tool, which now supports multi-stage mass spectrometry data analysis which enables identification of structure specific fragment pathways. The program now includes comprehensive support to perform multi-stage/sequential mass spectrometry data analysis, which involves refragmentation of product ions. Multi-stage mass analysis provides structural information that is useful in structure elucidation of metabolites, glycopeptides, and glycans. It aids in discrimination of glycans having similar characteristic fragment ions at MS/MS level. It resolves heterogeneity of carbohydrate distribution and branching pattern of complex glycans such as isobaric isomers.

PREMIER Biosoft International

For info: 888-847-7494 | www.premierbiosoft.com

PROTEIN EXTRACTION

Four new kits that are designed to simplify the extraction of proteins from cells and tissues are now available. Fast and easy to use, individual DUALXtract kits are available for total protein extraction, the extraction of integral membrane proteins and membrane-associated proteins, and the isolation of cytoplasmic and nuclear proteins. DUALXtract Mammalian Cell Total Protein Extraction Reagent provides gentle one-step extraction of total protein, while the DUALXtract Nuclear and Cytoplasmic Protein Extraction Kit rapidly isolates cytoplasmic and nuclear proteins from cultured cells and tissues. The DUALXtract Total Membrane Protein Extraction Kit quickly isolates high quality membrane and cytoplasmic protein fractions from mammalian cells and tissues, with no cross-contamination. The DUALXtract Membrane Protein Optimization Kit can be used to quickly identify optimal extraction conditions for membrane proteins of interest and is suitable for the extraction of native, functional membrane proteins from mammalian, fungal, and bacterial cells.

Dualsystems Biotech AG

For info: +41-(0)-44-738-50-00 | www.dualsystems.com

PROTEIN DIGESTION KITS

Two new sample preparation kits are designed to advance a "universal" sample preparation protocol for mass spectrometry-based proteome research. Filter-Aided Sample Prep (FASP) Protein Digestion Kits enable complete, reproducible solubilization, and digestion of both fluid and tissue sample proteomes, and extend mass spectrometry-based proteome research methods into the previously inaccessible realms of the insoluble and formalin-fixed paraffin-embedded (FFPE) ("biobank") proteomes. By enabling the use of strong detergents within mass spectrometry sample preparation workflows, the FASP Protein Digestion Kit offers a standardized sample preparation workflow that works for both soluble and insoluble proteins in fluids and tissues. The FFPE-FASP Protein Digestion Kit's composition is similar, but contains supplemental materials and protocol steps to guide researchers through additional tissue sample and protein treatment steps to ensure compatibility of FFPE samples with downstream mass spectrometry sample preparation and analysis workflows.

Protein Discovery, Inc.

For info: 865-521-7400 | www.proteindiscovery.com

Electronically submit your new product description or product literature information! Go to **www.sciencemag.org/products/newproducts.dtl** for more information.

Newly offered instrumentation, apparatus, and laboratory materials of interest to researchers in all disciplines in academic, industrial, and governmental organizations are featured in this space. Emphasis is given to purpose, chief characteristics, and availability of products and materials. Endorsement by *Science* or AAAS of any products or materials mentioned is not implied. Additional information may be obtained from the manufacturer or supplier.

ASSISTANT/ASSOCIATE PROFESSOR
Department of Nutrition and Food Science
College of Agriculture and Natural Resources
University of Maryland

The Department of Nutrition and Food Science at the University of Maryland, College Park invites applications for a nine-month, tenure-track position as assistant or associate professor in nutrition.

Responsibilities: (1) The successful candidate will be expected to sustain/develop an independent nutrition research program that focuses on the role of nutrition and dietary factors in the etiology, prevention, and treatment of chronic diseases such as obesity, cardiovascular disease, diabetes, or cancer. (2) This individual will develop an outstanding research program that employs modern clinical and/or laboratory approaches to prevent and ameliorate human chronic disease by dietary means. (3) The location of the university provides excellent opportunities for collaboration with scientists at several nearby institutions including the National Institutes of Health, the U.S. Department of Agriculture Beltsville Human Nutrition Research Center, and the University of Maryland Medical School. (4) The successful candidate must also have demonstrated ability or potential to teach and mentor graduate students as well as undergraduate dietetics and nutrition students effectively, possess excellent interpersonal and communication skills, and have the ability to work with others in a collegial team atmosphere.

Qualifications: (Required) Candidates must have an earned Doctorate in nutrition or related field. (Preferred) Certification as a Registered Dietitian is highly desirable. Salary/Benefits: Salary will be commensurate with education and experience. The University of Maryland offers an extensive benefits package. Application: Applicants are to send a current (signed) curriculum vitae, representative publications, official transcripts, and the names and contact information for three professional references (include mailing address, telephone number, and e-mail address), and a cover letter describing the candidate's strengths, accomplishments, and future research plans to **e-mail: jobs.umd.edu.** If you have any further questions, contact **Dr. David K. Y. Lei,** the Chair of the Search Committee at **e-mail: dlei@umd.edu.** Closing Date: March 15, 2011, or until an acceptable candidate is identified.

The University of Maryland is an Equal Opportunity/Affirmative Action Employer. Minorities and Women are encouraged to apply.

GEOSCIENCES FACULTY SEARCH 2010–2011—Stony Brook University's Department of Geosciences invites applications for a tenure-track **ASSISTANT PROFESSOR** faculty position in the field of remote sensing with a specialty in planetary spectroscopy. Seeking a candidate with the potential for collaboration augmenting the Department's current research strengths in spectroscopy, planetary science, mineralogy, and environmental science, and who will be an effective teacher in undergraduate and graduate courses in the areas of remote sensing, planetary science, and general geology. The successful candidate must have a Ph.D. in the geosciences, planetary sciences, or a related field at the time of appointment and preference will be given to those with postdoctoral experience. The successful candidate must have demonstrated potential to establish an internationally recognized, externally funded research program that would include mentoring of graduate and undergraduate students. To apply, submit a cover letter, curriculum vitae, research and teaching statements, and the names and contact information of three references to: **Chair of Search Committee, Department of Geosciences, 255 Earth and Space Sciences Building, Stony Brook University, Stony Brook, NY 11794-2100.** Preferred: Electronic submissions in one PDF document through the online system. For a full position description, application procedures, or to apply online, visit **website: http://www.stonybrook.edu/jobs** (**Reference #F-6619-10-12**). Applications will be accepted until the position is filled; however for best consideration, please submit materials by January 17, 2011. *Stony Brook University/SUNY is an Equal Opportunity/Affirmative Action Employer.*

POSITIONS OPEN

The Genomics Research Center, Academia Sinica
Taipei, Taiwan

Nominations and applications are invited for all levels of **RESEARCH FELLOW** and **RESEARCH SPECIALIST** position. Extensive working experience on glycomics and glycoproteomics is highly preferred.

For consideration, please send a copy of curriculum vitae, including a list of publications, two to three references, and a cover letter describing your area of interest, and for a Principal Investigator position, a brief statement of research plan to:

Director, Dr. Chung-Hsuan Chen
Genomics Research Center
Academia Sinica
128 Academia Road, Section 2
Nankang Dist., Taipei 115, Taiwan
Tel: +886-2-2789-9922
E-mail: winschen@gate.sinica.edu.tw
Website: http://www.genomics.sinica.edu.tw/

FACULTY POSITION in
Genetics, Instructor Level
Harvard Medical School

The New England Primate Research Center (NEPRC), Harvard Medical School seeks an outstanding scientist with expertise in genetics/genomics, especially as it relates to health and disease. The NEPRC currently has active programs in the genetics of psychiatric and addictive disease, comparative primate genomics, and genetics of viral pathogenesis. A Doctoral degree in an appropriate discipline, postdoctoral/professional experience, and evidence of outstanding research potential are required. Candidates will be appointed at the faculty rank of Instructor and will develop an independent research program with guidance and mentorship from senior investigators. A three-year financial award will cover salary and defray research costs while the candidate competes for extramural funding through conventional grant mechanisms. Applications should be addressed to: **Instructor Initiative Genetics Search Committee, Harvard Medical School, New England Primate Research Center, P.O. Box 9102, Southborough, MA 01772-9102.** Applicants should include their curriculum vitae, summary of past accomplishments and future plans, and arrange for at least three references to be sent directly to the search committee. Electronic submissions as PDF files are encouraged and should be sent to **e-mail: neprcgeneticsinstructor@hms.harvard.edu.** Applications will be accepted until the position is filled. *Harvard Medical School and the New England Primate Research Center are Equal Opportunity Employers, committed to diversity in the workplace.*

FACULTY POSITION in
Plant Signaling Mechanisms

The University of North Texas (UNT) seeks candidates at the **ASSOCIATE** or **FULL PROFESSOR** level with an active research program in plant cell biology or genetics. The successful candidate must have a strong record of obtaining extramural funding and will be an integral part of a new initiative in "Plant Signaling Mechanisms" targeted by the UNT administration for support. Exceptional startup funding and salary will be provided. This position will be one of four senior-levels hires being recruited to UNT to enhance an existing core of research activities in the plant sciences. New research initiatives, including three that involve life science disciplines, were announced in September 2008 by the UNT administration. For further information, see **websites: http://www.biol.unt.edu/signaling/** and **http://research.unt.edu/clusters/.** All applicants must hold a Doctoral degree in a chemical- or life-science related discipline and must apply online at **website: http://facultyjobs.unt.edu.** For questions, contact **Kent Chapman,** Search Committee Chair, at **e-mail: chapman@unt.edu.** Applications will be reviewed beginning March 25, 2011, and will continue until the search is closed. *UNT is an Affirmative Action/ADA/Equal Opportunity Employer.*

POSITIONS OPEN

DIRECTOR of
METACyt Biochemical Analysis Center
Indiana University

The Department of Chemistry seeks applications at the Associate or Senior Scientist rank for Director of the METACyt Biochemical Analysis Center, effective July 1, 2011. A Ph.D. in Chemistry with emphasis in mass spectrometry (MS) and multiple years of postdoctoral experience is required; the salary is commensurate with experience. The successful candidate will be expected to interact with the wide range of users in a service role as well as mentor and supervise postdoctoral and Bachelor's level associates, and perform routine maintenance on METACyt HPLC and MS instrumentation while developing new collaborations both on and beyond the Indiana University (IU)-Bloomington campus in the areas of glycomics, proteomics, and metabolomics. The Director will team with leadership in the IU Mass Spectrometry Laboratory and IU Proteomics Facility to coordinate the growth and expansion of mass spectrometry-related resources on the IU-B campus. Opportunities for developing training curricula or new courses are available if the candidate so desires.

The deadline for receipt of applications is March 1, 2011. Please submit a cover letter, curriculum vitae, and arrange to have three letters of recommendation sent to: **David P. Giedroc, Chair, Department of Chemistry, Indiana University, 800 E. Kirkwood Avenue, Bloomington, IN 47405,** or send as PDF files to **e-mail: chemchair@indiana.edu.** *Indiana University is an Affirmative Action/Equal Opportunity Employer and especially encourages applications from women and members of minority groups.*

POSTDOCTORAL RESEARCH ASSOCIATE and **RESEARCH ASSISTANT** positions are available for two motivated individuals with strong work ethics and research interest in Molecular Nutrition. Both positions are full-time with benefits located in the Department of Health and Nutritional Sciences at South Dakota (SD) State University Brookings campus, a public land grant research University. Ongoing projects look into cellular mechanism of biological activities of dietary components and natural products in context of inflammatory diseases, metabolic syndrome, and cancer. Questions related to nutrition and health are being studied using a combination of molecular and cell biology approaches and animal disease models. The laboratory is supported by NIH, USDA, and SD state funding and is very well-equipped. Postdoctoral candidates must possess a Ph.D. and excellent scientific writing skills. Research Assistant position primarily involves research support for which previous exposure to laboratory setup and Biological research is a must but does not require a Ph.D. Please submit recent curriculum vitae, a one-page statement of long-term career goals, and three letters of reference to **e-mail: moul.dey@sdstate.edu.**

St. John's University, Queens, New York Pharmaceutical Sciences Department is seeking applications for **THREE NON-TENURE-TRACK** and **ONE TENURE-TRACK** position; Ph.D. required and postdoctoral experience preferred. Non-tenure positions responsibilities include teaching anatomy and physiology, public health, and biochemistry. Tenure-track position responsibilities include establishing a research program to attract funding, mentoring, and teaching graduate and undergraduate students in pharmaceutics, biopharmaceutics, and industry pharmacy. Electronically send curriculum vitae and three letters of recommendation to **e-mail: trombetl@stjohns.edu.**

RESEARCH ANALYST—Division of General Internal Medicine, University of Michigan Ann Arbor, Michigan. Provide consultation to multiple project managers and research scientists on issues of data management, study design, and analytical methods for health service research projects, among other duties. Minimum of a Master's degree in epidemiology, economics, statistics, or related; experience with management and analysis of longitudinal health services data and complex survey and simulation data using either SAS or STATA. Apply to **Brittany Weatherwax, e-mail: bweather@umich.edu.**

UNIVERSITY OF MICHIGAN

DEAN
SCHOOL OF NATURAL RESOURCES AND ENVIRONMENT
UNIVERSITY OF MICHIGAN
ANN ARBOR

The University of Michigan invites applications and nominations for the position of Dean of the School of Natural Resources and Environment (SNRE). The School's over-arching objective is to contribute to the protection of the Earth's resources and the achievement of a sustainable society. Through research, teaching, and outreach, faculty, staff and students of the School are devoted to generating knowledge and developing policies, techniques, and skills to help practitioners manage and conserve environmental resources to meet the full range of human needs on a sustainable basis. We believe this is best accomplished through the joining of multiple disciplines and approaches in a creative research and teaching atmosphere.

Faculty and students are drawn from an unusually wide range of disciplinary backgrounds and professional experiences, representing the natural and social sciences and numerous professional fields. Research programs aim at understanding environmental processes and developing engineering, design, business, and policy solutions to environmental problems in settings that range from regional to international; these programs involve diverse partners, from private sector to government and non-profit. The School provides instruction through Master's and doctoral programs, multiple dual degree programs, and an undergraduate program offered jointly with the University's College of Literature, Science, and the Arts.

The Dean is the chief academic and administrative officer of the School and reports directly to the Provost and Executive Vice President for Academic Affairs. The Dean provides leadership for the planning and implementation of the School's academic, research and outreach programs. The Dean is expected to effectively represent the School to internal and external constituencies and to secure funds from a variety of sources. Qualifications must be appropriate for appointment as full professor with tenure, and include demonstrated commitment to and/or experience in achieving the School's mission with a diverse student body and faculty. We seek highly qualified candidates from professional and academic backgrounds.

Nominations and applications will be reviewed continuously beginning in January 2011. Individuals from traditionally underrepresented groups are encouraged to apply. Inquiries, nominations, and applications consisting of a letter, curriculum vitae, and the names and contact information of three references, should be submitted, preferably in electronic form, to:

Dan Brown, Ph.D.
Chair, SNRE Dean Search Advisory Committee
Professor of Natural Resources and Environment
University of Michigan
503 Thompson Street, Room 3074
Ann Arbor, MI 48109-1340
email snre-search-chair@umich.edu

or to the University's consultants for this search:

AUERBACH ASSOCIATES

Judith A. Auerbach and Kit J. Nichols
385 Concord Avenue, Suite 103
Belmont, MA 02478
(617) 451-0095
Electronic submissions preferred: email vicki@auerbach-assc.com

The University of Michigan is an equal opportunity/ affirmative action employer.

NIFA

UNITED STATES DEPARTMENT OF AGRICULTURE
NATIONAL INSTITUTE OF FOOD AND AGRICULTURE

The National Institute of Food and Agriculture (NIFA) in the Department of Agriculture (USDA) was recently reorganized to a structure with four Institutes. Each of the Institutes is co-led by an Assistant Director and a Principal Scientist. The Assistant Director provides leadership for the administration of programs that comprise the Institute. The Principal Scientist provides the scientific leadership to programs assigned to the Institute. More information about NIFA can be found at **http://www.nifa.usda.gov/**. NIFA is seeking to fill the following four Principal Scientist positions, as either permanent **(PERM)**, term **(TERM)**, or under an **Intergovernmental Personnel Act (IPA)** appointment:

Principal Scientist of the Institute of Bioenergy, Climate, and Environment (PERM) (NIFA-SL: 10-06)
Principal Scientist of the Institute of Bioenergy, Climate, and Environment (TERM) (NIFA-SL: 10-07)

Principal Scientist of the Institute of Food Production and Sustainability (PERM) (NIFA-SL:10-08)
Principal Scientist of the Institute of Food Production and Sustainability (TERM) (NIFA-SL: 10-09)

Principal Scientist of the Institute of Food Safety and Nutrition (PERM) (NIFA-SL: 10-10)
Principal Scientist of the Institute of Food Safety and Nutrition (TERM) (NIFA-SL:10-11)

Principal Scientist of the Institute of Youth, Family, and Community (PERM) (NIFA-SL: 10-12)
Principal Scientist of the Institute of Youth, Family, and Community (TERM) (NIFA-SL:10-13)

Principal Scientist positions are Senior Level (SL) positions. The Federal salary ranges from $119,554 to $179,700. A copy of each job announcement may be located on the Office of Personnel Management web page at **http://www.usajobs.opm.gov/**. As specified in each job announcement, applicants must meet mandatory qualifications and address specific technical qualifications. Veterans preference applies, and U.S. citizenship is required. The job announcements listed above identify these four positions as a Permanent or a Term position (which is a competitive appointment for a period of more than one year but not more than four years). Candidates applying for permanent and term appointments should clearly identify in your application the type(s) of appointment desired, indicate the corresponding vacancy announcement number(s), and submit the documents required in the job announcements through USAJOBS.

In addition, NIFA will consider filling these positions under an **Intergovernmental Personnel Act (IPA)** appointment. The IPA allows for a temporary assignment (detail) of skilled employees from local, State and Indian tribal government, institutions of higher education and other eligible organizations to Federal Government agencies. IPAs remain employees of their permanent organizations; appointments can be made for up to two years and may be extended an additional two years under specific conditions. Cost of the assignment (including salary, benefits, relocation cost, travel and per diem expenses) are negotiated between participating organizations. **Applicants applying only for an IPA appointment should submit a resume and address the specific technical qualifications identified for the position(s). To obtain the technical qualifications and/or receive additional information relating to IPA appointments contact Rhonda Pratt (301-504-1475)**.

All applications must be received by **January 31, 2011**. For more information about the application process, contact **Deborah Crump (301-504-1448)**. To learn more about NIFA, contact **Betty Lou Gilliland (202-720-5506)**.

HOWARD HUGHES MEDICAL INSTITUTE

GRANTS FOR BIOMEDICAL RESEARCH

INTERNATIONAL EARLY CAREER SCIENTISTS

Science is a multinational, cross-cultural endeavor that connects researchers across the borders created by discipline and continent. The Howard Hughes Medical Institute (HHMI) believes it is vital to encourage the careers and scientific creativity of scientists working abroad. HHMI is announcing an International Early Career Scientist Program, which will support up to 35 outstanding scientists working in selected countries outside the United States who are, or have the potential to become, scientific leaders.

Five-year basic biomedical reseach grant

Application deadline: February 23, 2011, at 2 p.m. ET, U.S.

Application information: http://www.hhmi.org/research/competitions

The International Early Career Scientist Program will select and support highly qualified scientists working in selected countries outside the United States who are in the critical beginning stages of their independent careers. HHMI international early career scientists will receive five-year grants—$250,000 in the first year and $100,000 for each of the following four years.

Successful applicants will have trained through the postdoctoral level in a vigorous basic research environment. Eligible candidates must have trained in the United States at the doctoral, medical, or postdoctoral level. Applicants are expected to have outstanding scientific training records and exceptional potential for significant productivity and originality in their independent careers.

HHMI recognizes that a supportive research environment is crucial to launching a successful research program, so awards will be made only to institutions that can clearly support the research activities of the grant recipient.

Applicants must meet the following eligibility requirements:

- Hold a doctoral degree or medical degree and have completed postdoctoral research training.
- Have trained at the doctoral, medical, or postdoctoral level in the United States.
- Hold a full-time position as an independent researcher at a research-oriented university, medical school, or nonprofit institution in any of the following countries: Argentina, Brazil, Chile, China, Czech Republic, Egypt, Hungary, India, Italy, Mexico, Poland, Portugal, Russia, South Africa, South Korea, Spain, Taiwan, Turkey.
- Have made significant contributions in fundamental biomedical research on basic biological processes or disease mechanisms, and have been the first or senior author on at least two peer-reviewed, English-language, original research publications.
- Have started their first independent research position on or after January 1, 2004.
- Control their own research direction, laboratory space, and funding and devote most of their professional time to research, mentoring, and teaching.

HHMI, a nonprofit medical research organization, plays a powerful role in advancing biomedical research and science education. To learn more, visit www.hhmi.org.

HHMI
HOWARD HUGHES MEDICAL INSTITUTE

Tenure-Track Faculty Position: Mechanical Engineering

The School of Engineering at the University of Vermont (UVM) invites applications for a tenure-track faculty position in its Mechanical Engineering Program at the level of Assistant Professor for a fall 2011 start date. The School is seeking a faculty member whose research focus lies in the engineering of functional materials with applications to the medical and biological sciences, bio-mimetic or bio-compatible materials, bio-inspired engineering design, cellular or medical materials applications, or related areas.

The successful candidate will have undergraduate and advanced degrees in mechanical engineering or a closely related engineering field. The new faculty member will maintain an active program of externally funded research and graduate student advising and will actively contribute to undergraduate and graduate instruction in engineering mechanics and materials engineering. Potential for interdisciplinary research collaborations will be highly valued; significant opportunities for collaboration exist with other academic units across campus, including: Mathematics & Statistics, Computer Science, the College of Medicine, the Materials Science Program, the Biomedical Engineering Program, and the Complex Systems Center. High-performance computing facilities are available to researchers within the Vermont Advanced Computing Center.

The School has excellent faculty and students in civil, electrical, environmental, and mechanical engineering, is a leader in interdisciplinary research partnerships, and offers innovative approaches to engineering education. In recent years, the School has seen significant growth in undergraduate and graduate student enrollment and research funding. The University is located in Burlington, Vermont, rated as one of the best small cities in America. UVM is an Affirmative Action/Equal Opportunity employer and welcomes applications from women and underrepresented ethnic, racial and cultural groups and from people with disabilities. The School is committed to building a culturally diverse educational environment and is interested in candidates who can contribute to the diversity and excellence of the academic community through their research, teaching, and/or service; therefore a commitment to diversity and inclusion is required. Applicants are requested to include in their cover letter information about how they will further this goal.

The application package should include a cover letter, detailed curriculum vitae, the names and contact information of at least three references, a statement describing current/future research activities and directions, and a statement describing teaching interests and teaching philosophy. Applications must be submitted through the UVM website **www.uvmjobs.com** (Search requisition **#033848**). Screening of applications will continue until the position is filled.

UVM recently identified three "Spires of Excellence" in which it will strategically focus institutional investments and growth over the next several years. These spires are all relevant to this position, and are Complex Systems; Neuroscience, Behavior and Health; and Food Systems. Candidates whose research, scholarship, and/or creative work interests align or intersect with these areas are especially encouraged to apply. More information on these areas is available on the web site at:

https://www.uvm.edu/~tri/?Page=csys.php (complex systems)
https://www.uvm.edu/~tri/?Page=nbh.php (neuroscience)
http://www.uvm.edu/~tri/?Page=foodsys.php (food systems)

Founded in 1791, UVM has been called one of the "public ivies" and is consistently ranked as one of the top public service universities in the United States. The University is located in Burlington, Vermont, also rated as one of the best small cities in America. The greater Burlington area has a population of about 125,000 and enjoys a panoramic setting on the shores of Lake Champlain, between the Green Mountains of Vermont and the Adirondack Mountains of New York. Burlington and the surrounding area provide an environment rich in cultural and recreational activities for individuals and families, with multiple opportunities for interactions with local industry and communities.

Smithsonian Tropical Research Institute

RESEARCH POSITIONS IN ARCHAEOLOGY AND MARINE SCIENCE

The Smithsonian Tropical Research Institute (STRI; www.stri.si.edu), headquartered in the Republic of Panama, invites applicants interested in conducting research in the new world tropics to fill one permanent research position in Archaeology and one in Marine Science. Candidates should have a strong publication record and demonstrated success in obtaining grants. The successful candidates are expected to develop strong research programs, supervise students, collaborate with other staff, and provide service to the Institute.

STRI maintains modern research facilities, a library with extensive holdings in the natural and anthropological sciences, and support centers in Panama City, together with diverse stations for marine and terrestrial field work throughout the tropics. Staff scientists maintain cooperative research programs within a world-wide network of academic institutions. Opportunities for mentoring young scientists are available through a vigorous fellowship program, and formal teaching is possible through educational programs with affiliated universities.

Archaeology: We seek an archaeologist interested in doing research on prehistoric adaptations of native peoples to tropical forests; anthropogenic transformations of the landscape; plant domestication; archaeozoology; innovations in subsistence technologies; and the development of social, cultural and economic systems. Mid-level candidates are preferred but applicants at any level will be considered.

Marine Science: We seek a broadly trained marine scientist who addresses fundamental research questions and whose interests complement those of the existing staff. Applicants at any level will be considered.

Minimum Qualifications: A Ph.D. in a relevant field, a demonstrated record of research excellence, and a commitment to communicating science to the public.

To Apply: Interested candidates should submit a single pdf containing a summary of research accomplishments and interests, curriculum vitae, five significant reprints, and the names and contact information of three referees. **Please send applications electronically to strimarinejob@si.edu or strianthrojob@si.edu**. Address inquiries to **Dr. Fernando Santos-Granero, Chair, Search Committee on Archeology at: santosf@si.edu** or **Dr. Rachel Collin, Chair, Search Committee on Marine Science at: collinr@si.edu**. Review of applications will begin on **February 15, 2011**, and interviews will commence shortly thereafter.

STRI is an Equal Opportunity Employer and appointments are made regardless of nationality.

FRED HUTCHINSON
CANCER RESEARCH CENTER
A LIFE OF SCIENCE

Human Biology Division Director

The Division of Human Biology at the Fred Hutchinson Cancer Research Center (FHCRC) is soliciting applications for a dynamic and visionary Division Director who can lead the expansion of the solid tumor research program within the Division and across the Center. FHCRC, in partnership with the University of Washington and Children's Hospital and Regional Medical Center, is an established NCI-designated comprehensive cancer center with vibrant research programs that include studies of cancer pathogenesis, prevention, early detection, treatment, and outcomes. An important area for development involves the integration of basic, clinical, and population sciences with translational studies of solid tumor biology.

The ideal candidate will have demonstrated excellence and leadership in translational research emphasizing cancer biology that spans the interface between laboratory, clinical, and/or population-based studies. All aspects of cancer-related research are of interest, from those utilizing large-scale genetic and genomic approaches to those focused on a mechanistic understanding of cancer pathogenesis. The candidate must be able to lead the expansion of the Human Biology Division through additional faculty recruitment, emphasizing translational research in solid tumors, while also fostering the broader research portfolio of the Division.

The Human Biology Division encompasses a diversity of interdisciplinary, collaborative research at the interfaces of basic, clinical, and population sciences in order to further our understanding of human biology, cancer, and other complex human disorders. The Division occupies state-of-the-art research laboratories on a beautiful lakeside campus. The Center offers outstanding shared resources, including genomics, proteomics, imaging, and animal models. The Center has active training programs for graduate students, postdoctoral fellows and clinically oriented trainees, and offers exceptional opportunities for scientific interactions with other investigators in the Seattle area.

Additional information about the Division and Center can be found at: **http://www.fhcrc.org/science/humanbio/** and **http://www.fhcrc.org/science/**

Candidates should submit a curriculum vitae, research and leadership statements, and contact information for three references to:

Human Biology Division Director Search
Fred Hutchinson Cancer Research Center
Mailstop: C3-168
1100 Fairview Avenue North
P.O. Box 19024
Seattle, WA 98109-1024
or:
dljackso@fhcrc.org

Applications will be considered as received until **February 15, 2011** or the position is filled.

The Fred Hutchinson Cancer Research Center is an Equal Opportunity Employer committed to work force diversity. Applications from female and minority candidates are strongly encouraged.

VICTORIA UNIVERSITY OF WELLINGTON

Victoria University delivers internationally-acclaimed results in teaching and research, as well as programmes of national significance and international quality.

As one of Wellington's largest and most established employers, we're committed to providing our staff with opportunities for rewards, recognition and development, all within a dynamic and inclusive culture where innovation and diversity are highly valued.

PROFESSOR IN ECOLOGY, EVOLUTION OR BIODIVERSITY

School of Biological Sciences

Wellington, New Zealand

We seek a senior academic or research scientist with a strong track record in internationally recognised research, with significant experience in both securing and leading externally-funded research programs together with experience in teaching and supervision of students.

The successful candidate will be expected to promote Victoria University of Wellington as a leading provider of research by advancing national and international research networks and leading university activities in outreach programmes in Ecology, Evolution or Biodiversity. Applicants may be able to collaborate with the Allan Wilson Centre for Molecular Ecology & Evolution, and/or one of the Victoria University of Wellington Applied Research Centres (The Centre for Marine Environmental & Economic Research, or The Centre for Biodiversity & Restoration Ecology).

We would welcome applications from specialists in a wide range of fields related to Ecology, Evolution or Biodiversity. These research areas include bioinformatics, conservation biology, terrestrial ecology, marine biology or molecular ecology. Experience of academic leadership is expected for all professorial candidates.

For a copy of the job description visit http://vacancies.vuw.ac.nz/ or for further information contact Associate Professor Phil Lester, phil.lester@vuw.ac.nz

Applications close 31 January 2010

Victoria University of Wellington is an EEO employer and actively seeks to meet its obligations under the Treaty of Waitangi.

For more information and to apply online visit
http://vacancies.vuw.ac.nz

Reference A397-10M

TE WHARE WĀNANGA O TE ŪPOKO O TE IKA A MĀUI
VICTORIA
UNIVERSITY OF WELLINGTON

UNIVERSITY OF MINNESOTA

Medical School

DULUTH CAMPUS

Head, Department of Biomedical Sciences
University of Minnesota
Medical School Duluth
Duluth, MN

www.med.umn.edu/Duluth/

The University of Minnesota Medical School Duluth, a campus of the University of Minnesota Medical School, invites applications and nominations for the position of Head of a newly created Department of Biomedical Sciences. The Department of Biomedical Sciences is being created via the merger of several basic science departments. The department is a key element of a new strategic plan for the University of Minnesota Medical School Duluth that more closely aligns the research efforts of the school's departments with the educational mission of our school to train rural and Native American physicians and serve the health needs of rural and Native American communities. The Head of Biomedical Sciences is expected to play a significant role in overseeing and establishing a vigorous new Biomedical Sciences department.

Qualifications

Required Qualifications:

- Ph.D., M.D., or equivalent degree in a biomedical sciences field.
- A significant publication and external funding record.
- Record of achievement that meets the standards for tenure and rank as set by the Medical School's promotion and tenure policy.
- Experience teaching health professional and graduate students.
- Excellent verbal and written communication skills.

Preferred Qualifications:

- History of distinguished research achievement, employing translational basic science, clinical, or population-based approaches to addressing health issues relevant to rural or Native American populations. Examples of health issues relevant to these populations include, but are not limited to, heart disease, hypertension, type two diabetes, obesity, kidney disease, respiratory disease, neurodegenerative diseases such as Alzheimer disease and Parkinson disease, stroke, cerebrovascular disease and cancer.
- Demonstrated ability to effectively lead and manage an academic or research program.
- Experience mentoring faculty and students.
- Ability to work cooperatively across programs and campuses for common goals.
- Demonstrated commitment to serving individuals from diverse backgrounds.

Applications and Nominations

Applications, nominations and questions should be addressed to:

Eileen P. Blake
Alexander, Wollman & Stark
eblake@alexanderwollmanstark.com
610-399-5284 Telephone
610-399-5285 Fax

Interested candidates should send a current CV and Letter of Interest. All communications will be held confidential. Electronic submission is preferred.

The University of Minnesota shall provide equal access to and opportunity in its programs, facilities, and employment without regard to race, color, creed, religion, national origin, gender, age, marital status, disability, public assistance status, veteran status, sexual orientation, gender identity, or gender expression.

ASSISTANT/ASSOCIATE PROFESSOR

Department of Molecular Medicine and USF Health Byrd Alzheimer's Institute

The USF Health Byrd Alzheimer's Institute and Department of Molecular Medicine at the USF Health College of Medicine are partnering to identify a candidate for a tenure track position at the rank of Assistant or Associate Professor. A successful applicant will employ structural, molecular and/or computational approaches to develop a mechanism-based drug discovery program related to neurodegenerative disease. The USF Health Byrd Alzheimer's Institute is a unique enterprise that allows investigators to participate in basic and clinical studies directly related to Alzheimer's disease and other dementias in one building. The Institute is the largest of its kind in the world. The Department of Molecular Medicine and USF Health Byrd Alzheimer's Institute are located in a vibrant and expanding USF Health Complex on the main campus of the University of South Florida that includes the Colleges of Medicine, Nursing, and Public Health, and the H. Lee Moffitt Comprehensive Cancer Center and Research Institute. USF is a nationally recognized research campus with extramural grants and contract activity in excess of $350 million annually and is home to several Centers for Excellence in Biomedical Research and state-of-the-art facilities. Over the past 3 years, the state of Florida committed an additional $450 million to the existing medical research budget, and as a result, USF is now part of a collaborative research corridor running through the heart of the sunshine state.

Successful candidates for this position are expected to develop and maintain a competitively funded research program, and to participate in medical and graduate education. To support these expectations, the department offers strong institutional salary support, competitive start-up packages, excellent core facilities, and a collegial atmosphere to create an environment that promotes success. Academic rank and salary are commensurate with qualifications and experience. The successful candidate must have a doctorate in a biomedical sciences discipline with at least two years postdoctoral experience. Appointment at the level of Associate Professor requires a minimum of five years experience at the Assistant Professor level, a nationally-recognized and federally funded research program and experience mentoring graduate students.

Please send a cover letter, curriculum vitae, research plan, statement of teaching philosophy, and arrange three reference letters to be sent by e-mail (with attached PDFs) to Ms. Maxine Roth at **mroth@health.usf.edu** Review of applicants will begin immediately and continue until the position is filled. **Dr. Chad Dickey, Search Committee Chair, University of South Florida-Health, 12901 Bruce B. Downs Blvd. MDC7, Tampa, Florida 33612-4799**

USF Health is committed to increasing its diversity and will give individual consideration to qualified applicants for this position with experience in ethnically diverse settings, who possess varied language skills, or who have a record of research that support diverse communities or teaching a diverse student population. The University of South Florida is an EO/EA/AA Employer. For disability accommodations, contact Maxine Roth at (813) 396-0746 a minimum of five working days in advance. According to FL law, applications and meetings regarding them are open to the public.

USF HEALTH

JAAS 江苏省农业科学院

Jiangsu Academy of Agricultural Sciences

Seeking Distinguished Scientists in Various Agriculture Areas

Jiangsu Academy of Agricultural Sciences (JAAS) is a professional agricultural research and extension institution that has been established since 1932. JAAS ranks at the top of provincial agricultural academies in China in terms of the comprehensive strength in agriculture. JAAS's headquarter and main research facilities are located in Nanjing, Jiangsu, China.

Currently, there are 3 distinguished full professor positions available for application in the following areas: breeding, food processing, bioenergy, facility agriculture, and large-scale farming for modern animal husbandry. Applicants should have a faculty position already beyond the assistant professor level in a university or the equivalent position in a research institution. In addition, all candidates should demonstrate excellent records of research accomplishment and have a command of bilingual language for English and Chinese, both in spoken and written.

Successful applicants will be offered a competitive package, including sufficient laboratory space, startup funding, relocation fee and competitive salary commensurate with experience, in addition to a housing allowance, and other employee benefit. Applicants can go to www.jaas.ac.cn for application details.

In addition, more information for other regular faculty positions from JAAS relevant to a variety of disciplines in agriculture is also available at www.jaas.ac.cn.

Contact information

E-mail: rsc-gbk@jaas.ac.cn; Tel: 086-25-84390037

Rochester, NY

RIT Rochester Institute of Technology

CHESTER F. CARLSON CENTER FOR IMAGING SCIENCE

Endowed Professorship

There is a faculty opening as a senior tenure-track/tenured endowed professorship in the Chester F. Carlson Center for Imaging Science (CIS) in the area of biomedical imaging. Over the next 5 years, RIT is committed to major growth and investment in research and education in the interdisciplinary arena of applied biological science, encompassing biomedical engineering, biological and medical imaging, biophysics, biomedical computation, and biotechnology. Applicants in any related application area or modality are of interest. Current related research efforts in CIS focus on magnetic resonance and ultrasound imaging, visual perception, and cognitive science. The Greater Rochester, New York Region is home to more than 70 biotech companies, with a concentration in vision science and medical imaging. The CIS biomedical faculty has long-standing collaborative relationships with the University of Rochester Medical Center and the SUNY Upstate Medical Center. RIT and Rochester General Health System (RGHS) have a partnership in educational and research programs that includes sharing of expertise and facilities. RIT has formed the Institute of Health Sciences and Technology that will commence operations next fall and will house joint RIT-RGHS research and educational programs. The person recruited for this position will take a prominent role in the growth of the CIS program in biomedical imaging, working collaboratively with the other faculty and labs, as well as in the generation of externally funded research projects, supervision of graduate research, laboratory expansion, and the development and teaching of related courses.

QUALIFICATIONS:

The following are required for the position: Doctoral degree, a substantial peer-reviewed publication record, and a history of successful research leadership in biomedical imaging or related fields at the level of PI demonstrated through externally funded projects; experience in the development of theory or methods for biomedical imaging, including acquisition, processing, and application; ability to teach and interest in teaching at the undergraduate and graduate level, including supervision of students and development of curricula. The ability to communicate well in speech and writing and synergy with existing research areas to promote collaboration are highly desirable.

Each CIS faculty member is expected to collegially contribute to the growth of the imaging science program through appropriate service activities in community outreach, industrial interaction and academic governance. An ability and interest in contributing to a community committed to diversity is desired.

APPLICATION INSTRUCTIONS FOR IRC43820:

Apply online at **http://apptrkr.com/172535**. Upload via this website application material as one PDF file that includes your cover letter; a summary of education and professional background; list of publications and research grants; summary of teaching and research experience; a list of three professional references and a brief personal statement on expected future research and teaching activities. A statement of your experience with and interest in cultural diversity should also be included. Materials should be addressed to Search Committee Chair, Center for Imaging Science.

You can contact the search committee with questions on the position at: biofacultysearch@cis.rit.edu.

Candidates should visit www.cis.rit.edu for more information and to view the detailed job postings.

Applications will be reviewed on a rolling basis and the position will remain open until filled.

The Rochester Institute of Technology is an equal opportunity/affirmative action employer. Members of protected classes and individuals with the ability to contribute in meaningful ways to the university's continuing commitment to cultural diversity, pluralism, and individual differences are encouraged to apply.

The University of Oslo is Norway's largest university with 6000 employees and 26500 students. We offer interesting career opportunities and a good work environment.

UiO : University of Oslo

Functional Genomics and Cell Signaling: Group Leader position with start-up package at the Biotechnology Centre of Oslo

Applications are invited for a group leader position at the Biotechnology Centre of Oslo (BiO, www.biotek.uio.no). BiO is a centre for molecular biology, biotechnology and bio-informatics within the University of Oslo. A call is now open for a new group leader to start at BiO in 2011. The successful candidate for the position will be offered a fixed-term, 5-year contract, which is renewable for up to 5 additional years subject to evaluation.

The successful applicant for the position will be responsible for building up a strong research group and initiate a new independent research program in functional genomics with focus on genetic analysis of signaling pathways, imaging of signaling, or chemical biology and high throughput cell biology. Relevant research areas also include other aspects of functional genomics and biotechnology. Qualification requirements include a PhD or equivalent degree, appropriate postdoctoral training, experience with supervision and a track-record of high-impact publications in top journals of biology or medicine.
In addition, considerable weight will be put on the research plan proposed by the candidate and on how this will integrate and synergize with the activity in the region.

For further information and a more comprehensive job description visit our website www.biotek.uio.no. Please contact Centre Director, Professor Kjetil Taskén (kjetil.tasken@biotek.uio.no) with inquiries. Applications should be addressed to the Director and sent electronically as a single pdf-file to the Biotechnology Centre of Oslo at recruitment@biotek.uio.no to arrive no later than

15th of February, 2011

marked REF. NO.: 2010/13469.

Welcome seeking
For full details, see
www.uio.no/english/about/vacancies/

HEAD, SCHOOL OF BIOLOGICAL SCIENCES

The Rochester Institute of Technology invites applications for Head of the School of Biological Sciences. As chief academic, fiscal and administrative officer for the School, the Head is expected to provide leadership, advocacy, oversight, and management for the entire Academic Unit. We seek candidates with excellent people skills and demonstrated commitment to undergraduate teaching and research, who understand, respect and value all of the Biological Sciences. The Head will be responsible for enabling student success and fostering the growth of faculty scholarship and grantsmanship. The successful candidate will hold a Ph.D., have an established record of publications, grants, and prior administrative experience, and should have qualifications consistent with the rank of tenured full professor. The exact area of scholarship within the Biological Sciences is open but should align with one of the School's focus areas.

The School of Biological Sciences currently has 29 faculty and six administrative and technical staff, and nearly 700 students. We offer undergraduate degrees in Biology, Biotechnology, and Medical Sciences, and both undergraduate and Masters degrees in Bioinformatics, and Environmental Science. In addition to these degree programs, the School supports a year-round undergraduate research program in all of these areas.

Applicants for this position should apply online at **http://apptrkr.com/170218**. Search for IRC 42555 and upload your letter of interest; a vita; a position statement describing your leadership style, philosophy of teaching and research, and the relationship between them, and a statement of your experience with and commitment to RIT's core values, honor code, and statement of diversity. Please arrange to have 3 letters of reference sent to robert.rothman@rit.edu (preferred) or mailed to Dr. Robert Rothman, School of Biological and Medical Sciences, Rochester Institute of Technology, 85 Lomb Memorial Drive, Rochester, NY 14623. Review of applications will begin on January 15, 2011 and continue until the position is filled, with a start date of July 1, 2011. The Rochester Institute of Technology is an equal opportunity/affirmative action employer. All qualified individuals with the ability to contribute in meaningful ways to the university's continuing commitment to its core values, honor code and diversity statement are encouraged to apply.

UNIVERSITY OF CAMBRIDGE

A world of opportunities
www.cam.ac.uk/jobs/

The Professorship of Plant Systematics and Evolution and The Directorship of The Cambridge University Botanic Garden

Applications are invited for the Professorship of Plant Systematics and Evolution from senior academics whose work falls within the general field of the Professorship to take up appointment as soon as possible.

The successful candidate will also be the Director of the Cambridge University Botanic Garden, one of the UK's finest collections of living plants, which provides an excellent opportunity to develop research and teaching programmes that are relevant to taxonomy, systematics and evolution as well as conservation and biodiversity. There will also be the opportunity for the Director to be the Curator of the University Herbarium.

Further information is available at: www.admin.cam.ac.uk/offices/academic/secretary/professorships/ or contact the Academic Secretary, University Offices, The Old Schools, Cambridge, CB2 1TT, (email: ibise@admin.cam.ac.uk), to whom a supporting statement should be sent, together with details of current and future research plans, a curriculum vitae, a publications list and form CHRIS/6 (parts 1 & 3 only with details of three referees) so as to reach him no later than 18 February 2011.

Informal enquiries may be made to Professor Sir David Baulcombe, Head of the Department of Plant Sciences (oo203@cam.ac.uk) or Professor Keith Richards, Chair of the CUBG Syndicate (keith.richards@geog.cam.ac.uk).

The University is committed to Equality of Opportunity.

UCRIVERSIDE

Department of Entomology – 041
College of Agriculutural and Natural Sciences

Assistant Professor and Assistant Entomologist in the area of Vector Biology/Medical Entomology, University of California, Riverside. Position available July 1, 2011, 9-month appointment, 50% Instruction and Research /50% Organized Research. Appointment level and salary commensurate with experience. Ph.D. in Entomology or related discipline required. The successful candidate must have strong training and experience with modern approaches to the study of aspects of vector biology. A program of research could include basic and applied studies of vector population genetics, genetics of insecticide resistance, host-vector-pathogen relationships, transmission biology, strategies for vector and disease management. The position offers unique opportunities to apply molecular techniques to the understanding of disease dynamics. Studies may include a combination of laboratory and field activities with the goal of mitigating the impact of vector-borne disease in California and abroad. Teaching responsibilities include supervision of graduate students, participation in undergraduate biological science instruction in medical entomology, curricula associated with genetics as well as a graduate course taught in an area of interest. Teaching and research interactions within interdepartmental programs are encouraged. Participation in development and instruction of new curricula associated with the School for Global Health is encouraged.

Send curriculum vitae, transcripts, statement of research interests, reprints, manuscripts in press, and have four letters of recommendation sent to: **Dr. William E. Walton, Search Committee Chair, Department of Entomology, University of California, 3401 Watkins Dr., Riverside, CA 92521; e-mail: william.walton@ucr.edu; phone (951)-827-3919**. Review of applications will begin on **January 31, 2011**; however, this position will remain open until filled. Information about the Entomology Department and an expanded position description can be found on the website: **http://www.entomology.ucr.edu**.

The University of California is an Affirmative Action/Equal Opportunity Employer committed to excellence through diversity, and strongly encourages applications from all qualified applicants, including women and minorities.

UCRIVERSIDE

Department of Entomology – 041
College of Agriculture and Natural Sciences

Assistant Cooperative Extension Specialist and Assistant Professor in the area of Urban/Structural Entomology, University of California, Riverside. Position available July 1, 2011, 11-month appointment, 75% Cooperative Extension Specialist/25% Instruction and Research. Appointment level and salary commensurate with experience. Ph.D. in Entomology or related discipline required. The successful candidate must have strong training and experience with modern approaches to the study of Urban/Structural IPM. A program of research could include basic and applied studies of invasive species, insect toxicology, molecular physiology, environmental toxicology, and behavior. The appointee will be responsible for coordinating conferences, training workshops, and outreach activities. Experience using modern innovative and successful communication methods and ability to deliver a web-based knowledge environment about urban entomology are desirable. Teaching responsibilities include supervision of graduate students, and participation in undergraduate biological science instruction in general and urban entomology. Interactions with the other research groups in interdepartmental programs are encouraged.

Send curriculum vitae, transcripts, statement of research interests, reprints, manuscripts in press, and have four letters of recommendation to: **Dr. Michael K. Rust, Search Committee Chair, Department of Entomology, University of California, 3401 Watkins Dr., Riverside, CA 92521; e-mail: michael.rust@ucr.edu; phone (951)-827-5327**. Review of applications will begin **January 31, 2011**; however, this position will remain open until filled. Information about the Entomology Department and an expanded position description can be found on the website: **http://www.entomology.ucr.edu**.

The University of California is an Affirmative Action/Equal Opportunity Employer committed to excellence through diversity, and strongly encourages applications from all qualified applicants, including women and minorities.

ETH

Eidgenössische Technische Hochschule Zürich
Swiss Federal Institute of Technology Zurich

Assistant Professor (Tenure Track) of Biomolecular Engineering

The Department of Biosystems Science and Engineering (www.bsse.ethz.ch) at ETH Zurich invites applications and nominations for an outstanding candidate in the area of biomolecular engineering. Ideally, the candidate should have a strong background in biomolecular engineering, preferably with proteins in a context of biological systems engineering, and demonstrate the potential for building an excellent independent research group in the field with a focus on experimental approaches.

D-BSSE of ETH Zurich is located in Basel, the heart of the BioValley area providing excellent opportunities for collaboration within this strong life science research community at the academic, clinical and pharmaceutical level. Its main research thrust is the understanding and engineering of biological systems for medical or chemical purposes, which generates numerous opportunities for interactions. Collaborations with the SystemsX.ch community (www.systemsx.ch), the Swiss initiative in systems biology, are encouraged. The new chair at the D-BSSE will be funded by the Misrock Foundation.

The educational goal of D-BSSE is to teach students at both the undergraduate and graduate levels by integrating expertise and knowledge from biologists, chemists, physicists, engineers, computer scientists and mathematicians, along with industrial collaborators. The successful candidate will be expected to teach undergraduate level courses (German or English) and graduate level courses (English).

Assistant professorships have been established to promote the careers of younger scientists. The initial appointment is for four years with the possibility of renewal for an additional two year period and promotion to a permanent position.

Please address your application together with a curriculum vitae, a list of publications and a statement of research and teaching interests **to the President of ETH Zurich, Prof. Dr. Ralph Eichler, no later than March 31, 2011.** With a view towards increasing the number of female professors, ETH Zurich specifically encourages qualified female candidates to apply. **In order to apply for this position, please visit: www.facultyaffairs.ethz.ch.**

UCDAVIS

Assistant Professor of Animal Microbiology/ Immunology, Department of Animal Science

The University of California at Davis is pleased to announce recruitment for a tenure-track faculty position in Microbiology/Immunology. The successful candidate will join the Department of Animal Science in the College of Agricultural and Environmental Sciences at the rank of Assistant Professor. Criteria for appointment include: a Ph.D. or equivalent, a strong interest in microbiology/immunology of poultry (preferred) or livestock, a record of excellence in scholarly research, and demonstrable potential to establish a competitively funded research program relevant to animal health, pre-harvest food safety or disease ecology of the production environment. The appointee will be responsible for teaching an undergraduate course on concepts in immunology and domestic animal health, be actively involved in undergraduate advising, curricular development and department and university service. The appointee is also expected to guide and mentor graduate students and participate in the outreach programs of the department and college.

The Davis campus of the University of California maintains state-of-the-art research facilities and provides ready access to a diverse array of poultry and livestock, including inbred research lines. The position is a nine-month tenure track appointment, with an eleven-month term appointment offered and continued contingent upon successful personnel review.

Applicants should submit materials via the following website: **https://secure.caes.ucdavis.edu/Recruitment/**. Additional inquiries can be directed to **Professor K. C. Klasing, Recruitment Advisory Committee Chair, Department of Animal Science, One Shields Avenue, University of California, Davis, CA 95616, telephone (530) 752-1901, kcklasing@ucdavis.edu**. The position will remain open until filled but to ensure consideration, applications should be received by **February 15, 2011**.

UC Davis is an Affirmative Action/Equal Employment Opportunity Employer and is dedicated to recruiting a diverse faculty community. We welcome all qualified applicants to apply, including women, minorities, veterans, and individuals with disabilities.

NIFA

UNITED STATES DEPARTMENT OF AGRICULTURE NATIONAL INSTITUTE OF FOOD AND AGRICULTURE

The National Institute of Food and Agriculture (NIFA) in the Department of Agriculture (USDA) was recently reorganized to a structure with four Institutes. Each of the Institutes is co-led by an Assistant Director and a Principal Scientist. The Assistant Director provides leadership for the administration of programs that comprise the Institute. The Principal Scientist provides the scientific leadership to programs assigned to the Institute. More information about NIFA can be found at **http://www.nifa.usda.gov/**.

NIFA is seeking to fill the position of **Assistant Director of the Institute of Food Safety and Nutrition** (NIFA:SES:10-14). This is a Senior Executive Service (SES) position. The salary ranges from $119,554 to $179,700, commensurate with experience.

A copy of the job announcement may be located on the Office of Personnel Management web page at **http://www.usajobs.opm.gov/**. As specified in the job announcement, applicants must meet mandatory qualifications and address specific executive core and technical qualifications. Veterans preference applies.

All applications must be received by **February 14, 2011**. For information about the application process, contact **Deborah Crump** (**301-504-1448**). To learn more about NIFA, contact **Betty Lou Gilliland** (**202-720-5506**).

U.S. CITIZENSHIP REQUIRED.
USDA IS AN EQUAL OPPORTUNITY PROVIDER AND EMPLOYER.

Associate or Full Professor in Cancer Biology

The Jackson Laboratory, a private, nonprofit, mammalian genetics research institute and NCI-designated Cancer Center in Bar Harbor, Maine, is seeking senior cancer researchers (equivalent to Associate and Full Professor) to join our expanding Cancer Center.

Our exceptionally collaborative faculty is supported by outstanding scientific services, unparalleled mouse and bioinformatics resources, pre- and post-doctoral training programs, and an internationally recognized courses and conferences program covering a wide range of topics in human biology and disease, emphasizing the mouse as a genetic model. Research within The Jackson Laboratory Cancer Center uses the mouse as a tool for modeling and understanding the organization, dynamics and function of the mammalian genome and the mechanisms that regulate genome stability. We directly test the effects of genomic perturbations on cancer initiation, progression, and response to therapy in the context of the whole organism, where we can define the interactions between cancer cells and the host environment. We are actively developing scientific programs with both internal and external partners that apply our strengths in basic cancer research to translational research.

Characteristics of successful candidates will include:

- ***A Ph.D., D.V.M., or M.D. and an established research program in cancer biology***
- ***Proven ability to maintain a competitively funded research program***
- ***Enthusiasm for mentoring junior faculty***

Experience in forging successful partnerships between basic and translational research centers is a plus.

Applicants should submit a curriculum vitae, including a record of mentoring relationships, and a statement of research plans and interests online to: www.jax.org/careers, click on Faculty Positions, then on Cancer Biology — Associate or Full Professor position #2595. Applications must be received no later than April 1, 2011.

For information about The Jackson Laboratory Cancer Center go to: http://research.jax.org/cancer/index.html

The Jackson Laboratory is located in Bar Harbor, Maine on Mt. Desert Island. Surrounded by Acadia National Park, the community offers beautiful scenery and abundant opportunities for outdoor recreation including hiking, biking, kayaking, sailing and cross-country skiing. It also has exceptional schools, good health care access and ample cultural opportunities. It's a great place to live, work, play and raise a family.

The Jackson Laboratory is an EOE/AA employer.

The Jackson Laboratory
Leading the search for tomorrow's cures

600 Main Street,
Bar Harbor, Maine 04609

Northeastern University

Cluster Hire in Sustainability

Joint Hires between the Colleges of Engineering; Science; Business; Arts, Media and Design; and Social Science and Humanities at Northeastern University

Northeastern University seeks outstanding candidates for multiple interdisciplinary positions in fields broadly relating to the core mission of Sustainability, with a focus on the complementary areas of Urban Sustainability and Energy Sustainability. In the area of Urban Sustainability, subjects of interest include, but are not limited to, development of sustainably optimized building and infrastructure components; high performance architecture; sustainable strategies for distributed lifeline systems; innovative materials; healthy living within the constructed environment; regional simulation and assessment for applications in sustainable engineering; supply chain modeling; and urban ecologies, urban sustainability planning, and brownfield redevelopment. In the area of Energy Sustainability, subjects of interest include, but are not limited to, power engineering, energy storage, transformation and management, energy generation technologies, biofuels and energy efficiency. Appointments at the rank of Full or Associate Professor are anticipated. Northeastern University will also consider a multidisciplinary cluster hire, where several candidates elect to form a team which proposes innovative and translational research directions responding to one or more of these positions.

Candidates are expected to work with faculty members across the University, and particularly across the relevant Colleges, in developing scholarship and funding opportunities at the intersection of traditional disciplines. Successful candidates will hold tenure and joint appointments within departments in one or more of the participating colleges.

Northeastern University is ideally located in the heart of Boston, in close proximity to a number of major academic institutions and innovative technology companies and installations. Northeastern's affiliated departments and research centers maintain strong collaborative interactions with many of these institutions. The University is also home to a number of NSF-, DHS- NIST- and NIH-supported core research centers. Northeastern is highly committed to interdisciplinary, experiential and use-inspired research geared toward addressing global and societal challenges while embracing global opportunities.

Candidates should have a doctoral degree in relevant fields pertaining to issues of urban and/or energy sustainability. Candidates should also exhibit strong scholarly achievements for developing interdisciplinary connections; and a record as an accomplished and innovative educator with the ability to teach in more than one of the participating colleges. It is anticipated that successful candidates are leading an active ongoing research program as evidenced by a strong record of publication in prominent peer-reviewed journals, mentorship of pre- and postdoctoral trainees, and by possession of a strong record of substantial, sustained and currently transferable extramural research funding.

Candidates are sought from a wide range of disciplines for these interdisciplinary positions in sustainability, and applicants are asked to submit materials online by visiting **http://www.northeastern.edu/provost/faculty/positions.html** and clicking on **Access Faculty Positions**. Applications should include a cover letter, a statement of current and future research interests, *curriculum vitae*, and contact information for at least three references. Screening of applications begins **January 31, 2010** and will continue until the position is filled. More information regarding this position may be obtained by contacting **sustainability_search@neu.edu**.

Northeastern University if an Equal Opporunity/Affirmative Action, Title IX, and and ADVANCE Institution. Minorities, women, and persons with disabilities are strongly encouraged to apply. Northeastern University embraces the wealth of diversity represented in our community and seeks to enhance it at all levels. Northeastern University is an E-Verify Employer.

Faculty Position
Assistant/Associate Professor/Professor
at the
Department of Physiology

The National University of Singapore invites applications for full-time tenure-track faculty positions in the Department of Physiology. Currently the department has research programmes in the following areas: The **Cancer Biology** Programme focuses on the study of apoptosis, experimental therapeutics, metastasis, DNA damage and repair, and telomere biology. The **Immunology** Programme is involved in the study of immune mechanisms in the inflammatory process, T cell biology and development and immunotherapy. The **Neuroscience** Programme focuses on molecular, cellular and system neurobiology with current strengths in the neurobiology of pain, the structure-function relationship of voltage-gated ion channels and neurodegenerative diseases. The **Quantitative Physiology and Engineering** Programme involves the study and manipulation of the structural-function relationship of cells and tissue so as to enable tissue repair and regeneration.

Candidates are expected to hold a Ph.D. or M.D. with post-doctoral experience and a track record of extramurally funded independent research.

Appointees will be expected to compete for independent research funding and are required to participate in undergraduate and graduate level teaching of medical, dental, pharmacy and life science students.

Remuneration and level of appointment will commensurate with qualifications and experience.

Interested candidates should send their resume, research plan and names of six referees by **15 February 2011** to:

Dr. Tuck Wah Soong
Head, Department of Physiology
Yong Loo Lin School of Medicine
National University of Singapore
Block MD9, 2 Medical Drive, Singapore 117597
Email: **phshead@nus.edu.sg**
Fax: (65) 6778 8161

Only shortlisted candidates will be invited for an on-site visit and interview

Details are available at **http://medicine.nus.edu.sg/phys/Recruitment_Teaching.html**
For call enquiries: (65) 6516 1878

Department of Physiology
NUS Yong Loo Lin School of Medicine
A member of the National University Health System

SYSTEMATIC ENTOMOLOGIST

The Smithsonian Institution's National Museum of Natural History seeks a systematist to conduct an integrative, collections-based research program focused on terrestrial arthropods or aquatic insects. The successful candidate is expected to develop an internationally recognized research program utilizing modern methods, which may include bioinformatics, in pursuing systematic research on Coleoptera, Diptera, Heteroptera, or another terrestrial arthropod or aquatic insect group, with relevance to phylogenetics, genetics, evolution, morphology, behavior, biogeography, biodiversity, ecology, or related fields. Frequent publication of highly regarded papers in competitive, peer-reviewed journals is expected, as is curation of collections in specialty area, service to the scientific community in leadership capacities, acquisition of external funding, engagement in outreach activities, and mentorship of students.

The position will be filled at the GS-12 level (salary range is $74,872–$79,864 per year commensurate with experience). For application procedures see: **www.sihr.si.edu** or **www.usajobs.opm.gov** and refer to Announcement **11A-JW-296508-DEU-NMNH** for a Research Entomologist, or contact **Jan Williams, 202-633-6363, willija@si.edu**. Applications must be received by **February 15, 2011**. Applicants will be notified by e-mail when their application is received. U.S. citizenship is required.

The Smithsonian Institution is an Equal Opportunity Employer.

Chaired Professor Position
Children's Hospital Boston and Harvard Medical School

The Vascular Biology Program at Children's Hospital Boston is seeking applications for a chaired faculty position at the level of Professor in a field related to the study of Vascular Biology. The successful candidate will be appointed as the James and Thea Stoneman Professor of Vascular Biology at Harvard Medical School. Candidates for this position will hold a Ph.D. and/or M.D. degree and will have an internationally recognized record of research excellence and a successful history of obtaining independent funding. Opportunities to collaborate with scientists and clinicians whose areas of expertise extend from fundamental cellular and molecular mechanisms to clinical and translational research in the field of vascular biology will be available. Applicants whose primary interest is in vascular biology and/or diseases that have a vascular component are encouraged to apply.

Interested applicants should forward their curriculum vitae and inquiries to:

Faculty Search Committee
Vascular Biology Program
Karp Family Research Building,
Room 11.124
Children's Hospital Boston
300 Longwood Avenue
Boston, MA 02115

Children's Hospital Boston is an Equal Opportunity Affirmative Action Employer. Applications from qualified women and underrepresented minorities are encouraged.

The University of Georgia

THREE FACULTY POSITIONS IN FUNGAL BIOLOGY

The University of Georgia invites applications for three tenure-track positions in the biology of fungi and fungus-like organisms to join a highly interactive multidepartmental group of plant and microbial biologists.

1) The **Department of Plant Biology** in the Franklin College of Arts and Sciences seeks applicants at the level of assistant professor, though candidates may also be considered at the level of early associate professor. We are especially interested in applicants studying the biology, genetics, cellular biology, functional genomics, phylogenomics or ecology of plant-associated fungi, including mycorrhizal fungi.

2) The **Department of Microbiology** in the Franklin College of Arts and Sciences seeks applicants at the level of assistant professor, though candidates may also be considered at the level of early associate professor. We are especially interested in applicants studying fungal diversity and ecology; fungal interactions with plants, animals or other microbes; fungal natural products and their impact on the environment, food or human health; manipulation of fungi for industrial and environmental applications, such as biofuel production and bioremediation; and other areas in basic and applied fungal biology.

3) The **Department of Plant Pathology** in the College of Agricultural and Environmental Sciences seeks applicants at the assistant or associate professor level. We are especially interested in applicants studying plant-fungal interactions to facilitate management of economically important plant diseases, understanding the ecological and genetic dynamics of host-pathogen resistance, and using contemporary approaches to elucidate the phylogeny of plant-pathogenic fungal species.

Applicants at the assistant professor level should have a Ph.D. degree and postdoctoral research experience. Applicants at the associate professor level should also have a record of independent scientific productivity. Successful applicants will be expected to establish (assistant professor) or continue and expand (associate professor) a vigorous externally funded research program and to instruct and mentor undergraduate and graduate students. To apply, the following should be submitted at **https://www.plantbio.uga.edu/positions/**: (1) a single PDF containing a cover letter which includes a statement of the position(s) the candidate is applying for, a curriculum vitae, and 1-2 page statements of research interests and teaching philosophy; (2) a single PDF containing reprints of three research papers; (3) three letters of recommendation submitted directly by the references. For questions, please contact **Stephanie Chirello** at **schirello@plantbio.uga.edu** or **706-542-1820**. Review of applications will begin **February 7, 2011**, and the search will remain open until the positions are filled.

The Franklin College of Arts and Sciences, the College of Agricultural and Environmental Sciences, their many units and the University of Georgia are committed to increasing the diversity of faculty and students and sustaining a work and learning environment that is inclusive. Women, minorities and people with disabilities are encouraged to apply. The University of Georgia is an EEO/AA Institution.

Chinese Academy of Sciences
Max-Planck-Gesellschaft

The Max-Planck-Gesellschaft (MPG) with support of the Chinese Academy of Sciences (CAS)

intends to establish

MAX PLANCK RESEARCH GROUPS

at the

CAS-MPG PARTNER INSTITUTE FOR COMPUTATIONAL BIOLOGY (PICB)

in Shanghai

Applications are invited for the position of Max Planck Research Group Leaders for young scientists in China or abroad who have achieved a degree of international recognition in their field, preferably in Computational approaches to Genomics, Epigenomics, Functional genomics, and biomolecular simulations in Protein Sciences, as well as Biostatistics, and Biomathematics. The initial contract will cover five years with the possibility of an extension. It includes a five-year core budget (research positions, running costs, and investments).

The CAS-MPG Partner Institute for Computational Biology, Shanghai Institutes for Biological Sciences, Chinese Academy of Sciences, is a joint non-profit research institution founded by the Chinese Academy of Sciences and the German Max Planck Society. See the home page of the institute (http://www.picb.ac.cn/) for more information. The proximity to experimentally oriented, internationally competitive research institutes on the campus of the Shanghai Institutes for Biological Sciences, CAS, allows close scientific cooperation and interaction between theoretical and experimental research.

Applications should include a tabular CV, a list of publications with reprints of three selected papers, a description of major scientific achievements and a summary of future research plans. Successful candidates should be prepared to attend a symposium to be held on Mar. 8-9, 2011 in Shanghai. Travel and accommodation expenses will be covered.

The Max Planck Society is committed to equal opportunities and to employing individuals with disabilities.

The deadline for application is **Jan. 23, 2011**.

Applications should be sent to:

Barbara SPIELMANN
E-mail: spielmann@gv.mpg.de
Dr. Barbara Spielmann
Max Planck Society
Hofgartenstraße 8
D-80539 München, Germany
Phone: +49-89-2108-1365
Fax: +49-89-2108-1041

CHEN Yi
E-mail: ychen@picb.ac.cn
Ms. Chen Yi
MPG-CAS Partner
Institute for
Computational Biology
320 Yueyang Lu
Shanghai 200031, China
Phone: +86-21-5492-0456
Fax +86-21-5492-0451

Chinese Academy of Sciences
Max-Planck-Gesellschaft

The Max-Planck-Gesellschaft (MPG)

is searching for the

Head of a Paul Gerson Unna Research Group of the Max Planck Society

in the field of

Skin and hair follicle morphogenesis, molecular biology of the ageing skin, and related areas.

The group will be located at the

CAS-MPG PARTNER INSTITUTE FOR COMPUTATIONAL BIOLOGY (PICB)

in Shanghai

The initial contract will cover five years with the possibility of an extension. It includes a five-year core budget (research positions, running costs, and investments).

The CAS-MPG Partner Institute for Computational Biology, Shanghai Institutes for Biological Sciences, Chinese Academy of Sciences, is a joint non-profit research institution founded by the Chinese Academy of Sciences and the German Max Planck Society (see http://www.picb.ac.cn/). The proximity to experimentally oriented, internationally competitive research institutes on the campus of the Shanghai Institutes for Biological Sciences, CAS, allows close scientific cooperation and interaction between theoretical and experimental research.

Applications should include a tabular CV, a list of publications with reprints of three selected papers, a description of major scientific achievements and a summary of future research plans. Successful candidates should be prepared to attend a symposium to be held on Mar. 8-9, 2011 in Shanghai. Travel and accommodation expenses will be covered.

The Max Planck Society is committed to equal opportunities and to employing individuals with disabilities.

The deadline for application is **Jan. 23, 2011**.

Applications should be sent to:

Barbara SPIELMANN
E-mail: spielmann@gv.mpg.de
Dr. Barbara Spielmann
Max Planck Society
Hofgartenstraße 8
D-80539 München, Germany
Phone: +49-89-2108-1365
Fax: +49-89-2108-1041

CHEN Yi
E-mail: ychen@picb.ac.cn
Ms. Chen Yi
MPG-CAS Partner
Institute for
Computational Biology
320 Yueyang Lu
Shanghai 200031, China
Phone: +86-21-5492-0456
Fax +86-21-5492-0451

SYMPOSIUMS

COURSE

NORTHWESTERN UNIVERSITY
FEINBERG
SCHOOL OF MEDICINE

NEURO-ONCOLOGY
RESEARCH FACULTY
OPEN RANK TENURE-TRACK

Northwestern Brain Tumor institute (NBTI),
Department of Neurological Surgery and
Lurie Cancer Center

As part of the Feinberg School of Medicine of Northwestern University, the Northwestern Brain Tumor Institute, the Department of Neurological Surgery and the Lurie Cancer Center announce a search for a full-time neuro-oncology research open-rank, tenure or non-tenure eligible faculty appointment at Northwestern's downtown Chicago campus. Outstanding candidates employing innovative molecular/cellular approaches to oncogenesis research, genomics, proteomics, metabolics of brain tumors, or molecular diagnostics or therapeutics are encouraged to apply.

Laboratory space adjacent to many other neuroscience and cancer research laboratories is available, with a genuine opportunity to expand to current level of research productivity in a collaborative milieu. The appointee will have access to 33 advanced shared facilities including imaging, transgenic and knockout projects, monoclonal antibodies, histology, IHC, ISH sequencing and genotyping, genomics micro-arrays, computational biology, structural biology, translational biotechnology, and access to a large volume of repositories housing human brain tumor tissue and other specimens. In addition, the candidate will join multi-disciplinary, multi-faceted members of the National and International Neurology, Neuro-Oncology, and Oncology Groups including ECOG, ACOSOG, RTO, etc.

The Ph.D or M.D. appointee to Neurological Surgery is expected to have an independently funded research program and participate in graduate and medical school teaching. An M.D. appointee would have the opportunity to participate in limited clinical activities, if desired. Salary is negotiable based on candidate qualifications.

This recruitment is part of a growing commitment to neuroscience research at Northwestern University. Additional information about The Feinberg School of Medicine, the Northwestern Brain Tumor Institute, the Department of Neurological Surgery and the Lurie Cancer Center can be found on our web pages: **www.medschool.northwestern.edu** and **www.northestern.edu/nuin**.

Interested candidates should submit the following materials as part of the application:

1) Current CV and list of publications
2) Brief statement of research interests (three pages or less)
3) Three letters of reference sent on applicant's behalf

Applications should send all materials to:

Dr. James Chandler
Neuro-Oncology Research Faculty Search Committee
(#16044)
Department of Neurological Surgery
676 N. St. Clair, Suite 2210
Chicago, IL 60611

Or e-mail to: k-makielski@northwestern.edu

Completed applications must be received by **March 1, 2011**. Appointment start date will be negotiable.

Northwestern University is an Affirmative Action/Equal Opportunity Employer. Hiring is contingent upon eligibility to work in the United States. Women and minorities are encouraged to apply.

The Ohio State University www.osu.edu

THE OHIO STATE UNIVERSITY

Dean of the College of Dentistry

The College of Dentistry at The Ohio State University invites nominations and applications for the position of Dean of the College of Dentistry.

The Ohio State University has one of the most comprehensive health sciences campuses in the United States and includes the colleges of Dentistry, Medicine, Nursing, Optometry, Pharmacy, Public Health, Veterinary Medicine; five hospitals, University Hospital, University Hospital East, the Arthur G. James Cancer Hospital and Richard J. Solove Research Institute, the Richard M. Ross Heart Hospital, and The Ohio State University Harding Hospital; numerous research centers and institutes; and a network of more than 30 community-based primary and specialty care facilities throughout central Ohio.

The College of Dentistry is fully accredited, with 95 full-time faculty members and 257 staff members, and engages in academic programming, research and health care delivery. The College's total budget for FY10 was $25.6 million, not including external/restricted funding.

The educational program of the College is managed by faculty and organized into eight divisions: endodontics; oral and maxillofacial surgery; oral biology; orthodontics; pediatric dentistry; periodontology; dental hygiene; and restorative/prosthetic dentistry and primary care.

The dean is the chief executive officer of the College and responsible for advancing the College's academic mission of teaching, research, and service. The dean reports to the executive vice president and provost and is a member of the University's Council of Deans. The dean also serves as chair of the Hospital Dental Service and as president of the Dental Faculty Practice Association, Inc.

Faculty in the College are engaged in a broad and diverse array of basic and clinical research. Basic research includes dental materials science, immunology, molecular microbiology, neuroscience, oral cancer, and psychoneuroimmunology. Faculty serve as mentors to: M.S. students in all of the dental specialties, combined DDS-PhD students, PhD students in oral biology, and PhD students in programs outside the college.

Nominees and applicants with a DDS degree or equivalent are preferred. Candidates must qualify for a tenured appointment as professor in the College. The preferred candidate will have a record of high level administrative leadership within a complex dental educational and clinical enterprise demonstrating successful initiatives. Personal accomplishments should be evident in research and/or dental sciences. In addition, a commitment to diversity should be evident and is expected. Candidates should become familiar with the University's six priorities at: http://oaa.osu.edu/assets/files/documents/Geegoals.pdf.

Salary and other considerations will be consistent with the University's commitment to recruiting the best-qualified individual.

Nominations, inquiries, or applications may be sent in confidence to

Dr. Melvin D. Shipp, Chair
Advisory Committee for the Search for the Dean
of the College of Dentistry
A400 Starling Loving Hall , 338 West 10th Avenue
Columbus, OH 43210

Nominations and applications will be received until a new dean is selected, with the expectation of having someone in place by Summer 2011.

To build a diverse workforce, The Ohio State University encourages applications from individuals with disabilities, minorities, veterans, and women. EEO/AA employer.

POSITIONS OPEN

THE SARAH AND DANIEL HRDY FELLOWSHIP in Conservation Biology
Department of Organismic and Evolutionary Biology
Harvard University

The Department of Organismic and Evolutionary Biology (OEB) invites applications or nominations for the Sarah and Daniel Hrdy Visiting Fellowship in Conservation Biology. The Hrdy Visiting Fellowship is available either at the **SENIOR FACULTY** level or at the **JUNIOR FACULTY** (i.e., postdoctoral) level for one or two semesters. Duties include teaching one course and/or giving lectures in conservation biology, as well as research and collaboration with members of the Harvard community. Recipients of this fellowship are expected to have a strong and transformative effect on the study of conservation biology at Harvard, from the undergraduate to the senior teaching level. The fellowship includes a stipend with modest additional funds for research and teaching. Applicants should contact a faculty sponsor(s), with whom they will collaborate, before applying. Applications should include a cover letter with a statement of intent, curriculum vitae, and representative publications, and applicants should arrange to have three letters of reference sent.

Please submit applications online at **website: https://webapps.sciences.fas.harvard.edu/apply/oeb-hrdy-2010/.**

Applicants should contact a faculty sponsor(s), with whom they will collaborate, before applying. Applications should include a cover letter with a statement of intent, curriculum vitae, and representative publications, and applicants should arrange to have three letters of reference sent.

Further information about OEB is available at **website: http://www.oeb.harvard.edu** and address questions about the application/nomination process to **Mr. Christopher Preheim** in OEB at **e-mail: cpreheim@oeb.harvard.edu.**

Review of applications will begin on **February 21, 2011**.

Harvard University is an Affirmative Action/Equal Opportunity Employer. Applications from women and minority candidates are strongly encouraged.

ASSISTANT/ASSOCIATE PROFESSOR of Toxicology
University of Connecticut, Storrs, CT

The Department of Pharmaceutical Sciences at the University of Connecticut, School of Pharmacy invites applications for a tenure-track faculty position in neurotoxicology at the Assistant or Associate Professor level, starting August 23, 2011. We are seeking a scientist with a strong background in research and teaching with a focus on the effects of xenobiotics on the nervous system and/or developmental neurotoxicology. This will complement the interests of the faculty in the Department of Pharmaceutical Sciences, which includes integrative approaches to elucidate mechanisms of drug or toxicant action, drug discovery and design, and pharmaceutical technology. The Department is housed in a new 200,000 square foot state-of-the-art building in the science quad of the University of Connecticut and encourages faculty interdisciplinary interactions with other programs of the University such as Physiology/Neurobiology and the Molecular and Cell Biology Program. The successful candidate is expected to develop a strong extramurally funded research program and to effectively participate in teaching at the graduate and professional levels. A competitive salary and startup funds will be provided. Qualifications: Applicants must possess a Ph.D. degree or equivalent; strong oral and written communication skills, and a strong background in research and teaching with a focus on the toxic effects of xenobiotics on the nervous system and/or developmental neurotoxicology. Preferred Qualifications: Contribute through research, teaching, and/or public engagement to the diversity and excellence of the learning experience.

Applicants should submit a cover letter, curriculum vitae, brief statement of research and teaching interests, names, telephone numbers and full addresses of three references via Husky Hire at **website: http://www.jobs.uconn.edu.** Screening of applications will begin immediately and continue until the position is filled. *The University of Connecticut is an Equal Employment Opportunity/Affirmative Action Employer.*

POSITIONS OPEN

A three-year **POSTDOCTORAL FELLOWSHIP** position is available to study iron transport mechanisms and membrane trafficking in polarized epithelial cells using advanced imaging approaches. For more information on our research, check **Margarida Barroso** on **website: http://www.Linkedin.com.**

The optimal applicants should have hands-on experience in molecular biology techniques (ex. molecular cloning, transfection, or RNAi techniques) and an interest in learning advanced imaging techniques. In our lab, candidates will have the opportunity of using confocal and TIRF microscopy to perform quantitative imaging techniques, such as FRET, FRAP, and others. The work is highly analytical and requires good technical expertise and computer skills. Preferred candidates are individuals with a recent Ph.D. degree with a track record of productivity as evidenced by publications and good command of English. The successful candidates will be offered competitive salary and health coverage.

Please e-mail a cover letter describing your past research experience, curriculum vitae, and the names and contact information of two references to:

Margarida Barroso, Ph.D.
Assistant Professor
Center for Cardiovascular Sciences
Albany Medical College
47 New Scotland Av
Albany, NY 12208
E-mail: barrosm@mail.amc.edu

AMC supports a diversified, smoke-free environment and is proud to be an Equal Opportunity/Affirmative Action Employer, encouraging women and minorities to apply. In support of a safe, drug-free environment, criminal background checks and drug testing are part of our hiring process.

ASSISTANT OR ASSOCIATE PROFESSOR
Division of Informatics
University of Alabama at Birmingham

The Department of Pathology, at the University of Alabama at Birmingham (UAB) is seeking an outstanding candidate (M.D., M.D.-Ph.D., or Ph.D.) for a tenure-earning Assistant/Associate Professor position. Rank will be commensurate with qualifications and experience. The successful candidate will join a newly formed Division of Informatics in the Department of Pathology. This individual will be expected to develop a research program in informatics, computational biology, image analysis, or bioinformatics and to participate in informatics training initiatives. UAB has integrated graduate programs across multiple disciplines, which is also reflected in multidisciplinary centers and opportunities for joint appointments, for example, in the school of engineering. There is a particular interest in applications attuned to the integrative challenges of systems-level analysis and the personalization of medicine. Interested candidates should submit a cover letter that includes research interest/experience, curriculum vitae, bibliography, and the names of three references to: **Jonas Almeida, Professor, Department of Pathology, University of Alabama at Birmingham, 619 S. 19th Street WP P230, Birmingham, AL 35233-7331; e-mail: pathinformfac@mail.ad.uab.edu.** Evaluation of applications will occur as they are received and will continue until the position is filled.

The University of Alabama at Birmingham is an Affirmative Action/Equal Opportunity Employer and welcomes applications from qualified women and minorities.

CAREER OPPORTUNITY—Doctor of Optometry (O.D.) degree in 27 months for Ph.D.s in science and M.D.s. Excellent career opportunities for O.D.-Ph.D.s and O.D.-M.D.s in research, education, industry, and clinical practice. This unique program starts in March of each year, features small classes, and 12 months devoted to clinical care.

Contact the Admissions Office, **telephone: 800-824-5526** at: **The New England College of Optometry, 424 Beacon Street, Boston, MA 02115.** Additional information at **website: http://www.neco.edu, or by e-mail: admissions@neco.edu.**

POSITIONS OPEN

TENURE-TRACK FACULTY POSITION in Developmental Biology
Baylor College of Medicine

The Department of Molecular and Human Genetics at Baylor College of Medicine, located in the Texas Medical Center in Houston, seeks an outstanding, basic researcher at the level of **ASSISTANT** or **ASSOCIATE PROFESSOR** with expertise in Developmental Biology. We are particularly interested in candidates who use flies, worms, mice, or other model organisms to tackle important questions broadly related to developmental biology using genetic approaches. The Department ranks first in number of NIH grants among Genetics departments at U.S. medical schools and fosters a rich collaborative environment with other departments and institutions at the Texas Medical Center. The successful candidate will also be a member of the Graduate Program in Developmental Biology, ranked among the best in the United States.

Applicants must hold a Ph.D. and/or an M.D. degree, and are expected to develop an internationally recognized, extramurally funded research program and be active in graduate student training and education. The successful candidate will receive a very generous startup package and highly competitive salary. To apply, please send a single PDF file titled with the applicant's first and last name including a cover letter, curriculum vitae, and a short research summary (three page maximum). All application materials should be sent electronically to **e-mail: agabriel@bcm.edu.**

Receipt Deadline: February 15, 2011.

Virginia Commonwealth University, School of Medicine, Department of Physiology & Biophysics is recruiting a **MASS SPECTROSCOPIST** (Ph.D. required) as a tenure-track position at the **ASSOCIATE PROFESSOR** level. Candidate must have state-of-the-art knowledge of macromolecular mass spectrometry demonstrated by publications and extensive collaborations. Demonstrated ability to attract federally funded shared instrumentation grant awards and independent R01 funding is required. Candidate must have a strong record of assisting funding efforts of biomedical scientists. The successful candidate is expected to utilize mass spectrometry to strengthen research on the MCV campus and to interface with mass spectroscopists on the Monroe campus. Teaching experience and a training record of graduate students is highly desirable. Demonstrated experience working in and fostering a diverse faculty, staff, and student environment or commitment to do so as a faculty member at VCU.

Applicants should electronically submit curriculum vitae, a one-page statement of past accomplishments, a one-page statement of future plans, and a cover letter and contact information for four references to: **Dr. Jason P. Rife,** Chair of the Search Committee (**e-mail: jprife@vcu.edu**), Virginia Commonwealth University, Richmond, Va. Deadline for applications is February 7, 2011, with the expectation to fill the position by July 10, 2011.

Virginia Commonwealth University is an Equal Opportunity/Affirmative Action Employer. Women, persons with disabilities, and minorities are encouraged to apply.

POSTDOCTORAL ASSOCIATE (Two Positions)—Stony Brook University's Department of Neurobiology and Behavior is seeking two postdoctoral associates. Proposed studies combine optogenetic and electrophysiological techniques to probe cholinergic circuitry as part of an NIH Directors Pioneer Award-supported program. Candidates must hold a Doctoral degree or the equivalent degree from a foreign university. Preferred qualifications include an M.D. and/or Ph.D. degree in neuroscience or related field and have prior experience with in vivo electrophysiology. For a full position description, application procedures, or to apply online, visit **website: http://www.stonybrook.edu/jobs (Job Reference #WC-R-6634-10-12-S).** *Stony Brook University/SUNY is an Equal Opportunity/Affirmative Action Employer.*

Making gasoline power history

Researchers at Northeastern University's Center for Renewable Energy Technology have received a $6.38 million grant from the U.S. Department of Energy to develop a less costly, more efficient fuel-cell catalyst. The goal: to bring a new generation of more affordable all-electric cars to market by 2018—and help make at least one kind of fossil fuel go the way of the dinosaur.

Our broad range of interdisciplinary research turns discoveries into solutions, with a focus on global challenges in health, security, and sustainability.

northeastern.edu/research

Northeastern University

cell sciences®

Buy two - Get three!

Buy two recombinant proteins and get an additional protein free for a limited time on any of our popular items listed below. Mention offer code RP342 when ordering. Visit www.cellsciences.com for details.

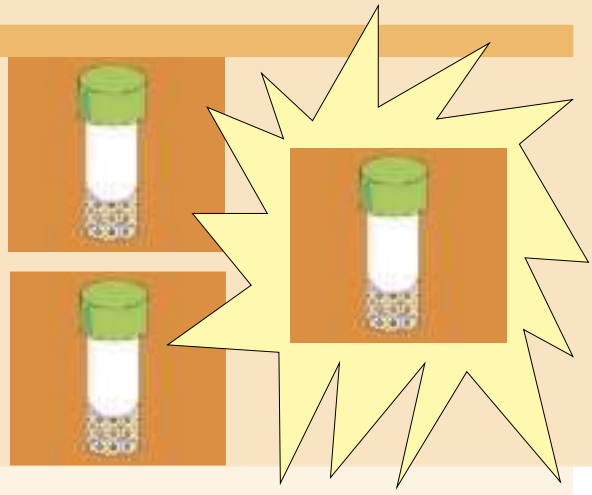

www.cellsciences.com

Recombinant human proteins

BD1 (47 aa)
BD2
BD3
BD4
BLC/BCA1/CXCL13
BMP2
BMP4
CCL14
CD40 Ligand
CNTF
CXCL1
CXCL10/IP10
CXCL11/I-TAC
CXCL2
CXCL3/MIP2 beta
EGF
ENA78/CXCL5
Eotaxin
Eotaxin-2
Exodus-2
FGF1 (aa 141)
FGF7
FGF10/KGF2
FLT3 Ligand
Fractalkine
GCSF
GH1
GM-CSF
IFN alpha 2b
IFN beta 1b
IFN gamma
IGF1
IGFBP3
IL1 alpha
IL1 beta
IL1RA
IL2
IL3
IL4
IL6
IL8 (72 aa)
IL8 (77 aa)
IL10
IL11
IL12
IL13
IL15
IL17
IL21
IL31
IL33
LEC
MCP1
MCP2
MCP4
M-CSF
MEC/CCL28
MIA-2
MICA
MIF
MIG
MIP-1 alpha
MIP-1 beta
MIP-3 alpha/CCL20
MIP-3/CCL23
MIP-4/CCL18
MIP-5/CCL15
NAP-2/CXCL7
Noggin
NRG1
NT4
RANTES
SCF
SDF-1 alpha
TARC/CCL17
TNF alpha
TPO
VEGF

Recombinant mouse proteins

CXCL2
CXCL16
EGF
FGF2
GM-CSF
IFN gamma
IL2
IL3
IL4
IL11
IL33
LIX/CXCL5
MCP2
Noggin
SDF-1 beta
SF20
TNF alpha
VEGF

Recombinant rat proteins

EGF
FGF2
IFN gamma
SDF-1a/CXCL12
SDF-1b/CXCL12

Other recombinant proteins

Protein A/G
Staphylokinase
Streptokinase

Offer good for any combination of three items on the list above. Products are for research use only. Not for human use. Not for use in diagnostic or therapeutic procedures.

CELL SCIENCES INC • 480 NEPONSET STREET, BUILDING 12A, CANTON, MA 02021 • INFO@CELLSCIENCES.COM

TOLL FREE: (888) 769-1246 • TEL: (781) 828-0610 • FAX: (781) 828-0542 • WEB: WWW.CELLSCIENCES.COM

GE Healthcare
Life Sciences

Inspired to Äccelerate scale-up

Inspired by your need for fast and predictable scale-up, we introduce ÄKTA™ avant 150, the latest development in our ÄKTA avant series.

Optimize your process with ÄKTA avant 25 and then scale-up seamlessly to ÄKTA avant 150 by automatically converting your methods using UNICORN™ 6.1 software.

ÄKTA avant is designed to fully exploit the advantages of our modern BioProcess™ media like MabSelect™ and Capto™.

Dedicated column formats ensure seamless scalability from process development to manufacturing – from prepacked HiScreen™ columns to HiScale™ to AxiChrom™ with Intelligent Packing.

Want to know more? Register today to receive a copy of the ÄKTA avant 150 Data File.
www.gelifesciences.com/pr-avant

imagination at work

First published Sept. 2010
GE Healthcare Bio-Sciences AB, Björkgatan 30, 751 84 Uppsala, Sweden
GE09-10

abcam®

What color will help you today?

Abcam offers hundreds of DyLight® conjugated secondary antibodies that complement our products in a wide range of applications.

- Bright fluorescence
- Excellent photostability
- Stable at pH4 - 9
- Pre-adsorbed formats

For all your secondary antibody needs visit:
www.abcam.com/secondary_antibody

DyLight® is a trademark of Thermo Fisher Scientific Inc. and its subsidiaries.

Emission spectra of DyLight® fluorochromes.
Line colors represent the approximate visible colors of the wavelength maxima.

Abcam Inc.
1 Kendall Square, Ste 341
Cambridge, MA 02139-1517
USA

Tel: 1-617-225-2272
Toll free: 1-888-77-ABCAM
Toll free Fax: 1-866-739-9884

GLYCOPROTEOMICS:

THE SWEET SMELL OF WE'RE-GETTING-THERE

Quick: What's the most abundant posttranslational modification on eukaryotic proteins? It's not phosphorylation. Some 50 percent of eukaryotic proteins, and not just those on the cell surface, are dusted with sugars like some molecular pastry. Those glycan modifications mediate intermolecular and intercellular binding events from fertility to immunity. Yet for years, researchers in the sugar and protein communities have operated independently of one another, cataloging sugars free of protein, or proteins free of sugar, and ne'er the twain shall meet. Today, though, the two communities are bridging their technical divide. "We are in a transition now," says James Paulson, principal investigator of the Consortium for Functional Glycomics. Glycoproteomics, he says, "is becoming mainstream." **By Jeffrey M. Perkel**

CREDIT: CAMERON SLAYDEN/*SCIENCE*

Glycoproteomics might be "becoming mainstream," but it's not there yet, and it won't come easy. Proteomics—cataloging and quantifying proteins from a biological sample en masse—is more or less routine. Glycomics, proteomics' glycan analog, is considerably more challenging, but it too is doable.

Put them together, though, and the problem becomes exponentially greater, a reflection of the fact that glycoproteomics encompasses two completely different classes of molecules—molecules with very different chemistries, compositions, and structures. The technology key to solving the problem: Mass spectrometry.

"Without mass spectrometry, to a large extent, glycosciences would still be in the dark ages," says Richard Cummings, chair of biochemistry at **Emory University School of Medicine** and a coordinator of the **Consortium for Functional Glycomics** (CFG). Mass spectrometry, Cummings explains, allows researchers to analyze exceptionally small amounts of sample. "Virtually sub-micrograms to nanograms of material can be sequenced," he says.

That's a good thing, for when it comes to glycoproteins, quantity is hard to come by. It's not a question of expression; even low-abundance proteins are easily seen by today's sensitive mass specs. The problem is heterogeneity: Different protein molecules contain different glycans at the same location, often with different stoichiometries.

"Many glycoproteins have 10, 20, 30, and in worst case, hundreds of glycosylation sites within a single glycoprotein," says Stuart Haslam of **Imperial College London.** "Some of those sites will be occupied, and some will not, and each can have a variety of glycans associated with it." One 2007 study from Haslam's research director, Anne Dell, documented over 100 different modifications on one site on a single protein in the mouse zona pellucida.

The strategy to deal with that heterogeneity—not to mention the general complexity of glycans themselves—has traditionally been simplification. Glycomics researchers tend to clip the sugars from their protein anchors and study those carbohydrates in isolation. Proteomics researchers mostly do the same, analyzing the proteins glycomicists choose to ignore.

More recently, though, a small but growing set of publications demonstrate that it is actually possible to study glycans in the context of their protein scaffolds. Though researchers cannot yet do so in a high throughput proteomics mode, they're getting close. "I will be very surprised if in this year and in 2011 we don't see a lot of … studies mapping glycans onto proteins," says Lance Wells, a member of the Complex Carbohydrate Research Center at the **University of Georgia.**

COMPLEX CARBOHYDRATES, COMPLEX CHEMISTRY

Glycoprotein sugars are not the stuff of baking and coffee. Sugars, says Paulson, are "the third alphabet" of molecular biology (the others being nucleic acids and protein). Theirs is an alphabet of mannose and fucose, of N-acetylglucosamine and sialic acid, and it is one that often is expressed not in letters but hieroglyphics of diamonds, circles, and squares. These "cartoons," as they are called, are both easier to read and write than the chemical entities they describe: oligosaccharides like "GalNAcα1-4GalNAcα1-4(Glcβ1-3) GalNAcα1-4GalNAcα1- 4GalNAcα1-3Bacβ1-NAsn."

That alphabet can assume practically limitless arrangements. Synthesized *sans* template by enzymes called glycosyltransferases, glycan modifications run the gamut from simple monosaccharides to complex branching trees, with myriad continued »

UPCOMING FEATURES

Forensic Technologies—March 4

Genomics: Synthetic Genomics—March 25

Small Devices—April 1

FEATURED PARTICIPANTS

Agilent Technologies
www.agilent.com

Bruker Daltonics
www.bdal.com

California Institute of Technology
www.caltech.edu

Consortium for Functional Glycomics
www.functionalglycomics.org

Emory University School of Medicine
www.med.emory.edu

Imperial College London
www.imperial.ac.uk

Life Technologies
www.lifetechnologies.com

New England Biolabs
www.neb.com

Seikagaku Biobusiness Corporation
www.seikagakubb.co.jp/english/

Sigma-Aldrich
www.sigmaaldrich.com

Thermo Fisher Scientific
www.thermoscientific.com

University of Georgia
www.uga.edu

University of Gothenburg
www.gu.se/english

University of New Hampshire
www.unh.edu

Vector Laboratories
www.vectorlabs.com

compositions and chemical linkages. "There may be well over 10,000 carbohydrate structures in the human glycome," says Cummings.

One variable, for instance, is the glycan-peptide bond. Glycans couple to proteins primarily in two ways, though dozens of different linkages have actually been des cribed, says Cummings. In *O*-linked glycans, sugars are linked to the protein backbone through the hydroxyl oxygens of serine and threonine residues; *N*-linked carbohydrates couple via the nitrogen atoms in asparagine side chains.

With so many variables, glycosylation provides "a massive exponential enhancement to the information content in the genome," Cummings says. The molecular adage, one gene-one protein, still holds, but glycosylation turns that notion on its head. Glycodelin, for instance, is expressed both in males and females, in two very different glycoforms. In women, the glycoprotein is a contraceptive; in men, it promotes sperm-egg binding.

Clearly, comprehensive analysis of glycan modifications is required. Yet how deep that analysis should be remains an open question. Paulson, for instance, says it's likely that in many cases what matters is not so much the exact chemical nature of a particular glycan modification as that any modification is present at all. "Biological variation doesn't necessarily mean functionally important," Paulson says. "Do you really want to know the structure of every possible variation that can occur? The answer is absolutely no, because it's not biologically relevant."

Plus, actually solving a glycan's complete structure—not just its composition, but also its order and inter-unit linkages—is a complex, time-consuming exercise, something many proteomics researchers are either unwilling or unable to do. Yet the payoff is an entirely new level of information. "By doing glycomics you actually know what structures are there—if you do it well," says Wells. One researcher who does it best, he says, is Anne Dell, whose lab untangled the glycodelins; Wells calls Dell "one of the mothers [of glycobiology]." Another standout, he says, is Vern Reinhold.

SUGARS AND SCARS

Reinhold, a chemist at the **University of New Hampshire,** is a glycomicist; he focuses on glycans in the absence of protein. His philosophy, in essence, is that when it comes to glycans, knowledge is power. "You cannot understand the structure of a carbohydrate until you look at every intervening linkage between each monomer, because they all vary," he says. "It can vary by one residue and [that may] be the effective residue that gives the carbohydrate its function."

Imagine, Reinhold explains, a tree made of colored Lego bricks and spray-painted white is sitting at the top of a flight of stairs. A kitten knocks it over onto the top step, where it shatters into large sections. As the kitten continues to play, it knocks each section further down the staircase until only individual pieces remain. Disaster? Hardly. All you need is a little intuition.

The Legos that are not white must have been internal to the structure, for instance, whereas the fully painted pieces resided on the surface. By comparing these fragments with a record of pieces known to be part of the structure—the instruction manual used to build the tree, say—a clever child can rebuild their masterpiece. "From known fragments we could follow the pieces back up the stairs, matching end-pieces to 're-synthesize' the tree," Reinhold explains.

In the lab, sample preparation and analysis steps create a number of molecular clues. Glycan-protein attachment points are reduced following either enzymatic release with PNGase F (for *N*-linked glycans; available through **Sigma-Aldrich** and **New England Biolabs**) or mild base treatment (for *O*-linked glycans). The molecules are then permethylated (the paint analog), which tags outward-facing and non-branched hydroxyls, and introduced into an ion trap mass spectrometer. Finally the mass spec—the stairs in this analogy—introduces a molecular "scar" by selecting glycans one by one and iteratively fragmenting and measuring them in an approach called MS(n).

In MS(n), the instrument fractures the glycans first along glycosidic bonds, and ultimately across the sugar rings themselves to reveal intramonomeric linkages—a series of fragments that, as with the Lego tree, may be matched against a library of known fragments. Armed with these data, and by working backwards up the molecular staircase, glycomicists can deduce the glycan's original structure.

TO THE GLYCOPROTEOME

At this point, a glycomicist's job is finished. Glycoproteomicists, though, face an even bigger challenge: assigning these glycomics data to the proteins the glycans once were attached to. Nobody can do that on a proteomics level yet, but researchers have decoded the glycobiology of individual proteins. In May 2010, for instance, Wells and his colleagues detailed the glycoprofile of alpha-dystroglycan (α-DG), an *O*-glycosylated protein that has been implicated in congenital muscular dystrophies. They published their findings in the *Journal of Biological Chemistry;* an independent team at the **University of Gothenburg,** Sweden, published a similar study the same day, in *Glycobiology.*

As Wells explains, researchers could already identify where on the protein glycosylation occurred, but not what specific chains were there. They also knew, in general, what kind of sugars they were looking for. The problem was putting all that information together.

Using glycomics, Wells' team identified 21 different *O*-linked glycans with abundances ranging from one-quarter of the total glycan, to less than 0.1 percent. Then, they attacked the protein itself. Tryptic peptides of the purified protein were introduced into the mass spec, weighed, and fragmented. Those that underwent a "neutral loss"—that is, the loss of a glycan—were fragmented again and again, each time peeling off one glycan until finally they reached the peptide itself, like chopping celery from the base of the stalk until you hit the greens. Because the researchers had already mapped the possible glycans, it was relatively easy to match the fragmentation patterns with that list to figure out which sugars went where.

The study, which CCRC colleague David Live calls "probably the most detailed analysis of a glycoprotein [ever published]," revealed, among other things, that α-DG contains four different glycans on serine-475 and two on threonine-478—a taste of the protein's saccharide heterogeneity, if you will. Yet it cannot easily be extended to high throughput proteomics, Wells says, because the informatics becomes too complex.

With α-DG, "We knew all the possible [glycan] structures that could be there, and we knew the protein. That allows us to confine our search space with two different parameters," he explains. But applying the same search algorithm to, say, a total cellular lysate wouldn't work, he says; "You're not going to have any confidence in any of those identifications."

MAKING MASS SPEC SMARTER

Wells' α-DG study was accomplished using an LTQ ion trap mass spec from **Thermo Fisher Scientific** (though other mass specs, such as those from **Bruker Daltonics, Life Technologies,** and **Agilent Technologies,** could also be used, he notes). In an ion trap, fragmentation is induced by collision with high-energy gas, which cleaves the weakest bond in a molecule first. Unfortunately, that is frequently the bond connecting posttranslational modifications to the peptide backbone. Researchers can thus isolate modified peptides, but when they go to determine where the modification actually is, they usually cannot find it.

There is an alternative, however. Electron transfer dissociation (ETD) cleaves peptide bonds while ignoring those between modifications and the peptide, allowing researchers to "step through [a peptide] and see whether an amino acid is glycosylated," says Live. The technique has "changed the game in terms of posttranslational modification site mapping. It's a huge, huge development," says Wells.

Wells, with collaborator Rosa Viner at Thermo Fisher Scientific, has used ETD to map *O*-GlcNAc modifications on proteins. Using antibodies to *O*-GlcNAc, the team isolated modified proteins and digested them into peptides. They then injected those peptides, only some fraction of which actually contain the desired modification, into a high-resolution Thermo LTQ Orbitrap Velos mass spec and allowed the instrument to probe them one at a time.

In a technique called HCD-triggered ETD, the instrument interrogates each ion, essentially asking, *are you a glycopeptide?* To do that, it hits each peptide once in HCD mode (high-energy collisional dissociation, another fragmentation technique) and scans for product ions that are diagnostic of glycans. If such signals are detected, the instrument switches to ETD mode to sequence the peptide; otherwise, the peptide is ignored, as it is not a glycopeptide.

Using this strategy, the team identified about 350 modified proteins, and mapped some 100 unique sites, Viner says. "It basically [makes] the mass spectrometer a little smarter," Wells says. "It's not wasting its time on things that we are not interested in, but it's actually spending more time on peptides that are glycosylated."

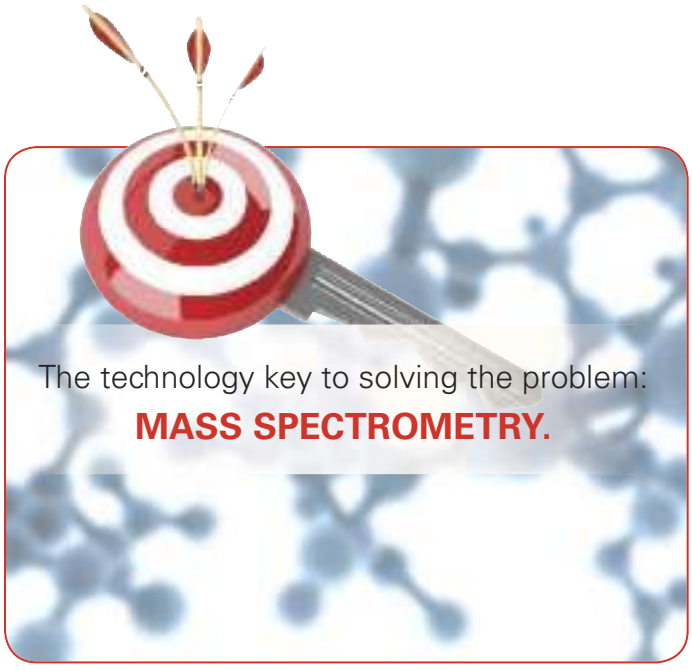

CAPTURING GLYCANS

Of course, to study glycopeptides, researchers first need to capture them lest their signal be drowned out by the noise. Using antibodies like Wells is one approach, but there are others. Some, for instance, oxidize glycans to chemically couple them (with their associated peptides) to hydrazide beads. Others use lectins—specific carbohydrate-binding proteins available from companies such as **Vector Laboratories** and **Seikagaku Biobusiness Corporation**—as affinity reagents. Earlier this year Matthias Mann and colleagues used a lectin-based peptide purification strategy to identify nearly 6,400 *N*-glycosylation sites on 2,352 proteins from mouse tissues.

Linda Hsieh-Wilson, professor of chemistry at the **California Institute of Technology,** uses enzyme engineering. Like Wells, Hsieh-Wilson is interested in *O*-GlcNAc-containing proteins. Her team engineered a glycosyltransferase enzyme that normally couples a sugar to *O*-GlcNAc to accept an "unnatural sugar"—UDP-galactose with a ketone or azide functional group. That functional group, she explains, "gives us a way to attach different chemical handles," from biotin (for purification) to fluorophores. (Life Technologies and Thermo Fisher Scientific market in vivo variants of this technology; Life Technologies' Click-iT Metabolic Labeling Reagents use an azide-alkyne conjugation reaction to label glycoproteins, while Thermo's GlcNAz, GalNAz, and ManNAz reagents couple via azide-phosphine chemistry.)

Hsieh-Wilson calls this approach "chemoenzymatic labeling," in that an enzyme performs the first step, but the second step is pure chemistry. The best part, she says, is its specificity; the enzyme will only tag those proteins containing the specific modification of interest. But that specificity is something of a double-edged sword; extending the technique to target other modifications is, she admits, "the hard part."

In a field as complicated as glycoproteomics, it's just one of many.

Jeffrey M. Perkel is a freelance science writer based in Pocatello, Idaho.

DOI: 10.1126/science.opms.p1000051

MASS SPECTROMETER

The LCMS-8030 combines the power of triple quadrupole mass spectrometry with unmatched speed to provide the ideal complement to its UHPLC systems. The LCMS-8030 features ultrafast multiple reaction monitoring transitions, enabling data acquisition with up to 500 different channels per second. The improvements to the electronics provide ultrafast mass spectrum measurement speeds of 15,000 µ/sec without sacrificing sensitivity or resolution, and ultrafast polarity switching (15 msec) for the most information without signal deterioration. Patented UFsweeper technology accelerates ions out of the collision cell by forming a pseudo-potential surface. The result is high-efficiency collision-induced dissociation and ultrafast ion transport, reducing the sensitivity losses and cross talk observed on other systems. The LCMS-8030's robust design allows maximum uptime, resulting in a system that can handle most complex matrices. Maintenance of the desolvation line without breaking vacuum minimizes instrument downtime.

Shimadzu Scientific Instruments, Inc.
For info: 800-477-1227 | www.ssi.shimadzu.com

PROTEOGLYCAN KIT

Glycosaminoglycans (GAGs) are polysaccharides consisting of repeated dimers. All but hyaluronic acid possess sulfate bases and exist in living organisms in the form of proteoglycans. The new Sulfated GAG Quantitation Kit allows easy quantification of sulfated GAGs in tissues such as cartilage, cultured chondrocytes, and chondrocyte culture solution. Based on a colorimetric determination method using 1,9-dimethylmethylene blue, the new kit is capable of measuring amounts in the 2.5 to 80 µg/mL range within a wide standard curve. Provided in a standard 96-well plate format that can be stored for up to one year, the kit facilitates simple, simultaneous processing of multiple samples. Additionally, a selection of new standards for a broad range of glycobiology and glycoanalysis has been launched, including oversulfated chondroitin sulfate, dermatan sulfate, hyaluronic acid from porcine skin, and heparan sulfate from porcine mucosa.

AMS Biotechnology
For info: +44-1235-828200 | www.amsbio.com

GLYCAN/GLYCOPEPTIDE DATA ANALYSIS

SimGlycan is a high throughput glycan and glycopeptide structure elucidation tool, which now supports multi-stage mass spectrometry data analysis which enables identification of structure specific fragment pathways. The program now includes comprehensive support to perform multi-stage/sequential mass spectrometry data analysis, which involves refragmentation of product ions. Multi-stage mass analysis provides structural information that is useful in structure elucidation of metabolites, glycopeptides, and glycans. It aids in discrimination of glycans having similar characteristic fragment ions at MS/MS level. It resolves heterogeneity of carbohydrate distribution and branching pattern of complex glycans such as isobaric isomers.

PREMIER Biosoft International
For info: 888-847-7494 | www.premierbiosoft.com

PROTEIN EXTRACTION

Four new kits that are designed to simplify the extraction of proteins from cells and tissues are now available. Fast and easy to use, individual DUALXtract kits are available for total protein extraction, the extraction of integral membrane proteins and membrane-associated proteins, and the isolation of cytoplasmic and nuclear proteins. DUALXtract Mammalian Cell Total Protein Extraction Reagent provides gentle one-step extraction of total protein, while the DUALXtract Nuclear and Cytoplasmic Protein Extraction Kit rapidly isolates cytoplasmic and nuclear proteins from cultured cells and tissues. The DUALXtract Total Membrane Protein Extraction Kit quickly isolates high quality membrane and cytoplasmic protein fractions from mammalian cells and tissues, with no cross-contamination. The DUALXtract Membrane Protein Optimization Kit can be used to quickly identify optimal extraction conditions for membrane proteins of interest and is suitable for the extraction of native, functional membrane proteins from mammalian, fungal, and bacterial cells.

Dualsystems Biotech AG
For info: +41-(0)-44-738-50-00 | www.dualsystems.com

PROTEIN DIGESTION KITS

Two new sample preparation kits are designed to advance a "universal" sample preparation protocol for mass spectrometry-based proteome research. Filter-Aided Sample Prep (FASP) Protein Digestion Kits enable complete, reproducible solubilization, and digestion of both fluid and tissue sample proteomes, and extend mass spectrometry-based proteome research methods into the previously inaccessible realms of the insoluble and formalin-fixed paraffin-embedded (FFPE) ("biobank") proteomes. By enabling the use of strong detergents within mass spectrometry sample preparation workflows, the FASP Protein Digestion Kit offers a standardized sample preparation workflow that works for both soluble and insoluble proteins in fluids and tissues. The FFPE-FASP Protein Digestion Kit's composition is similar, but contains supplemental materials and protocol steps to guide researchers through additional tissue sample and protein treatment steps to ensure compatibility of FFPE samples with downstream mass spectrometry sample preparation and analysis workflows.

Protein Discovery, Inc.
For info: 865-521-7400 | www.proteindiscovery.com

Electronically submit your new product description or product literature information! Go to **www.sciencemag.org/products/newproducts.dtl** for more information.

Newly offered instrumentation, apparatus, and laboratory materials of interest to researchers in all disciplines in academic, industrial, and governmental organizations are featured in this space. Emphasis is given to purpose, chief characteristics, and availability of products and materials. Endorsement by *Science* or AAAS of any products or materials mentioned is not implied. Additional information may be obtained from the manufacturer or supplier.

DEEPWATER HORIZON

GULF OF MEXICO OIL SPILL

A CONFERENCE ON LESSONS LEARNED: CHARTING OUR FUTURE

BASE PHOTO: NOAA

EARLY REGISTRATION DEADLINE JANUARY 24

SPEAKERS

DR. JANE LUBCHENCO
Under Secretary of Commerce for Oceans and Atmosphere and NOAA Administrator
OPENING KEYNOTE

JOHN H. HANKINSON, JR.
Executive Director
President's Gulf Coast Ecosystem Restoration Task Force

JOHN HOFMEISTER
Founder and CEO,
Citizens for Affordable Energy, Inc.
Former CEO of Shell Oil Company

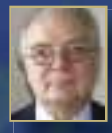

RANDY BAYLISS
The Bayliss Consultancy
State OnScene Coordinator for the Exxon Valdez Oil Spill

CONFERENCE CO-CHAIRS

ROBERT H. WEISBERG
Distinguished University Professor of Physical Oceanography, University of South Florida

WILLIAM T. HOGARTH
Acting Director, Florida Institute of Oceanography

MICHAEL P. CROSBY
Senior Vice President for Research, Mote Marine Laboratory

KEY TOPICS

GEOTECHNICAL ENGINEERING • REGIONAL OCEANOGRAPHY • CHEMICAL WEATHERING-BIOLOGICAL CONSUMPTION • DISPERSANTS • ECOLOGICAL CONSEQUENCES AND TOXICITY • ECONOMIC AND SOCIAL IMPACTS • HUMAN HEALTH ISSUES • STAKEHOLDERS, SCIENCE AND POLICY

FEBRUARY 9-11, 2011

HILTON ST. PETERSBURG BAYFRONT, ST. PETERSBURG, FLORIDA

FOR MORE INFORMATION AND TO REGISTER GO TO:

www.oilspill.usf.edu

SPONSORED BY

USF UNIVERSITY OF SOUTH FLORIDA

MOTE MARINE LABORATORY www.mote.org

STATE OF FLORIDA Oil Spill Academic Task Force

Partnerships for Innovation ORAU

Reagent Proteins

A DIVISION OF Pfenex Inc.

Your single source for proteins

Supplying Reagent, Pre-clinical and cGMP Grade Proteins to the Biopharmaceutical and Vaccine Development Community

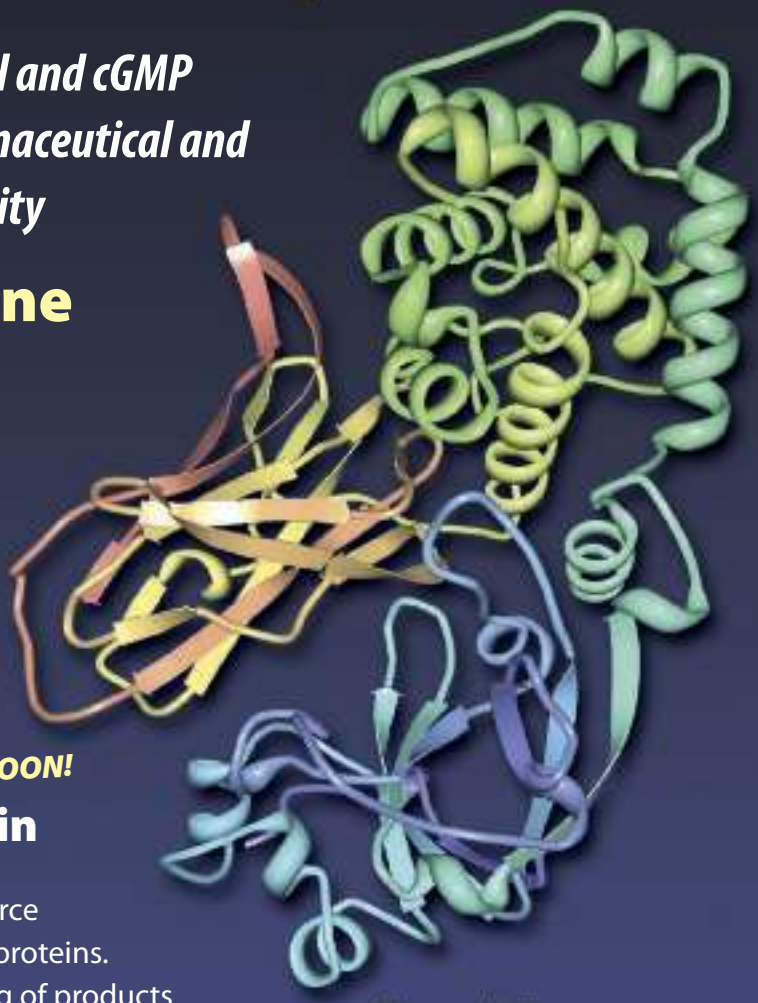

Recombinant Vaccine Components

- **CRM197**
- ***P. aeruginosa* rEPA**
- **Cholera Toxin B**
- ***E. coli* LTB**
- ***C. difficile* Toxin B**

COMING SOON!

- **Circumsporozoite Protein**

Reagent Proteins is now your single source for reagent, pre-clinical and cGMP grade proteins. See our new website for a complete listing of products and special discounts of up to 30% on recombinant human proteins.

Also available…

Cytokines
Growth Factors
Chemokines
Enzymes

Win an iPad !

Make a purchase by Feb 28, 2011 for a chance to win an iPad!

www.reagentproteins.com